QUATERNARY GEOLOGY OF THE GERMAN NORTH SEA AND WESTERN IRISH SEA MUD BELT: REVISED STRATIGRAPHIES, GEOTECHNICAL PROPERTIES, SEDIMENTOLOGY AND ANTHROPOGENIC IMPACTS

Mark J.C. Coughlan

This thesis is submitted in fulfilment of the requirement of the degree of Doctor of Philosophy

National University of Ireland, Cork
School of Biological, Earth & Environmental Sciences (Discipline of Geology)
College of Science, Engineering & Food Science.

Head of School: Dr. Sarah Culloty
Research Supervisor: Prof. Andy J. Wheeler
Co-Research Supervisor: Prof. Dr. Tobias Mörz
Research Advisor: Dr. Boris Dorschel

Vol 1 of 2
(Main text)

February 2015

TABLE OF CONTENTS

★Chapter is currently restricted access. For further information please refer to Mark Coughlan (mark.j.c.coughlan@gmail.com) or Prof. Andy Wheeler (a.wheeler@ucc.ie) .

DECLARATION

I hereby declare that this thesis has not been submitted or previously accepted as an exercise for a degree at any other university. This work is the result of my own research, except where otherwise stated.

This thesis is submitted in fulfilment of the requirement of the degree of Doctor of Philosophy at the National University of Ireland, Cork in the School of Biological, Earth & Environmental Sciences (Discipline of Geology), College of Science, Engineering & Food Science.

Signed ……..… (Mark Coughlan)

Date ……

ACKNOWLEDGEMENTS

I've found the whole PhD experience to be more a journey of self-discovery and hard slog than a course of enlightening study at times. For that journey I couldn't have asked for a better companion than Andy Wheeler, who was more than a supervisor, he was whatever was required at any particular stage: friend, motivation, drinking-buddy, inspiration, confidant, kick-in-the-ass, devil's advocate, supporter, guru. I can't thank him enough for getting me into research and the opportunities and experiences since.

A very special thanks goes to my research advisor Boris Dorschel. Again, he is more to me than the title suggests; a constant source of inspiration, guidance and friendship. He thought me the most important thing to remember in times of doubt in research: "if we knew what we were doing it wouldn't be called research!".

Vielen dank must go to my co-supervisor Tobias Mörz, his team and all at MARUM that I encountered there. Particular thanks go to Dierk Hebbeln for helping to make it happen also. It was an incredible year academically and otherwise.

My sincerest gratitude also goes to all my co-authors and collaborators, Steve McCarron, Henko de Stigter, Henk de Hass, Wim Boer, Piet van Gaever, Colm Lordan, Daniel Hepp for their stimulating discussions and sterling help. Similarly, to all who helped me with sampling and analyses I'd like to acknowledge Inka Meyer, Holger Kuhlman, Vera Lukies, Cormac Ryan, Antoinette McCarthy, Markus Eisele, Furu Mienis and J-B Stuut.

Similarly I'd like to thank my colleagues, staff and students from the School of BEES and in particular all in "Geology" past and present including all my "old" mentors and friends Ed, John Gamble, Reavy, Pat, Bettie, Ken, Alistair, Ivor and Richard, without forgetting the two Marys. Especially thanked are Cora McKenna for generally looking out for me (and everyone else!), Messrs. Willie & Dave McCarthy for all the laughs, chats (scientific and otherwise) and pints as well as Rory O'Donnell and Katrien Van Landeghem for precious help in my early days. Of course I can't forget my fellow marine geology pioneers Aaron "Field Calculator" Lim and Marian "no fish, no lamb, no duck" McGrath, having shared an office and boatspace we know each other TOO well. To the newbies (Brenton, Aidan, Mohit) I'm sure you'll keep the proud flag of geology postgrad shenanigans and endeavour flying for years to come. Above all though I must profoundly thank Mieke Thierens for being there in the beginning to show me the ropes, the middle to give me a floor to sleep on in Bremen and the end to keep me going and see it through. A truly gentle spirit.

To all "the lads" for their friendship and support over the years even though most probably haven't a clue what this thesis is about least read it. A special word for Bren to show it is possible to come out the other end…(we'll always have the castle) "It was not only a house of revelry. It was to be the hearth of a new life. And in that name all our sins were committed".

To Melanie for being so understanding and supportive, especially in the end when I started to show some of the strain because no man is deserving of a woman's love.

Lastly, but most of all, words cannot express enough thanks to my parents because "whatever else is unsure in this stinking dunghill of a world a mother's love is not", and without their love, support and guidance I'd dread to imagine where'd I'd be.

CHAPTER 1

"I've put in so many enigmas and puzzles that it will keep the professors busy for centuries arguing over what I meant, and that's the only way of insuring one's immortality" - James Joyce.

INTRODUCTION

1.1 EUROPEAN CLIMATE DEVELOPMENT OF THE MID TO LATE QUATERNARY

During the Mid to Late Quaternary (approximately the last 500,000 years), the climate development of NW Europe has been characterised by fluctuation between glacial and interglacial conditions leading to the present "interglacial" or warm period; the Holocene (Ehlers and Gibbard, 2003; Gibbard and Cohen, 2008; Ehlers et al., 2011). The trigger for this cyclicity is owed to the oblique, eccentric and precession orbit of the Earth around the Sun resulting in so-called Milankovitch cycles with periodicities of 100,000, 41,000 and 23,000 years. The strength and variability of solar radiation itself (i.e. sunspot cycles) also has a bearing on long term (centennial) climatic changes. Additionally, shorter term changes in climate (decadal) may be brought on by more abrupt events such as volcanic eruptions. A more recently prominent factor is referred to as "anthropogenic forcing". This latest shift in climatic conditions is believed to be driven largely by anthropogenic activities including enhanced warming as a result of "greenhouse" emissions, depletion of the ozone, urban growth and atmospheric pollution (IPCC, 2007). As a result there has been increased advocating to classify this latest climatic and environmental shift as a new period in the geological record referred to as the "Anthropocene" (Crutzen and Stoermer, 2000).

Ice sheets are known to have advanced into northern Europe at several stages of the Quaternary, interceded by periods of marine transgression. Traditionally, three major glacial episodes have been recognised during the Mid to Late Quaternary. These have been identified locally in the marine and terrestrial records of northern Europe and related to Marine Isotope Stages (MIS). These include the Elsterian/Anglian Stage (MIS 12), Saalian/Wolstonian Stage (MIS 10 - 6) and

Weichselian/Devensian (MIS 5d – 2) (Gibbard and Cohen, 2008; Toucanne et al., 2009). The ice sheets formed during these glacial periods did not react passively to climatic changes, but, played an active role in altering and driving regional and global climate change (Clark et al., 1999). They also had a strong modifying effect on palaeoenvironments and landscape formation (Toucanne et al., 2009).

The present warm period (i.e. the Holocene) was believed to be, in comparison to preceding periods, a time of relative climatic stability. However, in recent years, studies have shown that the Holocene can be divided into relatively cooler periods alternating with time intervals where climatic conditions ameliorated (O'Brien et al., 1995; McDermott et al., 2001). This climatic variation during the Holocene is believed to be the result of natural variation as a result of circumpolar vortex expansion and ocean-atmosphere interactions with the North Atlantic Oscillation (NAO) the principal driving factor. The Greenland ice CORE from NorthGRIP (NGRIP) indicate the Holocene began at 11,700 cal yr b2k (before AD 2000) (Walker et al., 2009). The earliest part of the Holocene witnessed a dramatic increase in temperature and rapid transition to interglacial conditions. This relatively warm climatic phase is recognised as the Holocene Thermal Maximum (HTM) or Holocene Thermal Optimum (HTO) is recorded between 11 and 5 ka BP by numerous proxy records (Kalis et al., 2003; Caseldine et al., 2006; Renssen et al., 2012). The rest of the Holocene is characterised by a general cooling in climatic conditions through the Roman Warm Period (RWP), Dark Ages Cold Period (DACP), Medieval Warm Period (MWP), Little Ice Age (LIA) and on to the present Modern Optimum (MO) where an increasing anthropogenic influence becomes noticeable (Schönwiese, 1988).

1.2 PALAEOARCHIVE SETTINGS IN NW EUROPE

Measuring present climatic and environmental conditions can be done directly using various instrumentation. Recreating past environmental conditions on any sort of resolution, however, requires an adequate archive and developed proxies. Such archives occur across a range of geographical and geological settings in NW Europe both terrestrially and in the marine realm.

Terrestrially, records of climatic variation in NW Europe (particularly during the Holocene) have been well established using tree rings (Stuiver and Braziunas, 1993), ice cores (O'Brien et al., 1995), speleothems (McDermott et al.,1999,2001), peatlands (Blundell et al., 2008; Langdon et al., 2012; Plunkett, 2006; Swindles et al., 2010, 2009, 2007; Turney et al., 2005) and based on early human settlements (Turney et al., 2006). Offshore, marine records can be reconstructed using sedimentary archives (Bond et al., 1997, 2001; Hass, 1993, 1996), scleroclimatology (Butler et al., 2010) and cold water coral settings (Thierens et al., 2010) . However, identifying archives in undisturbed settings which offer a complete record can be difficult, particularly in shallow shelf settings. This is particularly true for records tracking glacial/interglacial changes given the erosive nature of glacial advance and retreat and associated marine transgressions. The same is true in hydrodynamic settings where sediment erosion or transport is the dominant processes. Despite this, two notable settings can offer the potential to record long and short term climatic and environmental change, often to a high resolution. These are low-energy depositional settings and tunnel valleys.

Low-energy depositional settings have been identified and utilised as archives tracking climatic, hydrographical and environmental change in the North Sea (Hass, 1993; 1996; Hebbeln et al., 2003; 2006) and on the Portuguese Shelf (Martins et al., 2007; Lantzsch et al., 2009a, 2009b). In these settings, areas of fine-grained sediment accumulation (referred to as a "mud belt") were identified. These depocentres act as regional sediment traps in otherwise dynamic and high energy shallow sea settings. Usually, in such settings, although glacial material is often found at the very base where glaciation has occurred, it is Holocene sediment that is predominately deposited there. As a result, these mud belts can offer high resolution archives of Holocene climatic change.

Tunnel valleys, by contrast, tend to span several glacial/interglacial cycles. Tunnel valleys are found on formerly glaciated terrains and consist of incisions that are up to 100 km long, 5 km wide and 400 m deep. The exact formation mechanism of tunnel valleys is still widely debated with various theories proposed including direct glacial erosion, sub-glacial meltwater and both steady state and episodic/catastrophic proglacial discharge (Huuse and Lykke-Andersen, 2000 and references therein). Regardless of formation, during their history these valleys may have become

reactivated fully or partly during successive glaciations or episodes of ice-sheet advances. Subsequently, they offer ideal sites for the accumulation and preservation of both glacial and interglacial sediments that would have otherwise been stripped or reworked by proceeding glacial periods and/or marine transgressions. This can be recognised on seismic profiles with several erosion horizons and fill episodes recognised in a particular valley profile.

1.3 MOTIVATION, AIMS AND STRUCTURE

In order to fully discern and quantify these modern, anthropogenic induced changes it is important to the understand background environmental processes that they are superimposed upon and the natural variability of these processes over both long and short timescales. This will help to not only distinguish anthropogenically induced change from natural but also aid in the prediction of future development.

Epicontinental seas in shallow shelf settings in NW Europe are particularly prone to anthropogenic influence through pollution, fisheries and offshore construction such as windfarm development. Similarly, they are located at mid-latitudes which have been repeatedly affected by glacial advance and retreat during the Quaternary. Marine sedimentary sequences from these settings can offer high resolution records of climatic and environmental change during the Quaternary.

In this study the German sector of the North Sea and the Northern Irish Sea (Western Irish Sea Mud Belt in particular) are the focus areas where extensive data has been collected in recent years associated with surveying for offshore windfarm development.

Having identified tunnel valleys and low-energy depositional settings as potential palaeoarchives, the research objectives of this study are two-fold:

- If tunnel valleys afford accommodation space for sediment accumulation to occur, what are the main controls on their generation and what is the influence of their structure on the lateral and horizontal distribution of Quaternary sediments in the German North Sea? And,

- If sediment accumulation has been occurring in the Western Irish Sea Mud Belt since the end of the Last Glacial Maximum then what are the main controls on Holocene sediment accumulation here and what can it tell us about the evolution of bed stress conditions over time?

.

In order to answer these questions, the main aim of this study is to re-evaluate the current geological models for the German North Sea Sector (GNSS) and the Western Irish Sea Mud Belt (WISMB) using new and novel data that would enhance our understanding of past climatic and environmental conditions in these areas. This will involve a multi-proxy approach involving a wide range of sedimentological, geochemical, geotechnical and geophysical techniques with a view to:

- Characterise these areas geologically and develop a robust litho- and chronostratigraphy.
- Evaluate the palaeoenvirnonmental record of these settings to assess marine and nearshore terrestrial change during the Quaternary.
- Evaluate the anthropogenic impact on these areas

These aims are addressed in four manuscripts put forward in chapter 2, 3 4 and 5 of this thesis.

Chapter 2 focuses on the Quaternary deposits in the GNSS with the aim of revising the stratigraphic framework utilising new geophysical and geological data and by applying a novel approach incorporating geotechnical data. Particular focus is paid to tunnel valleys and their sedimentary successions as potential palaeoarchives.

Similarly, **Chapter 3** aims to characterise the WISMB by utilising a similar approach involving new and novel geological, geophysical and geotechnical data to enhance the current sedimentary architecture model. This will form the basis for further palaeoenvironmental studies.

Chapter 4 sees the application of a rigorous and in-depth analyses of geophysical data and core material using a multitude of proxies to reconstruct the Mid to Late Holocene depositional history of the WISMB and evaluate it as a palaeoarchive.

Developing on Chapter 4, **Chapter 5** investigates more recent changes in the sedimentological and geochemical composition of surface and near-surface sediments in the WISMB through anthropogenic activities.

The particular materials and methods pertinent to each study are presented and outlined in the relevant chapters. Considering that each manuscript is being prepared for peer-reviewed publication, the contribution of each co-author is mentioned in an introductory paragraph along with a description of how that manuscript fits in with the theme and development of the thesis.

1.4 GEOGRAPHIC SETTING AND DEVELOPMENT OF THE IRISH SEA

The Irish Sea is a, largely, tidally controlled basin located between southern Scotland, Wales, England and Ireland extending from the northern approaches of the Celtic Sea in the south to the North Channel separating the north of Ireland from southwestern Scotland (Fig. 1.1). It is a formerly glaciated shelf having last experienced glaciation from approximately 28,000 years BP until the end of the Last Glacial Maximum (LGM) approximately 17,000 years BP with shallow glaciomarine to marine conditions potentially between 21.0 – 16.0 cal kyr BP according to Roberts et al. (2006). During the LGM icesheets had merged across much of Northern Britain and Ireland, heading south through the Irish Sea, which acted as a conduit, where it eroded north-south trending tunnel valleys into bedrock (Wingfield, 1988; Eyles and McCabe, 1989). It also blanketed much of the Irish Sea with glacigenic deposits (Eyles and McCabe, 1989; Jackson et al., 1995) . Following disintegration of the ice sheet at the end of the LGM, global sea level generally rose and incurred into the Irish Sea area but isostatic rebound in the north of the Irish Sea meant an intricate relationship between global post-glacial sea level rise and crustal movement (Roberts et al., 2006) Despite glacial isostatcic adjustment (GIA) modelling suggesting this incursion occurred having breached a land bridge further south between Britain and Ireland (Lambeck, 1996a), evidence for such a land bridge still remains unresolved (Furze et al., 2014). By 6,000 years BP the area was fully marine (Lambeck, 1996b).

The Quaternary sediments in the Irish Sea generally form a drape over the underlying bedrock. These sediments mainly consist of reworked glacial and post-glacial sediments that form a complex distribution of various sediment types (Belderson, 1964; Dobson et al., 1971; Jackson et al., 1995). The present day distribution of seabed sediments is related to bed stress conditions. These bed stress conditions are a reflection of tidal dynamics which are primarily determined by the geometry of the Irish Sea basin. Bathymetrically the Irish Sea can be divided into five zones (Belderson and Stride, 1966; Jackson et al., 1995):

- Estuaries and coastal embayments with depths of high water mark to 10 m.
- Inner shelf platforms with depths of 10 to 60 m.
- The Western Trough which runs sinuously from the North Channel to St. George's Channel forming a zone up to 80 km wide and between 60 to 140 m water depth.
- Enclosed deeps that are generally 30 km long and from 10 to 165 m deeper than the general seafloor. These are glacially formed tunnel valleys which have not been infilled by sediment.
- Rocky prominences including outcrops of rock at headlands, islets and shoals and can occur at depths of 75 up to 130 m depth.

At present, the sea has access to the Atlantic Ocean through the North Channel to the north and St. George's Channel in the south with a central trough connecting the two running through the Irish Sea. It is through these two channels that tides enter the Irish Sea with the two tidal branches meeting to the southwest of the Isle of Man to form a standing wave field (Belderson and Stride, 1966). From the dengenerate amphidrome (where a bedload parting zone has been inferred) at the Wicklow-Cahore Point interval of the Irish Coast, tidal ranges increase away from this location in a northerly and southerly direction (Robinson, 1979; Van Landeghem et al., 2009). For the most part, the bed stress conditions created by these residual tidal currents exceed the energy thresholds that allow sediment to be actively eroded or induced to transport with the result that their direction are marked by migratory sediment-wave fields ending in areas of sediment accumulation; the Eastern and Western Irish Sea Mud Belt (EISMB and WISMB) in the north and Celtic Sea in the south (Belderson, 1964; Van Landeghem et al., 2009). As a result, seafloor sediments of the Irish Sea

can be divided into three types; lag or modern day erosion, sediments in transport and present day deposits (Holmes and Tappin, 2005).

Unlike the rest of the Irish Sea, which is well mixed by strong tides, the WISMB stratifies in Spring and Summer of each year. This is the result of a combination of weak tides and relatively deep water producing insufficient mixing usually generated by tides and so fails to overcome the input of surface buoyancy created by solar heating(Hill et al., 1997). Bed stress current velocities within the area generally do not exceed the 0.5 ms^{-1} to mobilize the class of sediment found there and tidal currents are largely weak at < 0.3 ms^{-1} (Hill et al., 1997; Holmes and Tappin, 2005). A seasonal gyre is known to develop in the area which increases near surface water current velocities and has been noted to have an effect on seafloor sediment and its dynamics (Callaway et al., 2009; Horsburgh et al., 2000). This is particularly true in the case of Callaway et al. (2009) who noted the formation of scour hollows at the base of bedrock structures on the seabed of the WISMB, north-east of the study area mentioned here. Their data suggested the currents in the area were responsible for the development of scour, often enhanced by the development of the gyre in addition to perturbations to the bottom current regime brought about by the obstacle of the bedrock. Furthermore, hydrogeographical modelling work carried out by Olbert et al., (2012) based on climatic changes predict a strengthening of the western Irish Sea gyre in time. Belderson (1964) also postulated that continued deposition in the area could result in a shallowing of water which would in turn cause a gradual increase in the near-bottom current velocity until the deposition of mud eventually becomes inhibited resulting in a "sand over mud" sequence. The structure and character of the Western Irish Sea Mud Belt is developed in chapters 3, 4 and 5.

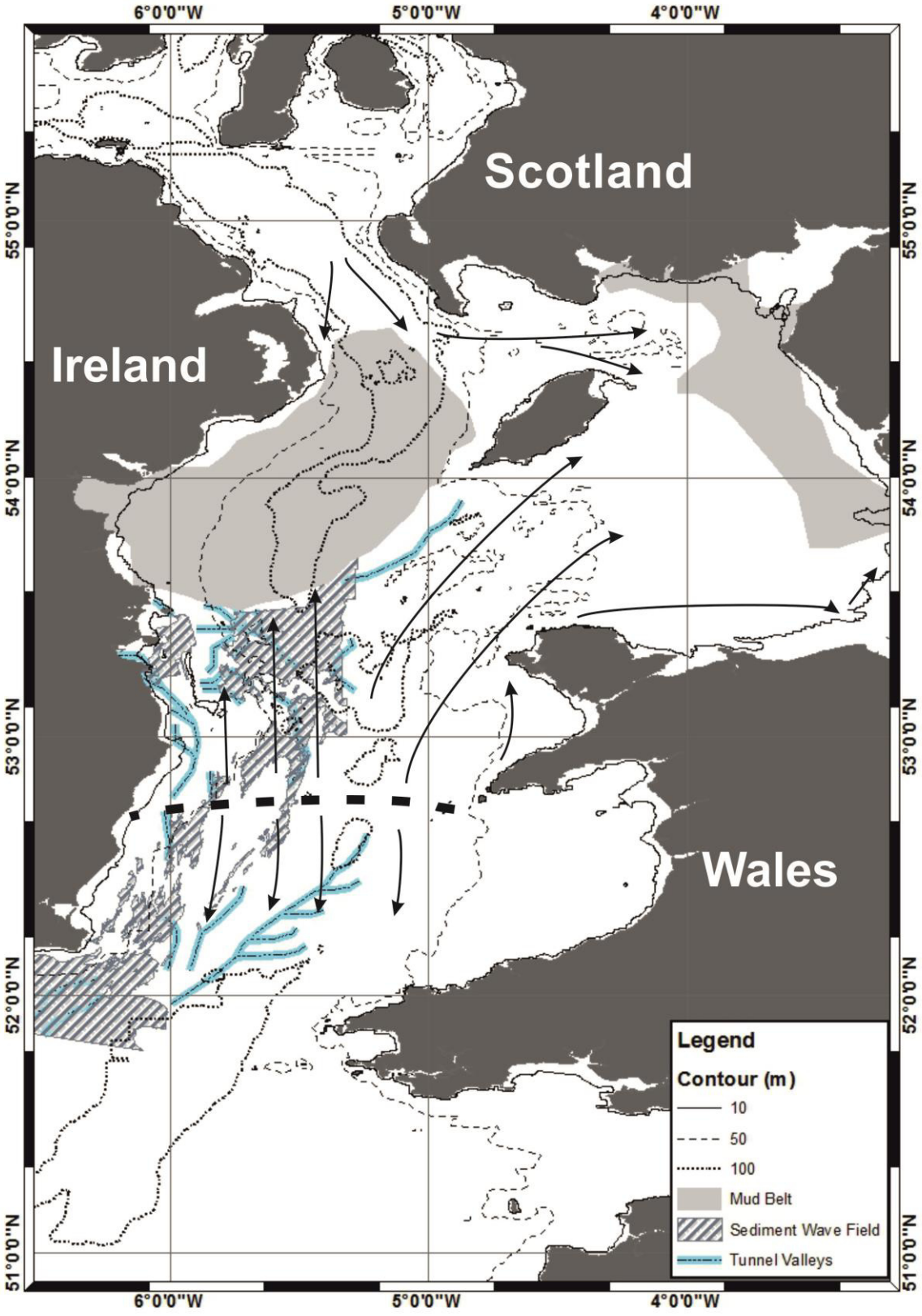

Figure 1.1 Map of the Irish Sea. Highlighted are areas of active deposition (Mud Belt) and noted sediment wave fields in the Irish sector of the Irish Sea indicating sediments in transport. Tunnel valleys are also noted (after Eyles and McCabe, 1989). Defined sediment pathways from residual tidal currents are marked by black arrows with bedload parting marked by dashed lines (Pingree and Griffiths, 1979).

1.5 GEOGRAPHIC SETTING AND DEVELOPMENT OF THE GERMAN NORTH SEA

The North Sea is also a semi-enclosed, epicontinental sea of the North Atlantic, almost surrounded on all sides by land. It is connected to the Atlantic Ocean to the north via the Norwegian Trench and the southwest through the English Channel. The North Sea has been heavily influenced by repeated glaciation during the Quaternary, an account of which can be found in chapter 2 (section 2.2)

In the southern North Sea, the German sector extends between 53° and 56°N latitude and 3° and 9°E longitude (Fig. 1.2). It is bordered to the east and south by the Danish and German coastline, to the north by a line of banks bordering the southern edge of the Norwegian Channel and extends westwards as far as Dogger Bank (Caston, 1979a). Its Quaternary geological development can be summarised as having an early stage characterised by marine to fluvio-deltaic sedimentation during the Early Pleistocene, a stage characterised by repeated ice advances and intervened by marine transgressions during the Middle and Late Pleistocene and a final stage of melting ice with the development of present day landscape and sedimentary environments in the Last Glacial Maximum and onset of the Holocene (Streif, 2004). These episodes of glaciation and marine inundation have resulted in accumulations of up to 1 km of deposits, making the German North Sea sector a major sediment repository (Caston, 1979b; Gibbard et al., 1988). Thicknesses of Holocene sediments in the German North Sea are relatively thin, between 0 - 10 m showing a maximum thickness of 16 m in the Elbe palaeovalley which runs through large parts of the sector (Figge, 1980).

In general, it is a relatively shallow and featureless area with water depth up to 60 m. Presently, the tidal circulation within the North Sea moves counter clockwise with inflow through the north and lesser southwest channels. The tidal stream is reflected off the southern coast of the North Sea with currents ranging from 75 to 125 cm s^{-1} (Zeiler et al., 2000). Whilst the majority of the seabed is featureless, the uppermost Holocene sands are known to be mobile, especially in coastal and near coastal areas with sand ridges and banks noted off the East Frisian Islands (Zeiler et al., 2000).

The sub-seabed is characterised by extensive tunnel valleys generated during the multiple phases of glaciation during the Quaternary (Cameron et al., 1987; Huuse and Lykke-Andersen, 2000; Lutz et al., 2009; Ehlers et al., 2011). These features are generally infilled and offer no seabed expression but often contain intricate sedimentary infill.

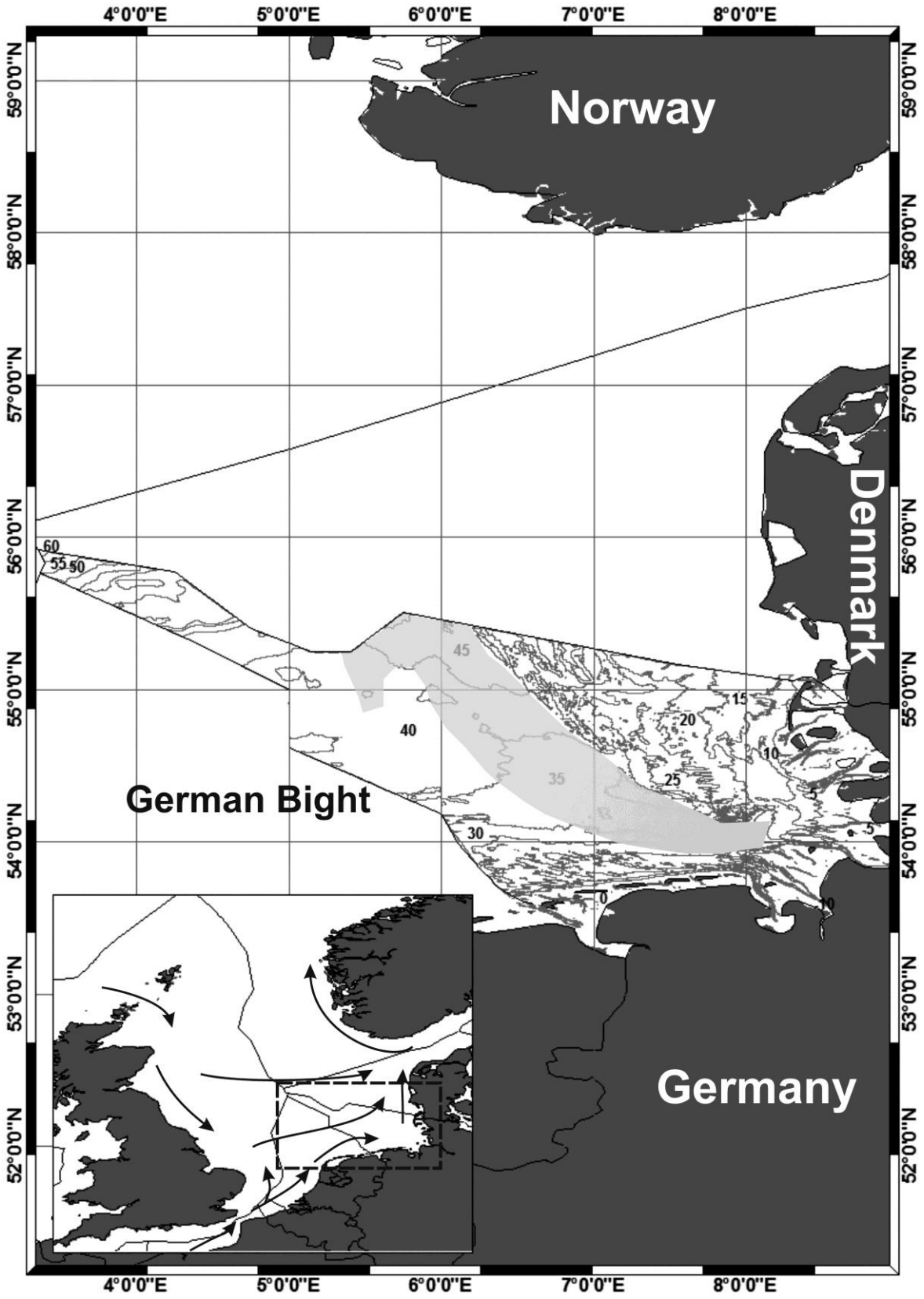

Figure 1.2 Map of the North Sea. Inset map shows location of German Economic Exclusion Zone (EEZ) with idealised tidal current directions indicated by black arrows. Main map shows EEZ with bathymetric contours and position of Elbe palaeovalley (after Figge, 1980).

1.6 ANTHROPOGENIC DEVELOPMENT WITHIN THE NORTH SEA AND IRISH SEA

The location of the Irish Sea between two populous coasts means that it is heavily subject to anthropogenic activity and influence. Dense industrial concentration along both coasts results in high levels of effluent output into the Irish Sea which has resulted in eutrophication in places (Allen et al., 1998; Evans et al., 2003). Another prominent anthropogenic input is radionuclide input resulting from low-level waste discharge from the Sellafield nuclear processing plant on the east coast of the Irish Sea at Cumbria. Operations at the plant have been on-going since 1951 with various levels of discharge over the years (Gray et al., 1995).

Demersal otter trawling is one of the most widespread fishing activities in Irish waters with fishing effort having increased substantially since the 1950s. The primary target is the "Norway Lobster" or "Dublin Bay Prawn" (*Nephrops norvegicus*) which is a highly prized commercial species. Landings of *Nephrops* from the north-east Atlantic for the past number of years have been roughly 60,000 t and in 2011 Irish *Nephrops* landings were worth approximately 36 million Euro at first sale. As a result *Nephrops* fisheries are very important to the Irish economy. However, intensive trawling is being increasingly recognised as having a heavy impact on not only the seabed structure but also habitats (Ball et al., 2000; Palanques et al., 2001). Hence, the sustainability of *Nephrops* stock and their habitat is a key priority for the fisheries industry.

Both the Irish Sea and North Sea offer strong potential sites for developing offshore renewable energy sites, namely wind farms. The utilization of this energy source (in addition to other such renewables as hydro power, direct solar power, wave, biomass, geothermal and tidal) produces little or no carbon dioxide as well as other such greenhouse gases identified as the main drivers of global climate change today, widely considered the most pressing environmental issue of the modern age. The Irish State is committed to achieving a target of 16% of all its energy needs (heat, transport, electricity) to come from renewable sources by 2020 under Directive 2009/28/EC as part of the EU's commitment to the Framework Convention on Climate Change signed at Kyoto in 1997. Ireland has at its disposal ample potential from renewable sources to achieve this goal, particularly in its offshore sector (i.e. offshore wind, wave and tidal energy). The greatest potential for offshore

wind energy in particular lies off the western coast. However, water depth increases too rapidly and so installations have to be located close to land where wave exposure is high and connection to the grid presents a problematic issue. The south coast is generally unfeasible due to a lack of shallow water close to shore and the close proximity of bedrock or rock exposure to the seabed. The east coast (i.e. Irish Sea) provides the necessary shallow water conditions to make wind energy viable as well as high energy hydrodynamic regimes which make tidal energy a possibility (Appendix A). The majority of developed projects have targeted the banks located in the Irish Sea, adjacent to the east coast of Ireland. This includes most notably the construction of seven turbines at Arklow Bank located roughly 11.7km offshore in an average water depth of 20m. Each capable of generating up to 3.6MW, totalling 25MW altogether. Phase 2 of the Arklow Bank project is currently dormant but environmental impact assessments (EIA's) and site surveys are currently being carried out at Codling Bank, Dundalk Bay and the Kish and Bray Banks in the Irish Sea as well as Skerd Rocks on the west coast for the potential construction of turbines. With increasing technology in this sector the construction of wind farms in water depths between 30-40m is becoming more and more feasible. This pushes locations for potential wind farms further offshore away from banks where sedimentary environments are less mobile and therefore scour is less of a problem (Appendix A). The utilisation of offshore wind power is considerably more advanced in the German North Sea sector. By the beginning of 2014, 520 MW of offshore wind capacity was connected to the grid in Germany. Currently five separate wind farms are operational in the German North Sea with a further eight under construction.

REFERENCES

Allen, J.R., Slinn, D.J., Shammon, T.M., Hartnoll, R.G., Hawkins, S.J., 1998. Evidence for eutrophication of the Irish Sea over four decades. Limnology and Oceanography 43, 1970–1974.

Ball, B.J., Fox, G., Munday, B.W., 2000. Long- and short-term consequences of a Nephrops trawl fishery on the benthos and environment of the Irish Sea. ICES Journal of Marine Science 57, 1315–1320.

Belderson, R.H., 1964. Holocene sedimentation in the western half of the Irish Sea. Marine Geology 2, 147–163.

Belderson, R.H., Stride, A.H., 1966. Tidal current fashioning of a basal bed. Marine Geology 4, 237–257.

Blundell, A., Charman, D.J., Barber, K., 2008. Multiproxy late Holocene peat records from Ireland: towards a regional palaeoclimate curve. Journal of Quaternary Science 23, 59–71.

Bond, G., Kromer, B., Beer, J., Muscheler, R., 2001. Persistent solar influence on North Atlantic climate during the holocene. Science 294, 2130–2135.

Bond, G., Showers, W., Cheseby, M., Lotti, R., Almasi, P., DeMenocal, P., Priore, P., Cullen, H., Hajdas, I., Bonani, G., 1997. A Pervasive Millennial-Scale Cycle in North Atlantic Holocene and Glacial Climates. Science 278, 1257–1266.

Butler, P.G., Richardson, C. a., Scourse, J.D., Wanamaker, A.D., Shammon, T.M., Bennell, J.D., 2010. Marine climate in the Irish Sea: analysis of a 489-year marine master chronology derived from growth increments in the shell of the clam Arctica islandica. Quaternary Science Reviews 29, 1614–1632.

Callaway, A., Smyth, J., Brown, C.J., Quinn, R., Service, M., Long, D., 2009. The impact of scour processes on a smothered reef system in the Irish Sea. Estuarine, Coastal and Shelf Science 84, 409–418.

Cameron, T.D.J., Stoker, M.S., Long, D., 1987. The history of Quaternary sedimentation in the UK sector of the North Sea Basin. Journal of the Geological Society 144, 43–58.

Caseldine, C., Langdon, P., Holmes, N., 2006. Early Holocene climate variability and the timing and extent of the Holocene thermal maximum (HTM) in northern Iceland. Quaternary Science Reviews 25, 2314–2331.

Caston, V.N.D., 1979a. The Quaternary Sediments of the North Sea, in: Banner, F.T., Collins, M.B., Massie, K.S. (Eds.), The North-West European Shelf Seas: The Sea Bed and the Sea in Motion. I. Geology and Sedimentology. Elsevier, Amsterdam, pp. 195–270.

Caston, V.N.D., 1979b. A new isopachyte map of the Quaternary of the North Sea, in: Oele, E., Schüttenhelm, R.T.E., Wiggers, A.J. (Eds.), The Quaternary History of the North Sea. University of Upsala, Uppsala, pp. 23–28.

Clark, P.U., Alley, R.B., Pollard, D., 1999. Northern Hemisphere Ice-Sheet Influences on Global Climate Change. Science 286, 1104–1111.

Crutzen, P.J., Stoermer, E.F., 2000. The Anthropocene. Global Change Newsletter 41, 17–18.

Dobson, M.R., Evans, W.E., James, K.H., 1971. The sediment on the floor of the southern Irish Sea. Marine Geology 11, 27–69.

Ehlers, J., Gibbard, P.L., 2003. Extent and chronology of glaciations. Quaternary Science Reviews 22, 1561–1568.

Ehlers, J., Grube, A., Stephan, H.-J., Wansa, S., 2011. Pleistocene Glaciations of North Germany — New Results, in: Quaternary Glaciations-Extent and Chronology. pp. 149–162.

Evans, G.L., le B. Williams, P.J., Mitchelson-Jacob, E.G., 2003. Physical and anthropogenic effects on observed long-term nutrient changes in the Irish Sea. Estuarine, Coastal and Shelf Science 57, 1159–1168.

Eyles, N., McCabe, A.M., 1989. The Late Devensian (<22,000 BP) Irish Sea Basin: the sedimentary record of a collapsed ice sheet margin. Quaternary Science Journal 8, 307–351.

Figge, K., 1980. Das Elbe-Urstromtal im Bereich der Deutschen Bucht (Nordsee). Eiszeitalter und Gegenwart 30, 203–211.

Furze, M.F. a., Scourse, J.D., Pieńkowski, A.J., Marret, F., Hobbs, W.O., Carter, R. a., Long, B.T., 2014. Deglacial to postglacial palaeoenvironments of the Celtic Sea: lacustrine conditions versus a continuous marine sequence. Boreas 43, 149–174.

Gibbard, P.L., Cohen, K.M., 2008. Global chronostratigraphical correlation table for the last 2 . 7 million years. Episodes 31, 243–247.

Gibbard, P.L., Rose, J., Bridgland, D.R., 1988. The history of the Great Northwest European rivers during the Past Three Million Years. Philosophical Transactions of the Royal Society of London. Series B, Biological Sciences 318, 559–602.

Gray, J., Jones, S.R., Smith, A.D., 1995. Discharges to the environment from the Sellafield site, 1951-1992. Journal of Radiological Protection 15, 99.

Hass, H.C., 1993. Depositional processes under changing climate: Upper Subatlantic granulometric records from the Skagerrak (NE-North Sea). Marine Geology 111, 361–378.

Hass, H.C., 1996. Northern Europe climate variations during late Holocene: evidence from marine Skagerrak. Palaeogeography, Palaeoclimatology, Palaeoecology 123, 121–145.

Hebbeln, D., Knudsen, K.-L., Gyllencreutz, R., Kristensen, P., Klitgaard-Kristensen, D., Backman, J., Scheurle, C., Jiang, H., Gil, I., Smelror, M., Jones, P.D., Sejrup, H.-P., 2006. Late Holocene coastal hydrographic and climate changes in the eastern North Sea. The Holocene 16 , 987–1001.

Hebbeln, D., Scheurle, C., Lamy, F., 2003. Depositional history of the Helgoland mud area, German Bight, North Sea. Geo-Marine Letters 23, 81–90.

Hill, A.E., Brown, J., Fernand, L., 1997. The summer gyre in the Western Irish Sea: Shelf sea paradigms and management implications. Estuarine, Coastal and Shelf Science 44, Supple, 83–95.

Holmes, R., Tappin, D.R., 2005. DTI Strategic Environmental Assessment Area 6, Irish Sea, seabed and surficial geology and processes.

Horsburgh, K.J., Hill, A.E., Brown, J., Fernand, L., Garvine, R.W., Angelico, M.M.P., 2000. Seasonal evolution of the cold pool gyre in the western Irish Sea. Progress in Oceanography 46, 1–58.

Huuse, M., Lykke-Andersen, H., 2000. Overdeepened Quaternary valleys in the eastern Danish North Sea: morphology and origin. Quaternary Science Reviews 19, 1233–1253.

IPCC, 2007. Climate Change 2007 : An Assessment of the Intergovernmental Panel on Climate Change, Change. Cambridge University Press.

Jackson, D.I., Jackson, A.A., Evans, D., Wingfield, R.T.R., Barnes, R.P., Arthur, M.J., 1995. United Kingdom offshore regional report: the geology of the Irish Sea. British Geological Survey, London.

Kalis, A.J., Merkt, J., Wunderlich, J., 2003. Environmental changes during the Holocene climatic optimum in central Europe - human impact and natural causes. Quaternary Science Reviews 22, 33–79.

Lambeck, K., 1996a. Limits on the areal extent of the Barents Sea ice sheet in Late Weichselian time. Global and Planetary Change 12, 41–51.

Lambeck, K., 1996b. Glaciation and sea-level change for Ireland and the Irish Sea since Late Devensian/Midlandian time. Journal of the Geological Society 153, 853–872.

Langdon, P.G., Brown, A.G., Caseldine, C.J., Blockley, S.P.E., Stuijts, I., 2012. Regional climate change from peat stratigraphy for the mid- to late Holocene in central Ireland. Quaternary International 268, 145–155.

Lantzsch, H., Hanebuth, T.J.J., Bender, V.B., 2009a. Holocene evolution of mud depocentres on a high-energy , low-accumulation shelf (NW Iberia). Quaternary Research 72, 325–336.

Lantzsch, H., Hanebuth, T.J.J., Bender, V.B., Krastel, S., 2009b. Sedimentary architecture of a low-accumulation shelf since the Late Pleistocene (NW Iberia). Marine Geology 259, 47–58.

Lutz, R., Kalka, S., Gaedicke, C., Reinhardt, L., Winsemann, J., 2009. Pleistocene tunnel valleys in the German North Sea: spatial distribution and morphology. Zeitschrift der Deutschen Gesellschaft für Geowissenschaften 160, 225–235.

Martins, V., Dubert, J., Jouanneau, J., Weber, O., Ferreira, E., Patinha, C., Alveirinho, J.M., Rocha, F., 2007. A multiproxy approach of the Holocene evolution of shelf – slope circulation on the NW Iberian Continental Shelf 239, 1–18.

McDermott, F., Frisia, S., Huang, Y., Longinelli, A., Spiro, B., Heaton, T.H.E., Hawkesworth, C.J., Borsato, A., Keppens, E., Fairchild, I.J., van der Borg, K., Verheyden, S., Selmo, E., 1999. Holocene climate variability in Europe: Evidence from δ18O, textural and extension-rate variations in three speleothems. Quaternary Science Reviews 18, 1021–1038.

McDermott, F., Mattey, D.P., Hawkesworth, C., 2001. Centennial-Scale Holocene Climate Variability Revealed by a High-Resolution Speleothem δ18O Record from SW Ireland. Science 294 , 1328–1331.

O'Brien, S.R., Mayewski, P.A., Meeker, L.D., Meese, D.A., Twickler, M.S., Whitlow, S.I., 1995. Complexity of Holocene Climate as Reconstructed from a Greenland Ice Core. Science 270 , 1962–1964.

Palanques, A., Guille, J., Puig, P., 2001. Impact of bottom trawling on water turbidity and muddy sediment of an unfished continental shelf. Limnology and Oceanography 46, 1100–1110.

Plunkett, G., 2006. Tephra-linked peat humification records from Irish ombrotrophic bogs question nature of solar forcing at 850 cal. yr BC. Journal of Quaternary Science 21, 9–16.

Renssen, H., Seppä, H., Crosta, X., Goosse, H., Roche, D.M., 2012. Global characterization of the Holocene Thermal Maximum. Quaternary Science Reviews 48, 7–19.

Roberts, D.H., Chiverrell, R.C., Innes, J.B., Horton, B.P., Brooks, A.J., 2006. Holocene sea levels , Last Glacial Maximum glaciomarine environments and geophysical models in the northern Irish Sea Basin , UK 231, 113–128.

Robinson, I.S., 1979. The tidal dynamics of the Irish and Celtic Seas. Journal of Geophysical Research 56, 159–197.

Schönwiese, C.D., 1988. Grundlagen und neue Aspekte der Klimatologie. Frankfurter Geowissenschaftliche Arbeitan, Frankfurt.

Streif, H., 2004. Sedimentary record of Pleistocene and Holocene marine inundations along the North Sea coast of Lower Saxony , Germany. Quaternary International 112, 3–28.

Stuiver, M., Braziunas, T.F., 1993. Sun, ocean, climate and atmospheric 14CO2 : an evaluation of causal and spectral relationships. The Holocene 3 , 289–305.

Swindles, G.T., Blundell, a., Roe, H.M., Hall, V. a., 2010. A 4500-year proxy climate record from peatlands in the North of Ireland: the identification of widespread summer “drought phases”? Quaternary Science Reviews 29, 1577–1589.

Swindles, G.T., Charman, D.J., Roe, H.M., Sansum, P.A., 2009. Environmental controls on peatland testate amoebae (Protozoa: Rhizopoda) in the North of Ireland: Implications for Holocene palaeoclimate studies. Journal of Paleolimnology 42, 123–140.

Swindles, G.T., Plunkett, G., Roe, H.M., 2007. A multiproxy climate record from a raised bog in County Fermanagh , Northern Ireland : a critical examination of the link between bog surface wetness and solar variability 22, 667–679.

Thierens, M., Titschack, J., Dorschel, B., Huvenne, V.A.I., Wheeler, A.J., Stuut, J., Donnell, R.O., 2010. The 2 . 6 Ma depositional sequence from the Challenger cold-water coral carbonate mound (IODP Exp . 307): Sediment contributors and hydrodynamic palaeo-environments. Marine Geology 271, 260–277.

Toucanne, S., Zaragosi, S., Bourillet, J.F., Gibbard, P.L., Eynaud, F., Giraudeau, J., Turon, J.L., 2009. A 1.2 Ma record of glaciation and fluvial discharge from the West European Atlantic margin. Quaternary Science Reviews 28, 2974–2981.

Turney, C., Baillie, M., Clemens, S., Brown, D., Palmer, J., Pilcher, J., Reimer, P., Leuschner, H.H., 2005. Testing solar forcing of pervasive Holocene climate cycles. Journal of Quaternary Science 20, 511–518.

Turney, C.S.M., Baillie, M., Palmer, J., Brown, D., 2006. Holocene climatic change and past Irish societal response. Journal of Archaeological Science 33, 34–38.

Van Landeghem, K.J.J., Uehara, K., Wheeler, A.J., Mitchell, N.C., Scourse, J.D., 2009. Post-glacial sediment dynamics in the Irish Sea and sediment wave morphology: Data–model comparisons. Continental Shelf Research 29, 1723–1736.

Walker, M., Johnsen, S., Rasmussen, S.O., Popp, T., Steffensen, J., Cwynar, L.E.S.C., Hughen, K., Gibbard, P., Hoek, W.I.M., Lowe, J., Andrews, J., Bjo, S., 2009. Formal definition and dating of the GSSP (Global Stratotype Section and Point) for the base of the Holocene using the Greenland NGRIP ice core , and selected auxiliary records. Journal of Quaternery Science 24, 3–17.

Wingfield, R.T.R., 1989. Glacial incisions indicating Middle and Upper Pleistocene ice limits off Britain. Terra Research 1, 538–548.

Zeiler, M., Schulz-Ohlberg, J., Figge, K., 2000. Mobile sand deposits and shoreface sediment dynamics in the inner German Bight (North Sea). Marine Geology 170, 363–380.

CHAPTER 2

A REVISED STRATIGRAPHIC FRAMEWORK FOR THE QUATERNARY DEPOSITS OF THE GERMAN NORTH SEA SECTOR: A GEOLOGICAL - GEOTECHNICAL APPROACH

Theme

Quaternary sediments from across the North Sea have been used extensively in reconstructing various glacial periods, marking the extent of ice sheets and their active processes, as well as the intermittent marine transgressions associated with ice sheet retreat and interglacial periods. Similarly, tunnel valleys have been identified as features which allow accommodation space for sediment deposition, potentially spanning glacial/interglacial cycles, that also protect these sediments from subsequent erosion and reworking. As such they are sediment palaeoarchives recording sequential stages of ice advance, disintegration, retreat and post glacial activity. In this chapter we compare the sedimentary succession of tunnel valleys found in the German North Sea sector against the record of background sedimentation from laterally deposited sediments in order to investigate if they garner new insights into Quaternary palaeoenvironmental settings. We do so using new and novel geological, geophysical and geotechnical techniques and data.

Contributors

Mark Coughlan is the first author on this manuscript having undertaken evaluation of this data and written all drafts of the manuscript.

Andrew J. Wheeler is the lead supervisor on this PhD project, arranged the collaboration between UCC and MARUM for this project, contributed to the discussion and proof read every draft of this manuscript.

Daniel A. Hepp aided in the interpretation of CPT data, contributed to the discussion and read all draft manuscripts.

Tobias Mörz Supplied all the data used in this study through numerous surveys he undertook in collaboration with industrial partners. He contributed to the discussion and proof read all stages of this manuscript

Dierk Hebbeln arranged the collaboration and helped secure funding for this project. He also proof read the final manuscript draft.

CHAPTER 2

A REVISED STRATIGRAPHIC FRAMEWORK FOR THE QUATERNARY DEPOSITS OF THE GERMAN NORTH SEA SECTOR: A GEOLOGICAL - GEOTECHNICAL APPROACH

ABSTRACT

This study is a synthesis of the lithostratigraphy, geotechnical properties, geometry and distribution of Quaternary deposits of the German North Sea sector. It is based on large datasets from four separate areas across the German North Sea sector and consists of seismic grids, cores and in-situ cone penetration tests (CPTu). Nine buried valleys and two shallow channels were identified from seismic profiles with three stages of valley generation inferred. Infill of these tunnel valleys consisted of meltwater sands, reworked till remnants, marine and lacustrine fine-grained sediments. Elsewhere, extensive tabular units have formed consisting of marine and outwash sands. Two saltdomes were also recognised which have had an effect on valley formation and uplifting of sediments. The integration of seismic, core and geotechnical data has allowed for a revision of the Mid to Late Quaternary stratigraphy of the German North Sea sector.

KEYWORDS: German continental shelf, Quaternary, seismic stratigraphy, lithostratigraphy, tunnel valley, cone penetration testing, deposit geometry.

This chapter is based on: Coughlan, M., Wheeler, A.J., Hepp, D.A., Mörz, T., Hebbeln, D. (submitted). A revised Stratigraphic Framework for the Quaternary Deposits of the German North Sea Sector: a Geological - Geotechnical Approach. *Quaternary Science Reviews*.

2.1 INTRODUCTION

In comparison to neighbouring countries the offshore Quaternary stratigraphy of the German North Sea remains largely under-investigated (Cameron et al., 1987). This can be attributed to the paucity of scientifically published information and data relating to the upper 100m or so of the German North Sea sub-surface as early surveys experienced poor recovery from sedimentary sequences, limited seismic depth penetration and resolution and the geomorphological context for features was not easily identifiable (Graham et al., 2008). As a result, generally oversimplified lithostratigraphies were presented (e.g. Sindowski, 1970).

A key step in further developing offshore stratigraphy is the mapping (and subsequent infill description) of Quaternary tunnel valleys. Tunnel valleys are overdeepened and irregular channels which, generally, have no surface expression on the seafloor in the North Sea (Ehlers and Wingfield, 1991; Huuse and Lykke-Andersen, 2000; Kluiving et al., 2003; Lutz et al., 2009). They are believed to be formed beneath or adjacent to large continental ice-sheets (Ó' Cofaigh, 1996) and are found across all sectors of the North Sea as well as the rest of Northern Europe both on- and offshore (Ehlers and Linke, 1989; Piotrowski, 1994; Huuse and Lykke-Andersen, 2000). Three separate generations of valley formation documented in the areas were correlated with known stages of ice advance into the area during the Elsterian (twice) and the Saalian (Ehlers and Linke, 1989; Huuse and Lykke-Andersen, 2000; Kluiving et al., 2003; Kristensen et al., 2007). The exact formation of these valleys can be explained by a variety of mechanisms including hydrostatic driven sub-glacial meltwater and groundwater drainage, catastrophic meltwater discharge (or Jökulhlaups), glacial erosion, river erosion during glacial lowstand, aggradation of delta channels and tidal scour (Ehlers et al., 1984; Ehlers and Wingfield, 1991; Huuse and Lykke-Andersen, 2000; Praeg, 2003). Huuse and Lykke-Andersen (2000) compiled an extensive map of existing and new data regarding the occurrence, inferred age and orientation of valleys across the North Sea. The timing of their formation can usually be deduced by their depth and can be further constrained by studying their fill (Cameron et al., 1987; Wingfield, 1990; Huuse and Lykke-Andersen, 2000; Hepp et al., 2012). The interior structure of these tunnel valleys often exhibit various stages of erosion and deposition reflecting a long history with multiple events recorded in the stratigraphy and expressed in seismic data (Lutz et al., 2009). This fill can be highly variable with glacial tills, deltaic

sands, tidal clays and silts, glaciofluvial, glaciolacustrine and marine sedimentation all recorded (Cameron et al., 1987; Huuse and Lykke-Andersen, 2000; Kluiving et al., 2003; Praeg, 2003). Tunnel valleys are, therefore, depressions with the potential to preserve information regarding sedimentary depositional history which may be otherwise erased, eroded or reworked by overriding glaciers or marine transgressions. Hence, they often record lithologies that are rarely (if at all) seen elsewhere in both offshore and onshore deposits, most notably Lauenburg Clay as well as Eemian and Holsteinian interglacial deposits (Cameron et al., 1987; This study).

The advent of increased interest in renewable energy in the offshore sector has brought new advances in offshore site investigation and yielded a new suite of data focusing on the geological and mechanical properties of the upper sedimentary layers in addition to extensive geophysical surveys. As a result, the study of offshore stratigraphy has benefitted from increased groundtruthing by sediment cores with in-situ measurements (such as Cone Penetration Tests or CPTu) along with an increased density and much improved resolution of seismic imaging allowing for a dependable interpretation of sedimentary processes and models. Similarly, data and information relating to the geology of the entire German North Sea sector from the seabed to several metres (and even kilometres) depth is being collated and digitised through the Geopotenzial Deutsche Nordsee (GPDN) project (www.gpdn.de).

This paper focused on four study areas within the German Exclusive Economic Zone (EEZ) where new data provides, for the first time, a detailed evaluation of depositional history and stratigraphy. These areas reveal a stratigraphic sequence comprising laterally extensive tabular units incised by palaeovalleys with multiple fills. Consistencies and details from the four study areas allow for regional stratigraphic correlation across the German EEZ.

This paper aims to reappraise the stratigraphy and geometry of the Quaternary deposits of the German EEZ by linking new seismic data with recovered core lithostratigraphies and geotechnical properties. Furthermore, these analyses will garner new insights into depositional history and palaeoenvironments.

2.2 QUATERNARY HISTORY OF THE NORTH SEA

The Quaternary cover of the German North Sea is characterised by a high degree of lateral and vertical complexity with heterogeneous facies assemblages. This heterogeneity is largely localised and controlled by a variety of basin wide and local factors making a lateral correlation of individual Quaternary successions difficult. The complexity of Quaternary deposits within the area can be explained by its history characterised by repeated ice advances intervened by marine transgressions and periglacial landscapes. This resulted in a variety of environmental settings ranging from glacial terrestrial and fluvial to lacustrine as well as brackish and marine environments with associated erosion, reworking, relocation and deposition. Major glaciations were identified onshore by studies of moraine fronts and tills. These glaciation episodes also generated an extensive channel or tunnel valley network both on- and offshore. The relative chronology of these features constrained by cross-cutting relationships, relative depth and infill allowed them to be related to glaciation episodes identified by the onshore studies.

The oldest sediments across the area are dense sands accumulated during the late Neogene/early Pleistocene in a large delta which developed across the North Sea (Cameron et al., 1987; Streif, 2004; Kuhlmann et al., 2006). It is upon these sands that the Quaternary sediments mentioned in this study rest.

Subsequent periods of glaciation occurred during the Elsterian, Saalian and Weichselian, the latter of which never extended as far south as the German North Sea (Ehlers and Gibbard, 2003; Streif, 2004; Svendsen et al., 2004). During these periods of glaciation much of the global marine water reservoir was locked up in terretrial ice and so sea level was much lower than it was now, somewhere in the region of 110 - 130 m lower (Streif, 2004). However, during the intervening Holsteinian and Eemian, sea level was higher and more in accordance with current levels (Streif, 2004; Litt et al., 2007). The final stage of ice melting during the Weichselian and onset of the Holocene marine transgression led to the development of present day environments.

The Elsterian represents the oldest recorded glaciation within the North Sea and is most prominently represented by a unconformity which generally occurs at a depth of less than 50 m below the land surface or the seafloor of the North Sea which is 80 - 90 m below present sea level

(Streif, 2004). It has been unequivocally correlated to MIS 12 by Gibbard and Cohen (2006) as well as Toucanne et al. (2009) and marks not only the beginning of repeated glacial advance and retreat on the north-western European margin but also a major switch in sedimentation from non-glacial to predominately glacial deposition. Additionally, the Elsterian is noted as a time of extensive valley formation with some reaching a length of more than 100 km, as deep as 500 m and as wide as 8 km, cutting into early Pleistocene and Tertiary deposits (Cameron et al., 1987; Wingfield, 1990; Ehlers and Wingfield, 1991; Huuse and Lykke-Andersen, 2000; Laban and Meer, 2004; Lutz et al., 2009). The Elsterian is largely believed to have comprised of, at least, two major advances (referred to as Elster 1 and Elster 2 in this study) which were interceded by an ice-free stage (Lutz et al., 2009; Stewart and Lonergan, 2011) during the course of which, the drainage system of the North Sea was rearranged with the majority of rivers blocked and forced to flow west into the Fleuve Manche (Toucanne et al., 2009; Ehlers et al., 2011). Despite the relatively large amount of seismic data for Elsterian glaciation, there is relatively little sedimentological evidence offshore, most likely due to lack of borehole penetration and reworking rather than non-deposition (Graham et al., 2008; Hepp et al., 2012). For the most part the channels are infilled by relatively fine-grained meltwater sands with small quantities of basal gravels (Grube et al., 1986; Smed, 1998; Ehlers et al., 2011). Till rarely occurs at the base of deep channels and when it does it is explained as having slumped from the glacier base (Ehlers et al., 1984). Richter (1962) was able to classify the Elsterian glacial by its clast petrology and decalification characteristics. Clast petrology in particular distinguished the two types of Elsterian till with one showing a dominance of Norwegian material, whilst the other exhibited a prevalence of Baltic material. Similarly, fine gravel analysis was used for differentiating the Elsterian from younger tills (Ehlers and Linke, 1989). Typical facies consists of brown-grey compacted material with a predominance of quartz in the coarse sand fraction (Grube et al., 1986). However, it is the Lauenburg Clay that provides the most useful stratigraphic marker from the Elsterian and was deposited following ice sheet melting with the formation of large ice-dammed lakes formed allowing for silt and clay deposition. These deposits are also found in the Netherlands and can reach thicknesses of over 150 m (Ehlers et al., 2011). The progressive deposition of the Lauenburg clay is reflected by older layers being rich in dropstones and mixed with sand with sorting increasing towards the top where a varve-like sequence of laminated sediments is found (Ehlers et al., 1984).

These glaciolacustrine silts and clays generally grade up into the marine and glaciomarine facies with arctic-boreal fauna of the early Holsteinian marine transgression which finished with the deterioration of climate at the onset of the Saalian. In Germany, the Holsteinian represents the first marine transgression since the Miocene with lake deposits showing a complete interglacial vegetational succession from subarctic - boreal through temperate to boreal conditions (Ehlers et al., 2011). The coastline of the Holsteinian North Sea was seaward of the East Frisian barrier islands with a small inlet extending into the tidal Jade Bay (Streif, 1990). The transgression progressed as far inland as 16 km, following the valleys formed during the Elsterian which were partly filled with meltwater sediments (Linke, 1993; Hinze et al., 1995). In the Hamburg region, the Holsteinian started with open water conditions with fauna indicating a water depth of 20 - 30 m (Streif, 2004). In the middle part of the succession there is evidence for warmer, shallow water with brackish conditions. More saline and deeper water conditions are observed in the uppermost part of the sequence (Knudsen, 1994). According to Linke (1993), the Holsteinian sea invaded in a single, uninterrupted rapid transgression with a vertical amplitude of more than 55 m and an average sea level rise of at least 1 m per 100 years. At this point the sea-level high stand may have lasted up to 5,000 years. Deposits in Germany usually occur at 20 - 30 m below sea level. Offshore in the southern North Sea, Holstein deposits form a discontinuous unit of very fine, fine to medium-grained marine sand with bands of silt and clay with marine shells (Cameron et al., 1987). Generally these layers are 25 m thick but locally can be 40 m. Toward the south, along the Franco-Belgium coast, shallow marine deposits were formed during a transgression from the south-west (Long et al., 1988; Balescu et al., 1997).

The subsequent Saalian was characterised by a number of climatic oscillations featuring a series of glacial advances and includes at least one warm event of interglacial character and so is referred to as the Saalian Complex (Ehlers et al., 2011). Whilst evidence for three Saalian advances in northern Germany has been well established (Ehlers et al., 1984; Grube et al., 1986; Ehlers and Linke, 1989; Piotrowski, 1994), the local stratigraphies do not match and hence issues arise with regard to classification when authors combine the three recognised tills to describe the two major sub-stages; the Drenthe and the Warthe. To avoid these complications, Ehlers et al (1984) described these three in terms of 'older', 'middle' and 'younger' till and argues for their consistent use. Grube et al. (1986), however, argue that the term "Older Saalian Glacial Stage" is less useful

outside the extent of younger Saalian sediments and uses a classification referring to Lower, Drenthe and Warthe stages. The initial warm stage (or Domnitz Interglacial) is separated from the underlying Holsteinian by sands of the Fuhne cold stage and is overlain by till of the first Saalian glacial sequence. In the North Sea, the first glaciation consisted of the British Ice Sheet deflecting the Baltic Ice Stream in the central North Sea towards the north and south (Böse et al., 2012). A second glaciation produced an erosional surface across the majority of the North Sea with a series of tunnel valleys suggesting an ice limit at around 56°N (Wingfield, 1990). Overlying this erosive surface are glacigenic sediments including till and glaciomarine deposits (Stoker et al., 1985; Cameron et al., 1987; Sejrup et al., 1987). Tills present offshore of the Netherlands and Denmark in the southern North Sea have been used in the past to infer a more extensive glacial occupation of the North Sea basin during the later Saalian (Carr, 2004). Similarly, studies of tunnel valleys and coastal sediments have provided minimum constraints on a southerly ice-sheet at 54°N (Kluiving et al., 2003; Kristensen et al., 2007). At its maximum, ice covered Denmark, parts of northern Germany and into the Netherlands (Cameron et al., 1987; Laban and van der Meer, 2004). The various extents and dynamics of the various ice advances during the Saalian are outlined in Ehlers (1990). Generally, Saalian tills differ from Elsterian till by possessing a lower quartz and higher limestone content. Additionally, in most cases, the content of shales and sandstones is slightly lower than in Elsterian till. However, Saalian tills show a large, unsystematic petrographic variability which makes correlation and definition difficult (Piotrowski, 1994). The Older Saalian glaciation in northern Germany is the equivalent of the Dutch Drenthe and the Polish Odra Glaciation (Ehlers et al., 2004). The till is characterised by Baltic indicators such as Palaeozoic limestone with some dolomites. A good account of till distribution is given in Ehlers et al. (1984, 2004). The advance covered most of Lower Saxony and reached the Lower Rhine. The Middle Saalian ice advance began in north Germany with the deposition of meltwater sands which accumulated in vast outwash fans unlike during the Elsterian when they were concentrated in buried tunnel valleys (Ehlers et al., 2004). Generally, the Middle Saalian is regarded as part of the Warthe substage and is referred to as Warthe I by Stephan (1982). The typical till of the Middle Saalian glaciation can be distinguished from the Older Saalian Glaciation by its higher content of Upper Cretaceous material. Following the Middle Glaciation, the ice front melted back to the north-east again. Evidence of

younger tills can be seen through northern Germany (Ehlers et al., 1984) but for the most part the German North Sea sector remained ice free (Ehlers, 1990).

Marine deposits belonging to the following Eem interglacial can be found at various sites in the southern North Sea but, there is a paucity of information from offshore cores. These consist of up to 20 m thick shallow marine to intertidal sand and clay in Britain. In the Dutch sector of the North Sea fully marine sediments can be found consisting of fine- to medium-grained, locally gravelly sands with a noticeably higher shell content than Holsteinian and Holocene deposits (Cameron et al., 1987). Similar deposits occur in the coastal region of Belgium, however, there is no evidence for such deposits along the French coast (Sommé, 1979). In Germany, terrestrial Eem deposits have been found in many places, for example, as mapped by Hermsdorf and Strahl (2008) for the Brandenburg and Berlin area, which includes up to 566 locations. Similarly to the west of the Börnhoved Lakes, fossil Eemian horizons have been recorded consisting primarily of deeply leached brown soils (Piotrowski, 1994). They record the average Eemian surface at around 16 - 18 m above sea level. Sediments of Eem age are exposed at a cliff in the River Elbe in Lauenburg primarily consisting of peat which hasn't been overlain by younger till demonstrating the Elbe wasn't crossed by Weichselian ice sheets here (Ehlers et al., 2004). Along the German North Sea coast the Eemian record is largely incomplete with only the upper section reconstructed on the basis of the Eemian pollen zones and counts of annual laminations (Knudsen, 1988) with the majority of deposits forming in troughs within the glaciated topography (Turner, 2000).

During the Weichselian cold stage, the sea level was more than 35 m below its present level in the southern North Sea area (Streif, 2004). Towards the northern sector of the North Sea, substantial glaciation occurred with the confluence of British and Scandinavian ice sheets at around 70,000 years BP (Carr, 2004). Much of the evidence for this is found as a subglacially deformed till in the northern part of the North Sea (Graham et al., 2010). Scotland and southern Norway were extensively glaciated prior to 39 cal ka and after 50 cal ka with the central North Sea most likely not glaciated with grounded ice failing to reach the shelf edge (Sejrup et al., 2009). Subsequently, between 39 and 29 ka, climate ameliorated with several interstadials before maximum Weichselian glaciation of the North Sea occurred between 29 and 25 ka followed by decoupling of the Fennoscandian and British icesheets resulting in the development of a marine embayment in the

northern North Sea (Sejrup et al., 2009). The phase of climatic deterioration which led to fully glacial conditions from 22,000 - 18,000 years BP caused sea-level to fall to 110 - 130 m below present level resulting in the German North Sea being largely ice free as the coastline retreated 600 km to the north, leaving the southern North Sea exposed as a periglacial plain (Streif, 2004; Graham et al., 2008). As a result the topography of the terrain at this time was characterised by lakes, dead ice hollows, melt water valleys and channels, outwash cones and plains as well as moraines (Böse et al., 2012).

A general amelioration of the climate occurred around 18,000 years BP which initiated a general rise in sea level in the North Sea which continued until the present day (Cameron et al., 1993). The subsequent progress of the marine transgression and inundation of land areas following the Weichselian caused a coastline displacement of about 600 km inland which can be divided into 3 phases (Gerdes et al., 2003; Streif, 2004). Sea level changes depended on existing ice-sheet coverage and dynamics between the British and Scandanavian ice-sheets (Graham et al., 2008). The first phase occurred from approximately 18,000 to 10,250 years BP and comprises of a sea level rise from a lowstand of about 130 to 72 m below present sea-level. This inundation gradually covered the North Sea basin. Evidence for this can be found in the central North Sea by way of palaeochannels characterised by transgressive overlaps of clastic glaciomarine to marine sediments that lie directly on terrestrial, glaciofluvial and morainic Pleistocene deposits. The earliest of these is recorded by Konradi (2000) in the narrow funnel-shaped "Heligoland Channel" which occurs as a relict in the Elbe Palaeovalley (Figge, 1980). Here, marine mollusc shells were found at a depth of 72 m below sea-level and dated at 10,250+/- 90 years BP. The second phase of transgression lasted from 10,250 to 7,100 years BP during which time tidal flat sediments became widespread in the southern North Sea between 9,000 and 8,000 years BP. At roughly 8,000 years BP the area was connected with the Middle Atlantic via the Dover Strait and fully marine conditions existed after 7,000 years BP (Eisma et al., 1981). The subsequent Holocene sequences consisted of fine- to medium-grained shell bearing shallow marine sand which is underlain by tidal flat sediments in places. Locally, limnic muds and peat occur at the base of Holocene sequences. In many places brackish marine sediments rest on an erosional contact with Pleistocene deposits. The third phase began at 7,500 years BP and has continued to today. It is characterised by 25 m of sea level rise (Streif, 2004). Zeiler et al. (2000) divided the distribution of

Holocene sediments in the German North Sea into three zones. The total amount of these sediments was calculated to be 17.8 +/- 11.3 x 10^9 m^3. Within zone 1 (0 - 10 m water depth), the maximum sediment thickness is 10 +/- 2.5 m consisting of large tidal sand tongues. Zone 2 is restricted to water depths of 10 – 15 m and characterised by a thin sand sediment cover of 0.4 - 1.5 m. In deeper waters (>15 m, zone 3), the sediment thickness increases to about 2 - 3 m with a local maximum thickness of 5 - 6 m observed. A Holocene chronology for the German North Sea was based on peat deposits which formed between 8,000 and 3,000 years BP when the relative sea-level rise slowed to less than 50 cm per year (Behre, 2004, 2007). However, this was based on a relatively stable tectonic regime. Vink et al. (2007) revised this data and compared it with geophysical modelling to suggest that Northwest Germany was subject to a total isostatic lowering of 7.5 m between 8 – 4.8 cal. ka BP when compared with Belgium. This variation in tectonic subsidence in the North Sea could account for higher than expected rates of sedimentation and called for a consideration of regional scale models when investigation relative sea-level changes. Alappat et al. (2010) used Optically Stimulated Luminescence (OSL) in combination with ^{14}C dating to show that during the terrestrial to marine transition, sedimentation in a predominately periglacial, fluvial environment continued to occur throughout the latest Weichselian and Early Holocene (approx. 16 - 8,000 years BP) right up to the elevation-dependent time of transgression. Due to the present day wave and current conditions the uppermost layer of Holocene deposits is generally mobile (Zeiler et al., 2000)

2.3 EXISTING STRATIGRAPHIC FRAMEWORK FOR GERMAN NORTH SEA

The existing stratigraphic framework for the offshore Quaternary deposits of the German North Sea sector was defined by Sindowski (1970; Fig. 2.1). This was based on 23 cores which were subsequently correlated across the area. Sindowski (1970) presents a series of cross-sections comprising 10 units derived from a stratigraphic framework incorporating each glacial and interglacial stage (Fig. 2.1). However, Sindowski's (1970) defined stratigraphy suffers from a limited number of cores and a lack of understanding of their topographical context. Predominately, this refers to their position inside or outside a series of buried valleys. The inability to relate new core

details and seismic data within the Sindowski (1970) model is what prompted this re-evaluation of the stratigraphy of the Quaternary deposits of the German North Sea sector. Based on a superior and adequate dataset for four separate areas, this study defines a more robust stratigraphic framework for the Quaternary deposits of the German North Sea sector taking due cognizance of the presence of buried valleys. Furthermore we take a new approach, comparable to similar advances in stratigraphic correlation undertaken in the Dutch North Sea Sector, in correlating seismic, downcore lithological and geotechnical parameters (Bot et al., 2005).

Epoch	Stage	Layer	Layer Thickness	Soil
Holocene	Holocene	Upper Marine Layer	1-15 m	Mostly grey fine sand and silty fine sand (silt) with molluscan residues, strongly calcareous.
Pleistocene	Weichselian	Limnic - Fluvial Layer	0-17 m	Upper Layer: clayey-sandy muds or humic materials Lower Layer: fine to medium sand with gravel component
	Eem	Middle Marine Layer	4-20 m	Fine to medium sand with gravel
	Saalian	Basin Deposit Glacial Layer Upper Glacio-fluvial Layer	0-3 m 1-10 m >2 m	Dark clay Grey, sandy glacial till or boulder poor bedload Fine to medium sand with little gravel component
	Holstein	Lower Marine Layer	>2 m	Fine to medium sands
	Elsterian	Basin Deposit Lower Glacio-fluvial Layer	To 30 m >2 m	Dark banded clays (Lauenburger Clays) Fine to medium sand with little gravel component

Figure 2.1 Established stratigraphic framework of German North Sea (after Sindowski, 1970).

2.4 MATERIALS AND METHODS

Seismic profiles, sediment cores and in-situ cone penetration tests (CPTu) gathered across four areas within the German Exclusive Economic Zone (EEZ) for the primary purpose of offshore wind farm development are used in this study (Fig. 2.2). The extensive dataset, with excellent seismic grid density and ample borehole sampling, provides a unique dataset enabling a revision of our knowledge of the German North Sea.

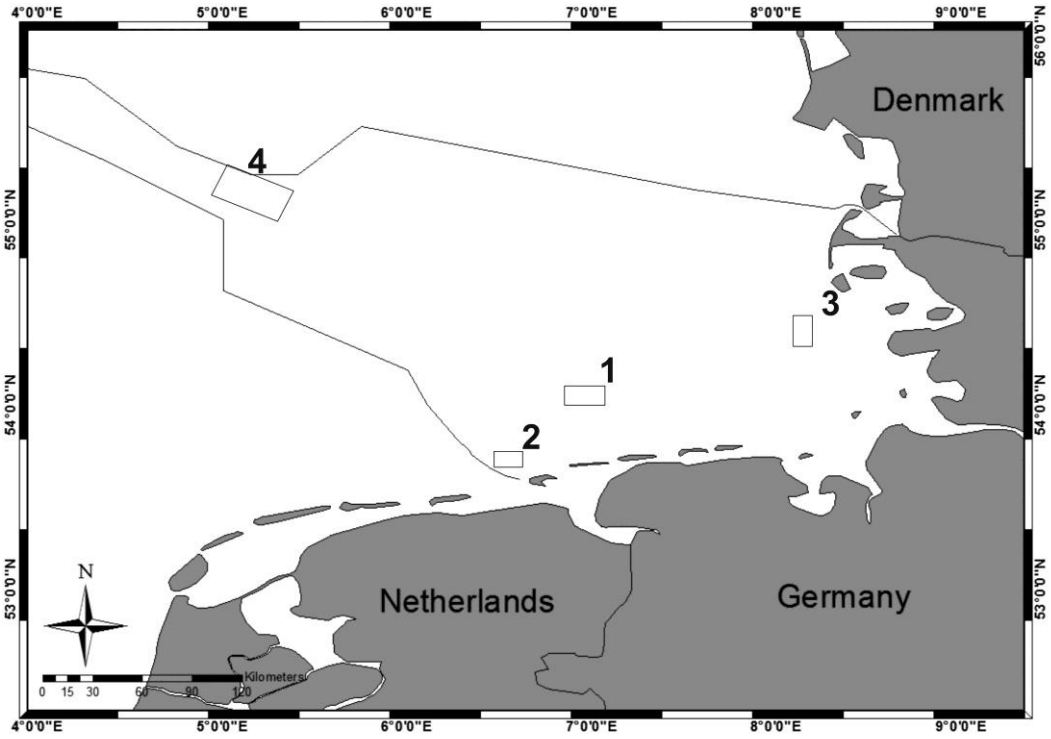

Figure 2.2 Location of study areas within the German EEZ.

Traditionally, correlation between recovered sedimentary cores based on comparable sedimentology can be used to establish the lateral extent of sedimentary units and their thicknesses. However, this methodology can be limited by a lack of knowledge regarding the context of the location of the recovered sequences, especially in areas containing buried valleys. The use of seismic data helps identify subsurface morphological features and their relative importance with respect to sedimentary architecture.

The approach outlined in this study adds a third step to the process that involves the inclusion of recorded in-situ geotechnical data. This element allows for a refinement of lithostratigraphic units identified in cores and, similarly, for easier correlation between these units and their position in the sub-surface from seismic images.

2.4.1 Seismic Data

A variety of seismic source and acquisition techniques were used to gather the data presented here, all of which were undertaken as part of site investigations for windfarm development from 2005 to 2012.

In Area 1 and Area 3, both single channel (boomer) and shallow water multiple channel seismic (Bremen MCS system) data were acquired in the study area. Boomer data penetrated the uppermost 10 - 20 m of the sediment column with very high resolution. The Bremen MCS data imaged deeper structures with a better multiple suppression, a better ability to resolve steep dipping reflectors and provided sound velocity information.

Boomer data were acquired using an Uwak 05b (Nautik Nord) and an AA301 (Applied Acoustic Engineering) boomer plate, respectively, operating at an energy level of 300 J. The data were received using a short single channel streamer with 20 hydrophones and recorded using a Coda 360 (Codaoctopus) recording system. This configuration provided a maximum shot rate of 3.5 shots per second, which offered good horizontal resolution.

The Bremen MCS system consisted of an analogue streamer system with 48 channels, which were distributed with a 1 m channel spacing along a 50 m long active section. Each channel consisted of one hydrophone. With this design, the streamer was able to record acoustic signals with omnidirectional incidence angle without signal distortion and thus was perfectly adjusted to operation in a very shallow water environment. The incoming data were digitized using custom designed marine multichannel seismic recording system at a sample rate of 0.25 ms. The seismic source was a two-chamber Micro-GI-Gun, which provided a near bubble-free source signal in a frequency range of 50 to 600 Hz. The very small chamber volume of the Micro-GI-Gun of 0.1 litre

restricted the source signal amplitude compared to bigger air guns, but allowed a very high shooting rate of 1.5 to 2 seconds and therefore enabled a good lateral coverage of the survey area and high common midpoint fold despite the comparatively short streamer. The total signal penetration of this gun at 150 bars reached 500 - 600 ms in the German North Sea. The data processing flow was specifically adapted to the needs of high resolution shallow water seismic with special emphasize on the correction of residual statics.

Similarly, in Areas 2 and 4 boomer data was gathered using single and multichannel systems. A CSP P Applied Acoustics Underwater Technology (CSP-P300) source was used with a range of 50 to 350 J. Data was also received using a short single channel streamer with 20 hydrophones and recorded using a Coda 360 (Codaoctopus).

2.4.2 Sediment Cores

Across the areas coring was conducted from a drillship and jack-up platforms each using different sample tools. In Area 1, undisturbed samples were recovered using a 70 mm diameter push core sampler (36 cores) or a 110 mm diameter percussion drive sampler. The length of each core is about 50 m (cut up into 1 m sections) and the recovery is more than 90% for all lithologies. All core sample sites are located on seismic lines, so there is a direct seismic cross section-sediment correlation. Immediately after coring, the sediment cores were opened and geotechnically tested and sedimentologically described.

In Area 2 and Area 4, rotary directional drilling was used which included the use of the Seaclam seabed frame from re-entry allowing core lengths of up to 50 m. During operation, WIP/WISDOM downhole tools were employed. The WIP sampler is capable of taking a soil sample of either 72 mm or 53 mm depending on conditions and has a maximum sample length of 0.98 m. Dry drilling was also employed in these areas with samples taken using a Nordmeyer BPE 150 hammer sampler. Maximum length of the liner sample was 1000 mm with a diameter of 100 mm.

2.4.3 Cone Penetration Tests

For Area 1, wireline downhole or top-pushed CPTu were conducted parallel to each coring site at a distance of 2 - 10 m. CPTu consists of a cone at the end of a series of rods pushed into the ground at a constant rate. Measurements continually or intermittently record the resistance of penetration to the cone. These measurements include cone resistance, sleeve friction and pore water pressure. Cone resistance (q_c) is the total force acting on the cone divided by the projected area of the cone. The total force acting on the sleeve divided by its surface area produces the sleeve friction (f_s) and the quotient of sleeve friction and cone resistance is the friction ratio, which allowed for the distinguishing of overconsolidated clay from loose sand.

The wireline downhole CPTu was performed in a quasi-continuous mode with no, or only minimal, gaps between the pushes. Dictated by conditions, either a 10 cm^2 3 m stroke, a 10 cm^2 1 m stroke or a 5 cm^2 2.5 m stroke CPTu unit was used. The different tools have thrust capacities of 45 MPa and 90 MPa, respectively.

The hydraulic penetrometer pusher used calibrated electric cones of 10 cm^2 or 15 cm^2 with a maximum nominal thrust of 200 kN and a cone tip capacity of 100 kN. The process was terminated when required penetration was achieved or the maximum available safe thrust capacity of the equipment was reached.

In Area 2 and Area 4, the “Wheeldrive Seacalf” apparatus was used. Here, a 15 cm^2 probe was used measuring cone resistance, sleeve friction and pore pressure up to 31 m depth.

2.4.4 Stratigraphic Correlation Procedure

The stratigraphy of the offshore deposits was established by correlating seismic-stratigraphic units with core lithologies and CPT profiles. Initially seismic data was interpreted by identifying first order strong reflectors which often marked erosional horizons within the sequence including buried valley walls, as well as sediment density contrasts and hence major lithological changes. These reflectors thereby defined seismo-stratigraphic unit boundaries. Similarly, observations were made with

regard to the nature of reflective amplitude and their lateral continuity. Sedimentary profiles preserved in cores were divided up into lithostratigraphic units based on similarities in sedimentary properties. Grouped patterns in downcore CPT values (homogenous or heterogeneous) were then related to both seismo-stratigraphic and downcore lithostratigraphic interpretation.

Finally, for each site, formal stratigraphic units were finalised by correlating seismo-stratigraphic unit boundaries, CPT and downcore lithological profiles using KINGDOM software. This approach of applying a correlation of seismic reflectors, geotechnical parameter patterns and core lithological changes proved robust on a core by core level for either channelized and non-channelized sequences. Furthermore, meaningful units could be interpolated between core sites with seismic imaging enabling the development of a more resolute background sedimentation (non-channelised or regional) stratigraphy.

2.5 RESULTS

In this section we present a synthesis of a significant body of data collected from four areas: 320 seismic lines, 72 cores (length: <50 m) and 196 CPTu profiles. From this data we generate a new stratigraphic framework for the German EEZ. To aid the geological explanations of the four areas we present the new stratigraphic framework briefly and informally. This is followed by a detailed analysis of the four areas and a demonstration of the new stratigraphy. In the discussion, the new stratigraphy is given formal unit names and compared to established nomenclature.

2.5.1 Seismo-stratigraphic Units

Seven major seismic reflectors are identified from seismic profiles in the four study areas. Three of these reflectors (R3, R6 and R7) equate with three generations of valley formation in the area during the Quaternary (Fig. 2.3). Other reflectors (R1, R2, R4 and R5) are widespread marking sequence boundaries at the base of tills or marine transgressive surfaces (Fig. 2.3). Given the broad range of seismic data collection techniques, discerning the individual seismic nature of each

unit proved too difficult. However, some units did display a characteristic unit signature such as an inverted reflector coinciding with the presence of peat layers seen at corresponding depths in core profiles. The R2 reflector lies above the most recent stage of valley generation (see for example Fig. 2.5). A summary of the seismo-stratigraphic units and their bounding reflectors is presented in Figure 2.3.

2.5.2 Downcore Lithostratigraphy

Dense Neogene sands form the "bedrock" upon which Quaternary units rest. A summary of these units outlined below is shown in Figure 2.3.

The oldest Quaternary sediments encountered are a common deep valley fill that comprised of two sub-units. The lower unit is composed primarily of dense fine to medium sands and is ascribed here to Unit Vb. The overlying Unit Va is comprised of dark laminated clays, silts and fine sands.

Above Unit V is another bipartite unit (Unit IV) resting on top of the R5 reflector. The basal Unit IVb dominated Unit IV and is found in most cores where the Unit IV is present, characterised by sands with a relatively high marine shell component with occasional clayey layers. Seismic data suggests this unit is widespread and not confined to palaeovalleys. Unit IVa is predominately mud grade often with humic and clay layers typical of deposition in lacustrine conditions.

The overlying Unit III is composed predominately of laminated silty and clayey sediments, with varying degrees of fine to medium sands and sometimes gravel which, occur both in shallow valleys and depressions as well as forming tabular beds. The basal Unit IIIc consists of fine to medium sands and gravel layers. This is overlain by Unit IIIb, which is a fine to medium sand with some gravel layers present that shows fining upwards sequences and often contains components of till. The top Unit IIIa is dominated by calcareous clayey and silty sediments, often alternating with silt to fine sand.

Unit II is composed of fine to medium grade clean sands that are generally well sorted. Coarser material such as gravels and cobbles can often be found at the erosive base of this unit marking the transition to Unit III, correlatable with R2.

Unit I predominately consists of sands but can be sub-divided into three lithologically distinct subunits. The basal Unit Ic marks the transition to the underlying Unit II. It is composed of peats varying in thickness from a few centimetres to 2 m with different degrees of decomposition. The overlying Unit Ib is dominated by sands with different proportions of silt and clay and some organic components. The uppermost Unit Ia is composed of fine to medium sands which are often shell rich. The uppermost two units are generally loose and mobile, the thickness of which varies between <1 m to 20 m depending on the topographical context. Often, they occur infilling shallow channel systems in the upper part of the sub seabed.

2.5.3 Geotechnical Correlations and Formal Stratigraphic Units

The lithostratigraphic units were correlated with in-situ CPT data which gives a unique signature for each lithostratigraphic unit. This greatly facilitates correlation between units and with seismic data. The following units had the following cone resistance values which are also graphically displayed in Figure 2.3.

Unit Vb has high to very high (up to 80 MPa) cone resistance values, whereas the overlying Unit Va has low cone resistance values of 5 – 10 MPa.

Unit IVb has cone resistance values of between 40 – 80 MPa, and is similarly overlain by Unit IVa which, generally, exhibits a low cone resistance of approximately 5 MPa.

The base of Unit III often exhibits a spike in cone resistance up to 80 MPa correlatable with R4 and Unit IIIc basal gravels. The remainder of Unit IIIc has variable and increasing cone resistance values ranging from 5 – 50 MPa. Unit IIIb has mainly high but variable cone resistance values between 10 – 50 MPa but mostly >30 MPa. In contrast, Unit IIIa has low cone resistance values between 1 – 10 MPa although variable.

Cone resistance values for Unit III give a strong contrast to Unit IIIa with average values of around 40 MPa, falling off at the top.

Cone resistance values for Unit I are low, between 1 – 5 MPa.

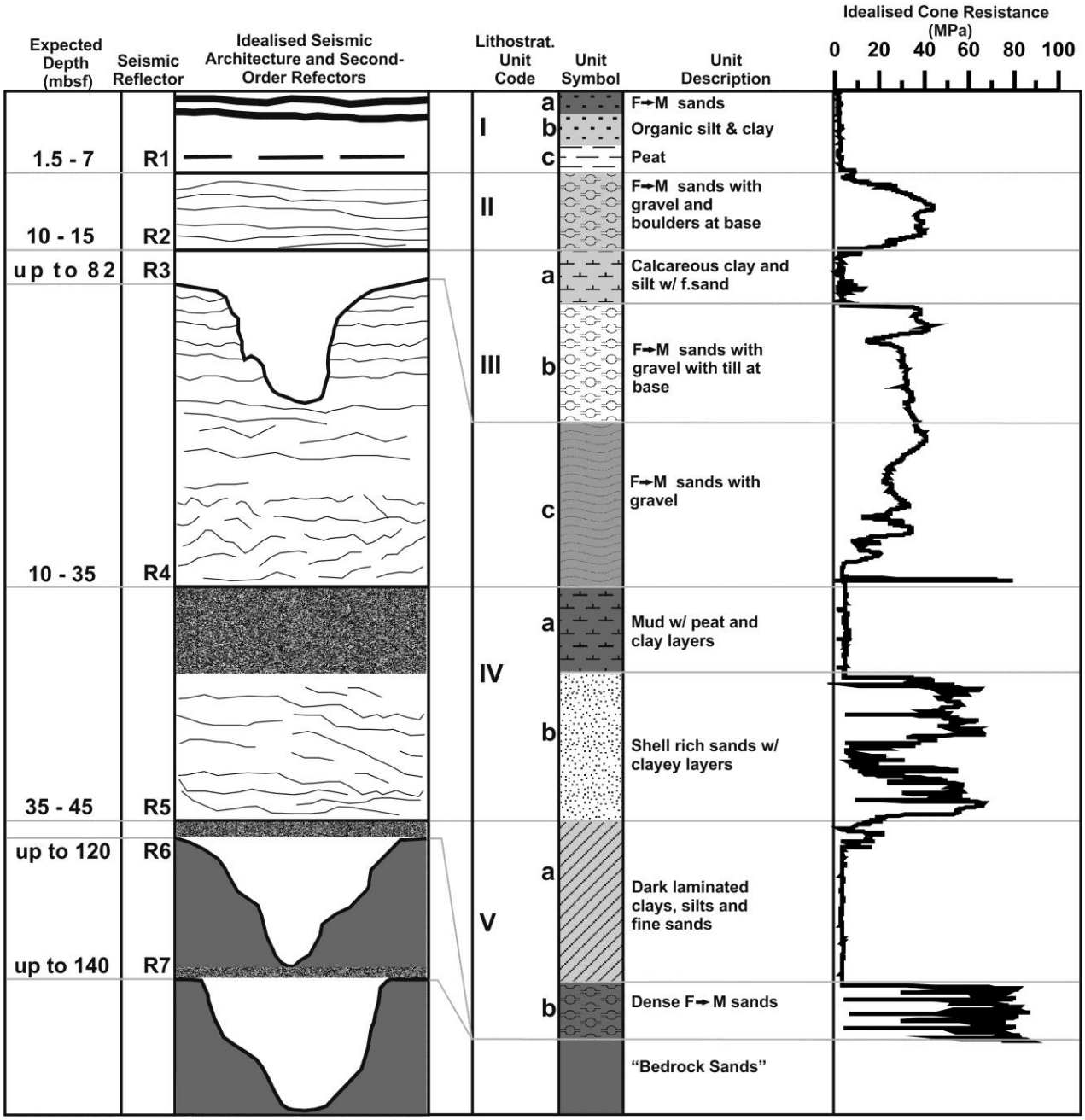

Figure 2.3 Litho-, seismic and geotechnical stratigraphy from results of this study. See section 2.5 for explanation.

2.6 DESCRIPTION OF STUDY AREAS

Details from the four study areas are presented below. Figure 2.2 above shows their location.

2.6.1 Area 1

Area 1 is located to the south of the German North Sea sector, roughly 40 km to the north of the east Frisian island of Juist, covering an area of 146 km^2 (Fig. 2.4). In this area, seismic surveys have identified three buried valleys cut into the dense Neogene sands prevalent throughout the area by various phases of glaciation (Fig. 2.5; Hepp et al., 2012). In addition to these features, a shallow meandering structure was also mapped in the eastern side of the section. The largest valley in the area has an E-W orientation, is roughly 38 km long with a depth of up to 150 m. A shallower valley runs parallel to this and both cross cut a deeper, N-S trending valley in the western section of the area. Based on this cross-cutting relationship, the depth of the valley base and subsequent valley fill, the N-S trending valley is interpreted as having been formed earliest with the major E-W trending valley formed during a later glaciation. The shallow meander system in the east is interpreted as part of a river system which developed postglacial.

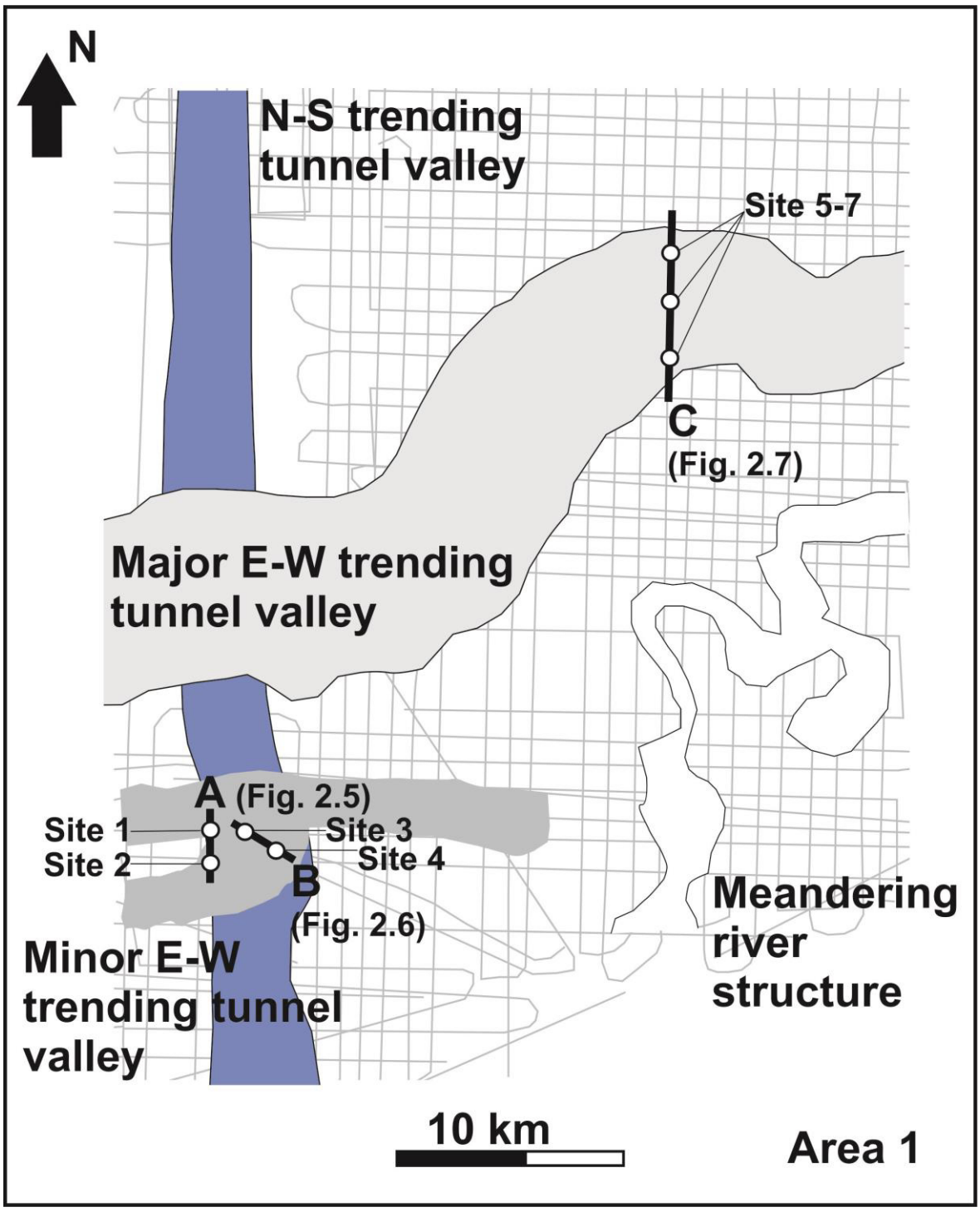

Figure 2.4 Details of the seismic grid for Area 1 and a 2D projection of features found there. Seismic lines and core sites included in this study are also highlighted and labelled. See section 2.6.1 for explanation.

Units I and II are seen throughout the area overlying the dense Neogene sands which form the deeper strata into which these valleys have been cut. Unit I has a maximum thickness of 2 m whilst Unit II varies between 5.5 and 10 m.

In the southern area, where the minor E-W valley cross cuts the N-S valley, gravels and boulders associated with Unit IIIb are found at the base of the E-W valley at Sites 1 and 2. Furthermore, at Site 2, Unit IIIb grades upwards into Unit IIIa which has a thickness here of approximately 5 m. The base of the minor E-W valley is marked by a strong reflector (R3) beneath which at both Sites 2 and 1, Unit Va is found with a thickness of 3 - 4 m and subsequently underlain by thick sequences of Unit Vb (Fig. 2.5).

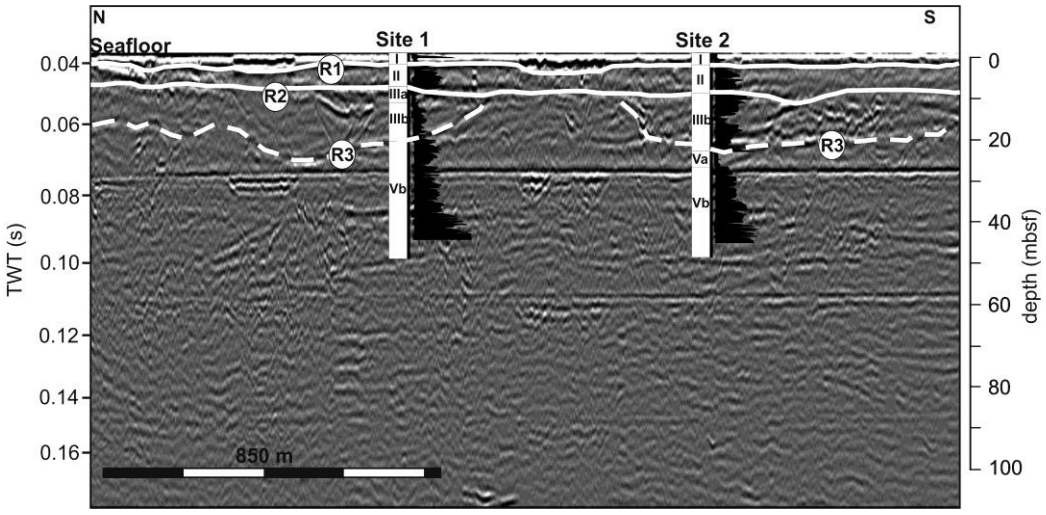

Figure 2.5 Seismic line A from Area 1. Superimposed are downcore CPT profiles for cone resistance for Site 1 and Site 2 with corresponding lithological units. The dashed line highlights valley walls associated with the R3 reflector.

Elsewhere in this area, the base of the minor E-W valley is again seen as a strong basal reflector in seismic profiles (R3) and represented by basal gravels and boulders of Unit IIIb at Sites 3 and 4 (Fig. 2.6). Here, Unit IIIb has a thickness of approximately 4 m at Site 3 and 1 m at Site 4 before grading into 7 m and 1 m thick accumulations of Unit IIIa respectively.

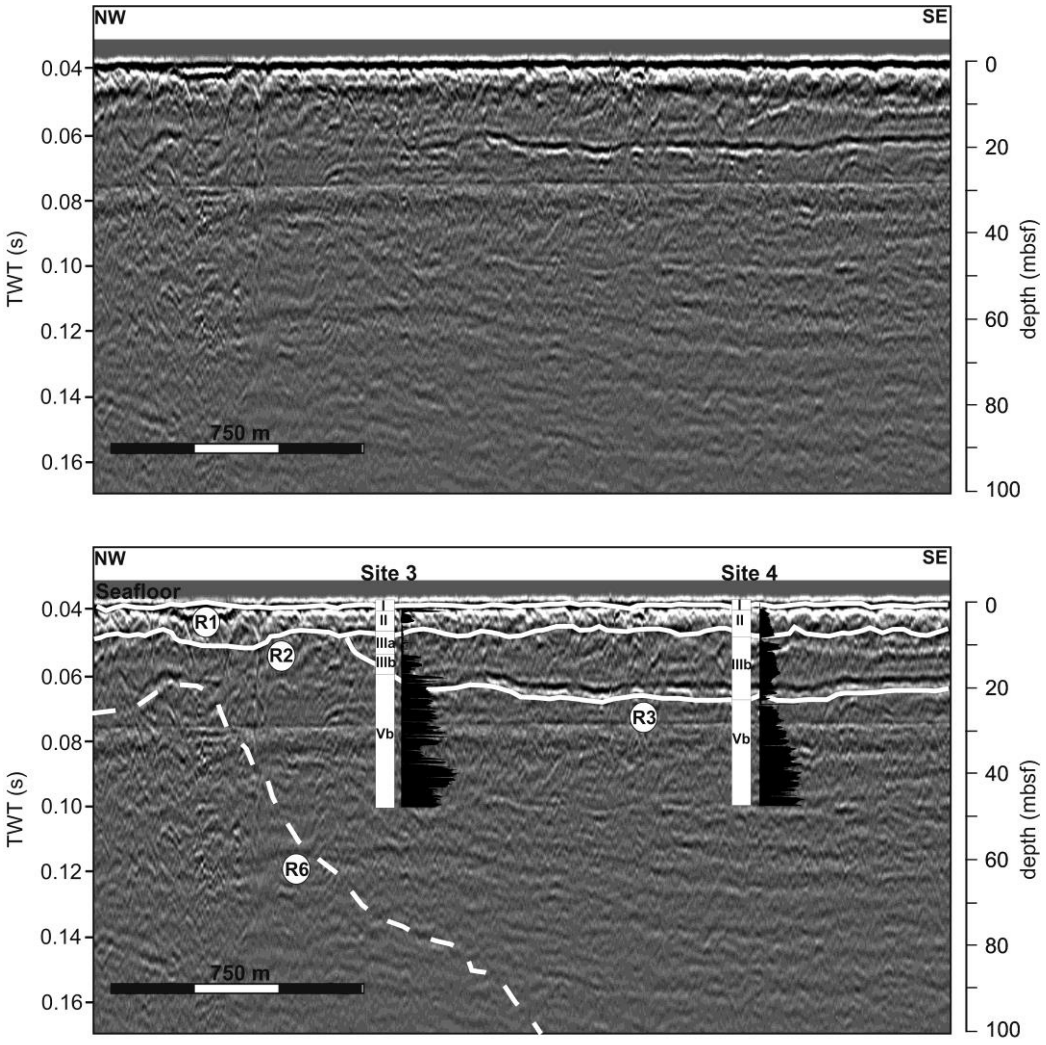

Figure 2.6 Seismic line B from Area 1. Above is the uninterpreted line, below has seismic reflectors marked on. Superimposed are downcore CPT profiles for cone resistance for Site 3 and Site 4. The dashed line highlights valley wall associated with R6 reflector.

Further north, where the major E-W valley cross-cuts the older N-S valley a different scenario arises. The base of the valley was seen on only a few seismic images and may reach depths of 350 metres below seafloor (mbsf; Fig. 2.7). Again, Units I and II cover the top of this valley at thicknesses of 3 and 5 - 14 m respectively with the erosive base of Unit II forming a strong reflector. Similarly, the valley walls are well defined; however, another discrete infill body is recognised in the upper 40 m of the main valley centre and also marked by a strong reflector (R3). In the valley centre, the succession consists of an approximately 20 m thick accumulation of Unit IIIa overlying Unit IVa with the transition marked by a strong seismic reflector as seen at Site 6 (Fig. 2.7). Unfortunately, this core did not penetrate the base of Unit IVa. Sites 5 and 7 saw cores taken from the flanks of this valley. On the southern flank at Site 7 beneath the basal reflector of Unit II

(R2) is a 33 m thick succession of Unit Va, consisting of stiff clays with fine sand layers in the lower part and silty clay alternating with silt to fine sand with shell deposits in the upper part. Overall, the sequence fines upward with laminae becoming more spaced. The base of this unit is marked by a disconformity in the core and considerable increase in cone resistance from 5 up to 90 MPa, marking the transition to Unit IVb which, in this instance, consists of dense sands and reworked till.

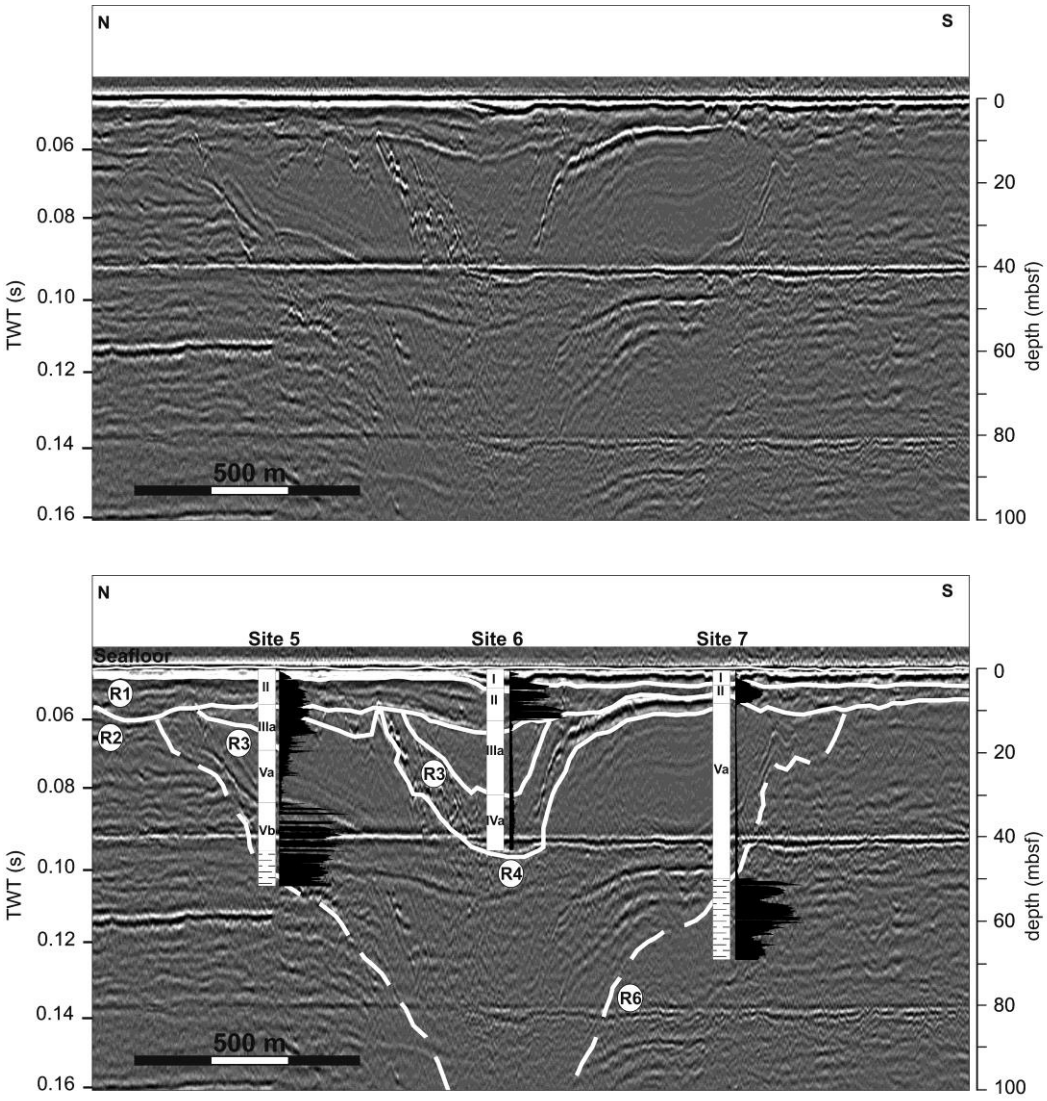

Figure 2.7 Seismic line C from Area 1. Above is the uninterpreted line, below has seismic reflectors marked on. Superimposed are downcore CPT profiles for cone resistance for Site 5, Site 6 and Site 7. The dashed lines represent valley walls associated with R6.

2.6.2 Area 2

Area 2 is located close to the German/Netherlands border in the waters near the Riffgatt windfarm development some 15 km north-west of the island of Borkum, covering an area of 6 km^2 (Fig. 2.2 and Fig. 2.8). Geologically it presents a similar scenario to Area 1 whereby a thin veneer (0 - 1 m) of Unit 1a overlies 5 - 10 m accumulations of Unit II. Unit II in turn rests either on Neogene "bedrock sands" or dense sands of Unit Vb (Fig. 2.9).

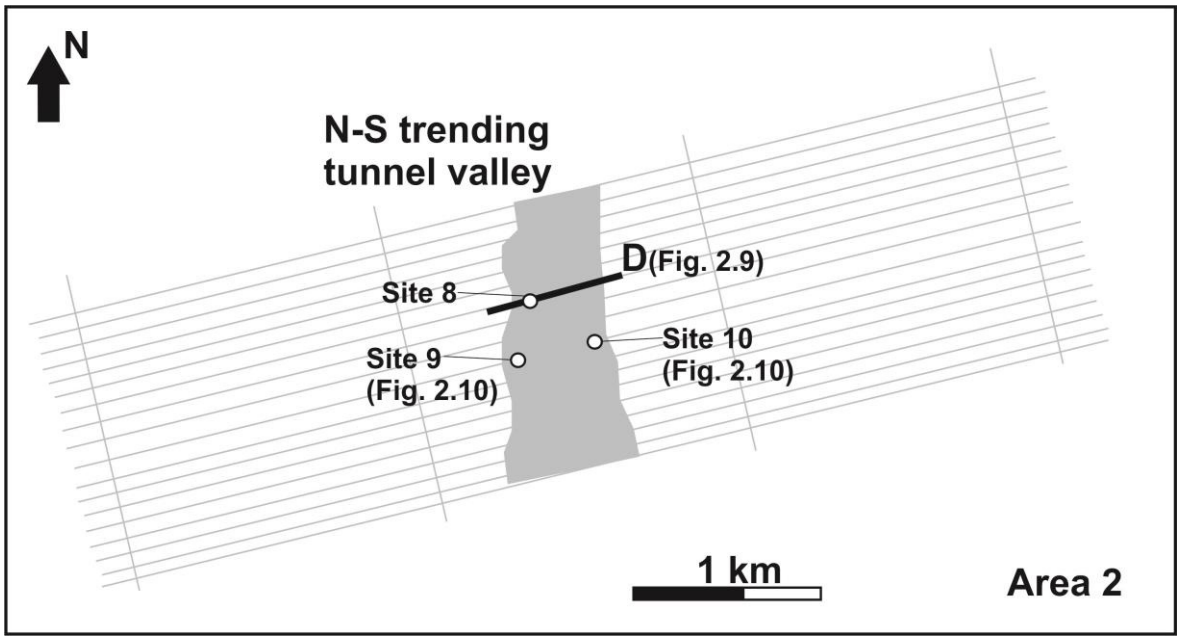

Figure 2.8 Details of the seismic grid of Area 2 and a 2D projection of buried valleys found there. Seismic lines and core sites included in this study are also highlighted and labelled.

On seismic profiles a relatively shallow (20 to 30 m deep) channel is seen beneath Unit II cutting into the Neogene sands or Unit Vb with a north south orientation (Fig. 2.8 and Fig 2.9).

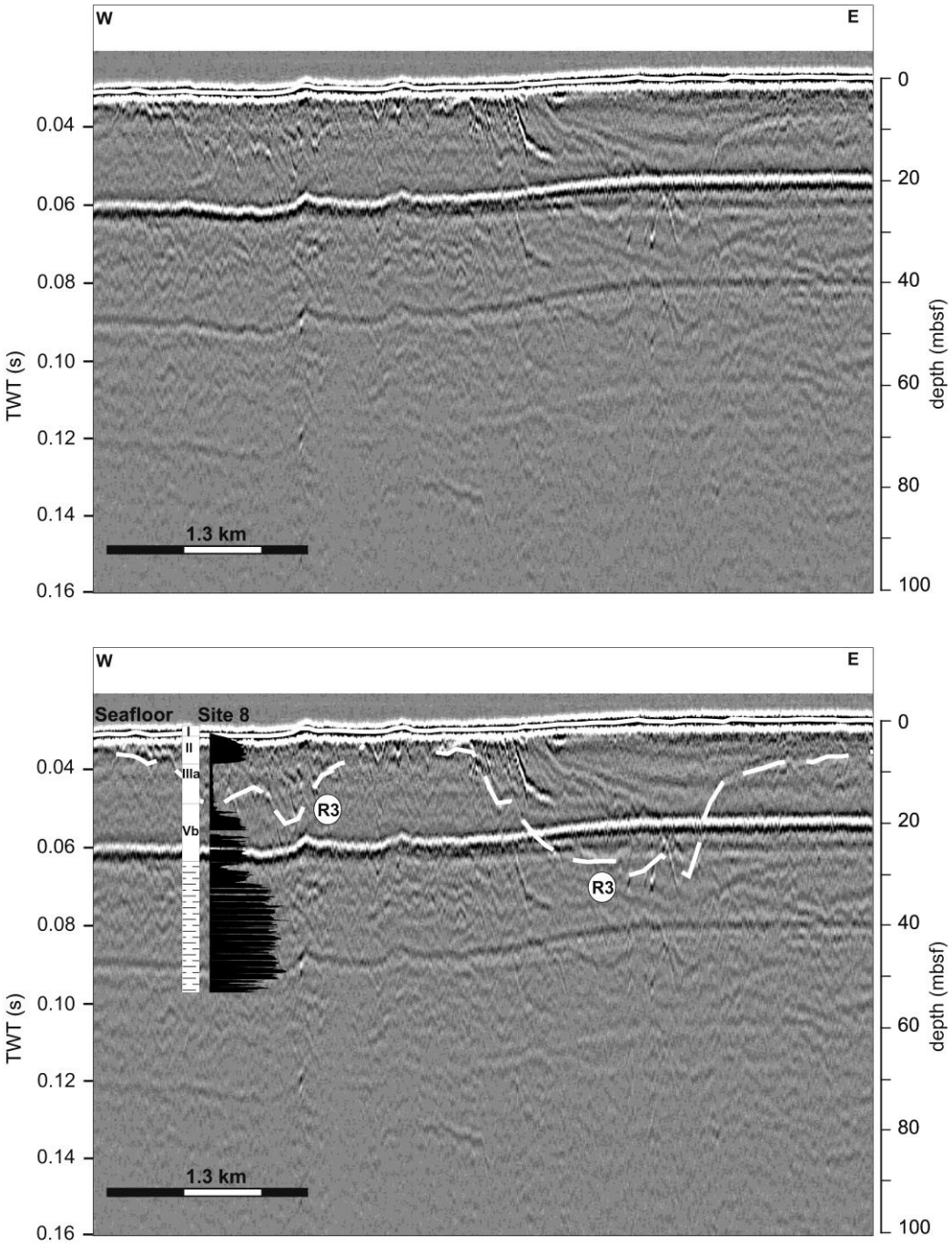

Figure 2.9 Seismic line D from Area 2. Above is the uninterpreted line, below has seismic reflectors marked on. Superimposed are downcore CPT profiles for cone resistance for Site 8. The dashed line represents valley walls associated with R3.

At Site 9 and Site 10 a valley infill of Unit IIIa can be seen underlying covers of Unit Ia and Unit II (Fig. 2.10). Beneath the R3 reflector marking the valley base there is distinct jump in cone resistance representing the transition to the tabular extensive Unit Vb which overlies the Neogene sands at these two sites (Fig. 2.10).

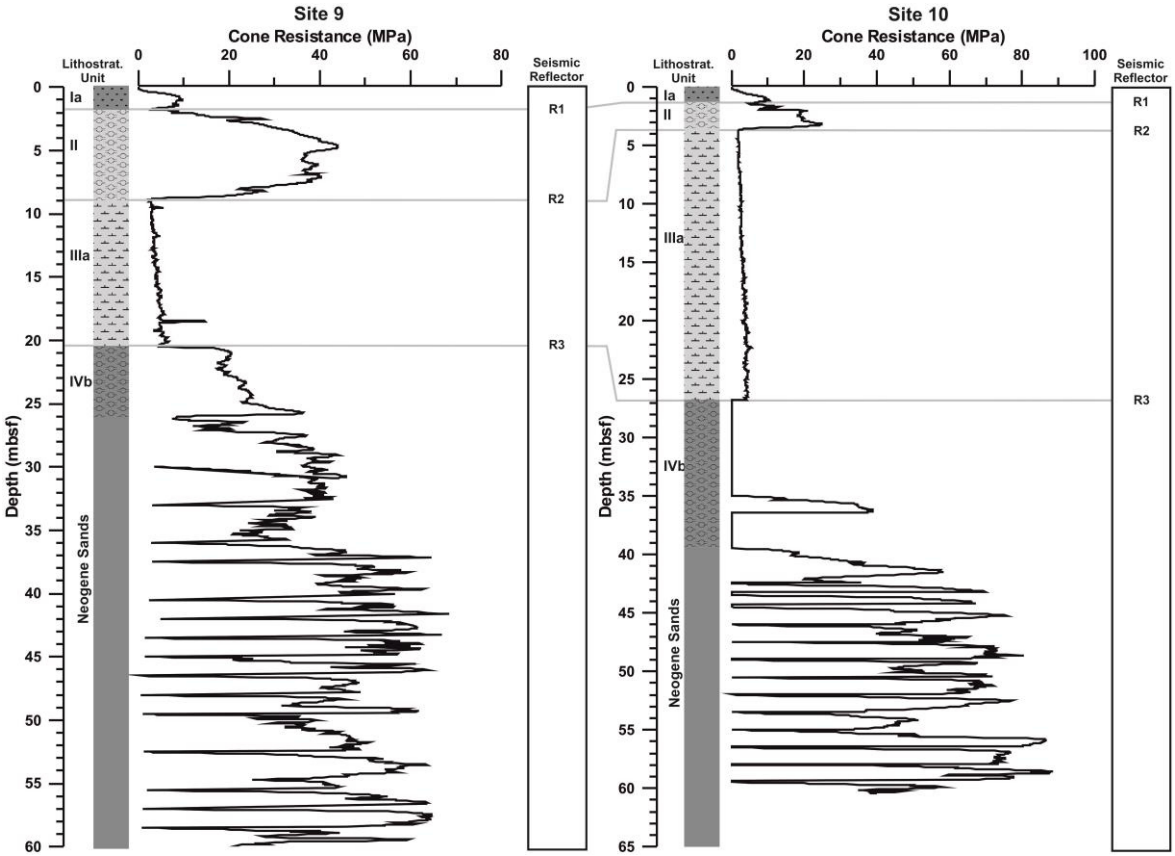

Figure 2.10 Downcore CPT profiles for cone resistance and lithology for Site 9 and Site 10. Superimposed are seismic reflectors marking unit boundaries. See Fig. 2.2 for core legend.

2.6.3 Area 3

Area 3 is located approximately 28 km northwest of Helgoland in the German North Sea sector, covering an area of 26 km^2 (Fig. 2.2 and 2.11). Similar to the other areas, seismic investigations have been able to identify unit boundaries and a number of features which control their distribution. Tabular elements of Units I, III, IV and V are extensively well developed here and have been uplifted in places by the presence of a saltdome (Fig. 2.11 and 2.12).

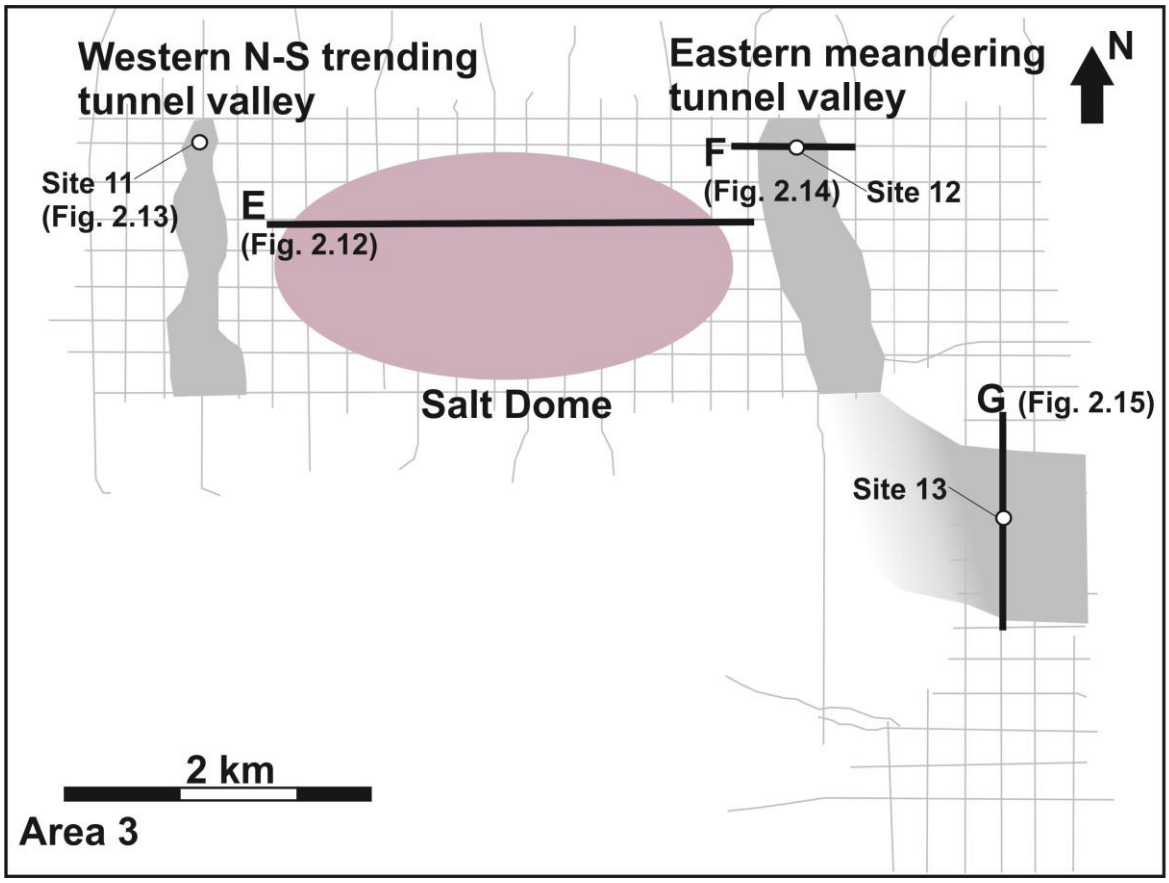

Figure 2.11 Details of the seismic grid for Area 3 and a 2D projection of buried valleys found there and position of a salt dome (in pink). Seismic lines and core sites included in this study are also highlighted and labelled. Inferences on course of certain tunnel valleys found in this area are marked by faded grey.

Adjacent to this saltdome are two valleys or channels of differing depths. The first runs in an N-S orientation on the west side of the saltdome and is relatively shallow at 30 - 40 mbsf cutting into Unit III with the valley deeper at the northern end of the survey limit. A core at Site 11 was taken from the northern end of this channel (Fig. 2.13). The upper 4 m is composed of Unit I with Unit Ia dominating the upper 3 m with basal peat comprising the bottom metre. The transition to the underlying Unit IIIb is marked by a strong basal reflector for Unit I (associated with the basal peat) and a subsequent rise in cone resistance from <5 MPa up to 50 MPa and a change to fine to medium sands with some gravels. The base of this shallow channel is interpreted to be at approximately 30 mbsf whereby in the core there is a change in cone resistance and lithology to a thick (20 m) accumulation of dense sands of up to 50 MPa with occasional peat and silty layers typical of Unit IVb. A peaty layer occurs at approximately 46 - 48 mbsf followed by a jump in cone resistance of up to 80 MPa marking Unit Vb.

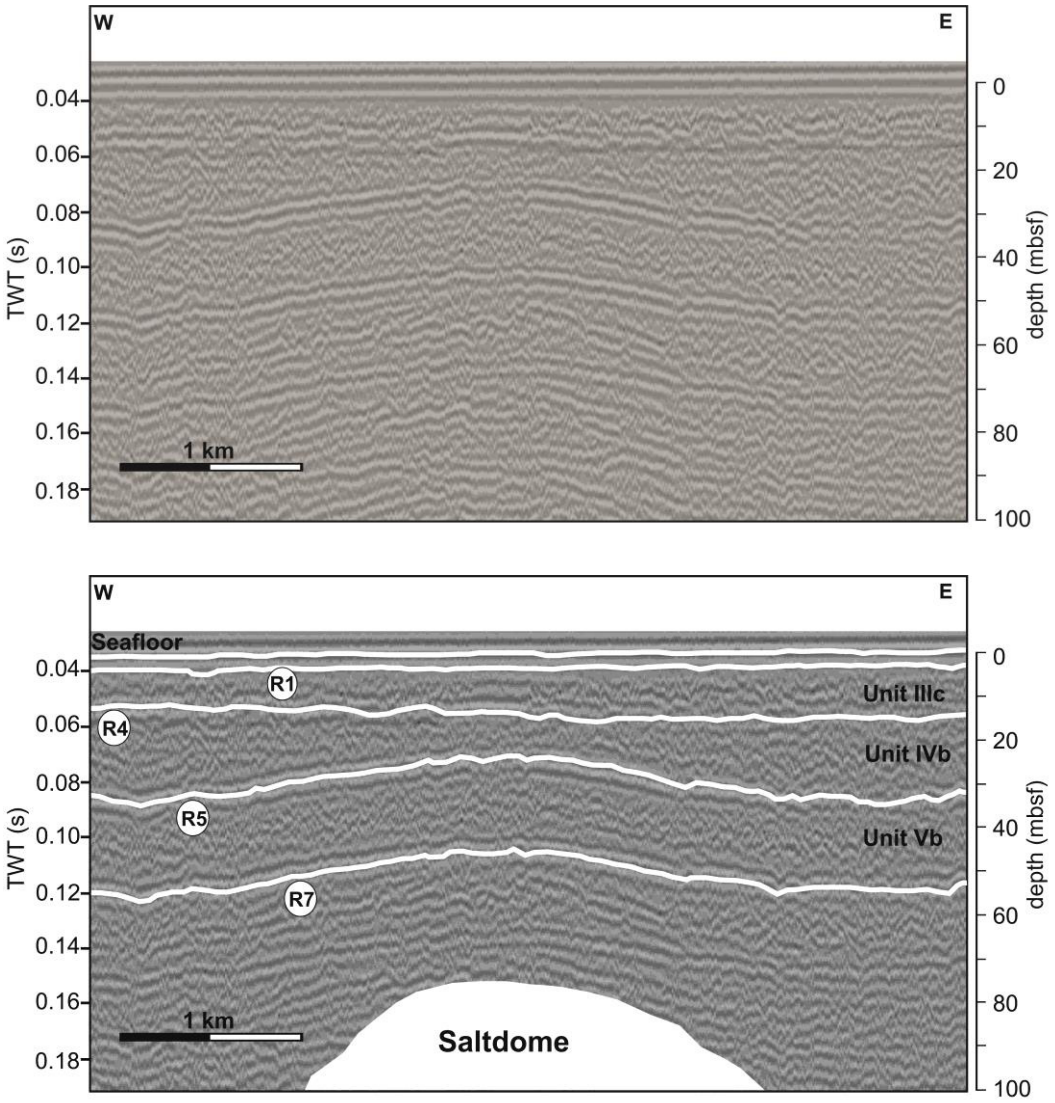

Figure 2.12 Seismic line E from Area 3. Above is the uninterpreted line, below has seismic reflectors marked on.

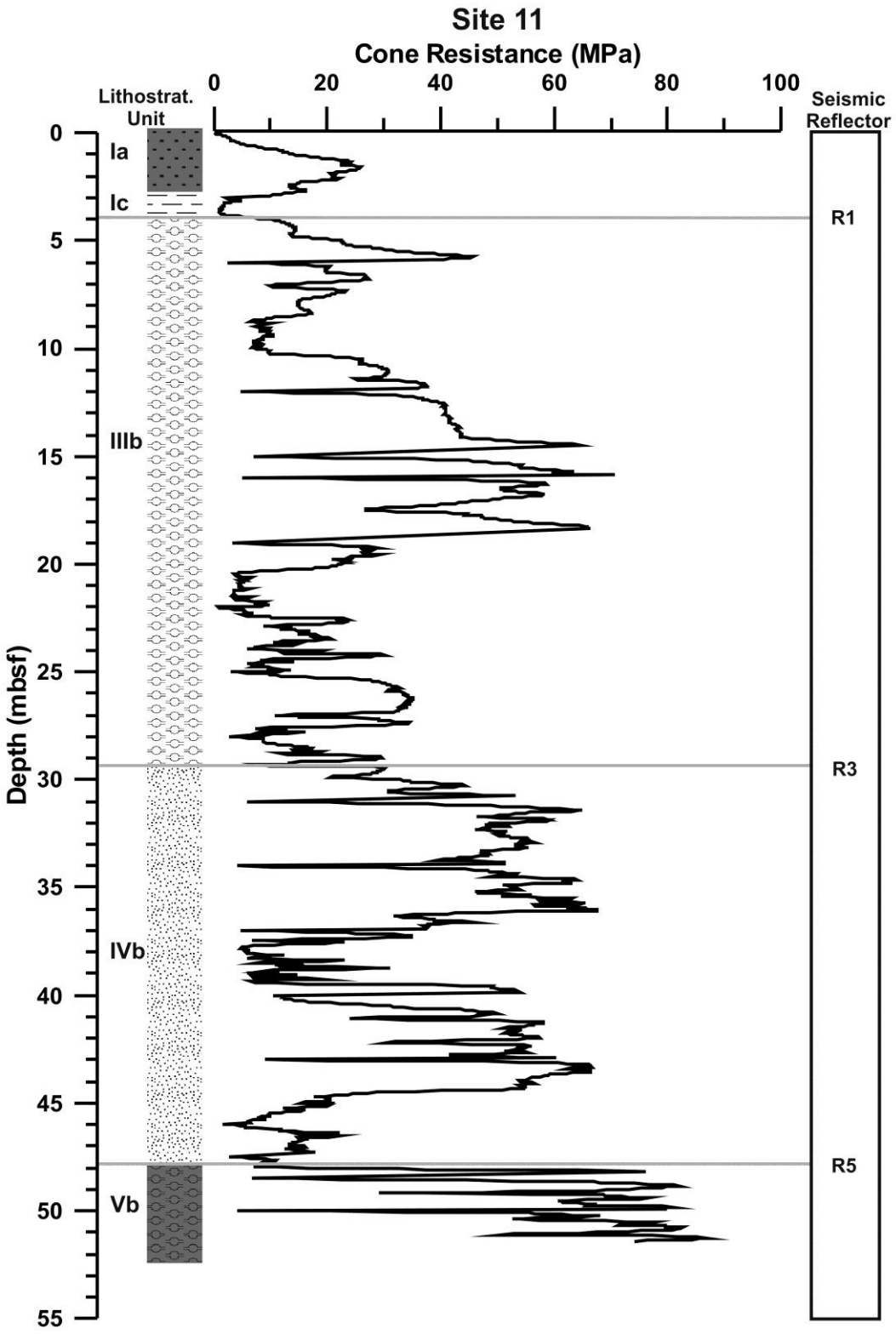

Figure 2.13 Downcore CPT profile for cone resistance and lithology for Site 11. Superimposed are seismic reflectors marking unit boundaries.

To the east and south-east of the saltdome (Fig. 2.14 and 2.15 respectively) lies another buried valley with a more substantial depth of up to 120 mbsf that cuts Units III, IV and IV. From the west

end of the survey area moving east, the valley has an N-S orientation parallel to the strike of the saltdome, similar to the shallow channel in the west side of the area. However, the valley then changes direction and takes on an E-W trend (Fig. 2.11). This presumed change in orientation cannot, however, be confirmed by seismic investigation due to a paucity of data but is inferred based on similar depths, structure and channel infill from cores at Site 12 and Site 13 (Fig. 2.14 and 2.15). Both cores show between <1 and 3 m thick accumulations of Unit I marked. In both instances, the transition from Unit I to the underlying Unit IIIa and IIb, which makes up the valley fill, can be seen by an initial drop in cone resistance followed by a jump in cone resistance and the change to more sand dominant lithogies.

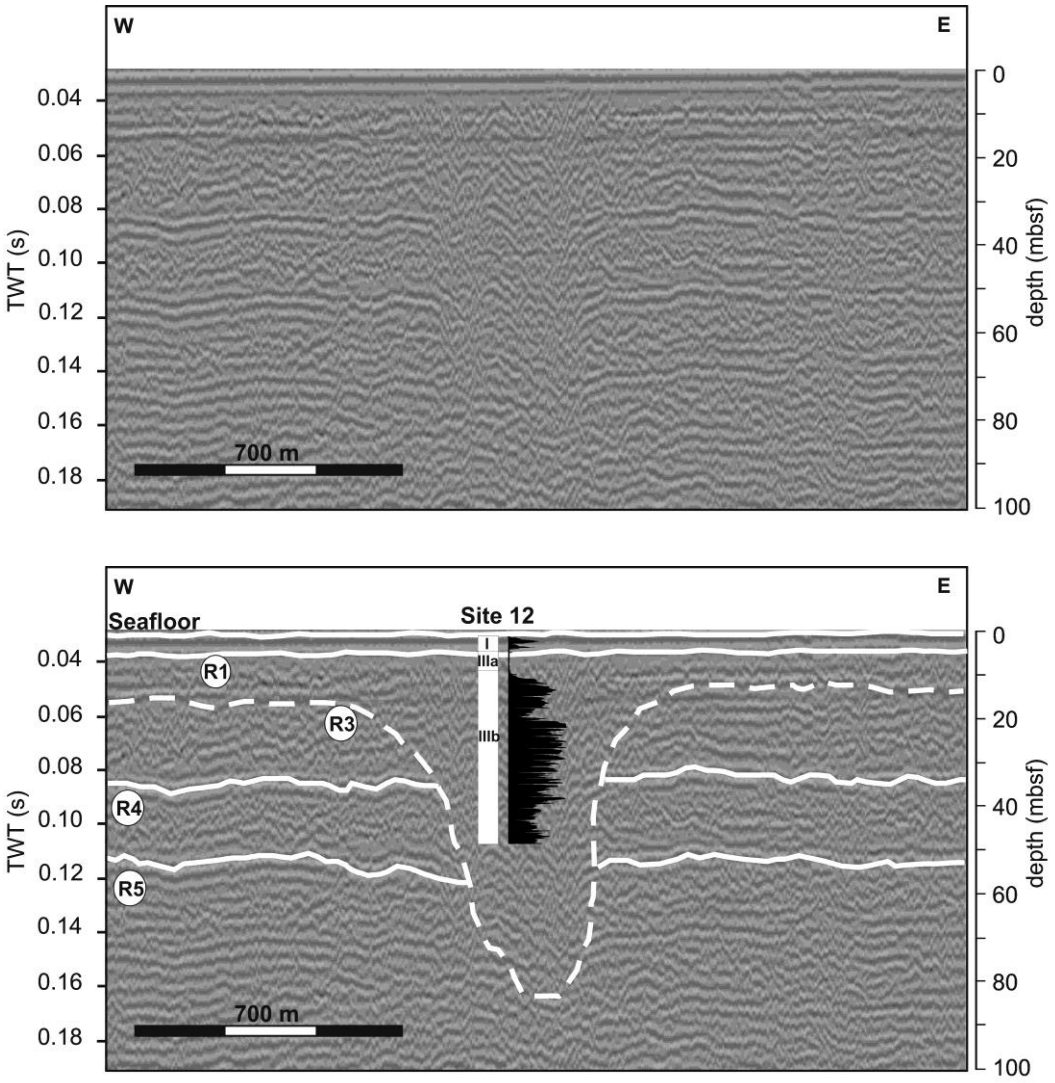

Figure 2.14 Seismic line F from Area 3. Above is the uninterpreted line, below has seismic reflectors marked on. Superimposed is the downcore CPT profiles for cone resistance for Site 12.

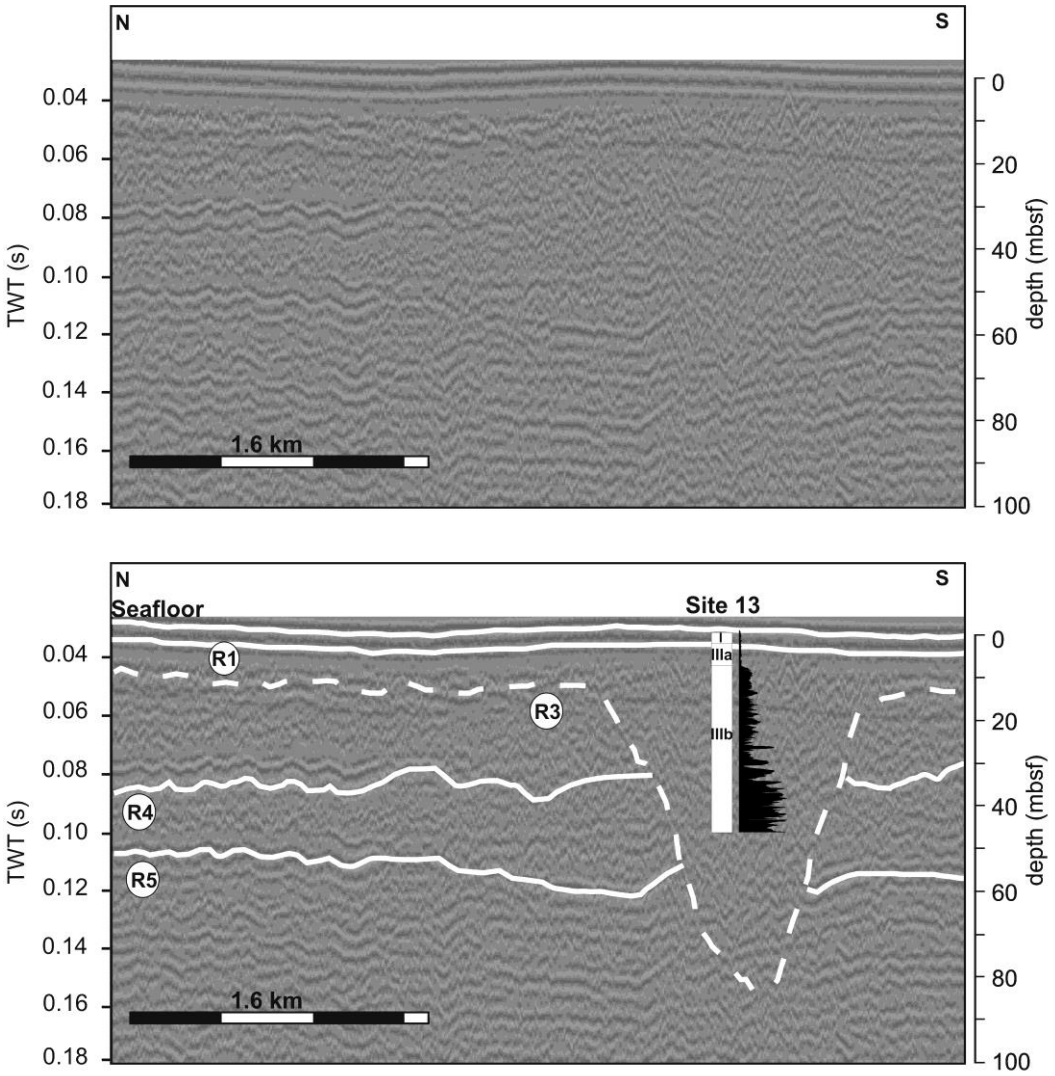

Figure 2.15 Seismic line G from Area 3. Above is the uninterpreted line, below has seismic reflectors marked on. Superimposed is the downcore CPT profile for cone resistance for Site 13.

2.6.4 Area 4

Area 4 is located in the northwest corner of the German North Sea sector close to the entrance of the "Duck's Bill" (“Entenschnabel”), some 1,200 km northwest of the Island of Borkum covering an area of approximately 74 km^2 (Fig. 2.2 and 2.16). The western end of the area is dominated by a salt dome which reaches a depth of over 250 mbsf and in many instances can be seen to affect overlying strata by doming them upwards. Two generations of deep valley formation can be seen on seismic images with between 3 - 4 deep valleys recorded and a shallow channel also. These valleys have been cut into dense Neogene sands which form the deeper strata across the area.

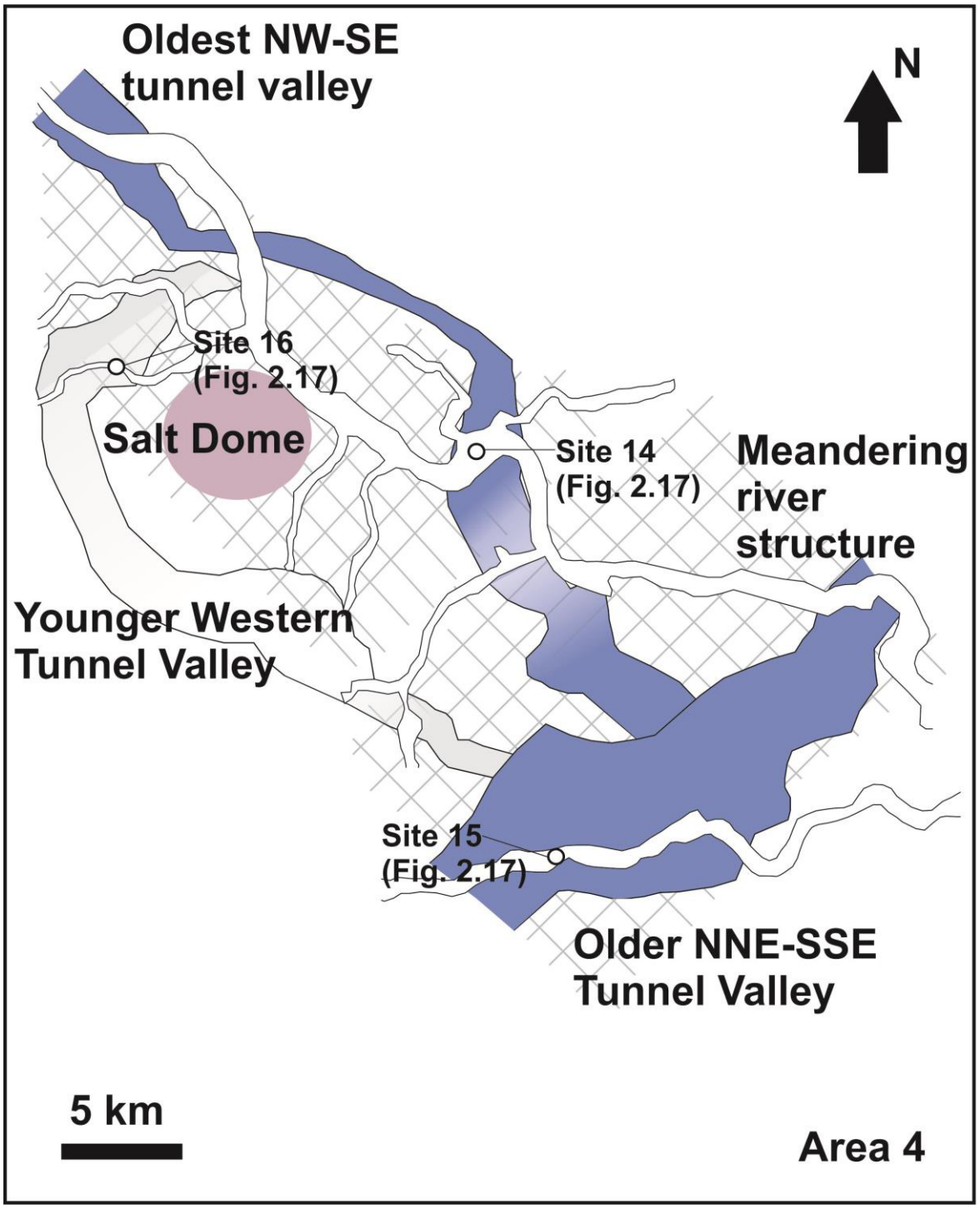

Figure 2.16 Details of the seismic grid for Area 4 and a 2D projection of buried valleys found there and position of a salt dome. Seismic lines and core sites included in this study are also highlighted and labelled. Inferences on valley orientation are marked by faded to transparent colouration.

The oldest valley was located centrally within the area running in a northwest - southeast orientation to a depth of approximately 200 mbsf and a width of 140 m. Another deep valley runs in a NNE-SSE direction at the eastern end of the area. Both these valleys were inferred as Elster 1 in

age due to their occurrence at the base of Unit IV and subsequent Unit V infill. A third valley was noted on various seismic profiles in the western part of the section to a depth of 130 mbsf. This valley was suggested to be Elster 2 in origin as it is cut into the top of Unit Va with a Unit Vb fill. The shallow valley seen predominately in the eastern part of the area cuts into Unit III and is interpreted as being part of the Elbe Palaeovalley ("Elbe-Urstromtal"), a drainage stream formed during the Weichselian glaciation at a time when the German North Sea sector was free of ice (Figge, 1980; Graham et al., 2008).

Unit I is once again ubiquitous across the area and ranges in thickness from 1 - 20 metres with the controlling factor on thickness being the presence and subsequent depth of the shallow channel associated with the Elbe Palaeovalley. This is particularly relevant to Units Ib and Ic and is best seen at Site 14 where they form relatively thick (up to 20 m) accumulations whereas elsewhere they can be comparatively thin (1 - 4 m) or even absent. Downcore at Site 14, Unit I is underlain by Unit IIIa. It is into Unit IIIa which the shallow channel controlling Unit I thickness is cut (Fig. 2.17). Unit III is between 8 - 40 m thick; again depending on the prevalence of the shallow channel associated with the Elbe Palaeovalley. The transition from Unit IIIa to the underlying Unit IVb is marked by a dramatic jump in cone resistance values from approximately 5 MPa up to 80 MPa. It has a thickness of between 13 - 20 m approximately and consists of dense sands with shell material. A further rise in cone resistance values is again seen in the transition from Unit IVb to Vb with values reaching up to 100 MPa consisting of very dense sands with little or no shell material. This unit has a thickness of roughly 10 m before a drop in cone resistance to 5 MPa marks the change to Unit Va comprising of dark silty clays. In the seismic profile for Site 14, Unit Vb overlies the buried valley seen in the central part of the area with Unit Va making up the valley fill as far as was sampled.

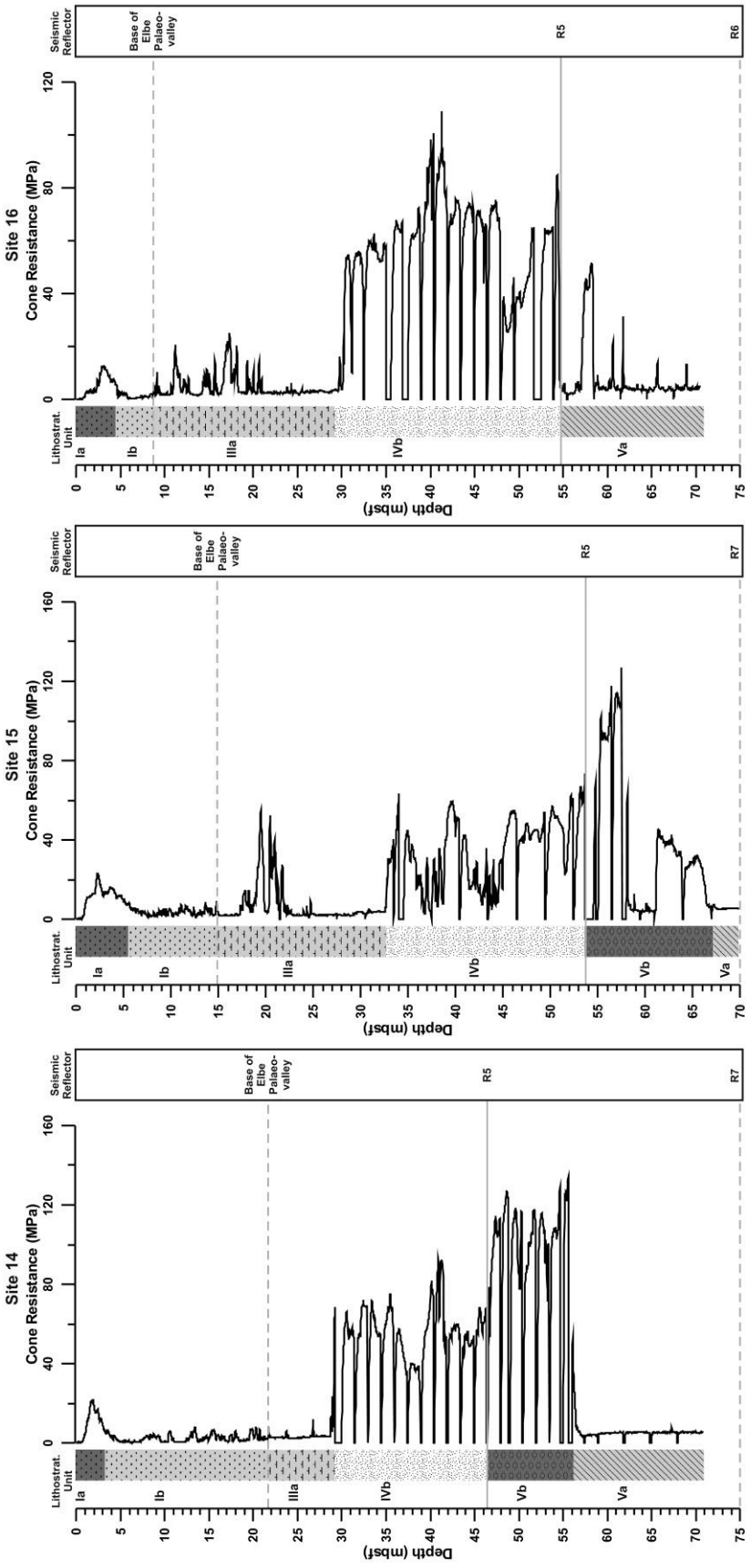

Figure 2.17 Downcore CPT profile for cone resistance and lithology for Site 14, Site 15 and Site 16. Superimposed are seismic reflectors marking unit boundaries.

A similar scenario can be seen at Site 15 taken from NNE-SSW trending valley in the eastern end of the section (Fig. 2.17). Units Ia and Ib make up the upper 15 m or so before a change in lithology to Unit IIIa which continues to a depth of 32.5 m and on into the underlying Unit IVb and subsequently Unit Vb. At the base of Unit Vb, and cut into the dense Neogene sands, is another valley of Elster 1 age with a Unit Va typical fill of predominately silty clays with some coarser sands.

A core at Site 16 was taken from the valley in the western side of the area (Fig. 2.16 and Fig. 2.17). The sequence here was slightly different than previous cores with peat associated with Unit Ic recorded at the base of the shallow valley at a depth of approximately 7 m underlying Units Ia and Ib. Missing from this sequence is Unit Vb. This is due to the fact that the valley here is younger than the other two in this area and subsequently been down cut into Unit Va and subsequently the Neogene sands. The valley is then infilled with Unit Va as far as was sampled.

2.7. DISCUSSION

2.7.1 Revised Stratigraphic Framework

Detailed mapping using extensive core, CPTu and seismic data from the Quaternary deposits of the German North Sea Sector facilitated a reconstruction of the sedimentation history for the areas studied and a stratigraphic framework to be established that is comparable across the North Sea (Fig. 2.18). Only certain units are extensively developed as tabular elements (Units II, IIIc, IVb, and Vb; Fig. 2.12) and are generally separated by planar erosional surfaces seen on seismic profiles representing unconformities (reflectors R1, R2, R4, R5). Others are confined as valley fill with transition between units seen in core lithologies and on CPTu profiles. No area showed a complete succession of units, further emphasising the complexity of sedimentary successions in the German North Sea Sector. Unit I was ubiquitous occurring generally as a veil-like covering on the seafloor. Due to a lack of micropalaeontological work and absolute dating, units were relatively dated based on lithological properties and stratigraphic relationship. The informal stratigraphic framework in

Figure 2.2 is reproduced below (Fig. 2.19) with inferred facies interpretations and ages (see also section 2.7.2).

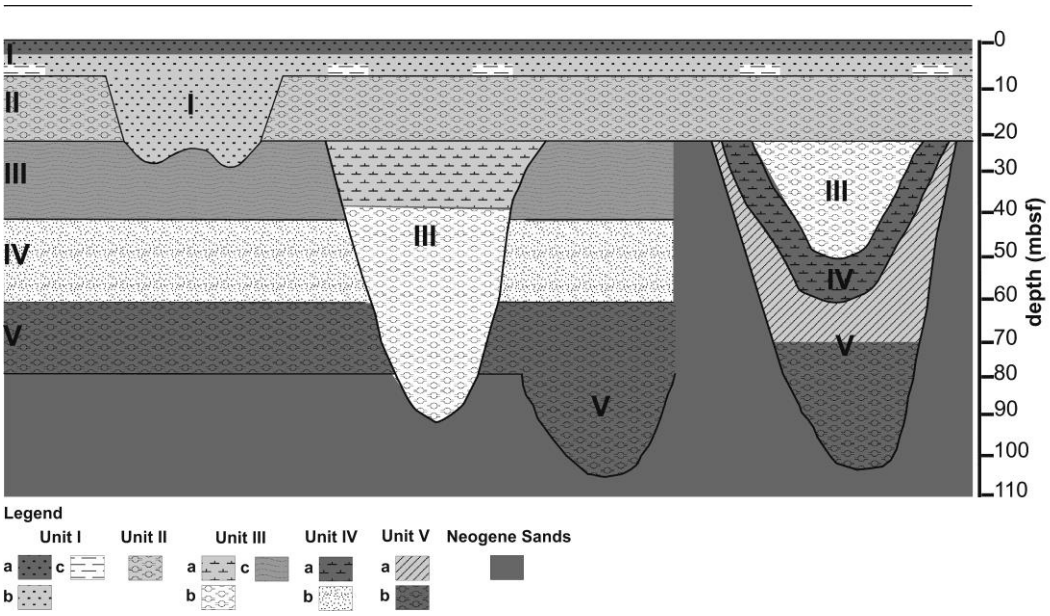

Figure 2.18 Scheme of Mid to Late- Quaternary deposits and stratigraphic units on German North Sea Shelf. See section 2.7.1 and 2.7.2 for explanation.

Units are also compared with existing stratigraphies form the British and Dutch North Sea sectors and given formal stratigraphical names here (Fig. 2.19 and Fig. 2.20). The stratigraphical nomenclature used comprised of formations and members. A formation is the primary unit of lithostratigraphy and is generally regarded as the smallest mappable unit (Stoker et al., 2011). In this study, formations were taken as units displaying lithological characteristics that distinguish it from adjacent formations and have a recognisable top and base. Typically this distinction relates to identifying glacigenic or nonglacigenic deposits. Members are classified as a rank below a formation and always form part of a formation. These were defined on the basis of lithological, geotechnical or seismic character and generally have a more localised expression. Typically formations are defined by a type section or area (Stoker et al., 2011). Given that this study focused on offshore sediments using such a definition proved difficult. Therefore, many of the formation and member names are attributed to the nearest geographical feature to the area that best defines it (often an island), or derived from annotated fishing ground maps.

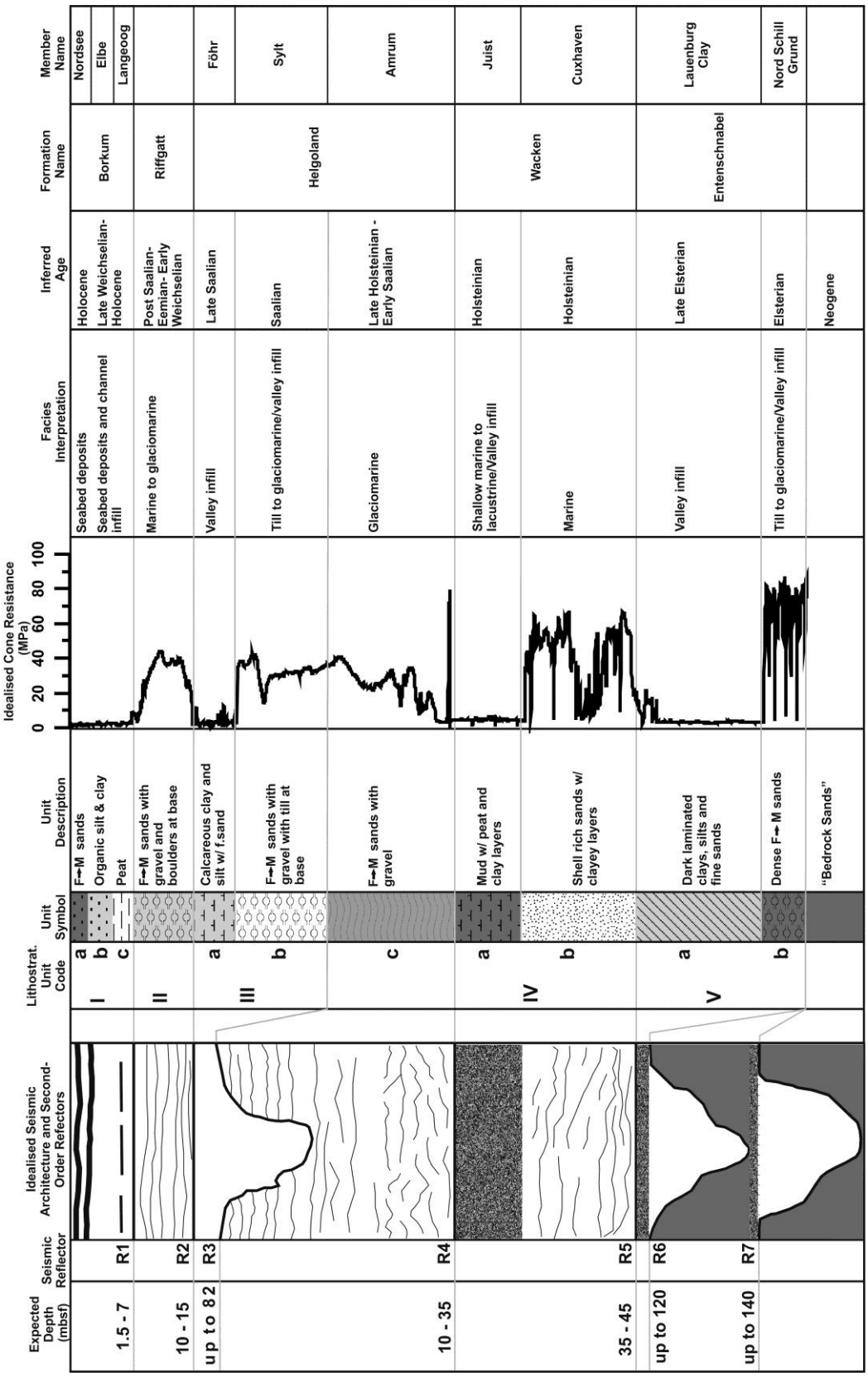

Figure 2.19 Extended version of Figure 2.2 and 2.21 complete with ltho-, seismo and geotechnical stratigraphic units from this study, their formational names, facies interpretation and inferred ages.

<table>
<tr><th colspan="2">Unit Code (This Study)</th><th>Formation Name (This Study)</th><th>Member Name (This Study)</th><th>German North Sea Stratigraphic Framework (Sindowski, 1970)</th><th>Quaternary Formations of Britain and The Netherlands (Long et al., 1988)</th></tr>
<tr><td rowspan="3">I</td><td>a</td><td rowspan="3">Borkum</td><td>Nordsee</td><td rowspan="3">Upper Marine Layer</td><td rowspan="2">Southern Bight Fm.</td></tr>
<tr><td>b</td><td>Elbe</td></tr>
<tr><td>c</td><td>Langeoog</td><td>Elbow Fm.</td></tr>
<tr><td colspan="2" rowspan="2">II</td><td rowspan="2">Riffgatt</td><td rowspan="2"></td><td>Limnic-Fluvial Layer</td><td>Twente Fm.</td></tr>
<tr><td>Middle Marine Layer (??)</td><td>Eem Fm. (??)</td></tr>
<tr><td rowspan="3">III</td><td>a</td><td rowspan="3">Helgoland</td><td>Föhr</td><td>Basin Deposit</td><td>Tea Kettle Hole Fm.</td></tr>
<tr><td>b</td><td>Sylt</td><td>Glacial Layer</td><td rowspan="2">Cleaver Bank Fm.</td></tr>
<tr><td>c</td><td>Amrum</td><td>Upper Glacio-Fluvial Layer</td></tr>
<tr><td rowspan="2">IV</td><td>a</td><td rowspan="2">Wacken</td><td>Juist</td><td></td><td></td></tr>
<tr><td>b</td><td>Cuxhaven</td><td>Lower Marine Layer</td><td>Egmond Fm.</td></tr>
<tr><td rowspan="2">V</td><td>a</td><td rowspan="2">Entenschnabel</td><td>Lauenburg Clay</td><td>Basin Deposits</td><td>Peelo Fm.</td></tr>
<tr><td>b</td><td>Nord Schill Grund</td><td>Lower Glacio-Fluvial Layer</td><td>Swarthe Bank Fm.</td></tr>
</table>

Figure 2.20 Comparison of stratigraphy nomenclature from this study with that of Sindowski (1970) for German EEZ and Long et al. (1988) for Quaternary deposits in the British and Dutch North Sea sectors. See section 2.7.1 and 2.7.2 for explanation.

In the British and Dutch sectors of the North Sea, sediments associated with the Elsterian glaciation are represented by the Swarte Bank Formation and largely found preserved in tunnel valley settings (Cameron et al., 1987; Praeg, 2003). This formation consists of basal unit of gravelly coarse sand, slump beds and, locally, till. Overlying this are clays with beds of silty clay and fine-grained sand (Long et al., 1988). In this study these deposits are similar in nature and structure to the Nord Schil Grund Member of the Entenschnabel Formation. According to Long et al. (1988) and in this study, these units are overlain by glaciolacustrine clays comparable to the P*otklei* or Peelo

Formation in the Netherlands and Lauenburg Clay in northern Germany. In this study it is classified as the Lauenburg Clay Member of the Entenschnabel Formation.

Holsteinian deposits in the Dutch North Sea sector are represented by shelly, fine- to medium-grained sands with thin beds of silt and clay, referred to as the Egmond Ground Formation (Long et al., 1988). In the southern sector of the U.K North Sea, deposits believed to be Holstein and comparable with Hoxnian dated deposits consist of shallow-marine clay (Long et al., 1988). In this study interglacial sediments akin to the Egmond Ground Formation were found and named as the Cuxhaven Member. Shallow marine to lacustrine sediments were also identified and named as the Juist Member. Together these two units form the Wacken Formation.

The complex nature of the Saalian complex is reflected in the variety within the nomenclature used to describe the deposits. In the central North Sea two phases of Saalian glaciation have been constructed (Ehlers, 1990). For the earliest phase till was found offshore of the Netherlands overlain by shallow marine sands. For the later phase evidence through large parts of the central and northern North Sea can be found in a single glacial erosion surface overlain by glacigenic sediments of till and glaciomarine sediments within the Fisher, Coal Pit and Ferder Formations (Graham et al., 2008). However, in the southern North Sea (particularly in the Dutch sector) Saalian deposits are proglacial (Cleaver Bank Formation) or periglacial (Tea Kettle Hole Formation) in nature (Long et al., 1988). The Cleaver Bank Formation consists of proglacial silty clays with silt and sand laminar with fluvioglacial fine grained outwash sands. The Tea Kettle Formation consists of well sorted, very fine- or fine-grained wind-blown sands. In this study the Saalian deposits were divided predominately classified as the Helgoland Formation consisting of three members: Amrum, Sylt and Föhr Members representing glaciomarine, proglacial to glaciomarine and periglacial conditions respectively.

The Riffgatt formation of this study is interpreted as marine to glaciomarine in nature. The lack of absolute chronological dating in this study meant that further interpretation was difficult. No definitive Eem related deposits were identified and as the unit occurs above R3 (late Saalian valley generation) this unit is inferred as post-Saalian to Weichselian in age. As a result this unit is most likely to correlate with the Eem and Twente Formation. The former comprising of intertidal and

shallow marine sands and clays, the latter of periglacial, glaciolacustrine and glaciomarine sands deposited near the ice margin (Long et al., 1988; Stoker et al., 2011).

The Borkum Formation largely incorporates the Holocene starting with basal peats of the Langeoog Member (this study) which is largely akin to the Elbow Formation which is also composed of freshwater basal peat inferred as latest Weichselian in age (Stoker et al., 2011). The Elbe and Nordsee Members in this study are modern mobile marine sediments similar to the Southern Bight Formation of Stoker et al. (2011) or the mobile sands of Zeiler et al. (2000).

2.7.2 Late Upper and Middle Pleistocene Reconstruction

Thick accumulations of dense, deltaic sands are the oldest formation seen across the North Sea having been deposited in a marine shelf environment during the late Neogene/ Early Pleistocene prior to the onset of alternating interglacial/glacial periods. These form the deeper strata upon which later Mid to Late Pleistocene deposits rest and the Elsterian valleys are incised into. Their wide-scale distribution across the North Sea suggests that the depositional environment was largely uniform and extensive at this stage (Cameron et al., 1987). The subsequent Mid to Late Pleistocene period, however, is characterised by alternating conditions associated with repeated glacial advance and intervening marine transgressions and interglacial environments (Ehlers et al., 1984; Cameron et al., 1987; Carr, 2004) (Fig. 2.19). The reach southward of ice sheet advance during each glaciation varied in extent as presented by Huuse and Lykke-Andersen (2000) (Fig. 2.21)

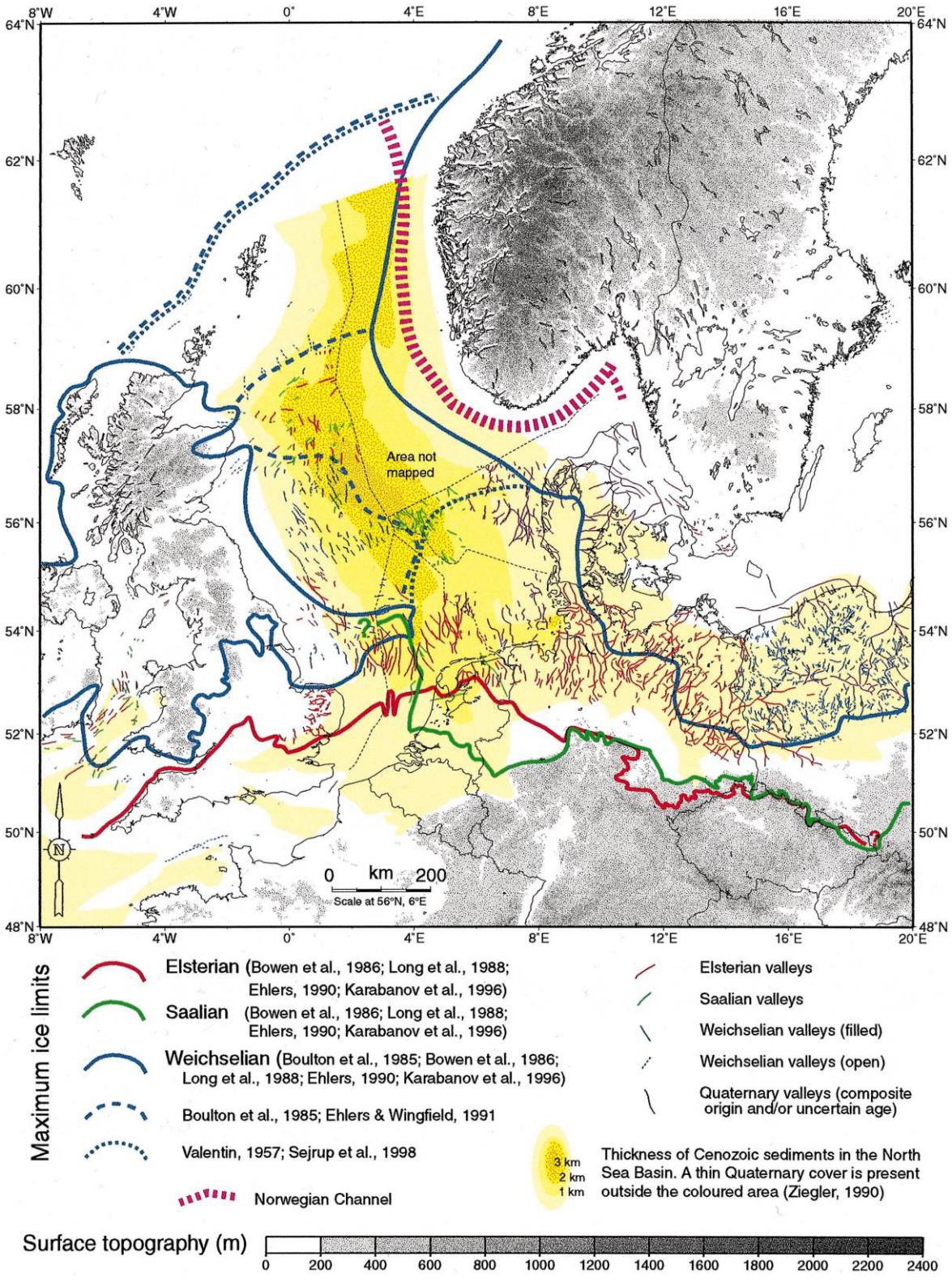

Figure 2.21 Extent of ice sheet advance during the Quaternary from Huuse and Lykke-Anderson (2000)

This transition from predominately marine sedimentation to glacial/interglacial conditions is recorded regionally by the seismic reflector R7 which corresponds with the first glacial advance of the Mid to Late Pleistocene during the Elsterian. Subsequently, the ice receded before a second advance occurred marked by the reflector R6. Both these periods are known times of valley generation (Ehlers and Linke, 1989; Huuse and Lykke-Andersen, 2000; Kluiving et al., 2003; Kristensen et al., 2007). During the Elsterian there was widespread glaciation across the North Sea, including the German Shelf (Ehlers et al., 1984; Grube et al., 1986). The prevailing conditions are represented by glaciomarine sands (Nord Schill Grund Member of the Entenschnabel Formation) that are seen resting above the R7 and R6 reflector as well as infilling the related valley structures.

During late Elsterian ice-sheet melting, large ice-dammed lakes are known to have formed on the North Sea plain (Ehlers et al., 1984). These lakes allowed for the quiet deposition of silts and clays referred to as Lauenburg Clay (Ehlers et al., 2011). These deposits are represented by the Lauenburg Clay Member of the Entenschnabel Formation (Unit Va) that show their greatest thicknesses in the buried valleys. Variations in composition throughout this unit represent the sequential deterioration of the ice sheet with some gravel and sandy layers found at the bottom which, subsequently, grade into better sorted clays and silts that are similar to varves in terms of lamination.

Climatic amelioration causing ice-sheet retreat with the subsequent Holsteinian Interglacial began with the transition from subarctic to boreal conditions (Ehlers et al., 2011). With it came the first marine transgression since the Miocene, marked by the reflector R5. The transgression is known to have progressed as far inland as 16 km and is believed to have encroached in a single, uninterrupted transgression (Linke, 1993; Hinze et al., 1995). Overlying this reflector are the deposits of the Wacken Formation (Unit IV). The resulting sediments are largely shelly sands of the Cuxhaven Member (Unit IVb) representing the marine conditions of this stage and occur exclusively in the Elsterian excavated valleys overlying the Entenschnabel Formation glaciomarine and glaciolacustrine sediments. Lacustrine settings may have also existed within depressions left in the valleys during the later stages of the Holstein as sea level began to fall again. This is

represented by the mud dominated Juist Member (Unit IVa) that contains clay and laminated varve-like sediments (Hepp et al., 2012; This study).

Whilst the subsequent Saalian period is characterised by a number of climatic oscillations resulting in three recorded ice advances into the North Sea, only one (the Drenthe) is known to have entered the German Sector resulting in an erosional surface across the area with a series of tunnel valleys suggesting an ice-sheet limit at around 56°N (Ehlers et al., 1984; Stoker and Long, 1984; Cameron et al., 1987; Ehlers et al., 1989; Wingfield, 1990; Ehlers and Wingfield, 1991). Data in this paper reveals early glaciomarine conditions are recorded as the related sands of the Amrum Member of the Helgoland Formation (Unit IIIc) which is extensively formed as a tabular unit. The advancement of ice into the area is recorded by the reflector R3 and the formation of five valleys seen in Areas 1, 2 and 4. Only one valley, which cuts into the Amrum Member, is seen in Area 3 as well as the Wacken and Entenschnabel Formations, whereas in Area 2 it cuts into Neogene sands. In Area 1 two valleys are recorded, both with an E-W trend, the first one is seen utilising an older Elsterian structure whereas a second one in the south cross cuts a similar Elster 1 valley. This would suggest that, similar to during the Elsterian, valley formation was followed by the deposition of meltwater sands (Sylt Member) and in some places extensive accumulations of glaciolacustrine or shallow glaciomarine silts and clays (Föhr Member).

Whilst in his stratigraphic framework Sindowski (1970) identified Eemian deposits, subsequent workers have noted the lack of such deposits in the German Sector (Streif, 2004). Here we were similarly unable to describe such units. The North Sea experienced a further glaciation during the Weichselian; however, the German sector is thought to have remained ice-free with sea-level dropping 110 - 130 m below its current height (Streif, 2004). As climatic conditions improved and the ice sheet decayed, sea ice may have reached as far south as 55°N (Cameron et al., 1987). During this stage of ice-sheet deterioration, clean, well-sorted sands were deposited in outwash or discharge river systems flowing across the ice-free plains. This event is recorded by Unit II which is generally confined to near coastal areas, namely Areas 1 and 2 where it is marked by a strong, erosive basal reflector (R2) and often with basal gravels. There is a marked decrease in the thickness of the Riffgatt Formation (Unit II) from east to west moving distally from the ice-sheet front. Shallow incisions in the upper 10 m associated with palaeochannels formed during the late

Weichselian/early Holocene were also noted. Similarly, any potential Eemian related deposits may be found at the base of this unit but are indistinguishable. Hence, this unit is defined as being post-Saalian and most likely related to Weichselian outwash sands.

A further improvement in climatic conditions occurred around 18,000 BP that initiated a general rise in sea level in the North Sea which, inundating the relatively barren terrain created during the preceding Weichselian glaciation, continued until the present day (Cameron et al., 1993). This is represented across the area by the ubiquitous Borkum Formation, varying in thickness from 1 - 10 m approximately. Thicker deposits are generally found closer to the German coast, notably in Area 3, but also a relatively thick (up to 20 m) accumulation is seen at Area 4 where the Elbe Palaeovalley has eroded into underlying Saalian deposits of the Sylt Member allowing more accommodation space. Various stages in the change in conditions associated with the end of the Weichselian and onset on the Holocene and subsequent marine transgression is well recorded in the Borkum Formation. Locally, peats and silts (Langeoog Member) marks the base of the sequence resting on an erosional contact (R1) with underlying Pleistocene sediments. The further rise in sea-level as the transgression progressed resulted in the deposition of silts and clays (Elbe Member) finally capped by the thin mobile sands of the Nordsee Member which also form the contemporary seabed (Zeiler et al., 2000).

2.7.3 Valley Generation and Infill

Tunnel valleys generally form perpendicular to the ice-advance front which, in the case of the Elsterian and Saalian, results in a commonly NW-SE and N-S trend respectively. This was true for the majority of recorded valleys in the areas with the exception of the major E-W Elster 2 related valley seen in Area 1 (Hepp et al., 2012; This study). Similarly, in Areas 3 and 4 where we see saltdome formation, the course of the valleys in these areas is seen to be deflected around the contours of the saltdome (Fig. 2.11 and Fig. 2.16).

All recorded valleys offer no modern seafloor expression as they have been subsequently filled and capped by either the Borkum and/or Riffgatt Formation. In their past these valleys may have

become reactivated fully or partly during subsequent glaciations or ice sheet advances (Piotrowski and Kraus, 1997). As a result, they offer ideal accommodation space for the accumulation and preservation of interglacial and glacial sediments that would have otherwise been stripped or reworked by subsequent glacial periods and/or marine transgressions. For instance, the Lauenburg Clay Member, Juist Member and Sylt Member are only found as valley fills. The multiple erosion horizons and fill episodes recorded in valley seismic profiles (Lutz et al., 2009), and is perhaps best seen in the major east-west valley in Area 1 that is fully investigated by Hepp et al. (2012). Hepp et al. (2012) noted a sedimentary sequence within an Elster 2 excavated valley recording initial Elsterian meltwater sands (Nord Schill Grund Member) and laminated clays and silts (Lauenburg Clay Member) before a second reflector marks the erosive base of the Holsteinian marine transgression overlain by associated shallow marine and lacustrine sediments (Juist Member). In the upper part of the valley evidence for a secondary shallow valley may also be seen suggested to be Saalian in age.

The general infill of these valleys reveals a common succession containing basal units often consisting of gravels and/or dense sands which were deposited synchronously or shortly after valley generation, namely the Nord Schill Grund Member. Similarly, these are regularly overlain by finer sediments deposited in glaciolacustrine or shallow glaciomarine/marine settings like those associated with the Lauenburg Clay (Ehlers et al., 2011) i.e. Lauenburg Clay Member of this study. This sequence of infill has also been recognised in profiles of onshore valleys (Ehlers and Wingfield, 1991; Piotrowski, 1994). The Lauenburg Clay is widely distributed in North Germany and into the Netherlands where it is the equivalent of the “Potklei” or Peelo Formation. It is a widely recognised stratigraphic marker for the late Elsterian and is usually associated with buried valley fills overlying sandier deposits (Ehlers and Linke, 1989; Huuse and Lykke-Andersen, 2000). Its occurrence outside of buried valleys is rarely recorded and wasn’t identified in core profiles outside valley structures in this study. The clay over sands sequence is most notably seen in the cross cutting minor E-W valley and N-S valley in Area 1. The N-S valley is filled predominately by the Nord Schill Grund Member and overlain by a relatively thin (3 - 4 m) accumulation of Lauenburg Clay Member that has been overconsolidated suggesting ice-loading. Above the Lauenburg Member is marked by the strong basal reflector of the cross-cutting E-W valley (R3), again, filled by the Föhr and Sylt Members that are normally consolidated suggesting they haven't been subjected

to similar pressure. Since the Drenthe stage of the Saalian, ice-advance was the last known to affect the area, it can be assumed the shallower valley is related to this ice-advance and the subsequent fill is at least syn- or post- Saalian with the older, deeper valley of Elsterian age. Although only the upper few metres of the Elsterian valleys found in Area 3 were sampled they similarly record late stage glaciolacustrine silts and clays of the Lauenburg Clay Member. The common succession of the tunnel valleys in this study (with the exception, perhaps, of the major east-west valley of this study and Hepp et al. (2012)) may be the result of accommodation space and proximity to the retreating ice sheet. Whilst tunnel valleys have been known to reach depths of up to 400 m, those found in this study were seen to depths of a maximum 140 mbsf. During deglaciation, massive amounts of meltwater gravel and sand can be released which can often fill the majority of accommodation space available in a tunnel valley (Ehlers and Linke, 1989). Minor amounts of basal till underlying these meltwater deposits and significant deposits of glaciolacustrine material overlying them means these tunnel valleys may be essentially filled with subglacial and ice-proximal deposits. As ice-retreat continues and conditions become more ice-distal, deposition of sediments may bypass the filled tunnel valley and become deposited further south. Such tunnel valleys containing Elsterian, Holsteinian and Saalian related fill have been recorded onshore near Hamburg (Ehlers and Linke, 1989) and Kiel (Piotrowski, 1994).

2.8 CONCLUSIONS

Our extensive mapping of Quaternary deposits in the study areas of the German North Sea sector outlined above involved 72 core profiles of up to 50 m depth, 196 CPT profiles of same and some 320 seismic lines. They revealed broad similarities in the depositional history of these areas with several stages of valley generation, and subsequent infill, the main control on local level variations.

Sedimentary sequences of Quaternary deposits range in thickness from a few metres up to 60 m outside of valley fills. The most ubiquitous of units was that of the Borkum Formation covering all areas and representing the most recent marine transgression during the late Weichselian/early Holocene. Background Quaternary sedimentary cover was thinnest towards the south coast in

Areas 1 and 4 comprising of the Borkum and Riffgatt Formations overlying bedrock Neogene sands. Further north and east in Area 2 and Area 3 respectively more extensive development of other units (namely the Helgoland, Wacken and Entenschnabel Formations) was visible in both seismic and core profiles. With improved seismic data and higher core density we have better mapped the extent of these units in comparison to previous studies (i.e. Sindowski, 1970).

Whilst the buried valleys in this study reveal a common succession, their infill is markedly different in many cases to background sedimentation. The buried valleys succession records the disintegration of ice-sheets (predominately Elsterian) with outbursts of meltwater sands represented by Nord Schill Grund Member grading into finer units such as the Lauenburg Clay Member as energy waned and more quiet, ice-distal conditions were established. The paucity of softer units such as the Föhr, Juist and Lauenburg Clay Members outside of valley structures may not necessarily indicate non-deposition. Layers that are more extensively developed laterally (such as the Riffgatt Formation, Amrum, Cuxhaven and Nord Schill Grund Members) are typically composed of dense sands and tills representing a stark mechanical difference in particular shear strength properties. Therefore, the finer units of the Föhr, Juist and Lauenburg Clay Members would be more prone to erosion and hence their absence in non-tunnel valley stratigraphy may be fundamentally due to this contrast in mechanical properties. Following this theory, tunnel valley structures act as depocentres, protecting units that may have been laterally extensive but were subsequently eroded/reworked during events such as marine transgressions or ice-sheet readvance.

In previous studies, buried valley structures were not identified and so the relationship of valley infill to background stratigraphic units was often misinterpreted. For example, in Sindowski (1970), no valleys were recorded and the relationship between Lauenburg Clay with glaciomarine sands associated with the Elsterian (Nord Schill Grund Member this study) is ambiguous. In this study, we identified the Lauenburg Clay as solely a valley infill and not laterally extensive. Similarly, in Sindowski's work only extensive marine sands associated with the Holstein were identified. In this study (and Hepp et al., 2012) lacustrine deposits from the Holsteinian were also identified in cores from a valley in Area 1.

Despite the high degree of lateral and vertical facies variation caused by uplift by saltdomes and morphological variation as a result of valley or channel presence, it was possible to correlate units across large areas by encompassing new geotechnical techniques. Therefore, the mapping and description of buried valleys and their infill history involves a multi-disciplinary approach incorporating sedimentology and geophysics with geotechnical analysis a useful intermediary tool to marry the two and help in the description and correlation of units.

REFERENCES

Alappat, L., Vink, A., Tsukamoto, S., Frechen, M., 2010. Establishing the Late Pleistocene–Holocene sedimentation boundary in the southern North Sea using OSL dating of shallow continental shelf sediments. Proceedings of the Geologists' Association 121, 43–54.

Balescu, S., Lamothe, M., Lautridou, J.-P., 1997. Luminescence evidence for two Middle Pleistocene interglacial events at Tourville, northwestern France. Boreas 26, 61–72.

Behre, K.-E., 2004. Coastal development, sea-level change and settlement history during the later Holocene in the Clay District of Lower Saxony (Niedersachsen), northern Germany. Quaternary International 112, 37–53.

Behre, K.-E., 2007. A new Holocene sea-level curve for the southern North Sea. Boreas 36, 82–102.

Böse, M., Lüthgens, C., Lee, J.R., Rose, J., 2012. Quaternary glaciations of northern Europe. Quaternary Science Reviews 44, 1–25.

Bot, S. Le, Lancker, V. Van, Deleu, S., Batist, M. De, Henriet, J.P., Haegeman, W., 2005. Geological characteristics and geotechnical properties of Eocene and Quaternary deposits on the Belgian continental shelf: synthesis in the context of offshore wind farming. Netherlands Journal of Geosciences 84, 147–160.

Cameron, T.D.J., Bulat, J., Mesdag, C.S., 1993. High resolution seismic profile through a Late Cenozoic delta complex in the southern North Sea. Marine and Petroleum Geology 10, 591–599.

Cameron, T.D.J., Stoker, M.S., Long, D., 1987. The history of Quaternary sedimentation in the UK sector of the North Sea Basin. Journal of the Geological Society 144, 43–58.

Carr, S.J., 2004. The North Sea basin, in: Quaternary Glaciations-Extent and Chronology. pp. 261–270.

Ehlers, J., 1990. Reconstructing the dynamics of the North-west European Pleistocene ice sheets. Quaternary Science Reviews 9, 71–83.

Ehlers, J., Eissmann, L., Lippstreu, L., Stephan, H., Wansa, S., Landesamt, G., Hamburg, D.-, Natur, L., Chaussee, H., Flintbek, D.-, 2004. Pleistocene glaciations of North Germany, in: Quaternary Glaciations-Extent and Chronology. pp. 135–146.

Ehlers, J., Gibbard, P.L., 2003. Extent and chronology of glaciations. Quaternary Science Reviews 22, 1561–1568.

Ehlers, J., Grube, A., Stephan, H.-J., Wansa, S., 2011. Pleistocene Glaciations of North Germany — New Results, in: Quaternary Glaciations-Extent and Chronology. pp. 149–162.

Ehlers, J., Linke, G., 1989. The origin of deep buried channels of Elsterian age in Northwest Germany. Journal of Quaternary Science 4, 255–265.

Ehlers, J., Meyer, K.-D., Stephan, H.-J., 1984. The pre-Weichselian glaciations of north-west Europe. Quaternary Science Reviews 3, 1–40.

Ehlers, J., Wingfield, R., 1991. The extension of the late Weichselian / Late Devensian ice sheets in the North Sea Basin. Journal of Quaternary Science 6, 313–326.

Eisma, D., Mook, W.G., Laban, C., 1981. An Early Holocene Tidal Flat in the Southern Bight, in: Holocene Marine Sedimentation in the North Sea Basin. Blackwell Publishing Ltd., pp. 229–237.

Figge, K., 1980. Das Elbe-Urstromtal im Bereich der Deutschen Bucht (Nordsee). Eiszeitalter und Gegenwart 30, 203–211.

Gerdes, G., Petzelberger, B.M., Scholz-Böttcher, B.M., Streif, H., 2003. The record of climatic change in the geological archives of shallow marine , coastal , and adjacent lowland areas of Northern Germany. Quaternary Science Reviews 22, 101–124.

Gibbard, P.L., Cohen, K.M., 2008. Global chronostratigraphical correlation table for the last 2 . 7 million years. Episodes 31, 243–247.

Graham, A.G.C., Lonergan, L., Stoker, M.S., 2010. Depositional environments and chronology of Late Weichselian glaciation and deglaciation in the central North Sea. Boreas 39, 471–491.

Graham, A.G.C., Stoker, M.S., Lonergan, L., Bradwell, T., Stewart, M.A., 2008. The Pleistocene Glaciations of the North Sea Basin, in: Quaternary Glaciations-Extent and Chronology. pp. 261–278.

Grube, F., 1979. Obertiefte Täler im Hamburger Raum. Eiszeitalter und Gegenwart 29, 157–172.

Grube, F., Christensen, S., Vollmer, T., Duphorn, K., Klostermann, J., Menke, B., 1986. Glaciations in north west Germany. Quaternary Science Reviews 5, 347–358.

Hepp, D.A., Hebbeln, D., Kreiter, S., Keil, H., Bathmann, C., 2012. An east – west-trending Quaternary tunnel valley in the south-eastern North Sea and its seismic – sedimentological interpretation. Journal of Quaternary Science 27, 844–853.

Hermsdorf, N., Strahl, J., 2008. Eemian deposits in the Brandenburg area. Brandenburgische Geowissenschftliche Beiträge 15, 23–55.

Hinze, C., Höfle, H.C., Jordan, H., Mengeling, H., Meyer, K.-D., Rohde, P., Streif, H., 1995. Quatärgeologische Übersichtskarte von Niedersachen und Bremen 1: 5000,000. Hannover.

Huuse, M., Lykke-Andersen, H., 2000. Overdeepened Quaternary valleys in the eastern Danish North Sea: morphology and origin. Quaternary Science Reviews 19, 1233–1253.

Kluiving, S.J., Aleid Bosch, J.., Ebbing, J.H.., Mesdag, C.S., Westerhoff, R.S., 2003. Onshore and offshore seismic and lithostratigraphic analysis of a deeply incised Quaternary buried valley system in the Northern Netherlands. Journal of Applied Geophysics 53, 249–271.

Knudsen, K.L., 1988. Marine interglacial deposits in the Cuxhaven Area , N W Germany: a comparison of Holsteinian , Eemian and Holocene foraminiferal faunas. Eiszeitalter und Gegenwart 38, 69–77.

Knudsen, K.L., 1994. The marine Quaternary in Denmark: a review of new evidence from glacial-interglacial studies. Bulletin of the Geological Society of Denmark 41, 203–218.

Konradi, P.B., 2000. Biostratigraphy and environment of the Holocene marine transgression in the Heligoland Channel , North. Bulletin of the Geological Society of Denmark 47, 71–79.

Kristensen, T.B., Huuse, M., Piotrowski, J.A.N.A., Clausen, O.L.E.R., 2007. A morphometric analysis of tunnel valleys in the eastern North Sea based on 3D seismic data. Journal of Quaternary Science 22, 801–815.

Kuhlmann, G., Langereis, C., Munsterman, D., Jan van Leeuwen, R., Verreussel, R., Meulenkamp, J., Wong, T., 2006. Chronostratigraphy of Late Neogene sediments in the southern North Sea Basin and paleoenvironmental interpretations. Palaeogeography, Palaeoclimatology, Palaeoecology 239, 426–455.

Laban, C., van der Meer, J.J.M., 2004. Pleistocene glaciation in The Netherlands, in: Quaternary Glaciations-Extent and Chronology. pp. 251–260.

Linke, G., 1993. Zur Geologie und Petrographie der Forschungsbohrungen quo 1-5, der Bohrung Hamburg-Billbrook und des Vorkommens von marinem Holstein im Gebiet Neuwerk-Scharhörn. Geologisches Jahruch A, 35–76.

Litt, T., Behre, K.-E., Meyer, K.-D., Stephan, H.-J., Wansa, S., 2007. Stratigraphische Begriffe für das Quartär des norddeutschen Vereisungsgebietes. Quaternary Science Journal 56, 7–65.

Long, D., Laban, C., Streif, H., Cameron, T.D.J., Schuttenhelm, R.T.E., Paepe, R., 1988. The Sedimentary Record of Climatic Variation in the Southern North Sea [and Discussion]. Philosophical Transactions of the Royal Society of London. B, Biological Sciences 318 , 523–537.

Lutz, R., Kalka, S., Gaedicke, C., Reinhardt, L., Winsemann, J., 2009. Pleistocene tunnel valleys in the German North Sea: spatial distribution and morphology. Zeitschrift der Deutschen Gesellschaft für Geowissenschaften 160, 225–235.

Ó Cofaigh, C., 1996. Tunnel valley genesis. Progress in Physical Geography 20, 1–19.

Piotrowski, J.A., 1994. Tunnel-valley formation in northwest Germany--geology, mechanisms of formation and subglacial bed conditions for the Bornhoved tunnel valley. Sedimentary Geology 89, 107–141.

Piotrowski, J.A.N.A., Kraus, A.M., 1997. Response of sediment to ice-sheet loading in northwestern Germany: effective stresses and glacier-bed stability. Journal of Glaciology 43, 495–502.

Praeg, D., 2003. Seismic imaging of mid-Pleistocene tunnel-valleys in the North Sea Basin—high resolution from low frequencies. Journal of Applied Geophysics 53, 273–298.

Richter, H.P., 1962. Geschiebekundliche Gliederung der Elster-Kaltzeit in Niedersachen.

Sejrup, H.P., Aarseth, I., Ellingsen, K.L., Reither, E., Jansen, E., Løvlie, R., Bent, A., Brigham-Grette, J., Larsen, E., Stoker, M., 1987. Quaternary stratigraphy of the fladen area, central North Sea: A multidisciplinary study. Journal of Quaternary Science 2, 35–58.

Sejrup, H.P., Nygård, a., Hall, a. M., Haflidason, H., 2009. Middle and Late Weichselian (Devensian) glaciation history of south-western Norway, North Sea and eastern UK. Quaternary Science Reviews 28, 370–380.

Sindowski, K.-H., 1970. Das Quartär im Untergrund d e r Deutschen Bucht (Nordsee). Eiszeitalter und Gegenwart 1–18.

Smed, P., 1998. Die Entstehung der dänischen und norddeutschen Rinnentäler (Tunneltäler) - Glaziologische Gesichtspunkte. Eiszeitalter und Gegenwart 48, 1–18.

Sommé, J., 1979. Quaternary coastlines in northern France, in: The Quaternary History of the North Sea. Symposia Universitatis Upsaliensis, Annum Quingentesimum Celebrantis: 2, Uppsala, pp. 147–158.

Stephan, H.J., 1982. Glazialgeologische Untersuchungen in Sülichen Geestgebiet Dithmarschens. Schriften des Naturwissenschaftlichen Vereins für Schleswig-Holstein 50, 1–36.

Stewart, M.A., Lonergan, L., 2011. Seven glacial cycles in the middle-late Pleistocene of northwest Europe: Geomorphic evidence from buried tunnel valleys. Geology 39, 283–286.

Stoker, M.S., Balson, P.S., Long, D., Tappin, D.., 2011. An overview of the lithostratigraphical framework for the Quaternary deposits on the United Kingdom continental shelf.

Stoker, M.S., Long, D., 1984. A relict ice-scoured erosion surface in the Central North Sea. Marine Geology 61, 85–93.

Stoker, M.S., Long, D., Fyfe, J.A., 1985. The Quaternary succession in the central North Sea. Newsletters on Stratigraphy 14, 119–128.

Streif, H., 1990. Quaternary sea-level changes in the North Sea, an analysis of amplitudes and velocities, in: Earth's Totation from Eons to Days. Springer, Berlin, pp. 201–214.

Streif, H., 2004. Sedimentary record of Pleistocene and Holocene marine inundations along the North Sea coast of Lower Saxony , Germany. Quaternary International 112, 3–28.

Svendsen, J.I., Gataullin, V., Mangerud, J., Polyak, L., 2004. The glacial history of the Barents and Kara Sea region, in: Quaternary Glaciations-Extent and Chronology. pp. 369–378.

Toucanne, S., Zaragosi, S., Bourillet, J.F., Gibbard, P.L., Eynaud, F., Giraudeau, J., Turon, J.L., 2009. A 1.2 Ma record of glaciation and fluvial discharge from the West European Atlantic margin. Quaternary Science Reviews 28, 2974–2981.

Turner, C., 2000. The Eemian interglacial in the North European plain and adjacent areas. Netherlands Journal of Aquatic Ecology 79, 217–231.

Vink, A., Steffen, H., Reinhardt, L., Kaufmann, G., 2007. Holocene relative sea-level change , isostatic subsidence and the radial viscosity structure of the mantle of northwest Europe (Belgium , the Netherlands, Germany, southern North Sea). Quaternary Science Reviews 26, 3249–3275.

Wingfield, R., 1990. The Origins of Major Incisions Within the Pleistocene Deposits of the North Sea. Marine Geology 91, 31–52.

Zeiler, M., Schulz-Ohlberg, J., Figge, K., 2000. Mobile sand deposits and shoreface sediment dynamics in the inner German Bight (North Sea). Marine Geology 170, 363–380.

CHAPTER 3

GEOTECHNICAL AND GEOPHYSICAL INVESTIGATION OF THE WESTERN IRISH SEA MUD BELT

Theme

Having displayed the usefulness of in-situ geotechnical data (i.e. cone penetration testing) in conjunction with geophysical (seismic) and geological (core) data to create a robust stratigraphic framework for the GNSS in Chapter 2, Chapter 3 outlines our attempt to apply a similar technique in the Irish Sea. The chosen study area was the Western Irish Sea Mud Belt (WISMB), an area that has been relatively unstudied but, has been earmarked as a potential site for development of offshore wind farms. Geophysical and geological data gathered in 2009 was supplemented by geotechnical data using the MARUM GOST system in 2014. This data was then used to create a geological model for the area which would be used as a sound baseline study for subsequent investigations.

Contributors

Mark Coughlan partook in both surveys which gathered the data for this study. He is also the first author having undertaken evaluation of this data and written all drafts of the manuscript.

Andrew J. Wheeler is the lead supervisor on this project, was chief scientist for both surveys which gathered the data for this study and has extensively proof read drafts of this manuscript.

Boris Dorschel was present during the Irish Sea Marine Assessment survey (ISMA; CV0926, Appendix BI) and supervised the collection of the geophysical data. He also subsequently processed the geophysical data used in this study.

Tobias Mörz is head of the working group which developed the GOST system and supervised its operation during CE14001 (Appendix BIII). He also aided in the processing of the geotechnical data and its interpretation.

CHAPTER 3

GEOTECHNICAL AND GEOPHYSICAL INVESTIGATION OF THE WESTERN IRISH SEA MUD BELT

ABSTRACT

This study presents a synthesis of the lithostratigraphy, geotechnical properties and seismic profiles portraying the geometry and distribution of Quaternary deposits of the Western Irish Sea Mud Belt in an area being appraised for the potential development of offshore wind turbines. The study is based on large datasets (seismic, cores and cone penetration tests) gathered over the course of two major site surveys. These data are interrogated to create a robust geological model for an area that has previously suffered from a lack of direct sampling. Hence, new insights are proposed into the structure and composition of sediments found there and, for the first time, their geotechnical properties. Furthermore, a constraint mapping exercise was undertaken in addition to this geological study to assess the area for wind turbine sites. The direct implication of the geological and geotechnical structure of the sediments found here for foundation design is considered.

KEYWORDS: Irish Sea, Quaternary, Mud Belt, seismic stratigraphy, cone penetration testing, deposit geometry, geotechnics, wind turbines.

This chapter is based on: Coughlan, M., Wheeler, A.J., Dorschel, B., and Mörz, T. (in prep. Currently under embargo). Geotechnical and Geophysical Investigation of the Western Irish Sea Mud Belt.

3.1 INTRODUCTION

The Western Irish Sea Mud Belt (WISMB) is located at the termination of a sediment transport path, largely marked by sediment wave migration, driven by variations in bedstress conditions

which enter the North channel and St. George's channel of the Irish Sea. It is one of two such Mud Belts within the Irish Sea that mark areas where deposition is the dominant process under a low energy regime (Dobson, 1977; Pantin, 1977; 1978).

Despite a large body of work characterising the WISMB over the decades, there is a paucity of information regarding the character of sediment at depth aside from one British Geological Survey (BGS) borehole (89/15) from the Manx Depression southwest of the Isle of Man (Dickson and Whatley, 1993; Jackson et al., 1995). This drilled borehole logged some 38 m of Holocene clays overlying glaciomarine late Devensian silty muds of the Western Irish Sea Formation (Dickson and Whatley, 1993). The majority of other studies have used shallow cores characterising only the upper 6 m below the surface (Belderson, 1964; Pantin, 1977; Yuan et al., 1992; Chapter 4). Similarly, reports by Gavin and Doherty Geosolutions (2012) and Coughlan et al. (2011) (Appendix A) for INFOMAR found that, despite the wide coverage of core and grab sample data collected during the INFOMAR programme, again, it only extended to a maximum depth of 6 m and so there was a lack of data including sediment classification (and associated geotechnical data) at significant depth. This was particularly relevant in relation to developing offshore wind farm foundations where Cone Penetration Testing (CPT) is recommended to address this issue, with the WISMB recognised as an area of high priority.

Electric CPT has been in use for several decades having first been developed during the Second World War (Lunne et al., 1997). Since then it was developed into a useful and vital tool in the determination of soil stratigraphy and the identification of soil type both on- and offshore (Robertson and Cabal (Robertson), 2009). During operation, an instrumented cone located at the end of a series of rods, is pushed into the seabed at a constant rate. Subsequently, measurements are continuously collected for resistance of the sediment to the instrument, or cone resistance (q_c). In addition to cone resistance, the frictional resistance (f_s) on the outer surface of a cone sleeve is also continuously recorded as well as the pore pressure (u_2) via a piezocone penetrometer located behind the cone shoulder (CPTu). The friction ratio (R_f) is the ratio, expressed as a percentage, of the sleeve friction, fs, to the cone resistance, qt, both measured at the same depth.

Although no soil sample is obtained during CPTu operations, it is possible to infer how the sediments tested behave mechanically and so infer possible sediment types. The advantages of CPTu are that it provides fast and continuous profiling that is economical and productive and has a strong theoretical basis in interpretation. Hence, in this study, we investigate the nature of sediment in the WISMB based on CPTu data and relate it to sub-seabed facies and structures from a previous geophysical survey to garner new insights into the sedimentary architecture of the WISMB and its depositional history.

3.2 GEOLOGICAL SETTING

Initial studies in the WISMB found that thickness of mud ranged up to 33 m with the upper surface tending to follow the profile of the floor beneath it (Belderson, 1964). Deposits were thickest in depressions and no intermediate reflecting horizons between the seafloor and the strongly reflecting surface on which the muds rested (Late Devensian glacial till) was recognized. From this, Belderson (1964) deduced that the muds as a whole were either uniform as a whole or with slight progressive vertical variations in composition, as had been shown in core profiles, indicating past conditions were not radically different from the present day. Thinner deposits of these muds were noted at the margins of the WISMB and to the south where the reflecting horizon at the base became progressively shallower before becoming lost beneath the sand waves located there. The BGS Borehole 89/15 recorded 38 m of Holocene mud with sands at the base (Jackson et al., 1995). Pantin (1977) similarly demonstrated using grab samples, sediment cores and acoustic profiles that the WISMB stratigraphy consisted of bedrock overlain by a more or less continuous cover of boulder clay, which in turn, was overlain by marine sediment consisting primarily of mud. Vibrocores from some areas showed this mud separated from the boulder clay by a layer of coarse marine sands only a few tens of cms thick. He accepted that evidence for proglacial water-laid deposits, which was abound in the eastern Irish Sea Mud Belt (EISMB), was lacking or confined to one or two local depressions where there was a marked discontinuity assumed to be an unconformity. Above this unconformity, there was distinctive layering which was thought to be due to the presence of alternating sandy or gravel layers with mud. Belderson (1964) had postulated that any proglacial deposits, if present, had been masked by coarser deposits or had been

completely removed by strong tidal currents during the Holocene marine transgression. Pantin (1977) also accepted that the general absence of such deposits between the boulder clay and marine muds could indicate a significant phase of erosion in the area.

During the course of his study, Pantin (1977) recognized areas of acoustic turbidity on seismic profiles which he attributed to gas accumulation. He warned against the effect of the presence of this gas in distorting the appearance of bedrock into a “basin” or the “Becken Effect”. Williams et al. (1981) also recognized such shallow gas accumulations in the EISMB which limited the penetration of their seismic survey in places with the gas-charged sediments marked by strong reflectors and all reflectors below suppressed. As a result, seismic records varied and often forming a coherent image of sub-bottom conditions was difficult. Yuan et al. (1992) carried out a geophysical survey with a complementary coring and grab sample programme to target these areas displaying acoustic turbidity as well as areas with no apparent gas signature. From their survey they acknowledged Pantin’s (1977) interpretation of the general subsurface geology of the area. Similarly, they identified two major reflectors correlating with the upper bedrock surface and the base of Holocene sediments, both of which could be traced over large parts of the WISMB. They also identified the main shallow gas zone within the WISMB with gassy sediments occurring within a few metres of the seabed surface. The vertical thickness of these gas bearing sediments was difficult to observe due to the acoustic turbidity which blanketed underlying sediments referred to as “gas blanking” (Yuan et al., 1992). Other physical manifestations of gas migration on the seafloor included pockmarks. From their lab tests, Yuan et al. (1992) stated that the Holocene muds in the WISMB appeared to act mechanically, typical of such normally consolidated marine deposits with a high compressibility and high moisture content. Analyses on core samples from areas of perceived acoustic turbidity displayed evidence of gas within sediment pore space. The presence of this gas appeared to be of biogenic origin with the combination of warm waters during transgression and sediment traps giving rise to rapid fine-grained sediment accumulation containing large quantities of decaying organic matter. In their lab tests they showed that the compressional wave velocity is highly sensitive to small volume changes in gas concentration and may prove invaluable for detailed studies of the geotechnical significance of gassy sediments.

Jackson et al. (1995) also recognised the blanking effect of gas making it difficult to distinguish seismic units. Aside from bedrock, they identified three seismic facies within the WISMB. The chaotic facies has an amorphous signature, lacking reflectors or consisting of high-angle, impersistent and irregular reflectors. Deposits ranged in thickness from a few metres to 25 m occurring in basal incision infills and basal tabular-stratified units. Borehole analysis showed this unit to be dominated by gravels with muds, sands, cobble and boulders and was interpreted to have formed during glaciation in glaciolacustrine and glaciomarine, ice proximal conditions. The overlying prograded facies consisted of wedges of fine- to medium-grained sands. Seismically they were tabular-stratified deposits that exhibit prograding reflectors and were notably developed towards the margins of the WISMB. Here, they reach the seabed where they are reworked into bedforms, mostly sand waves. The facies was interpreted as being prodeltaic and glaciomarine, representing the passage from ice-proximal chaotic facies to a distal mud facies as ice retreated. Finally, the mud facies had a near-transparent acoustic character with parallel, subhorizontal reflectors forming tabular-stratified units of up to 80 m thickness. This facies was also recognised as containing dense concentrations of gas producing acoustic impedence on seismic profiles. Sporadic hyperbolic reflections were also noted interpreted as being caused by single cobbles or boulders and were regularly concentrated in layers. Cores from the area showed this facies to be black to greenish grey, shelly, sulphide- or glauconite-rich silts passing towards sandier deposits at the belt margins. This facies was interpreted as distal, glaciomarine deposits passing upwards into distal, marine conditions.

3.3 MATERIALS AND METHODS

3.3.1 Geophysical Investigation

A geophysical survey was carried out in September 2009 as part of the Irish Sea Marine Assessment (ISMA; CV0926, Appendix BI), which investigated the WISMB as well as other areas not relevant here (Fig. 3.1). During the survey onboard the R.V. Celtic Voyager, sub-bottom data was gathered using a Geo-Source 400 sparker system, which images to a depth of 50 m approximately. The system consisted of a 6 kJ pulsed power supply with the source comprising of

four electrode modules evenly spaced in a planar array. The return signal was picked up in a Geo-Sense single channel hydrophone array. Multibeam echosounder (MBES) data was also gathered using the Simrad EM3002D multibeam echosounder. The EM 3002 is a high resolution shallow water multibeam echosounder with dynamically focused beams suitable for 0.5 to 150 m water depth acquiring bathymetry and backscatter data. The transducers are hull mounted and, depending on the accuracy of positioning, the horizontal accuracy (x, y) is usually less than 50 cm and the vertical accuracy (z) less than 15 cm for the processed bathymetry data. Data processing was performed on board with the CARIS HIPS and SIPS software package.

In the post processing stage, reflectors were manually picked and traced along each seismic profile line in CorelDraw. At each fix point along a seismic profile, the depth to these reflectors was calculated using the formula:

$$(TWT \div 2) \times (0.001) \times (V)$$

where:

TWT = Two-way travel time in milliseconds

V = velocity of sound through the particular medium.

In the case of the water column, the sound velocity value was derived from conductivity, temperature and density probing (CTD) which was found to be 1,500 m/s. For different sediment types the value varies from approximately 1,550 m/s in unconsolidated muds to 1,650 m/s in over-consolidated tills. As sediment composition in the area comprised of both sediment types an average sound velocity value of 1,600 m/s was used for calculation. Once each point was assigned a depth for each reflector identified, an Excel table was compiled with positional data for each point and the relevant reflector depths. A Geographical Information System (GIS) was built from the data in this Excel table and depths between fix points interpolated. The data could then be analysed visually in 2D in ArcGIS.

3.3.2 Groundtruthing Investigation

The high-quality MBES and seismic data was groundtruthed by 975 high-quality, digital photographs of the seabed from 15 areas, 269 surface grab samples and 20 vibrocores of up to 3 m length. Based on the results from the initial geophysical survey, targets were obtained for groundtruthing using a Shipek sediment sampler and a 3 m Geo-Resources 6000. These targets included shallow occurring reflectors and areas of acoustic turbidity, potentially thought to be shallow gas.

Samples retrieved from all vibrocores for downcore grain-size variation were taken every 5 cm, weighing circa. 2 grams, with particle-size analyses (PSA) performed using a Beckman Coulter LS 13 320 laser diffraction particle-size analyser at MARUM, University of Bremen, to provide information about for all cores. The laser diffraction PSA is equipped with an Aquous Liquid Module and an Auto Prep Station and determines particle grain-sizes from 0.4 to 2000 µm. Analyses was carried out on bulk sediment samples.

In the case of surface grab-samples, the particle-size distribution of the siliciclastic fraction was measured on a Malvern Mastersizer 2000 laser-granulometer with Autosampler and Hydro G dispersion unit at the National Oceanography Centre Southampton. The siliciclastic fraction was obtained through the removal of organic matter and the carbonate phase by oxidation (10% H_2O_2) and dissolution (10% HCL) respectively. A 5% Calgon (Sodium Hexametaphosphate) solution was added for disaggregation and the sample agitated on a shaker. No comparative study was made between core and grab samples. The carbonate and organic fraction was removed from grab samples with the intention of studying sediment transport dynamics whereas an analysis on core material was carried out on bulk samples for the purpose of studying geotechnical properties. Similarly, a comparison was carried out on ten samples at different horizons in the cores to see the difference between bulk and carbonate/organic free samples. No significant difference was found.

Statistical parameters extracted from determined PSA data including modal and mean grain-size, sorting and sediment type were calculated according to Folk and Ward (1957) using the GRADISTAT software (Blott and Pye, 2001).

3.3.3 Cone Penetration Testing Investigation

In January 2014, a further survey was undertaken in collaboration between UCC and MARUM, this time with the goal of gather CPTu data utilising the Geotechnical Offshore Seabed Tool (GOST). Geophysical data from the ISMA survey was to form the basis of the planned CPT campaign using the GOST (CE14001; Appendix BIII). Based on extensive interrogation and review of the seismic data from the ISMA survey, 15 sites were chosen across the area as locations for further CPT investigation. One further site was chosen from outside the study area, to the south, for comparative purpose. In total these 16 sites were chosen as they presented the best representation of the variety of geological conditions found in the area (Fig. 3.1). These included shallow cropping reflectors where it was possible to target all sedimentary units, areas of acoustic turbidity believed to be related to gas charged sediments and locations at which to groundtruth bedrock depth. Similarly, where possible, sites were chosen were there was a strong seismic control on the sub-surface structure. Predominately, this refers to sites located at the intersection of two seismic profiles and/or sites where cores have been previously retrieved.

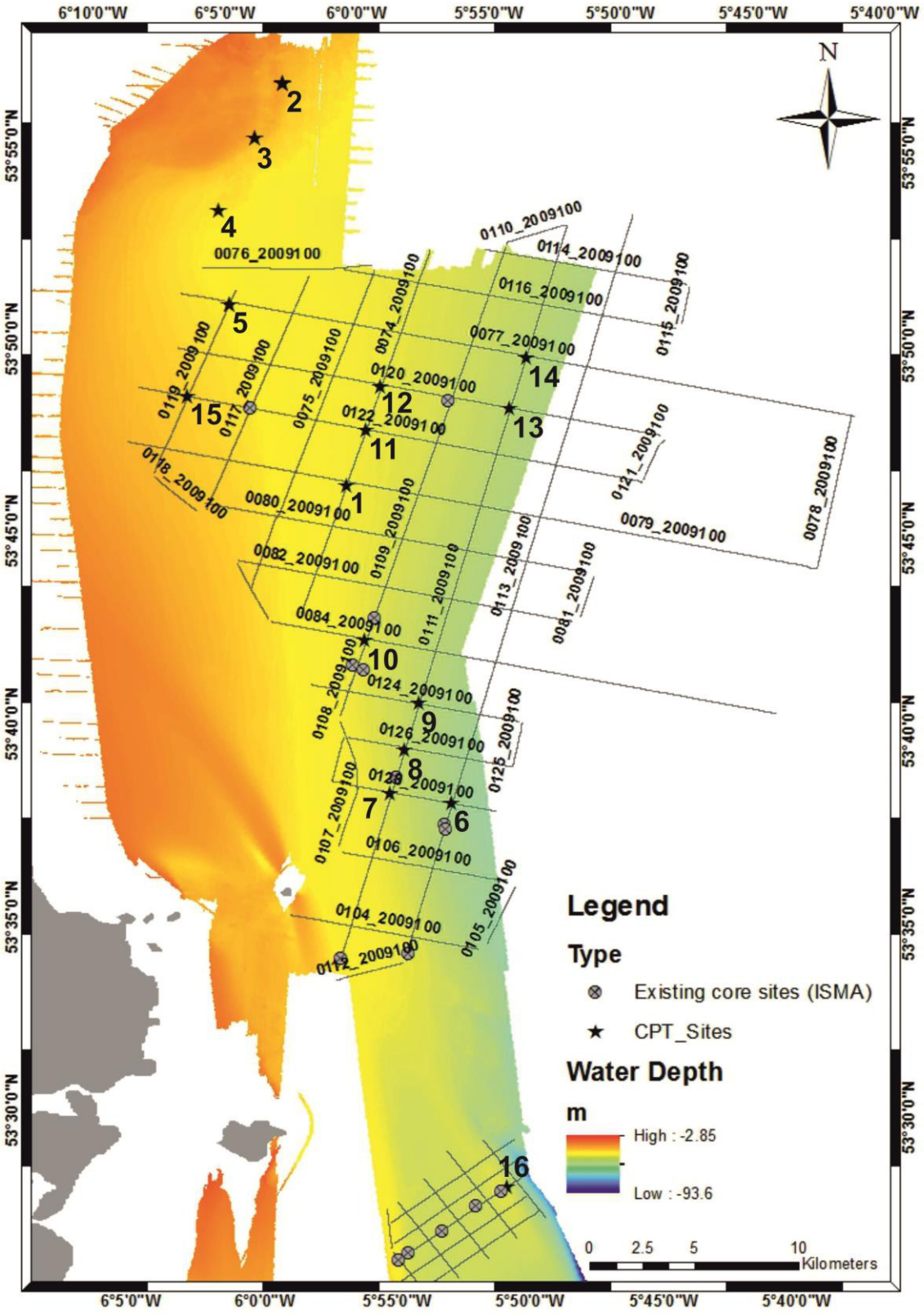

Figure 3.1 Site location map for CPT sites with existing seismic lines in grey existing core sites indicated by crossed circles.

The Geotechnical Offshore Seabed Tool (GOST), designed and developed at the MARUM Institute, University of Bremen in Germany, is an innovative geotechnical tool used to characterise the subsoil by means of "push-in tools" such as cone penetration testing or CPT. It is designed to operate from the seafloor in water depths of up to 4,000 m with a penetration depth of 6 – 40 m. Its primary focus is as an offshore site investigation tool in aid in foundation design, cable/pipeline route surveys and environmental mapping. During continuous operations, GOST can be slightly lifted from the seafloor during transit times and so allow for maximum use of valuable shiptime as there is no need for full recovery and subsequent redeployment at new sites. The GOST itself weighs between 2 and 8 tonnes depending on the addition of weighted plates for extra stability. It has its own mobile winch with a mobile hydraulic power unit allowing for easy and quick deployment using a three point suspension. It has 8,000 kg of hydraulic push power with infinitely variable hydraulic pressure of 0 – 200 bar. The cone tip has a cross section of 5 cm^2 and is composed of hardened stainless steel. Recording measurements such as tip resistance, sleeve friction, differential pore pressure, inclination and acceleration, it has a resolution of 0.06 MPa allowing for a range up to 120 MPa. Additionally, it is fitted with sensors for heat conductivity. Exact control on push velocity during penetration allows for data to comply to the highest international including DIN 4904 requirements. The interface is a digital one of industrial RS485 BUS using direct A/D converting of a measured variable with overvoltage and reverse protection.

Raw CPT data was calibrated through an individual calibration file with a linear calibration equation for every input signal in the form:

$$y=a*x+b,$$

where a is the gradient and b the intercept.

All data was zeroed through the zero-file which was recorded shortly before each test. During the next step double depth values where averaged to get a mean value and deleted. Artificial outliers were manually replaced by NaN (Not a Number). Since the data were altered through the deceleration and acceleration of GOST at the end of each push and at the start of the next push a

short section is replaced by NaN. The thickness of this section differs between the locations with the section usually 3 mm at the end of the push and 5 mm at the beginning of the next push. To get equal depth intervals, and allow a vertical shift of the sleeve data, the data were then interpolated to a depth interval of 1 cm. The sleeve data were shifted 7 cm upward which is the distance between the theoretical cone and sleeve center. The apparent depth was corrected by the measured inclination for every data point. Where temperature data were available (i.e. compression cones) the data were corrected for temperature effects.

The main application of CPTu data is to identify lithological changes in the sub surface and characterize sediment types. Typically, sands exhibit high cone resistance and a low friction ratio whilst clays display a low cone resistance and high friction ratio. Additionally, the use of pore pressure measurements during CPTu can further improve sediment identification. Very stiff, overconsolidated clays can give very low or negative recorded pore pressures as the cone is pushed through, as can very dense fine or silty sands. Contractive silts can give high recorded positive pore pressures as the cone is pushed through, whereas dilative silts may also give low or negative recorded pore pressures.

In addition to the primary CPTu parameters of cone resistance, sleeve friction and pore pressure, secondary parameters can also be derived. These include undrained shear strength (s_u) which can be calculated using empirical approaches (Lunne et al., 1997). In this study the equation:

$s_u = (q_t - \sigma_{v0})/N_{kt}$ was used

where: q_t is cone resistance corrected for pore pressure, σ_{v0} the total overburden pressure and N_{kt} an empirical correction factor.

For normally consolidated marine clays the N_{kt} value is between 11 - 19 with an average of 15 (Lunne and Kleven, 1981) with over consolidated clays measuring 17. Lunne et al. (2002) reported an N_{kt} value of 15 for lodgement till which was adopted by O'Kelly (2014) for the Dublin Boulder Clay (DBC) who also noted that an N_{kt} of 20 would provide conservatism for design. For silts, N_{kt}

values vary between 15 –30. For the purpose of this study, as we have two distinct lithologies at least of marine mud and glacial till, an N_{kt} value of 15 was adopted as an average to satisfy all possible lithological types thought to be in the study area (Steenfelt and Sørensen, 1995).

It is not possible to accurately predict sediment types based on grain size distribution from CPTu recorded values. However, by comparing values for cone resistance, friction ratio and pore pressure it is possible to classify sediment units according to how they behave mechanically or as Soil Behaviour Types (Robertson et al., 1986). In this study, Soil Behavior Type (SBT) zones were defined according to Robertson et al. (1986) based on cone resistance and friction ratio values. For each data collection point (every 1 cm) where cone resistance, sleeve friction and pore pressure was recorded it is possible to define an SBT zone. Furthermore, since both cone resistance and sleeve friction are influenced by increasing effective overburden with increasing depth, CPTu data requires normalization against this effect of effective overburden. A refined chart for SBT types based on normalised CPT data was proposed by Robertson (1990). Similarly, this normailised chart, although widely applicable, provides only a guide to the soil behavior type and is not a definitive prediction.

3.3.4 Constraint Mapping Exercise

Whilst geological conditions are a vital component in siting wind turbines, socio-economic factors can also have an impact. To supplement our geological evaluation of the study area, a constraint mapping exercise was also undertaken to assess the extent of socio-economic activities and other constraints which may impact on the siting of turbines. Data was gathered from a variety of sources and compiled in a GIS which allowed for a dynamic and flexible comparison of data and aid in producing a finalised map. A summary of data considered in this exercise is presented in Table 3.1.

Data Type	Data Source
Wind Speed, Direction, Frequency	Marine Institute
Wave Height, Direction, Period and Power	Marine Institute
Tidal Range and Period	Marine Institute
Offshore Weather Reports	Marine Institute and Met Eireann
Special Areas of Conservation (SAC)	National Parks and Wildlife Service
Special Protected Areas (SPA)	National Parks and Wildlife Service
Commercial Navigation	Irish Maritime Development Office
Fisheries	Marine Institute
Pipelines and Cables	Kingfisher Information Service, Department of Petroleum Affairs
Shipwrecks	Underwater Archaeological Unit
Military Exclusion Zones	Department of Defence

Table 3.1 Description and source of data used in constraint mapping exercise.

3.4 RESULTS

3.4.1 Seafloor Setting

The seabed within the study area slopes eastward to a depth of 55 m (Fig. 3.2). No obvious bedforms were recorded within the study area, although MBES data revealed small-scale sediment waves outside the area to the south passing northwards into a relatively uniform seabed (Fig. 3.2). Some pockmarks were noted in the southern and northeastern sections of the area (Fig. 3.2). These features were believed to be associated with gas escape from shallow accumulations (Yuan et al., 1992).

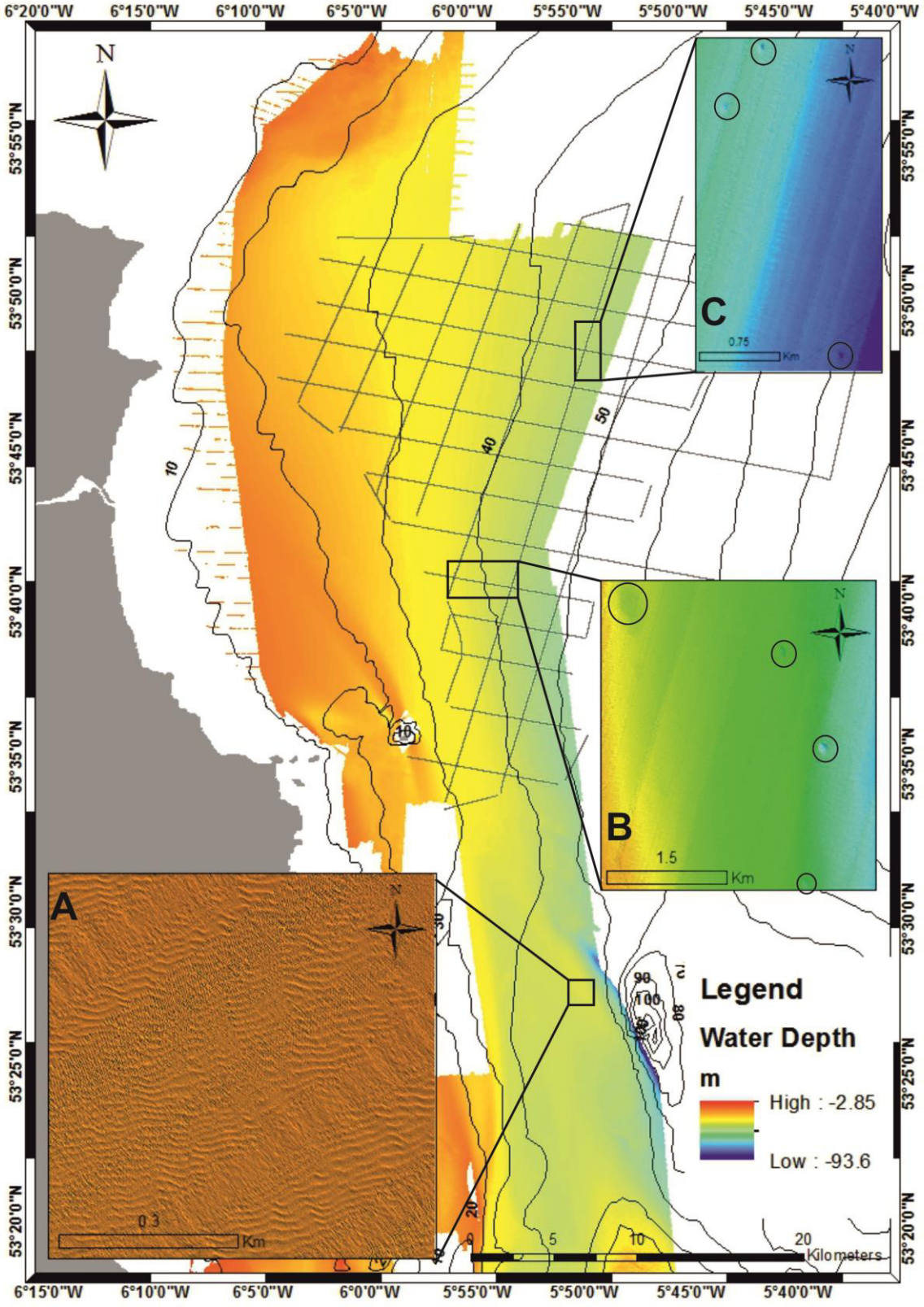

Figure 3.2 Seafloor setting. Main map shows water depth across the study area. Panel A highlights sediment waves located to the south. Panel B and C highlight pockmarks indicating gas escape.

Particle-size analyses on grab samples confirmed the fine-grained nature of seafloor sediment (Fig. 3.3). All samples were poorly to very poorly sorted with subtle changes in sediment distribution showing a general progressive northward decrease in grain-size. Starting in the south-west of the area, modal grain-size is 120.8/138.7 µm with mean grain-size 90 - 120 µm (Fig. 3.3). Towards the centre of the area, modal grain-size shows values of 52.73, 60.54, 69.51, 79.81, 91.64 and 105.21 µm with mean grain-size ranging from 20 - 115 µm. In the north-east section of the area modal values decrease further to values of 5.8, 6.64 and 8.75 µm with mean values between 0 and 20 µm.

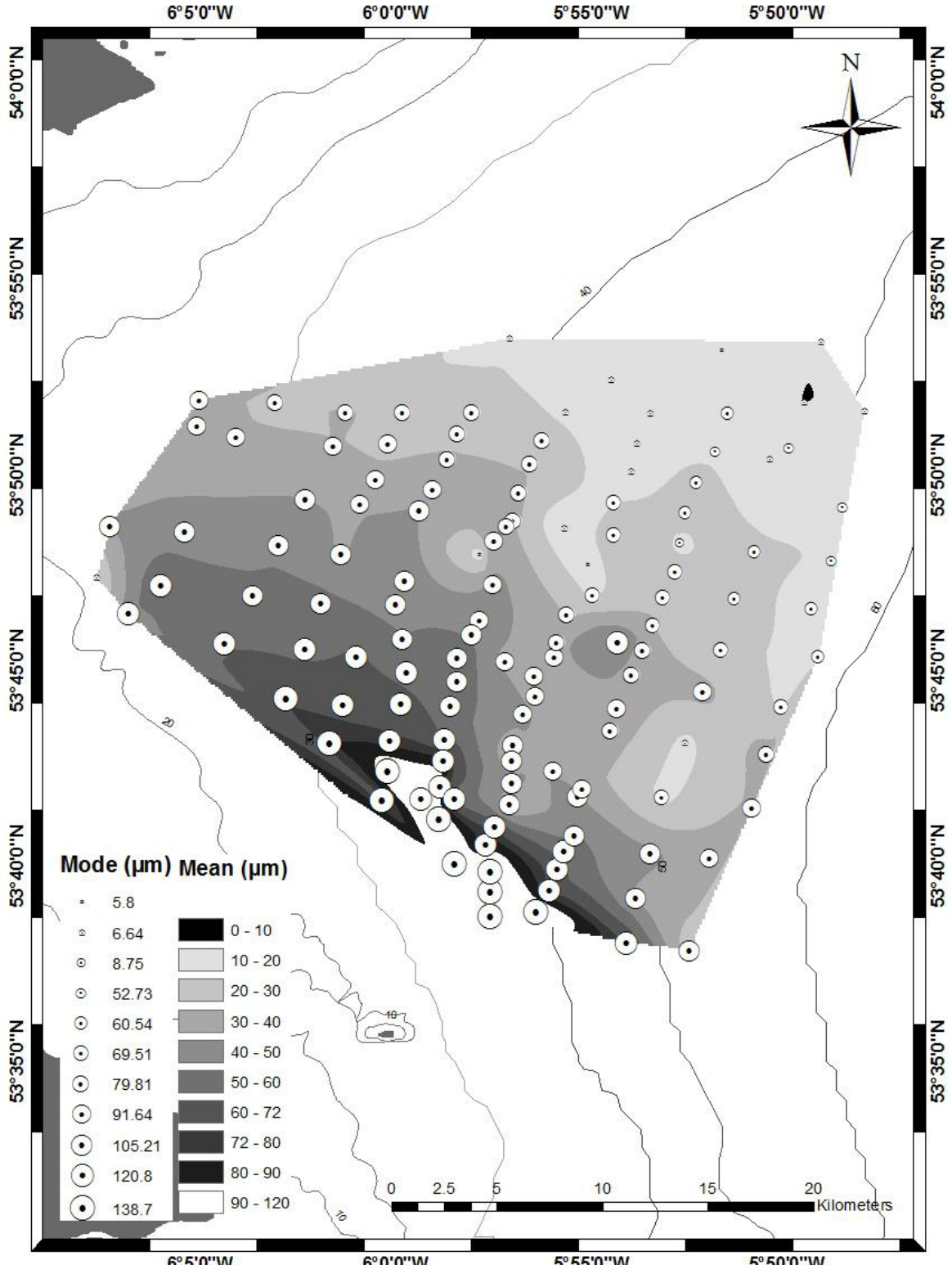

Figure 3.3 Grain size distribution. Both mean and modal grain size distribution are presented here. Mode is represented by representative circles. Mean grain size data has been interpolated from point data.

The study area is mainly covered with muds to fine sands with the sediment types of muddy sand, sandy mud, slightly gravelly mud and slightly gravelly sandy mud (all according to Folk and Ward

(1957)) showing a distinct progression from south to north (Fig. 3.4). Seabed photography confirmed the relatively featureless and fine grained nature of the seabed but did expose a microtopography that is related, for the most part, to epifaunal burrowing.

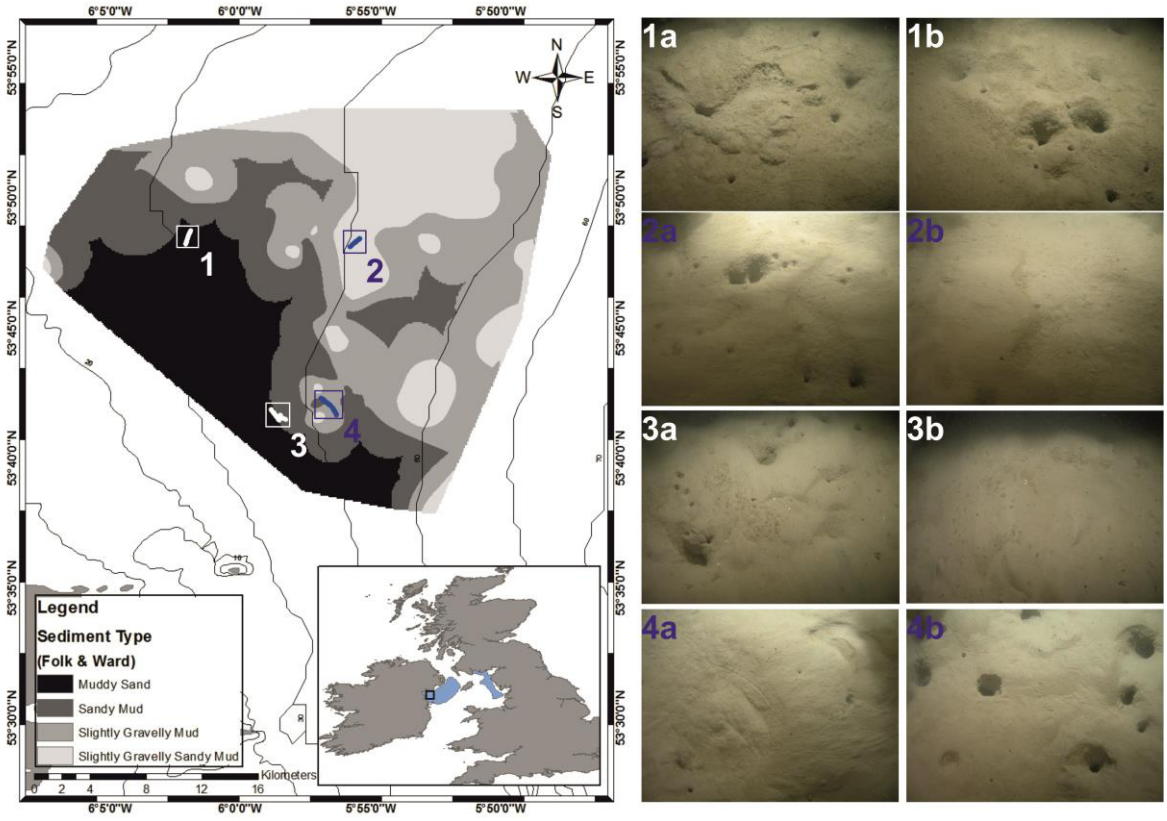

Figure 3.4 Left panel highlights sediment type distribution across the study area according to Folk and Ward (1957) classification. To the right are digital styles highlighting the muddy nature of substrate in the area and evidence for biotubation.

3.4.2 Seismic Facies and Groundtruthing

From seismic profiles, two major seismic reflectors (R1 and R2) were recorded which could be traced laterally across the study area. These reflectors in turn marked the base of two dominant seismic facies (S1 and S2, see chapter 4).

R2 was inferred as the top of bedrock with depths calculated presented in Figure 3.5. However, in many areas the certainty of R2 identification was low due to acoustic turbidity and the associated

"gas blanking" effect. Generally, depth to bedrock was shallowest in the north- and southernmost aspects of the area showing its greatest depths (up to 45 m) towards the centre.

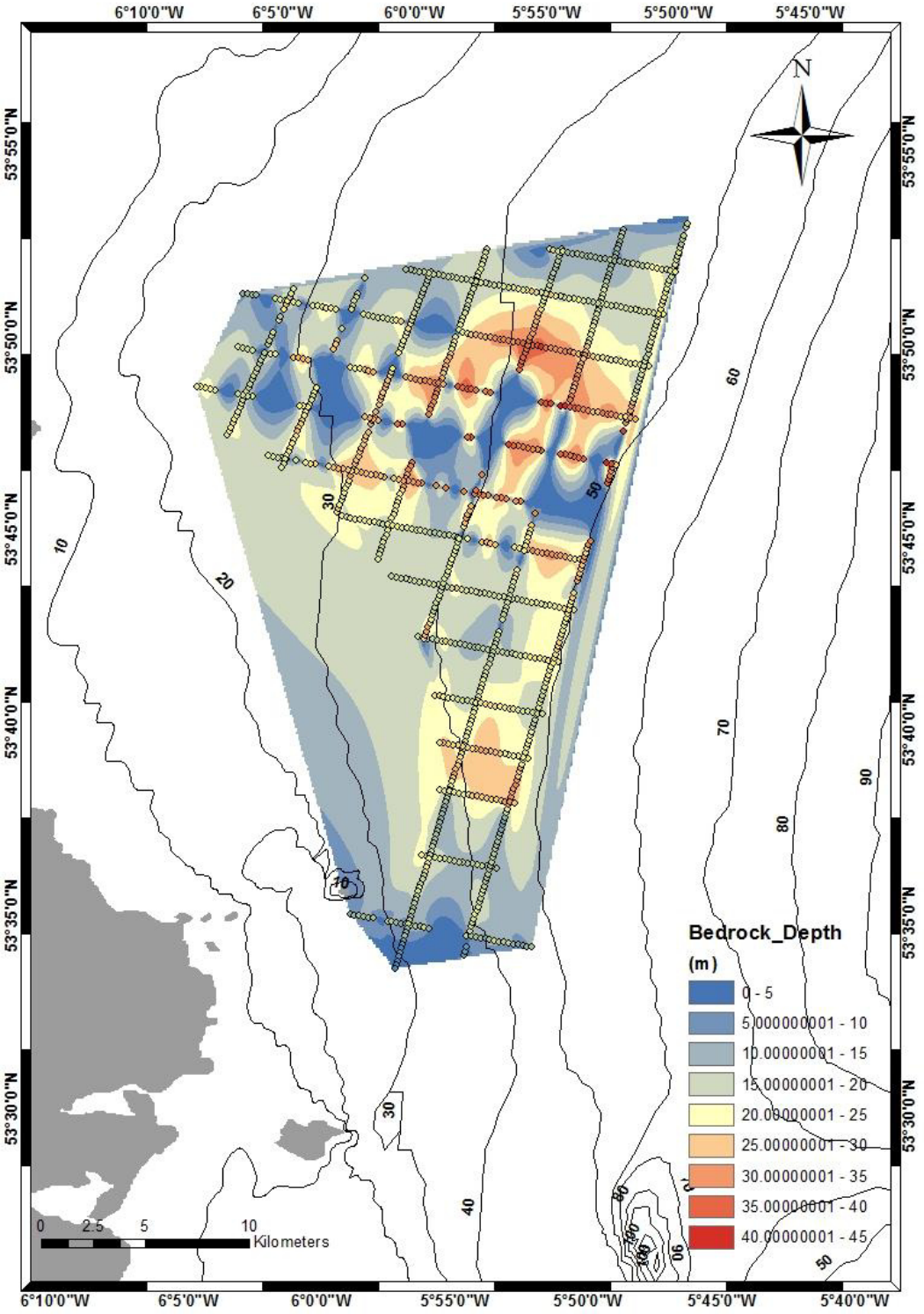

Figure 3.5 Bedrock depth (in metres below seabed) distribution map from seismic interpretation.

Overlying R2 is S2, a unit lacking internal horizontal laminations. For the most part the unit exhibits an amorphous structure (Fig. 3.10). However, in some places clear and laterally continuous structures were identified, mostly in the upper part of S2. This is likely to indicate erosive horizons and, thus, two multiple stages of deposition. Thickness of this unit ranged from 1.5 to 24 m with variation depending on the undulating nature of underlying bedrock. Often the base of the unit was synchronous with R1 indicating the unit may be relatively shallow and close to the seabed in places.

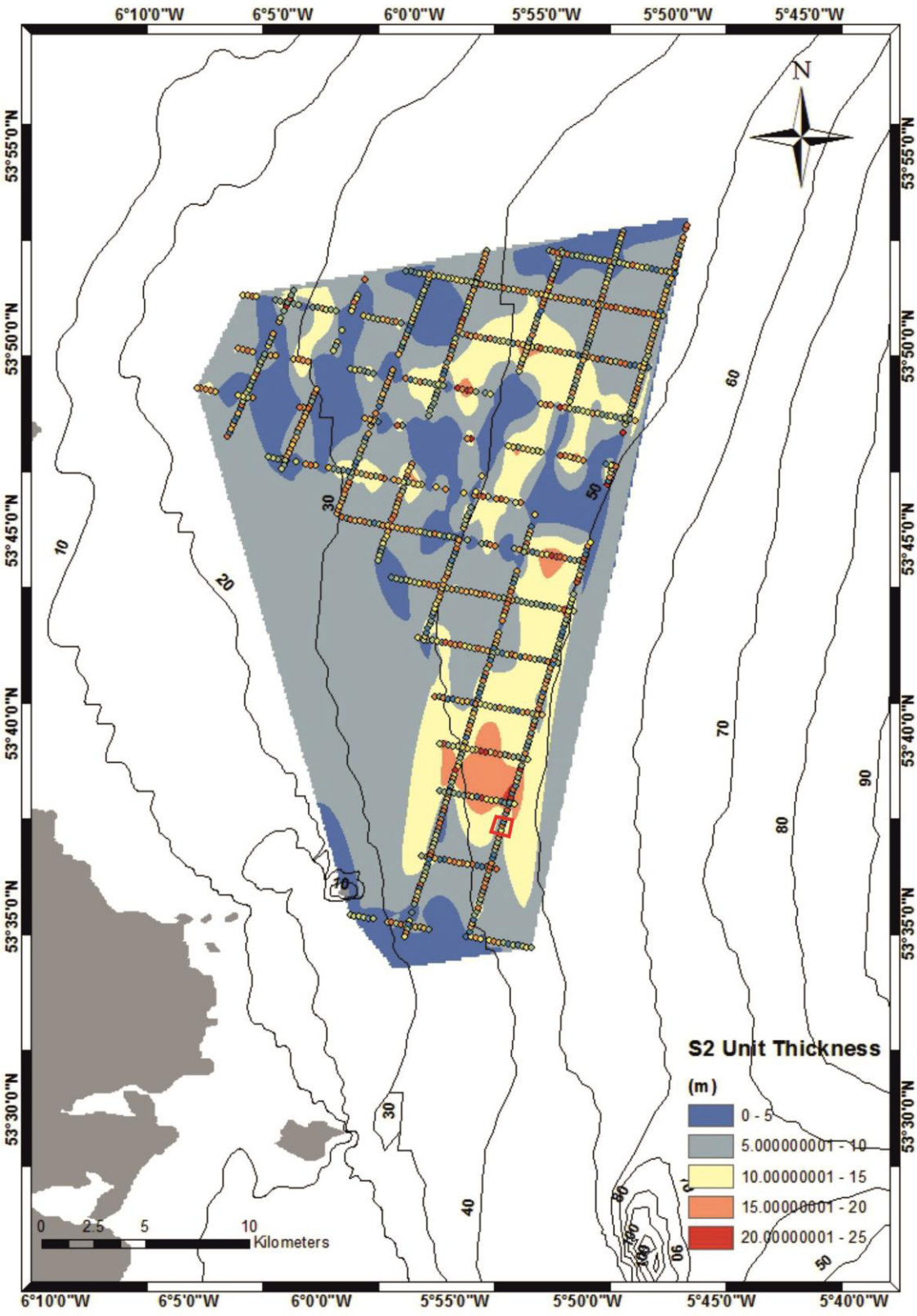

Figure 3.6 Isopach distribution (in metres) of S2. The seismic line segment highlighted by the red box is presented in Figure 3.7.

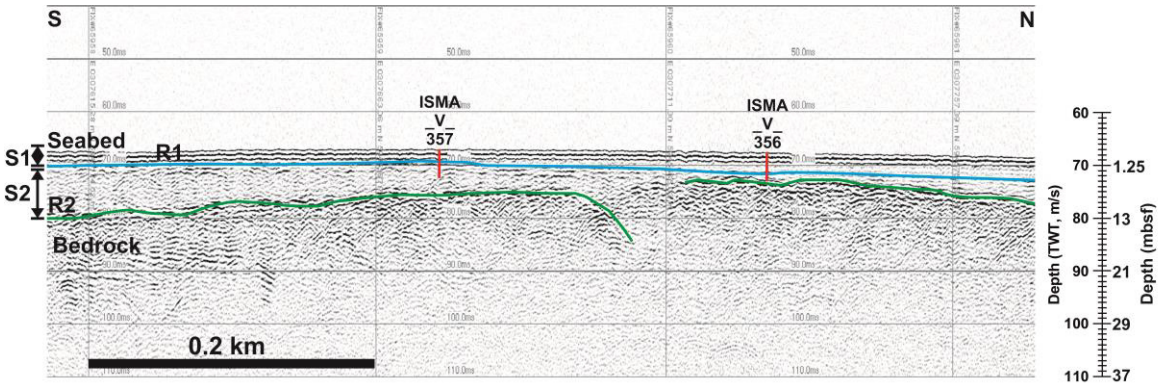

Figure 3.7 Seismic profile highlighted in Figure 3.6 with interpretations. Core profile for ISMA_V_356 and ISMA_V_357 is presented in Figure 3.8.

Two cores (ISMA_V_356 and ISMA_V357, Fig. 3.8) to the south of the study area, which are believed to have penetrated the R1 reflector and sampled the upper part of S2, display silty muds similar to those of S1 grading downcore towards glacial material consisting of pebbles (0.5 - 1 cm) and cobbles (up to 10 cm) in a stiff clay matrix (Fig. 3.8F).

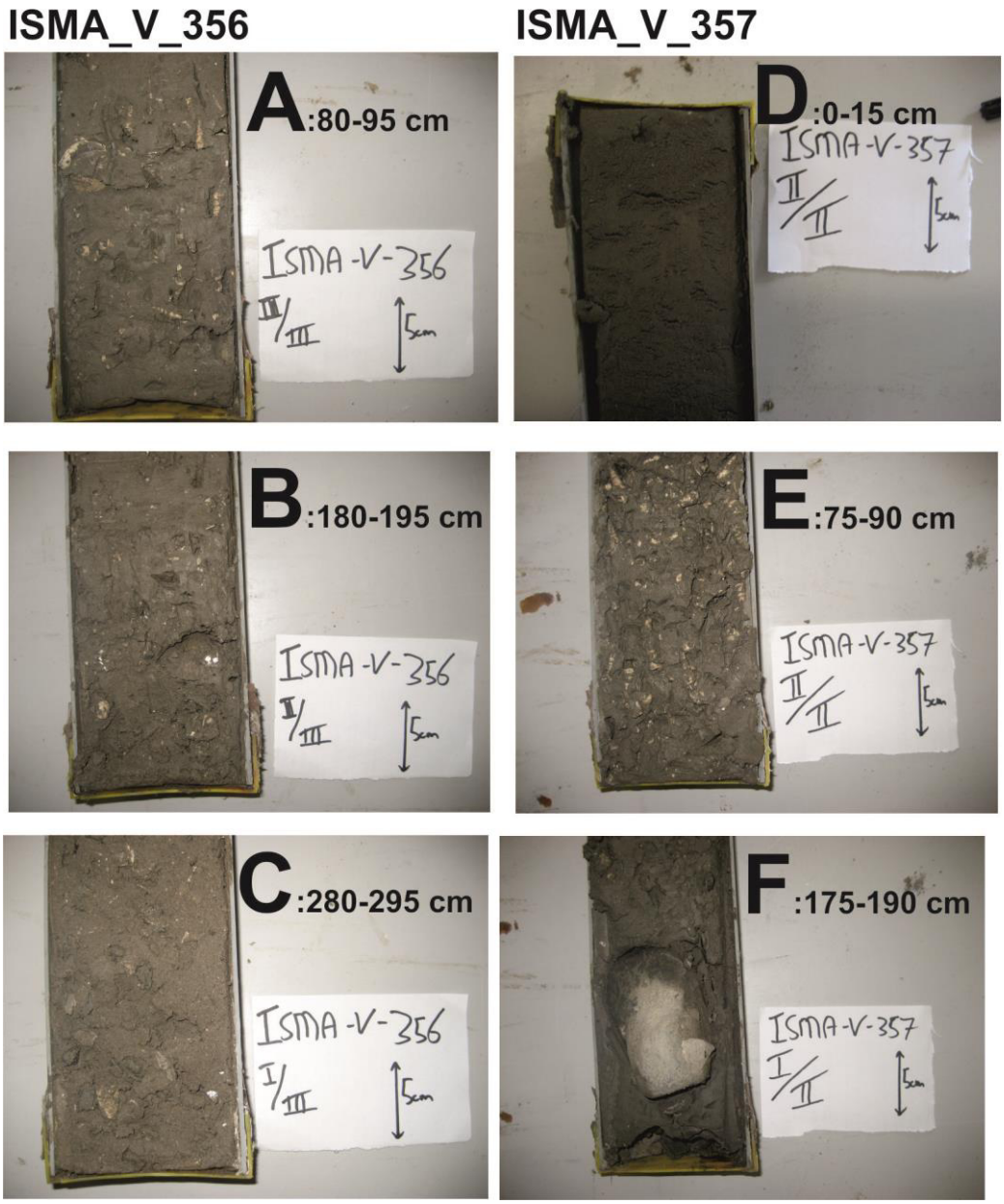

Figure 3.8 Core profiles for ISMA_V_356 and ISMA_V_357. Note shelly silty-sands in A, B, C and E. Olive green/brown silty mud in D and a sizeable cobble (14 cm) set in a stiff, dark-grey clayey matrix in F.

The first strong reflector (R1) after seabed varied in depth from 0.8 to 26.5 metres below seafloor (mbsf). It is largely horizontal in nature and shows greatest depth towards the centre of the WISMB. Lying above R1 is seismic facies 1 (S1) (Fig. 3.9 and Fig. 3.10).

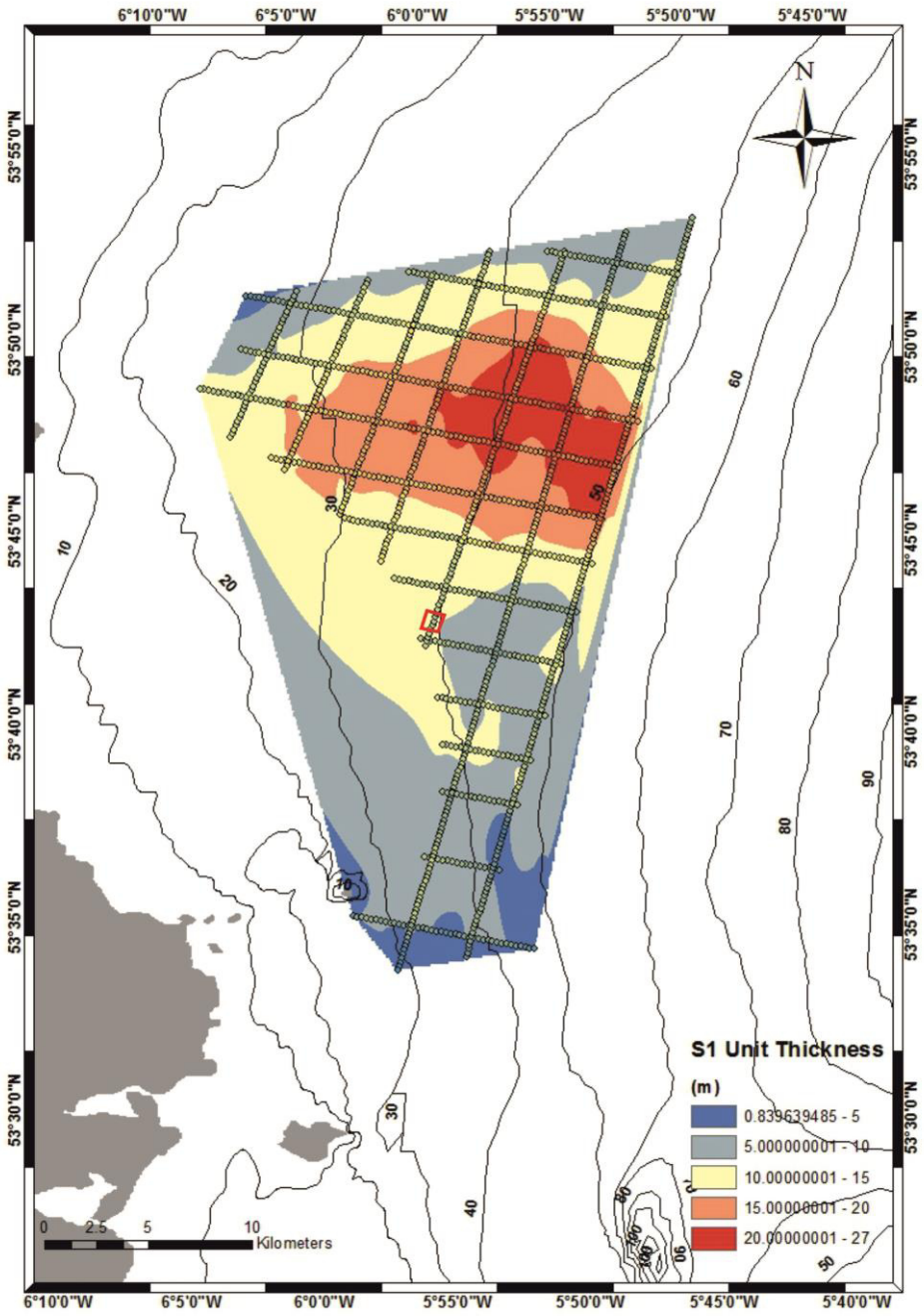

Figure 3.9 Isopach distribution (in metres) of S1. The seismic line segment highlighted by the red box is presented in Figure 3.10.

S1 is the youngest unit and contains little internal structure other than faint, horizontal parallel laminae which would indicate the unit is made up of flatly bedded sediment with no signs of erosion (Fig. 3.10). Within certain seismic profiles, the lower sections of S1 showed enhanced reflectors creating a sharp boundary with the surrounding material. Hence, R1 was often dissipated and the transition to S2 not as definitive. Similarly, it was difficult to infer R2 (Fig. 3.13)

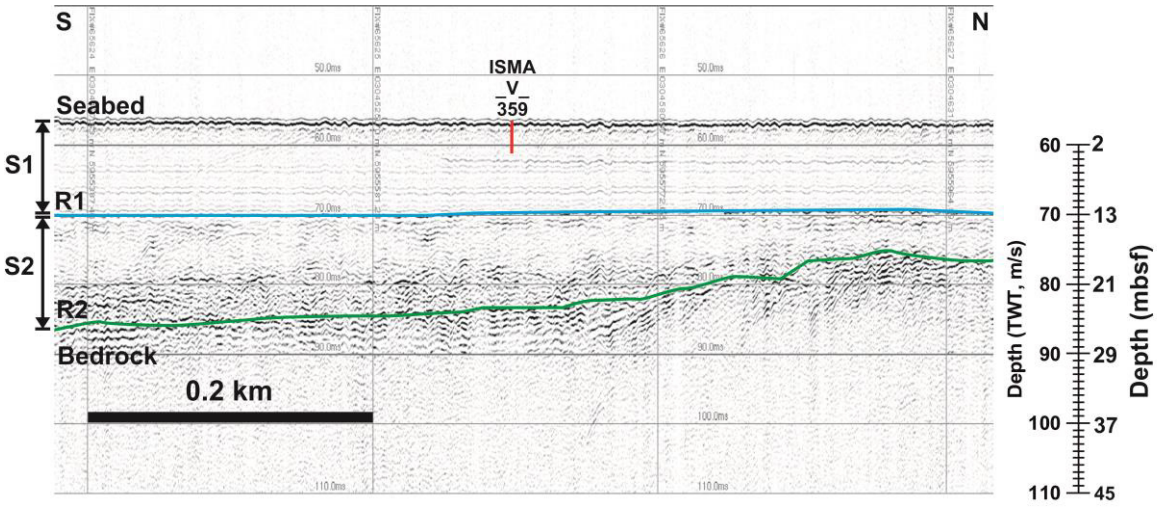

Figure 3.10 Seismic profile highlighted in Fig. 3.9 with interpretations. Core profile for ISMA_V_359 is presented in Figure 3.11.

Shallow 3 m cores were taken during the ISMA cruise revealing the uppermost part of this facies, at least, to consist of normally consolidated, olive-grey to brown silty to sandy muds predominantly with some shell-rich horizons (mainly of the gastropod *Turritella communis*). Given the homogenous seismic nature of this unit, it is assumed the lower part of S1 is relatively similar in composition.

An example of this unit is presented in Figure 3.11 (in this case core ISMA_V_359) along with grain-size distributions from analyses. Despite the seemingly homogenous distribution evident from visual inspection, analyses revealed a downcore decrease in dominant grain size class from sand at the top to silt at the base.

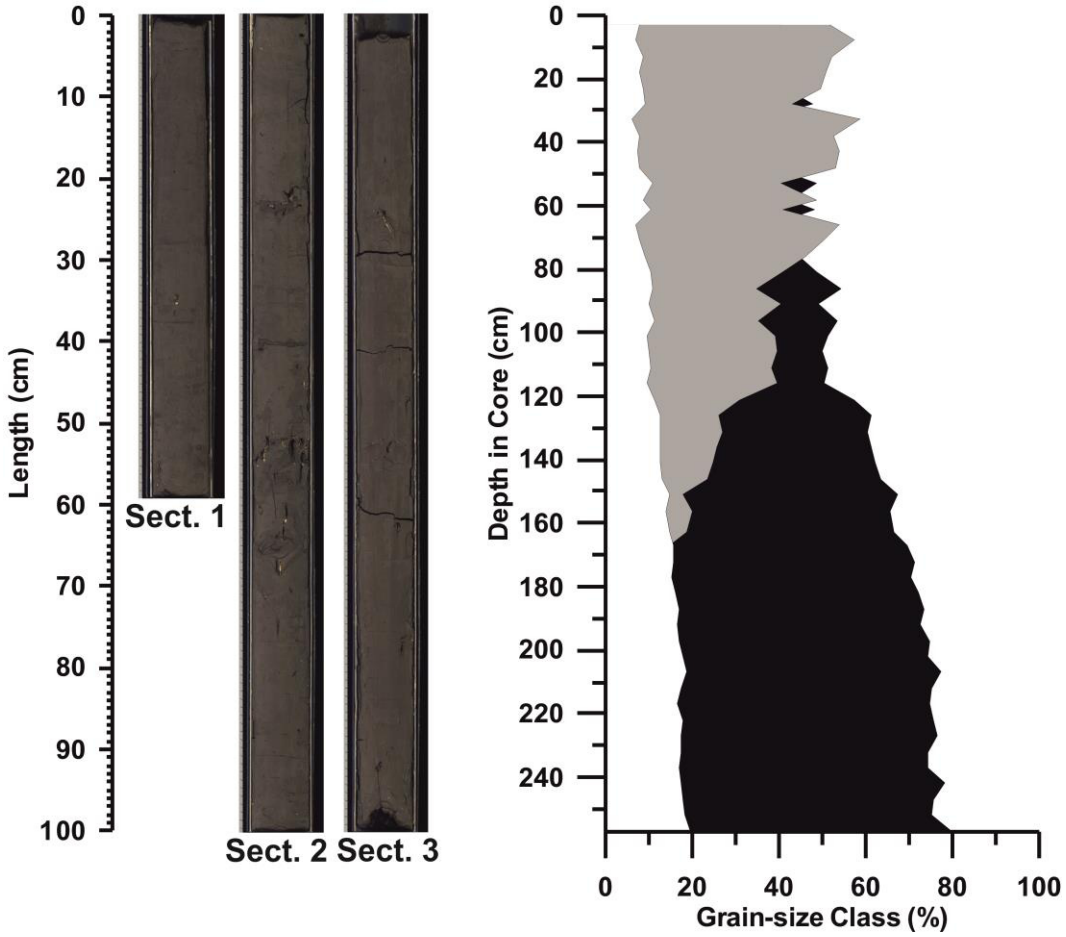

Figure 3.11 To the left is a linescan image for ISMA_V_359 showing a homogenous, silty, brown sediment. On the right is a downcore grain-size distribution for the same core. Grain-size classes are presented in volume percent with white representing clay (<2 µm), black representing silt (2-63 µm) and sand coloured in grey (>63 µm).

There is multiple evidence for accumulations of biogenic gas in the area including pockmarks seen on MBES data (Fig. 3.2). Whilst the pockmarks seen in the northeast occurred within an area where shallow gas was also seen on seismic profiles, our data would suggest there was no direct correlation between the features and evidence for shallow gas at the same locations in the southern section (Fig. 3.12). Hence, the southern pockmarks are most likely best explained as relicts from previous gas escape. On seismic profiles, gas accumulations are identified as areas of acoustic turbidity (Fig. 3.13). This acoustic turbidity, or “gas blanking”, has the effect of obscuring subsurface detail. Often, where gas is detected, there are enhanced reflectors which create a sharp boundary with the surrounding material. It is below this turbidity where detail of deeper reflectors is lost, in this case, R2 (Fig. 3.13). Figure 3.12 shows the distribution of these gas charged sediments indicating a strong concentration towards the northern-centre section of the

study area. Figure 3.13 shows these sediments on a typical seismic profile, highlighting the fact that the R2 reflector becomes indiscernible below such sediments.

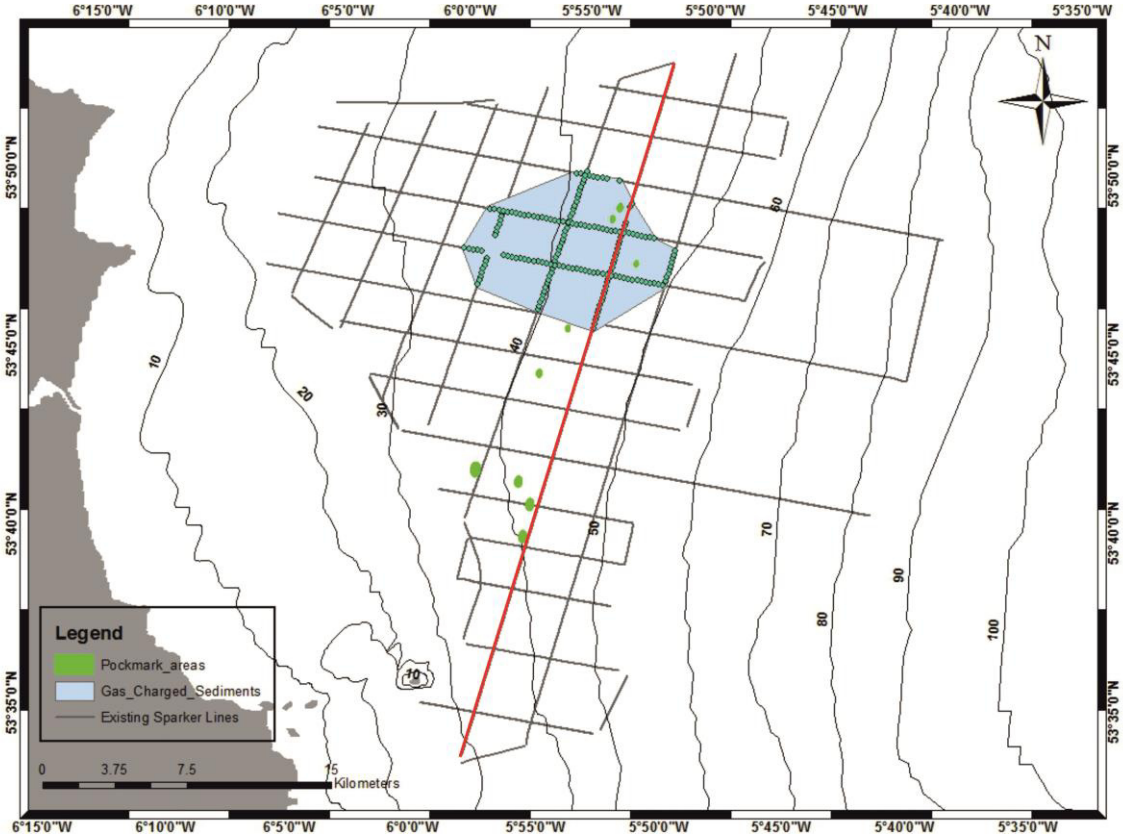

Figure 3.12 Distribution of gas charged sediments marked by acoustic turbidity on seismic profiles are highlight in blue. A profile displaying this feature is highlighted in red and presented in Figure 3.13.

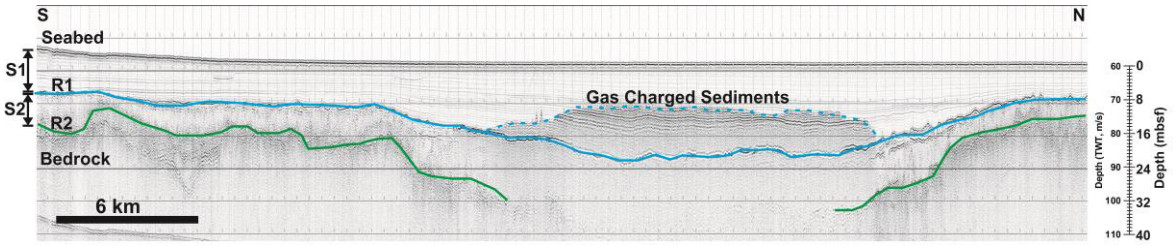

Figure 3.13 Seismic profile highlighted by red line in Fig. 3.12 showing gas charged sediments.

3.4.3 Geotechnical Units

In this section we assess the CPTu trends of cone resistance, sleeve friction, friction ratio and pore pressure, as well as the derived parameters of shear strength, SBT and SBTn, in order to generate

an overview of lithological units found in the area. We then present the distribution of these units at each of the sites investigated in this study (Fig. 3.14 – 3.31) and finally relate the lithological units and CPTu profiles to subsurface units on seismic profiles (Fig. 3.32 – 3.38) where possible. The seismic data related to Sites 2, 3 and 4 is industry sensitive and so cannot be presented here. What is noted, however, is that depth to bedrock at these three sites was relatively shallower in comparison to the remaining sites.

A strong trend was seen in the cone resistance profiles for Sites 1 – 15 consisting of low (0 – 1 MPa) values for the uppermost part of the profile (on average down to 10 mbsf) before a marked increase and a larger degree of variation in the profile with values fluctuating between 1 – 20 MPa The general exceptions to this trend were Site 2a, 2b, 3, 4, 5a and 5b, or the sites with the thinnest coverage of sediment and had the shortest CPTu profiles.

Similar to CPTu data, s_u profiles exhibit a large degree of homogeneity in the upper section with values overall generally <50 kPa and usually <25 kPa. Despite this, there is a clear trend of q_c (and subsequently s_u) increasing with depth and a marked change in lithology coinciding with changes in pore pressure. S_u values for this new lithology exhibit a high level of heterogeneity with increased values of > 100 kPa and up to 1,250 kPa indicative of hard or dense overconsolidated sediments such as glacial deposits.

Six SBT zones were identified on 11 of the 16 CPTu profiles taken from the area. The remaining five profiles had insufficient sleeve friction data to compile a robust SBT analysis. The majority of profiles exhibited a similar trend with SBT zones 1 (Sensitive, fine grained), 2 (Organic soils-peats) and 3 (Clays-silty clay to clay) dominating the upper section before gradating towards a coarser and more consolidated zone heavily influenced by SBT zones 3 and 4 (Silt mixtures-clayey silt to silty clay) with zones 5 (Sand mixtures-silty sand to sandy silt) and 6 (Sands- clean sand to silty sand) also present. A total of six SBTn zones were also identified on CPTu profiles. A comparable trend with SBT zones was found with SBTn zone 1 (sensitive fine grained), 2 (organic material) and 3 (clay) dominate throughout and in the uppermost sections for the most part. Further down in the CPTu profiles, there was a transition to increased influence of zone 4 (Silty clay to clay), 5 (Clayey silt to silty clay) and 6 (Sandy silt to clayey silt).

Based on CPTu characteristics, SBT zones, SBTn zones and relative depth, three geotechnical units were identified. Unit 1 (L1) is the uppermost unit and is typically characterized by low cone resistance (<1 MPa) with pore pressure greater than 0 MPa and less than 1 MPa. It is dominated by SBT zones 1, 2 and 3 and is usually found to depths of up to 20 mbsf. Unit 2 (L2) is not widespread and seen only at Sites 12, 13, 14 where it underlies L1. The transition from L1 to Unit 2 (L2) is usually indicated by a drop in pore pressure. It exhibits a similarly low cone resistance but a lower pore pressure value of typically <0 MPa. It is comprised of SBT zones 1 and 2. Usually underlying Unit 1 is Unit 3 with the transition between both also seen in the drop in pore pressure. Subsequently, L2 typically exhibits pore pressure values of <0 or just greater than 0. In contrast, L2 shows an increase in cone resistance values of 0 - 20 MPa. It is comprised predominantly of SBT zones 3 and 4 with the presence of zones 5 and 6 also notable.

Unit	SBT zone	SBTn zone	Cone resistance (MPa)	Pore pressure (MPa)
L1	1: Sensitive, fine grained	1: Sensitive fine grained	< 1 MPa	0 – 1 MPa
	2: Organic soils-peats	2: Organic material		
	3: Clays-silty clay to clay	3: Clay		
L2	2: Organic soils-peats	2: Organic material	< 1 MPa	< 0 MPa
	3: Clays-silty clay to clay			
L3	3: Clays-silty clay to clay	3: Clay	1 – 20 MPa	0 – 1 MPa
	4: Silt mixtures-clayey silt to silty clay	4: Silty clay to clay		
	5: Sand mixtures-silty sand to sandy silt	5: Clayey silt to silty clay		
	6: Sands-clen sand to silty sand	6: Sandy silt to clayey silt		

Table 3.2 Summary of litho- and geotechnical units with typical associated SBT and SBTn zones asa well as cone reistnace and pore pressure values.

Locations for CPTu sites are shown in Fig. 3.1 with data for cone resistance, sleeve friction, friction ratio, pore pressure, SBT, SBTn and undrained shear strength values for each site is presented in figures 3.14 to 3.32.

Site 1

Site 1 is located near the centre of the study area and comprises a profile 28.77 mbsf (Fig 3.1 & Fig. 3.14). The upper 16 mbsf is comprised of L1 characteristic sediments, dominated by SBT zone 1, 2 and 3 with low (<1 MPa) cone resistance and sleeve friction. Below 16 mbsf, there is a continuing increase in cone resistance with a similar increase in pore pressure until 25 mbsf. In this section, the SBT zones most prevalent are 3 and 4 with some instances of 5 and 6 corresponding with L3. At 25 m there is a notable drop in pore pressure back to 0 MPa. Pore pressure continues at 0 MPa until 28 mbsf where there is a drop to < 0 MPa corresponding with an increase in cone resistance of up to 17 MPa. SBT at this depth level is predominately zone 6.

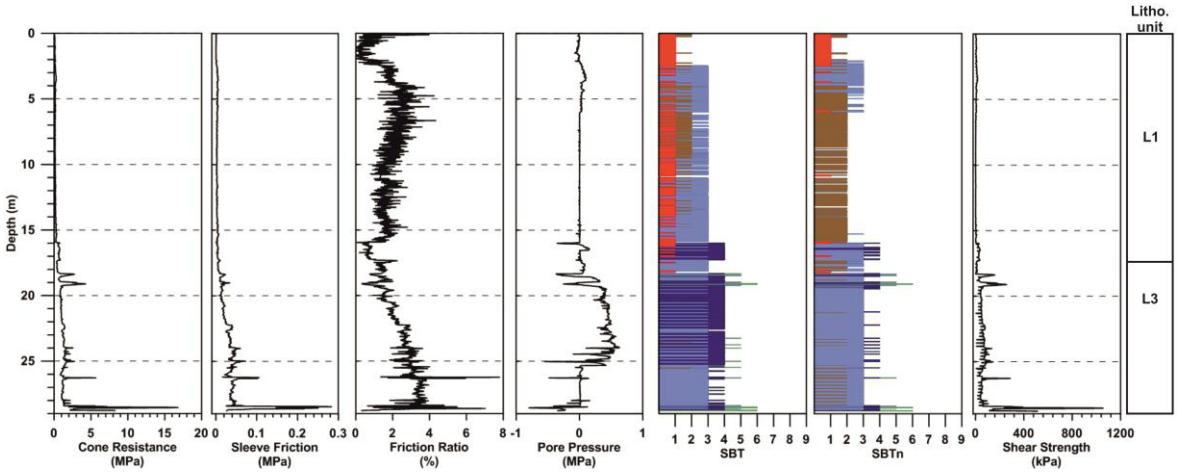

Figure 3.14 CPTu profiles for Site 1.

Site 2

Site 2 is located to the north-west of the area (Fig. 3.1). Here, there were three attempts with CPT, two of which were relatively successful producing profiles of 3.12 mbsf (2a) and 3.19 mbsf (2b) (Fig. 3.15 & Fig. 3.16). However, in both instances sleeve friction and pore pressure failed to record hence no SBT could be defined for these profiles. Instead, an interpretation of lithology was derived from cone resistance. For Site 2a, cone resistance started off low at < 1MPa before gradually increasing to 4 MPa at 2.9 mbsf. Below this, there is a strong increase up to 24 MPa. For 2b, values initially started at <3 MPa. After 2.2 mbsf there is a marked increase reaching a peak of 10 MPa just below 3 mbsf.

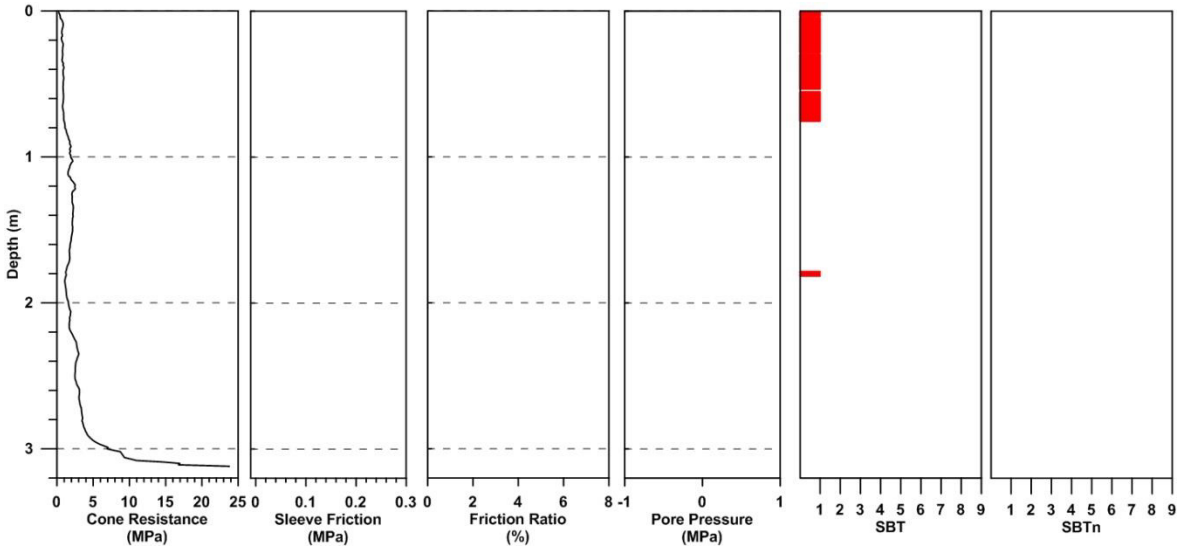

Figure 3.15 CPTu profiles for Site 2a.

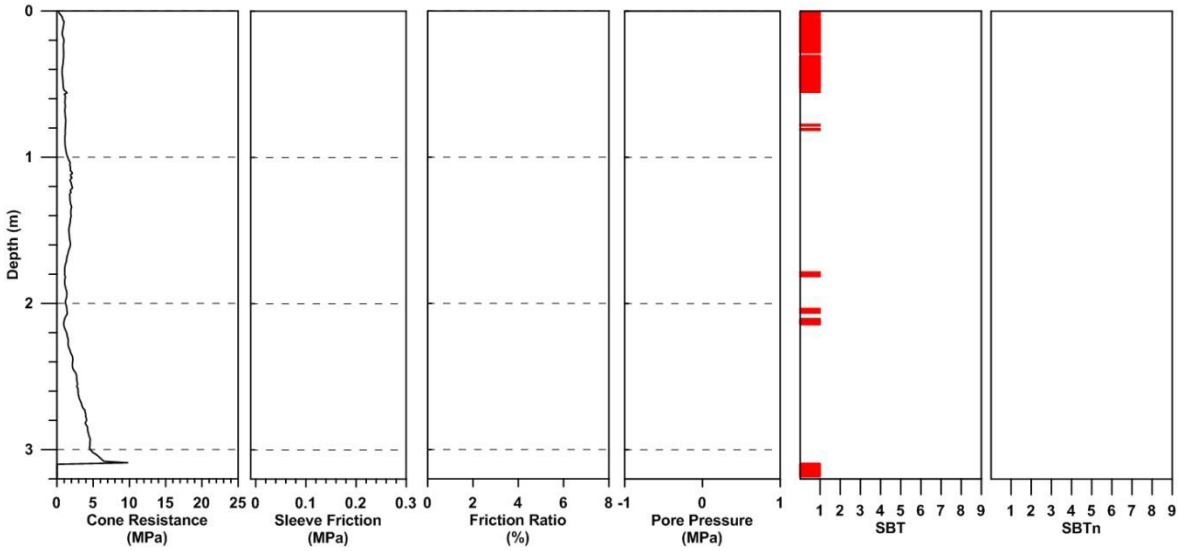

Figure 3.14 CPTu profiles for Site 2b

Site 3

Two attempts at CPTu were made at this site with one successful producing a profile of 3.25 mbsf (Fig. 3.17). Similarly again, sleeve friction and pore pressure were never recorded and so it was not possible to establish SBT zones for this site. Cone resistance did record an overall gradual increase from the beginning of the profile, eventually reaching a peak of 19 MPa at 3.25 mbsf.

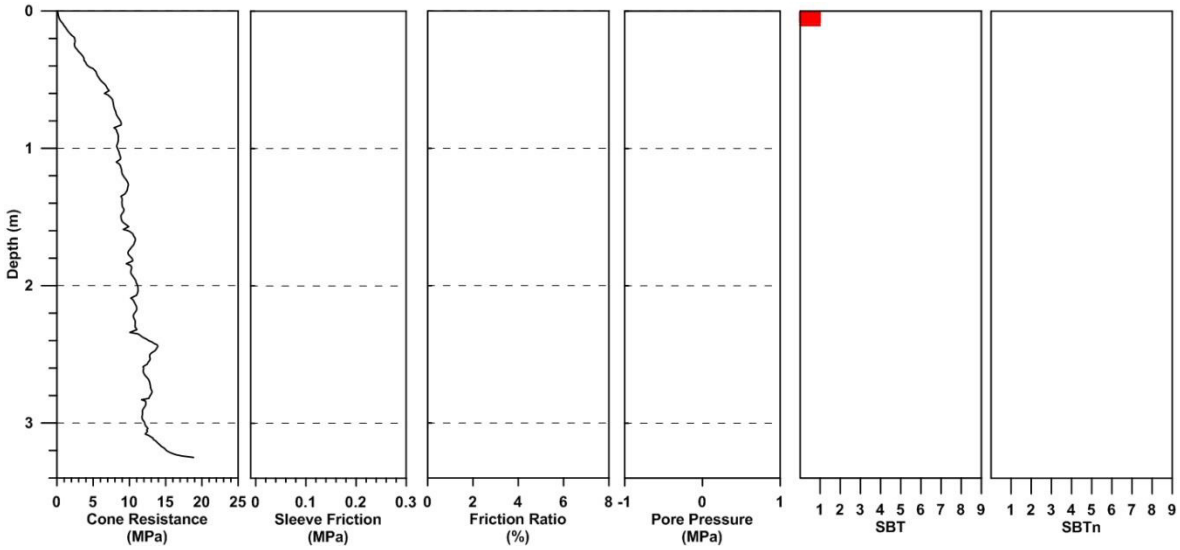

Figure 3.17 CPTu profiles for Site 3.

Site 4

Located south west from Sites 2 and 3, Site 4 was similarly shallow reaching a depth of 3.78 mbsf (Fig. 3.18). Sleeve friction and pore pressure measurements also failed to record here. The cone resistance profile shows a low (<1 MPa) reading for the upper 1.65 m before the start of a gradual increase to a broad peak of 22 MPa at around 2.25 mbsf. Values decrease once more to <5 MPA at 2.8 mbsf before a further increase until 25 MPa is reached at 3.78 mbsf.

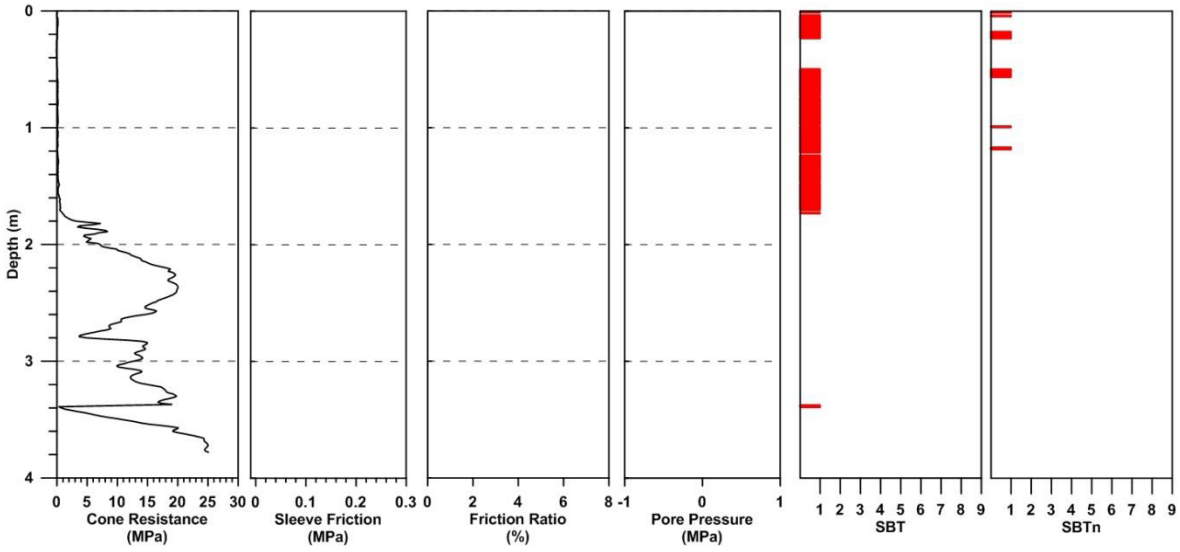

Figure 3.18 CPTu profiles for Site 4

Site 5

Two attempts were made at Site 5 yielding profiles of 8.87 mbsf (5a) and 4.4 mbsf (5b) comprising of cone resistance data with some pore pressure measurements also recorded (Fig. 3.19 & Fig. 3.20). The upper 8 m of 5a exhibit low cone resistance values of <1 MPa and low pore pressure values of ~0 MPa, similar to L1. Below 8 mbsf, pore pressure measurements ceased recording, corresponding with an increase in cone resistance of up to 17 MPa. For 5b, similarly low values of cone resistance (<1 MPa) were prevalent for the upper 2.2 mbsf. Values rose thereafter up to 7 MPa before sharply falling off to <2 MPa followed by another increase with fluctuation between 3 and 12.5 MPa until the end of the profile.

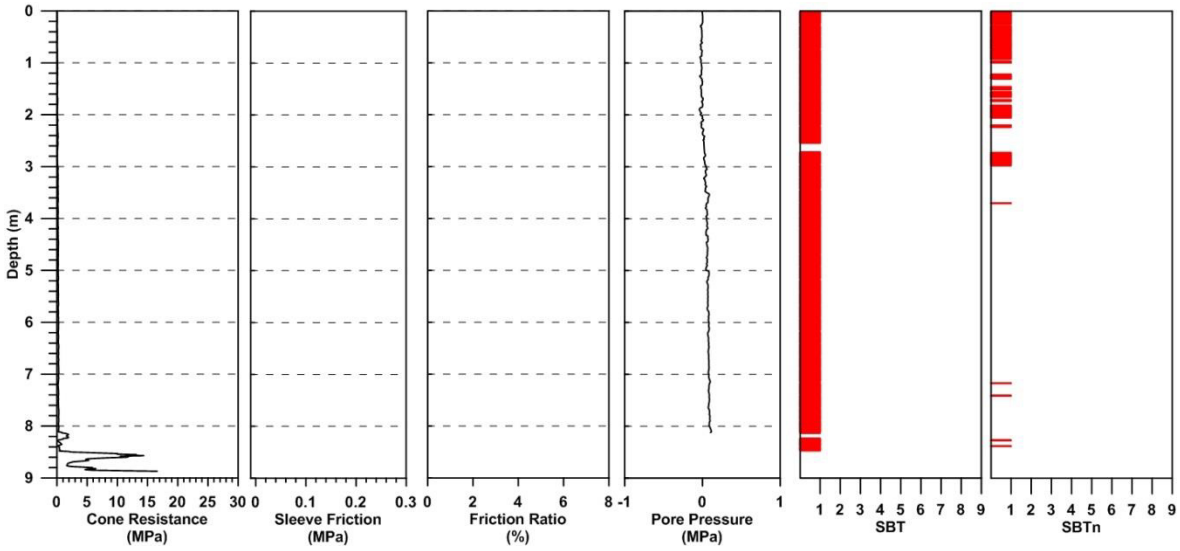

Figure 3.19 CPTu profiles for Site 5a.

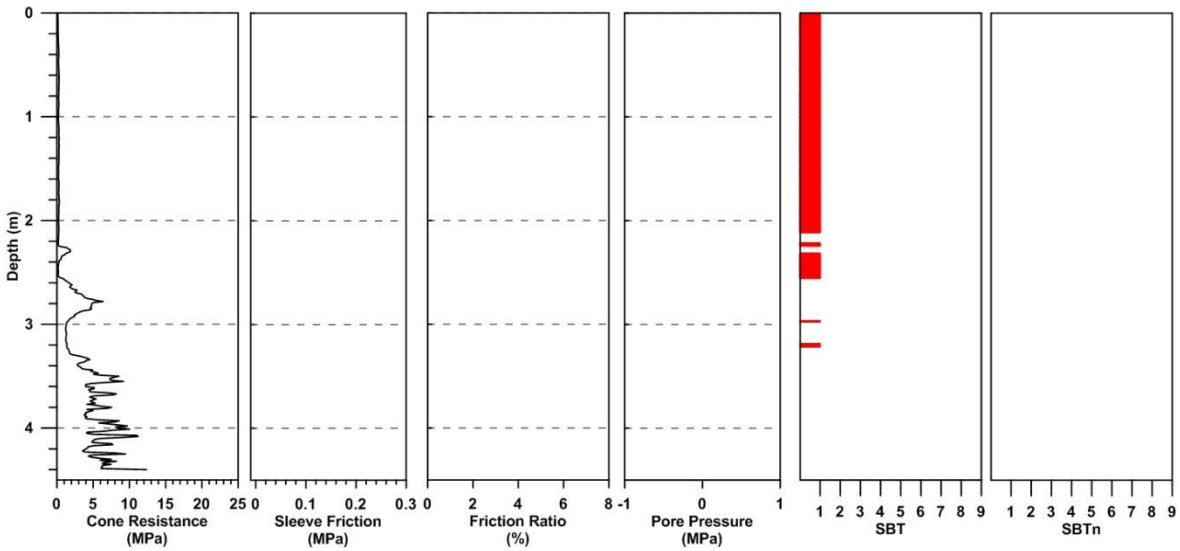

Figure 3.20 CPTu profiles for Site 5b.

Site 6

Site 6 is located at the south east corner of the study area (Fig. 3.1). Here a 23.75 m profile was retrieved (Fig. 3.21). Cone resistance values throughout remain low at generally <1 MPa with pore pressure at 0 or with two minor drops at 7 and 13 mbsf. The profile is composed of 60.3% SBT zone 1 with 19.3% and 12.9% of zone 1 and 2 respectively to suggest that this site profile is almost entirely composed of L1 related sediments. The remaining 7.5% comprised of SBT zone 4 which was largely found below 14 mbsf.

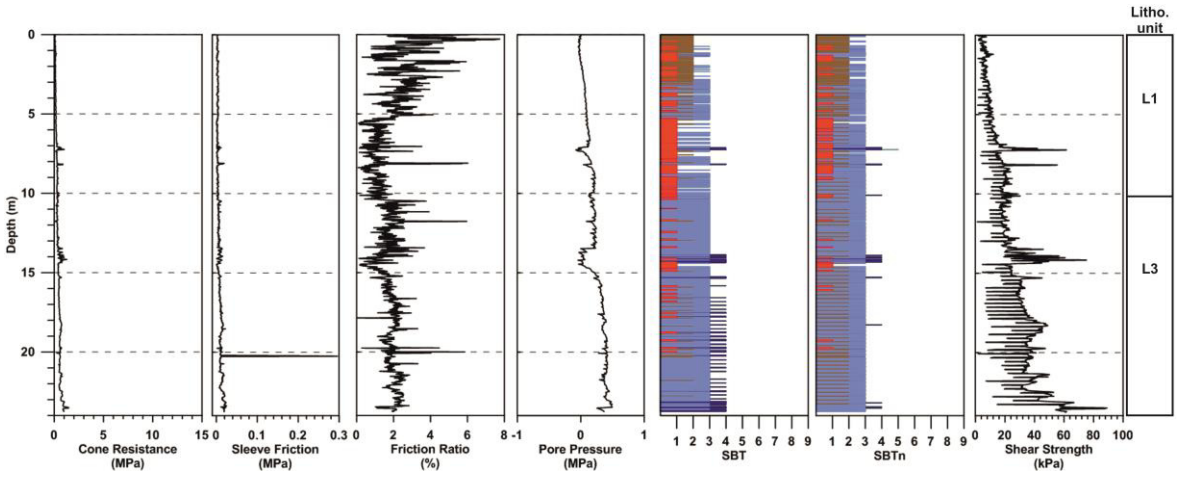

Figure 3.21 CPTu profiles for Site 6

Site 7

Site 7 is located 2.6 km to the west of Site 6 (Fig. 3.1). At this site, a 15.93 mbsf profile was retrieved, the upper 7.8 m of which comprised of low cone resistance (<1 MPa) SBT zone 1, 2 and 3 sediments synonymous with L1 (Fig. 3.22). The transition to L3 is marked by a drop in pore pressure to ≤0 MPa. There is also a corresponding increase in cone resistance to ~3 MPa and a 11 MPa peak at 15.93 mbsf. From 10 to 11 mbsf, the L3 unit is dominated by SBT zone 5, after which it is predominantly zones 3 and 4.

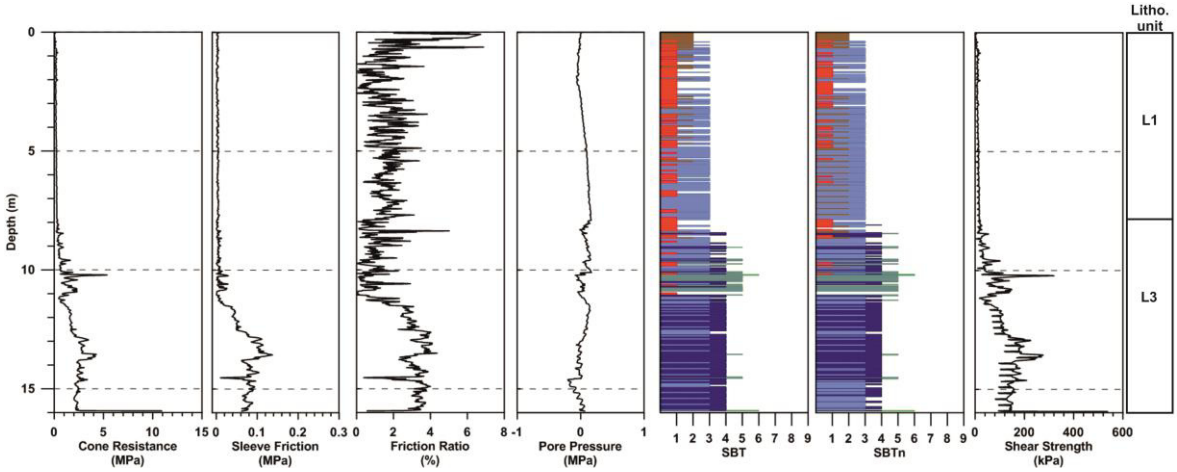

Figure 3.152 CPTu profiles for Site 7.

Site 8

Site 8 is located further north and comprises a 19.01 mbsf profile consisting primarily of L1 related sediments for the upper 12 mbsf that display low cone resistance (generally <1 MPa) and pore pressure values which generally do not drop below 0 MPa (Fig. 3.1 and Fig. 3.23). Below 12 mbsf there are minor increases in cone resistance up to 4 MPa with more fluctuation in pore pressure corresponding with a shift from SBT zone 1, 2 and 3 dominated L1 to zone 3, 4 and 5 dominant L3 sediments.

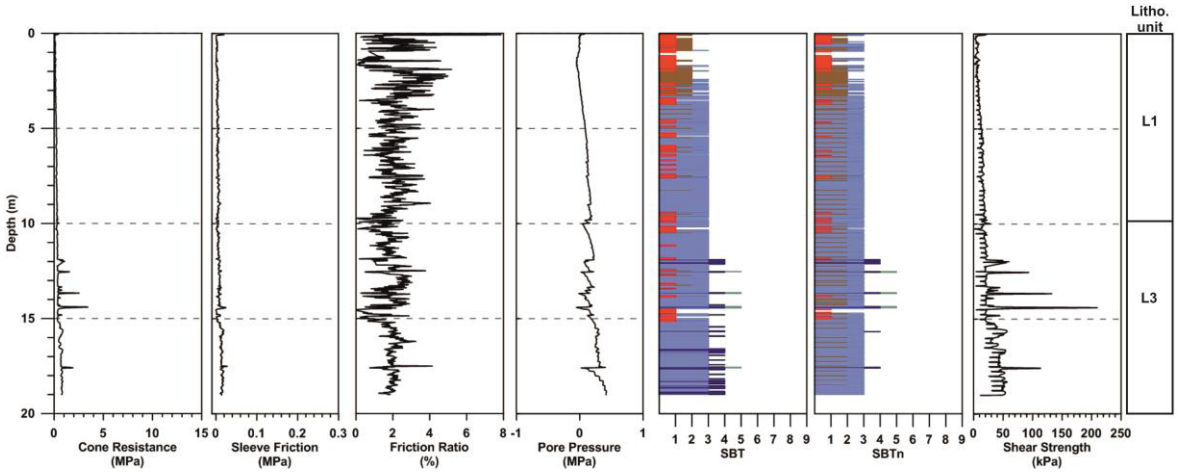

Figure 3.23 CPTu profiles for Site 8.

Site 9

Site 9 is located further north along the same seismic line (Fig. 3.1). Here, the 19.02 mbsf profile shows a similar trend to Site 8 with low cone resistance (<1 MPa) L1 sediments dominating the

upper 9 mbsf before a drop in pore pressure signals the transition to higher cone resistance (up to 3 MPa) and SBT zone 3 and 4 dominated L3 sediments (Fig. 3.24).

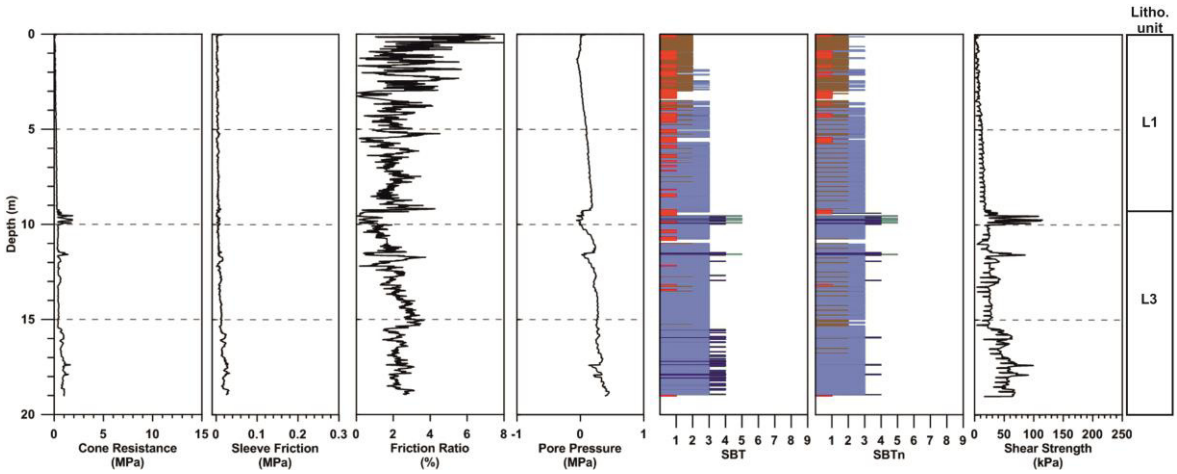

Figure 3.24 CPTu profiles for Site 9.

Site 10

Site 10 also exhibits a similar profile to a depth of 19.86 mbsf, with the upper 10.50 mbsf composed of L1 sediments (Fig. 3.25). From 10.5 mbsf to the end of the profile is composed of L3 sediments with a distinct increase in cone resistance seen at 18.50 mbsf corresponding with a drop to negative pore pressure values and mainly SBT zone 4, 5 and 6 L3 related sediments.

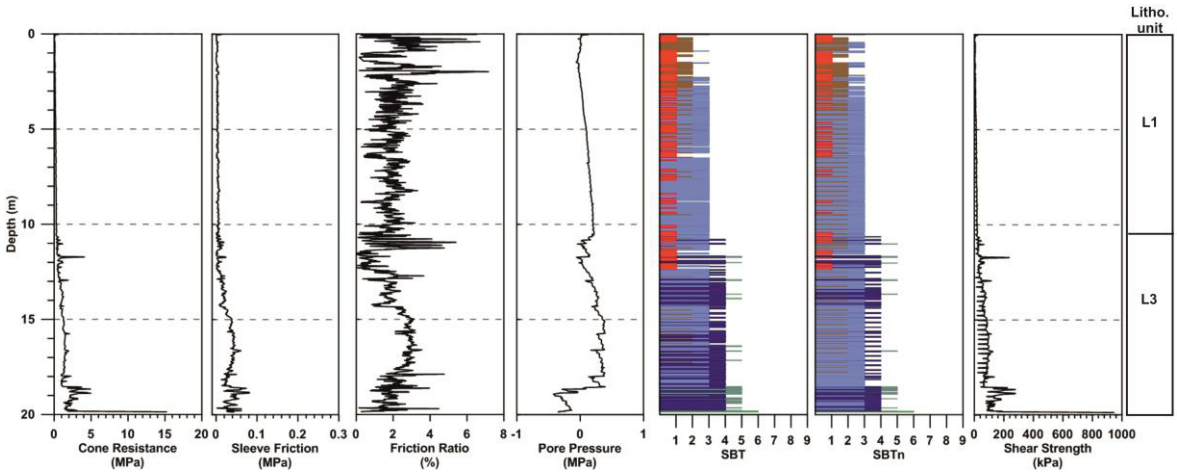

Figure 3.25 CPTu profiles for Site 10.

Site 11

Site 11 is located north of Site 1 at the centre of the study area (Fig. 3.1). It comprises of a 25.98 mbsf profile with L1 sediments dominating the upper 16.5 mbsf (Fig. 3.26). Below 16.5 mbsf, a drop in pore pressure to negative values indicates the transition to L3 sediments which persist to the end of the profile.

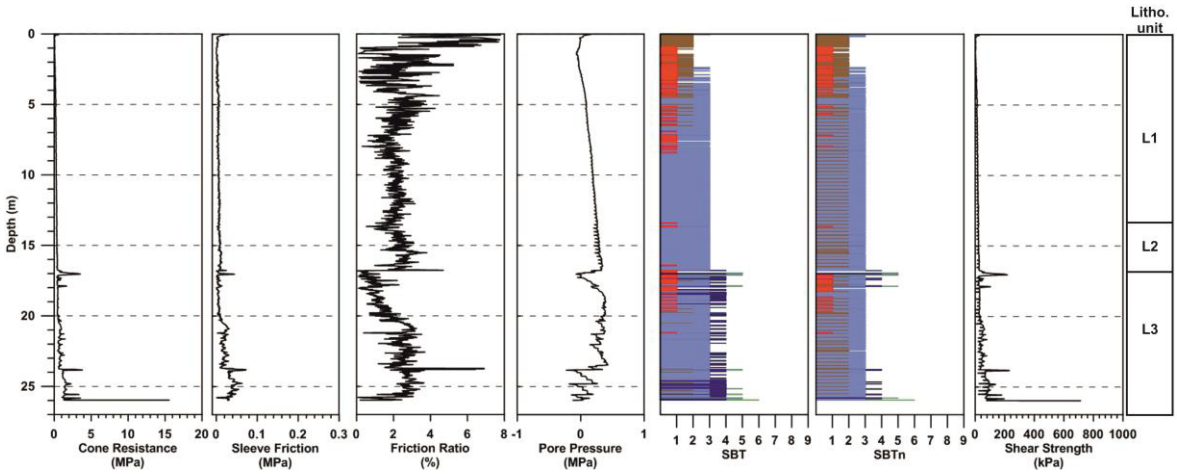

Figure 3.26 CPTu profiles for Site 11.

Site 12

Site 12 comprises a 26.03 mbsf profile, 75.5% of which is SBT zone 3 sediments. Low cone resistance (<1 MPa) persist throughout indicating it is mostly composed of L1 sediments. However, a drop in pore pressure at 18 mbsf corresponds with a change in SBT zones characterizing this section of the profile as L2 related sediments (Fig. 3.27).

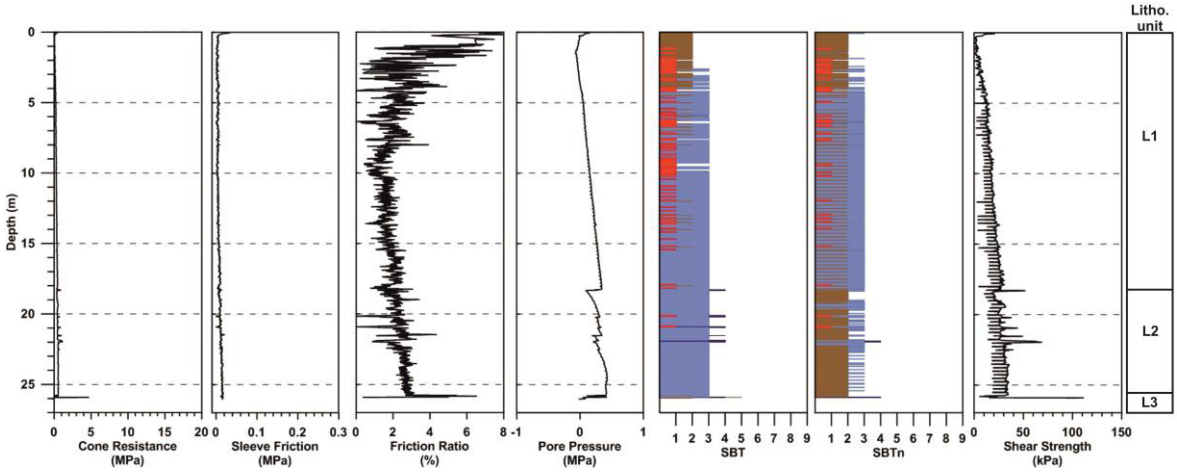

Figure 3.167 CPTu profiles for Site 12.

Site 13

A similar profile as Site 12 is seen at Site 13 with L1 sediments comprising the upper 23 mbsf, followed by a drop in pore pressure and L2 sediments persisting to the end of the profile at 30.05 mbsf (Fig.3. 28).

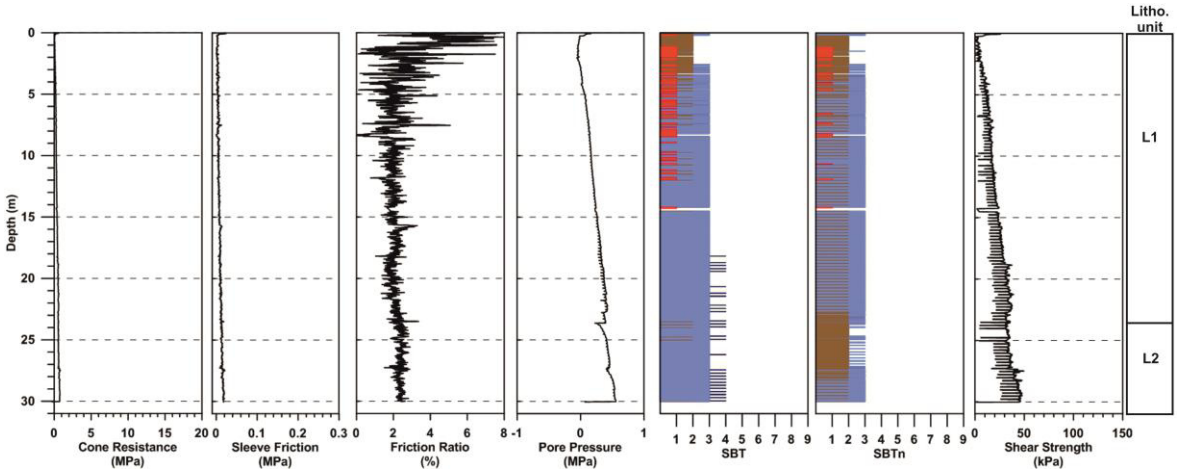

Figure 3.178 CPTu profiles for Site 13.

Site 14

Site 14 is located at the north east corner of the study where a 26.71 mbsf profile was retrieved, 25 mbsf of which comprised low cone resistance L1 sediments (Fig. 3.29). A significant drop in pore pressure and increase in cone resistance up to 22 MPa marks the transition to L3 sediments that comprise the lower 1.71 mbsf.

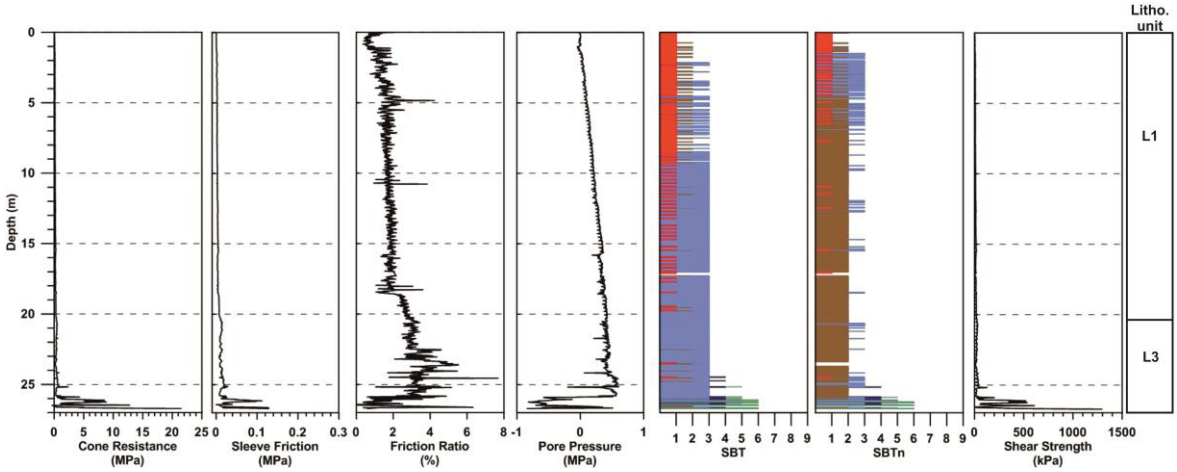

Figure 3.29 CPTu profiles for Site 14.

Site 15

Site 15 is located further south along the same seismic line as Site 5 where a considerably longer profile of 18.31 mbsf was recorded (Fig. 3.30). The upper 12 mbsf of the profile consists of L1 sediments with a drop in pore pressure indicating the change to L3 type sediments. A further significant drop in pore pressure occurs at 16 and 17 mbsf coinciding with an increase in cone resistance of up to 15 MPa.

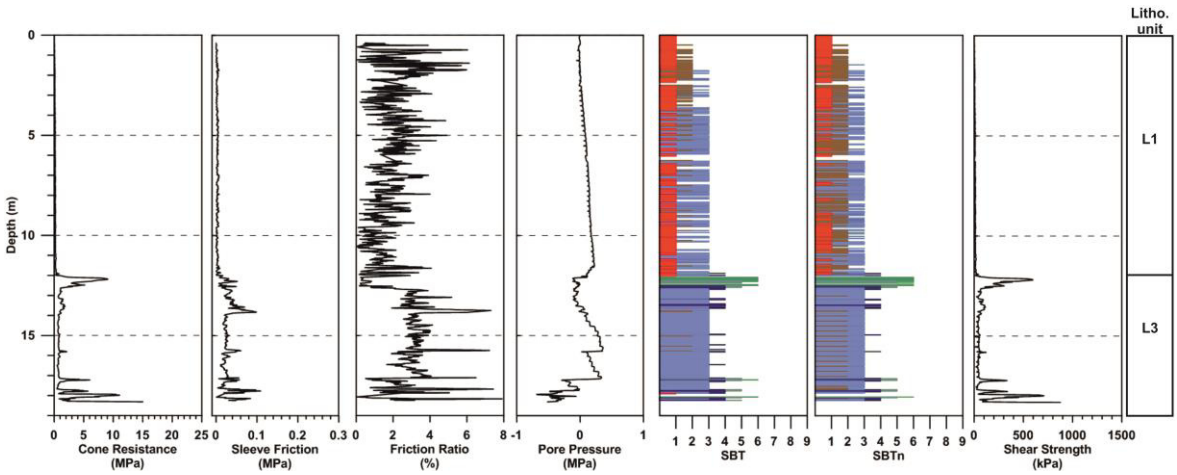

Figure 3.30 CPTu profiles for Site 15.

Site 16

Site 16 is, in fact, located outside the WIMSB towards the area of Lambay Island (Fig. 3.1). A profile was taken here in order to act as a comparison to sites in the WISMB as it represents a different geological setting with mobile sands located at the surface and considerably greater

thickness of sediment. A 20 mbsf profile was retrieved here consisting of low (generally <1 MPa) cone resistance sediments with shear strengths of up to 100 kPa most likely representing unconsolidated, loose sands with an increase in density with depth (Fig. 3.31).

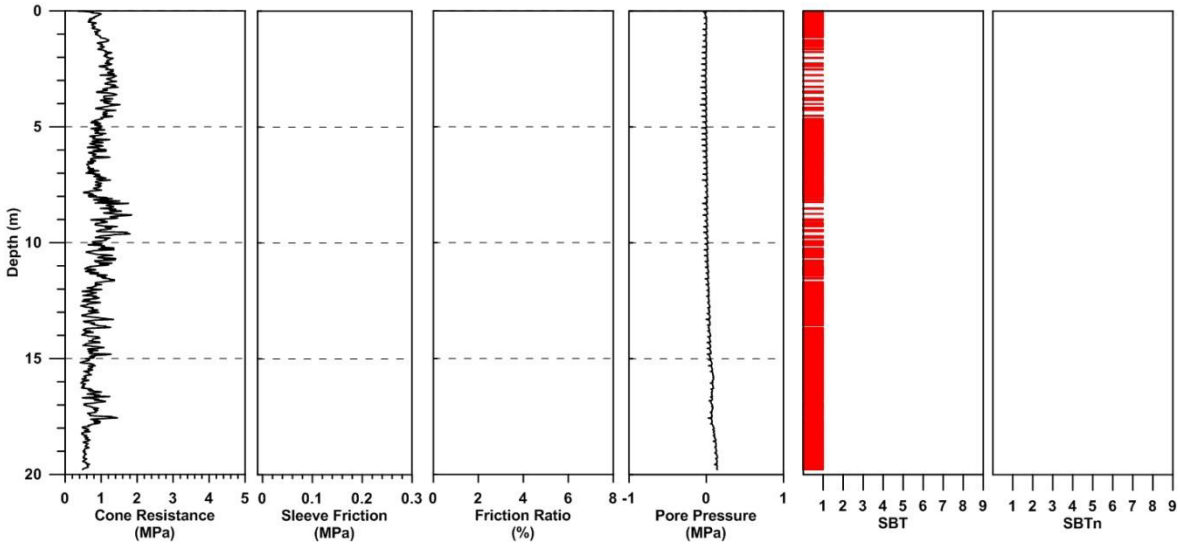

Figure 3.181 CPTu profiles for Site 16.

3.4.4 Distribution of Units at Sites and Correlation Method

Stratigraphic units based on CPTu parameters were then correlated with seismic-stratigraphic data by comparing depths of the geotechnical boundaries (in CPTu profiles) with the depths of seismic-stratigraphic and seismic facies boundaries at the same offshore location (Fig. 3.32 to 3.35).

Good correlation was generally seen between unit L1 and seismic facies S1. Similarly, in areas of acoustic turbidity associated with gas charged sediments showed a dominance of unit L2 at the corresponding depths in CPTu profiles. Unit L3 was correlated with seismic facies unit S2.

No seismic data was readily available to Sites 2, 3 and 4 for which to present a correlation with CPTu profiles.

Line 074, Sites 1, 11 and 12

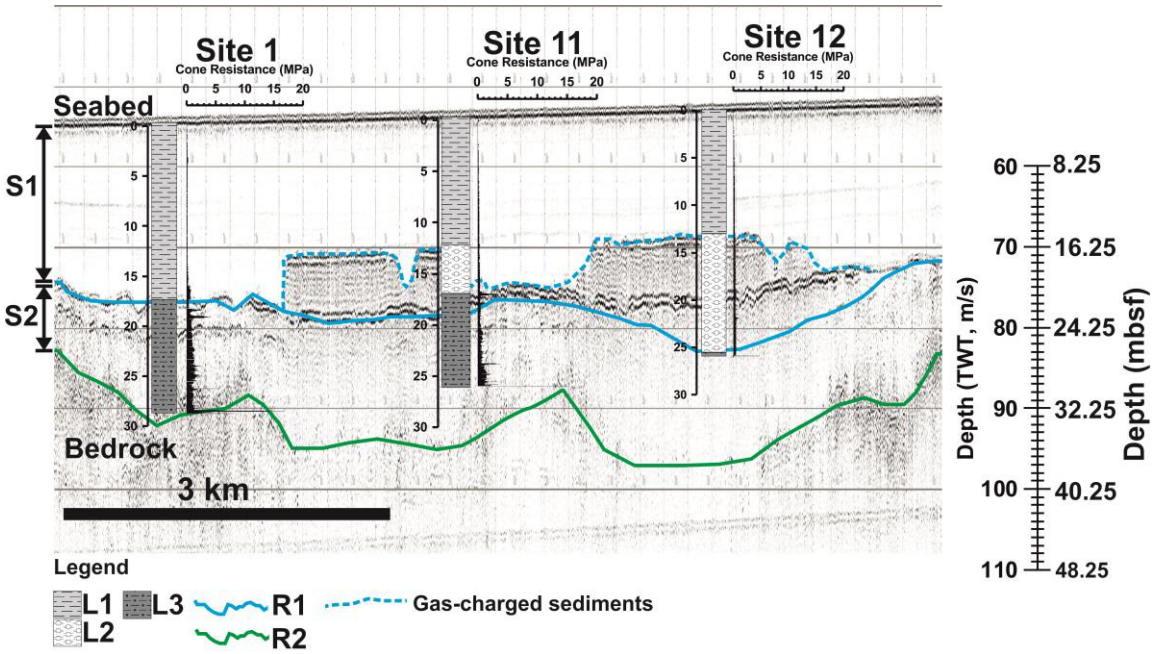

Figure 3.32 Line 074, Sites 1, 11 and 12. Depth in metres below seafloor (mbsf) is approximate.

The presence of gas-charged sediments inferred from seismic profiles was also seen in the CPTu profiles taken at Site 11 and Site 12. Site 11, in particular, showed good correlation between CPTu boundaries and corresponding seismic boundaries at the same depth (Fig. 3.32). At Site 12, whilst gas-related sediments were seen on the CPT profile, there was no transition to L3 sediments coinciding with the S2 seismic unit until deeper in the profile. This may be the result of gas blanking of the reflector in seismic profiles. The profile at Site 1 showed good correlation between L1 sediments in CPTu profile with S1 facies on the seismic profile and, similarly, between L3 and S2.

Line 111, Sites 7. 8 and 9

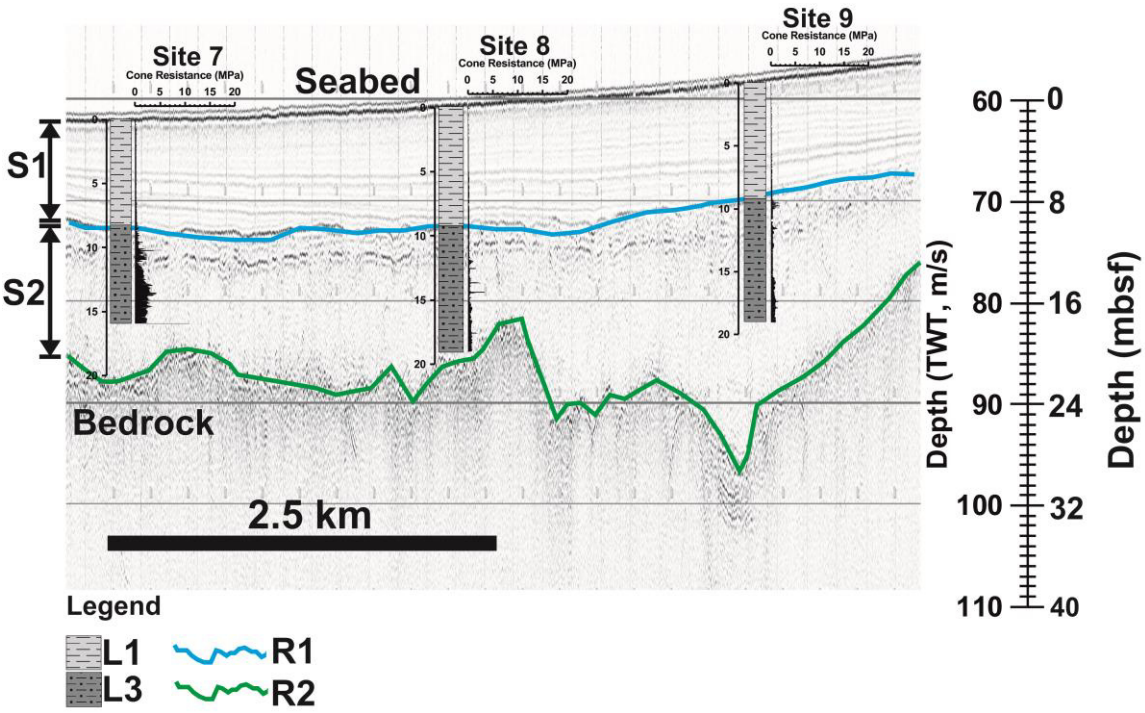

Figure 3.33 Line 111, Sites 7. 8 and 9 **.** Depth in metres below seafloor (mbsf) is approximate.

Sites 7, 8 and 9 all lie on seismic line 111 and show good correlation between L1 and S1 and L3 and S2 at suitable depth (Fig. 3.33). Whilst L1 shows a strong homogeneity across the three profiles, L3 shows more heterogeneity with higher cone resistance values for the unit seen at Site 7.

Line 111, Sites 13 and 14

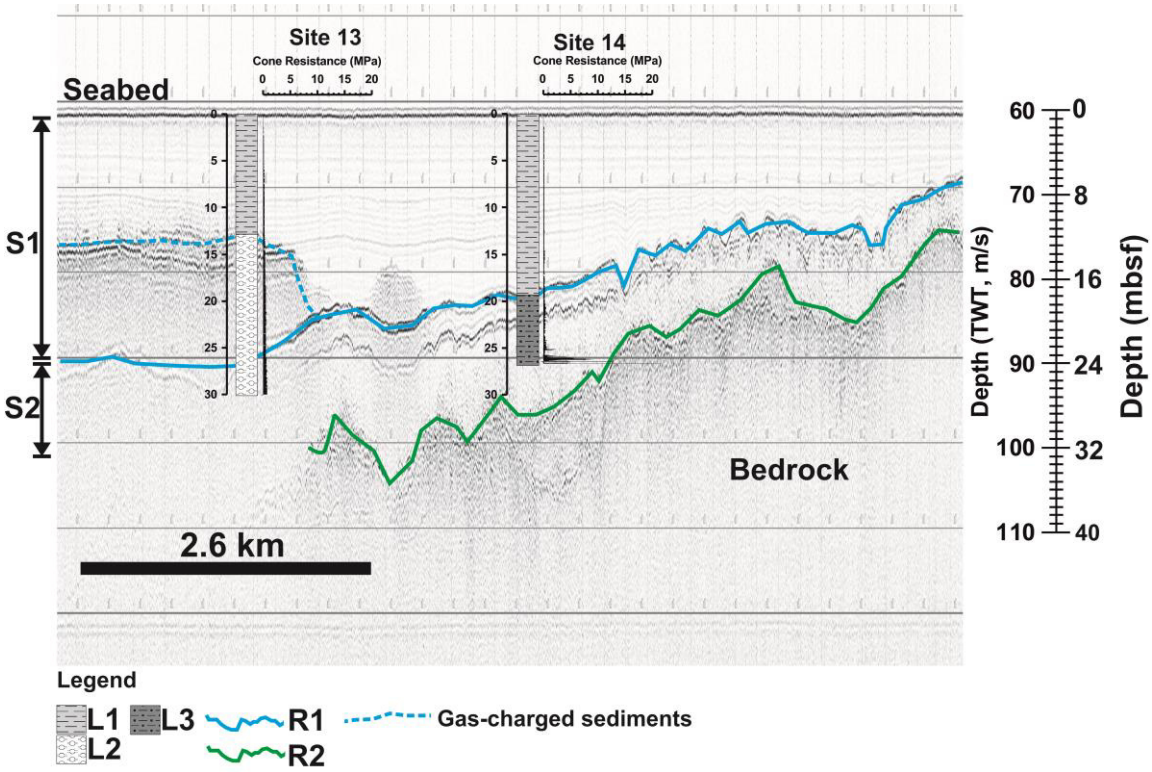

Figure 3.194 Line 111, Sites 13 and 14. Depth in metres below seafloor (mbsf) is approximate.

Gas-charged sediments were also observed on seismic line 111 (Fig. 3.34). On this profile, the R2 reflector was, again, blanked by the presence of shallow gas. These sediments were penetrated by the CPTu at Site 13 and are reflected by the presence of L2 type sediments from approximately 15 mbsf depth until the base of the profile. Similarly, whilst the profile appeared to penetrate the R1 reflector here there was no corresponding transition to L3 sediments as seen at Site 14 where this reflector was inferred at 20 mbsf depth from seismic and CPTu profiles.

Line 109, Site 10

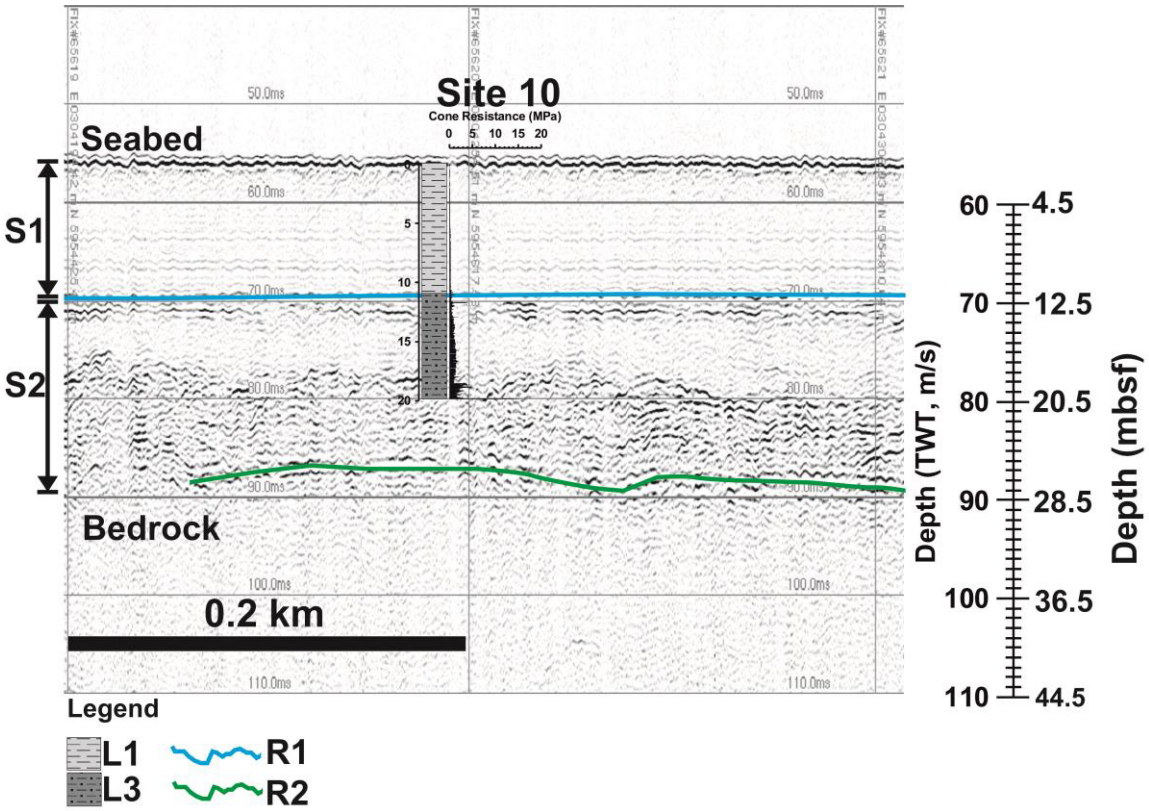

Figure 3.205 Line 109, Site 10. Depth in metres below seafloor (mbsf) is approximate.

At Site 10, the R1 reflector was inferred at approximately 12.5 mbsf from seismic profiles which was subsequently confirmed by CPTu profiles (Fig. 3.35). Interestingly at this site, within the S2 seismic facies there appears two distinctive sets of reflectors with the transition between the two at approximately 20 mbsfl. A similar change in cone resistance is seen as an increase in the CPT profile at this same depth indicating two geotechnically distinct lithologies within this heterogeneous unit.

Line 113, Site 6

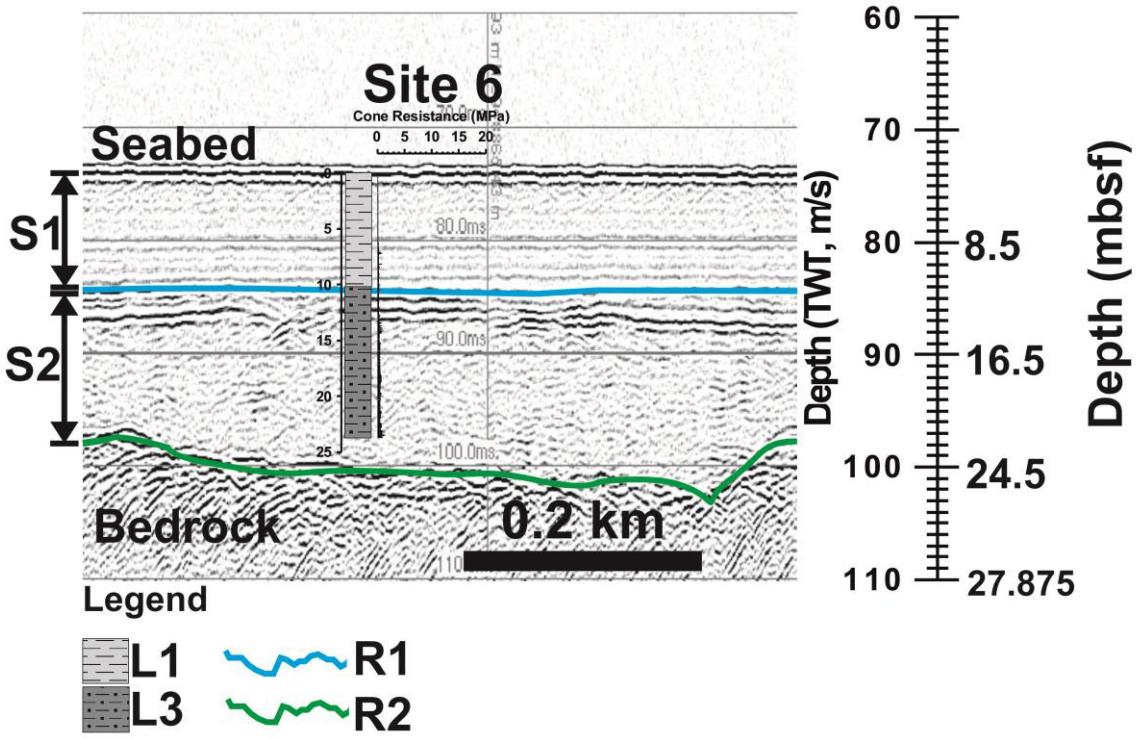

Figure 3.216 Line 113, Site 6. Depth in metres below seafloor (mbsf) is approximate.

The profile at Site 6, taken along line 113, shows a large degree of homogeneity although an increase in cone resistance does correspond with the transition to S2 and presence of LS sediments (Fig. 3.36).

Line 119, Site 15

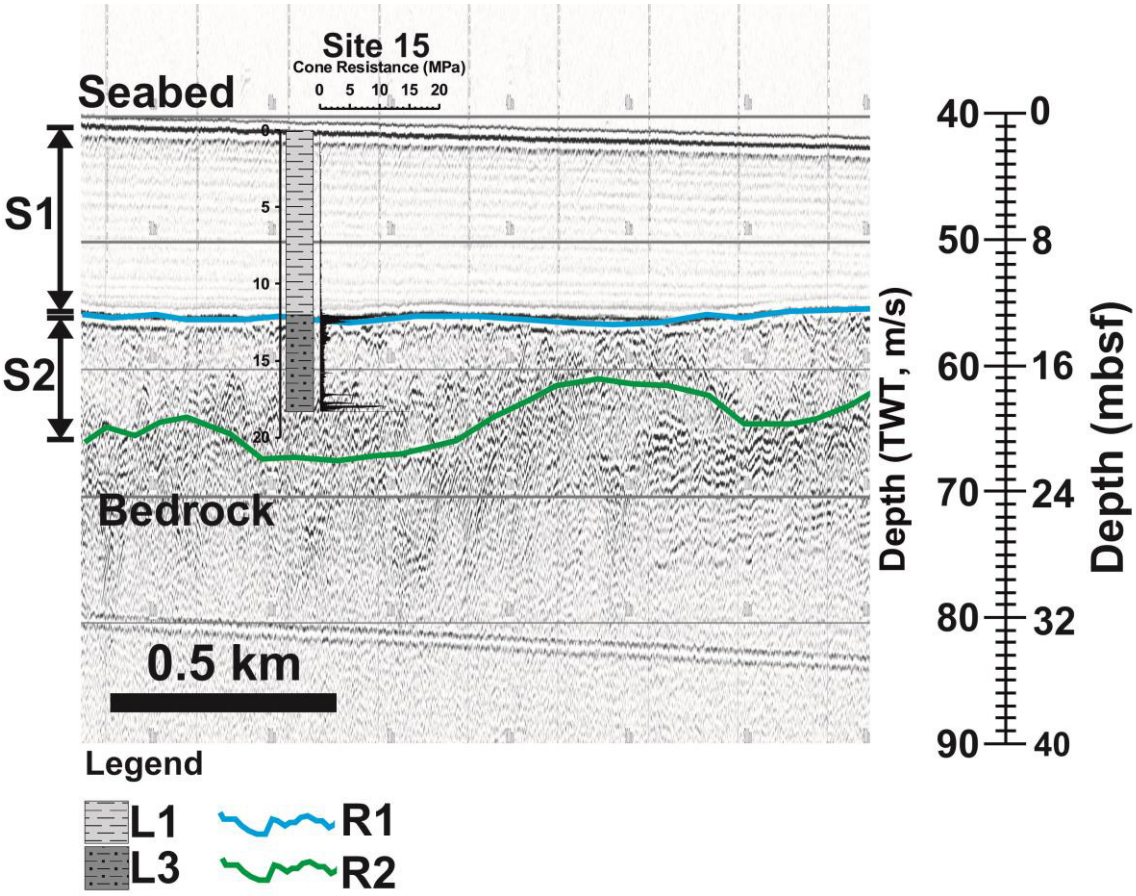

Figure 3.227 Line 119, Site 15. Depth in metres below seafloor (mbsf) is approximate.

Line 119, Site 5

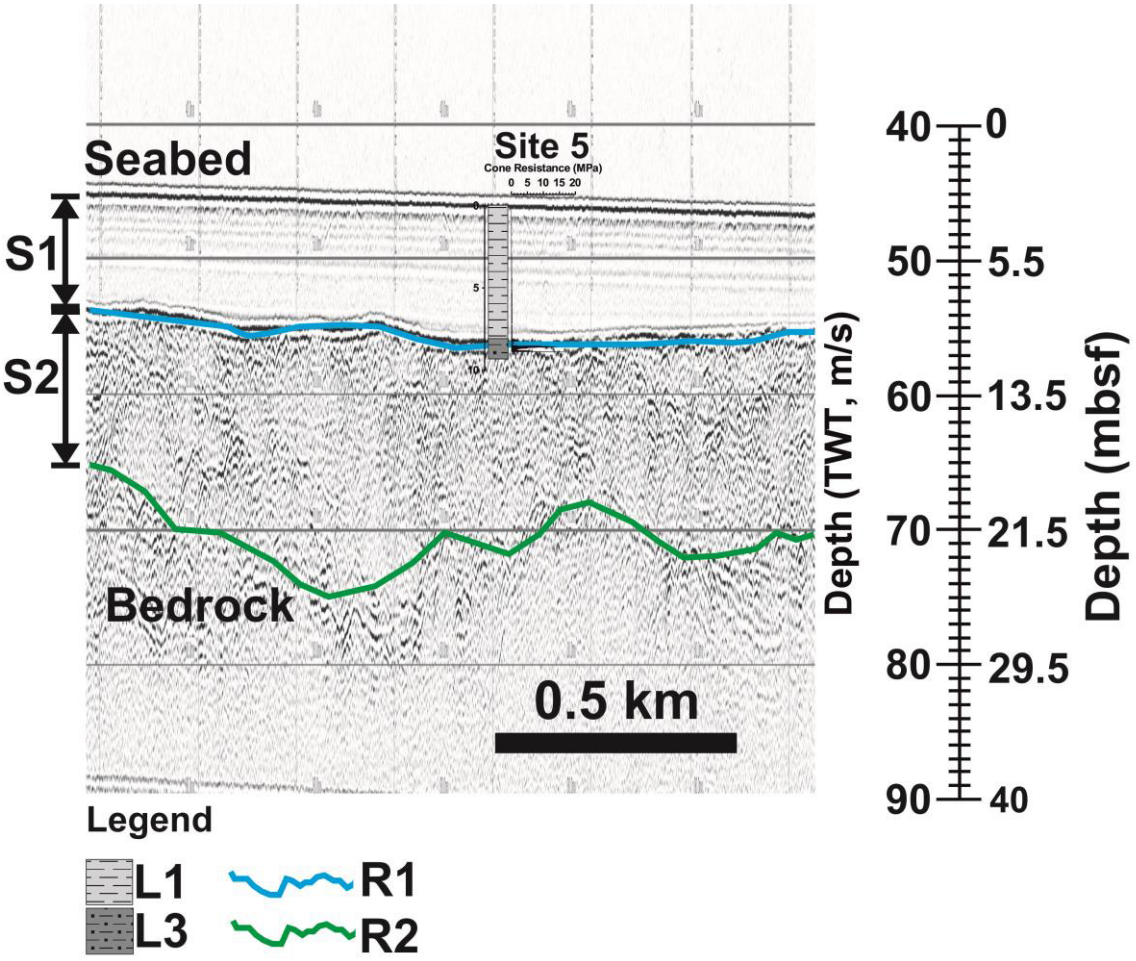

Figure 3.38 Line 119, Site 5. Depth in metres below seafloor (mbsf) is approximate.

The CPT profiles at both Site 5 and Site 15 show an abrupt increase in cone resistance corresponding with penetration of the R1 reflector at the same depth (Fig. 3.37 and Fig. 3.38).

3.4.5 Constraint Map

Aside from being extensive trawled for *Nephrops norvegicus* (see chapter 5) there are other socio-economic activities also in the study area (Fig. 3.39). Between the coast, and impinging on the western edge of the study area, lies a Department of Defence danger area exclusion zone. Running through the centre of the study area is a Department of the Marine special exclusion zone and there is a navigation channel running through the northern part of the site. There is no SAC or SPA located within the survey site although quite a few shipwrecks are reported. However, no evidence of any shipwrecks was found on MBES or any acoustic mapping data suggesting the

locations of these lost vessels are erroneous or that the shipwrecks have been significantly degraded.

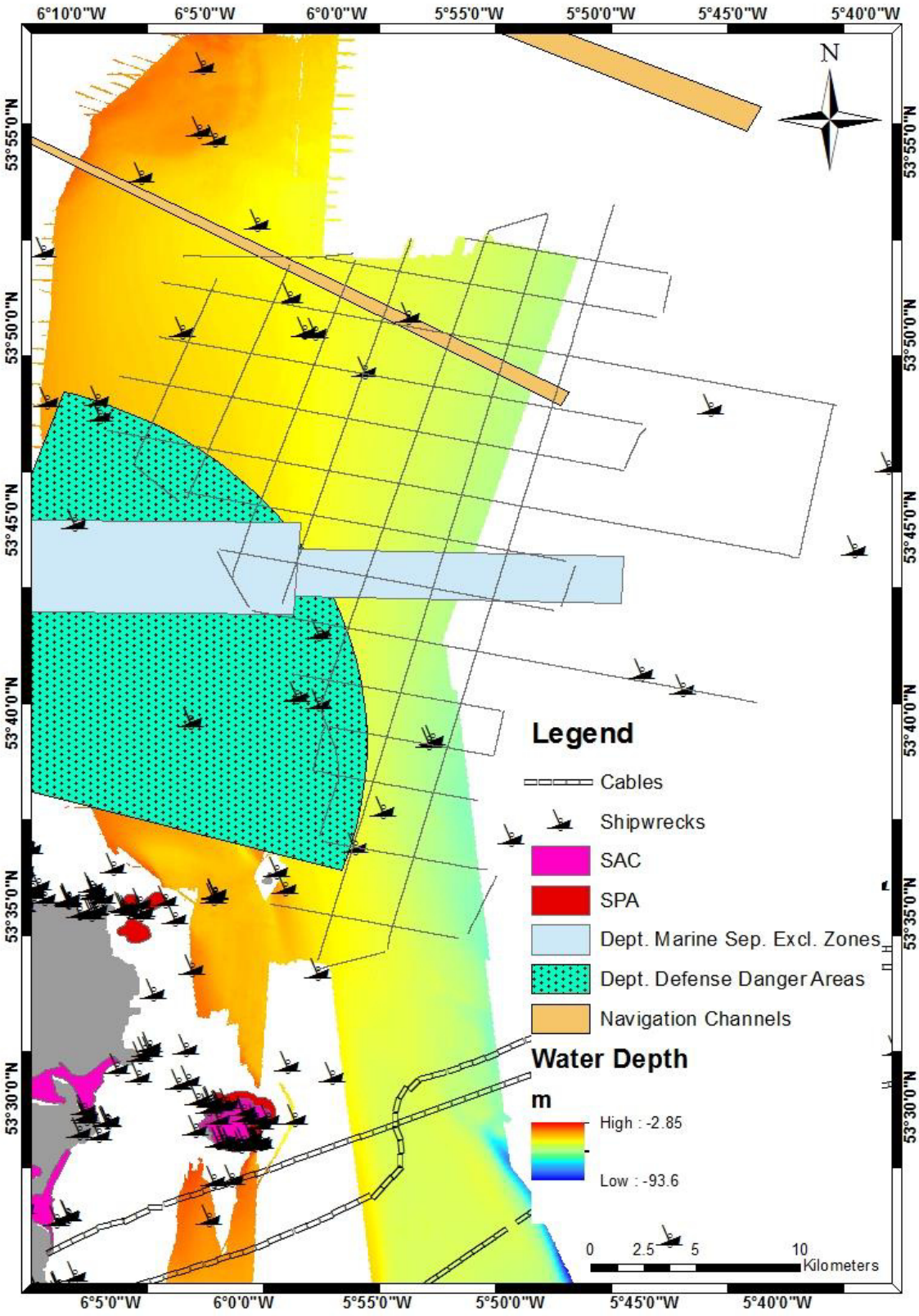

Figure 3.39 Constraint map.

3.5 DISCUSSION

3.5.1 Geological-Geotechnical-Geophysical Relationships with Inferences on Geological and Environmental History

Our seismic interpretation largely conforms with previous work consisting of a lower glacial layer (S2) associated with the Irish Sea Ice Stream (ISIS) during the Last Glacial Maximum (LGM) that ubiquitously rests on undulating bedrock. This is subsequently overlain by a marine mud layer (S1) marked by an erosive base associated with the Holocene marine transgression and subsequent Holocene marine conditions persisting to present (Belderson, 1964; Pantin, 1977; Yuan et al., 1992). The seismic homogeneity of the upper S1 layer was confirmed by a similar level of homogeneity seen in CPT profiles with L1 consisting largely of fine-grained material as suggested by SBT and SBTn zones and confirmed by core profiles for the upper section at least. The low cone resistance and largely positive pore pressures would also suggest that these are unconsolidated sediments.

Acoustic turbidity seen on seismic profiles was mainly confined to the northern section of the area (Fig. 3.12). CPTu profiles taken from this area (namely Site 12, 13 and 14), exhibit sediments that are genetically similar to L1 sediments but with a slight variation in recorded pore pressure values and SBT and SBTn zones. These are the sediments classified as L2 and have been affected by the presence of shallow gas. The presence of shallow gas in the WISMB was mapped by Yuan et al. (1992) who discerned that the lateral extent of gas bearing sediments could be mapped seismically, however, the exact vertical thickness was unknown due to the effect of “gas blanking”. In addition, they found from lab based experiments that the presence of gas had an effect on sediments by replacing pore fluid and subsequently expanded as a result of overburden. The transition between L1 and the inferred gas charged sediments of L2 is marked by an initial drop in pore pressure followed by a delayed increase. These L2 sediments were found to predominately behave mechanically like SBT and SBTn zone 2, or organic sediments with low or negative pore pressures that have been related to dilative silts (Lunne et al., 1997). It is most likely the presence of gas that is primarily responsible for the recorded pore pressure response. A comparable

response in pore pressure was noted by (Seifert, 2010) who used it to confirm the presence of free gas in sediments in the North Sea where acoustic turbidity was also seen on seismic profiles. Shear strength values for this unit showed a similar trend with an initial decrease at the top of the unit with a gradual recovery to previous values. Gas has been identified as having an effect on s_u predominately as it replaces seawater in voids giving a differing compressibility (Seifert, 2010 and references therein). This trend may be explained by the presence of gas although it is unclear as to whether or not increasing gas content increases or decreases s_u values (Brandes, 1999; Wheeler, 1988). Wheeler (1988) in particular noted that an increase or decrease in s_u depended largely on the values of consolidation pressure and the initial pore water pressure. The effect of gas was also noted in the relation of seismic reflectors to CPTu profiles. At Sites 12 and 13 there was a noticeable discrepancy between the calculated depth to the R1 reflector and identifying the same transition to L3 sediments in CPTu profiles. This is due to the "Becken" or "gas blanking" effect suggested by Pantin (1977) and Yuan et al. (1992). However, these gas-charged sediments have a distinctive CPTu signature by way of a drop in pore pressure and dominance of SBT and SBTn zone 2 in the profiles (i.e. L2 sediments). Thus, by using CPTu profiles, it is possible to constrain the position of these gas-charged sediments at depth, and similarly the transition to new lithological units, where seismic profiles may be misleading.

Very little core material has been retrieved from the WISMB relating to L3 owing to its depth below seafloor; hence the unit remains relatively underdescribed. In addition, no substantial amount of material was recovered from any of the sites mentioned in this study in order to fully groundtruth seismic and CPTu profiles. Similarly, no previous work has been carried out in relation to CPTu values and offshore deposits in the WISMB. However, CPT has been used successfully for investigating glacial till deposits of the Dublin Boulder Clay (DBC) in County Dublin, a lodgement till associated with the ISIS (O'Kelly, 2014). Similarly, offshore CPT was used extensively in investigating heterogeneous till deposits in Denmark with s_u values of below 50 kPa to >1,000 kPa (Steenfelt and Sørensen, 1995). These till materials included gravels, cobbles, boulders and lenses of sand and gravel. Despite the lack of material from this unit, geological inferences are made here from CPTu profiles. The heterogeneity seen seismically in S2 is also displayed in L3; its lithostratigraphical equivalent. Erosive horizons with laterally extensive, prominent reflectors

suggesting distinctive stages of deposition are substantiated by a similar heterogeneity in CPT profiles, characterised by a scattering of intermittent peaks. Such various stages of deposition, and hence heterogeneity, is related to various stages of the disintegration of the ISIS at the end of the LGM. Lower elements of L3 exhibit high values of q_c (up to 15 MPa) coinciding with a notable drop in pore pressure to almost -1 at Sites 1, 10, 14 and 15. Such high q_c and negative pore pressures are typical of heavily overconsolidated clay such as associated with lodgement till. Further spikes in q_c in L3 (such as at Sites 1, 7, 10, 11, 14 and 15) are not accompanied by the same level of pore pressure decrease. In fact, for the most part, pore pressure recovers after an initial drop. Such an inconsistent pattern and lower pore pressure drop is assumed to be the result of seams of dense sand/gravel present. These features are interpreted as outwash deposits associated with the disintegration of the ISIS, prior to the onset of fully marine conditions associated with the Holocene transgression. This is confirmed by the fact that the deposits largely lie below the seismic reflector R1 which is interpreted as marking the initial Holocene transgression. Without core sample to verify this, this layer may also be interpreted as one of particularly high clast content. Whilst for the most part sediments associated with L3 are classified as SBT zone 3, 4 or 5 according to Robertson et al. (1986), who recognized that very stiff, heavily overconsolidated fine-grained sediments tend to behave more like coarse grained soil in so far as they tend to dilate under shear and so can have a high undrained shear strength, thus classifying them as Silty Clay to clay or Clayey silt to silty clay or SBT zones 4 and 5 respectively.

3.5.2 An application: recommendations for the selection of wind farm sites

In this section an attempt is made to evaluate the study area geologically, and using our constraint mapping exercise, as a site for potential wind turbine construction. Whilst geological investigation plays an important role in these evaluations, ultimately any project will depend on a full engineering assessment. Hence, any recommendations made here are purely based on geological background information and would require a full, engineering based verification.

An in-depth knowledge of the seabed geology is particularly important to offshore renewable energy resource development as it heavily influences anchoring and foundation construction for

installations which in turn affects cost, one of the main drivers in such projects. In essence, geotechnical surveys groundtruth the data seen in the geophysical survey to confirm the geological/geophysical model and should provide all the necessary seabed data to supplement the design project for foundations as well as cable burial and protection. Whilst the technology governing offshore foundations is rapidly evolving allowing it to adapt to varying conditions, three dominant foundation choices are used for offshore wind turbines in Europe. Gravity bases are used in the majority of wind turbine projects with their principal function to use the dead weight of the structure to counteract movement created by environmental loading. They are suitable at sites with relatively shallow water depths and where the sediment is both competent and laterally consistent. Any lateral heterogeneity can pose a significant risk as can shallow soft deposits prone to scour. Monopile foundations are generally used in water depths of less than 30 m and are often used in the offshore wind sector. Usually, they are driven between 20 to 30 m into the seabed. In water depths of greater than 30 m (and up to 70 m) tripod (three-legged) or jacket (four-legged) structures are deployed. Although considerably more stable than monopole structures they represent a significant cost increase.

In this study, CPTu derived values were used to characterise sediment in terms of resistance and shear strength. The upper unit L1 displayed a high degree of homogeneity but relatively low shear strengths of generally < 10 kPa. In addition, thicknesses of this unit varied from <1 to 27 m. The underlying L3 unit displayed thicknesses of 1.5 to 24 m but with a high degree of heterogeneity and considerably higher shear strengths of >250 kPa.

For all foundation designs (but particularly monopile structures) scour presents a troublesome engineering consideration. The initiation of scouring on the seabed occurs when flow velocity exceeds the gravitational, frictional as well as any cohesive forces which may hold the sediment together. Thus, once the fluid shear stress exceeds a critical value then sediment particles are said to be hydraulically scoured with even a slight increase in flow velocity causing a small degree of sediment motion known as incipient motion (Callaway et al., 2009). The critical shear value referred to is a function of mean particle size and the submerged density of the sediment although a number of other factors influence its parameters; notably the angle of repose of bed sediment.

From our acoustic mapping of the seabed through MBES, and similarly in high-resolution digital photography of the seabed, we saw no evidence for sediment movement or the presence of erosion or scour on the seabed within the WISMB. However, sediments to the south of WISMB were noted to be in motion through the presence of small-scale sediment waves. In general, current velocities within the Mud Belt fail to exceed 0.5m/s and, hence, are not powerful enough to initiate sediment particle movement (Callaway et al., 2009). In saying so, the introduction of an obstruction (e.g. foundation pile) may induce vortex evolution and shedding with self-propagating scour occurring as increased amounts of sediment are eroded until such time that equilibrium is reached with depth. This was shown to be true in the northern WISMB by Callaway et al. (2009) who observed significant scour at the Pisces Reef system; a set of three igneous intrusions which outcrop on the seabed. They acknowledged the effect of a seasonal gyre on intensifying bottom currents on an annual basis which augmented erosion.

Water depth is an important factor in site identification for installations. Construction costs of offshore installations increases with water depth and so generally a 35 m water depth is not exceeded. Nevertheless, evolving technology is pushing installations to potentially greater depths. In the study, area water depths close to the coast remain quite shallow at 20 m and greatly deepen reaching depths of up to 60 m towards the eastern section of the area.

Outside of physical considerations, there are also socio-economic constraints which influence the area. For example; a Department of Defence exclusion zone occurs at the very western edge of the area with a Department of the Marine special exclusion zone running through the centre. Similarly, an established navigation channel runs through the northern section of the area (see Fig. 3.39). Intensive fisheries for the Dublin Bay Prawn also takes place in this area (chapter 5).

3.6 CONCLUSIONS AND SITE RECOMMENDATIONS

Information regarding the geological and geotechnical characteristics of retrieved sediments at depth in the Irish Sea is lacking. The use of in-situ geotechnical tools, such as CPTu, offers the chance to help characterise and interpret sediments in relatively simple geological settings such as WIMSB where seismic profiles are available. In the WISMB, using the MARUM GOST system, it was possible to not only characterise sediments geotechnically but also verify seismic reflectors such as lithological boundaries and bedrock. This data was also used to assess the area as a potential site of construction for offshore windfarm turbines.

Geologically, CPTu data verified two dominant units in the WISMB consisting of homogenous, marine muds overlying heterogeneous glacial deposits associated with the disentegration of the ISIS. Whilst no samples were directly retrieved, CPTu profiles indicated a high level of heterogeneity within the glacial deposits, suggesting they are considerably more complex than stated in previous works and require an extensive sampling programme to confirm this. These glacial deposits most likely comprise of till at the base, overlying bedrock, grading upwards into dense meltwater related sands and silts. CPTu measurements also indicated the high likelihood that the acoustic turbidity associated with the lower section of the upper marine mud layer to be gas-charged sediments associated with shallow methane accumulation seen elsewhere in the area by other workers. Whilst no considerable reduction in shear strength was noted in these gas-charged sediments, gas under pressure has been known to reduce shear strength. Piled foundations sited above such sediments are likely to be affected by unpredictable bearing properties in addition to providing escape routes for gas migration. Similarly, the quantity of gas in these deposits is currently unknown but in significant accumulations they offer potential geohazards.

It is difficult to classify the site as suitable for constructing a windfarm as it will depend on budget and the type of foundation chosen. Outside of geological reasoning the site offers good wind potential (8 - 10 m/s at 100 m above sea-level), is located relatively close to major urban areas along the east coast (particularly Dublin Bay and Drogheda Bay which are regarded as priority bay

areas) and in adequate water depths (up to 50 m, generally <35 m). Other important considerations include navigation channels, a Department of the Defence exclusion zone and Department of the Marine exclusion zone all found in or near the area. The area is also extensively trawled with trawling gear reaching depths of up to 30 cm. As a result, any cables associated with the windfarm will need to be entrenched to of at least 2 m depth in order to avoid contact.

The water depth of >20 m in many areas of the site and the generally low shear strength upper unit would discount the use of monopile foundations. In such conditions gravity foundations would be the preferred option. However, the heterogeneous nature of the underlying glacial unit and its proximity to the surface in many places means that ultimately the safest option would be for jacket (three- or four-legged structures) foundations. The seabed in the area is generally smooth and largely free of boulders and gravel or any erosive features. However, scour has been recorded elsewhere in the WISMB and so is an important consideration to mitigate against. Some predictive modelling based on the geotechnical data derived from CPT and seismic data presented here would help considerably with this issue

REFERENCES

Belderson, R.H., 1964. Holocene sedimentation in the western half of the Irish Sea. Marine Geology 2, 147–163.

Blott, S.J., Pye, K., 2001. GRADISTAT: a grain zize distribution and statistics package for the analysis of unconsolidated sediments. Earth Surface Processes and Landforms 26, 1237–1248.

Brandes, H.G., 1999. Predicted and measured geotechnical properties of gas-charged sediments. International Journal of Offshore and Polar Engineering 9, 219–225.

Callaway, A., Smyth, J., Brown, C.J., Quinn, R., Service, M., Long, D., 2009. The impact of scour processes on a smothered reef system in the Irish Sea. Estuarine, Coastal and Shelf Science 84, 409–418.

Coughlan, M., Wheeler, A.J., Dorschel, B., 2011. Offshore Renewable Energy Site Suitability Mapping (ORESSuM).

Dickson, C., Whatley, R., 1993. The Biostratigraphy of a Holocene borehole from the Irish Sea Ostracod species, in: Proceedings of the 2nd Euroopean Ostracodologists Meeting. British Micropalaeontological Society, London, Glasgow, pp. 145–148.

Dobson, M.R., 1977. The geological structure of the Irish Sea, in: Kidson, C., Tooley, M.J. (Eds.), The Quaternary History of the Irish Sea. Seel House, Liverpool, pp. 13–26.

Folk, R.L., Ward, W.C., 1957. Brazos River Bar: a study in the significance of grain size parameters. Journal of Sedimentary Petrology 27, 3–26.

Jackson, D.I., Jackson, A.A., Evans, D., Wingfield, R.T.R., Barnes, R.P., Arthur, M.J., 1995. United Kingdom offshore regional report: the geology of the Irish Sea. British Geological Survey, London.

Lunne, T., Kleven, A., 1981. Role of CPT in North Sea foundation engineering, in: Cone Penetration Testing and Experience, Proceedings of a Session Sponsored by the Geotechnical Division at the ASCE National Convention. St. Louis, Missouri, pp. 76–107.

Lunne, T., Robertson, P.K., Powell, J.J.M., 1997. Cone Penetration Tesing In Geotechnical Practice. Blackie Academic & Professional.

Lunne, T., Robertson, P.K., Powell, J.J.M., 2002. Cone Penetration Testing in Geotechnical Practice. Spon Press.

O'Kelly, B.C., 2014. CPT testing in Dublin Boulder Clay, in: Proceedings of the Third International Symposium on Cone Penetration Testing (CPT '14). Las Vegas, Nevada, USA, pp. 2–50.

Pantin, H.M., 1977. Quaternary sediments of the northern Irish Sea, in: Kidson, C., Tooley, M. j (Eds.), The Quaternary History of the Irish Sea. Seel House, Liverpool, pp. 27–54.

Pantin, H.M., 1978. Quaternary sediments from the northeast Irish Sea: Isle of Man to Cumbria. Bulletin of the Geological Society of Great Britain 64, 43.

Robertson, P.K., 1990. Soil classification using the cone penetration test. Canadian Geotechnical Journal 27, 151–158.

Robertson, P.K., Cabal (Robertson), K.L., 2009. Guide to Cone Penetration Testing fo Geotechnical Engineering. Greggg Drilling & Testing, Inc.

Robertson, P.K., Campanella, R.G., Gillespie, D., Greig, J., 1986. Use of Piezometer Cone data, in: In-Situ '86 Use of In-Situ Testing in Geotechnical Engineering, GSP 6. ASCE, Reston, VA, pp. 1263–1280.

Seifert, A., 2010. In situ detection and characterisation of fluid mud and soft cohesive sediments by dynamic piezocone penetrometer testing. University of Bremen.

SOLUTIONS, G.& D.G., 2012. Foundation Risk & Geotechnical Uncertainty Mapping for future Offshore Wind Farm Developments " D3 : Final Report ."

Steenfelt, J.S., Sørensen, C.S., 1995. CPT- Contraption for probing in tills?, in: Proceedings of International Symposium on Cone Penetration Testing (CPT '95). Linköping, Sweden, pp. 307–312.

Wheeler, S.J., 1988. The undrained shear strength of soils containing large gas bubbles. Géotechnique 38, 399–413.

Williams, S.J., Kirby, R., Smith, T.J., Parker, W.R., 1981. Sedimentation studies relevant to low level radioactive effulent dispersal in the Irish Sea. II. Sea bed morphology, sediments and shallow sub-bottom stratigraphy of the eastern Irish Sea.

Yuan, F., Bennell, J.D., Davis, A.M., 1992. Acoustic and physical characteristics of gassy sediments in the western Irish Sea. Continental Shelf Research 12, 1121–1134.

CHAPTER 4

MID TO LATE HOLOCENE DEPOSITIONAL HISTORY OF THE WESTERN IRISH SEA MUD BELT

Theme

In the study from Chapter 3, the geological model for the WISMB was established using seismic and in-situ geotechnical data. The findings were that the WISMB represented an area of seemingly continuous sedimentation since the end of the Last Glacial Maximum comprising Holocene muds overlying glacial deposits. In this chapter, we adopt a more fine-scale approach to the interpretation of environmental conditions by applying multi-proxy analyses of three cores from the area.

Contributors

Mark Coughlan partook in the survey (ISMA; CV0926, Appendix B) which gathered the data for this study and carried out labwork for PSA, XRF, MSCL and foraminiferal analysis. He is also the first author having undertaken evaluation of all data and written all drafts of the manuscript.

Andrew J. Wheeler is the lead supervisor on this project, was chief scientist for the survey which gathered the data for this study and has extensively proof read drafts of this manuscript.

Boris Dorschel was present during the survey and supervised the collection of the geophysical data. He also subsequently processed the geophysical data used in this study.

Stephen McCarron provided the Multi-scan core logging (MSCL) facilities used in this study, aided in the gathering of data through this method and in the interpretation of results.

Wim Boer, Piet Van Gaever and Henk de Haas carried out the gamma spectrometry work used in this study, helped in the interpretation of results and contributed to the discussion.

Antoinette McCarthy carried out picking and identification of foraminifera from samples of ISMA 358.

Cormac Ryan processed surface grab samples for PSA.

Tobias Mörz provided the particle-size analysis facilities for this study and proof read the final manuscript.

CHAPTER 4

MID TO LATE HOLOCENE DEPOSITIONAL HISTORY OF THE WESTERN IRISH SEA MUD BELT

ABSTRACT

With increasing focus on anthropogenic driven climatic and environmental change during the Holocene, there is a clear need for undisturbed records recording both natural, background fluctuation and human induced change both on a localised and regional scale. Marine records are increasingly being utilised to reconstruct such records, particularly in shallow shelf settings where terrestrial and near shore changes can also be recorded due to their proximity to continental land masses. The Irish Sea is a formerly glaciated shelf experiencing marine conditions since the end of the Last Glacial Maximum (LGM). Presently, the Irish Sea is a relatively high energy, tide dominated basin with the Western Irish Sea Mud Belt (WISMB) being one of the few areas of predominately active sediment deposition. In this study a palaeoenvironmental reconstruction from the WISMB deposition archive is presented based on a multi-proxy analysis of three marine sediment cores and geophysical data. This investigation included grain-size, geochemical, multi-sensor core logging, gamma spectrometry, AMS ^{14}C dating and foraminiferal analyses and

facilitated a study of the mid- to late-Holocene development of the WISMB and surrounding area. The reconstruction of this record revealed two marked environmental shifts at 4, 500 years and 100 years BP approximately. Both these shifts can be correlated with marked changes in European climatic conditions during the Holocene. The intervening time-period revealed overall increased bottom currents and fluctuating environmental conditions coinciding with varying climatic conditions in the late Holocene. Increased sedimentation rates and changes in sediment composition in the last 100 years also point to distinctive environmental changes reflecting both natural events, such as increased storm events, and local human impacts including bottom trawling.

KEYWORDS: Irish Sea, Holocene, Mud Belt, climate variability, benthic foraminifera, AMS ^{14}C, grain-sizes, gamma spectrometry.

This chapter is based on: Coughlan, M., Wheeler, A.J., Dorschel, B., McCarron, S., Boer, W., van Gaever, P., de Haas, H. and Mörz, T. (Submitted). Mid to Late Holocene Depositional History of the Western Irish Sea Mud Belt. *Marine Geology*.

4.1 INTRODUCTION

European Holocene climate variability has been well established using a variety of proxies from both the terrestrial and marine realm including tree rings (Stuiver and Braziunas, 1993), marine records (Bond et al., 1997, 2001) and ice cores (O'Brien et al., 1995). These capture fluctuations between periods of relative warm and cold, particularly in the mid- to late Holocene (Stuiver & Braziunas, 1993; O'Brien et al., 1995; Bianchi & McCave, 1999). The isolation of Ireland by its positioning on the north-west fringe of Europe means its maritime climate is largely dominated by a prevailing westerly airflow without the influence of continents and major ice masses. As a result, it is in an ideal location to record potential climatic variations brought about by variations in the North Atlantic Oscillation (NAO) as well as previous freshwater pulses into the North Atlantic (McDermott et al., 2001; Turney et al., 2005). In Ireland, these variations in Holocene climatic conditions have been reconstructed using high-resolution speleothem studies (McDermott et al., 1999, 2001), peatland successions (Turney et al., 2005; Plunkett, 2006; Swindles et al., 2007, 2009, 2010; Blundell et al., 2008; Langdon et al., 2012), lake records (Diefendorf et al., 2006; Holmes et al.,

2010; Ghilardi and O'Connell, 2013) and the study of early human settlements (Turney et al., 2006). Work has also focused on records of such change during the Holocene from marine sediments in the North Atlantic, off the western Irish coast (Bond et al., 1997, 2001; Øvrebø et al., 2005) and the Celtic Sea (Austin and Scourse, 1997; Scourse et al., 2000, 2002).

In shallow shelf settings, conditions can be energetic and areas of continuous sedimentation where deposition is the dominant mechanism scarce. This is particularly true of such tide dominated, mid latitude shelf seas as the Irish Sea. Here, seasonal thermal stratification is the dominant hydrodynamic phenomena (Austin and Scourse, 1997; Scott et al., 2003; Scourse et al., 2002). Stratification is controlled by seasonal heating of the sea exceeding the effects of tidal stirring which, in turn, also influences peak bed stress vectors and, therefore, sediment distribution (Scourse, 2013). Where strong tidal mixing occurs, and resulting peak bed stress vectors are high, net sediment erosion and transport occurs. However, where shelf basins occur beneath seasonally stratified water bodies, peak bed stress vectors are low and fine-grained sediments are allowed to accumulate (Scourse and Austin, 2002; Scourse et al., 2002). Such palaeoarchive conditions exist in the Western Irish Sea Mud Belt (WISMB; Fig. 4.1) which holds the potential to recreate detailed records of climatic and environmental change (Dickson and Whatley, 1993). However, studies into the Irish Sea depocentre marine records for Holocene climatic and environmental change are few in number in comparison with similar areas in Northern Europe such as the North Sea (Hass, 1993, 1996; Hebbeln et al., 2003, 2006). Analogous mud belt settings in the Celtic Sea have been investigated by Austin and Scourse (1997), Scott et al. (2003), Scourse et al. (2002). From their studies, the onset of stratification in the Celtic Sea occurred after 10,660 yr cal BP and before 7,100 yr cal BP, most likely between 8990 and 8440 yr cal BP based on mixing model ages (Scourse et al., 2002). This stable isotope based transition also corresponded with a shift in sediment deposition from sand to predominately mud with such a transition also common across present day frontal regions like the WISMB (Jackson et al., 1995; Chapter 3). The subsequent evolution of stratification can be constrained by different foraminiferal assemblages which represent mixed or stratified conditions (Austin and Scourse, 1997; Scott et al., 2003). At present, the main controls on shelf stratification are water depth and tidal stream amplitude. Therefore, the

principal control on the timing of this stratification threshold over time is largely relative sea-level (Scourse and Austin, 2002; Scourse et al., 2002).

In this study, we aim to investigate the nature of the sediment record in the WISMB and develop a high-resolution palaeorecord of environmental change during the Holocene through a multi-proxy approach. This approach was applied to three vibrocores recovered from the WISMB with correlation between the three cores was made possible by multi-sensor core logger (MSCL), X-ray fluorescence (XRF) and grain-size data. Subsequently, two cores were subjected to detailed stratigraphic analysis by way of gamma spectrometry and accelerator mass spectrometry (AMS) ^{14}C dating.

4.2 AREA SETTING

The Irish Sea is predominately a tidally active area with tides entering through St. George's Channel in the south and the North Channel after which they follow distinct migratory pathways (Pingree and Griffiths, 1979; Robinson, 1979). For the most part, these tides are strong enough to exceed sediment thresholds allowing for sediment erosion and transport (Van Landeghem et al., 2009). The WISMB is located at the northern termination of such a transport path, largely marked by sediment-wave migration, which has its origins further south (Belderson, 1964) (Fig. 4.1). It is one of two such Mud Belts within the Irish Sea (the other in the eastern half of the Irish Sea) that mark areas where deposition is the dominant process under a low energy regime (Dobson, 1977; Pantin, 1977;1978) (Fig 4.1).

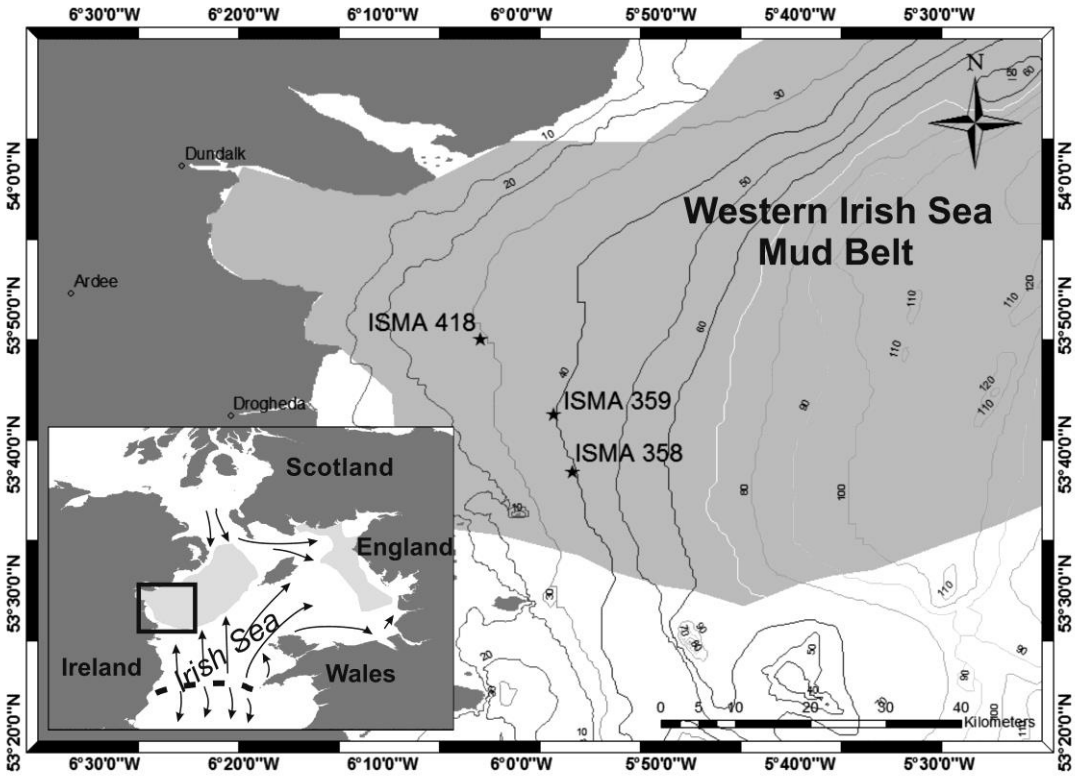

Figure 4.1 Location of WISMB in the Irish Sea. Inset map: Irish Sea with dashed line denoting sediment separation zone and arrows indicating sediment transport paths according to Pingree and Griffiths (1979). The WISMB and EISMB are highlighted in grey with the target area of this study indicated by the black box. Main map: Study area close up showing bathymetry lines and core locations.

As such, it is a depocentre consisting of predominately Holocene muds and silts overlying glacial tills deposited during the melting of the Devensian ice-sheet (Belderson, 1964; Jackson et al., 1995). It lies between the east coast of Ireland and the Isle of Man, as far south as Lambay Island and north as far as Carlingford Lough with water depths ranging down to 100 m. Fine-grained sediment infill forms a lens shaped body dominated by muds towards the centre, surrounded by material which becomes increasingly sandy and eventually grades into gravels with varying degrees of sand and mud, interpreted as representing reworked glacial material (Belderson, 1964). At some sites bedrock outcrops through the mud cover onto the sea floor (Callaway et al., 2009) as well as boulder clay occurring close to the surface under a thin covering of mud (Jackson et al., 1995). A British Geological Survey (BGS) borehole (89/15) taken from the Manx Depression southwest of the Isle of Man was logged with samples taken for palaeoclimatic studies (Dickson

and Whatley, 1993). The subsequent investigation, based on ostracod assemblages, revealed temperate, presumed Holocene, deposits to a depth of 38.25 m that overlie an erosive surface. Below this erosive surface to a depth of 57.5 m were Devensian silty muds with an essentially cold water fauna. Below 57.5 m were Devensian sands yielding lower Jurassic fauna of Hettangian to Lower Pliensbachian age with the lack of Quaternary specimens suggesting that this material was either part of a till or material washed from a till (Dickson and Whatley, 1993).

Notwithstanding work carried out by a number of workers on the sedimentological and hydrological regime that suggests both the eastern and western Mud Belts are active zones of sedimentation (Belderson, 1964; Belderson and Stride, 1966; Pantin, 1977; 1978), Kirby et al. (1983) surmised that much of the evidence suggesting that both areas of actively depositional was circumstantial without a definite source for the fine sediment to support continued sedimentation. The presence of a sub-surface maximum for ^{137}Cs in a studied core by Mitchell et al. (1999), however, supports the hypothesis that significant sedimentation is taking place currently in the WISMB although, Mitchell et al. (1999) could give no insights into the nature or provenance of deposited sediment.

Estimated sedimentation rates calculated for the area vary. Based on ^{14}C dating of the carbonate fraction, Kershaw (1986) established a zone of near constant ^{14}C age of 7780 to 8620 years occurring in the upper 55cm, deduced as a zone of mixing, after which the ^{14}C age decreased linearly to give a sedimentation rate of 0.018 cm a^{-1}. Below the 160 cm mark the sedimentation rate was calculated at 0.007cm a^{-1}. Mitchell et al. (1999) report sedimentation rates to be between 0.4 and 0.73 cm a^{-1} based on ^{210}Pb profiles for the upper 60 cm although accepted that these may be lower than actual values due to the effect of physical or biological mixing . In addition, ^{137}Cs data from the same cores gave rates of 1.9 cm a^{-1} having identified a sub-surface maximum at a depth of approximately 20 cm. By comparison, ^{239,240} Pu profiles on the other hand showed little variation for the uppermost 20 cm with sedimentation rates calculated at 1.5 and 1.7 cm a^{-1}, whilst ^{241}Am values were almost identical indicating rates of 1.5 cm a^{-1}.

4.3 MATERIALS AND METHODS

The core material and geophysical data presented in this study were gathered in September 2009 as part of the Irish Sea Marine Assessment (ISMA; CV0926, Appendix B). During the course of this survey, some 352.65 km^2 of the Irish Sea seabed was mapped using Simrad EM3002D multibeam echosounder onboard the R.V. Celtic Voyager. In addition, 534 km of sparker seismic lines were shot using a Geo-Source 400 Sparker Seismic System with a single channel hydrophone array. Data processing was performed on board with the CARIS HIPS and SIPS software package.

This high-quality acoustic mapping data was supplemented by 975 high-quality, digital photographs of the seabed from 15 areas, 269 surface grab samples and 20 vibrocores of up to 3 m length. Three of these vibrocores were taken from the WISMB and form the basis of this study (Table 4.1).

Core ID	Latitude	Longitude	Water Depth (m)	Core Length (cm)
ISMA 358	53°38.6974"N	05° 56.4116”W	44.8	285
ISMA 359	53°42.8173"N	05° 57.664"W	42	260
ISMA 418	53°48.2333"N	06° 02.9527"W	33.5	249

Table 4.1 Core information for cores used in this study

4.3.1 Computerised Tomography X-ray and Digital Line Scanning

All cores were imaged using the Computerised Tomography (CT) X-ray Scanner housed at MARUM, University of Bremen with a maximum resolution of ~ 1 mm. Subsequently, eFilm visual software was used to interrogate the data in order to identify internal primary sedimentological structures and secondary features such as bioturbation. Digital images of these open cores were also taken using the Geoscan III on the Multi-sensor core logger (MSCL) scanner at MARUM. The colour line camera is a 3 CCD device using 3 x 2048 pixel CCD arrays and a beam -splitter. The linescan software produces visual colour images but also colour data in RGB and CIE-L*, a*, b*. These high resolution digital images were used to identify physical evidence of bioturbation and also aid in facies recognition along with identifying potential structures within the sediment column such as layering and bioturbation.

4.3.2 Foraminiferal Analyses

A foraminiferal analysis was carried out on ISMA 358 and ISMA 359. Samples taken for foraminiferal analyses consisted of slices of sediment measuring approximately 2 cm in thickness and weighing between 40 - 90 g, depending on density. These were taken at 10 cm intervals through the core. These samples were wet sieved using >63 µm, >125 µm and >250 µm meshes. Samples were then oven dried before being picked under a light microscope. The >250 µm size class was chosen for this study due to the good abundance of species and preservation with at least 300 specimens picked per sample where possible. Identification of benthic forams was based on compiled microfossil descriptions (Murray, 1971; 1979) and a number of key papers including Murray (1970; 2000; 2003) and Murray and Alve (2011).

4.3.3 Multi Scan Core Logging

After being split lengthways, all cores were analysed at 1 cm intervals for gamma ray attenuation, P-wave velocity, magnetic susceptibility and colour spectrometry using the non-destructive GEOTEK multi-sensor core logger (MSCL) at the National University of Ireland, Maynooth to aid in identifying lithological changes and core correlation (Weber et al., 1997).

4.3.4 X-ray Fluorescence Scanning

For all cores, X-ray Fluorescence (XRF) Core Scanner data were collected every 2 cm downcore using a generator setting of 20 kV, 0.087 mA directly at the split core surface of the archive half with XRF Core Scanner 1 at the MARUM- University of Bremen. The split core surface was covered with a polypropylene foil to avoid contamination of the XRF measurement and desiccation of the sediment. The data reported here was acquired by XRF Core Scanner I at MARUM using a

KEVEX Psi Peltier Cooled Silicon Detector and a KEVEX X-ray Tube 52500008-02 with the target material titanium (Ti), iron (Fe), potassium (K) and calcium (Ca). Analyses focused on these elements to aid in palaeoenvironmental reconstructions (Röhl et al., 2000; Bahr et al., 2005).

4.3.5 Particle-Size Analysis

Samples weighing roughly 2 grams were taken every 5 cm to be used in particle-size analyses (PSA) using a Beckman Coulter LS 13 320 laser diffraction particle-size analyser at MARUM, University of Bremen, to provide information about downcore grain-size distribution for all cores. The laser is equipped with an Aquous Liquid Module and an Auto Prep Station and determines particle grain-sizes from 0.4 to 2000 µm. Analyses was carried out on bulk sediment samples generally although ten samples were analysed for both the bulk and carbonate free fractions and compared. There was no siginificant difference between these samples.

In the case of surface grab-samples, the particle-size distribution of the siliciclastic fraction was measured on a Malvern Mastersizer 2000 laser-granulometer with Autosampler and Hydro G dispersion unit at the National Oceanography Centre Southampton. The siliciclastic fraction was obtained through the removal of organic matter and the carbonate phase by oxidation (10% H_2O_2) and dissolution (10% HCL) respectively. A 5% Calgon (Sodium Hexametaphosphate) solution was added for disaggregation and dispersion accompanied by mechanical shaking. No comparison between grab samples and core samples was undertaken in this study.

Statistical parameters including modal and mean grain-size, sorting and sediment type for PSA distributions were calculated according to Folk and Ward (1957) using the GRADISTAT software (Blott and Pye, 2001).

4.3.6 Age Model

To constrain an age model for the cores, further analyses were carried out on ISMA 418 and ISMA 359 using AMS ^{14}C and gamma spectrometry. AMS ^{14}C dates were determined on ten samples of the gastropod *Turritella communis. T. communis* shells were present throughout both cores and considered more reliable for dating as opposed to the bulk sediment carbonate fraction which is susceptible to reworking and bioturbation or recycling of carbon (Kershaw, 1986; Bourrin et al., 2007). In total, ten *T. communis* shells were taken from horizons where XRF and PSA data indicated perceived changes in the environmental setting with analyses carried out at Queen's University, Belfast. Initially, 155 micro litres of 1% HCL acid per 10 mg of shell was used to remove 33% of the shell weight with 25 - 30% of the shell etched off the surface to remove any calcite contamination before they were hydrolysed to CO_2. All ages were calibrated using Calib version 6.1.0 software, based on MARINE09 dataset, with a ΔR value of -2 ± 38 yrs calculated from the Marine Reservoir Correction Database (Reimer et al., 2009).

Analyses were undertaken for ^{210}Pb, ^{137}Cs, ^{226}Ra and ^{241}Am by way of gamma spectrometry at the Royal Netherlands Institute for Sea Research (Royal NIOZ) to investigate anthropogenic radionuclide levels in the core profile. Sixteen samples from both ISMA 359 and ISMA 418 were taken at intervals of 5 cm for the upper 40 cm and every 10 cm thereafter until the 160 cm mark. Each sample taken measured between 12 – 20 g and was subsequently separated into fine (<63 µm) and coarse (>63 µm) fraction using the Atterberg sedimentation tube method. The fine fraction was used in analyses owing to the fact that using the fine fraction enhances measured activities and negates uncertainties regarding grain-size variations. Gamma spectrometry was carried out with a Canberra Broad Energy Range High Purity Germanium Detector (BEGe). The detector was connected to a computer via a Digital Spectrum Analyser (DSA-1000) and the data were calculated with Genie 2000 gamma spectroscopy software. The samples were accurately weighed and added to a Petri dish with a diameter of 6 cm and a height of 1.5 cm, depending on the availability the volume was 1 - 6 ml. Calibration, monitor standards and samples were prepared in the same geometry. The Petri dishes were sealed airtight to equilibrate the samples for at least three weeks before counting. Samples were counted for 2 to 5 days depending on the amount of sample to

obtain good counting statistics. The detector was externally calibrated with a Geological Certified Reference Material IAEA/RGU-1 with reference date of 01-01-1988. Quality control was performed using a monitor standard IAEA-300.

4.4. RESULTS

4.4.1 Sub-Seabed Structure

Seismic investigations reveal Palaeozoic-Carboniferous bedrock (Pantin, 1977), forming an irregular, lopolithic depression underlying the area overlain by sediments varying in thickness from <10 - 30m (Chapter 3). Sediment thickness is greatest towards the centre of the area and gradually wedges out. Within the succession, three distinct seismic units are recognisable bounded by two major reflectors being the bedrock surface (R2) and the base of Holocene sediments (R1) (Fig. 4.2). These surfaces can be traced laterally across the area (Chapter 3).

The lowest unit (Unit 3) underlies the strong R2 reflector and has limited internal reflectors representing the Palaeozoic-Carboniferous basement. Overlying this are sediments which have an amorphous signature consisting of reflectors that are high angle, impersistent and irregular or are lacking entirely (Unit 2). The unit is interpreted to be dominantly gravels with muds, sands and cobbles and is thought to have formed during glaciation in glaciolacustrine and glaciomarine, ice-proximal settings (Jackson et al., 1995). This was confirmed in other core profiles taken south of the area investigated here (Chapter 3).

The uppermost unit, Unit 1, is predominately near-transparent with parallel, subhorizontal reflectors on seismic images. It is interpreted as post glacial, Holocene deposits deposited in a marine environment, marked at the base by sandier deposits representing the transition from ice-proximal to distal marine following ice retreat (Jackson et al., 1995). Within certain seismic profiles, the lower sections of Unit 1 showed enhanced reflectors creating a sharp boundary with the surrounding material (Fig. 4.2). These were interpreted as gas-charged sediments based on the work of Yuan et al. (1992) who identified such features, associated with a gas front in the area, on sub-bottom images and in core profiles (Chapter 3).

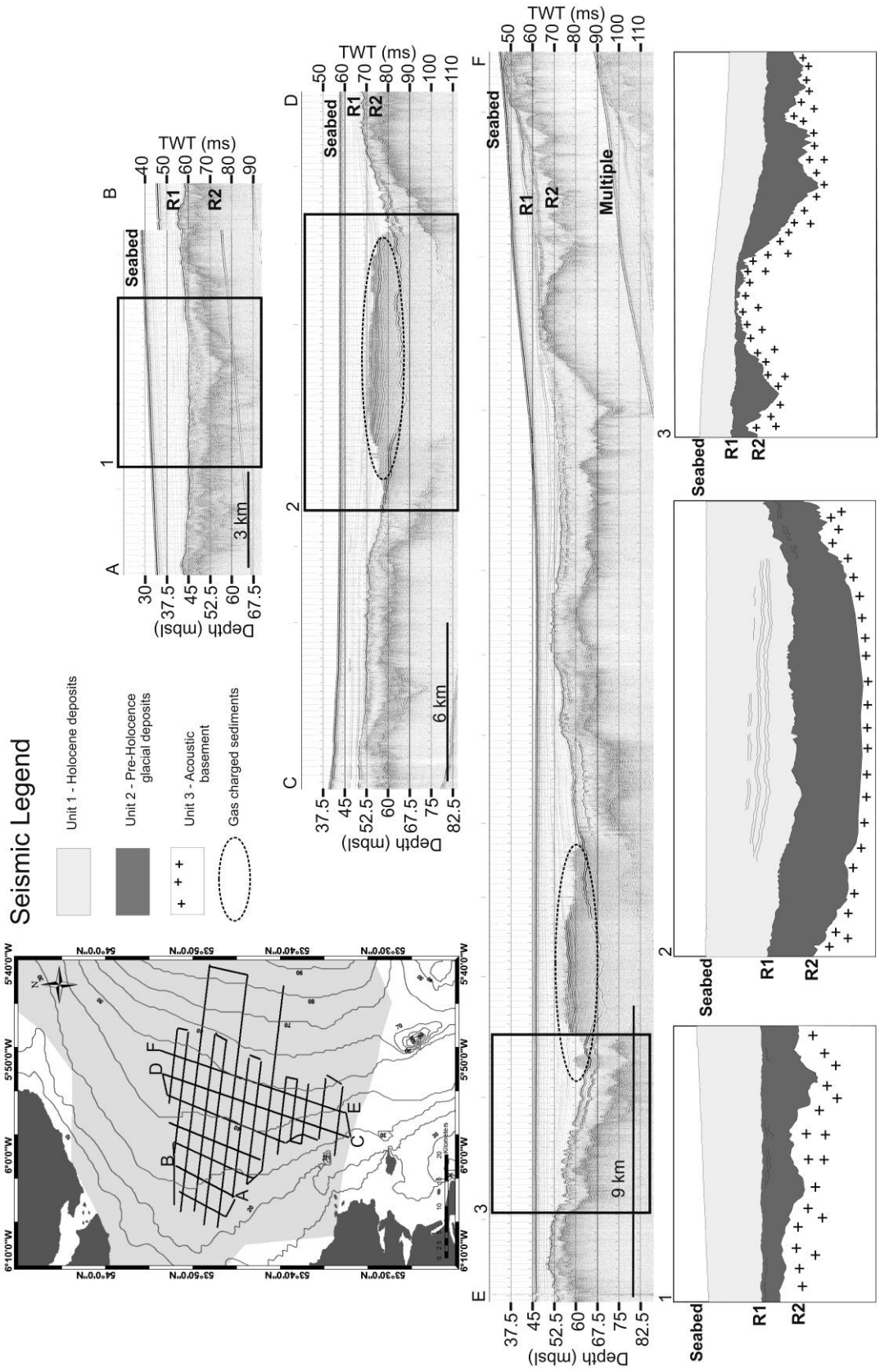

Figure 4.2 Seismic data presentation. Inset map: sparker seismic grid across the study area with highlighted profiles A-B, C-D and E-F presented below. Presented lines display interpreted reflectors and seismic units (see section 4.1 for explanation) with depths in metres below sea level (mbsl) and two way travel time (TWT). Gas charged sediments are identified by dashed circle.

4.4.2 Seafloor Setting

The study area covers roughly 26 x 20 km with water depths down to 50 m (Fig. 4.3 and Fig. 4. 4). Backscatter and MBES data revealed small-scale sediment waves south of the WISMB passing northwards into a uniform seabed of fine-grained sediments. Particle-size analyses on grab samples confirmed the fine-grained nature of seafloor sediment with sediment types of muddy sand, sandy mud, slightly gravelly mud and slightly gravelly sandy mud (all according to Folk and Ward, 1957) dominating the area (Fig. 4.3). All samples were poorly to very poorly sorted with subtle changes in sediment distribution showing a general progressive northward decrease in grain-size. Starting in the south-west of the area, modal grain-size is 120.8/138.7 µm with mean grain-size 90 -120 µm (Fig. 4.3). Towards the centre of the area, modal grain-size shows values of 52.73, 60.54, 69.51, 79.81, 91.64 and 105.21 µm with mean grain-size ranging from 20 - 115 µm. In the north-east section of the area modal values decrease further to values of 5.8, 6.64 and 8.75 µm with mean values between 0 and 20 µm.

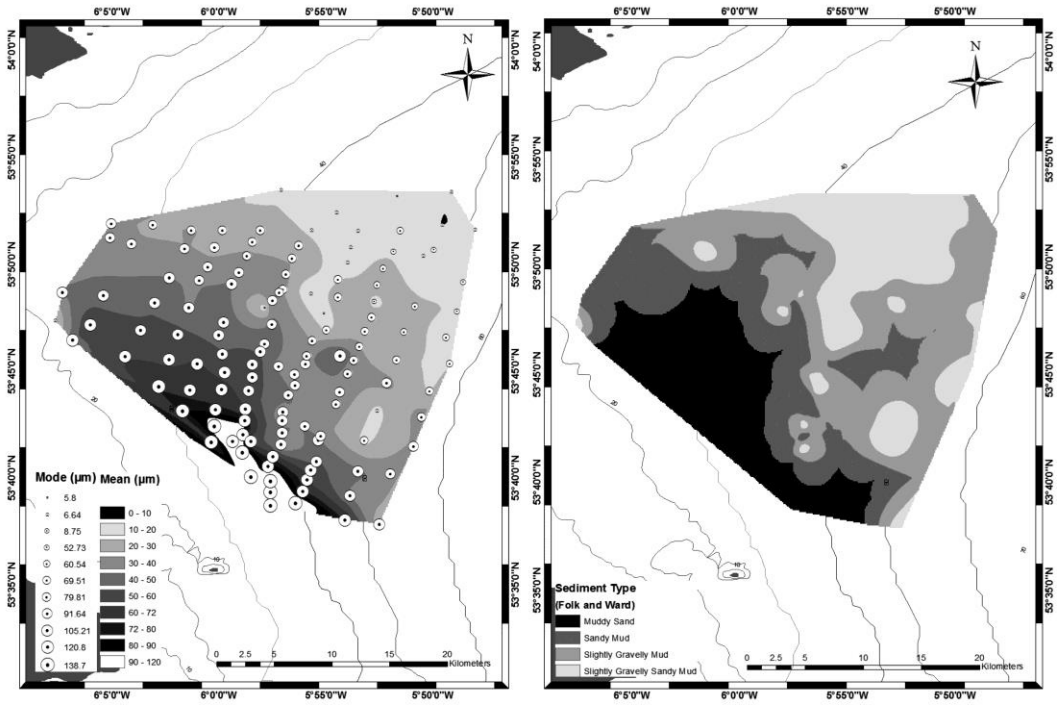

Figure 4.3 Particle-size distributions from grab samples across the study area. Left panel: modal grain-size for each grab sample location indicated by size of representative filled circle in the corresponding legend. Mean grain-size for each sample location is presented as a sediment distribution map using interpolation of the data. Right panel: sediment type (according to Folk and Ward, 1957) distribution based on interpolation of point data. Individual grab sample locations are indicated by circles.

Evidence for sediment waves at the southern edge of the WISMB (Fig. 4.4) was confirmed by seabed photography which also exposes a microtopography that is related, for the most part, to epifaunal burrowing (Fig. 4.4). Mottling of the seabed was also seen which may be linked to bioturbation or gas seepage in the area. Few other features were recorded other than evidence of seabed trawling (Fig. 4.4, Chapter 5) and occasional pockmarks forming as a result of shallow gas accumulation (Yuan et al., 1992, Chapter 3). The area is extensively and intensively trawled for *Nephrops norvegicus* with the seabed potentially trawled, on average, between five to ten times a year (Fox et al., 1996, Chapter 5). Density of *Nephrops* distribution varies locally and seasonally depending on sediment type and the energy regime (Ball et al., 2000, Chapter 5).

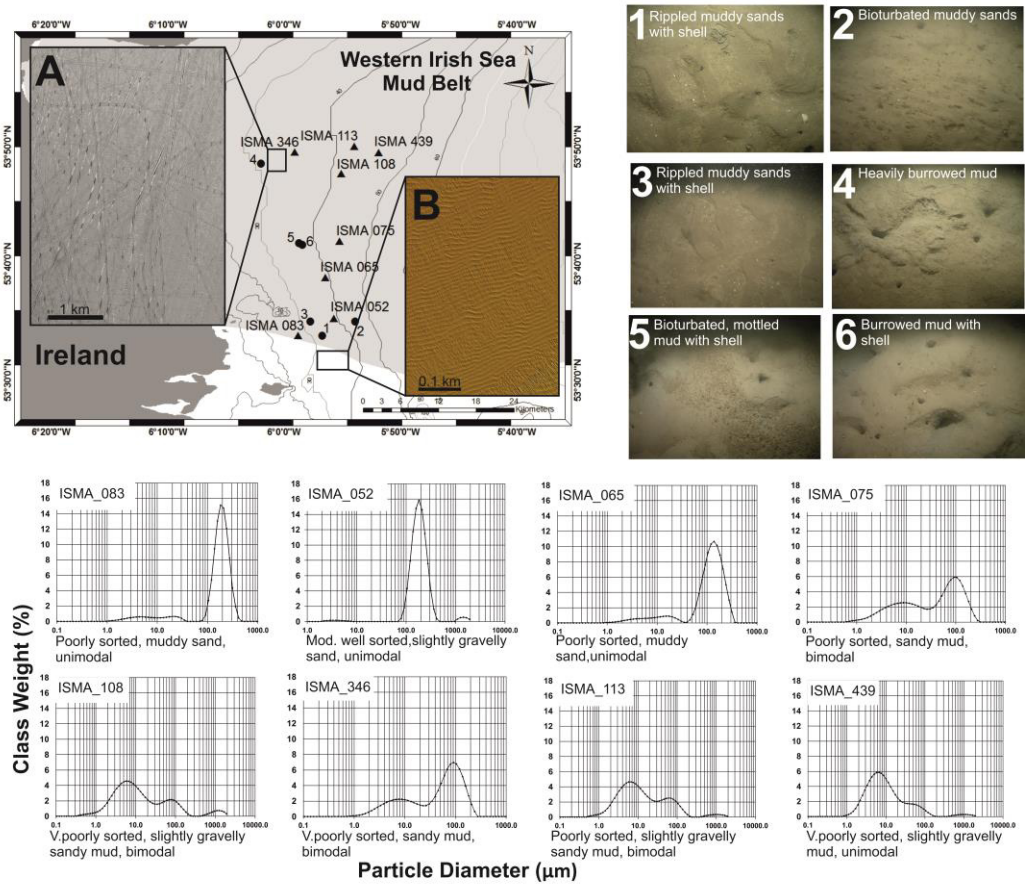

Figure 4.4 Sea floor characterisation of the WISMB. Top left panel: A is a backscatter image highlighting trawl marks in the area. B is a MBES image showing sand waves located south of the WISMB. Also included are triangles marking highlighted grab samples (see also bottom panel) and circles marking seabed photography (see also right hand panel). Right panel: corresponding seabed imagery with brief facies description. Bottom panel: corresponding particle-size distribution plots for highlighted samples indicating an overall northward decrease in grain-size.

4.4.3 Core Description

All cores contain homogenous, fine-grained (silty) sediments displaying a dark olive-grey colour (Fig. 4.5). Variations in colour were attributed to bioturbation. Macrofauna occurred throughout all cores with the gastropod *Turritella communis* the most dominant. The occurrence of these shells was patchy but often with rich horizons on the scale of centimetres and becoming less abundant towards the top of each core. CT X-ray revealed the full extent of these *T. communis* rich layers. No primary fabric was recorded in the cores from visual inspection, line scans or CT X-ray. However, significant evidence for sediment disturbance was seen in both cores, manifested as laterally discontinuous contrasting bands of light and dark colouration and was most prominent in the upper 30 cm approximately of all cores. This was assumed to be as a result of bioturbation as burrowing *Nephrops* are prominent in the area.

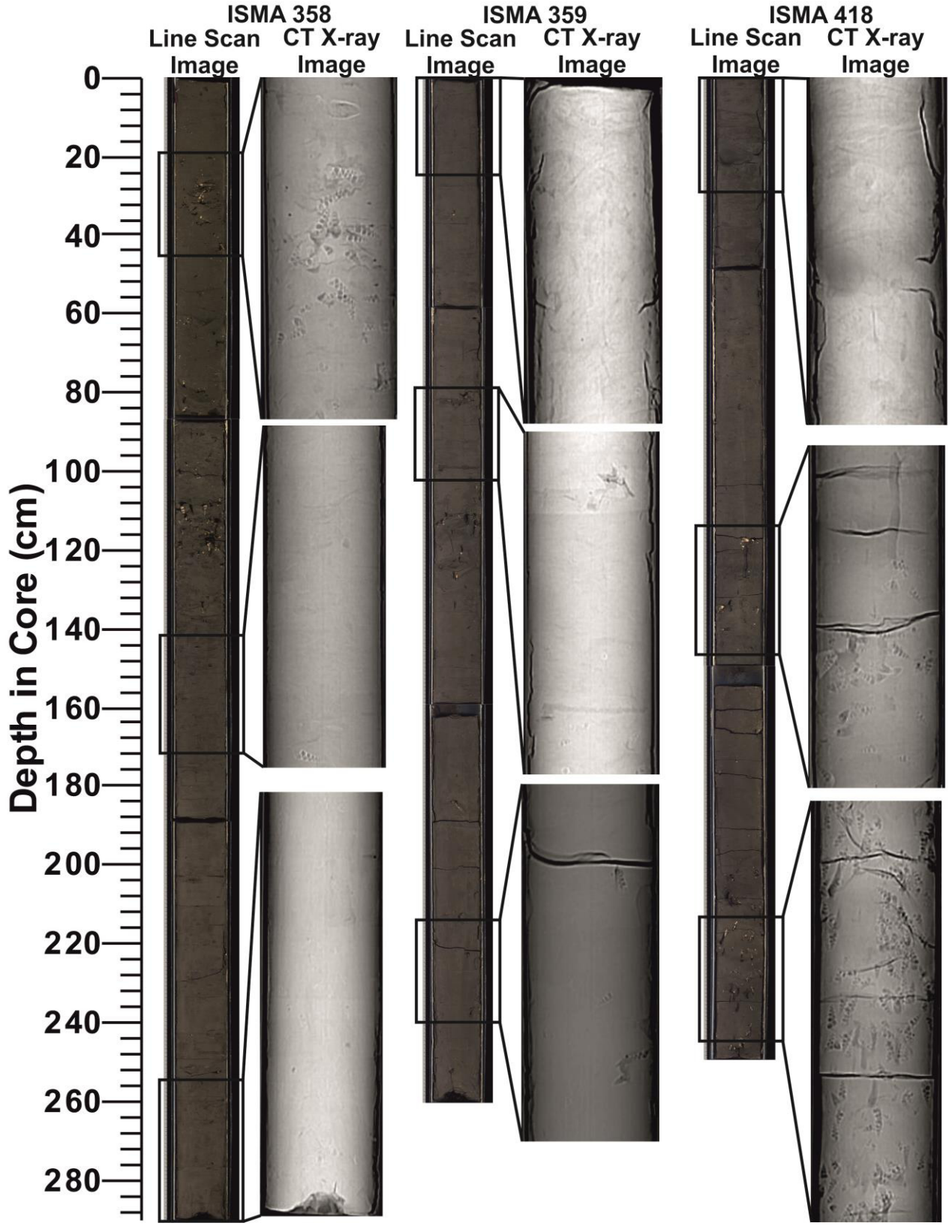

Figure 4.5 Macro core descriptions. Line scan imagery for each core mentioned in this study with CT X-ray images for highlighted sections. See section 4.3 for explanation. Note evidence of bioturbation in uppermost sections of each core.

4.4.4 Foraminiferal Stratigraphy

Foraminiferal counts performed on ISMA 359 with relative abundance counts are present in Figure 4.6. Whilst the relative abundance of key indicator species varied significantly over the course of the core ISMA 359, *Ammonia beccarii* (Linné) *(Ammonia batavus)* proved to be the most dominant, often accounting for >70% of the overall abundance. This is not very surprising considering that it is an opportunistic species that can tolerate a wide variability in temperature, salinity and oxygen (Scourse et al., 2002). The remaining 30% of counts identify a number of species with greater downcore variability. Three zones were established reflecting sections of the core where species assemblages showed similarities.

4.4.4.1 Zone F1 (140 - 255 cm)

This zone is dominated by *A. beccarii, Textularia sagittula* (Defrance group) and *Textularia aggultinans* with minor amounts of *Siphotextularia flintii* (Cushman), *Quinqueloculina lata* (Terquem), *Lagena interrupta* (Williamson)*, Eggerella scabra* (Williamson) and *Nonionella turgida* (Williamson). It can be divided further into two subzones based on relative frequencies of *Q. lata* and *S. flintii*.

Subzone F1a (255 - 184 cm); this zone sees a peak of *Q. lata* at 242 cm which subsequently decreases thereafter. There are also relatively low levels of *S. flintii* and *E. scabra Subzone F1b* (184 - 140 cm); sees a marked increase in *S. flintii* primarily as well as *E. scabra* and *L. interrupta* with decreases in *Q. lata.*

4.4.4.2 Zone F2 (140 - 80 cm)

Zone 2 is again dominated by *A. beccarii*, *T. sagittula* and *T. agglutinans* (despite showing an overall decrease in both), along with a pronounced peak in *S. flintii* at 112 cm. This peak also mirrors peaks in such minor elements such as *Quinqueloculina seminulum* (Linné), *Bulimina gibba/elongata* (Fornasini/d'Orbigny), *Brizalina spathulata* (Williamson) and *Pyrgo williamsoni* (Silvestri) that are not represented elsewhere in the core and coincides with the emergence of other species allowing this zone to be subdivided into two. Accessory species here include *Q. lata*,

Planorbulina mediterranensis (d'Orbigny), *Lagena substriata* (Williamson), *L. interrupta, Dentalina subcurata* (Montagu), *Bulimina marginata* (d'Orbigny), *Cibicides Lobatulus* (Walker and Jacob) and *Pyrgo depressa* (d'Orbigny). *Q. lata* and *L. interrupta* both display deceases from the preceding F1 zone with this zone also marking the emergence of *Elphidium excavatum* (Terquem) as well as *L. substriata* and *P. mediterranensis*.

Subzone F2a (140 - 112 cm); this zone witnesses the decrease in *L. interrupta* before the emergence of *L. substriata.*

Subzone F2b (112 - 80 cm); the peak in *S. flintii* at this point also coincides with the growing emergence of *E. excavatum*, *E. scabra* and *Ammoscalaria pseudospiralis* (Williamson). There is also a peak in *P. mediterranensis* at 84 cm.

4.4.4.3 Zone F2 (140 - 80 cm)

A. beccarii, again, dominates this zone with levels recording 70% abundance. S. *flintii* and *T. saggitula* show an overall decrease in this zone with *T. aggultinans* fluctuating between 8 and <2 %. However, it is the increase in *E. excavatum*, *E. scabra* and *A. pseudospiralis* that best define this zone. Levels of *E. excavatum* steadily increase from zone F2 to peak at 18% at 72 cm in the core before generally decreasing to the top of the core with some minor fluctuation. *A. pseudospiralis* also increases to peak at 63 and 34 cm. These two peaks coincide with peaks in *N. turgida* at the same horizons, the lower of which (63 cm) also corresponding in higher levels of *P. depressa*, *B. marginata* and *Dentalina legume* (Linné). Similarly, *E. scabra* peaks at 8% at 34 cm in the core. Other species present include *L. substriata* (showing its highest levels in the core), *D. subcurata*, *Elphidium gerthi* (Van Voorthuysen), *P. mediterranensis* (showing a general decrease in comparison to F2b levels to the top of the core) and *C. Lobatulus* (showing an overall increase).

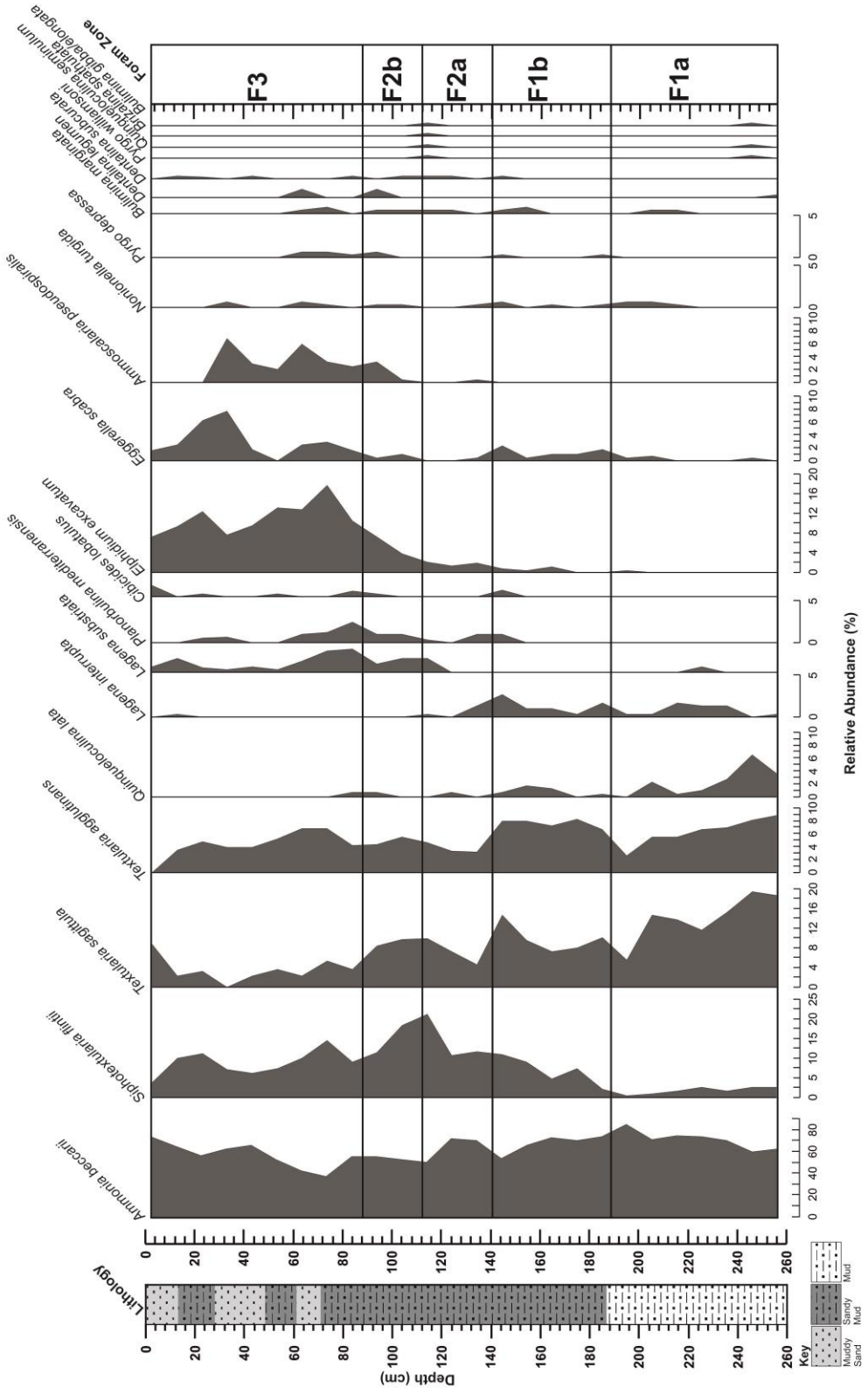

Figure 4.6 Foraminiferal analyses for ISMA 359. To the left had side of the graph is a core log showing core lithology from PSA. The percentage relative abundance of selected major taxa is presented with foraminiferal zonation based on major assemblage changes (see section 4.4.4 for explanation).

4.4.4.4 Core ISMA 358 comparison

A comparative study was made on ISMA 358 with results presented in Figure 4.7. Similar to ISMA 359, *A. beccarii* was also identified to be the most prominent species in this core. The three foraminiferal zones identified in ISMA 359 were similarly recognised in ISMA 358 based on the presence of key indicator species. Zone F1a was noted from 266 - 235 cm in ISMA 358 based on the relatively high presence of *Q. lata* with minor amounts of *S. flintii, Q. semiulum* and *P. williamsoni*. Zone F1b was recognised from 235 - 170 cm with decreasing numbers of Q*. lata* contrasted with a continuing up-core increase in *S. flintii* and a peak in *L. interrupta* at 184 cm depth. *Q, seminulum* exhibited a continuing decrease in this zone.

Zone F2 was also recorded in ISMA 358 and, similarly, could be subdivided into F2a and F2b. Whilst *A. beccarii* still dominated at almost 70% relative abundance, F2a as noted from 170 - 139 cm by the increase in *S. flintii* of up to 15%. Zone F2b in ISMA 358 is also marked from 139 - 90 cm by an increase in *E. excavatum* and *A. pseudospiralis* which exhibits a peak at 95 cm depth. *B. maginata* is also present throughout this section at levels less than 5%.

Zone F3 encompasses from 90 cm to the top of the again and is, again, defined by a continued increase in *E. excavatum*, a strong presence of *A. pseudospiralis* and a marked decrease in levels of *S. flintii* and *T. aggluntinans*. In this section, *P. mediterranensis* also exhibits a marked increase, as does *T. agglutinans*. P*. mediterranenis, Q. lata* and *B. marginata* showed a continued presence with the former decreasing towards the top of the core from 6% to <2%.

Strong similarities in these species trends facilitated the correlation of ISMA 359 with ISMA 358 and in substantiating the palaeoenvironmental record.

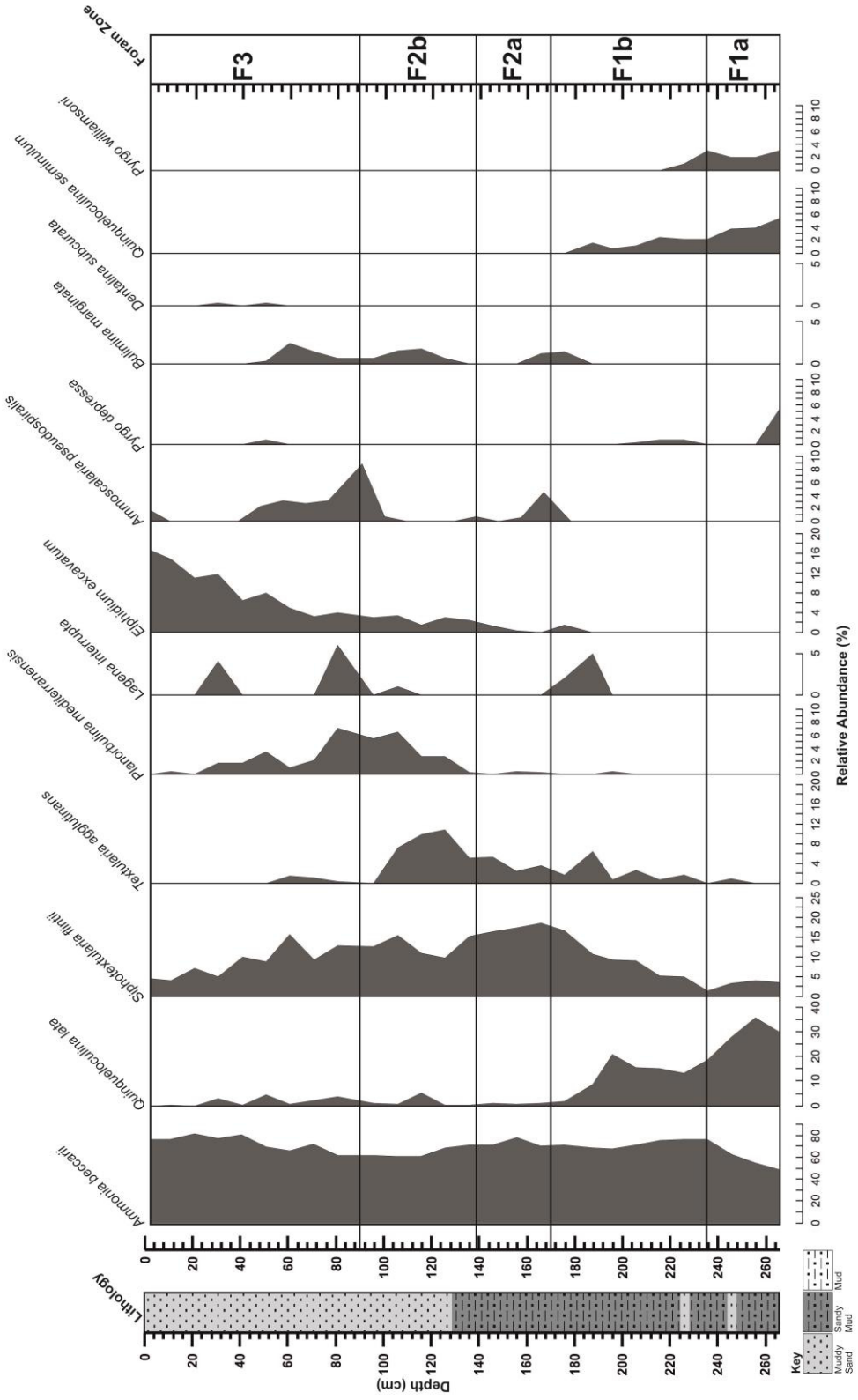

Figure 4.7 Foraminiferal analyses for ISMA 358. Similar to Figure 4.6, on the left is a core log with derived lithologies. Elsewhere is presented percentage relative abundance of selected major taxa with foraminiferal zonation (see section 4.4.4.4 for explanation).

4.4.5 Core Grain-size, Geochemical and Physical Properties

4.4.5.1 Basic Grain-Size Parameters

Overall the particle-size distributions for the three cores studied can be described as poorly to very poorly sorted with values ranging from 3.36 - 5.52 with an average of 4.8 for ISMA 358, 3.88 - 5.36 with an average of 4.7 for ISMA 359 and 4.47 - 5.28 with an average of 4.9 for ISMA 418 (Fig. 4.8 – 4.10). Similarly all cores were dominated by silt to fine sand material. Mean and modal grain-size was also investigated to assess major grain-size variations along with clay, silt and sand percentages (Fig. 4.8 – 4.10). For ISMA 358, individual samples are very poorly sorted exhibiting a uni-modal distribution for the upper 134 cm roughly and a dominance of tri-modal peaks in samples thereafter until the base of the core (Fig. 4.8). This coincides with a change from more sand dominated sediment distribution in the upper part (up to 75%) to a mud (percentage clay and silt) dominant base. Within this upper 134 cm section, modal values show a stepped decrease from 147 µm to 134 µm at 28 cm depth with a further decrease to values of 122 and 111.1 µm at 84 cm. Mean grain-size values also show an overall decrease from 74 µm at the top to 22 µm at the 134 cm mark. From 134 cm to the base of the core modal values show more variability fluctuating between 84 and 111 µm with mean values generally between 13 and 30 µm.

Grain-size samples for ISMA 359 display a variance in uni-, bi-, tri- and poly-modal peaks in the upper 115 cm before a dominance in tri-modal distribution for the lower portion (Fig. 4.9). This coincides with a shift towards a dominance of mud which reaches almost 100% at the base of the core. A similar trend to ISMA 358 is seen with consistent modal values of 111.1 µm and 121.94 µm until a step decrease at 81 cm to values of 101.2 µm and 92.2 µm until 115 cm depth. Mean grain-size for this section exhibits more variability with values between 24 and 42 µm in the uppermost 88 cm before decreasing to between 21 and 25 µm until 115 cm depth. From 115 cm until the end of the core exhibit a continued overall decrease with modal values between 83.98 - 27.42 µm and mean values from 19.6 - 7.04 µm.

ISMA 418 is dominantly sandy mud throughout with individual samples displaying a very poorly sorted bi- and tri-modal distribution (Fig. 4.10). Mean grain-size varies between 17 and 34 µm with no significant increase or decrease downcore. Modal grain-size also remains relatively consistent at 111.1 µm until 130 cm where there is a slight overall decrease to values of 101.21, 92.2 and 84 µm until the end of the core. The sand content remains relatively constant throughout between 30 - 50% and showing a slight decrease downcore.

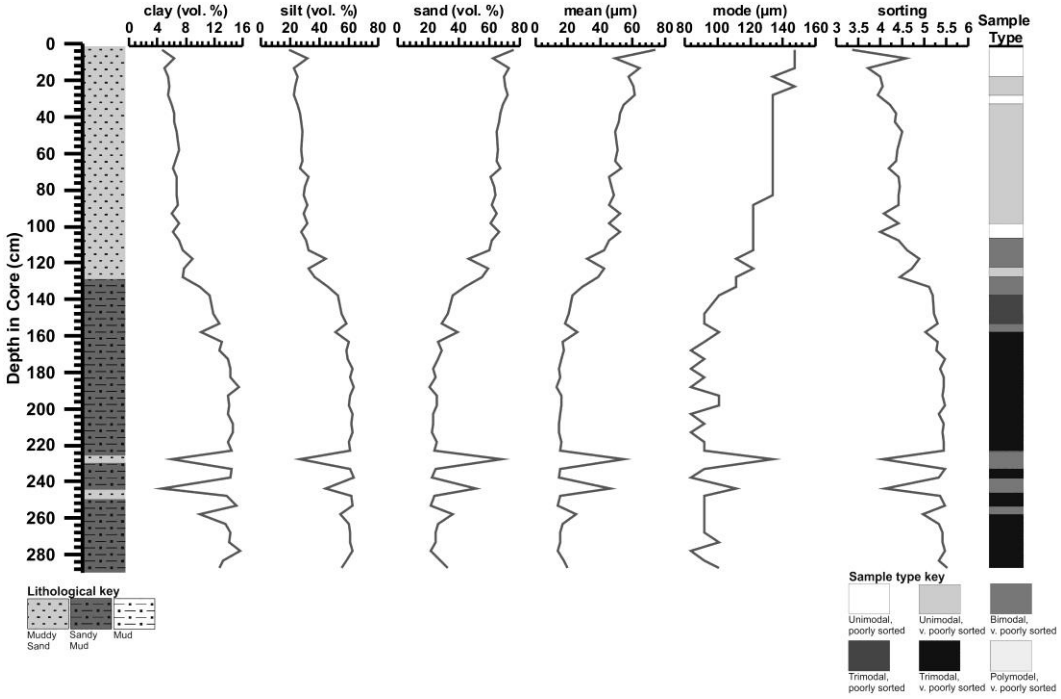

Figure 4.8 ISMA 358 particle-size results. Displayed are downcore variations of basic particle-size parameters. Clay (<2 µm), silt (2-63 µm) and sand (>63 µm) size fractions in volume % (vol. %). All measurements are depth in core in centimetres. Downcore mean and modal grain-size are also presented (both in µm) along with sorting. Sorting values are between poor and very poor. To the left is a core log showing sediment type according to Folk and Ward (1957) and to the right is a sample type log indicating sorting and peak modality (see section 4.4.5.1 for explanation).

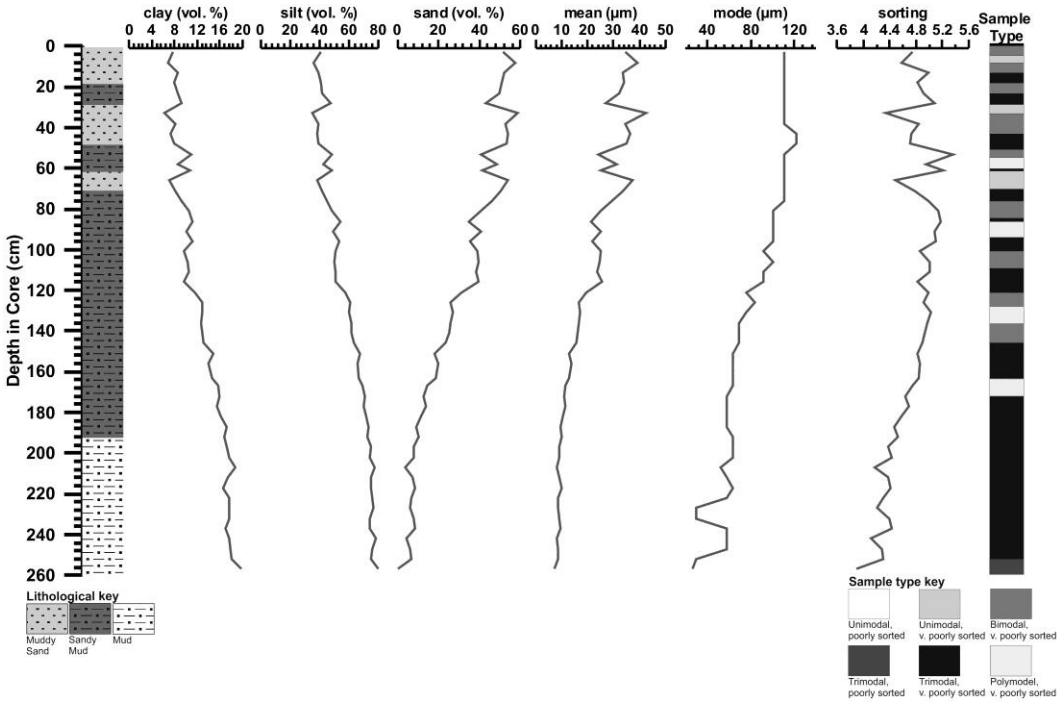

Figure 4.9 ISMA 359 particle-size results. Displayed are downcore variations of basic particle-size parameters. Clay (<2 µm), silt (2-63 µm) and sand (>63 µm) size fractions in volume % (vol. %). All measurements are depth in core in centimetres. Downcore mean and modal grain-size are also presented (both in µm) along with sorting. Sorting values are between poor and very poor. To the left is a core log showing sediment type according to Folk and Ward (1957) and to the right is a sample type log indicating sorting and peak modality (see section 4.4.5.1 for explanation).

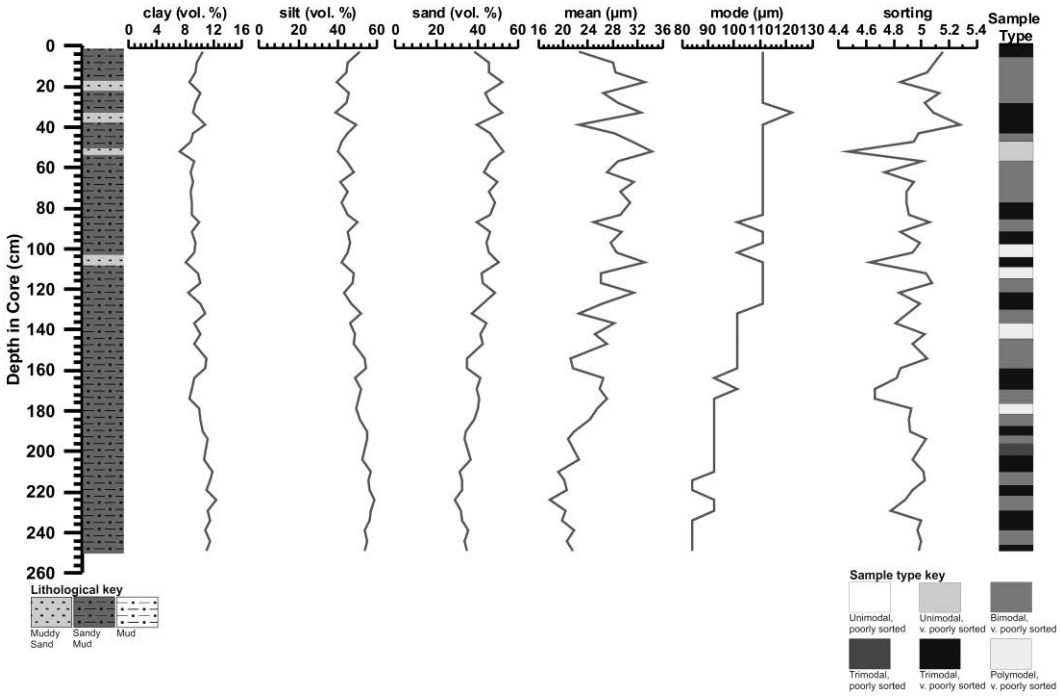

Figure 4.10 ISMA 418 particle-size results. Displayed are downcore variations of basic particle-size parameters. Clay (<2 µm), silt (2-63 µm) and sand (>63 µm) size fractions in volume % (vol. %). All measurements are depth in core in centimetres. Downcore mean and modal grain-size are also presented (both in µm) along with sorting. Sorting values are between poor and very poor. To the left is a core log showing sediment type according to Folk and Ward (1957) and to the right is a sample type log indicating sorting and peak modality (see section 4.4.5.1 for explanation).

4.4.5.2 Lithological Sub-Division

Stratigraphic division of the cores was made possible by using discrete grain-size parameters, geochemical, physical and foraminiferal data (see Fig. 4.11, 4.12 & 4.13). McCave et al. (1995) recognised the sortable silt mean ($\overline{SS}$) of the terrigenous fraction to be a sound proxy for relative bottom current velocity, even in shallow marine environments (McCave et al., 2006). In this study the $\overline{SS}$ of the bulk sortable silt fraction was used as there was no significant difference between it and the carbonate-free, terrigenous fraction. The coarse fraction (>63 µm) was used to investigate increased intensity of bottom currents generally over time or as a result of high energy events (e.g. storms) and is shown in Figures 4.11 – 4.13.

Magnetic susceptibility (MS) values provide evidence of changes in sediment provenance (Richter et al., 2001; Pérez-Cruz and Urrutia-Fucugauchi, 2009). The uniform nature of MS values suggests

a similar geological provenance of the sediment for all cores studied (Fig. 4.11 – 4.13). Measurements are reported as 10^{-5} SI units.

Fe, Ti and K-intensities are linked to siliclastic components and so variations in these elements reflect the contribution of terrestrial material. In contrast, Ca-intensities reflect biogenic and/or authigenic precipitated carbonate. Hence, ratios between the two sets of elements can act as a representative indicator highlighting variations in the relative riverine input and carbonate sedimentation (Bahr et al., 2005). All ratios (Fe, Ti and K with Ca) showed a similar trend. However, since Ti is inert against diagenetic alterations, Ti/Ca ratio was used as a proxy for riverine input along with MS (see Fig. 4.11 – 4.13).

Based on similarities between these proxies and grain-size distributions, it was possible to discern three lithostratigraphic (LS) units that show a strong correlation with foram zones.

4.4.5.2.1 LS Unit 1

LS Unit 1 was only found in cores ISMA 358 and ISMA 359. In ISMA 358 it encompasses from the base of the core to 170 cm approximately (Fig. 4.11). The mean $\overline{SS}$ value for this unit in ISMA 358 was 27 µm, with peaks of 30 µm at 224, 242 and 258 cm. Similar peaks at the same horizons were found in the >63 µm fraction which shows an average value of approximately 22%. Values for MS fluctuated between 12 and 17 10^{-5} SI units with a general decrease towards the top of the unit. The Ti/Ca ratio from the base of the section to the top displays an overall increase with values between 0.11 and 0.14.

In ISMA 359, LS Unit 1 began at the base of the core to 150 cm depth approximately (Fig. 4.12). The average $\overline{SS}$ value was also 27 µm, showing an increase towards the top of the unit from 188 cm upward with values up to 30 µm. The >63 µm fraction ranged from 0% at the base to 15% at the top. MS values similarly fluctuated throughout this unit, generally between 12 and 17 10^{-5} SI units. Ti/Ca ratios also show a close affinity with those in LS Unit 1 of ISMA 358 with values ranging from 0.11 to 0.14. However, in the case of ISMA 359, from approximately 192 cm to the top of the unit values generally decrease.

4.4.5.2.2 LS Unit 2

In ISMA 358, LS Unit 2 begins at 170 cm approximately and extends up-core until 90 cm depth (Fig. 4.11). The base of this unit sees a continual increase from 27 µm to peak near 34 µm at the top of the unit for $\overline{SS}$ values. The >63 µm fraction also continuously increases from 20 to 65%. MS values show further fluctuation in this unit, but with lower values of 6 to 15 10^{-5} SI units, generally decreasing towards the top of the unit. The Ti/Ca ratio exhibits a sharp decline from 0.14 at the base to 0.08 at the top of the unit.

LS Unit 2 manifests itself in ISMA 359 from 150 to 80 cm (Fig. 4.12). Similar to in ISMA 358, $\overline{SS}$ values increase from 29 µm at the base to a peak at 120 cm of 33 µm, decreasing thereafter to around 30 µm near the top of the unit. The >63 µm fraction continues to increase in this section with a gradual increase from 150 cm to 124 cm where a step increase occurs from 25 to 40% with values staying around 40% to the top of the section here. A similar trend in MS and Ti/Ca ratios can also be seen in Section 2 of ISMA 359 with a decrease in the range of MS values from 8 to 15 10^{-5} SI units with a notable decrease at 136 cm. The Ti/Ca ration also decreases over the course of this unit from 0.12 to 0.08 at the top.

Section 2 comprises from the base of ISMA 418 to 90 cm depth (Fig. 4.13). The $\overline{SS}$ in this unit for ISMA 418 is generally coarser than ISMA 358 or ISMA 359 showing a more pronounced fluctuation between 31 to 34 µm and no obvious overall increase or decrease. The >63 µm displayed an overall increase from 27% at the base to close to 50% at the top. For the lower part of this unit (260 - 200 cm) MS values vary but with an average of 4 10^{-5} SI units. Towards the top of the unit, values fluctuate greatly from 0 to 12 10^{-5} SI units, but at 116 cm show greater consistency with an average value of 10 thereafter. The Ti/Ca ratio shows less dramatic variation with an average value of 0.08 for the entirety of the unit.

4.4.5.2.3 LS Unit 3

The base of LS Unit 3 in ISMA 358 is marked by a gradual decrease in $\overline{SS}$ values from 32 to 30 µm at 50 cm (Fig. 4.11). Values, on average, stay at 30 µm until the top of the unit. The percentage of the >63 µm fraction continues to gradually increase from 60% at the base to 75% at the top. MS values continue to fluctuate around an average of 10 10^{-5} SI units. The decrease in the Ti/Ca ratio halts at the base of this unit and only shows minor fluctuation thereafter between 0.04 and 0.07.

By contrast the base of LS Unit 3 in ISMA 359 is marked by an increase in $\overline{SS}$ with peaks of up to 33 µm at 66, 46 and 32 cm (Fig. 4.12). The percentage of the >63 µm fraction also continues to increase and maintains levels above 40% for the first time in the core. MS values show a consistency of around 11 10^{-5} SI units to the top of the core. The Ti/Ca ratio shows an initial increase from the base from 0.08 to 0.10 until approximately 40 cm. Values then decrease to 0.06 at the top of the core.

Values for $\overline{SS}$ in LS Unit 3 of ISMA 418 continue to fluctuate between 30 and 33 µm. Fluctuation is also observed in the >63 µm where values range from 40 to 55%. The base of LS Unit 3 at 90 cm is marked by an increase in MS values from 12 to 15 10^{-5} SI units at the top. The Ti/Ca ratio also exhibits a general increase with greater fluctuating in values between 0.07 and 0.12.

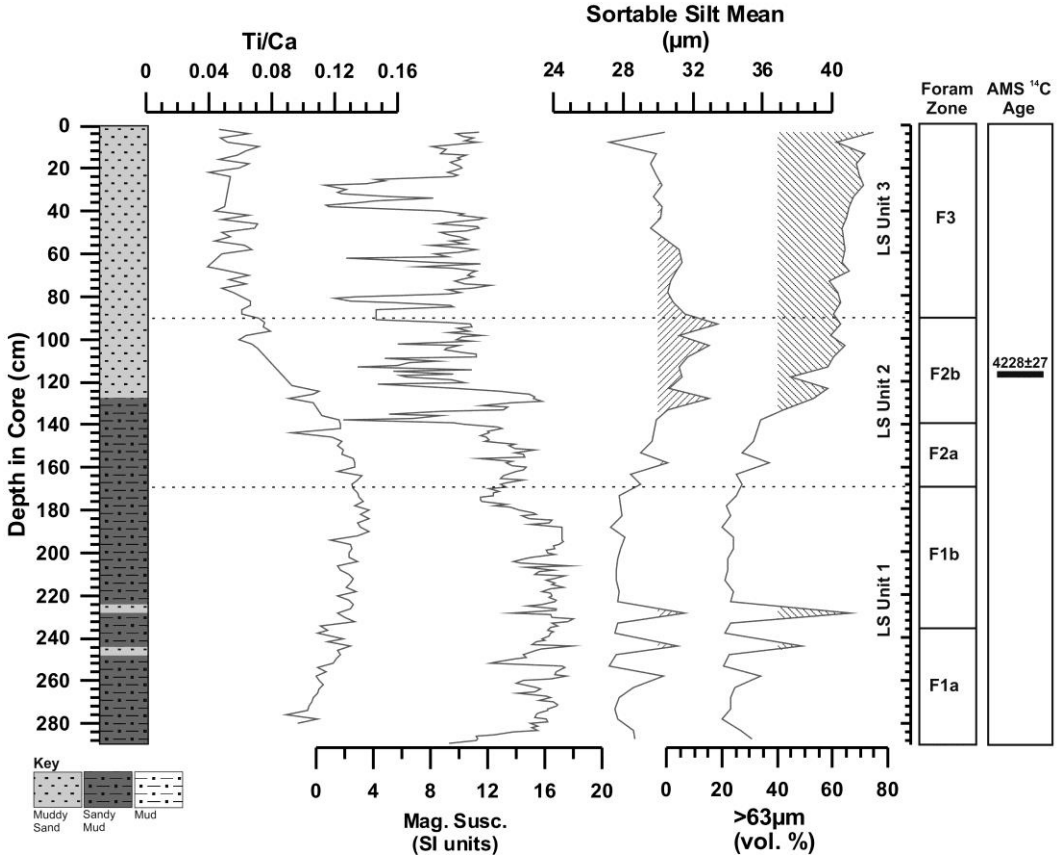

Figure 4.11 Lithological sub-division of ISMA 358. Presented is downcore data for Ti/Ca ratio, magnetic susceptibility (Mag. Susc. in 10^{-5} SI units), sortable silt mean (mean of the 10-63 µm fraction) and the >63 µm fraction (in volume %). Explanations for each proxy are given in section 4.5.2. Hatching on the sortable silt mean trend highlights values >30 µm. Similarly, hatching on >63 µm fraction highlights >40% volume. Dash lines highlight the division of the core in three Lithological (LS) Units explained in section 4.4.5.2. Beside this are foraminiferal zones for the same core and a singular AMS ^{14}C date showing cal. years BP with error.

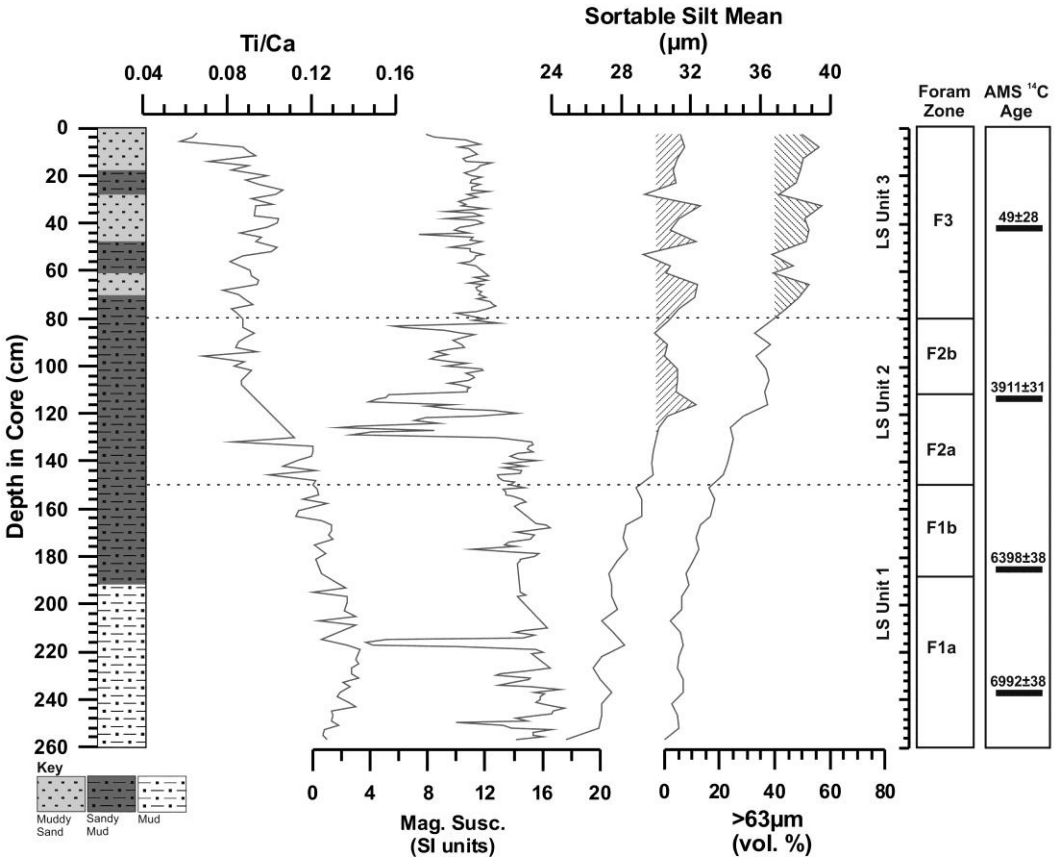

Figure 4.12 Lithological sub-division of ISMA 359. Presented is downcore data for Ti/Ca ratio, magnetic susceptibility (Mag. Susc. in 10^{-5} SI units), sortable silt mean (mean of the 10-63 µm fraction) and the >63 µm fraction (in volume %). Explanations for each proxy are given in section 4.4.5.2. Hatching on the sortable silt mean trend highlights values >30 µm. Similarly, hatching on >63 µm fraction highlights >40% volume. Dash lines highlight the division of the core in three Lithological (LS) Units explained in section 4.5.2. Beside this are foraminiferal zones for the same core with four AMS ^{14}C date showing cal. years BP with error.

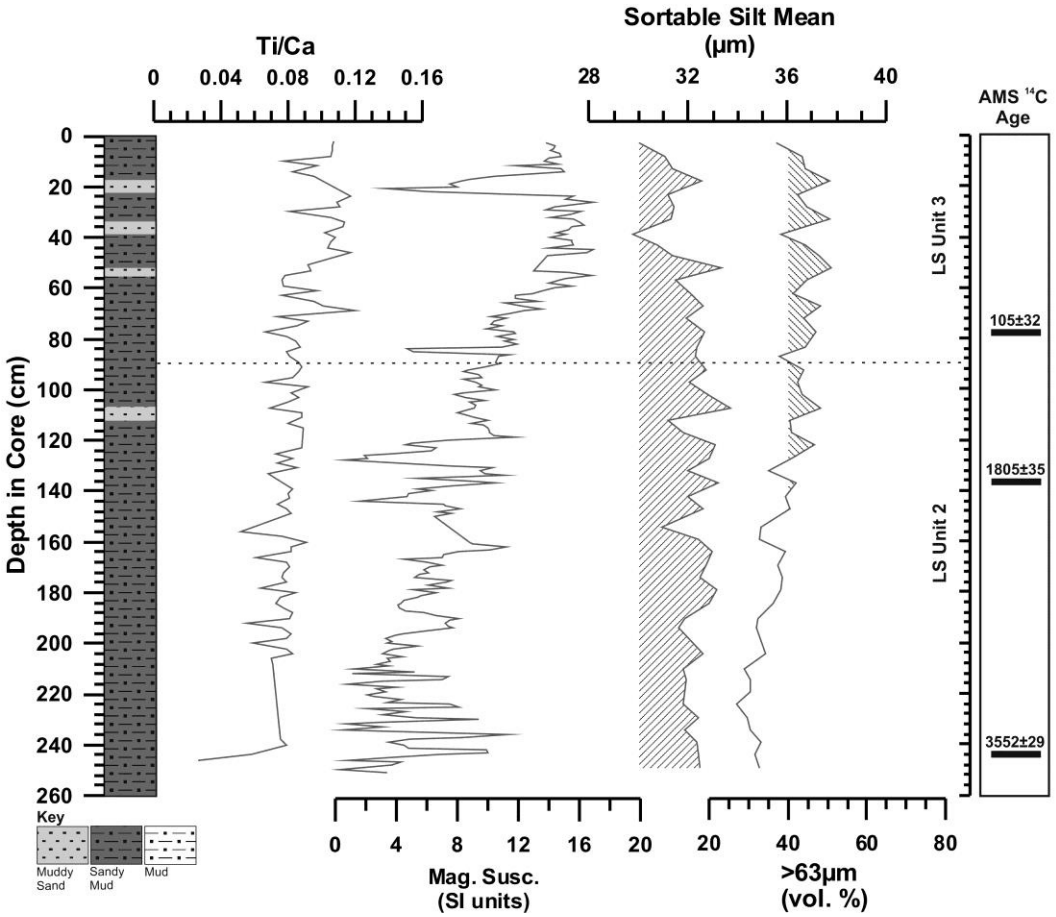

Figure 4.13 Lithological sub-division of ISMA 359. Presented is downcore data for Ti/Ca ratio, magnetic susceptibility (Mag. Susc. in 10^{-5} SI units), sortable silt mean (mean of the 10-63 µm fraction) and the >63 µm fraction (in volume %). Explanations for each proxy are given in section 4.4.5.2. Hatching on the sortable silt mean trend highlights values >30 µm. Similarly, hatching on >63 µm fraction highlights >40% volume. Dash lines highlight the division of the core in two Lithological (LS) Units explained in section 4.5.2. No foraminiferal analyses was performed on this core. Beside the lithological division are three AMS ^{14}C date showing cal. years BP with error.

4.4.6 Age Model

The age models for cores ISMA 359 and ISMA 418 (Fig. 4.14 and 4.15 respectively) was based on AMS ^{14}C dating as well as ^{210}Pb and ^{137}Cs analysis by way of gamma spectrometry. A further isolated AMS ^{14}C date was carried out on ISMA 358 to aid in chronology correlation (Table 4.2).

Core	Depth (cm)	Raw ^{14}C Age BP	±	Calibrated Age Years BP	AMS $\delta^{13}C$	$F^{14}C$	±
ISMA 359	42	449	28	49	-0.8	0.9457	0.0033
ISMA 359	65	4982	34	5308	0.4	0.5379	0.0023
ISMA 359	113	3936	31	3911	5.5	0.6126	0.0024
ISMA 359	185	5997	38	6398	-2.4	0.474	0.0022
ISMA 359	237	6502	38	6992	-3.3	0.4451	0.0021
ISMA 358	116	4153	27	4228	3.7	0.5964	0.002
ISMA 418	77.5	489	32	105	2.6	0.941	0.0037
ISMA 418	136	2190	35	1805	-2.4	0.7614	0.0033
ISMA 418	207	3719	27	3630	4.5	0.6294	0.0021
ISMA 418	244	3651	29	3552	3.4	0.6348	0.0023

Table 4.2 Tabulated data for AMS ^{14}C results.

Average sedimentation rates were deduced from ^{14}C dating by plotting calibrated ages with sediment depth, assuming a linear trend between points. In truth, more discrete changes in the sedimentation rate most likely occur between dated points given the relatively low resolution of sampling. Profiles were regressed using a linear regression fit in order to calculate mean rates for the whole core in each instance. According to the AMS ^{14}C dates, both cores can be divided into a high sedimentation upper part and a lower sedimentation lower part. Despite one instance in each core of 'older' material overlying younger, there is a net downcore increase in ^{14}C ages suggesting that the sediment columns in both instances are accretionary. For core ISMA 359 (Fig. 4.14) in particular, the bottom three dates align to produce a constant sedimentation of 0.03 cm a^{-1} before a jump occurs in the upper 40 cm indicating an increased sedimentation rate of 0.86 cm a^{-1}. According to the dates, the upper 40 cm is inferred to have been deposited within the last 80 years or so. The lack of age constraint on the upper most section can be explained by the lack of potentially datable material. Whilst *T. communis* was relatively abundant in the lower section there is a notable decrease towards the surface. Dating of the bulk carbonate fraction was not considered due to the potential effect of physical reworking by bioturbation in the area highlighted as by Kershaw (1986) and seen on our own CT X-ray images. A similar paucity of *T. communis* was recorded in ISMA 418, however, a possible age of 105 ± 38 years was recorded in the upper 80 cm to give a sedimentation rate of approximately 0.74 cm a^{-1}, whilst the lower dates lined up to give rates of 0.08 and 0.07 cm a^{-1} over the last 3,600 years BP (Fig. 4.15).

Downcore profiles for ^{137}Cs show remarkable similarities in both cores and also correlate with a similar core from the area studied by Mitchell et al. (1999). Both cores show an observed peak at ~20 cm depth before decreasing downcore to negligible levels at between 80 - 120 cm (Fig. 4.14 and 4.15). ^{137}Cs is an anthropogenic radionuclide produced by nuclear reaction and so its first appearance in the natural environment began with nuclear armaments testing in the early 1950s. Introduction of ^{137}Cs directly into the Irish Sea from Sellafield related discharge began with operations at the plant in 1951 with maximum discharge of ^{137}Cs peaking in 1978 and has been in decline since (Gray et al., 1995). Assuming the subsurface peak at 20 cm corresponds to this event and the first instance of ^{137}Cs corresponds to initial nuclear testing, we can hence derive a two-part sedimentation rate from our profile. Whilst the rates differ from the AMS ^{14}C dates, they do support the idea of a generally higher sedimentation rate in the upper portion of both cores. Taking the top of the cores as representing 2009, we can calculate average sedimentation rates of 2.1 cm a^{-1} and 2.7 cm a^{-1} for the 1952-1978 interval of cores ISMA418 and ISMA359, respectively, and 0.8 cm a^{-1} and 1.0 cm a^{-1} for the 1978-2009 interval. Here, we see an obvious discrepancy between the two intervals with a decrease in sedimentation inferred for the last 30 years or so. However, ^{137}Cs is highly mobile and subjective to the influence of bioturbation. Even so, if we assume that the first occurrence of ^{137}Cs has been shifted downwards by 20 cm (the typical burrowing depth of *Nephrops norvegicus*) we still calculate average sedimentation rates of 1.3 cm a^{-1} and 1.9 cm a^{-1} for the 1952-1978 interval of cores ISMA 418 and ISMA 359, respectively, higher than the average rates calculated for the upper part of the cores.

The activity of ^{210}Pb was also measured by way of gamma spectrometry in the upper 120 cm in both cores and was shown to generally decrease downcore (Fig. 4.14 and 4.15). Interestingly, levels of excess ^{210}Pb at the top of both cores has a considerably lower activity than the levels reported from surface sediments from the same area by Mitchell et al. (1999). Whilst the top of the profiles seem to be missing and the remainder appearing quite jagged, fitting of the observed ^{210}Pb curves with a conventional exponential model yields average sedimentation rates of 2.0 cm a^{-1} and 2.4 cm a^{-1} for cores ISMA418 and ISMA359, respectively (Fig. 4.14 and 4.15). This is similar to the average rates obtained from the ^{137}Cs profiles for the 1952-1978 interval.

The change in sedimentation regime can be explained by two potential scenarios. The first is gradual or stepwise decrease in sedimentation rate with deposition continuing until present, or secondly cessation of net deposition around early 1990s. Evidence from radionuclide profiles would support the latter given the top of the excess ^{210}Pb profile is essentially missing. In addition, there is the considerable ^{137}Cs activity at the top of both cores more akin to a level typical of the mid 1980s than for any later date especially when considering ^{137}Cs discharge from Sellafield and concentration in Irish Sea waters has shown an almost complete reduction of ^{137}Cs from the late 1980s onwards (Mitchell et al., 1999; Charlesworth et al., 2006).

In terms of establishing an age model, the integration of radionuclide based and AMS ^{14}C dated chronologies can prove quite difficult. However, in this instance, both methods reflected the same marked changes in sedimentation for the upper portion. Whilst AMS ^{14}C was useful for dating throughout the core, gamma spectrometry was instrumental in refining changes in the upper portion where a more dominant anthropogenic signal is seen. A full account of radionuclide profiles, their interpretation and relation to anthropogenic impacts may be found in chapter 5.

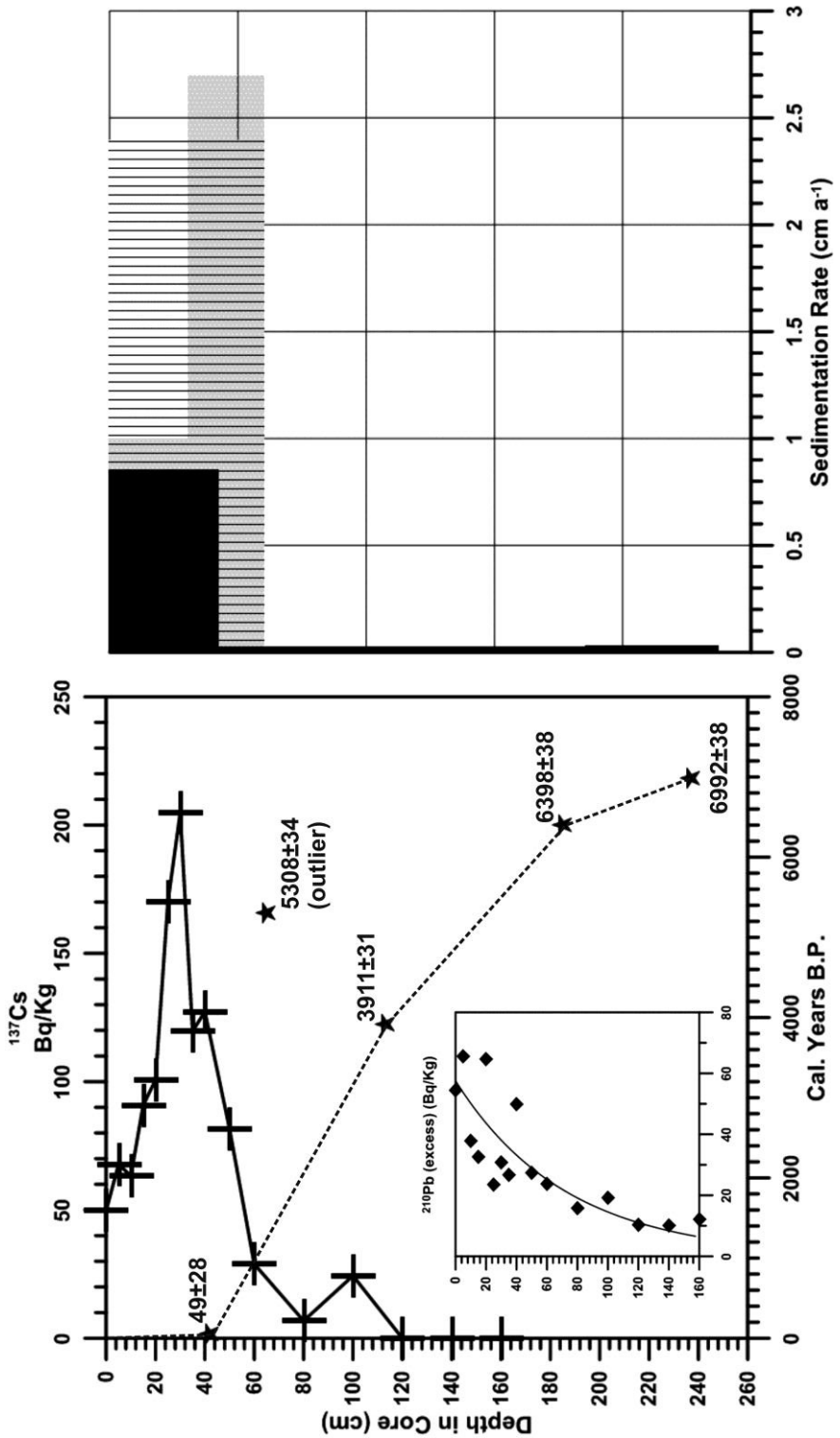

Figure 4.14 Age model for ISMA 359. Left panel: closed stars represented AMS ^{14}C dated samples of the gastropod *T. communis* with dates in calibrated years BP with error. One dated sample was noted to be an outlier due to its position at the edge of the core, most likely due to smearing during the coring process. The upper graph represents measured ^{137}Cs levels with crosses marking sample points in the core. The inset graph here displays ^{210}Pb levels with an exponential model fit applied. Right panel: derived sedimentation rates (in cm a^{-1}) for AMS ^{14}C (solid black, based on linear interpolation), ^{137}Cs (grey cross hatch) and ^{210}Pb (vertical stripe hatch). See section 4.4.6 for full explanation.

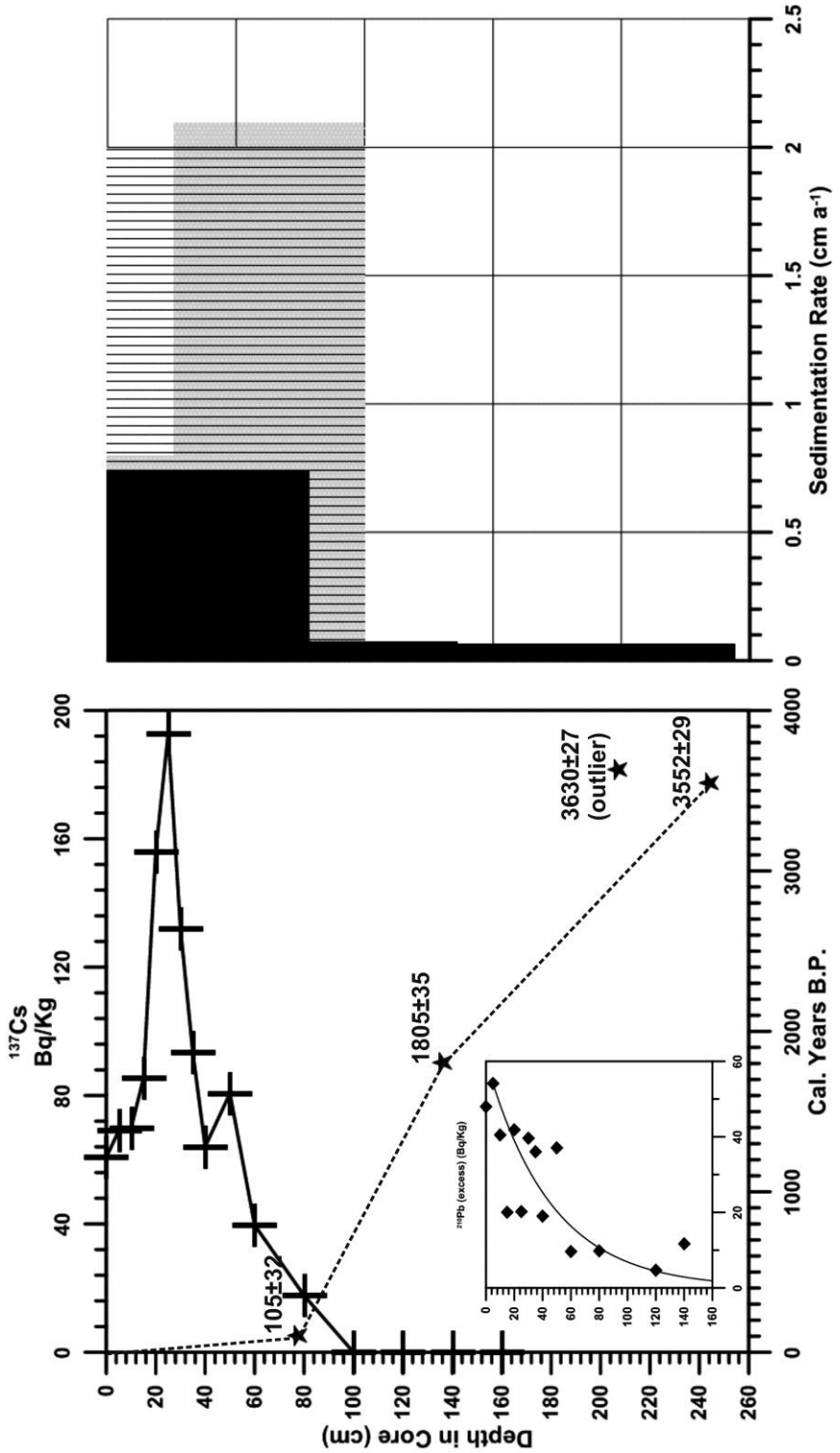

Figure 4.15 Age model for ISMA 418. Left panel: closed stars represented AMS ^{14}C dated samples of the gastropod *T. communis* with dates in calibrated years BP with error against core depth. One dated sample was noted to be an outlier due to its position at the edge of the core, most likely due to smearing during the coring process. The upper graph represents measured ^{137}Cs levels with crosses marking sample points in the core. The inset graph here displays ^{210}Pb levels with an exponential model fit applied. Right panel: derived sedimentation rates (in cm a^{-1}) for AMS ^{14}C (solid black, based on linear interpolation), ^{137}Cs (grey cross hatch) and ^{210}Pb (vertical stripe hatch). See section 4.4.6 for full explanation.

4.4.7 Core Correlation

The WISMB is a relatively low energy environment, predominately one of deposition and perceived to be a potential palaeo-archive. Therefore, an important question is to what extent is the record present throughout the area and is it coherent from location to location?

All cores showed a homogenous, silty sequence with no distinguishable changes in colour or other visual interpretation other than abundance of macrofauna, most notably *T .communis*. These distinctive layers abundant in *T. communis* occurred within cores ISMA 358, ISMA 359 and ISMA 418 at depths of 116 cm, 113 cm and 207 cm respectively which were subsequently dated using ^{14}C in order to help constrain the age model. It was shown that they exhibited ages which fell within a close range (Table 4.2 and Fig. 4.16.).

Initial correlation was performed using MSCL data and in particular gamma-ray attenuation measurements which correspond to density and, hence, may highlight discrete lithological changes. Nine-point running averages were applied to the data which displayed variations between 1.8 and 2.2 g cc^{-3} and allowed for an easier correlation (Fig. 4.16). Whilst this initial correlation using gamma density values proved to be tentative, it was only through further particle-size, geochemical and other physical property analyses outlined above in section 4.4.4 and 4.4.5 that a more robust correlation was made. The depth constraints of the three lithological sections in each core, and correlation between cores, are presented in Figure 4.16.

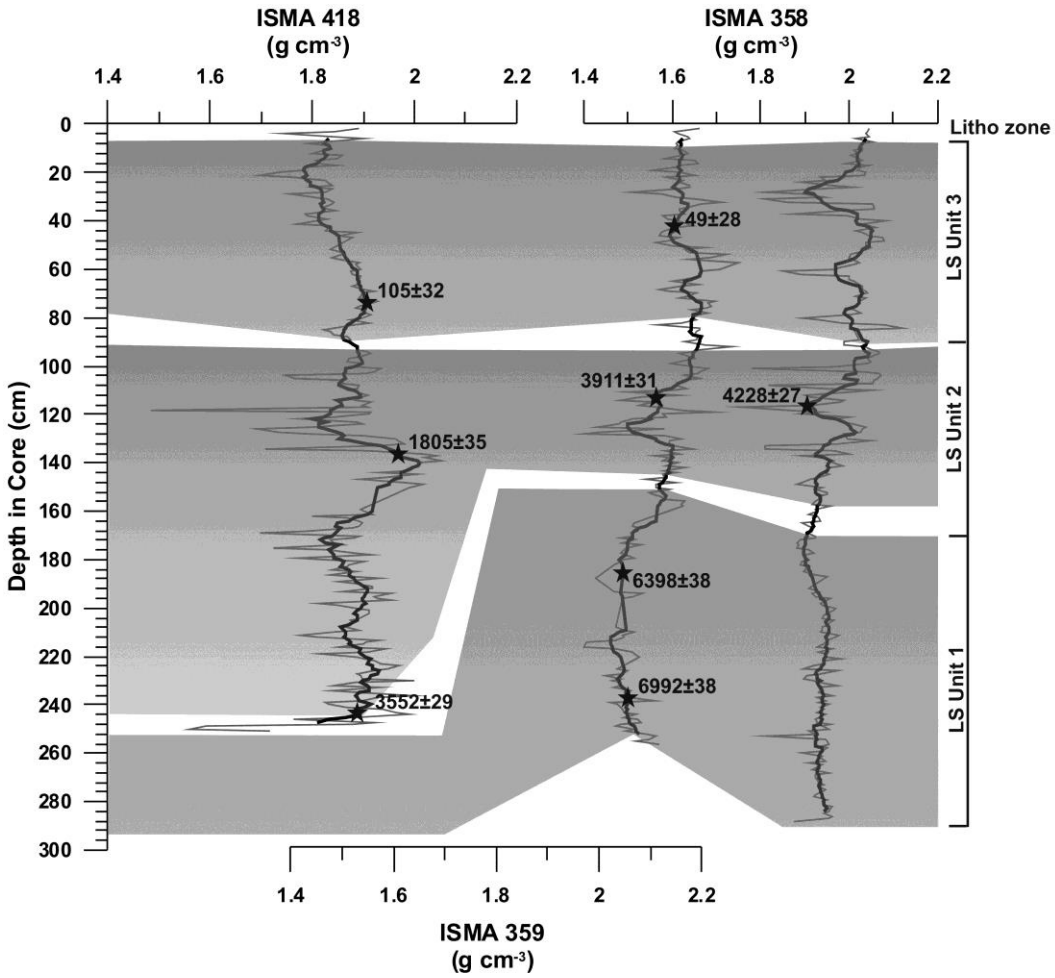

Figure 4.16 Core Correlation. MSCL derived density values (in g cm^{-3}) are presented and were used in an initial correlation. Also plotted are AMS ^{14}C ages versus depth in core with lithological section depths from section 4.5.2 superimposed to complete the correlation. See section 4.4.7 for explanation.

4.5. DISCUSSION

4.5.1 Lithostratigraphy

Gamma density values show little correlation with lithostratigraphic units and so are believed to better express variations in the deposition rate. Lithological sections in ISMA 358 and ISMA 359 showed a strong correlation in both nature of proxy trends and depth. However, such a definite correlation between these two cores and ISMA 418 could not be made and was hampered by dating constraints. Thus, it appears that whilst sediments of the WISMB as a whole represent a

coherent and relatively long depositional history which is largely correlatable across the area, individual cores can be subject to localised variations in processes which impact on the succession.

From the age model, the studied cores are believed to represent the last ca. 7 ka of depositional history in the WISMB with proxy records revealing a distinct variation in sedimentary conditions. Ultimately, the investigated cores can be divided into two main parts: a high-sedimentation, predominately anthropogenic signalled period in the upper part and a lower sedimentation, environmentally driven lower part. Within this lower portion is a further sub-division into a stable lower section and fluctuating upper section. The characteristics of all three sections from ISMA 359 and ISMA 418 are presented below in Fig. 4.17 on a 7,000 cal. years BP scale. Proxy data for ISMA 358 is not included due to the lack of dating constraints from that particular core. In addition, distinctive climatic periods (including the Little Ice Age, Medieval Warm Period and Dark Ages Cold Period) noted in other proxy records in Ireland by Swindles et al. (2013) and McDermott et al. (2001) are superimposed to discern a possible climatic influence on changes in environmental conditions.

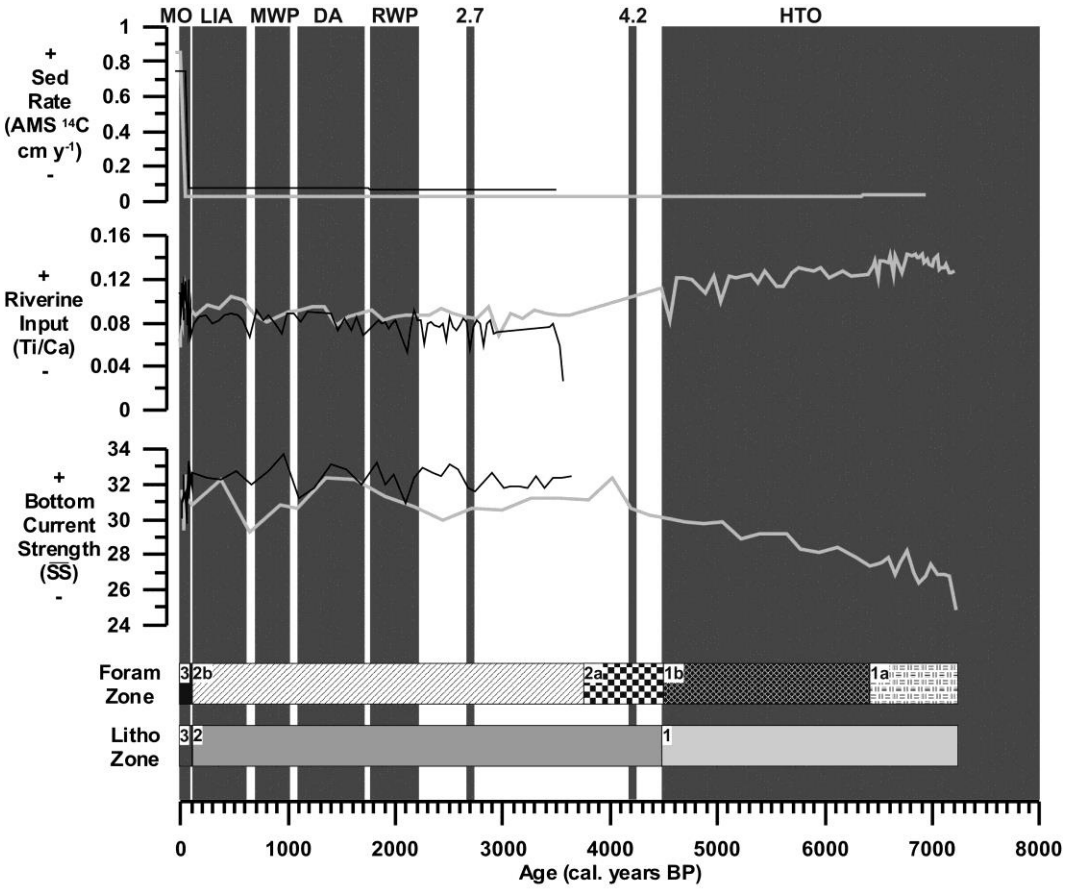

Figure 4.17 Diagram of the most important results and interpretations from this study. Results for bottom current strength ($\overline{SS}$), riverine input (Ti/Ca ratio) and sedimentation rate (derived from AMS ^{14}C) for ISMA 359 (solid grey line) and ISMA 418 (solid black line) are plotted against a calibrated timescale at the bottom. ISMA 358 was excluded due to lack of age constraint. Also included are corresponding litholostratigraphic units and foraminiferal zones explained in the text. Superimposed in grey blocks are notable climatic periods and events in the Holocene noted by Swindles et al. (2013) and McDermott et al. (2001) in Irish proxies. These include (from left to right, youngest to oldest) Modern Optimum (MO), Little Ice Age (LIA), Medieval Warm Period (MWP), Dark Ages Cold Period (DA), Roman Warm Period (RWP), the 2.7 ka event, the 4.2 ka event and the Holocene Thermal Optimum (HTO).

4.5.1.1 LS Unit 1: Stable Low Sedimentation Period at the Beginning of the Record (7,000 - 4,500 years BP)

The lowermost part of core ISMA 359 and ISMA 358 (>130 and 170 cm respectively; Fig. 4.8 and 4.9 respectively) consists of fine sediments that appear to have been deposited in a relatively low energy regime. Sedimentation rates for this unit are low, recorded at 0.03 cm a^{-1} for ISMA 359. Grain-size data reveal a subtle coarsening upward sequence from the base of the core. Similarly, $\overline{SS}$ exhibits a general increase from around 24 - 32 µm suggesting that whilst bottom currents

during this time were still relatively low, with time, they were beginning to increase up-core. The low bottom current interpretation is further support by the low sedimentation rate coupled with the generally low >63 µm fraction, which would suggest that winnowing was not taking place. This section of the core also shows the highest levels of sustained riverine input for the whole of both cores. It can be suggested that, from an environmental perspective, this was one of stable conditions with little storm related activity but perhaps sufficient precipitation leading to higher riverine input. However, the gradual increase in bottom currents and coarser material fraction increasing from 0 to between 20 and 40% suggests that these conditions were starting to change with time with increasing current speeds.

4.5.1.2 LS Unit 2: Fluctuating Middle Period (4,500 - 100 years BP)

The deterioration that marked the end of the lower unit is continued in the middle unit of ISMA 358 and ISMA 359 (90 - 170 and 80 - 130 cm respectively) and is also seen in core ISMA 418 (>90 cm depth). The most noticeable change in this part of the core is the considerable increase in energy, that appears to have begun around 3 - 4,000 years BP, and a shifted decrease in riverine input. Similarly, there is a noticeable decrease in the number of the macrofauna *T. communis*. Whilst $\overline{SS}$ varies in the middle section, overall it shows an increase with values ranging from 30-37 µm across the three cores. Discernible peaks are also noticeable in ISMA 359 at 116 cm and at 90 and 124 cm in ISMA 358 indicating alternate periods of relative high and low bottom current velocities. Coupled with the relatively low sedimentation rate (0.03 and 0.08 cm a^{-1} for ISMA 359 and ISMA 418 respectively) and the continued increase in the coarse fraction from 20 - 50 wt. % we can imply an increase in winnowing and the potential for erosional horizons and hiatuses in this section, although, there seems to be no physical manifestations in the core itself visible from linescans or CT X-ray images. Changes in all proxies and visible changes in core properties suggest the onset of a period of fluctuating environmental conditions.

4.5.1.3 LS Unit 3: High Sedimentation Upper Period (0 - 100 years BP)

This unit is best constrained chronologically due to the use of gamma spectrometry. The high sedimentation rate portion comprises the uppermost 0 - 90 cm approximately of each core, incorporating the last 100 years or so. This unit shows the highest sedimentation rates and contains the highest coarse fraction (>63 µm) of up to 70 wt. %. By contrast the $\overline{SS}$ shows an

overall slight decrease to between 27 - 38 µm across the three cores coinciding with an increase in the silt fraction. Ti/Ca and MS values are also higher compared to the preceding unit representing an increase in riverine input. CT X-ray images also reveal the most evidence for bioturbation in this section.

4.5.2 Depositional History and Inferred Environmental Forcing

Within the WISMB, bed stress conditions are the main control on sediment deposition. This bed stress is influenced by the interplay between water depth, tidal dynamics and solar heating resulting in stratification. Only two geologically reconstructed records of palaeostratification for north west Europe exist; the Celtic Sea (Austin and Scourse, 1997; Scourse et al., 2002) and Geordie Trough in the U.K North Sea (Evans et al., 2002). Stratification for the Celtic Sea was calculated at approx. 8,700 cal yr BP based on a mixing model, whilst at Geordie Trough it occurred later at approx. 5,800 cal yr BP. Given that sea level rise generally in NW Europe is believed to have ceased at approx. 6,700 cal yr BP (Lambeck, 1996), the difference in stratification at both sites was explained as a function of water depth with the deeper (118 m) Celtic Sea site stratifying earlier than the shallower (55 m) Geordie Trough site (Evans et al., 2002). In both sets of studies, the onset of stratification was defined using benthic foraminiferal assemblages supplemented by grain-size and stable isotopes as well as dating using AMS ^{14}C.

Analyses of benthic foraminiferal assemblages from this study were inconclusive in elucidating varying hydrographical conditions associated with the transition from mixed through frontal to stratified conditions as recorded by Austin and Scourse , 1997, Scourse et al. (2002) and Scott et al. (2003) in the Celtic Deep. Many of the key indicator species for the various assemblage types including *Stainforthia fusiformis, Cibicides lobatulus* and *Bulminia marginata* were either absent or occurred in relatively low numbers. This could be attributed to the fact that the >250 µm

fraction was used in the analyses as it had the most numerically abundant and well preserved foraminifera. However, species such as *Bulimina marginata* and *Stainforthia fusiformis* in particular are known to be <250 µm in size generally (Alve, 2003; Scott et al., 2003). Similarly, palaeotidal simulations by Uehara et al. (2006) suggest that the onset of stratification in the WISMB occurred between 10 - 9,000 cal yr BP with conditions similar to present fully developed by 7,000 cal yr BP at the latest (Fig. 4.18). Considering our record extends back 7,000 cal yr BP it is possible that it records deposition solely under stratified conditions.

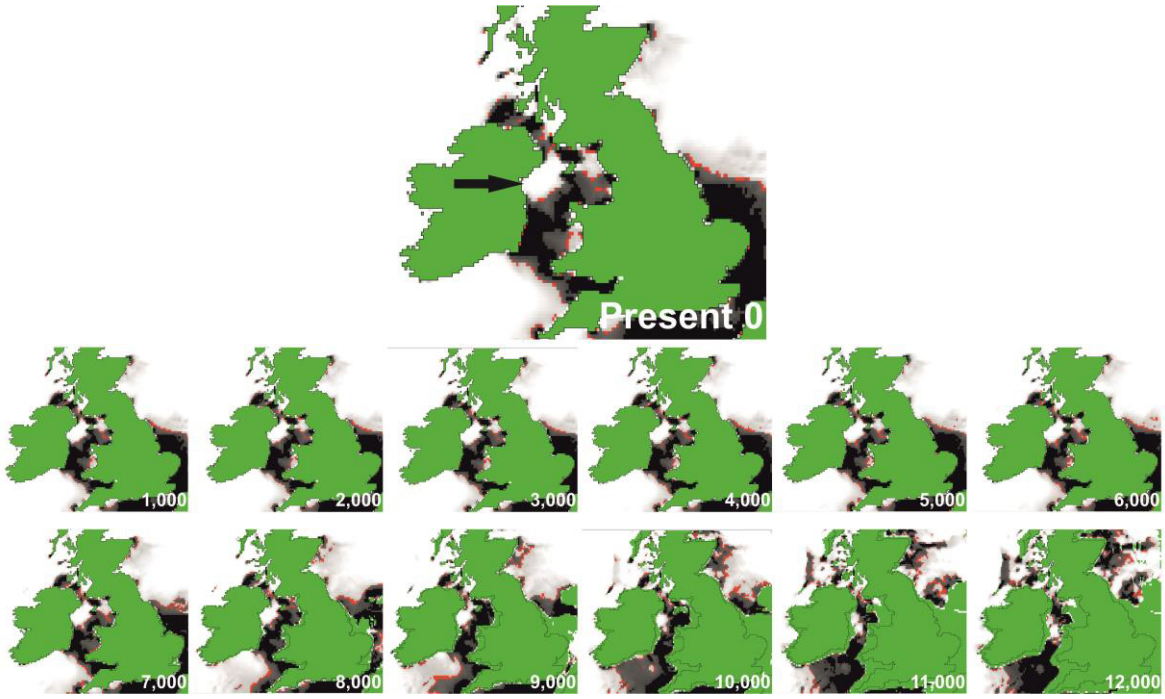

Figure 4.18 Stratification of the Irish Sea since the end of LGM. Time period in cal yr BP in the bottom right of each image with tidally mixed water in black, seasonally stratified water in white, frontal zones (tidal mixing fronts) in red. Top image shows position of study area indicated by black area within WISMB and stratification conditions at present.

However, there is still significant variation in all proxies represented by the various core sections and related time periods outlined above in section 4.5.1. To explain this fluctuation in environmental conditions, we attempt to develop the above section interpretations with reference to known climatic and environmental changes during the Holocene and test the fidelity of our record.

The beginning of the Holocene is marked with a distinct amelioration in climatic conditions referred to as the Holocene Thermal Optimum (HTO). The duration of this period varies upon geographic location but is generally considered to have lasted from 9,000 until 4,500 BP in Northern Europe with warm, stable conditions prevailing (Caseldine et al., 2006; Renssen et al., 2012). A significant deterioration in conditions occurred following the HTO around 5,000 yr BP, which also coincided with a significant period of human migration and a time when associated human activity would have had an impact on many proxy records (Kalis et al., 2003). It has been well documented in terrestrial records, particularly in elm populations and their dramatic decline during this period (Parker et al., 2002) as well as being linked with periods of extensive land clearance (Pilcher et al., 1971). The deterioration in conditions continued steadily until approximately 4,500 BP. This period also coincides with the proposed cessation of global sea level rise at 6,700 cal yr BP according to Lambeck (1996). Geological records on the Isle of Man suggest marine conditions between 8,700 and 8,200 cal yr BP with relative sea level rising from -3.86 m throughout the early Holocene up to a mid-Holocene maximum of +2.25 m between ca. 6,800 and 4,300 cal yr BP (Roberts et al., 2006). Similarly, in BGS borehole 89/15, ostracod assemblages for this time period suggest a sustained warm interval (Dickson and Whatley, 1993). This period of climatic stability and gradual cessation of sea level rise is well recorded in the core record as the low sedimentation of fine grained deposits unit at the base of ISMA 358 and ISMA 359 reflected in LS Unit 1. The high rates of riverine input coincide with related high periods of precipitation as a result of increased evaporation from the sea at this time (Langdon et al., 2012). This stability is also reflected in foram abundances where large populations of a few species seen in F1 (*A. beccarii*, *T. sagittula*, *T. aggluntinans* predominately). Foraminiferal data, in conjunction with greater numbers of macrofauna seen in this section, would suggest an increased organic load at this time which would promote such a low diversity as stronger competitors dominate. Similarly, the relatively high abundance of *Q. lata* (with peak at ~250 cm in ISMA 359) would point to increased bottom water salinity at this time.

The proceeding period is characterised by highly variable climatic conditions including two known times of glacial advances across Europe resulting in extensive cold periods referred to as the Dark Ages Cold Period (DA) and the Little Ice Age (LIA) (Grove, 1988). These cold periods were brought about by the advection southwards of polar fronts resulting in sustained periods of wintery

conditions with stronger wind forcing and increased storm activity (Lamb, 1977; Hass, 1993, 1996). Both these periods are recorded in a high-resolution spelothem and from troughs in bog oak numbers to have occurred from 1,700 - 1000 years BP and 600 - 100 years BP respectively (McDermott et al., 2001; Turney et al., 2006). In between these periods Europe witnessed more humid and warm conditions from 1,000 - 600 years BP ago known as the Medieval Warm Period (MWP) (Hughes and Diaz, 1994) as these polar fronts receded once more. In Ireland, this manifested itself as a peak in oak numbers which was witnessed around 800 years BP (Turney et al., 2006). Similarly from BGS bore hole 89/15, ostracod assemblage diversity shows a marked reduction during this period associated with the slow but oscillating decline to a cooler climate starting at around 5,000 BP (Dickson and Whatley, 1993). In an assessment of late Holocene palaeonvironmental history of the Skagerrak (North Sea) Hass (1996) concluded that variations associated with these well-established climatic periods were the main mechanism behind changes seen in particle-size distributions and stable oxygen isotope data. Hass (1996) was able to relate deposition of finer sediments with warm periods such as the MWP and Roman Climate Optimum (RWP) as a result of weaker currents due to less Atlantic water advection and less wind forcing. By contrast, coarser sediments were linked with extensive periods of cold such as the LIA and DA. LS Unit 2 is believed to represent this period of fluctuating conditions. Aside from the proxies investigated, the most noticeable, physical evidence from the data for this deterioration in conditions is the marked decrease in macrofauna, in particular, *T. communis*. Edwards et al. (1987) noted a similar decrease off the Scottish coast which he attributed to changing climatic conditions over the last 2 - 3000 years. Particle-size analysis reveals a noticeable shift towards a coarser $\overline{SS}$ in this section accompanied by an increase in the > 63 µm fraction. These changes in grain-size coincides with a decrease in Ti/Ca and MS values representing a sustained shift in sediment composition which reflects more localised change associated with the sediment source area, sediment transport pathways, riverine input or coastal erosion intensity. Values for $\overline{SS}$ vary throughout this unit but there is a mean increase in current velocities over time along with an overall coarsening in grain-size indicating a persistence of strong bottom current velocities this period. Such an increase would be expected during the LIA and DA with increased wind forcing due to stronger westerly winds, but would not be characteristic during such times as the MWP where lower current velocities would be expected. No geological data was available to constrain

the mid to late Holocene relative sea level (Roberts et al., 2006). Although, as mentioned, sea level rise is generally believed to have ceased by 6,700 cal ye BP (Lambeck, 1996) or 4,300 cal yr BP (Roberts et al., 2006) depending on modelled and geological data available. It may be the case that the strength of the dominant atmospheric forcing conditions during the LIA and DA only impacted slightly on bottom currents with the acting oceanic forces having a more consistent, regulatory effect. Variability in bottom conditions is also reflected in the species abundances of the foram record. Further evidence for a general increase in bottom current velocities in is seen in an increase of *P. mediterranensis* and *C. Lobatulus* in particular, which are both known to prefer to colonise in areas of strong bottom currents (Murray, 1971). Overall, species diversity is rich here. An increase in *E. excavatum* seen in F2b would indicate colder water temperatures associated with the LIA and the augmented unstable conditions it would have induced in bottom conditions with increased current speeds.

However, the low sedimentation rate for the middle and lower portion of the core derived from dating would suggest that the record here is likely incomplete, possibly due to periods of erosion associated with persistent higher bottom velocities during colder periods or periods of hiatus. In fact, Pantin (1978) described *T. communis* accumulations as lag deposits and evidence for erosion. Whilst we do see a general coarsening upwards in the core this can be explained by a number of climatic and environmental forcing factors. Similarly, there is no distinctive coarsening of material at the horizons where we retrieved our samples to be dated nor is there any physical evidence in the core or revealed by X-ray or line scanning. In addition, many of the *T. communis* shells throughout the core show little or no signs of abrasion as a result of transport. Another factor to consider in explaining the low sedimentation rate for the lower section of the cores is the effect of sediment compaction either by auto-compaction or even the coring method. Whilst the sediments appear to be normally consolidated, the effect of auto-compaction is well known to distort such data and may result in decreases in the apparent sedimentation rate of up to 60% (Scourse et al., 2002). This effect can be corrected for by measuring the liquid limit of the sediment to construct a porosity-depth profile and so show how a section of sediment would compact with increasing overburden with depth according to a sediment compression line (Burland, 1990; Skempton, 1969).

Conditions resembling modern day ones were established at roughly 100 years ago coinciding with the onset of the Modern Optimum (MO) (Schönwiese, 1988). The MO is generally considered to exhibit conditions similar to those found in the MWP (Hass, 1996). In this study LS Unit 3 is related to the MO based on AMS ^{14}C and gamma spectrometry dating and characterised by higher sedimentation rates, coarser sediments with continued fluctuation in the riverine input corresponding with an increase in Ti/Ca and MS values. The most striking feature of this time is the dramatic jump in sedimentation rate that was seen in both cores examined and identified by both AMS ^{14}C and radionuclide derived rates (Fig. 4.14, 4.15 and 4.17). This is most likely due to some degree of stratigraphic incompleteness. Stratigraphic incompleteness results from hiatuses, periods of non-deposition or erosion that reduce the amount of time and space preserved in a sediment column which is the norm for shallow marine strata (Sommerfield, 2006). Generally, deeper, or older, sediment intervals carry more hiatuses per unit length than time periods closer to the sediment-water interface. As a result, rates averaged over the full sediment column using AMS ^{14}C are generally lower than at the top. Similarly, mean sediment accumulation rates based on ^{210}Pb, ^{137}Cs or other short lived short-lived, radionuclide based chronometers are found to be invariably an order of magnitude higher than based on ^{14}C (Sommerfield, 2006). This is primarily due to stratigraphic incompleteness rather than any methodological differences or temporal variations in sediment delivery.

However, a number of environmental changes are reflected in the core during this period. The first is the higher number of storm events that have been recorded in the Irish Sea in the last 100 years (Wolf and Woolf, 2006; Olbert et al., 2012). This is supported by the higher (up to 70 wt. %) dominance of coarser (>63 µm) material. The most significant change in environmental conditions is best exemplified by F3 zone in the foram stratigraphy. This zone is characterised by a marked increase in *E. excavatum*, *E. scabra* and *A. pseudospiralis*. According to Goineau et al. (2011), *E. scabra* lives in muddy-to-sandy sediment that are enriched in low-quality organic matter. Similarly, Ernst et al. (2005) noted that *E. scabra* was capable of tolerating seasonally eutrophic conditions with Diz et al. (2006) marking it as a strong competitor for space in food in organic matter enriched and hypoxic sediments. The increase in abundance of *E. scabra* in LS Unit 3, particularly in the upper 40 cm of ISMA 359 with a peak at 32 cm, corresponds with the last 40 years approximately during which time this central part of the Irish Sea was beginning to see increased nutrient loading

(Allen et al., 1998). A similar record of increasingly eutrophication like conditions was also recorded in the foram record of the North Sea by Evans et al. (2002). The continued emergence and growth of other species such as *E. excavatum*, A. *pseudospiralis* and *A. beccarii* would suggest this zone to be one of lower salinity and increased unstable environmental conditions which are correlated with an increase in grain-size. *A. pseudospiralis* is known to indicate warmer water conditions which would be prevalent during the MO and hence account for the perceived drop in salinity.

Up to this point in our core it was possible to relate core changes to broad climatic shifts. In LS Unit 3, however, the change seen in grain-size and foram populations cannot be explained by climatic forcing alone. Since the 1960s, the estimated effort for the Irish fishing fleet for the area has increased dramatically from an estimated effort of 50,000 - 250,000 hours per year, especially with the use of beam trawl (C. Lordan, pers. comm.). The intensity of this trawling can be quite high which, no doubt, contributed to the sediment redistribution of the area and hence resulted in the deposition of increasingly coarse lag deposits. The effect of trawling is also seen from excess ^{210}Pb profiles which, when extrapolated, were interpreted to be missing the upper 17 - 53 cm of the succession (chapter 5.). Whilst, some of this loss may be explained by coring methods it doesn't account for the scale of potential loss seen here. Whilst an attempt was made to infer changes related to climatic factors, this uppermost section essentially exhibits an increasing human influence.

4.6. CONCLUSIONS

From our analyses of the three vibrocores taken from the Western Irish Sea Mud Belt the following conclusions can be made.

The dominant control on sediment deposition in the WISMB is bed stress which is inherently controlled by a combination tidal dynamics and climate resulting in seasonal stratification. The depositional history in the WISMB from the cores analysed show a record of environmental changes that can be related to broad climatic periods.

This record includes a period of climatic stability from the base of the core record (7,000 years BP) to approximately 4,500 years BP coinciding with the Holocene Thermal Optimum. Bottom velocities and higher energy events became more prevalent in general after this until 100 years BP as the record in all proxies becomes more variable due to fluctuating climatic conditions associated with the Dark Ages Cold Period, Medieval Warm Period and Little Ice Age.

However, the low sedimentation rate for the lower portion of the core derived from dating would suggest that the record here is likely incomplete as a result of environmental (periods of erosion/hiatus) or possibly mechanical (auto-compaction, coring method) effects.

By contrast, the record for the past 100 years or so can be tightly constrained using a combination of AMS ^{14}C dates and gamma spectrometry. During this period there is a remarkable increase in sedimentation with increased amounts of coarser material. This may be attributed to the combination of a number of factors including the higher frequency of storm-like events and higher riverine input due to increased precipitation over land. However, again, it is most likely a result of stratigraphic incompleteness and the averaging of rates over longer periods in the deeper, older part of the core.

This upper section of the record also offers substantial evidence for anthropogenic impacts on the area including the effect of trawling and input of radionuclides.

Hence, with further work including stable isotopes, additional AMS ^{14}C dating, more detailed foraminiferal studies in addition to carrying out a geotechnical analysis of the core to account for the effect of compaction and stratigraphic incompleteness, the WISMB offers a unique area in the Irish Sea to study the link between past, as well as future, climate forcing, oceanic circulations and terrestrial changes in addition to anthropogenic impacts.

REFERENCES

Allen, J.R., Slinn, D.J., Shammon, T.M., Hartnoll, R.G., Hawkins, S.J., 1998. Evidence for eutrophication of the Irish Sea over four decades. Limnology and Oceanography 43, 1970–1974.

Alve, E., 2003. A common opportunistic foraminiferal species as an indicator of rapidly changing conditions in a range of environments. Estuarine, Coastal and Shelf Science 57, 501–514.

Austin, W.E.N., Scourse, J.D., 1997. Evolution of seasonal stratification in the Celtic Sea during the Holocene. Journal of the Geological Society 154, 249–256.

Bahr, A., Lamy, F., Arz, H., Kuhlmann, H., Wefer, G., 2005. Late glacial to Holocene climate and sedimentation history in the NW Black Sea. Marine Geology 214, 309–322.

Ball, B.J., Fox, G., Munday, B.W., 2000. Long- and short-term consequences of a Nephrops trawl fishery on the benthos and environment of the Irish Sea. ICES Journal of Marine Science 57, 1315–1320.

Belderson, R.H., 1964. Holocene sedimentation in the western half of the Irish Sea. Marine Geology 2, 147–163.

Belderson, R.H., Stride, A.H., 1966. Tidal current fashioning of a basal bed. Marine Geology 4, 237–257.

Bianchi, G.G., McCave, I.N., 1999. Holocene periodicity in North Atlantic climate and deep-ocean flow south of Iceland. Nature 397, 515–517.

Blott, S.J., Pye, K., 2001. GRADISTAT: a grain size distribution and statistics package for the analysis of unconsolidated sediments. Earth Surface Processes and Landforms 26, 1237–1248.

Blundell, A., Charman, D.A.N.J., Barber, K., 2008. Multiproxy late Holocene peat records from Ireland : towards a regional palaeoclimate curve. Journal of Quaternary Science 23, 59–71.

Bond, G., Kromer, B., Beer, J., Muscheler, R., 2001. Persistent solar influence on North Atlantic climate during the holocene. Science 294, 2130–2135.

Bond, G., Showers, W., Cheseby, M., Lotti, R., Almasi, P., DeMenocal, P., Priore, P., Cullen, H., Hajdas, I., Bonani, G., 1997. A Pervasive Millennial-Scale Cycle in North Atlantic Holocene and Glacial Climates. Science 278, 1257–1266.

Bourrin, F., Monaco, A., Aloïsi, J.-C., Sanchez-Cabeza, J.-A., Lofi, J., Heussner, S., Durrieu de Madron, X., Jeanty, G., Buscail, R., Saragoni, G., 2007. Last millennia sedimentary record on a micro-tidal, low-accumulation prodelta (Têt NW Mediterranean). Marine Geology 243, 77–96.

Burland, J.B., 1990. On the compressibility and shear strength of natural clays. Géotechnique 40, 329–378.

Callaway, A., Smyth, J., Brown, C.J., Quinn, R., Service, M., Long, D., 2009. The impact of scour processes on a smothered reef system in the Irish Sea. Estuarine, Coastal and Shelf Science 84, 409–418.

Caseldine, C., Langdon, P., Holmes, N., 2006. Early Holocene climate variability and the timing and extent of the Holocene thermal maximum (HTM) in northern Iceland. Quaternary Science Reviews 25, 2314–2331.

Charlesworth, M.E., Service, M., Gibson, C.E., 2006. The distribution and transport of Sellafield derived 137 Cs and 241 Am to western Irish Sea sediments. The Science of the Total Environment 354, 83–92.

Dickson, C., Whatley, R., 1993. The Biostratigraphy of a Holocene borehole from the Irish Sea Ostracod species, in: Proceedings of the 2nd Euroopean Ostracodologists Meeting. British Micropalaeontological Society, London, Glasgow, pp. 145–148.

Diefendorf, A.F., Patterson, W.P., Mullins, H.T., Tibert, N., Martini, A., 2006. Evidence for high-frequency late Glacial to mid-Holocene (16,800 to 5500 cal yr B.P.) climate variability from oxygen isotope values of Lough Inchiquin, Ireland. Quaternary Research 65, 78–86.

Diz, P., Francés, G., Rosón, G., 2006. Effects of contrasting upwelling–downwelling on benthic foraminiferal distribution in the Ría de Vigo (NW Spain). Journal of Marine Systems 60, 1–18.

Dobson, M.R., 1977. The geological structure of the Irish Sea, in: Kidson, C., Tooley, M.J. (Eds.), The Quaternary History of the Irish Sea. Seel House, Liverpool, pp. 13–26.

Edwards, A., Xu, Z., Thompson, R., 1987. Sediments and physical oceanography of Airds Bay, Loch Etive. Marine Biology Association 38, 11.

Ernst, S., Bours, R., Duijnstee, I., van der Zwaan, B., 2005. Experimental effects of an organic matter pulse and oxygen depletion on a benthic foraminiferal shelf community. The Journal of Foraminiferal Research 35, 177–197.

Evans, J.R., Austin, W.E.N., Brew, D.S., Wilkinson, I.P., Kennedy, H.A., 2002. Holocene shelf sea evolution offshore northeast England 191.

Folk, R.L., Ward, W.C., 1957. Brazos River Bar: a study in the significance of grain size parameters. Journal of Sedimentary Petrology 27, 3–26.

Fox, G., Ball, B.J., Munday, B.W., Pfeiffer, N., 1996. The IMPACT II study: preliminary observations on the effect of bottom trawling on the ecosystems of the Nephrops grounds in N.W. Irish Sea, in: Irish Marine Science 1995. pp. 337–354.

Ghilardi, B., O'Connell, M., 2013. Early Holocene vegetation and climate dynamics with particular reference to the 8.2 ka event: pollen and macrofossil evidence from a small lake in western Ireland. Vegetation History and Archaeobotany 22, 99–114.

Goineau, A., Fontanier, C., Jorissen, F.J., Lansard, B., Buscail, R., Mouret, A., Kerhervé, P., Zaragosi, S., Ernoult, E., Artéro, C., Anschutz, P., Metzger, E., Rabouille, C., 2011. Live (stained) benthic foraminifera from the Rhône prodelta (Gulf of Lion, NW Mediterranean): Environmental controls on a river-dominated shelf. Journal of Sea Research 65, 58–75.

Gray, J., Jones, S.R., Smith, A.D., 1995. Discharges to the environment from the Sellafield site, 1951-1992. Journal of Radiological Protection 15, 99.

Grove, J.M., 1988. The Little Ice Age. Methuen, London.

Hass, H.C., 1993. Depositional processes under changing climate: Upper Subatlantic granulometric records from the Skagerrak (NE-North Sea). Marine Geology 111, 361–378.

Hass, H.C., 1996. Northern Europe climate variations during late Holocene: evidence from marine Skagerrak. Palaeogeography, Palaeoclimatology, Palaeoecology 123, 121–145.

Hebbeln, D., Knudsen, K.-L., Gyllencreutz, R., Kristensen, P., Klitgaard-Kristensen, D., Backman, J., Scheurle, C., Jiang, H., Gil, I., Smelror, M., Jones, P.D., Sejrup, H.-P., 2006. Late Holocene coastal hydrographic and climate changes in the eastern North Sea. The Holocene 16 , 987–1001.

Hebbeln, D., Scheurle, C., Lamy, F., 2003. Depositional history of the Helgoland mud area, German Bight, North Sea. Geo-Marine Letters 23, 81–90.

Holmes, J., Arrowsmith, C., Austin, W., Boyle, J., Fisher, E., Holme, R., Marshall, J., Oldfield, F., van der Post, K., 2010. Climate and atmospheric circulation changes over the past 1000 years reconstructed from oxygen isotopes in lake-sediment carbonate from Ireland. The Holocene 20 , 1105–1111.

Hughes, M., Diaz, H., 1994. Was there a “medieval warm period”, and if so, where and when? Climatic Change 26, 109–142.

Jackson, D.I., Jackson, A.A., Evans, D., Wingfield, R.T.R., Barnes, R.P., Arthur, M.J., 1995. United Kingdom offshore regional report: the geology of the Irish Sea. British Geological Survey, London.

Kalis, A.J., Merkt, J., Wunderlich, J., 2003. Environmental changes during the Holocene climatic optimum in central Europe - human impact and natural causes. Quaternary Science Reviews 22, 33–79.

Kershaw, P.J., 1986. Radiocarbon dating of Irish Sea sediments. Estuarine, Coastal and Shelf Science 23, 295–303.

Kirby, R., Parker, W.R., Pentreath, R.J., Lovett, M.B., 1983. Sedimentation studies relevant to low-level radioactive effulent dispersal in the Irish Sea. Part III. An evaluation of possible mechanisms for the incorporation of radionuclides into marine sediments.

Lamb, H.H., 1977. Climatic History and the Future. Methuen, London.

Lambeck, K., 1996. Glaciation and sea-level change for Ireland and the Irish Sea since Late Devensian/Midlandian time. Journal of the Geological Society 153, 853–872.

Langdon, P.G., Brown, A.G., Caseldine, C.J., Blockley, S.P.E., Stuijts, I., 2012. Regional climate change from peat stratigraphy for the mid- to late Holocene in central Ireland. Quaternary International 268, 145–155.

McCave, I.N., Hall, I.R., Bianchi, G.G., 2006. Laser vs. settling velocity differences in silt grainsize measurements: estimation of palaeocurrent vigour. Sedimentology 53, 919–928.

McCave, I.N., Manighetti, B., Robinson, S.G., 1995. Sortable silt and fine sediment size/composition slicing: Parameters for palaeocurrent speed. Paleoceanography 10, 593–610.

McDermott, F., Frisia, S., Huang, Y., Longinelli, A., Spiro, B., Heaton, T.H.E., Hawkesworth, C.J., Borsato, A., Keppens, E., Fairchild, I.J., van der Borg, K., Verheyden, S., Selmo, E., 1999. Holocene climate variability in Europe: Evidence from δ18O, textural and extension-rate variations in three speleothems. Quaternary Science Reviews 18, 1021–1038.

McDermott, F., Mattey, D.P., Hawkesworth, C., 2001. Centennial-Scale Holocene Climate Variability Revealed by a High-Resolution Speleothem δ18O Record from SW Ireland. Science 294 , 1328–1331.

Mitchell, P.I., Condren, O.M., Leo, L., Mcmahon, C.A., 1999. Trends in plutonium , americium and radiocaesium accumulation and long-term bioavailability in the western Irish Sea mud basin. Journal of Environmental Radioactivity 44, 223–251.

Murray, J.W., 1970. Foraminifers of the Western Approaches to the English Channel. Micropaleontology 16, 471–485.

Murray, J.W., 1971. An Atlas of British Recent Foraminiferids. Heinemann Educational Books, London.

Murray, J.W., 1979. British Nearshore Foraminiferids: Keys and Notes for the Identification of the Species. Academic Press, London.

Murray, J.W., 2000. Revised taxonomy, An Atlas of British Recent Foraminiferids. Journal of Micropalaeontology 19, 44.

Murray, J.W., 2003. An illustrated guide to the benthic foraminifera of the Hebridean Shelf, west of Scotland, with notes on their mode of life. Palaeontologica Electonica 5, 31pp.

Murray, J.W., Alve, E., 2011. The distribution of agglutinated foraminifera in NW European seas : Baseline data for the interpretation of fossil assemblages. Palaeontologica Electonica 14, 41p.

O'Brien, S.R., Mayewski, P.A., Meeker, L.D., Meese, D.A., Twickler, M.S., Whitlow, S.I., 1995. Complexity of Holocene Climate as Reconstructed from a Greenland Ice Core. Science 270 , 1962–1964.

Olbert, A.I., Dabrowski, T., Nash, S., Hartnett, M., 2012. Regional modelling of the 21st century climate changes in the Irish Sea. Continental Shelf Research 41, 48–60.

Øvrebø, L.K., Haughton, P.D.W., Shannon, P.M., 2005. Temporal and spatial variations in Late Quaternary slope sedimentation along the undersupplied margins of the Rockall Trough , offshore west Ireland. Norwegian Journal of Geology 85, 279–294.

Pantin, H.M., 1977. Quaternary sediments of the northern Irish Sea, in: Kidson, C., Tooley, M. j (Eds.), The Quaternary History of the Irish Sea. Seel House, Liverpool, pp. 27–54.

Pantin, H.M., 1978. Quaternary sediments from the northeast Irish Sea: Isle of Man to Cumbria. Bulletin of the Geological Society of Great Britain 64, 43.

Parker, A.G., Goudie, A.S., Anderson, D.E., Robinson, M. a., Bonsall, C., 2002. A review of the mid-Holocene elm decline in the British Isles. Progress in Physical Geography 26, 1–45.

Pérez-Cruz, L., Urrutia-Fucugauchi, J., 2009. Magnetic mineral study of Holocene marine sediments from the Alfonso Basin , Gulf of California - implications for depositional environment and sediment sources. Geofísica Internacional 48, 305–318.

Pilcher, J.R., Smith, A.G., Pearson, G.W., Crowder, A., 1971. Land Clearance in the Irish Neolithic: New Evidence and Interpretation. Science 172, 560–562.

Pingree, R.D., Griffiths, D.K., 1979. Sand transport paths around the British Isles resulting from M2 and M4 tidal interactions. Journal of Marine Biological Association of the UK 59, 497–513.

Plunkett, G., 2006. Tephra-linked peat humification records from Irish ombrotrophic bogs question nature of solar forcing at 850 cal. yr BC. Journal of Quaternary Science 21, 9–16.

Reimer, P.J., Bard, E., Bayliss, A., Beck, J.W., Blackwell, P.G., Bronk Ramsey, C., Buck, C.E., Cheng, H., Edwards, R.L., Friedrich, M., Grootes, P.M., Guilderson, T.P., Haflidason, H., Hajdas, I., Hatté, C., Heaton, T.J., Hoffmann, D.L., Hogg, A.G., Hughen, K.A., Kaiser, K.F., Kromer, B., Manning, S.W., Niu, M., Reimer, R.W., Richards, D.A., Scott, E.M., Southon, J.R., Staff, R.A., Turney, C.S.M., van der Plicht, J., 2009. IntCal13 and Marine13 Radiocarbon Age Calibration Curves 0–50,000 Years cal BP. Radiocarbon 51, 1111–1150.

Renssen, H., Seppä, H., Crosta, X., Goosse, H., Roche, D.M., 2012. Global characterization of the Holocene Thermal Maximum. Quaternary Science Reviews 48, 7–19.

Richter, T.O., Lassen, S., van Weering, T.C.., de Haas, H., 2001. Magnetic susceptibility patterns and provenance of ice-rafted material at Feni Drift, Rockall Trough: implications for the history of the British–Irish ice sheet. Marine Geology 173, 37–54.

Roberts, D.H., Chiverrell, R.C., Innes, J.B., Horton, B.P., Brooks, A.J., 2006. Holocene sea levels , Last Glacial Maximum glaciomarine environments and geophysical models in the northern Irish Sea Basin , UK 231, 113–128.

Robinson, I.S., 1979. The tidal dynamics of the Irish and Celtic Seas. Journal of Geophysical Research 56, 159–197.

Röhl, U., Sciences, G., Carolina, N., Hill, C., Norris, R.D., Wefer, G., 2000. New chronology for the late Paleocene thermal maximum and its environmental implications. Geology 28, 927–930.

Schönwiese, C.D., 1988. Grundlagen und neue Aspekte der Klimatologie. Frankfurter Geowissenschaftliche Arbeitan, Frankfurt.

Scott, G.A., Scourse, J.D., Austin, W.E.N., 2003. The Distribution of Benthic Foraminifera in the Celtic Sea: the significance of seasonal stratification. Journal of Foraminiferal Research 33, 32–61.

Scourse, J., 2013. Quaternary sea- level and palaeotidal changes : a review of impacts on , and responses of , the marine biosphere. Oceanography and Marine Biology: An Annual Review 1–70.

Scourse, J.D., Austin, W.E.N., 2002. Quaternary shelf sea palaeoceanography : recent developments in Europe. Marine Geology 191, 87–94.

Scourse, J.D., Austin, W.E.N., Long, B.T., Assinder, D.J., Huws, D., 2002. Holocene evolution of seasonal stratification in the Celtic Sea: refined age model, mixing depths and foraminiferal stratigraphy. Marine Geology 191, 119–145.

Scourse, J.D., Hall, I.R., McCave, I.N., Young, J.R., Sugdon, C., 2000. The origin of Heinrich layers: evidence from H2 for European precursor events. Earth and Planetary Science Letters 182, 187–195.

Skempton, A.W., 1969. The consolidation of clays by gravitational compaction. Quarterly Journal of the Geological Society 125, 373–411.

Sommerfield, C.K., 2006. On sediment accumulation rates and stratigraphic completeness: Lessons from Holocene ocean margins. Continental Shelf Research 26, 2225–2240.

Stuiver, M., Braziunas, T.F., 1993. Sun, ocean, climate and atmospheric 14CO2 : an evaluation of causal and spectral relationships. The Holocene 3 , 289–305.

Swindles, G.T., Blundell, a., Roe, H.M., Hall, V. a., 2010. A 4500-year proxy climate record from peatlands in the North of Ireland: the identification of widespread summer “drought phases”? Quaternary Science Reviews 29, 1577–1589.

Swindles, G.T., Charman, D.J., Roe, H.M., Sansum, P.A., 2009. Environmental controls on peatland testate amoebae (Protozoa: Rhizopoda) in the North of Ireland: Implications for Holocene palaeoclimate studies. Journal of Paleolimnology 42, 123–140.

Swindles, G.T., Plunkett, G., Roe, H.M., 2007. A multiproxy climate record from a raised bog in County Fermanagh , Northern Ireland : a critical examination of the link between bog surface wetness and solar variability 22, 667–679.

Turney, C., Baillie, M., Clemens, S., Brown, D., Palmer, J., Pilcher, J., Reimer, P., Leuschner, H.H., 2005. Testing solar forcing of pervasive Holocene climate cycles. Journal of Quaternary Science 20, 511–518.

Turney, C.S.M., Baillie, M., Palmer, J., Brown, D., 2006. Holocene climatic change and past Irish societal response. Journal of Archaeological Science 33, 34–38.

Uehara, K., Scourse, J.D., Horsburgh, K.J., Lambeck, K., Purcell, A.P., 2006. Tidal evolution of the northwest European shelf seas from the Last Glacial Maximum to the present. Journal of Geophysical Research 111.

Van Landeghem, K.J.J., Uehara, K., Wheeler, A.J., Mitchell, N.C., Scourse, J.D., 2009. Post-glacial sediment dynamics in the Irish Sea and sediment wave morphology: Data–model comparisons. Continental Shelf Research 29, 1723–1736.

Weber, M.E., Niessen, F., Kuhn, G., Wiedicke, M., 1997. Calibration and application of marine sedimentary physical properties using a multi-sensor core logger. Marine Geology 136, 151–172.

Wolf, J., Woolf, D.K., 2006. Waves and climate change in the north-east Atlantic. Geophysical Research Letters 33, 1–4.

Yuan, F., Bennell, J.D., Davis, A.M., 1992. Acoustic and physical characteristics of gassy sediments in the western Irish Sea. Continental Shelf Research 12, 1121–1134.

CHAPTER 5

RECORD OF ANTHROPOGENIC IMPACT IN THE WESTERN IRISH SEA MUD BELT

Theme

During the course of the study in chapter 4, it became apparent that there was an increasing anthropogenic influence and impact on the palaeorecord reconstructed from the cores. Geophysical data had also shown evidence for anthropogenic impacts through trawling. In this chapter we elaborate on these anthropogenic influences.

Contributors

Mark Coughlan partook in both surveys (ISMA; CV0926 & CV12006 Appendix BI and BII) which gathered the data for this study. He is also the first author having undertaken evaluation of this data and written all drafts of the manuscript.

Andrew J. Wheeler is the lead supervisor on this project, was chief scientist for the survey which gathered the data for this study and has extensively proof read drafts of this manuscript.

Boris Dorschel was present during the ISMA survey (CV0926, Appendix BI) and supervised the collection of the geophysical data. He also subsequently processed the geophysical data used in this study.

Colm Lordan provided VMS and other data relating to trawling efforts within the Irish Sea as well as contributing to the discussion.

Wim Boer, Piet Van Gaever and Henk de Haas carried out the gamma spectrometry work used in this study, helped in the interpretation of results and contributed to the discussion.

Tobias Mörz provided the particle-size analysis facilities for this study and proof read the final manuscript.

CHAPTER 5

RECORD OF ANTHROPOGENIC IMPACT IN THE WESTERN IRISH SEA MUD BELT

ABSTRACT

Six cores and a suite of geophysical data, surface grab samples and video photography were collected from the area of the Western Irish Sea Mud Belt (WISMB) to analyse radionuclide input and subsequently study the influence of bottom trawling and bioturbation on the surface and near-surface sediments. Significant changes in the sedimentation and geochemical regime in the WISMB were observed due to anthropogenic input (bottom trawling and radionuclides) supportive of the concept of the Anthropocene time-period. Levels of anthropogenic radionuclides were measured in two of the cores and used to construct a chronology based on relation to recorded levels of discharge from the Sellafield nuclear facility on the eastern (UK) seaboard of the Irish Sea. Only ^{137}Cs provided a useful basis for the chronology. Using this chronology and radionuclide data it was also possible to investigate the effect trawling had on the area which was visible on acoustic seabed mapping data. Ultimately, between 17 - 53 cm of the upper seabed is calculated to have been removed as a result of bottom trawling. The influence of bioturbation (which is similarly prominent from core scan data) on the record is further considered here.

KEYWORDS: Irish Sea, Anthropocene, Mud Belt, grain-sizes, gamma spectrometry, trawling, radionuclides.

This chapter is based on: Coughlan, M., Wheeler, A.J., Dorschel, B., Lordan, C., and Boer, W., van Gaever, P., de Haas, H. and Mörz, T. (in prep). Record of Anthropogenic Impacts in the Western Irish Sea Mud Belt.

5.1. INTRODUCTION

In recent times, the term Anthropocene is being widely debated to identify and qualify the late to recent time period where human impact on Earth systems is demonstrable. First coined in 2000 by Crutzen and Stoermer, the notion behind the Anthropocene has generated a lively discussion regarding human activity and its influence on the Earth system past, present and future (Oldfield et al., 2013). Definition of the Anthropocene, and its study, encompasses a wide range of disciplines from engineering to geological and environmental sciences as well as humanities and social sciences. From a geological perspective, studies in defining the Anthropocene are concerned with criteria which have traditionally been used in recognising stratigraphic units in the rock record, namely; lithostratigraphy, chemostratigraphy, sequence stratigraphy and biostratigraphy. In terms of lithostratigraphy, Anthropocene related distinction of units is largely focused with modification of sedimentary environments by human activities such as damming of rivers, urban development and deforestation and, offshore, trawling (Zalasiewicz et al., 2011). The process of trawling in disturbing seafloor sediments is estimated to affect an area of approximately 20 x 10^6 km^2, including most of the continental shelf or about 7% of the global seabed area (Zalasiewicz et al., 2011).

In order to define the start of the Anthropocene and significant events therein, much focus has been put on the use of chemostratigraphy. Similarly, this involves identifying human perturbation in global geochemical cycles to such an extent so as to leave a distinctive marker in the stratigraphic record. Arguably, it is the human impact on carbon and atmospheric CO_2 levels which represents the most influential and, therefore, important perturbation on the Earth system. However, one of the most readily distinctive, traceable and quantifiable is the input of anthropogenic radionuclides into

the environment. These are largely associated with fall-out as a result of nuclear weapons testing beginning in the 1950s, but also as direct output from nuclear power facilities.

Although the Anthropocene is still an informal term, and not yet fully recognised in the geologic time-scale, it is still an important idea in forcing humans to assess their relationship with the environment and Earth system (Cohen et al., 2013). If we are to combat the growing issue of climate change, and other adverse effects on our environment, it is important to document and understand this relationship on a past, present and future basis.

Despite widespread anthropogenic use of the Irish Sea, there are relatively few studies on the effects (Allen et al., 1998; Rogers et al., 1999; Veale et al., 2000; Evans et al., 2003). In this study, we investigate two prominent aspects of anthropogenic influence (namely trawling and radionuclide input) and aim to establish a chronology of these events and their impact on the Irish Sea seabed to date.

5.2. REGIONAL SETTING AND ANTHROPOGENIC HISTORY

The Irish Sea is a semi-enclosed tidal basin lying between Great Britain and Ireland (Fig. 5.1). As such, it is exposed to anthropogenic activities which threaten the natural resources found there and the environment itself. Fisheries activity is extensive throughout and particularly intensive in the fine-grained sediment area west of the Isle of Man referred to as the Western Irish Sea Mud Belt (WISMD) (Belderson, 1964; Kaiser et al., 1996). The relatively benign setting offered by this area, with its low energy regime and uniform fine-grained substrate, makes it an ideal habitat for many commercially fished species especially the Dublin Bay Prawn (*Nephrops norvegicus*) and various benthic macrofauna (Kaiser et al., 1996). The depth of the effect of trawling in this area may be up to 20 cm depending on the type of gear used (Kaiser et al., 1996). Studies regarding the effect of trawling in the area have largely focused on the effect it has on species population richness and community changes (Kaiser et al., 1996; Ball et al., 2000). Trawling efforts in the WISMB have increased by a factor of 2.5 since the 1970s with, on average, the seabed trawled from between five to even ten times a year (Brander, 1980; Fox et al., 1996). Considering this frequency of

activity, the potential alteration of the seafloor sediment structure could have costly implications in terms of long term habitat loss of commercial species (Kaiser et al., 1996).

Another prominent anthropogenic effect in the Irish Sea is radionuclide input. Sellafield (located in Cumbria, west coast of the UK) has been discharging low-level waste into the Eastern Irish Sea Mud Belt (EISMB) since 1952 (Gray et al., 1995). There is a well-established transport corridor for radionuclides from the EISMB to the WISMB via physical transport of contaminated particles and in the soluble form (Mitchell et al., 1999; Charlesworth et al., 2006). As a result, short lived radionuclides released from Sellafied are often recorded in the sediments of the WISMB (Kershaw et al., 1984; Mitchell et al., 1999; Charlesworth et al., 2006). In the EISMB, attempts at matching core profiles with Sellafield discharges using Pu quotients had met with little success (Kershaw et al., 1990 and references therein). This could be attributed to the effects of bioturbation, chemical conditions within the seabed or even intrabasinal sediment erosion and deposition (Aston et al., 1985; Kershaw et al., 1990). Kershaw et al. (1990), however, focused on a previously dredged harbour (namely Senhouse Dock, Mary Port Harbour) that was undisturbed by bioturbation and were able to successfully establish a comprehensive environmental history of Sellafield discharges and derive a chronology for the sediment sequence based primarily on ^{137}Cs and ^{241}Am.

5.3. MATERIALS AND METHODS

The core material and other data presented in this study were predominately gathered in September 2009 as part of the Irish Sea Marine Assessment (ISMA; CV0926, Appendix BI) and CV12006 survey (Appendix BII) in April 2012. During the course of the former survey, some 352.65 km^2 of the Irish Sea seabed was mapped using Simrad EM3002D multibeam echosounder onboard the R.V. Celtic Voyager. Data processing was performed on board with the CARIS HIPS and SIPS software package. This high-quality acoustic mapping data was supplemented by 975 high-quality, digital photographs of the seabed from 15 areas, 269 surface grab samples and 20 vibrocores of up to 3 m length. Two of these 20 vibrocores were taken from the WISMB which form the basis of this study (Table 5.1). During the course of the latter CV12006 survey, some 30

vibrocores were retrieved, four of which were taken from the WISMB and two at comparable GPS location as those recovered during the ISMA survey for the purpose of comparison and further geotechnical investigation (Table 5.1).

Core ID	Latitude	Longitude	Water Depth (m)	Core Length (cm)	Study ID
ISMA 359	53°42.8173"N	05° 57.664"W	42	260	Core 1
ISMA 418	53°48.2333"N	06° 02.9527"W	33.5	249	Core 2
CV12006_038	52°38.6993"N	05° 56.4873"W	42	258	Core 3
CV12006_039	53°42.7616"N	05° 57.5076"W	41	292	Core 4
CV12006_040	53°48.1247"N	06° 02.7625"W	35	285	Core 5
CV12006_041	53°48.3841"N	05° 55.4912"W	44	302	Core 6

Table 5.1 Core information

Supplementary data constraining the spatial extent of trawling activity was provided by Colm Lordan at the Marine Institute. This consisted of Vessel Monitoring Systems (VMS) data which automatically collects positional data from fishing vessels. The system has been installed on all fishing vessels >24 m since January 2000 according to European Commission legislation and on vessels >18 and >15 m since 2004 and 2005 respectively (Gerritsen and Lordan, 2011). Previously, VMS data has been used to assess the extent and frequency of the impact made by mobile fishing gear (Gerritsen et al., 2013). Additionally, Marine Institute data for estimated fishing effort (in hours) for the Irish Sea was also used.

5.3.1 Computerised Tomography X-ray and Digital Line Scanning

Core 1 and Core 2 were imaged using the Computerised Tomography (CT) X-ray Scanner housed at MARUM, University of Bremen with a maximum resolution of ~ 1 mm. Subsequently, eFilm visual software was used to interrogate the data in order to identify internal primary sedimentological structures and secondary features such as bioturbation. Digital images of these open cores were also taken using the Geoscan III on the Multi-sensor core logger (MSCL) scanner at MARUM. The colour line camera is a 3 CCD device using 3 x 2048 pixel CCD arrays and a beam -splitter. The linescan software produces visual colour images but also colour data in RGB

and CIE-L*, a*, b*. These high resolution digital images were used to identify physical evidence of bioturbation and also aid in facies recognition along with identifying potential structures within the sediment column such as layering and bioturbation.

5.3.2 Particle-Size Analysis

Samples weighing roughly 2 grams were taken every 5 cm to be used in particle-size analyses (PSA) using the Beckman Coulter LS 13 320 laser diffraction particle-size analyser at MARUM, University of Bremen, to provide information about downcore grain-size distribution for all cores. The laser is equipped with an Aquous Liquid Module and an Auto Prep Station and determines particle grain-sizes from 0.4 to 2000 µm. Analyses was carried out on bulk sediment samples.

In the case of surface grab-samples, the particle-size distribution of the siliciclastic fraction was measured on a Malvern Mastersizer 2000 laser-granulometer with Autosampler and Hydro G dispersion unit at the National Oceanography Centre Southampton. The siliciclastic fraction was obtained through the removal of organic matter and the carbonate phase by oxidation (10% H_2O_2) and dissolution (10% HCL) respectively. A 5% Calgon (Sodium Hexametaphosphate) solution was added for disaggregation and dispersion accompanied by MECHANICAL shaking.

Statistical parameters including modal and mean grain-size, sorting and sediment type for PSA distributions were calculated according to Folk and Ward (1957) using the GRADISTAT software (Blott and Pye, 2001).

5.3.3 Free-fall Cone Penetration Testing

Cores 3, 4, 5 and 6, collected during the CV12006 survey, were split lengthways once onboard and subjected to free-fall cone penetration tests (CPT). The free-fall CPT was equipped with four cones of varying weight and apex angle (400 g/30°, 100 g/ 30°, 60 g/60°, 10 g/60°). The selected weight

was suspended above the sediment surface by a permanent magnet. The cone was dropped from a set height into the sediment by release using a trigger allowing for replication of the experiment. Shear strength values were calculated using correlated penetration depths under the assumption that the strength of a soil at constant penetration of a cone is directly proportional to the weight of the cone (Houlsby, 1982).

5.3.4 Gamma Spectrometry

Analyses were undertaken for ^{210}Pb, ^{137}Cs, ^{226}Ra and ^{241}Am by way of gamma spectrometry at the Royal Netherlands Institute for Sea Research (Royal NIOZ) to investigate anthropogenic radionuclide levels in the core profile. Sixteen samples from both ISMA 359 and ISMA 418 were taken at intervals of 5 cm for the upper 40 cm and every 10 cm thereafter until the 160 cm mark. Each sample taken measured between 12 – 20 g and was subsequently separated into fine (<63 µm) and coarse (>63 µm) fraction using the Atterberg sedimentation tube method. The fine fraction was used in analyses owing to the fact that using the fine fraction enhances measured activities and negates uncertainties regarding grain-size variations. Gamma spectrometry was carried out with a Canberra Broad Energy Range High Purity Germanium Detector (BEGe). The detector was connected to a computer via a Digital Spectrum Analyser (DSA-1000) and the data were calculated with Genie 2000 gamma spectroscopy software. The samples were accurately weighed and added to a Petri dish with a diameter of 6 cm and a height of 1.5 cm, depending on the availability the volume was 1 - 6 ml. Calibration, monitor standards and samples were prepared in the same geometry. The Petri dishes were sealed airtight to equilibrate the samples for at least three weeks before counting. Samples were counted for 2 to 5 days depending on the amount of sample to obtain good counting statistics. The detector was externally calibrated with a Geological Certified Reference Material IAEA/RGU-1 with reference date of 01-01-1988. Quality control was performed using a monitor standard IAEA-300.

5.4. RESULTS

5.4.1 Area Characterisation

Particle-size analyses on grab samples revealed a predominately fine-grained seabed in the area with minor changes in sediment distribution showing a general progressive decrease in grain-size from muddy sands in the southwest towards slightly gravelly sandy mud in the northeast (see Fig. 5.1). Digital seabed imagery from video tows reinforced this picture of a relatively homogenous, fine-grained sediment distribution and exposed a microtopography that is related, for the most part, to epifaunal burrowing (Fig. 5.1)

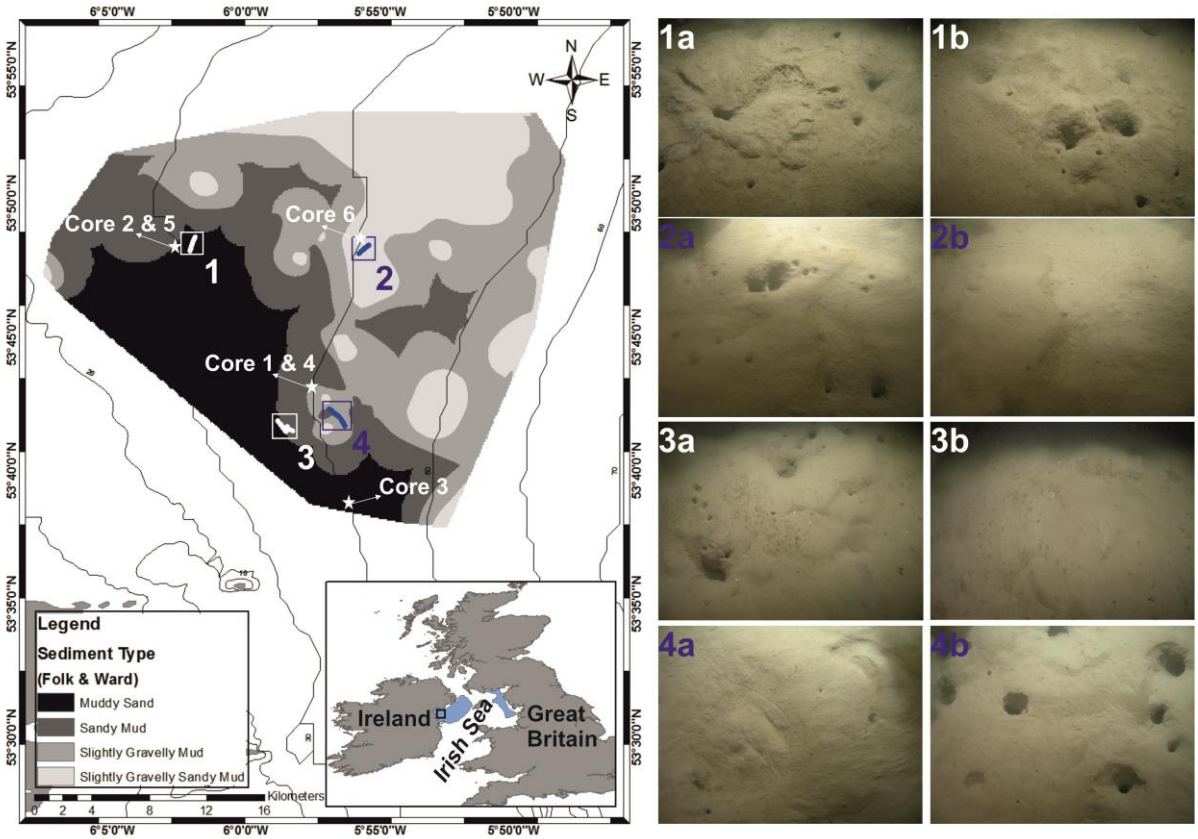

Figure 5.1 Inset Map: Location of study area within WISMB (marked in blue, EISMB also marked in blue). Main Map: Sediment distribution from PSA and locations of video transects (marked by numbered boxes) and core locations (marked by numbered stars). 1-4: Seabed photography of highlighted areas.

Evidence from backscatter and MBES data suggested a relatively featureless seabed aside from pockmarks associated with shallow gas escape (Yuan et al., 1992, Chapter 3) and extensive trawl marks (Fig. 5.2).

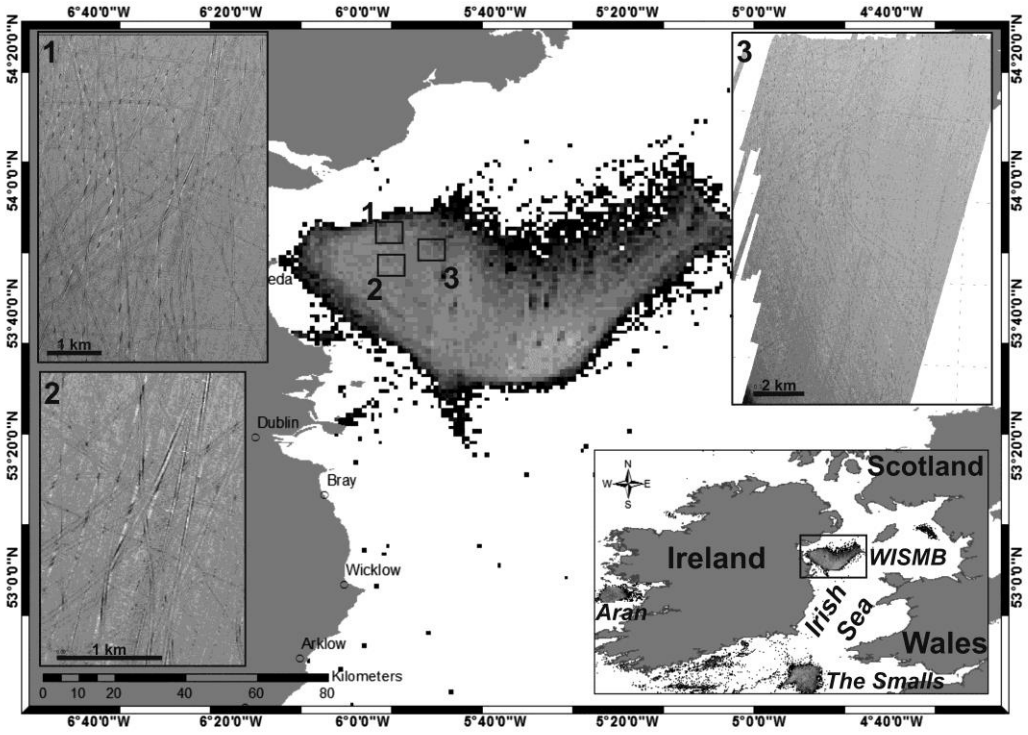

Figure 5.2 Inset Map: *Nephrops* directed fishing effort using VMS logbook data with WISMB highlighted. Main Map: Focus on WISMB with VMS logbook data highlighting trawling intensity in the area. 1-3: Trawling marks on the seabed from backscatter imagery.

5.4.2 Line Scans and CT X-ray

Line scans and CT X-ray were carried out on Core 1 and Core 2. All cores, however, contain homogenous, fine-grained (silty) sediments displaying a dark olive-grey colour. Variations in colour were attributed to bioturbation. Skeletal macrofauna remains occurred throughout all cores with the gastropod *Turritella communis* the most dominant. The occurrence of these shells was patchy but often with rich horizons on the scale of centimetres and becoming less abundant towards the top of each core. CT X-ray revealed the full extent of these *T. communis* rich layers (Fig. 5.3). No primary sedimentary fabric was recorded in the cores from visual inspection, line scans or CT X-ray. However, significant evidence for sediment disturbance was seen in both cores, manifested as

laterally discontinuous contrasting bands of light and dark colouration and was most prominent in the upper 30 cm approximately of both cores (Fig. 5.3). This was assumed to be as a result of bioturbation as burrowing *Nephrops* are prominent in the area (Fig. 5.1).

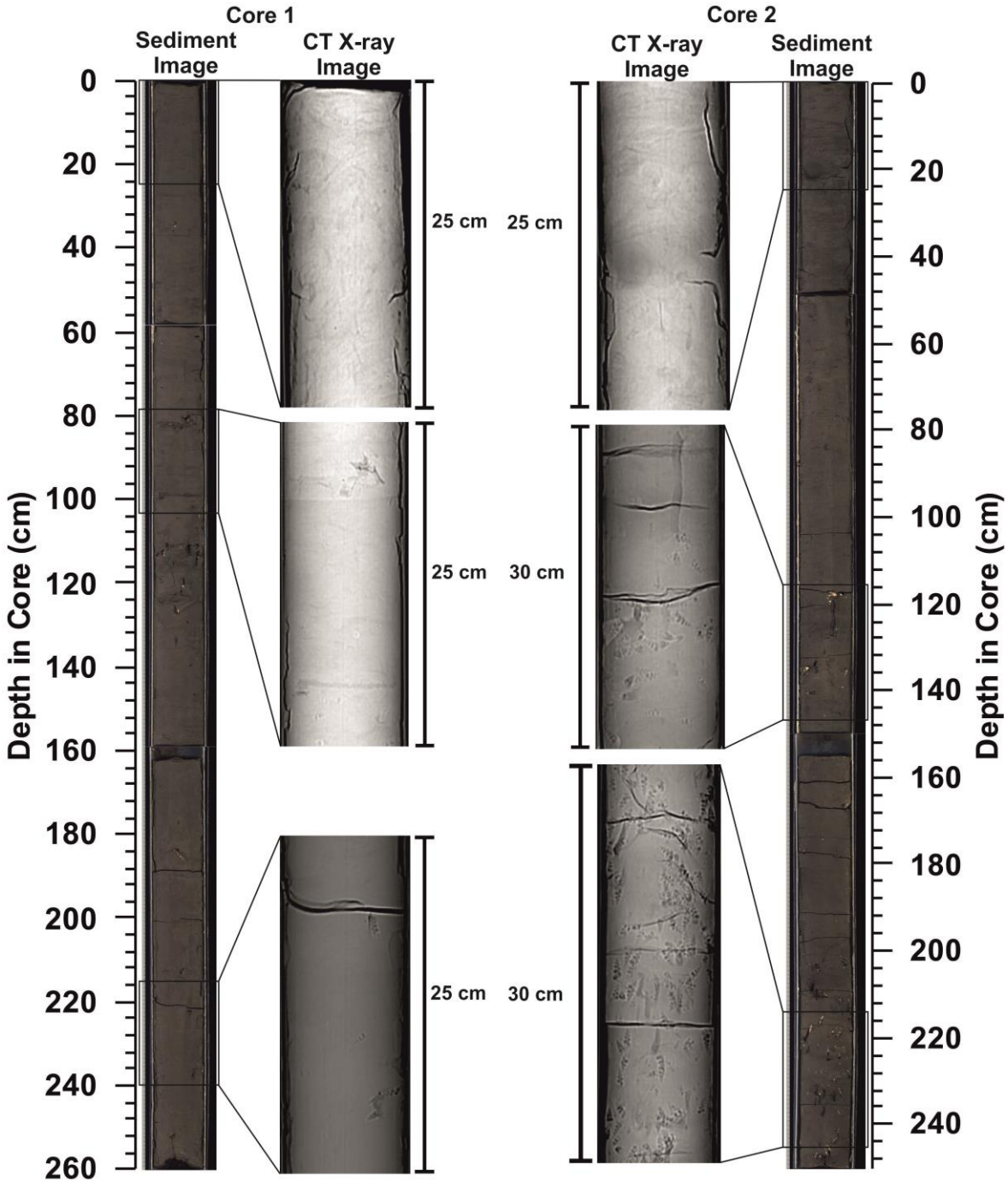

Figure 5.3 Line scans and CT X-ray for core 2 and Core 1. See section 5.4.2 for explanation.

5.4.3 Sediment Composition and Geotechnical Relationships

For the purpose of this study, sediment composition was investigated through changes in the cores of percentages of clay, silt and sand (Fig. 5.4). In addition, it was investigated if there was any meaningful relationship between sediment composition and geotechnical parameters, in this case, shear strength (Fig 5.4). Throughout all cores studied, levels of clay remained stable and relatively low (< 20%) with levels of silt and sand showing the most variation. Contrast between cores is also notable. Both Core 1 and Core 4 come from the same site location and exhibit a similar trend with a silt dominant base (up to 80%) gradually becoming sand dominant towards the top (up to 60%). Core 2 and Core 5 (similarly from the same core location) exhibit a comparable trend albeit less dramatic with silt (up to 50% at the base) being replaced towards the top of the core by sand (up to 60%) as the dominant grain-size class. Core 3 exhibits a dominance of silt at the base (60%) continuing to 170 cm depth when sand becomes the dominant component. Samples for the upper 60 cm of this core were missing prior to analyses and are not included here. Overall, Core 6 is more silt dominant throughout with levels remaining at around 60% with sand at 20% and clay at 10% on average.

Shear strength measurements, on the whole, vary between 0.5 and 27 kPa with an average of between 4.5 and 8.3 kPa for each core (Fig. 5.4). Similarly, values show a mean increase downcore for each profile. Peaks in the profile may be due to the presence of shelly material or burrowing activity at that level in the core rather than due to change in grain-size.

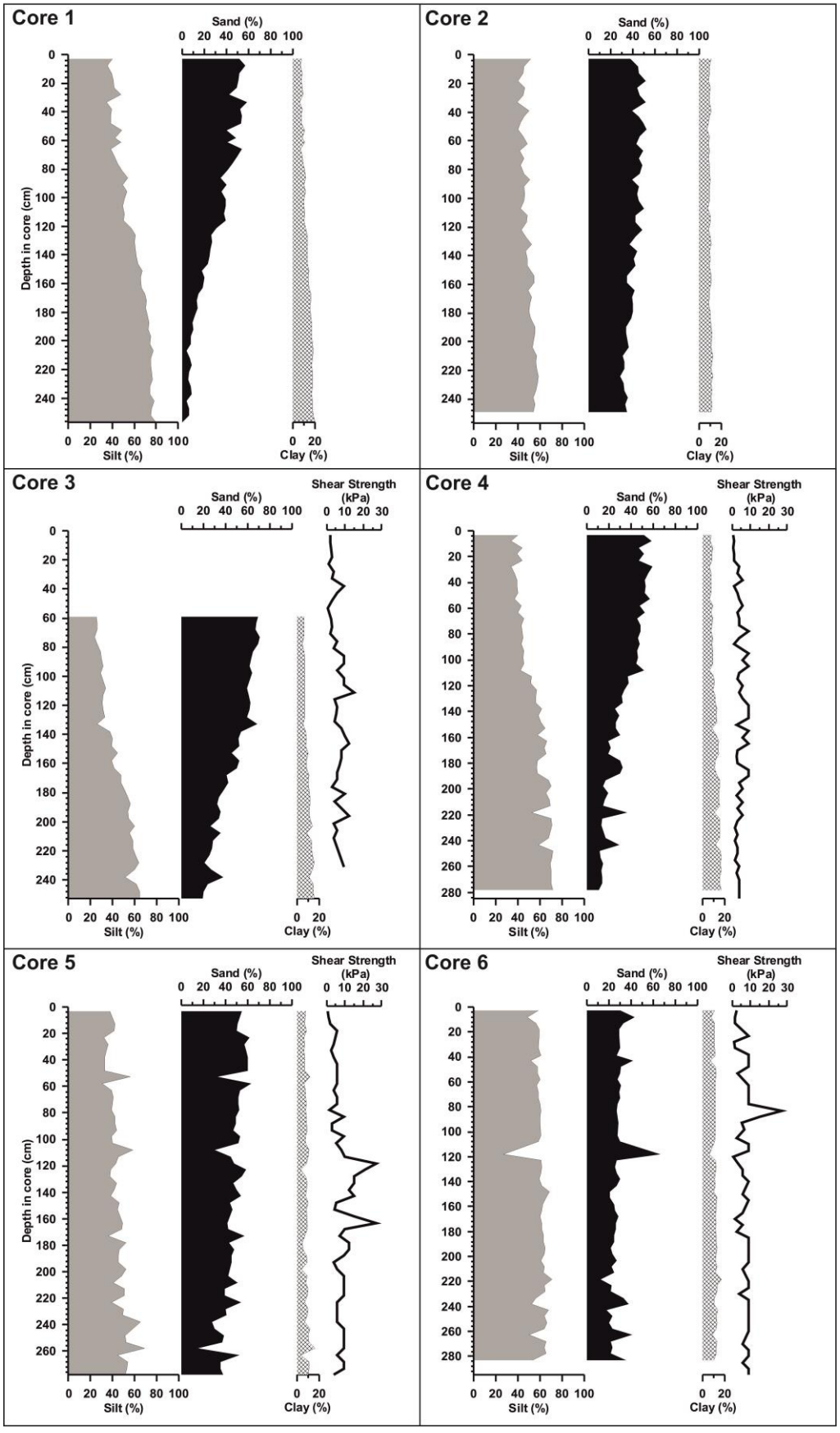

Figure 5.4. PSA (vol. % of individual grain-size classes) and CPT profiles for all cores presented in this study. Grey highlights % silt, black is % sand and hatch is% clay. See section 5.4.3 for explanation.

5.4.4 Radionuclide Profiles

All radionuclide profiles referred to in this study are presented in Figure 5.5. Most striking is the comparability in ^{137}Cs profiles between the two cores with the first occurrence of detectable levels at 100 cm in Core 1 and 80 cm in Core 2. Both cores show a conspicuous peak at 30 cm and 25 cm in Core 1 and Core 2 respectively with a sub-maximum peak at 44 in Core 1 and 52 cm in Core 2. From the main peak to the top of the core both profiles show a prominent decrease in ^{137}Cs levels.

In comparison, following initial detection of ^{241}Am in both cores, there is an steep increase similar to ^{137}Cs but with no subsequent decline. In fact, ^{241}Am remains at a relatively high level of activity possibly even increasing towards the top of both cores (Fig. 5.5). Levels of ^{226}Ra show steady profiles through both cores with distinct peaks at 16 cm in Core 1 and 12 cm in Core 2 with sub-maximum peaks at 40 cm and 36 cm respectively.

Profiles for excess ^{210}Pb show relatively high but strongly variable values in the upper ~50 cm of both cores, and a more regular exponential decrease further downcore. Fitting a conventional constant flux constant sedimentation (CF-CS, (Appleby and Oldfield, 1978)) model on the data yields sedimentation rates of 2.4 cm a^{-1} and 2.0 cm a^{-1} for Core 1 and Core 2 respectively (Fig. 5.5).

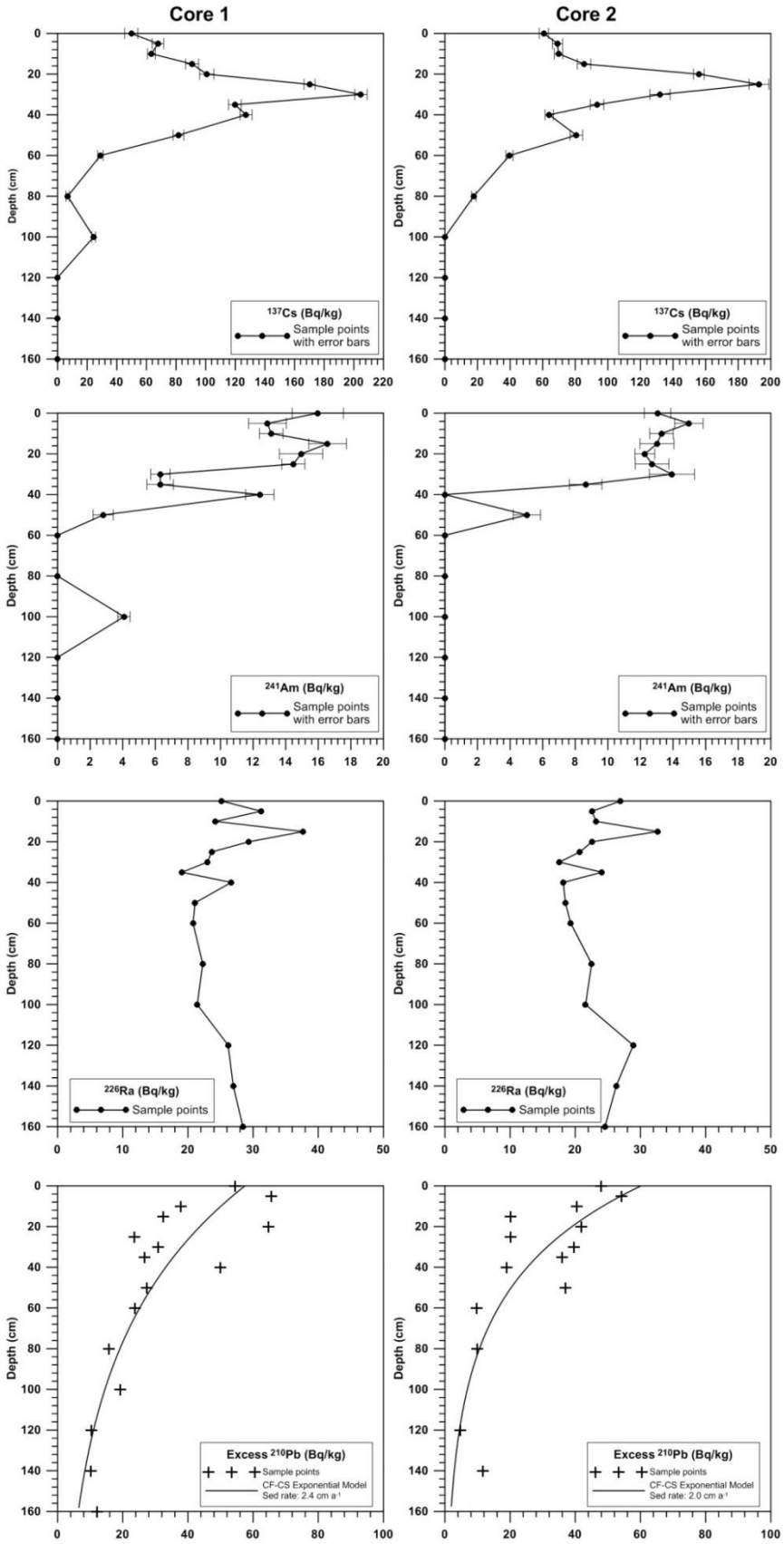

Figure 5.5 Radionuclide profiles for Core 1 and Core 2. 5.4.4 for explanation and 5.5.1 for discussion.

5.5. DISCUSSION

5.5.1 Sediment Chronology and Sellafield Discharges

Establishing a radionuclide based chronology in the Irish Sea is notoriously difficult. In their study, Kershaw et al. (1990) accepted that a number of factors could influence the relationship between radionuclide concentration in a layer of sediment and the supposed year of corresponding discharge from Sellafield, including; uncertainties in assigning a date to the sediment depth interval, fluctuations in the quantity discharged during that year, redistribution within the core by bioturbation, diffusion or diagenesis, dilution of the contemporary signal by 'older' material corresponding to earlier discharges, changes in particle size distribution, variations in accumulation rate, variations in chemical association in the effluent and alteration of sediment transport paths in the eastern Irish Sea.

Sellafield derived radionuclides have been recorded in WISMB sediments with a well-established migration path for radionuclides from the EISMB to the WISMB by way of the physical migration of contaminated particles and through dissolved transport (Kershaw et al., 1984; Aston et al., 1985; Mitchell et al., 1999; Charlesworth et al., 2006). Data presented in this study (namely ^{137}Cs profiles) show a considerable correlation with records of radioactive discharges of the same radionuclides from Sellafield (Kershaw et al., 1990; Gray et al., 1995) (Fig. 5.6). Similarly, despite their reservations, Kershaw et al. (1990) successfully established a correlation between downcore radionuclide levels and discharge rates for ^{241}Am and ^{137}Cs in particular.

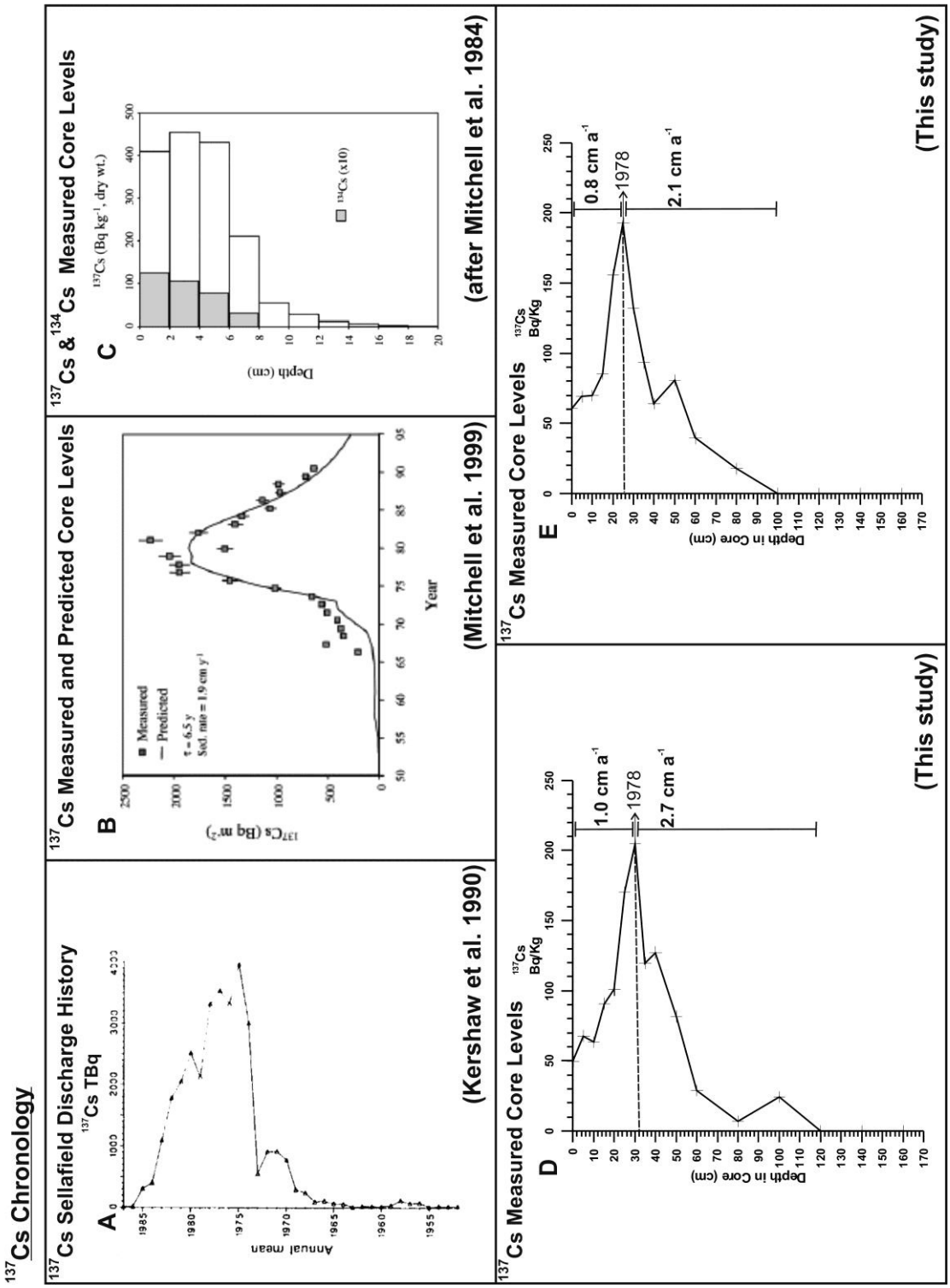

Figure 5.6 ^{137}Cs Chronology. A: Annual mean discharge of ^{137}Cs from Sellafield (from Kershaw et al. (1990)). B: Measured ^{137}Cs levels from a core studied in Mitchell et al. (1999) along with levels predicted by semi-empirical models from the same study. C: Measure ^{137}Cs levels from a core studied by Mitchell et al. (1984). D ^{137}Cs chronology for Core 1 (see 5.5.1 for explanation). C: ^{137}Cs chronology for Core 2 (see 5.5.1 for explanation).

Taking the profiles presented in Figure 5.5 and Figure 5.6, a ^{137}Cs sub-surface maximum is clearly visible at 30 cm and 25 cm in Core 1 and Core 2 respectively. A similar sub-surface peak in ^{137}Cs levels was also recorded at 20 cm in a core from the WISMB by Mitchell et al. (1999). In addition, Mitchell et al. (1984) record a sub-surface ^{137}Cs peak just beneath the surface in a core profile taken from the west of the Isle of Man in May 1982. The presence and corroboration of these sub-surface maxima would suggest that significant sedimentation is taking place in the WISMB. Based on semi-empirical modelling incorporating contributions of contemporary and historic discharges, Mitchell et al. (1999) predicted these maxima to correspond with the year 1981 with an implied sedimentation rate of 1.9 cm a^{-1}.

From our profiles (Fig. 5.5 and 5.6) it is possible to interpret the first detectable amounts of ^{137}Cs as correlating with the beginning of operations at Sellafield in 1952. Following this trend, the prominent peaks at 30 cm and 25 cm depth in Core 1 and Core 2 respectively equate with the peak in Sellafield ^{137}Cs discharge around 1978 (Gray et al., 1995). Similarly, sub-maximum peaks in both cores correlate with a period of increased discharges in the early 1970s, preceding this 1978 peak. In ^{137}Cs chronology, the Chernobyl accident of 1986 is often readily recognised in sedimentary profiles, even in Ireland (Jones and Scheib, 2007). However, from our data it appears to have been completely overprinted by the Sellafield signal. The input of ^{137}Cs to the Irish Sea from the Chernobyl fallout was estimated to be 10 TBq with negligible additional input thereafter (Hunt and Kershaw, 1990). The decline in ^{137}Cs levels in the top portion of each core also corresponds with an overall decrease in discharge from Sellafield post 1978 (Gray et al., 1995). With this in mind, and considering the top of the cores as representing 2009 (year of collection), it is possible to calculate average sedimentation rates of 2.7 cm a^{-1} and 2.1 cm a^{-1} for the time interval of 1952 - 1978 in Core 1 and Core 2 respectively. Similarly, we calculate rates of 1.0 cm a^{-1} and 0.8 cm a^{-1} for the same cores for the period of 1978 - 2009 (Fig. 5.6). By comparison, the excess ^{210}Pb curves yielded average sedimentation rates of 2.4 cm a^{-1} and 2.0 cm a^{-1} for Core 1 and Core 2 respectively which is close to values calculated for the 1952 - 1978 period in both cores. By contrast, a sedimentation rate of 0.73 cm a^{-1} was calculated by Mitchell et al. (1999) for the area based on their excess ^{210}Pb profiles and a constant rate of supply (CRS) model. They accepted, however, that this was an apparent rate and that the actual rates may be lower due to biological

and physical mixing disturbing the sediment column and leading to an overestimation of the sedimentation rate.

According to the record of Sellafield discharges, both ^{137}Cs and ^{241}Am were released from the beginning of operations in the early-1950s and peaked in the mid-1970s followed by a sharp decrease in subsequent years (Gray et al., 1995). Core profiles for both cores reflect this gradual increase from 1952 to the 1978 peak (see Fig. 5.5 and 5.6). However, only ^{137}Cs exhibits the subsequent decline in discharge whereas ^{241}Am remains relatively high. This difference in behaviour between the two radionuclides was also noted by Mitchell et al. (1999), who attributed it to differences in particle reactivity of the two radio isotopes and, subsequently, differing dispersion modes. Additionally, ^{137}Cs is the less particle-reactive of the two, and more soluble, thus spreading rapidly through the Irish Sea along with water circulation and hydrography. It is, therefore, flushed relatively rapidly from the area when discharges cease. By contrast, ^{241}Am is highly reactive in relation to particles and so binds rapidly to sediment in the immediate vicinity of the discharge site. From there, it is gradually released following resuspension of the surface sediment and subsequent transport. As a result, the deposits near the discharge site remain a source of ^{241}Am despite the fact that direct discharge has declined over time. In addition, MacKenzie et al. (1999) noted that levels of discharged ^{241}Am in the Irish Sea may be obscured by in-growth from ^{241}Pu and the redissolution of ^{137}Cs from surface sediments, constituting an additional source of ^{241}Am. In fact, McCartney et al. (1990) calculated that by 1988, up to 37% of ^{241}Am levels in the Irish Sea could be attributed to the in-growth of ^{241}Pu. With this in mind, only ^{137}Cs offers a sound basis with which to form a chronology based on core measured levels and recorded discharge levels.

5.5.2 Effects of Trawling

Accepting the ^{137}Cs signal as real and correlating with the Sellafield discharge history, from the radionuclide based chronology of the upper portion of the WISMB it was possible to calculate sedimentation rates in the area over the last 60 years approximately. As stated above, sedimentation rates for the 1952 - 1978 interval (2.1 - 2.7 cm a^{-1}) were significantly higher than the proceeding 1978 - 2009 period (0.8 - 1.0 cm a^{-1}). In addition, both these sets of sedimentation rates

are considerably higher than AMS ^{14}C derived rates for the lower portion of both cores (40 - 240 cm for Core 1 and 80 - 240 cm for Core 2) of 0.03 - 0.08 cm a^{-1} over a timescale of up to 7,000 yrs BP (Chapter 4). Furthermore, assuming the first occurrence of ^{137}Cs has been shifted downcore by 20 cm (typical burrowing depth of *N. norvegicus*) sedimentation rates for the 1952 - 1978 interval of Core 2 and Core 1 are 1.3cm a^{-1} and 1.9 cm a^{-1} respectively which are more in-line with a sedimentation rate of 1.9 cm a^{-1} for the area reported by Mitchell et al. (1999) based on ^{137}Cs levels. These new rates are still significantly higher than the average rates calculated for the upper part of the cores.

The apparent decrease in sedimentation post-1978 can be explained by two possible scenarios. The first involves a gradual or stepped decrease in the sedimentation rate to present but with deposition continuing. The second suggests a cessation of net deposition around the early 1990s. ^{137}Cs data suggests the second scenario is more viable as ^{137}Cs levels at the top of both cores were considered relatively high. So high, in fact, they occurred at levels much more akin from the mid-1980s according to data from Mitchell et al. (1999). Similarly, levels of ^{210}Pb are considerably lower than reported by Mitchell et al. (1999). Hence, in this respect, the uppermost sediment layers appear to be missing for both cores. Based on this evidence from ^{137}Cs and excess ^{210}Pb it would appear that the most recent two decades are not represented by the sedimentary stratigraphy. By extrapolating sedimentation rates for the 1952 - 1978 period it is estimated that somewhere between 17 - 53 cm of sediment is absent from the top of the core. Whilst it is accepted that some sediment would be lost during the coring process, this is not likely to explain the significant loss seen here.

One such mechanism which may account for such a loss is trawling. Fishing efforts in the Irish Sea (in particular bottom trawling) have increased dramatically over the past decades (C. Lordan, pers. comm.; Fig. 5.7). Of this activity, *Nephrops* targeted otter trawling on soft sediments accounts for one third of all trawling activity (Davie and Lordan, 2011). The focus of this activity is primarily the soft sediment dominated areas of the Aran Grounds, The Smalls and the WISMB as shown in Figure 5.2. During active trawling, depth of penetration of the seabed depends on the type of gear used as well as the sediment over which it is being towed (Hall, 1994; Kaiser et al., 1996). In soft, muddy sediments (such as in the WISMB) using *Nephrops* directed gear, the average penetration

can be between 15 - 30 cm (Power and Lordan, 2012). Such activity leaves behind visible marks (see Fig. 5.2), the persistence of which can depend on the sediment type and natural processes acting in the area (Power and Lordan, 2012).In the WISMB, underwater photography surveys by the Marine Institute found observations of trawl marks at 18% of stations (Lordan et al., 2011). Similar trawl marks were noted in the EISMB on side scan sonar by Williams et al. (1981). A study by Palanques et al. (2001) showed that these scars can remain for up to a year after the trawling event.

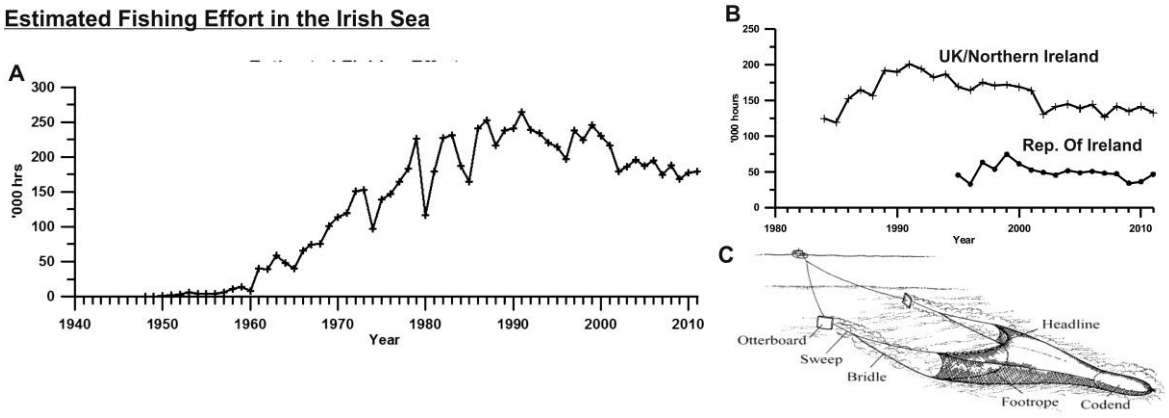

Figure 5.7 Estimated fishing effort in the Irish Sea. A: Estimated fishing effort of the Irish fleet in the Irish Sea since 1940. B: Estimated Nephrops directed trawling in the western Irish Sea. C: Schematic of an otter trawl (from Palanques (2001)).

Aside from these visible scars and the effects trawling has on species population richness and community changes (Kaiser and Spencer, 1996; Ball et al., 2000), it can also effect seabed conditions through loss of the upper surface (Palanques et al., 2001). In their study, Palanques et al. (2001) showed how between 2 - 3 cm of the seabed can be removed after a single trawl. As suggested from our own data, extrapolated excess ^{210}Pb profiles indicate that somewhere between 17 - 53 cm is absent. The study site in Palanques et al. (2001) was a previously untrawled, deep sea site. In comparison, ours is a heavily trawled, relatively shallow site with trawling occurring potentially from twice a day to five or even ten times a year (Brander, 1980; Fox et al., 1996). Hence, the intensity of trawling may account for the high level of seabed loss seen here. Similarly, the development of a seasonal gyre in the WISMB may exacerbate the issue as near bottom currents increase during this time aiding in the entrainment of sediment within the water column and its re-dispersal elsewhere (Hill et al., 1997; Horsburgh et al., 2000).

5.5.3 Influence of Bioturbation

Despite the seeming legitimacy of the chronology proposed above, significant consideration must be given to various biological and physical effects on the sediment in the WISMB which may impact on the record's fidelity. In the EISMB, Williams et al. (1981) recognised bioturbation as the dominant mechanism determining the sedimentary structure of the top 45 cm at least, with a decrease in ^{226}Ra profiles indicative of extensive mixing and reworking by organisms. In addition it plays an important role in incorporating radionuclides into the sedimentary column. As a result, they warned against the use of radionuclide accumulations for establishing sediment chronology until such time as an extensive study into animal, sediment and radionuclide interaction mechanisms was carried out. Also in the EISMB, Kershaw et al. (1988) noted significant bioturbation by *Callianassa subterranea* (Montagu) and the echiuran worm *Maxmülleria lankesteri* (Herdman).The former is known to excavate deep, extensive burrow systems (usually 20 cm and up to 1 m deep) and transport sediment to the surface (Stamhuis et al., 1997). Studies on the bioturbation of *Callianassa subterranea* found that four individuals had the capacity to expel 3500 g/m^2 dry weight of sediment from their burrows per year (Whitbaard and Duineveld, 1989). The latter, *M. lankesteri,* tends to remove fine particles from the sediment surface, subsequently depositing some of this material as fecal pellets in the upper 50 cm (Kershaw et al., 1988). Their burrow can extend down for 80 m into the sediment (Hughes et al., 1996a). Other studies on these echiuran worms found that they could expel up to 97 g dry sediment per burrow per day suggesting significant amounts of bioturbation (Hughes et al., 1996b).

The burrowing activity of *C. subterranea* in particular is noted to have had a significant influence on ^{210}Pb derived sedimentation rates in the North Sea where it is abundant (Zuo et al., 1989; de Haas et al., 1997). Here, in the Oyster Grounds, a phantom ^{210}Pb profile was recognised whereby the upper decimetres of the seabed consisted of "old" sediments with background levels partly mixed with "younger" material. X-ray radiographs confirmed the presence of bioturbation and Zuo et al. (1989) concluded that it was impossible to estimate sedimentation rates from ^{210}Pb as a result of this sediment mixing over the depth of the core. This phenomenon of transport of higher ^{210}Pb activity downward into seemingly older sediment has also been recognised by Smith and Schafer (1984) who used it as a means to investigate sediment mixing rates

In the WISMB, Kershaw (1986) established a zone of near constant age of 7780 to 8620 years based on ^{14}C dating of the carbonate fraction of core sediment samples occurring in the upper 55cm deduced to be a zone of mixing. This sharp boundary, marking the base of the bioturbated mixed layer, was confirmed in the WISMB by repeated sampling, but, not observed in the EISMB (Kershaw et al., 1988). This would suggest that bioturbation in the WISMB is restricted to the upper few decimetres and not as extensive as in the EISMB. In addition, whilst *C. subterranea* is well documented in the North Sea (with an average density of 46 individuals per m^2 according to Witbaard and Duineveld (1989)) its presence and distribution around the Irish coast is lacking in information (Power and Lordan, 2012). In fact, a study by Ball et al. (2000) into the effects of a *Nephrops* trawl on the benthos in two separate areas of the WISMB recognised *Nephrops* as the dominant species with varying degrees of richness of other macrofauna, but no recording of *C. subterranea* or *M. lankesteri* . Therefore, the most prominent agent of bioturbation in the WISMB is most likely *Nephrops norvegicus*. These tend to form simple burrows that are usually 20 - 30 cm deep (Hughes et al., 1996a).

Our own CT X-ray scans suggest that bioturbation is indeed present in core profiles. It is mostly confined to the uppermost 30 cm suggesting that bioturbation is, in fact, predominantly carried out by *N. norvegicus* (Fig. 5.3). Similarly, the irregularity of the excess ^{210}Pb could be due to an injection of recent material into older sediments by burrowers such as *Nephrops*. Our ^{226}Ra profiles were not conclusive in revealing different rates of bioturbation at both sites (Fig. 5.5). However, the seemingly good preservation of the Sellafield discharge signal for ^{137}Cs across both cores, and its corroboration with similar profiles elsewhere in the WISMB from Mitchell et al. (1984; 1999) would suggest that bioturbation isn't that intense.

Palanques et al. (2001) also noted a general coarsening and silt enrichment in their studied cores post trawling. Whilst a similar upward coarsening in core profiles can be found in our study, this most likely as a result of changing environmental conditions during the course of the mid- to late-Holocene (Chapter 4). It is therefore too difficult to differentiate between any potential sediment coarsening as a result of trawling against the background environmental-driven sedimentation. However, what is noticeable is the geotechnical relationship between shear strength and sediment composition (Fig. 5.4). Yuan et al. (1992) recognised the sediments found in the upper portion of

the WISMB as behaving mechanically as normally consolidated marine deposits. Average shear strength values for the cores studied lay between 4.5-8.3 kPa which is considered normal for such sediments (Christian et al., 1991). For each of the cores examined the lowest shear strength values occurred in the upper 20 cm with values less than 2 kPa (Fig. 5.4). Whilst trawling may contribute to this lowering of shear strength through extensive sediment mixing, the burrowing and feeding activities of benthic macro invertebrates can also affect the sediment column in a number of ways including biostratigraphy, textural features and geotechnical properties (Smith and Schafer, 1984). Decreases in shear strengths owing to bioturbation have been observed in silty mud sediments (Rowe, 1974) and in sandy sediments (Myers, 1977). Despite inferences from radionuclide profiles that bioturbation is relatively low, evidence for biological activity is visible in CT X-ray scans with the majority of it in the upper 20 - 40 cm (Fig. 5.3). Similarly, underwater photography from across the area reveals an abundant density of burrows present on the seafloor (Fig. 5.1). These burrows are generally excavated by *Nephrops* or burrowing fish and are larger than any other burrowing organism that may be found in the area (Davie and Lordan, 2011). Due to their size, large amounts of sediment may be expelled during initial construction of the burrow, with further maintenance capable of producing significant bioturbation of the sediment (Power and Lordan, 2012). Further downcore, values rise significantly to reach maximum peaks of up to 27 kPa. Whilst there is an increase in clay content downcore in each instance (which would increase shear strength given significant amounts) the sediment composition does not change sufficiently to account for this discrepancy in values between the top portion and the rest of the core. It has been postulated that in certain cases bioturbation may, in fact, result in an increase in shear strength within localised zones. It has been noted that burrowing macrofauna, particular at high population densities, can produce mucous secretions that bind sediment into vertical structures which may increase the sediment cohesion (Krantzberg, 1985). Whilst no clear evidence for such bioturbation was seen at similar horizons as shear strength peaks it cannot be discounted. Often the uppermost centimetres represent the “mixed layer” which is completely bioturbated and homogenised, characterised by low shear strengths (Löwemark and Werner, 2001). Below this is the transition layer where some burrows may be preserved and maintain localised high shear strength values. Christian et al. (1991) found undrained shear strengths as high as 47 kPa measured with free-fall cone on indurated Malaniid burrows. Finally, as sedimentation continues and, layers are successively

transferred upwards, the deepest burrows become preserved in the historical layer. During subsequent decomposition of burrows with burial, water contents are allowed to recover slightly and, ultimately, lead to a return of more normal, or even lower, levels for shear strength (Löwemark and Werner, 2001).

5.6. CONCLUSIONS

Despite the warnings of Williams et al. (1981), this study was able to establish a core based sediment chronology for the upper portion of the Western Irish Sea Mud Belt based primarily on levels of the anthropogenic radionuclide ^{137}Cs and correlations with published records of radioactive discharge from Sellafield. This chronology was repeated in two cores taken from the area and corroborated with a further two cores from previous studies by other authors. Subsequently, it was revealed that what appeared to be a relatively undisturbed core was, in fact, missing 17 - 53 cm of the sedimentary record from the top of the core or approximately the last two decades. Extensive trawling in the area for *Nephrops norvegicus* is suggested as the mechanism for this substantial loss of sediment. In addition, trawling has further affected the seafloor in the area by leaving visible trawl marks. A combination of trawling and bioturbation has also lowered the shear strength of sediment in the uppermost 20 cm which could potentially lead to further loss or remobilization of sediment from continued trawling or increased near bottom currents due to a seasonal gyre or other environmental/climatic changes in the area. Similarly, however, higher localised areas of shear strength may be attributed to indurated burrows.

Whilst the ^{137}Cs based chronology seems to hold up well, the spectre of bioturbation cannot be ignored. CT X-rays and ^{210}Pb do indicate biological activity but not, perhaps, as intense as reported by other authors. Yet, at the same time, bioturbation may result in a possible displacement of the profile by as much as 30 cm in the sediment column which is the average burrowing depth for *Nephrops norvegicus*. Other profiles for ^{241}Am and ^{226}Ra could not be corroborated with Sellafield discharge history.

Given the recent focus on recent anthropogenic induced environmental change, particularly in the marine realm, we would argue that the Western Irish Sea Mud Belt and this radionuclide based chronology is a prime area and tool to study for such changes in the Irish Sea including nutrient loading and use of stable isotopes.

REFERENCES

Allen, J.R., Slinn, D.J., Shammon, T.M., Hartnoll, R.G., Hawkins, S.J., 1998. Evidence for eutrophication of the Irish Sea over four decades. Limnology and Oceanography 43, 1970–1974.

Appleby, P.G., Oldfield, F., 1978. The Calculation of 210Pb dates assuming a constant rate of supply of unsupported 210Pb to the sediment. Catena 5, 1–8.

Aston, S.R., Assinder, D.J., Kelly, M., 1985. Plutonium in Intertidal Coastal and Estuarine Sediments in the Northern Irish Sea. Estuarine, Coastal and Shelf Science 20, 761–771.

Ball, B.J., Fox, G., Munday, B.W., 2000. Long- and short-term consequences of a Nephrops trawl fishery on the benthos and environment of the Irish Sea. ICES Journal of Marine Science 57, 1315–1320.

Belderson, R.H., 1964. Holocene sedimentation in the western half of the Irish Sea. Marine Geology 2, 147–163.

Blott, S.J., Pye, K., 2001. GRADISTAT: a grain zize distribution and statistics package for the analysis of unconsolidated sediments. Earth Surface Processes and Landforms 26, 1237–1248.

Brander, K., 1980. Fisheries management and conservation in the Irish Sea. Helgoländer Wissenschaftliche Meeresuntersuchungen 33, 687–699.

Charlesworth, M.E., Service, M., Gibson, C.E., 2006. The distribution and transport of Sellafield derived 137 Cs and 241 Am to western Irish Sea sediments. The Science of the Total Environment 354, 83–92.

Christian, H.A., Piper, D.J.W., Armstrong, R., 1991. Strength and consolidation properties of surficial sediments, Flemish Pass: effects of biological processes. Deep-Sea Research 38, 663–676.

Cohen, K.M., Finney, S.C., Gibbard, P.L., Fan, J.X., 2013. The ICS International Chronostratigraphic Chart. Episodes 36, 199–204.

Crutzen, P.J., Stoermer, E.F., 2000. The Anthropocene. Global Change Newsletter 41, 17–18.

Davie, S., Lordan, C., 2011. Definition, dynamics and stability of métiers in the Irish otter trawl fleet. Fisheries Research 111, 145–158.

De Haas, H., Boer, W., van Weering, T.C.E., 1997. Recent sedimentation and organic carbon burial in a shelf sea: the North Sea. Marine Geology 144, 131–146.

Evans, G.L., le B. Williams, P.J., Mitchelson-Jacob, E.G., 2003. Physical and anthropogenic effects on observed long-term nutrient changes in the Irish Sea. Estuarine, Coastal and Shelf Science 57, 1159–1168.

Folk, R.L., Ward, W.C., 1957. Brazos River Bar: a study in the significance of grain size parameters. Journal of Sedimentary Petrology 27, 3–26.

Fox, G., Ball, B.J., Munday, B.W., Pfeiffer, N., 1996. The IMPACT II study: preliminary observations on the effect of bottom trawling on the ecosystems of the Nephrops grounds in N.W. Irish Sea, in: Irish Marine Science 1995. pp. 337–354.

Gerritsen, H., Lordan, C., 2011. Integrating vessel monitoring systems (VMS) data with daily catch data from logbooks to explore the spatial distribution of catch and effort at high resolution. ICES Journal of Marine Science 68, 245–252.

Gerritsen, H.D., Minto, C., Lordan, C., 2013. How much of the seabed is impacted by mobile fishing gear? Absolute estimates from Vessel Monitoring System (VMS) point data. ICES Journal of Marine Science 68, 245–252.

Gray, J., Jones, S.R., Smith, A.D., 1995. Discharges to the environment from the Sellafield site, 1951-1992. Journal of Radiological Protection 15, 99.

Hall, J.S., 1994. Physical disturbance and marine benthic communities: life in unconsolidated sediments. Oceanography and Marine Biology 32, 179–239.

Hill, A.E., Brown, J., Fernand, L., 1997. The summer gyre in the Western Irish Sea: Shelf sea paradigms and management implications. Estuarine, Coastal and Shelf Science 44, Supple, 83–95.

Horsburgh, K.J., Hill, A.E., Brown, J., Fernand, L., Garvine, R.W., Angelico, M.M.P., 2000. Seasonal evolution of the cold pool gyre in the western Irish Sea. Progress in Oceanography 46, 1–58.

Houlsby, G.T., 1982. Theoretical analysis of the fall cone test. Géotechnique 32, 111–118.

Hughes, D., Ansell, A.D., Atkinson, R.J.A., 1996. Distribution, ecology and life-cycle of Maxmuelleria lankesteri (Echiura: Bonelliidae): A review with notes on field identification. Journal of Marine Biological Association of the UK 76, 897–908.

Hughes, D.J., Ansell, A.D., Atkinson, R.J.A., 1996. Sediment bioturbation by the echiuran worm Maxmuelleria lankesteri (Herdman) and its consequences for radionuclide dispersal in Irish Sea sediments. Journal of Experimental Marine Biology and Ecology 195, 203–220.

Hunt, G.J., Kershaw, P.J., 1990. Remobilisation of artificial radionuclides from the sediment of the Irish Sea. Journal of Radiological Protection 10, 147–151.

Jones, D.G., Scheib, C., 2007. A preliminary interpretation of Tellus airborne radiometric data.

Kaiser, M.J., Hill, A.S., Ramsay, K., Spencer, B.E., Brand, A.R., Veale, L.O., K, P., Rees, E.I.S., Munday, B.W., Ball, B., Hawkins, S.J., 1996. Benthic disturbance by fishing gear in the Irish Sea: comparison of beam trawling and scallop dredging. Aquatic Conservation: Marine and Freshwater Ecosystems 6, 269–285.

Kaiser, M.J., Spencer, B.E., 1996. The effects of beam-trawl disturbance on infaunal communities in different habitats. Journal of Animal Ecology 65, 348–358.

Kershaw, P.J., 1986. Radiocarbon dating of Irish Sea sediments. Estuarine, Coastal and Shelf Science 23, 295–303.

Kershaw, P.J., Swift, D.J., Denoon, D.C., 1988. Evidence of recent sedimentation in the eastern Irish Sea. Marine Geology 85, 1–14.

Kershaw, P.J., Swift, D.J., Pentreath, R.J., Lovett, M.B., 1984. The incorporation of plutonium, americum and curium into the Irish Sea seabed by biological activity. The Science of the Total Environment 40, 61–81.

Kershaw, P.J., Woodhead, D.S., Malcolm, S.J., Allington, D.J., Lovett, M.B., 1990. A Sediment History of Sellafield Discharges. Journal of Environmental Radioactivity 12, 201–241.

Krantzberg, G., 1985. The Influence of Bioturbation on Physical , Chemical and Biological Parameters in Aquatic Environments : A Review. Environmental Pollution 39, 99–122.

Lordan, C., Service, M., Doyle, J., Fitzgerald, R., 2011. Western Irish Sea Nephrops Grounds (FU15) 2011 UWTV Survey Report.

Löwemark, L., Werner, F., 2001. Dating errors in high-resolution stratigraphy: a detailed X-ray radiograph and AMS- 14 C study of Zoophycos burrows. Marine Geology 177, 191–198.

MacKenzie, A.B., Cook, G.T., McDonald, P., 1999. Radionuclide distributions and particle size associations in Irish Sea surface sediments: implications for actinide dispersion. Journal of Environmental Radioactivity 44, 275–296.

McCartney, M., Kershaw, P.J., Alley, R.B., 1990. The Behaviour of 210Pb and 226Ra in the Eastern Irish Sea. Journal of Environmental Radioactivity 12, 243–265.

Mitchell, P.I., Condren, O.M., Leo, L., Mcmahon, C.A., 1999. Trends in plutonium , americium and radiocaesium accumulation and long-term bioavailability in the western Irish Sea mud basin. Journal of Environmental Radioactivity 44, 223–251.

Mitchell, P.I., Gonzalo, M., Vidal-Quadras, A., n.d. Levels of radioactive caesium and potassium in the marine environment of Ireland, in: Actas de La IX Reunión Anual de La Sociedad Nuclear Espanola, Sevilla. pp. 1–20.

Myers, A.C., 1977. Sediment processing in a marine subtidal sandy bottom community. I. Physical aspects. Journal of Marine Research 35, 609–632.

Oldfield, F., Barnosky, a. D., Dearing, J., Fischer-Kowalski, M., McNeill, J., Steffen, W., Zalasiewicz, J., 2013. The Anthropocene Review: Its significance, implications and the rationale for a new transdisciplinary journal. The Anthropocene Review 1, 3–7.

Palanques, A., Guille, J., Puig, P., 2001. Impact of bottom trawling on water turbidity and muddy sediment of an unfished continental shelf. Limnology and Oceanography 46, 1100–1110.

Power, J., Lordan, C., 2012. A review of the effects of bottom trawling on soft sediments; sea pens and burrowing megafauna biotope complexes.

Rogers, S.I., Maxwell, D., Rijnsdorp, A.D., Damm, U., Vanhee, W., 1999. Fishing effects in northeast Atlantic shelf seas : patterns in fishing effort , diversity and community structure . IV . Can comparisons of species diversity be used to assess human impacts on demersal fish faunas ? Fisheries Research 40, 135–152.

Rowe, G.T., 1974. The effects of the benthic fauna on the physical properties of deep-sea sediments, in: Deep-Sea Sediments: Physical and Mechanical Properties. pp. 381–400.

Smith, J.N., Schafer, C.T., 1984. Bioturbation processes in continental slope and rise sediments delineated by Pb–210, microfossil and textural indicators. Journal of Marine Research 42, 1117–1145.

Stamhuis, E.J., Schreurs, C.E., Videler, J.J., 1997. Burrow architecture and turbative activity of the thalassinid shrimp Callianassa subterranea from the central North Sea. Marine Ecology Progress Series 151, 155–163.

Veale, L.O., Hill, A.S., Hawkins, S.J., Brand, A.R., 2000. Effects of long-term physical disturbance by commercial scallop fishing on subtidal epifaunal assemblages and habitats. Marine Biology 137, 325–337.

Witbaard, R., Duineveld, G.C.A., 1989. Some aspects of the biology and ecology of the burrowing shrimp Callianassa subterranea (Montagu) (Thalassinidea) from the southern North Sea. Sarsia 74, 209–219.

Williams, S.J., Kirby, R., Smith, T.J., Parker, W.R., 1981. Sedimentation studies relevant to low level radioactive effulent dispersal in the Irish Sea. II. Sea bed morphology, sediments and shallow sub-bottom stratigraphy of the eastern Irish Sea.

Yuan, F., Bennell, J.D., Davis, A.M., 1992. Acoustic and physical characteristics of gassy sediments in the western Irish Sea. Continental Shelf Research 12, 1121–1134.

Zalasiewicz, J., Williams, M., Fortey, R., Smith, A., Barry, T.L., Coe, A.L., Bown, P.R., Rawson, P.F., Gale, A., Gibbard, P., Gregory, F.J., Hounslow, M.W., Kerr, A.C., Pearson, P., Knox, R., Powell, J., Waters, C., Marshall, J., Oates, M., Stone, P., 2011. Stratigraphy of the Anthropocene. Philosophical Transactions of the Royal Society A: Mathematical, Physical and Engineering Sciences 369, 1036–1055.

Zuo, Z., Eisma, D., Berger, G.W., 1989. Recent sediment deposition rates in the oyster ground, North Sea. Netherlands Journal of Sea Research 23, 263–269.

CHAPTER 6

"Any intelligent fool can make things bigger, more complex, and more violent. It takes a touch of genius, and a lot of courage, to move in the opposite direction."— Albert Einstein.

SUMMARY

6.1 Findings

New geological and geophysical data for the North Sea and Irish Sea were supplemented by in-situ geotechnical data in this study to reappraise their stratigraphic framework. In general, for both areas, it can be concluded that in-situ geotechnical measurements (in this case Cone Penetration Testing or CPT) offer the ideal intermediary tool with which to marry geophysical (seismic) and geological (core) data in identifying lithological units and correlating them across an area.

Specifically, in relation to the German North Sea sector, with improved seismic data and higher core density better mapping of the the extent of these units was carried out in comparison to previous studies (i.e. Sindowski, 1970). Our study found that tunnel valleys exert a strong control over lateral and vertical sedimentary successions with their infill generally markedly different to background (or non-tunnel valley) sedimentation. In most cases the common succession of these tunnel valleys consisted of dense meltwater sands grading into finer units of low-energy clays and silts. Tunnel valleys can act as depocentres and sedimentary palaeoarchives with sedimentary units accumulating that may otherwise be eroded or reworked during subsequent erosive events like ice sheet advance or marine transgressions. This is best represented by the major E-W trending tunnel valley in Area 1 (section 2.6.1) where lacustrine-like sediments associated with the Holstein transgression (Juist Member of the Wacken Formation) are found. Outside of tunnel valley successions, sedimentary sequences of Quaternary deposits range in thickness from a few metres up to 60 m. The most ubiquitous of units was that of the Borkum Formation covering all areas and representing the most recent marine transgression during the late Weichselian/early Holocene.

Background Quaternary sedimentary cover was thinnest towards the south coast in Areas 1 and 4 comprising of the Borkum and Riffgatt Formations overlying bedrock Neogene sands. Further north and east in Area 2 and Area 3 respectively more extensive development of other units (namely the Helgoland, Wacken and Entenschnabel Formations) was visible in both seismic and core profiles.

In the Western Irish Sea Mud Belt, we employed a similar investigating combining geological, geophysical and geotechnical data. Here, we found our results to show that the sedimentary architecture is more complex than previously stated. This can be attributed to a paucity of information regarding the nature of sediments at depth in the WISMB. However, by employing the MARUM GOST CPT system we were able to geotechnically distinguish sediments up to 30 mbsf. The sedimentary succession likely comprises of till at the base, overlying bedrock, grading upwards into dense meltwater related gravels, sands and silts overlain by an upper marine mud layer often found to contain gas-charged sediments associated with shallow methane accumulation. With further analyses on this area of sediment accumulation using 3 m cores and a multi-proxy approach, a detailed palaeoenvironmental reconstruction for the Mid to Late Holocene was achieved. Natural environmental change was identified in our analysis which was related to known climatic periods. Generally, this comprised a low-sedimentation period of climatic stability from the base of the core record (7,000 years BP) to approximately 4,500 years BP coinciding with the Holocene Thermal Optimum. Bottom velocities and higher energy events became more prevalent in general after this until 100 years BP as the record in all proxies becomes more variable due to fluctuating climatic conditions associated with the Dark Ages Cold Period, Medieval Warm Period and Little Ice Age.

The use of gamma spectrometry, and in particular the anthropogenic radionuclide ^{137}Cs, allowed for a sedimentary chronology be established based on comparison with output levels from Sellafield nuclear plant. As a result, the past 100 years or so can be tightly constrained using a combination of AMS ^{14}C dates and gamma spectrometry. During this period there is a remarkable increase in sedimentation with increased amounts of coarser material. This may be attributed to the combination of a number of factors including the higher frequency of storm-like events and the

development of a seasonal gyre in the area. Similarly, higher riverine input is seen due to increased precipitation over land.

In addition, the use of gamma spectrometry also offered an insight into other anthropogenic impacts, namely trawling. Through our analysis, it was revealed that what appeared to be a relatively undisturbed core was, in fact, missing 17 - 53 cm of the sedimentary record from the top of the core or approximately the last two decades due to the effects of extensive trawling.

6.2 Recommendations

In the present thesis, the stratigraphic framework for the German North Sea sector was revised based on 72 core profiles of up to 50 m depth, 196 CPT profiles of same and some 320 seismic lines in comparison to Sindowski (1970) who used 23 cores. The majority of these data were gathered during various surveys relating to site investigations for offshore windfarm development. With the continued growth of this sector, and the prospect of further surveying, the potential for applying our approach and defining lithological units based on core along with seismic and CPT data can be applied to different areas and incorporated into our framework. Additionally, there is currently more existing core material, CPT profiles and seismic lines which could not be analysed during this study due to time constraints. Studying this extra data could help further delineate units such as the Riffgatt formation which show a large degree of heterogeneity.

Whilst the CPT investigation in the WISMB revealed a greater heterogeneity in the sedimentary succession than previously thought, there is a real need to groundtruth this data at depth using coring, drilling or other deep (>6 m) sampling methods. During the course of this study, the WISMB was assessed geologically for its potential as a site for offshore wind turbine construction. Although, ground conditions were found to be favourable and there was no recorded instance of extensive erosion or scour of the seabed, Callaway et al. (2009) has shown previously how an obstruction on the seabed in this area (i.e. rock outcrop) can increase current acceleration and subsequent vortex evolution and shedding resulting in the initiation of scour. As a result, the

WISMB would benefit greatly from predictive scour modelling, parameters for which could be derived from our own CPT data.

With regard to the Mid to Late Holocene palaeoenvironmental reconstruction, this was carried out on three main cores using a number of proxies. All cores used bear the potential for further analyses. Initially, the present sampling resolution of 5 cm for PSA could be increased to a higher density. Similarly, the 10 cm interval for foraminiferal sampling could be increased, with the >125 µm fraction also investigated. Further AMS ^{14}C dating (particularly in the upper parts of each core) would also help further constrain the age model. Stable isotopes would also aid in unravelling the palaeoenvironmental story.

Our ^{137}Cs based gamma spectrometry was compared with similar profiles by other workers and found to correlate strongly. Further such core profiles from other parts of the WISMB would help strengthen this chronology, as would a full qualitative and quantitative study of bioturbation processes and effects in the WISMB.

Sedimentation rates in the WISMB are recorded as increasing dramatically in the last 100 years approximately and our subsurface ^{137}Cs peaks would indicate that continued sedimentation is currently operating. Sediment traps or other physical devices measuring sedimentation rates would greatly help in validating this increase in sedimentation and proving sedimentation is, in fact, still on-going.

The low sedimentation rate for the lower portion of the core derived from dating would suggest that the record here is likely to be incomplete as a result of environmental (periods of erosion/hiatus) or possibly mechanical (autocompaction, coring method) effects. Whilst the sediments appear to be normally consolidated, the effect of auto-compaction is well known to distort such data and may result in decreases in the apparent sedimentation rate of up to 60% (Scourse et al., 2002). This effect can be corrected for by measuring the liquid limit of the sediment to construct a porosity-depth profile and so show how a section of sediment would compact with increasing overburden with depth according to a sediment compression line (Skempton, 1969; Burland, 1990).

REFERENCES

Burland, J.B., 1990. On the compressibility and shear strength of natural clays. Géotechnique 40, 329–378.

Callaway, A., Smyth, J., Brown, C.J., Quinn, R., Service, M., Long, D., 2009. The impact of scour processes on a smothered reef system in the Irish Sea. Estuarine, Coastal and Shelf Science 84, 409–418.

Scourse, J.D., Austin, W.E.N., Long, B.T., Assinder, D.J., Huws, D., 2002. Holocene evolution of seasonal stratification in the Celtic Sea: refined age model, mixing depths and foraminiferal stratigraphy. Marine Geology 191, 119–145.

Sindowski, K.-H., 1970. Das Quartär im Untergrund d e r Deutschen Bucht (Nordsee). Eiszeitalter und Gegenwart 1–18.

Skempton, A.W., 1969. The consolidation of clays by gravitational compaction. Quarterly Journal of the Geological Society 125, 373–411.

QUATERNARY GEOLOGY OF THE GERMAN NORTH SEA AND WESTERN IRISH SEA MUD BELT: REVISED STRATIGRAPHIES, GEOTECHNICAL PROPERTIES, SEDIMENTOLOGY AND ANTHROPOGENIC IMPACTS

Mark J.C. Coughlan

This thesis is submitted in fulfilment of the requirement of the degree of Doctor of Philosophy

National University of Ireland, Cork
School of Biological, Earth & Environmental Sciences (Discipline of Geology)
College of Science, Engineering & Food Science.

Head of School: Dr. Sarah Culloty
Research Supervisor: Prof. Andy J. Wheeler
Co-Research Supervisor: Prof. Dr. Tobias Mörz
Research Advisor: Dr. Boris Dorschel

Vol 2 of 2
(Appendices)

February 2015

APPENDICES

APPENDIX A

OFFSHORE RENEWABLE ENERGYSITE SUITABILITY MAPPING (ORESSUM) REPORT

INTRODUCTION

The ORESSuM report was undertaken in the first year of the PhD and was funded by the INFOMAR Programme of the Geological Survey of Ireland (GSI).

ORESSuM

Offshore Renewable Energy Site Suitability Mapping

Mark Coughlan, Dr. Andrew Wheeler and Dr. Boris Dorschel

March 2011

EXECUTIVE SUMMARY

High wind speeds coupled with energetic tidal regimes and strong waves exist off the coast of Ireland. It forms a large, relatively untapped renewable energy source that could help Ireland reach its green energy targets in the future. So far offshore wind energy has only been harnessed at Arklow Bank on the east coast whereas tidal and wave energy devices are still largely at the research and development stage.

In order to expand the offshore renewable energy sector Ireland needs to be able to provide detailed information and data from a variety of disciplines when it comes to site selection for offshore installations. In this regard a large amount of data pertinent to the offshore renewable energy sector has been collected over the decades, particularly as part of the INFOMAR program. This data forms a sound basis from which to create geological models for areas identified as being potential sites for development. However, there is scope for additional data collection, especially with reference to studying seabed dynamics. Practices such as the deployment of ADCP's and other such current velocity monitoring equipment during the course of site surveys would greatly enhance the comprehensiveness of the survey and its ability to provide the necessary data for not only the initial geological model but also subsequent studies such as scour modeling and sediment transport which, over time, need to be monitored throughout an installations lifetime.

Similarly, the importance of adequate sample collection is highlighted in the case studies mentioned within with particular reference made to the OSIG guidelines which serve as a useful reference with regard to site survey best practice.

By assessing the INFOMAR dataset and its ability to meet industry requirements it is possible to tailor future INFOMAR data collection and, in doing so, address one of Ireland's key policy objectives of enhancing the knowledge economy and renewable energy sector, which are the current government's perceived key economic drivers.

1. PROJECT BACKGROUND

1.1 Renewable Energy

Renewable energy comes from inexhaustible sources which are continually replaced (e.g. wind, hydro power, direct solar power, wave, biomass, geothermal and tidal). The utilization of these sources produces little or no carbon dioxide as well as other such greenhouse gases identified as the main drivers of global climate change today, widely considered the most pressing environmental issue of the modern age.

The Irish State is committed to achieving a target of 16% of all its energy needs (heat, transport, electricity) to come from renewable sources by 2020 under Directive 2009/28/EC as part of the EU's commitment to the Framework Convention on Climate Change signed at Kyoto in 1997. Ireland has at its disposal ample potential from renewable sources to achieve this goal, particularly in its offshore sector (i.e. offshore wind, wave and tidal energy)

1.2 Sites Around Ireland

The greatest potential for offshore wind energy in particular lies off the western coast. However, water depth increases too rapidly and so installations have to be located close to land where wave exposure is high and connection to the grid presents a problematic issue. Similarly, wave energy potential is greatest off the west coast and is a more feasible option here than wind. The south coast is generally unfeasible due to a lack of shallow water close to shore and the close proximity of bedrock or rock exposure to the seabed. The east coast provides the necessary shallow water conditions to make wind energy viable as well as depths with high energy hydrodynamic regimes which make tidal energy a possibility. However, this high energy also makes scour a destructive and limiting factor.

1.3 Current State of Irish Offshore Renewable Sector

In recent years tidal and ,in particular, wave energy have become the main focus of offshore renewable energy in Ireland whereas wind has become the most viable and hence most developed with installations constructed at Skerd Rocks, Codling Bank, and Arklow Bank, with further sites set to be developed at Dundalk Bay, Bray and Kish Banks. The Irish Government has set a target to

have 500MW of wave and tidal capacity in operation by 2020, transforming the island of Ireland into 'Europe's Battery'.

Research into tidal energy has been largely conducted in estuaries most notably Strangford Lough which has the worlds first commercial scale turbine commissioned in 2007. Issues identified with the installation of these turbines focus mostly on socio-economic factors and their operational layout. Socio-economic factors relate to navigation paths for commercial and recreational vessels being blocked. Usually, turbines are constructed in banks with lines of turbines one behind the other resulting in energy being dissipated once it passes the first line contributing to lower energy yields for subsequent lines of turbines. Areas within the Irish Sea have been identified where tidal energy is high and that are sufficiently distanced from shore so that the above constraints are negated. However, the high energy hydrodynamic regimes of these areas also have increased seabed scour which is a limiting factor in constructing foundations.

Ireland has a first-rate ocean energy research base represented by both academic and commercial interests with world class levels of expertise in project design, testing and mooring design. The Marine Institute, in association with Sustainable Energy Ireland, has established an Ocean Energy Test Site for scaled prototypes of wave energy devices in Galway Bay where, most notably, Ocean Energy Ltd. and Wavebob Ltd. are currently testing prototypes. The Sustainable Energy Authority of Ireland also plans to develop a National Wave Energy Test Site to be located off Annagh Head, west of Belmullet in County Mayo. This test site will provide a location for the temporary mooring and deployment of wave energy machines in order to monitor their ability to generate electricity and survive open ocean conditions.

Wind currently remains the most viable of all offshore renewable energy sources because of Ireland's large wind resource (up to 9m/sec in some places). The majority of these projects have targeted the banks located offshore of the eastern coast. This includes most notably the construction of seven turbines at Arklow Bank located roughly 11.7km offshore in an average water depth of 20m. Each capable of generating up to 3.6MW, totaling 25MW altogether. Phase 2 of the Arklow Bank project is currently dormant but environmental impact assessments (EIA's) and site surveys are currently being carried out at Codling Bank, Dundalk Bay and the Kish and Bray Banks in the Irish Sea as well as Skerd Rocks on the west coast for the potential construction of turbines.

With increasing technology in this sector the construction of windfarms in water depths between 30-40m is becoming more and more feasible. This pushes locations for potential windfarms further offshore away from banks where sedimentary environments are less mobile and therefore scour is less of a problem.

1.4 Scope of the Study

We will assess the current state of the offshore renewable energy sector in Ireland identifying the key datasets as identified by industry as being of vital importance in the construction of offshore renewable energy installations, investigating the availability of these datasets and assessing INFOMAR's ability to provide such datasets highlighting gaps

The chief data requirements referred to consider seabed geology and sedimentary dynamics related data. However, the scope of the study also considers socio-economic, ecological, metocean and general physical factors.

A number of case studies regarding data use in successful offshore projects are also presented.

2. METHODS

2.1 Industry Appraisal

Telephone interviews and email correspondence were carried out with people identified as having an interest and currently working in the offshore renewable sector in Ireland as well as abroad. Similarly the Irish Renewable Energy Summit 2010 was attended in order to network and speak first hand with industry players as well as gather information regarding the current state of the sector.

The information sought through these correspondences was;

- The company's current interest in Irelands offshore renewable energy sector;
- The perceived datasets required in offshore installation construction;
- Which of these datasets were sourced from INFOMAR or other state bodies;
- Which of these datasets were acquired by third party investigations and surveys;
- The level of satisfaction regarding dataset availability and usability;

- Any potential areas that company had earmarked for future site investigation.

2.1 Data Collection and Integration

The basic data source for this desktop study report comes from phone interviews, email correspondence and data exchange with key people involved in the offshore renewable energy sector and government bodies undertaken during early 2010. These correspondences provide technical and non-technical information as well as data pertinent to the industry. Available information and data, where possible, were summarised in excel spreadsheets, geo-referenced, incorporated into a GIS. The table below gives an overview of the available data sets and their sources utilized.

Data Type	Data Source
Seabed Sediment Classification	GSI (INFOMAR)
Bedforms and Topograhy	GSI (INFOMAR)
Faults	GSI (INFOMAR)
Water Depth (Bathymetry)	GSI (INFOMAR)
Wind Speed, Direction, Frequency	Marine Institute
Wave Height, Direction, Period and Power	Marine Institute
Tidal Range and Period	Marine Institute
Offshore Weather Reports	Marine Institute and Met Eireann
Special Areas of Conservation	National Parks and Wildlife Service
Special Protected Areas	National Parks and Wildlife Service
Commercial Navigation	Irish Maritime Development Office
Fisheries	Marine Institute
Pipelines and Cables	Kingfisher Information Service, Department of Petroleum Affairs
Shipwrecks	Underwater Archeological Unit
Military Exclusion Zones	Department of Defence

3. APPRAISAL OF INDUSTRY NEEDS

3.1 Introduction

Site suitability mapping is an integral part of the construction of offshore installations and requires data acquisition from across a variety of disciplines. INFOMAR offers a variety of mapping products for different offshore areas. However, very often companies are forced to carry out in-house surveys or hire private specialized groups to supplement publically provided data or gather data that is missing or outstanding.

By documenting industry data needs and subsequently assessing INFOMAR's ability to satisfy these needs it is possible in the future to tailor INFOMAR site surveying to maximize data collection potential hence increasing its data output helping make offshore renewable energy a more economically viable option in Ireland.

The various datasets and requirements we identified in consultation with industry can subsequently be grouped into the following broad headings:

- Geological Features (Section 3.2)
- General Physical Features (Section 3.3)
- Ecological Factors (Section 3.4)
- Socio-economic Factors (Section 3.5)

3.2 Geological Features

An in-depth knowledge of the seabed geology is particularly important to offshore renewable energy resource development as it heavily influences anchoring and foundation construction for offshore renewable energy installations which in turn affects cost, one of the main drivers in such projects. Generally speaking, Geological Features can be divided into three distinct headings:

1) Seafloor Morphology, including:
    - Seabed slopes and gradients
    - Bedforms
    - Seabed Dynamics
2) Quaternary Geology, including:
    - Sediment type and classification

- Depth of transition to bedrock

3) Solid Geology, including:
    - Bedrock description
    - Faults
    - Oil/gas accumulations

3.2.1 Seafloor Morphology

3.2.1.1. Seabed Dynamics

Seabed dynamics is primarily concerned with mobile sediment and the hydrodynamic regime which drives them. Essentially the prime concern associated with seabed dynamics is scour which destructively affects foundations of offshore installations. Negating scour is a costly issue in construction and where possible areas with high scour potential are excluded from site mapping. Predicting scour is largely done by modeling based on a series of geotechnical parameters measured in the sediment from the area under investigation.

3.2.1.2. Seabed Slopes and Gradients

Seabed gradients and slopes are also important in the site identification process as installation foundations are generally not constructed on slopes greater than 5^{o}.

3.2.1.3. Bedforms

Bedforms are the result of sediment mobility and hence are important to identify when establishing the hydrodynamic regimes, hence scour potential, of potential sites.

3.2.2 Quaternary Geology

Quaternary geology and associated structures heavily affect foundation design. Classification of these sediments can be carried out using acoustic techniques. Sub-bottom profiling can identify sedimentary strata continuity and thickness as well as sedimentary mega-structures. However, acoustic data must be supported by groundtruthing by way of coring and sampling.

3.2.2.1 Sediment Type and Classification

Information regarding seabed sediments is an important factor in offshore installation construction as analysis of sediment samples can influence foundation design. They may be used in geotechnical investigations to assess the various properties of the sediment including strength,

cohesion, liquefaction potential and scour potential as well as the extent of sediment mobility across an area. As a rule, dense sands and silts are preferred, although gravel is often acceptable.

Seabed sediment studies have been carried out most successfully utilizing a combination of broad scale remote sensing (i.e. acoustic backscatter) and small scale ground-truthing. Information regarding seabed sediments should be ideally consist of a shapefile containing polygons showing the dominant type of sediment. This data should be referenced to WGS84 and interpolated from the best available data for the area. Similarly, for developers who do not have access to adequate mapping software, a Google Earth kmz file available to download should be provided.

3.2.2.2. Depth of Transition to Bedrock

One of the prime concerns for offshore renewable energy installation construction is the depth to bedrock and subsequently its composition and competency. Again, this is primarily to assess suitability for foundation construction. Monopile foundations are preferred for windfarm development, usually reaching a depth of roughly 35m. Therefore it is important to carry out seismic surveys which image the sub-seabed to at least 50m. A potential error arising from sub-bottom profiling is the misinterpreting of glacial till as bedrock so groundtruthing becomes all the more important in that respect. Coring has the added advantage of providing physical samples for lab based geotechnical and physical property analysis.

3.2.3 Solid Geology

3.2.3.1. Bedrock Description

As mentioned the depth from seabed to bedrock is of importance in relation to foundation design and construction. In addition, the subsequent composition and competency of this bedrock is also important information.

Information regarding bedrock description should be delivered using a shapefile which uses polygons to show the predominant bedrock with information regarding type, age and formation name. The additional option of a Google Earth kmz file would be of use to developers who didn't have access to adequate mapping software.

3.2.3.2. Faults

Sub-seabed faults are naturally planes of weakness and knowledge of their locations is vital in siting installation construction. Although Ireland is seismically a quiet area, within the Irish Sea low magnitude events are often recorded. Similarly, faults can act as conduits allowing for the accumulation off shallow gas. Therefore the mapping of scarps and other features is important and can be done using multibeam and side scan sonar techniques.

3.2.3.3. Oil/Gas Accumulations

Gas, which may accumulate in the subsurface, proves problematic for site investigations and foundation installations. Some of the potential risks resulting from shallow gas accumulations include:

- Loss of vessel buoyancy
- Blowouts
- Gas kicks and minor flows
- Loss of drill/installation jack up
- Uncontrolled environmental emissions
- Technogenic hydrate formation

3.3 General Physical Features

Only certain general physical features are applicable to each of the three main types of offshore renewable energy. In addition, the limits or constraints the data associated with these features places on siting potential installations is less strict as the technology can often be tailored to meet varying conditions in the wind, wave or tidal regime at a certain site.

The main general physical features are:

1) Water depth, namely:
    - Seabed Bathymetry
2) Wind characteristics, including:
    - Wind speed
    - Frequency
    - Direction
3) Wave characteristics, including:
    - Average period
    - Wave height
    - Direction
    - Significant wave height exceeded 10% and 50% of the time
4) Tidal regime, including:
    - Maximum current amplitude
    - Spring tidal ranges
    - Tidal Period
5) Distance to shore
6) Landfall description
7) Offshore weather reports

3.3.1 Seabed Bathymetry

Water depth is an important factor in site identification for installations and so detailed and widespread bathymetric maps are a necessity. Construction costs of offshore installations increases with water depth and so generally greater than 35m water depth is not exceeded. In saying so, evolving technology is pushing installations to potentially greater depths.

Bathymetry should be delivered in an ASCII file as gridded data referenced to WGS84, interpolated from the best available data for the area and corrected to mean sea level as well as lowest astronomical tide. The gridded data should be prepared up to the high water line. The gridded data should be available in resolutions of 1 minute, down to 3 seconds. The additional option of a Google Earth kmz file for download would help those developers who do not have access to mapping software.

3.3.2 Wind Characteristics

Wind characteristics are an obvious important consideration for installing wind energy installations. Generally a wind speed of 9 ms^{-1} is preferred. Wind data recorded should consist of wind speed, direction, frequency and maximum gust. In order to assess the wind generating potential of an area there must be a continual dataset recording hourly for the past decade.

The Marine Institute has 6 weather buoys located around the Irish coast which constantly record wind speed and direction as well as the maximum gust. This data is available from the Marine Institute in an excel spreadsheet form (http://www.marine.ie/home/).

3.3.3 Wave Characteristics

The 6 Marine Institute buoys also collect wave data in the form of wave height, period, peak period, mean wave spread and mean direction. These data sets are provided by the Marine Institute as excel spreadsheets. Also available are shapefiles for the average practicable power (see Figure. A-3.1) and the average wave height (see Figure A-3.2). The data from these attributes were derived from the Marine Institute's Accessible Wave Energy Resource Atlas published in 2005.

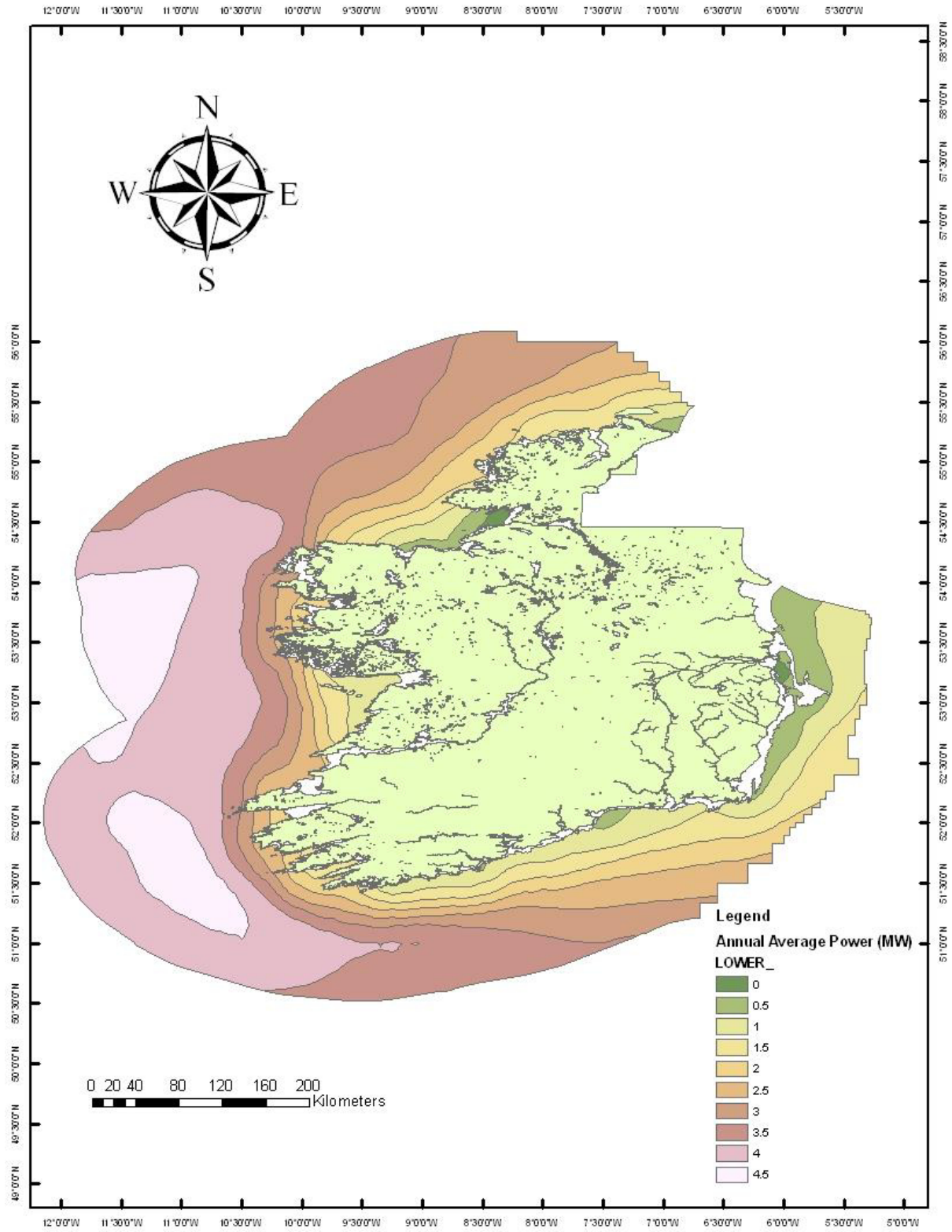

Figure A-3.1. Annual Average Wave Power

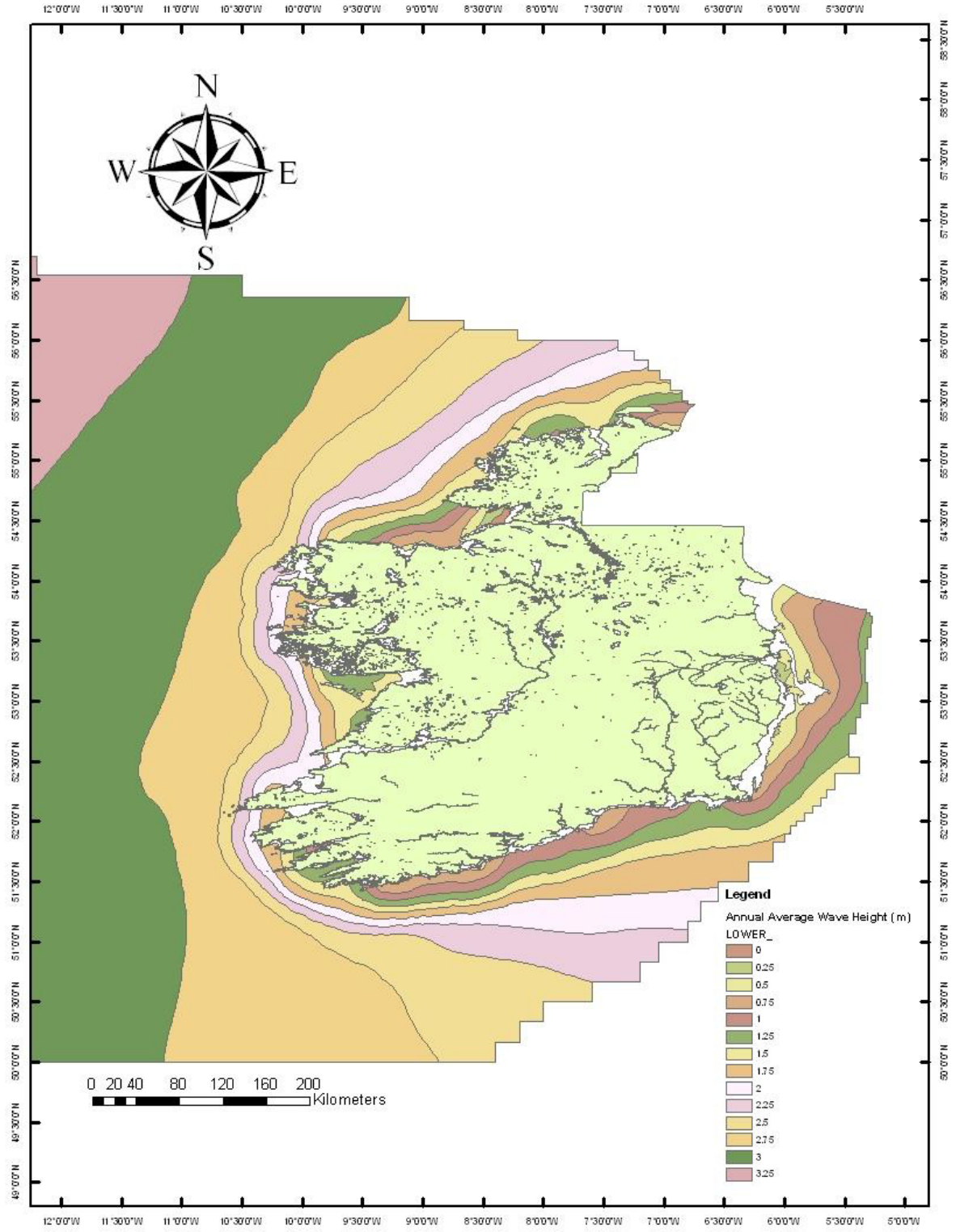

Figure A-3.2: Annual Average Wave Height.

3.3.4 Tidal Regime

In order to harness tidal energy an understanding of the hydrodynamic regimes is needed. ADCP deployments provide crucial hydrodynamic data that are necessary to calibrate tidal models. Tidal models can then input into understanding sediment dynamics in terms of migration and pathways.

Additional tidal data are provided by 13 tidal gauges located around the coast of Ireland. These data sets are online available from the Marine Institute at http://www.marine.ie/home/services/operational/oceanography/ TideGauge.htm

Figure A-3.3 Marine Institute Tidal Gauges.

3.3.5 Distance to Shore

Similar to water depth, the distance from an installation to shore (and subsequently grid connection) influences the cost of construction. Generally the distance from shore to these installations is between 10-20 km. In The Netherlands and the U.K, the 12 nautical mile zone is excluded from offshore windfarm development.

3.4 Ecological Factors

Ecological factors refer to marine mammals, birds and fish habitats, nursing grounds and migratory routes. As part of an Environmental Impact Assessment concerning the construction of offshore installations the primary areas of focus are the various species that either reside or pass through the area under investigation, their numbers and concentrations and seasonal variability.

3.4.1 Special Areas of Conservation (SAC's)

The National Parks and Wildlife Service is the national body charged with the conservation of a range of habitats and species in Ireland. Subsequently they identify and assess Special Areas of Conservation or SAC's which are areas in Ireland of upmost concern regarding wildlife conservation and are considered important not just in Ireland but also in Europe (see Figure A-3.4). SACs have a legal grounding in the EU Habitats Directive and cover an area of roughly 13,500 km² with 47% of this area concerning the marine and large lakes. In addition to the in and near shore SAC's, also offshore four SACs exist in water depth deeper than 500m.

3.4.2 Special Protection Areas (SPA's)

The National Parks and Wildlife Service also identifies Special Protection Areas (SPAs) that cover breeding, feeding, roosting and wintering areas of birds under the EU Birds Directive (see Figure A-3.5).

Shapefiles for SACs and SPAs are available from the National Parks and Wildlife Service.

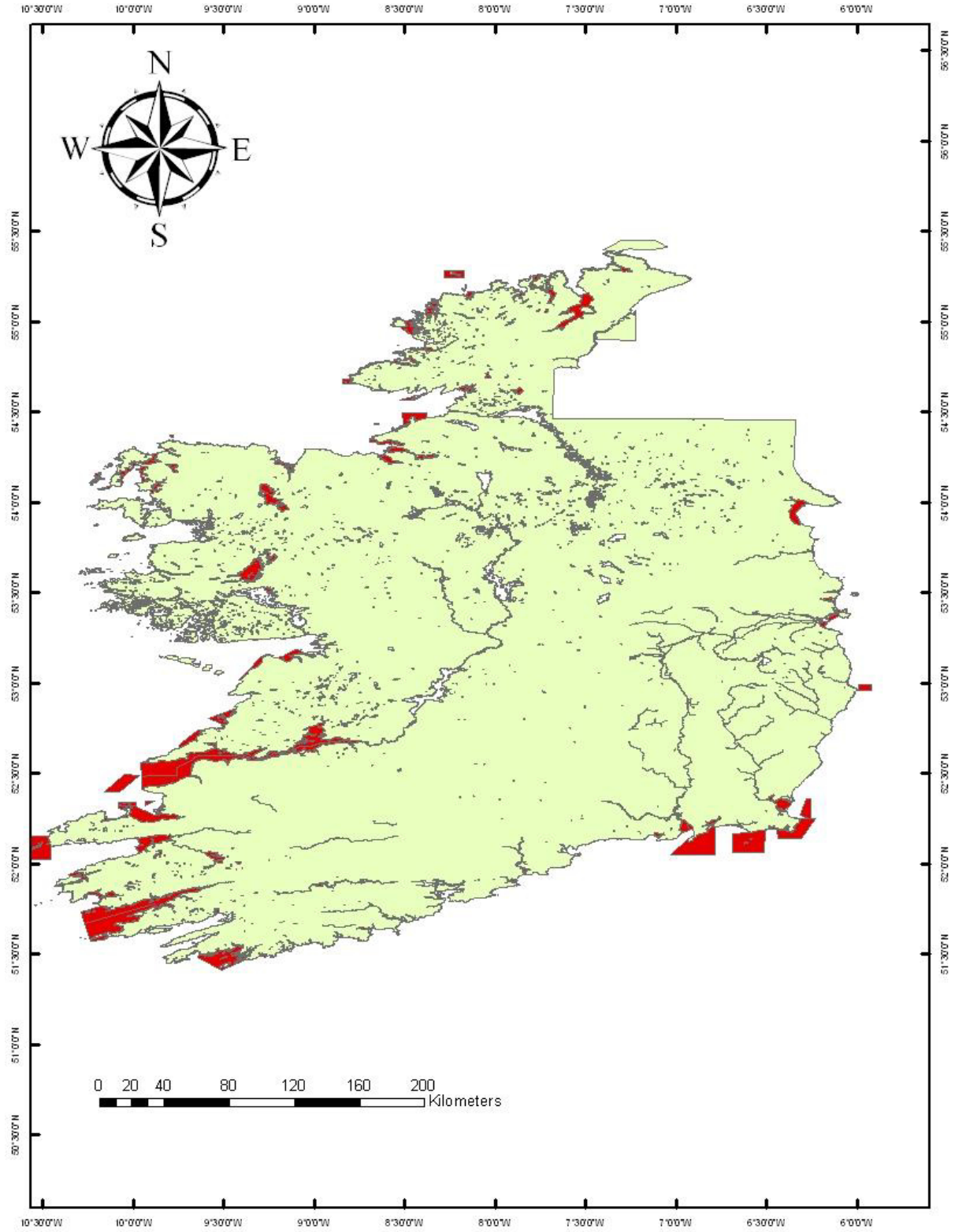

Figure A-3.4. Special Areas of Conservation.

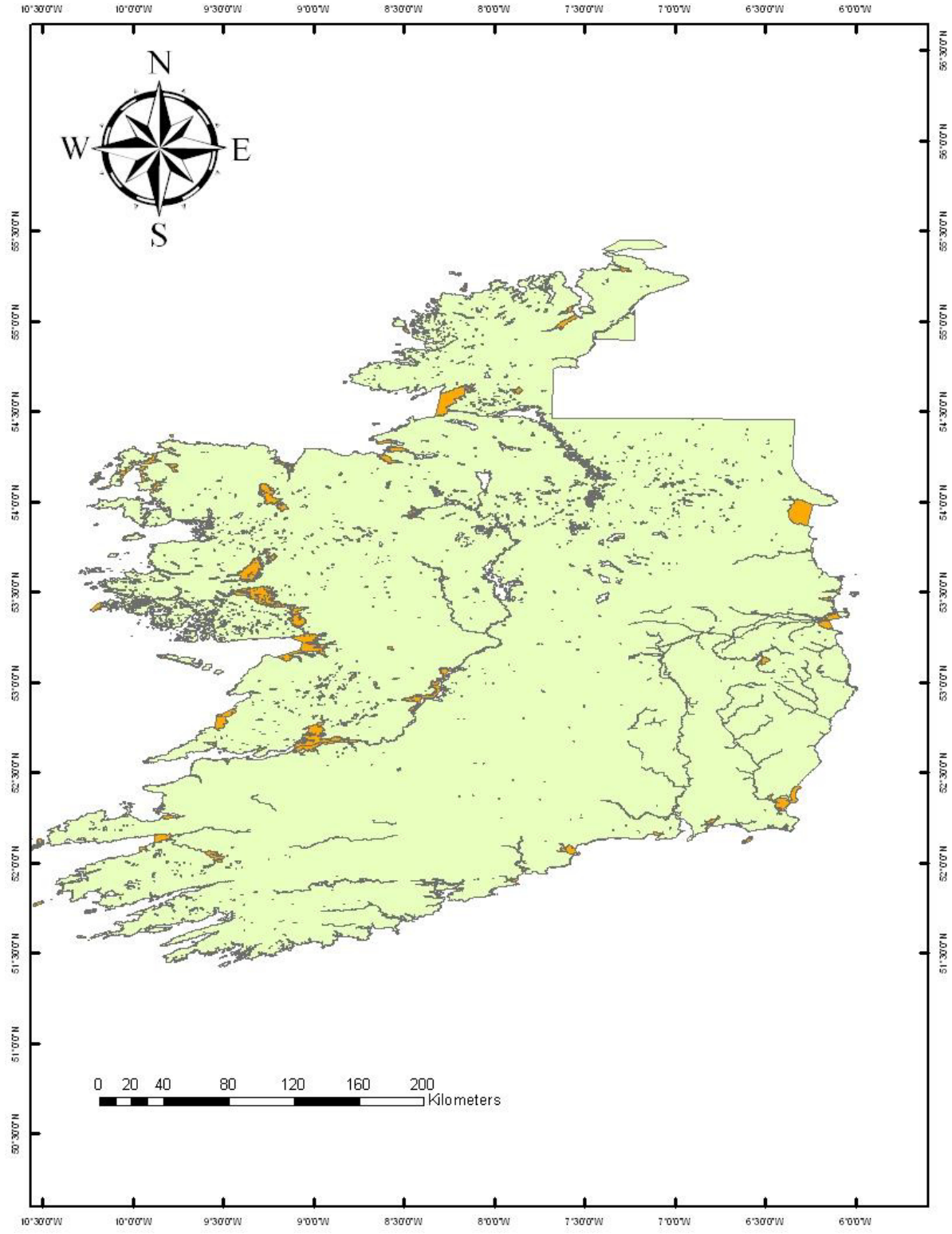

Figure A-3.5. Special Protection Areas.

3.5 Socio-economic Factors

Socio-economic factors represent constraints that usually discount an area as a potential site and include:

1) Commercial navigation, including:
    - Shipping lanes
    - Ferry routes
2) Fisheries
3) Dredging for aggregates
4) Recreational leisure
5) Distance to port
6) Oil/gas exploration
7) Pipelines and cables
8) Wrecks and other archeological sites
9) Military installations and firing ranges
10) Aviation

3.5.1 Commercial Navigation

A potential danger in the construction of offshore installations is the possibly of an accidental collision with vessels. Around the Irish coast, it is the Irish Sea which sees the most activity in terms of commercial navigation with ferries running from Ireland to the UK and France along the Dublin- Holyhead, Rosslare- Pembroke, Rosslare- Cherbourg and Rosslare- Roscoff routes (see Figure A-3.6). These routes see up to 10,000 crossings a year and represent an important source of national income through tourism. Figure A-4.6 shows the main commercial routes fro and to Ireland. Additional information regarding shipping channels, along with other merchant routes, can be obtained from The Irish Maritime Development Office (http://www.imdo.ie/imdo/).

3.5.2 Fisheries

In 2009 the Marine Institute published the Atlas of Commercial Fisheries around Ireland which assessed and reviewed Ireland's exploitation of the 75 various fish species in Irish waters under the EU's Common Fisheries Policy (CFP). Data regarding this publication is available from the Marine Institute as GIS shapefile and include such data as target fish, fishing methods and habitats (see Figure A-3.7 and Fig. A-3.8).

3.5.3 Cables

Underwater cables, pipelines and gas interconnectors are constraints for offshore installations. No offshore construction is allowed within a buffer-zone of generally 100m these features.

Most underwater cables, pipelines and gas interconnectors are located on the east coast of Ireland transporting oil and gas between Britain and Ireland (see Figure A-3.9) Information regarding these pipelines can be acquired from the UK Department of Energy and Climate Change (http://www.decc.gov.uk/) and the Petroleum Affairs Division (http://www.dcenr.gov.ie/Natural/Petroleum+Affairs+Division/).

Information on underwater cables can is provided by the Kingfisher Information Service (http://www.kisca.org.uk/). This information is available to download in a number of different formats.

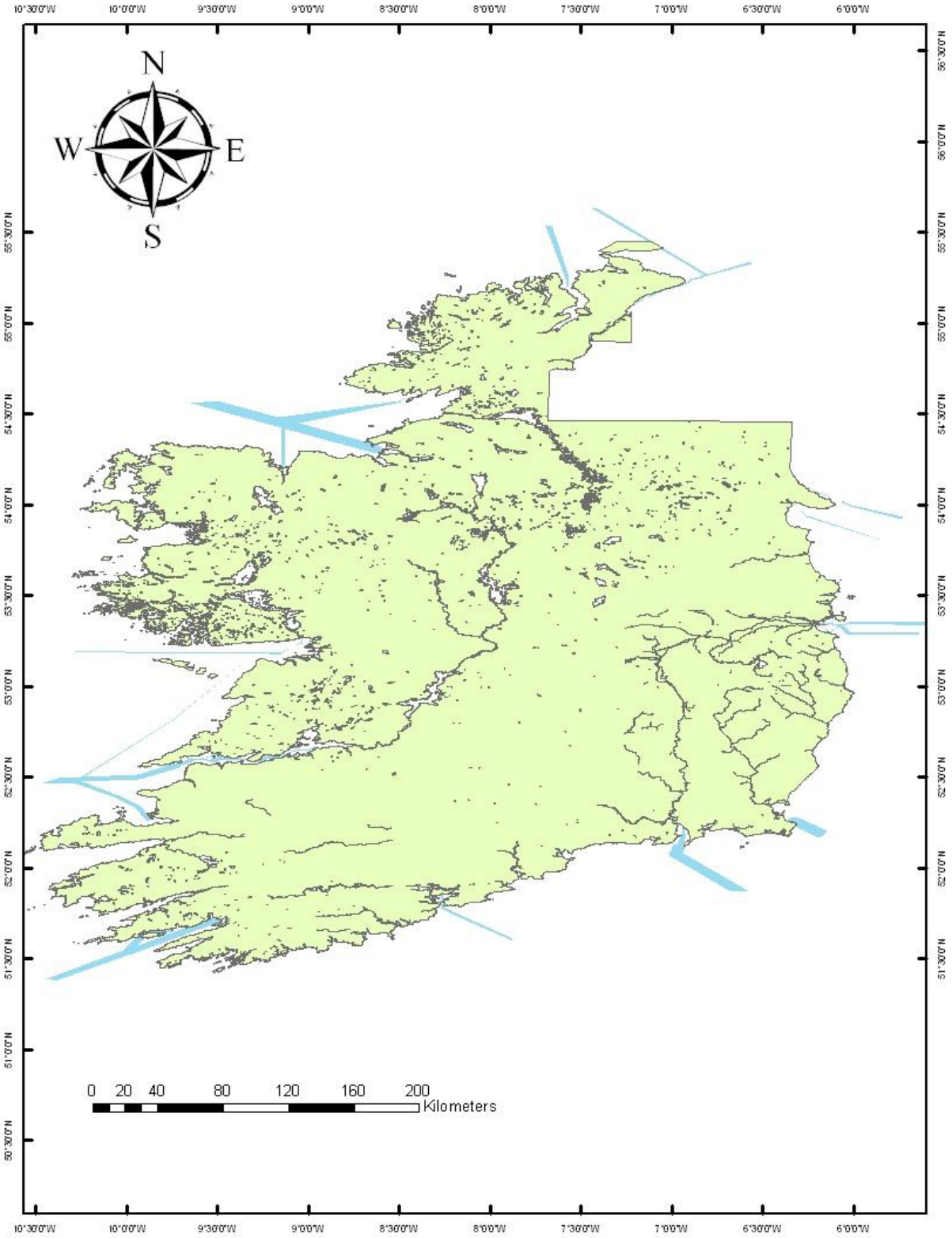

Figure A-3.6. Ferry Routes.

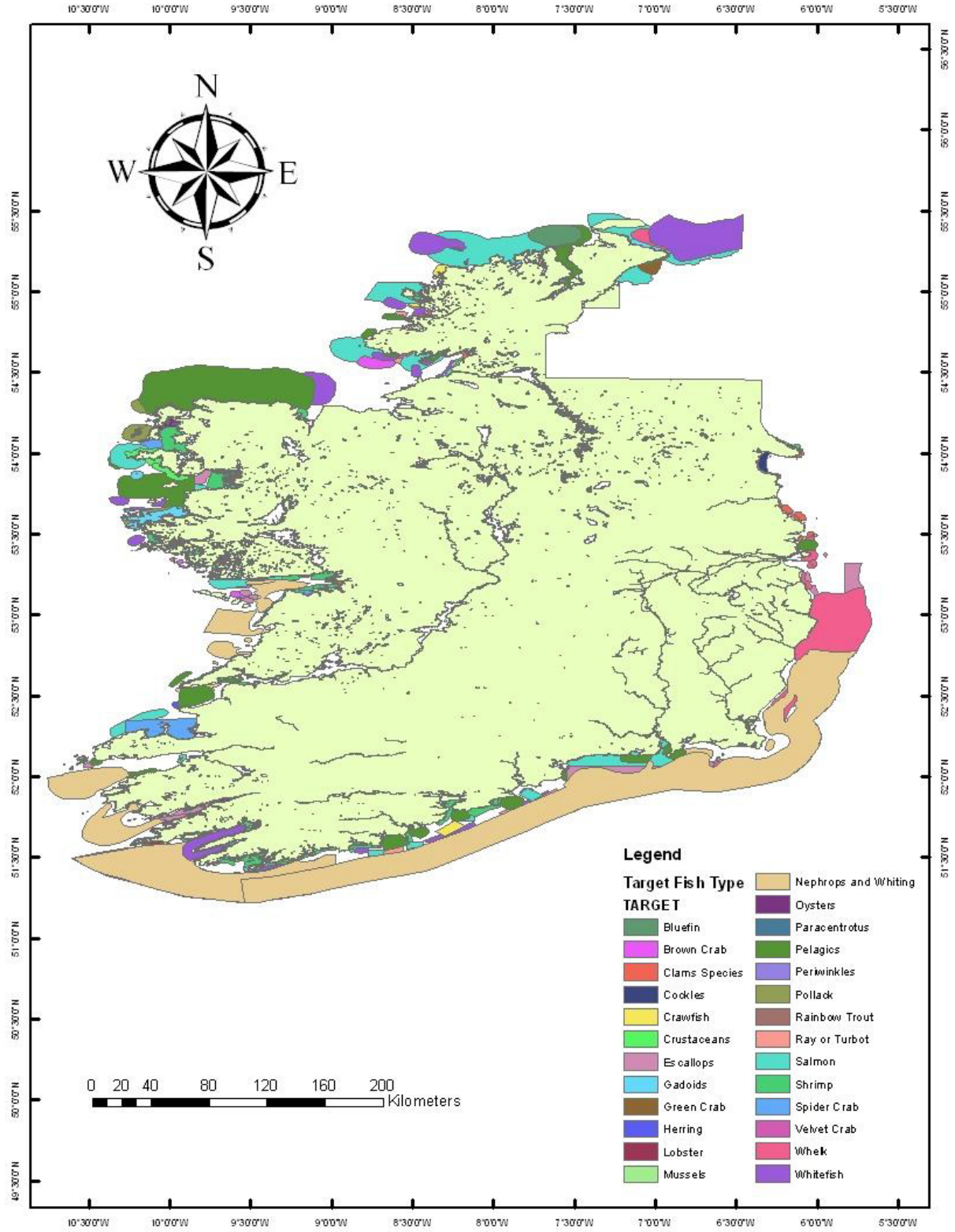

Figure A-3.7. Target Fish Type.

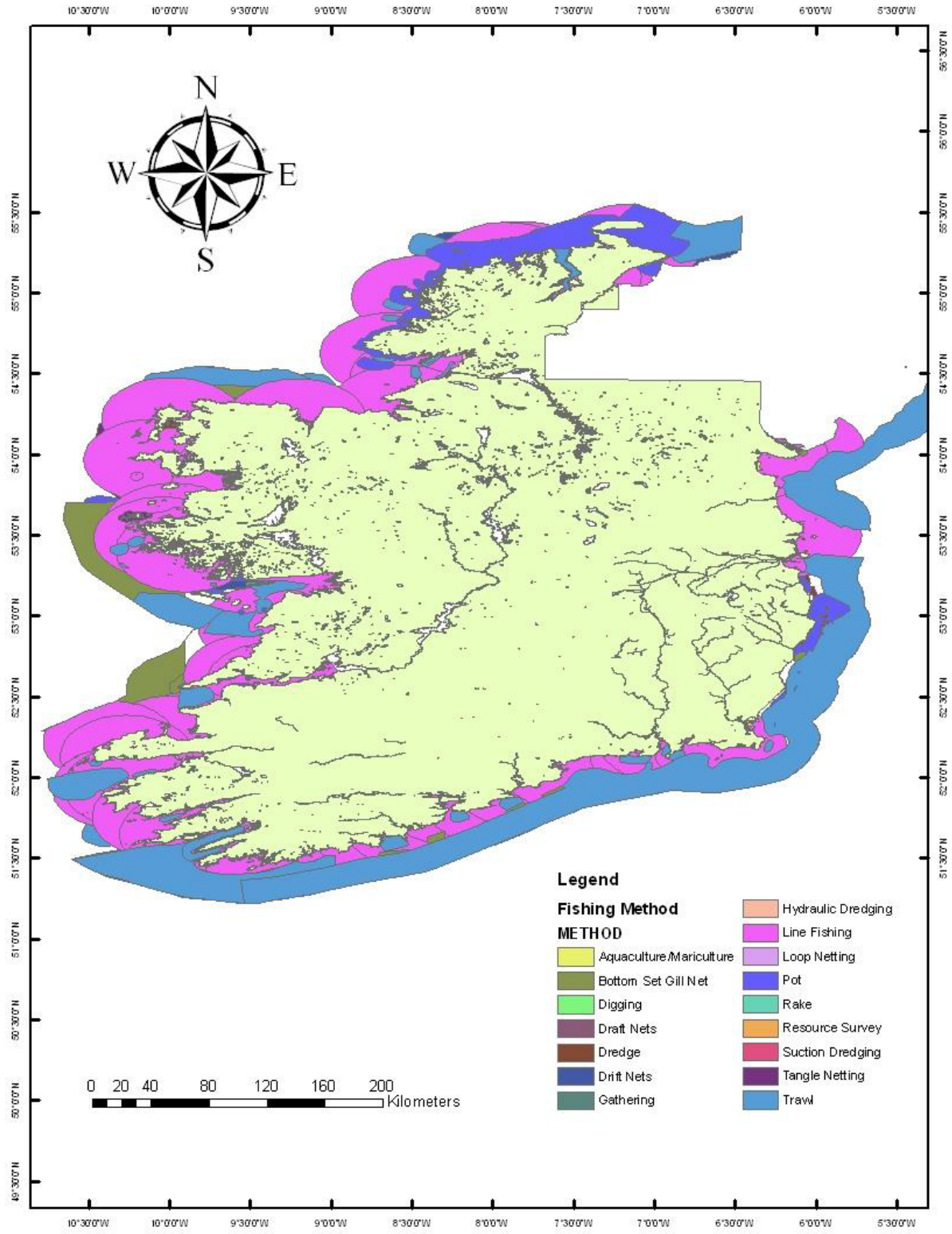

Figure A-3.8. Fishing Methods.

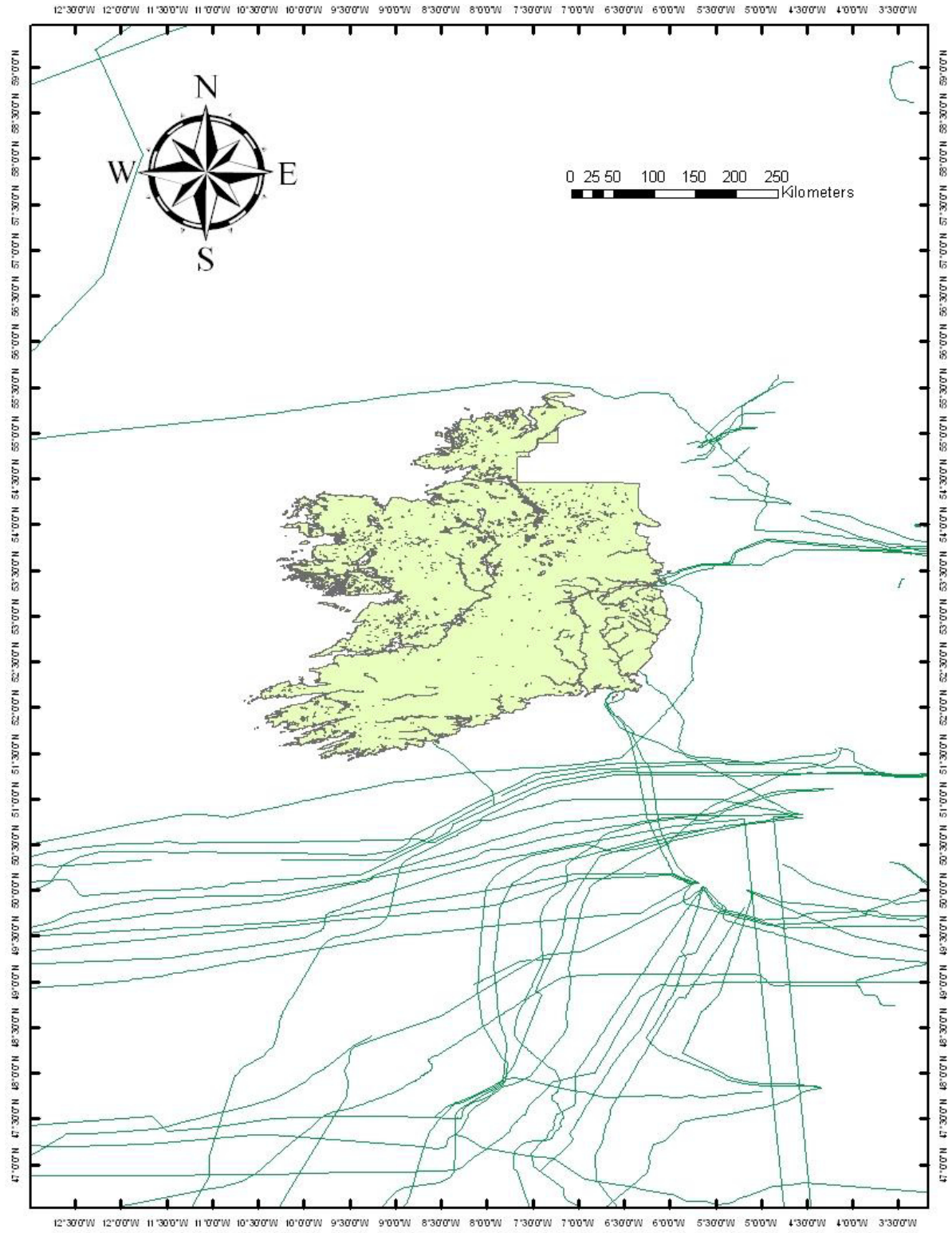

Figure A-3.9. Cables.

3.5.4 Shipwrecks

Shipwrecks and other archeological sites encountered during INFOMAR seabed mapping are duly logged and the locations are recorded in a GIS database. These data are available for download as

shapefiles (see Fig. A-4.10). Many shipwrecks are however not detected on the standard resolution bathymetry used and go unrecorded.

The shipwreck inventory pictured (Fig. A-3.10) contains roughly 250 wrecks. According to the Underwater Archeology Unit of The National Monuments Service there are between 1,500 to 2,000 wrecks located in Irish waters. These data come from a variety of sources including divers and fishing trawler reports, hydrocarbon exploration and admiralty charts amongst others. All shipwrecks reported are available for viewing from the National Monuments Service in the form of physical maps. Ongoing work by the National Monuments Service will make this data accessible in digital format early 2011.

As such there is no set exclusion zone set around shipwrecks. It depends on the nature of the wreck and extent of its debris. Usually the exclusion zone is in the region of 100 to 300m in diameter.

3.5.5 Military Installations and Firing Ranges

Military installations and in particular firing ranges pose an obvious constraint to offshore installations. Information regarding the location and extent of these ranges can be procured from the Department of Defence (www.defence.ie). See Figure A-3.11.

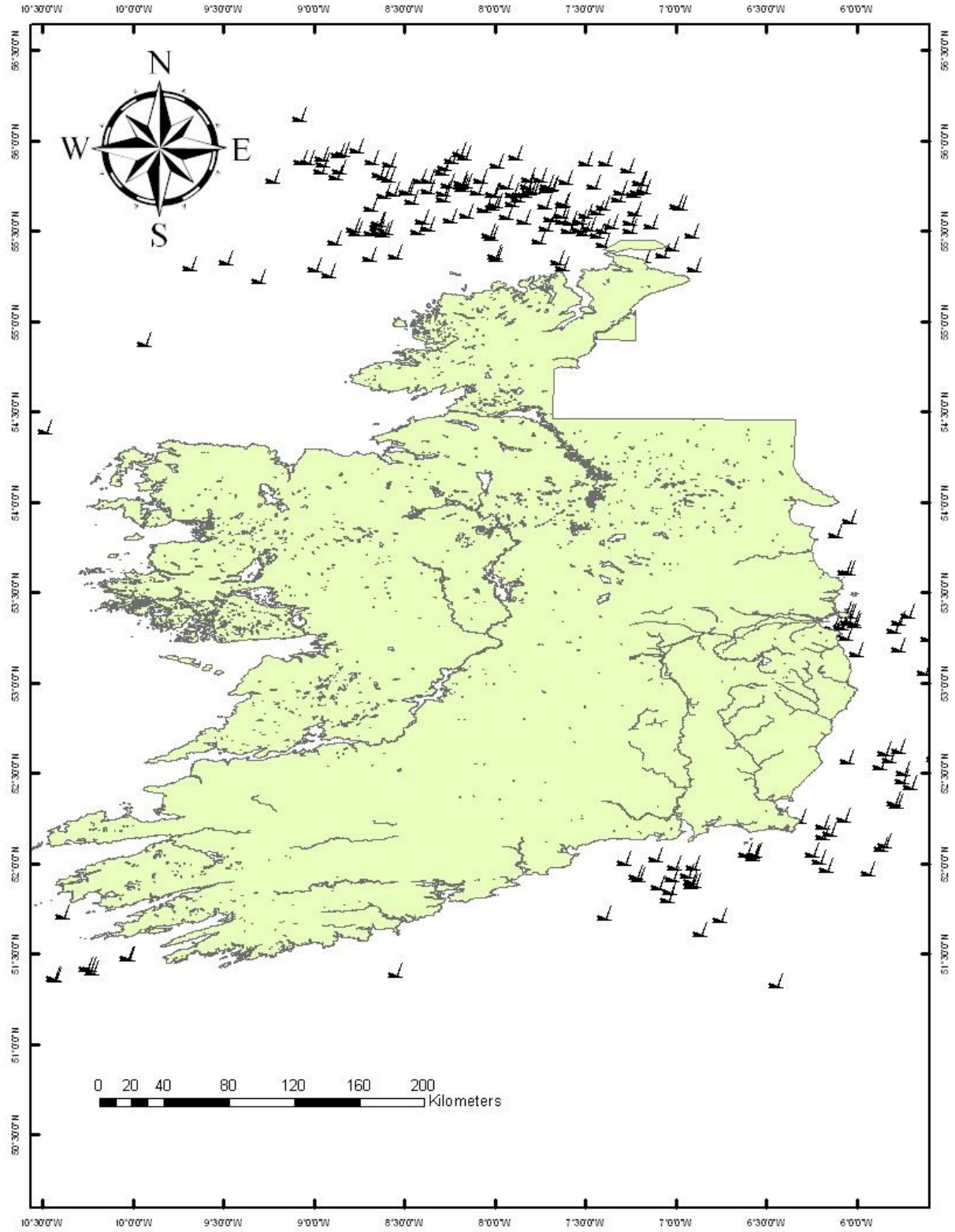

Figure A-3.10. Shipwreck Inventory (GSI).

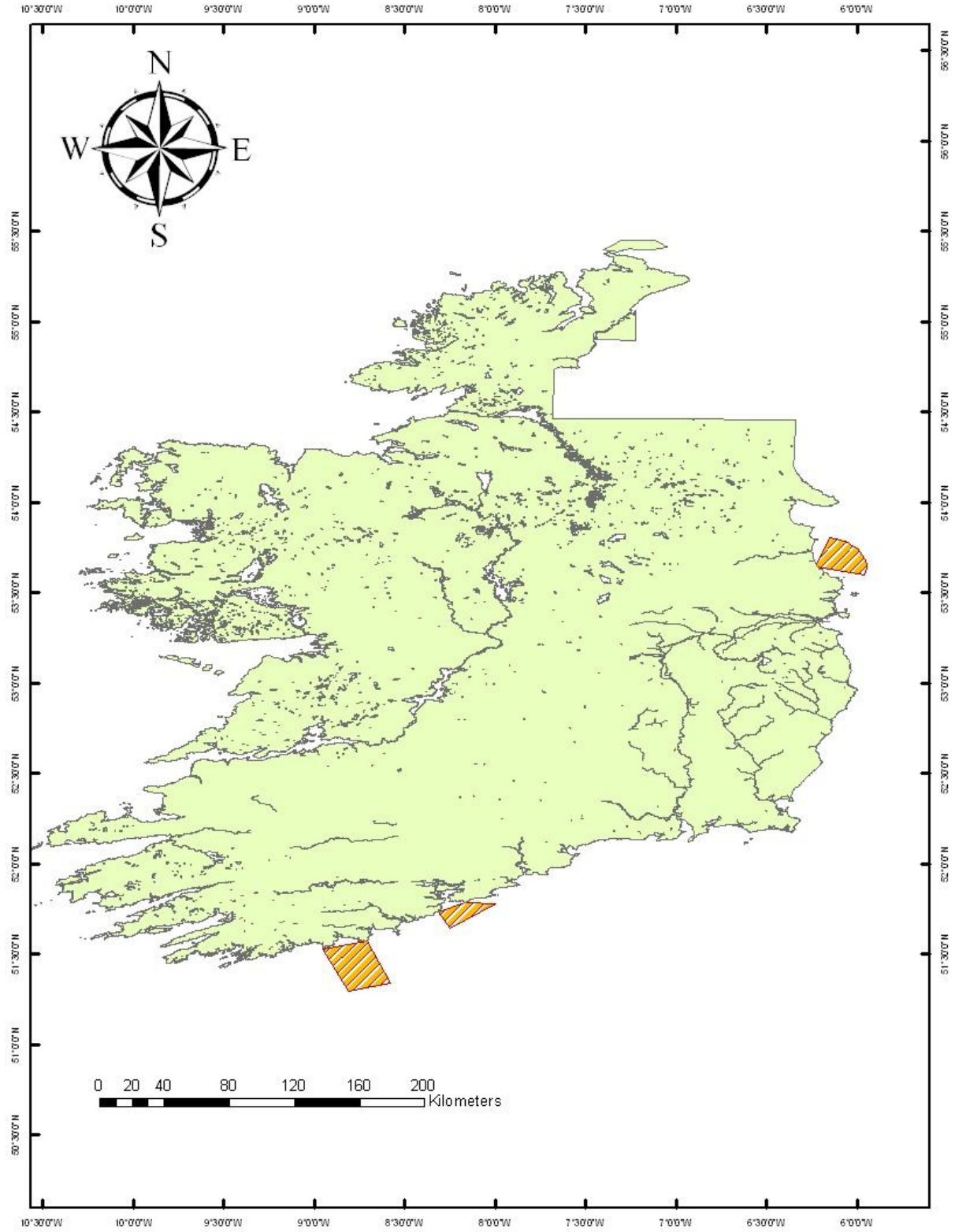

Figure A-3.11. Military Exclusion Zones.

4. ASSESSMENT OF INFOMAR DATASET COMPATIBILITY

The main focus of INFOMAR programme is to provide high resolution bathymetric maps. These products directly address offshore renewable industry needs. Water depth is a major constraint for

offshore installations and high resolution bathymetric information therefore crucial for planning and costing offshore devices.

Another part of the INFOMAR programme is to deliver a seabed sediment classification scheme. To date for the areas of Galway Bay, Bantry and Dunmanus Harbour, the Waterford coast, Cork Harbour, Sligo and Donegal coast as well as part of the East coast the sediments have been classified. However, these are unsupervised classifications and are based solely on acoustic properties and statistical analysis. Where groundtruthing data is available INFOMAR intend to apply this to the classification maps in order to improve their value with Bantry and Dunmanus identified as starting points. Similar to its sediment classification coverage, INFOMAR provides backscatter and multibeam bathymetry data for a limited area comprising of Cork Harbour, the Waterford and Wexford Coasts, much of the East Coast around Dublin and Louth, Galway Bay, the Donegal and Sligo coasts as well as much of the Kerry and Cork Coast from the Shannon Estuary as far south as Dunmanus. These data are available as gridded datasets with a 10m resolution.

These INFOMAR datasets provide essential information for hydrographic models necessary to predict current directions and velocities. In addition, a sediment classification is required to establish a more robust, up to date, dynamic geological model.

Geological factors such as seabed dynamics change over time and so it is vital to have up to date and accurate data. In this respect INFOMAR plays an integral role in developing offshore renewable energy. The datasets it provides form the basis for any modelling and geotechnical analysis essentially influencing site selection and foundation design as well as cable route selection.

Many of the datasets mentioned already pertaining to offshore renewable energy are utilised in constraint mapping exercises to identify sites with the best potential. The geological factors not only aid in this site identification process but also heavily influence anchoring and foundation design of offshore installations which in turn affects cost, one of the primary drivers for such projects. The INFOMAR programme already provides bathymetric, sedimentological and geological data sets.

Additional geological (seismic) data sets would however support the site selection process for

offshore installations. A summary gap analysis of the INFOMAR dataset can be found below in Table A-1.

Data	Recommended	INFOMAR	Suggestions
Multi- beam Echo Sounder	Frequency of 100 kHz or higher. Delivered in an ascii file as gridded data referenced to WGS84, interpolated from best available data corrected to MSL and LAT. Option of Google Earth .kmz file	95 kHz EM1002 or 200 kHz EM3002 system. Data corrected to LAT and available in grid (.ers), ascii (.dat), map (.png), Fledermaus (.scene), Google (.kmz), zipped ESRI ArcGIS GRIDS.	Adequate
Side-scan Sonar	Frequency of 100 kHz or higher	Edge tech side scan sonar	Adequate
Sub-bottom profiler	Boomer or alternative systems of comparable or better performance and sufficient signal penetration. Near surface resolution min. 1m Possibly supplemented by sub bottom profiler or chirp sonar in surface sediment layer vertical resolution min. 0.5m.	3.5 kHz SES Probe 500 pinger and 500 – 2000 Hz Geo-Spark 200 sparker with data available in .jpeg or .segy format	Adequate
Shallow Geotecnical Survey	Vibrocore and Cone Penetration Test (CPT) to depths of 6 -8m	Geo Resources 3000 + 6000 vibrocore with depths of 3-6m which are scanned, logged and stored.	Possibly deeper core. Provision of CPT data.
Video and Grab Survey	Video reconnaissance by way of drop down camera and seabed samples of <1m depth to ground truth and use in grain-size analysis.	Day, Shipek, Van Veen and Box Corer. Samples undergo particle size analysis.	Possible provision of seabed imagery.

Hydrodynamics Study	Deployment of acoustic wave and tidal monitor (ADCP or MiniLander). Deployment of wave buoy. Deployment of passive sediment traps. Gathering of CTD data.	Tidal and Wave data available from Marine Institute. CTD data also available.	Introduce site specific wave and current monitoring by way of ADCP data or equivalent. Make provision for deployment of sediment traps for hydrodynamic surveys

Table A-1- Data Gap Analysis

5. SITE SURVEY METHODOLOGY

5.1 Current Information

The importance of site investigation cannot be overstated as it is a critical step in the construction of offshore renewable energy installations. A study by the Delft University Wind Energy Research Institute found that 25% of total project capital expenditure is linked with the foundation design. Foundation design and cable route design in turn is ultimately decided by factors such as the sub-seabed geology and seabed dynamics.

As such, there are very few documents regarding guidelines or recommended best practice protocols when it comes to site investigation for offshore renewable energy installations. There are a few existing documents which are related to the subject and much information is drawn from site investigation methods for the offshore hydrocarbon exploration sector. These documents refer mostly to the geotechnical analysis aspect of site investigation and subsequently foundation planning and design and apply to different types of sites, structures and budgets.

A number of nations, most prominently Germany, Denmark and the Netherlands, have developed regulations regarding the construction of windfarms (and hence offshore windfarms by default) which are set down in law. As a result these regulations take precedence over other guidelines or recommended practice.

Other multidisciplinary groups (such as the Society for Underwater Technology) have looked at the issue of site investigation in relation to foundation behaviour and as a result of a series of conferences have produced a collection of publications on the matter, most notably “Offshore Site Investigation and Geotechnics, Confronting New Challenges and Sharing Knowledge” and “Offshore site Investigation and Foundation Behaviours: New Frontiers”.

Additional relevant documents give guidelines with respect to laboratory testing of geotechnical samples, including:

- Norsk Standards 8000 to 8017
- EN1997, Eurocode 7, Geotechnical Design.
- International Standards Organisation; Geotechnical Investigation and Testing, Identification and Classification of Soil, Part 1: Identification and Description ISO 14688-1:2002

- American Society of Testing and Materials, (2005) Volume 04.08, Soil and Rock (1) D420-D5779. Annual Book of ASTM Standards
- American Petroleum Institute
- British Standards Institution (1999) BS5930: Code of Practice for Site Investigation
- British Standards Institution 91990) BS1377:Methods of Tests for Soil for Civil Engineering Purposes

The basic components of a site investigation are the preliminary site assessment and geophysical and geotechnical studies. In addition, environmental baseline surveys and environmental impact assessments are required for offshore construction projects. These may also involve gathering seabed samples for chemical, biological and physical analyses. Notable overlap between such surveys and standard geophysical and geotechnical surveys require strategic survey planning in order to achieve a maximum efficiency of overall data collection.

5.2 Desktop Study

The first phase of a site investigation involves a desktop study collating all available data and information regarding the area from across a variety of disciplines to establish a base model. Based on the outcomes of this desktop study, it is possible to identify areas of information conflict or deficiency. Required data sets include:

- Geological databases
- Bathymetric information
- Geophysical databases
- Geotechnical databases
- Metocean data (tides, currents, wind, wave etc.)
- Seismic data
- Data on human activities (e.g. pipelines, wrecks, cables, aggregate dredging, navigation routes etc.)

Resulting from this desktop study the key outputs are usually:

- A constraint map for the area of interest
- An outline geological model for the area of interest
- Preliminary definition of key geological processes and their status (e.g. active, dormant etc.)
- Estimated metocean conditions
- Identification of major geotechnical risks

These outputs would form a baseline against which to identify changes in seabed process since the last data was recorded and establish an outline for possible additional survey and monitoring requirements as well as areas of insufficient information.

5.3 Geophysical Survey

The geophysical forms the basis of any geological model of an area. It provides the initial seabed and sub-seabed model which can then be groundtruthed by the geotechnical survey.

The objectives of the geophysical survey should be to:

- Provide an accurate bathymetric chart of the area of interest
- Chart natural seabed features and any obstructions, debris or wrecks
- Produce isopach charts for sedimentary units
- Map the depth to the rockhead. Seabed penetration to 50m or so is typical for geotechnical purposes
- Locate any structural complexities or geohazards within the shallow geological succession such as faulting, accumulations of shallow gas, buried channels etc.
- Provide detailed geological interpretation to show facies variations and structural feature changes via appropriate maps and sections
- Design a geotechnical sampling and testing programme following the completion of the geophysical survey
- Produce a comprehensive interpretation report on the survey results obtained to assist design of the offshore foundations/structure and cable burial.

The design of the survey should be based on the survey needs such as water depths and other physical requirements. The minimum requirements for each survey are outlined below.

	Geological Survey	Monitoring
Targets	Survey of bathymetric conditions	Recording of local depth changes (scouring)
Scope	Each turbine site to be covered at least once	Along offshore wind farm components (longitudinal lines on both sides) At least 200m to either side
Time-scale	Once	In the years after completion, once a year in spring
Method	Single-beam echosounder if the seafloor is relatively level, or multibeam system if it's rough. Positioning better than 5m + 5% of the water depth. Accuracy for reduced depths according to IHO Standards for Hydrographic Surveys	Multi-beam echosounder. Positioning better than 5m + 5% of water depth Accuracy of reduced according to IHO Standards for Hydrographic Surveys
Presentation of results	Bathymetric map of surveyed areas Reported water depths must be sound velocity corrected and related to chart datum (tidal correction) Data must also be provided in digital form	Bathymetric map of surveyed areas Reported water depths must be sound velocity corrected and related to chart datum (tidal correction) Data must be provided in digital form

Table A.2 Requirements for echosounder surveys

	Geological Survey	Monitoring
Targets	Survey of sediment types and structures Verification or calibration of interpretation by means of grab samples	Recording of erosion areas, scouring and obstructions Verification and/or calibration of interpretation by means of grab samples
Scope	Each energy installation component to be surveyed at least once Complete coverage of the area if the sea floor is heterogeneous	At least 200m to either side
Time-scale	Once	In the first years after completion, once a year in spring
Method	Frequency 100kHz or higher Coverage max 2x100m Recognition of cubic features > 1m Digital recording Cruise speed max. 4 knots Equipment positioning better than 10m	Frequency 100kHz or higher Coverage max. 2 x 75m Recognition of cubic features >1m Digital recording Cruise speed max. 4 knots Equipment positioning better than 10m
Presentation of results	Digital SSS mosaic of profiles (horizontal resolution 0.5m) Map with interpretation of the side scan sonar profiles Data have to be additionally provided in analogue form	Digital SSS mosaic of profiles (horizontal resolution 0.5m) Map with interpretation of the side scan sonar profiles

Table A.3 Requirements for side scan sonar (SSS) surveys

	Geological Survey
Targets	Determination of type and location of geological units
Scope	Each offshore installation component shall be covered by at least one longitudinal and one cross section Max. spacing of cross sections 2000m It is recommended that longitudinal sections comprise of 10m spacing along total foundation breadth and one cross section
Time-scale	Once
Method	Boomer or alternative systems of comparable or better performance and sufficient signal penetration. Near surface resolution min. 1m Possibly supplemented by sub bottom profiler or chirp sonar in surface sediment layer (e.g. along planned cable routes), vertical resolution min. 0.5m Cruise speed max. 4 knots Deployment up to sea state max. 4
Presentation of results	Profiles and profile interpretation such as geological longitudinal and cross sections Map showing spatial position of boundaries between geological units and structural elements (e.g. isolines map)

Table A.4 Requirements for seismic surveys

The above surveys are geared towards acquiring information with regard to foundation siting and design. A different set of requirements apply to surveying relating to routes for infield cables and power export cables. The main issues are concerned with horizontal cover and penetration in the investigation area as well as seabed hardness or trenchability. The technical requirements are outlined below.

	Route survey	Monitoring
Targets	Bathymetric and morphological investigation of the planned cable route Mapping of wrecks, other obstructions and ammunition Investigation into sediment composition, geological stratification and geotechnical properties of the upper sediment layer Mapping of existing cables and pipelines Determination of cable route and length	Detection of possible free spanning of cable Checking of rockfills or comparable cable safety features Measurement of cable depth

	Route survey	Monitoring
Scope	Complete coverage of 200m wide corridor	Monitoring of complete cable routes in the first years After a sufficient database is available, modified monitoring intervals may be applied for within the framework of the periodical inspections
Time-scale	Once	In the first years completion, once a year in spring
Methods	Multi-beam; positioning better than 5m + 5% of water depth and accuracy for reduced depths according to IHO Standards for Hydrographic Surveys Sidescan sonar; frequency 100 kHz or higher; measuring range max. 2 x 100 m; recognition of cubic features >1m; digital recording; cruise speed max. 4kn; sonar positioning better than 10m Sub-bottom profiler, chirp sonar or alternative systems of comparable or better performance Vibrocorer or CPT down to the planned burial depth, spacing to be determined on the basis of seismic data Magnetometer or active metal detection system	Cable tracking system or suitable other method for cables buried in sediment Multi-beam; positioning better than 5m + 5% of water depth and accuracy for reduced depths according to IHO Standards for Hydrographic Surveys Side scan sonar if necessary; frequency 100 kHz or higher; measuring range max. 2 x 100m; recognition of cubic features > 1m; digital recording; cruise speed max. 4 kn; sonar positioning better than 10m
Presentation of results	Map (horizontal scale 1:5000, vertical scale 1:200) showing all survey results	Map (horizontal scale 1:5000, vertical scale 1:200 showing all survey results)

Table A.5 Requirements for geological survey of cable routes

5.4 Geotechnical Survey

In essence geotechnical surveys groundtruth the data seen in the geophysical survey to confirm the geological/geophysical model and should provide all the necessary seabed data to supplement the design project for foundations as well as cable burial and protection.

The programmes for the geotechnical surveys usually comprise samples for further lab analysis and *in situ* tests such as cone penetration tests. The choice of sampling and testing locations will depend on the lateral and vertical variability of ground conditions as revealed by the geophysical survey and the preliminary site assessment. Project specific factors that can influence sample site selections are:

- Size, location and foundation type of any seabed structures
- Complexity of geological model
- Presence and distribution of geotechnical hazards
- Variability and uncertainty in geotechnical terms

In terms of foundation design for offshore installations, the main issues include:

- **Bearing capacity.** Regardless of the structure, the sediment must have sufficient capacity to carry the static and cyclic loads of the foundation with an acceptable margin for excessive displacements and failures.
- **Permanent displacements.** (e.g. settlement). The static load will cause initial displacements in addition to displacements brought on by consolidation and creep in the sediment beneath and outside the foundation. Cyclic loading from wave action will increase shear strain and dissipation of cyclically induced pore pressure causing additional permanent displacements.
- **Cyclic displacements.** Cyclic loads cause cyclic displacements of the sediment.
- **Foundation stiffness.** Necessary for structural dynamic analyses from wave and/or earthquake loading.
- **Soil reaction stresses.** Results from static and cyclic loads depending on the density of the sediment. Soil reaction stresses may redistribute with time due to creep and cyclic degradation of the soil modulus.

- **Penetration of skirts.**
- **Pile drivability.** Sufficient depth for foundation piles is essential.
- **Liquefaction potential analyses.** This is important in areas where sands and silts are present in areas which are seismically active or where heavy wave loading is expected**.**
- **Scour and erosion.** Waves and currents can cause scour and erosion around the base of foundations. It is most prominent in areas dominated by sands and typically increases as water depth decreases.
- **Punch through.** Rapid, uncontrolled penetration may occur in sediment where there is limited soil strength increase with depth, and in sediment where there is a strong layer of limited thickness overlies a weaker layer.

In order to address these issues, additional basic sediment and rock parameters have to be analysed.

Clay	Sand,Silt or Gravel	Rock
• General description • Layering • Grain size distribution • Organic material content • Mineralogy • Total unit weight • Atterberg limits • Water content • Remoulded shear strength • Sensitivity • Undrained shear strength • Carbonate content • Over consolidation ratio • Indicative shear	• General description • Layering • Grain size distribution • Maximum and minimum densities • Relative density • Water content • Organic material content • Angularity • Sediment stress history and over-consolidation ratio • Angle of shearing resistance • Drained angle of resistance	• General description • Rock quality designation • Water absorption • Total unit weight • Unit weight of solid blocks • Unconfined compression strength • Mineralogy • Carbonate content

strength • Sediment stress history		

Table A.6 Basic sediment and rock parameters

Design Issue	Parameter
Bearing capacity	• Monotonic shear strengths under different stress paths • Cyclic shear strength under combined average and cyclic shear stresses for triaxial and simple shear stress paths
Permanent displacements	• Compressibility • Permeability • Permanent shear strain and pore pressure under combined average and cyclic shear shear stresses for triaxial and simple shear stress paths • Compressibility after cyclic loading
Cyclic displacements	• Cyclic shear strain as function of cyclic shear stress under combined average and cyclic shear stresses for triaxial and simple shear stress paths • Initial shear modulus
Foundation stiffness	• Cyclic shear strain as function of cyclic shear stress under combined average and cyclic shear stresses for triaxial and simple shear stress paths • Initial shear modulus • Damping
Soil reaction stresses	• Monotonic and cyclic shear strengths • Compressibility under virgin loading and reloading • Cyclic and permanent shear strains and permanent pore pressure under combined average and cyclic shear stresses for triaxial and simple shear stress paths • Seabed topography, objects on the seafloor
Liquefaction potential	• Initial shear modulus • Cyclic shear modulus degradation curves • Damping • Coefficient of reconsolidation

Design Issue	Parameter
(For all the above)	• Cyclic shear strain and permanent pore pressure contour diagrams for at least one representative average shear stress (e.g. simple shear tests with (τ_a=0) • Coefficient of reconsolidation
Skirt penetration	• Undrained anisotropic monotonic shear strengths • Remoulded shear strength (or sensitivity) • Drained angle of shearing resistance • Residual interface angle of shearing resistance • CPT resistance • Seabed topography and objects on the seafloor • Boulders in the soil within the skirt penetration depth
Pile capacity and drivability	• Axial and lateral response • Shear strength • Sediment modulus or strain at 50% ultimate strength • CPT cone resistance
Scour/erosion	• Permeability • Water depth • Significant wave height • Wave peak period • Mean current velocity • Current direction • Grain size • Surface roughness • Density of sediment

Table A.7 Additional parameters for specific design issues

6. CASE STUDIES

The case studies outlined below represent pioneering work where techniques and practices were applied and subsequently lessons learned. In the case studies, different problems were encountered and the experience gained offer some solution to similar problems arise in future projects.

6.1 Sheringham Shoals

The Sheringham Shoal windfarm is located between 8 and 12 nautical miles (17 to 20km) off the coast of North Norfolk covering an area of 36km^2 approximately. Water depth ranges from 15 to 22m at lowest astronomical tide (LAT) with a tidal range of 5m roughly. A number of geophysical/geotechnical surveys were carried out on the area prior to construction between 2004 and 2007 as listed below.

Survey	Description	Data Application	Date
Hydrodynamics and sediment Study	Deployment of acoustic wave and tidal monitor; deployment of wave buoy; 5 grab samples	EIA – hydrodynamics and geomorphology Determination of metocean Conditions	Winter 2004 - 2005
Bird/marine mammal surveys	29 boat-based visual surveys; 7 aerial visual surveys	EIA – ornithology EIA – marine mammals	2004 - 2007
Acoustic, video and grab survey	Broad scale swathe bathymetry; side-scan; acoustic ground definition system; magnetometry with some seabed sample grabs	EIA – marine ecology Geophysical site characterisiation Provision of bathymetry data for site characterisation	Summer 2005
Benthic and epibenthic faunal surveys	Including 2, 7, 11m depth beam trawls	EIA – natural fisheries EIA – marine ecology	Summer 2005
Geophysical survey	Single channel analogue surface tow boomer survey of offshore wind farm site and cable route, comprising 133km of survey lines	Provision of geological data for site characterisation	Summer 2005
Shallow geotechnical survey	30 vibrocore samples and 19 CPTs up to depths of around 6 – 8m	Provision of geological/geotechnical data for site characterisation EIA – marine archaeology	Summer 2006
Drop-down video survey	Clear water box video of seabed	EIA – marine ecology EIA – hydrodynamics and geomorphology Fulfil ecological survey consent	Summer 2006
Magnetometer survey	Magnetometer survey of borehole locations	EIA – marine archaeology Fulfil health and safety requirements for geotechnical survey	Summer 2006
Geotechnical Survey	5 boreholes, 4 x 50m and 1 x 70m depth	Provision of geological/geotechnical data for site characterisation	Summer 2006

Table A.8 Surveys during development stages of Sheringham Shoal offshore wind farm

The data from these various surveys fed into the development of the EIA and facilitated front-end design (FEED) studies. Table A.7 also shows the large degree of overlap between surveys meeting environmental and engineering requirements.

The structure of the surveys and their timescales largely followed recommendations suggested by the OSIG guidance notes. The first stage was a desktop study to determine the geological makeup of the site from publicly available information. For the Sheringham Shoals, this was carried out by an independent geological specialist mostly from British Geological Survey (BGS) data. Based on this study, a geophysical survey, a shallow geotechnical survey and an acoustic, video and grab survey were planned.

After the completion of these surveys and analyses of the gathered data, isopach charts for the predicted levels of bedrock and overlying formations were produced. However, the geophysical survey had been hampered by bad weather and inadequate equipment; hence the raw data contained a significant amount of noise. Therefore, a number of assumptions had to be made to predict the deeper geology of the site, in particular, below 20m beneath the seabed. Similarly, strata predicted by the desktop study varied from those interpreted by the geophysical survey in terms of depth and structure. The successive geotechnical survey was planned in order to calibrate available geophysical data and gain a better understanding of deeper site geology. The key aims of the geotechnical survey were:

- Calibration of geophysical data to assist in the development of more accurate geological mapping of the site
- To obtain geotechnical properties for preliminary foundation design

During the course of the survey four 50m boreholes and one 70m borehole were completed in a 10 day period. Boreholes were drilled utilising a composite borehole system consisting of a repeated process of a push sampling of 1m intervals followed by a CPT of 3m.

An environmental statement was submitted by the operating company Scira after all necessary environmental surveys were successfully completed. However, following the completion of the geotechnical site investigation programme and subsequent analysis of results, the project was

found to be unable to model costs for the whole wind farm with complete accuracy. Two key reasons for this were:

- Uncertainty over the distribution and depth of soil types across the site
- Uncertainty regarding bedrock properties.

However, data gathered allowed for 'best' and 'worst' case scenarios to be formulated, allowing the risks to be quantified.

The uncertainty regarding soil types was subsequently traced back to inaccuracies in both the BGS survey data and the geophysical survey data and the key flaws regarding the geotechnical survey appeared to have emanated from the lack of penetrative depth of the equipment used and its inability to distinguish bedrock (in this case chalk) from clay. Poor data quality was blamed on bad weather at the time of collection.

Although poor weather conditions cannot always be anticipated, the use of a secondary data collection system would have mitigated against this effect. Subsequent advice to Scira recommended the use of air-gun survey equipment in addition to boomer as it gives deeper seabed penetration despite being comparatively expensive.

With regards to the geotechnical survey, samples proved to be important in identifying various geological layers that were correlated with CPT data in order to calibrate the geophysical data sets. In general, the push sampling system that was proved to be successful in sampling the clays and sands encountered which accounted for 70% of the total soils met. However, the structureless chalk which made up the bedrock proved mush harder to obtain undisturbed samples from. In retrospect the piggyback coring system they used was unsuited to this type of ground conditions.

Lessons were also learned from the selection of borehole location for the Sheringham Shoals project. Following expert advice, drilling sites were selected for intersection of survey lines from the site geophysical survey done in 2005 and available BGS data (see Figure A-6.1). They were also designed to target specific geological features that were expected to exist and calibrate both sets of geophysical data. Subsequently, areas within the corners of the site were left without boreholes. It

was later found that borehole findings did not match geophysical survey data or data available from the BGS database with regard to bedrock depth making it difficult to map the stratigraphy of the site area. It was admitted that the poor quality of the original geophysical data reduced significantly the usefulness of the geotechnical survey results. More equally spaced borehole pattern would have potentially resulted in a better understanding of geological features across the site.

Figure A-6.1. Borehole locations at Sheringham Shoal.

6.2 Scroby Sands

The Scroby Sands offshore wind farm is located 2.5km off Great Yarmouth in the North Sea consisting of 30 wind turbines each piled 30m into the seabed. Construction took place in just under a year with three export cables bringing power ashore.

Work carried out prior to the construction consisted of an intense programme of research and monitoring. The scientific objectives were:

- To collect datasets of waves and currents over a spring/neap cycle on the sandbanks for use in calibration and validation of numerical models for potential impacts of wind farms.
- To assess gross changes in sediment transport during winter and summer seasons pre- and post- construction to compare any effects due to wind farm construction.

- To undertake suspended sediment monitoring during wind farm construction using a combination of optical backscatter sensor (OBS) profiles and water samples in order to monitor potential effects of piling and ship movements.
- To produce a GIS showing the sedimentological and hydrodynamic distributions for use in interpretation. Maps of individual bedforms were created from interpreted side-scan sonar records from the Southern North Sea Sediment Transport Study (www.sns2.org). Five snapshots of the bedforms enabled the detection of any gross changes of sediment transport regime and allowed for a comparison of seasonal and inter-annual variations. This information also supported the zone management of the wind farm by monitoring and assessing the impact of scour protection around each monopole.
- To liaise with numerical modellers such as HR, ABPMer, Posfords and Halcrow to test their models against gathered datasets.

These objectives were achieved through a series of seabed surveys (namely side-scan sonar and swathe bathymetry) as well as the deployment of seabed landers (Cefas 'MiniLanders') before, during and after construction of the wind farm. The data sets were used to assess changes in seabed bathymetry, bedforms, currents, waves and suspended sediment concentrations and consequently disturbance of sedimentary environments and sediment transport paths.

As part of the EIA process, developers had to understand and quantify the relevant processes operating at the site. This was done by the following of investigations:

- A time-series of swathe bathymetric surveys over the entire site and the export cables routes. This was placed into a historic context based on analysis of historical charts;
- Shear-stress exceedance diagrams for key locations within the area along with the export cable route;
- Particle-size information for sediments from representative locations within the area and along export cables or alternatively, particle settling velocities;
- Estimation of the size and shape of scour pits and wakes and the nature of any emplaced scour protection;
- Estimation of the disturbance caused by the construction of the wind farm, e.g. jetting, ploughing, 'grouting in' or from seabed levelling for gravity-based structures;

- Assessment of sub-bottom geophysical acoustic data, to identify historic directions of sediment transport.

Prior to construction of the wind farm four MiniLanders were deployed around the site area collecting a series of datasets including water temperature, salinity, depth, tidal current speed and direction, significant wave height, wave period and turbidity throughout the water column. On each MiniLander, passive sediment traps were mounted ('Booner tubes') to collect ambient suspended sediment.

During construction and subsequent monitoring of the wind farm, a number of monitoring strategies were proposed in keeping with best practice:

- In locations of expected sediment transport for significant periods of time, a comprehensive swathe bathymetric survey was undertaken, ideally a time-series of surveys, allowing an analysis of sediment transport processes over the bank. Bi-annual seasonally linked surveys permit the quantification of key aspects of the sediment transport budget, the identification of net sediment transport pathways and any potential areas of net erosion or accumulation;
- In regions where sediment transport was expected to be weak, a selection of representative scour pits were monitored. If the scouring exceeded the predictions in the EIA, a more systematic swathe survey was undertaken across the area and repeated at appropriate time intervals;
- High-resolution swathe bathymetry surveys of scour pits and associated scour protection measures were undertaken to identify the extent, volume and integrity of any scour protection used. This allowed for the monitoring of any secondary scour pits caused by scour protection;
- Regular swathe bathymetric surveys of the export cable route checked for any cable free-spans (compromise of the cable), exposure (risk to shipping/fishing) or movement from the desired location;
- During pile-driving, grouting or cabling operations, suspended-sediment monitoring was carried out, especially if the surface sediments or the immediate subsurface sediments had a high proportion of easily re-suspendible components, had elevated levels of

contaminants or if the operations took place near a conservation site or within a Special Area of Conservation.

A time line depicting process monitoring in relation to stages of construction can be seen below.

	2003	2003	2003	2003	2004	2004	2004	2004	2005	2005	2005	2005
	Q1	Q2	Q3	Q4	Q1	Q2	Q3	Q4	Q1	Q2	Q3	Q4
Survey Technique												
Seabed Landers												
Side-scan Sonar												
Swathe Bathymetry												
Construction Activity												
Piling												
Turbines												
Cables												

Table A.9 Timeline of monitoring at Scroby Sands

Despite the large success of the monitoring programme in establishing a good knowledge base of seabed processes within the area, several oversights resulted in data gaps. Most notably;

- Swathe surveys were only undertaken during sufficiently calm weather.
- The aim of the survey was the broad-scale mapping of the entire sand bank upon which the wind farm was located and associated bedforms. As a result, accuracy close to monopiles (roughly up to 5m away) was most likely impaired due to backscattering from strong reflectors and shadow effects of the monopiles on the differential global positioning system (DGPS);
- The scope of the hydrodynamic and sediment transport programme was to cover physical scales which reflected the large size of the wind farm area resulting in smaller impacts (e.g. 0-10m scale) not being included;

- During the construction and cable-burial operations turbidity measurements were not recorded;
- Wave statistics were only taken during the pre-construction phase.

The lack of long-term wave statistics for the site and export cable routes made it difficult to assess extreme wave events. Similarly, long-term (>annual) changes and variability of sediment particle-size distributions across the site and cable route were necessary to establish sediment transport regimes and pathways.

Current and wave height/period time-series data recoded by the MiniLanders was subsequently converted into bed shear stress. Coupled with the critical erosion thresholds for various particles sizes (see Figure A-6.2)

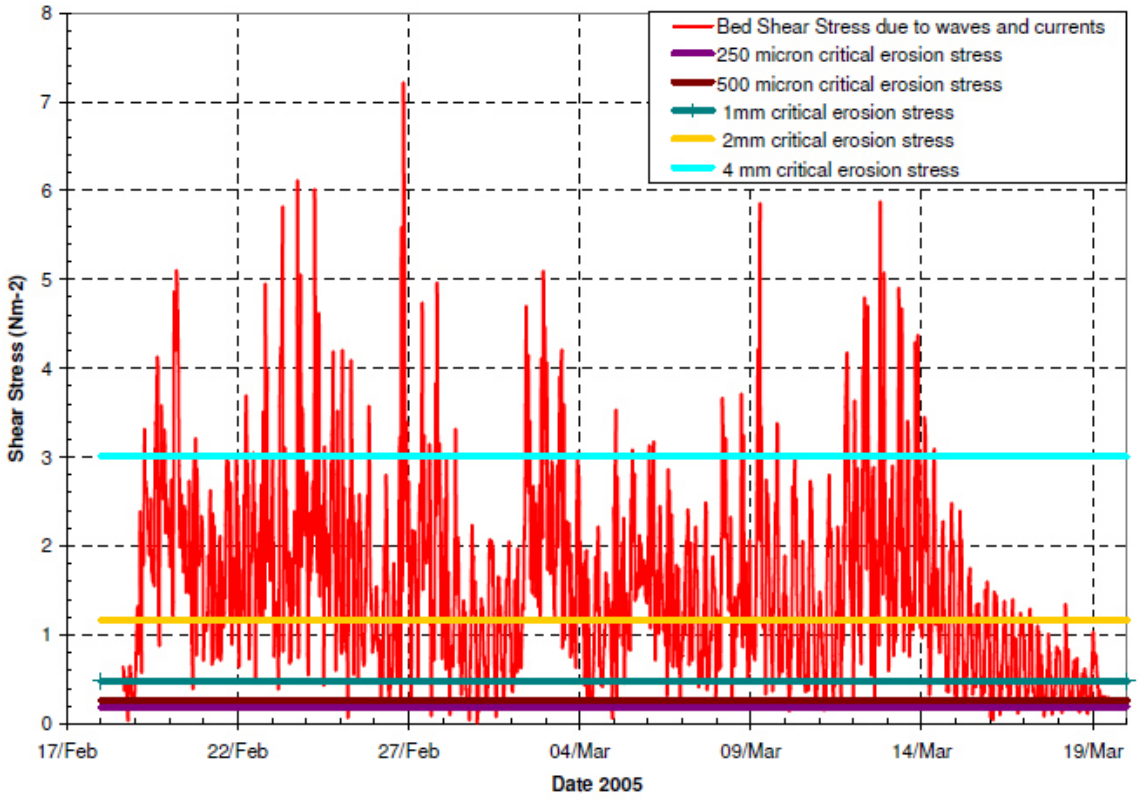

Figure A-6.2 Time-series of bed shear stress and particle critical erosion sizes (Soulsby, 1997).

From swathe bathymetry data, Digital Elevation Models (DTM) were generated. Based on the DTMs, volumetric analyses were performed for the entire area or from selected zones to identify

scour pits, scour pans and scour wakes. In order to quantify these changes, the differential volumes between older and younger DEMs were calculated.

Successive swathe surveys at various stages of construction also allowed for an assessment of the impact of monopiles on migrating sandwaves by comparing the position of sandwave crest at the various stages. By combining the results from swathe bathymetry and the MiniLander deployment, it was possible to generate a sediment dynamic model for the Scroby Bank. Data collect on waves, currents, tidal elevation and suspended sediment concentrations made it also possible to:

- Assess change in sediment transport magnitudes and pathways and;
- Assist verification and validation of wave and tidal numerical models in shallow water associated with sandbanks

7. CONCLUSIONS

7.1 Data Gap Analysis

Data	Recommended	INFOMAR	Suggestions
Multi- beam Echo Sounder	Frequency of 100 kHz or higher. Delivered in an ascii file as gridded data referenced to WGS84, interpolated from best available data corrected to MSL and LAT. Option of Google Earth .kmz file	95 kHz EM1002 or 200 kHz EM3002 system. Data corrected to LAT and available in grid(.ers), ascii (.dat), map(.png), Fledermaus (.scene), Google (.kmz), zipped ESRI ArcGIS GRIDS.	Adequate
Side-scan Sonar	Frequency of 100 kHz or higher	Edge tech side scan sonar	Adequate
Sub-bottom profiler	Boomer or alternative systems of comparable or better performance and sufficient signal penetration. Near surface resolution min. 1m Possibly supplemented by sub bottom profiler or chirp sonar in surface sediment layer vertical resolution min. 0.5m.	3.5 kHz SES Probe 500 pinger and 500 – 2000 Hz Geo-Spark 200 sparker with data available in .jpeg or .segy format	Adequate
Shallow Geotecnical Survey	Vibrocore and Cone Penetration Test (CPT) to depths of 6 -8m	Geo Resources 3000 + 6000 vibrocore with depths of 3-6m which are scanned, logged and stored.	Possibly deeper core. Provision of CPT data.
Video and Grab Survey	Video reconnaissance by way of drop down camera and seabed samples of <1m depth to ground truth and use in grain-size analysis.	Day, Shipek, Van Veen and Box Corer. Samples undergo particle size analysis.	Possible provision of seabed imagery.
Hydrodynamics Study	Deployment of acoustic wave and tidal monitor (ADCP or MiniLander). Deployment of wave buoy.	Tidal and Wave data available from Marine Institute. CTD data also	Introduce site specific wave and current monitoring

	Deployment of passive sediment traps. Gathering of CTD data.	available.	by way of ADCP data or equivalent. Make provision for deployment of sediment traps for hydrodynamic surveys

7.2 General Conclusions

General feedback from industry regarding the quality of information provided by INFOMAR was positive. As part of the various correspondences with industry, it was envisioned that potential sites of investigation and development should be considered for INFOMAR surveys in the near future. However, with the imminent publication of Irelands Strategic Environmental Assessment draft released in January, industry was awaiting its result and conclusions before deciding on future projects.

The existing datasets cover a variety of aspects relevant to the offshore renewable industry and form a solid basis on which to prepare a desktop survey prior to any geophysical or geotechnical survey.

A good desktop survey is a baseline against which subsequent data collected can be measured. Identifying data gaps and missing information allows for tailored data collection to be planned. This makes the data acquisition more efficient and allows for developing robust and reliable geological models. The importance of the desktop study was highlighted in the Sheringham Shoal case study.

In relation to data gaps, the main issues arose with regard to geotechnical data. Geotechnical data are of central importance for foundation constructions, in particular for the monopile foundations that are commonly used for wind turbines.

Information on seabed dynamics was also identified as a vital for offshore installation development. Currently, this information is largely unappreciated or lacking in data. Scouring is the primary concern in relation to seabed dynamics. This has been realised at the Arklow Bank windfarm

project where, following Phase 1, strong currents coupled with geotechnical sediment properties around the bank have caused severe scour problems at the foundations.

Data acquisition on seabed dynamics can be assisted by the use of multibeam water column imaging, a technique largely developed by the Canadian Hydrographic Survey. Patterns within water column scattering profiles give good indication of watermass distribution. Similarly, individual watermasses can be defined by variations in density (by measuring suspended particles) and sound speed as well as zones of turbulence and the presence of zooplankton species. The issues associated with this technique, however, are distinguishing genuine water column features from anthropogenic ones such as third party sonar interference, vessel engine and propeller noise and bubble wash down. Nonetheless, the data that is recorded proves useful in establishing a model for the water column which can subsequently feed into hydrodynamic and sediment transport studies.

General guidelines for site surveying for offshore renewable energy installations come from related documents of the offshore hydrocarbon exploration sector. However, the Offshore Site Investigation and Geotechnics Group (OSIG) of the Society of Underwater Technology (SUT) have developed a competent set of guidelines for data acquisition and equipment selection with regard to site selection for offshore renewable energy installations based on shared experience and knowledge of its authors and members. It is largely focused on data acquisition with regard to engineering and construction aspects of offshore project and neglects survey requirements for EIA purposes. These guidelines have been widely adopted for a number of offshore wind farm site investigations across England.

Although the OSIG outlines guidelines with regard to site investigation there is little scope for geotechnical surveys. The DNV (2004) is referenced to covers sediment investigation for offshore wind turbines and provides all necessary data for detailed design.

8. RECOMMENDATIONS

For future site investigations and surveys, it is clear that a multidisplinary approach is required with seabed dynamics and geotechnical parameters a key consideration. As suggested by OSIG guidelines, this will involve a multi-stage investigation with the first phase comprising of a desktop survey detailing all previously available data and information about the area. The second phase is to map the seafloor acoustically using a multibeam echosounder system (MBES) and side scan sonar (SSS). In conjunction with this survey, seismic data may also be acquired. It is suggested that seismic data should be recorded along survey lines spaced at 50m intervals with cross lines every 250m. It is highly suggested that the use of air-gun equipment and a secondary data collection system should be used during the geophysical survey as highlighted in the Sheringham Shoal case study. Swathe data should be recorded along survey lines spaced no more than 3 times water depth. Magnetic, resistivity and electromagnetic surveys, data should be recorded along lines as closely spaced as possible. Considering that the majority of potential new sites for offshore renewable energy lie within the 20m water depth zone, ideally, 100% covered with MBES should be obtained. If possible, current velocity meters (e.g. Acoustic Doppler Current Profiler (ADCP)) should be deployed. Ideally, ADCPs should be left on the seabed for a period of more than two tidal cycles, preferably covering the time interval of highest energy conditions (strong tidal events such as the spring and equinox tides). Information on predicted tides for forthcoming strong tidal events can be obtained from the meteorological office.

Following on from information gathered in the first leg of the survey, a detailed second survey can be planned to gather samples to groundtruth acoustic data sets. Biological sampling supports habitat mapping. In addition, a series of drop down video surveys can be carried out to groundtruth backscatter data, aid in habitat mapping and assist in facies classification. Additional survey for more extensive location sampling (e.g. coring) may also be carried out. Sampling and borehole location are selected based on the outcomes of the previous surveys, geotechnical expertise and the desktop study. The OSIG provides a good evaluation of the use of various seabed sampling and collecting equipment and their suitability for various sediment types (see Table A.10 – 12).

Soil Parameters	In-Situ Testing			Laboratory Testing		
	Type of Tests	Applicability		Type of Tests	Applicability	
		Sand	Clay		Sand	Clay
Interpolation of soil layering in between cores/borings/CPT's	Seismic reflection, (sub-bottom) profiling	3	3	N/A	N/A	N/A
Soil classification	Seismic reflection profiling	2	2	Grain size,	5	3
				Water content,	2	3
	CPT/PCPT*	4	4	Atterberg limits.	N/A	5
Soil density	CPT/PCPT*	3 to 4	2	Unit weight and water content measurement	1 to 2	5
Soil strength (Undrained shear strength)	CPT/PCPT*	N/A	3 to 4 (a)	Unconsolidated triaxial compression,	N/A	3 to 4
	In-situ Vane	N/A	4 to 5	Consolidated triaxial compression,	5 (b)	5
				Fallcone, pocket penetrometer, Torvane, Labvane, Direct Simple Shear	N/A	2
Friction angle (Drained shear strength)	CPT/PCPT*	3 to 4	2	Consolidated triaxial compression,	5(b)	5
				Direct Shear (Shear box), Direct Simple Shear	4	1
Sensitivity	CPT/PCPT*	N/A	2	Fall cone, labvane	N/A	5
	In-situ Vane	N/A	3			
Consolidation characteristics and permeability	PCPT*	1	3(c)	Oedometer	2(b)	5

Table A.10 Conventional Test Methods (after OSIG, 2005)

Suitability Scale

1. Poor or inappropriate
2. Acceptable for non-critical analyses
3. Moderately good
4. Good
5. Very good

Soil Parameters	In-Situ Testing			Laboratory Testing		
	Type of Tests	Applicability		Type of Tests	Applicability	
		Sand	Clay		Sand	Clay
Interpolation of soil layering in between borings/CPT's	Instrumented plough	3	3	N/A	N/A	N/A
	Seismic refraction profiling	(d)	(d)			
	Electrical resistivity profiling	(d)	(d)			
Soil density and stiffness	Electrical resistivity probe	2 to 3	1	Small strain effective stress testing	3 to 4 (e)	1
	Nuclear density probe	1 to 2	2 to 3			
	Seismic cone	3 to 4 (e)				
Soil strength and deformation	Pipe model test Plate load test	3 to 4	3 to 4	Direct simple shear	4 (b)	5
Rate effects / cyclic behaviour	Seismic Cone	3 to 4	3 to 4	Direct simple shear - static/cyclic	4 (a)	5
				Consolidated triaxial – static/cyclic	5 (b)	5
Permeability	PCPT* - dissipation tests BAT probe Piezoprobe	1	4	Special permeability tests	5 (b)	N/A
Thermal conductivity	Heat flow probe	4	4 to 5	Transient method	5 (b)	5
				Steady state method	5 (b)	5
				Mineralogy and porosity	4	4
Corrosion potential	Electrical resistivity cone	4	4	Electrical resistivity	4 (b)	4
Gas content	BAT/DGP (Deep Gas Probe)	4	4	Geochemical	5	5

Table A.11 Special Testing Methods (after OSIG, 2005)

Suitability Scale

1. Poor or inappropriate
2. Acceptable for non-critical analyses
3. Moderately good
4. Good
5. Very good

Type of Equipment *	Sample Quality		Recovery (relative to length of sample tube)	
	Sand (g)	Clay	Sand	Clay
Gravity Corer/Piston Corer	2	3	1	3 to 4
Vibro Corer	2 to 3	2 to 3 (g)	3 to 4	2 to 3
Grab Sampler	1 to 2	1	1 to 2	2
Box Corer (i)	1 to 2	5	1	5

Table A.12 Seabed Sampling Equipment (after OSIG, 2005)

Type of Equipment	Sample Quality		Recovery (relative to length of sample tube)	
	Sand (g)	Clay	Sand	Clay
Hydraulic Piston Sampler	3 to 4	5	3	5
Hydraulic Push Sampler	3 to 4	4 to 5	3	5
Hammer Sampler	2 to 3	2 to 3	3 to 4	3 to 4
Rotary Coring (j)	1	2 (i)	1	3 (l)

Table A.13 Downhole Sampling Equipment (after OSIG, 2005)

Suitability Scale

1. Poor or inappropriate
2. Acceptable for non-critical analyses
3. Moderately good
4. Good
5. Very good

Information with regard to geotechnical data required for offshore installation foundations is comprehensively outlined in the DNV (2007) and should be used as a reference.

The work carried out by INFOMAR provides a variety of datasets which are widely used by the offshore renewable energy industry to build good geological models. There is, however, more scope for collecting data that can contribute to developing further dynamic models (particularly sediment dynamics and scour) and subsequent site monitoring. Better information on geotechnical parameters of the sediments is also crucial for foundation design, the main financial concern of offshore renewable energy projects. By extending the time-scales of site surveys, it is possible to monitor seabed dynamics.

By following the guidelines set out by OSIG and DNV it is possible to develop a phased site survey methodology which is both efficient and productive in acquiring the relevant data necessary to develop an offshore installation.

REFERENCES

DARTNELL, P. & GARDNER, J.V (2004) Predicting Seafloor Facies from Multibeam Bathymetry and Backscatter Data*. Photogrammetric Engineering & Remote Sensing, Vol. 70,No 9, September 2004, pp. 1081-1091.*

Det Norske Veritas (2004), Offshore Standard: 'Design of Offshore Wind Turbine Structures' – 2007

Cefas (2006) Scroby Sands Offshore Wind Farm- Coastal Processes Monitoring. Final Report July 2006.

FISH, P. & LEACH, C. (2007) Experience and Lessons Learned from Procurement of Site Investigation Campaigns at Sheringham Shoal Offshore Windfarm. *Proceedings of the 6th International Offshore Site Investigation and Geotechnics Conference: Confronting New Challenges and Sharing Knowledge, 11-13 September 2007, London, UK.*

FUGRO (2005) Geotechnical and Geophysical Investigations for Offshore and Nearshore Developments. *International Society for Soil Mechanics and Geotechnical Engineering, September 2005.*

HAMILTON, E.L. (1980) Geoacoustic modeling of the sea floor. *The Journal of the Acoustical Society of America,* 68, 1313–1340.

HAWKINS, R.A., & MARKUS, A (1998). New Developments in Offshore Geotechnical Investigation. *Offshore Site Investigation and Foundation Behaviour SUT 1998.*

HOLMES, R. & TAPPIN, D.R. (2005) DTI Strategic Environmental Assessment Area 6, Irish Sea, seabed and surficial geology and processes. British Geological Survey Commissioned Report, CR/05/057. pp. 72.

HUGHES CLARKE, J.E (2006). Applications of Multibeam Water Column Imaging for Hydrographic Survey. The Hydrographic Journal, April 2006

MANWELL, J.F., MCGOWAN, J.G & ROGERS, A.L (2002) Wind Turbine Siting, System Design and Integration. *John Wiley & Sons Ltd 2002*

NORSOK STANDARD (2004) Marine Soil Investigations. G-001, REV. 2, October 2004.

OFFSHORE SOIL INVESTIGATION FORUM (2000) Guidance Notes on Geotechnical Investigations for Subsea Structures.

OFFSHORE SITE INVESTIGATION and GEOTECHNICS GROUP (OSIG). Guidance Notes on Site Investigation for Offshore Renewable Energy Projects.

POEHNER, J.R. &HAMMERSTAD, E. (1991). Combining Bathymetric Mapping, Seabed Imaging. Sea Technology 32(6): 17-25.

ROBINSON, E. & BYRNE, G. (2008) Methodology for Modelling Tidal Turbine Charactersitics.OCEANS 2008, pp.1-5

WANG, W. & BAI, Y (2010) Investigation on Installation of Offshore Wind Turbines. J.Marine Sci.Appl. (2010) 9:175-180

WHEELER, A.J., WALSHE, J. & SUTTON, G.D. (2001) Seabed mapping and seafloor processes in the Kish, Burford, Bray and Fraser Banks area, south-western Irish Sea. *Irish Geography,* 34, 194–211.

Appendix B

"Nobody knows what's going to happen. And then we film it. That's the whole concept"
- Steve Zissou

SURVEY CV0926 CRUISE REPORT

Appendix B

Research Cruise: RV Celtic Voyager – Survey CV0926; Irish Sea Marine Assessment (ISMA) 28th September – 18th October 2009

Ship's Crew	**Scientific Party (Leg 1)**
Philip Baugh – Master	Dr. Boris Dorschel – Chief Scientist
Brandon McGovern- 1st Mate	Dr. Katrien Van Landeghem – Scientist (Uni. Bangor)
Damien McCallig – Chief Engineer (Leg 1)	Slava Sobolev – Scientist (INFOMAR)
Brendan Barry – Chief Engineer/Bosun (Leg 1)	Fabio Sacchetti – Scientist (INFOMAR)
Thomas Byrne – 2nd Engineer	Brian Cohen – Scientist (INFOMAR)
Peter Greening – Officer of the Watch	Vince Kelly – Scientist (INFOMAR)
Mark Toner – Officer of the Watch	Conor Ryan – Marine Mammal Observer (UCC)
Philip Gunnip – AB	
Martin Goggin – AB	
Ollie Murphy – Cook	
	Scientific Party (Leg 2)
	Dr. Andy Wheeler – Chief Scientist (UCC)
	Xavier Monteys – Scientist (GSI)
	Mieke Thierens – Scientist (UCC)
	Anna Cole – Scientist (Gaelectric)
	Mark Coughlan – Scientist (UCC)
	Rory O Donnell – Scientist (UCC)
	Cormac Ryan – Scientist (UCC)

Compiled by
Dr. Andy Wheeler (Project coordination & Chief Scientist: Leg 2)
Dr. Boris Dorschel (Chief Scientist: Leg 1)
Scientific Party (data input, corrections to drafts and minor text)

EXECUTIVE SUMMARY

The Irish Sea Marine Assessment (ISMA) is a collaborative research survey undertaken by University College Cork, the INFORMAR programme (Geological Survey of Ireland & Marine Institute), and Gaelectric Developments Ltd. Its purpose is to produce integrated seabed and sub-seabed mapping products to assist in a fundamental understanding of the seabed and how in

changes through time, thereby deriving information pertinent to the development of offshore renewable energy resources.

Four study areas where surveyed:

The Codling Deep is a long north-south deep (or channel) tidal currents flow strong. The seabed it typified by both mobile sands and gravels, and areas covered by cobbles (stoney ground) rich in seabed life. The sub-seabed geology is complicated with localised drift bodies and numerous erosional surfaces.

The next three areas are relatively flat and experience decreasing current intensity resulting in a decrease in seabed sediment type particle size from sand (Lambay area) to fine sands (Rockabill area) to muds (Northern Mudbelt). All three areas show a sub-horizontal layers of deposits underlying the seabed consisting of upper sands to muds underlain by glacial tills (muds with boulders) and rock.

The Lambay area, covered in rippled sands with shell fragments, has a limited fauna with sponges, red fish and seaweed. The upper sand layer thins in middle of the area to expose lithified sediments at the seabed.

The Rockabill area is also covered with rippled sands that are compacted below the seabed with some fish and shell.

The Northern Mudbelt is a large area heavily burrowed by the commercial Dublin Bay Prawn. The sub-seabed shows shallow accumulation of (biogenic) gas (although not enough to form a geohazard).

Due to exceptional weather conditions and a 24 hour work routine, in total **352.65 km^2 (35,265 hectares) of seabed was mapped** to a precision of x/- 0.4 m horizontal and 0.1 – 0.15 m vertical. **534 km of sparker seimic lines** were shot imaging into the sub-seabed by 50 m. In **addition 2179**

km of pinger seismic lines (down to 30 m penetration) were taken. **269 sediment samples** were taken, **171 biological samples** were taken with an additional **7 faunal samples frozen for DNA studies**. **20 cores** where sunk into the seabed up to a depth of 3 m from which changes in the seabed through time will be studied and geotechnical properties of deposits that can also be traced deeper determined. In addition, we took **5 Reineck box-cores** which preserve the upper 30 cm for palaeoenevironmental and geotechnical studies. **975 good quality digital still photographs of the seabed** were taken in **15 areas** and a 1 month long measurements of variation in current speeds throughout the water column was also taken for one key location.

BACKGROUND

The Irish Marine Assessment (ISMA) survey is a joint collaboration between the University College Cork marine geology group (UCC), the Geological Survey of Ireland and the Marine Institute's "Integrated Mapping for Sustainable Development of Ireland Marine Resources" (INFOMAR) programme, and Gaelectric Developments Ltd. These four organisations have overlapping interests in mapping the Irish Sea for ongoing sediment transport studies, producing baseline coverages and for assessment renewable energy potential, respectively.

UCC has been involved in studying sediment transport and mobility in the Irish Sea since pioneering mapping of the Kish Bank in 1998. Since then it has concentrated on sediment dynamics in the south-western Irish Sea for a number of applied projects including two INTERREF project on habitat mapping (HabMap project) and aggregate resource evaluation (IMAGIN). These studies have culminated in 2 recent papers on sediment transport and sediment wave morphometrics and dynamics (Van Landeghem et al., 2009a; b). ISMA will allow UCC, in collaboration with the University of Bangor, to extend out spatial coverage of sediment transport studies along the entire western Irish Sea and also augment our record of repeat coverages to improve our understanding of sediment transport dynamics through time.

INFOMAR is a joint venture between the Geological Survey of Ireland and the Marine Institute following on from the Irish National Seabed Survey (INSS). INFOMAR concerned with producing

integrated mapping products covering physical, chemical and biological features of the seabed in productive and commercially valuable inshore waters. INFOMAR focuses on mapping 125,000 km^2 including 26 priority bays and three priority areas including the western Irish Sea. ISMA provides new coverage of previously unmapped seabed in one of the priority area (Irish Sea). Collaboration between INFOMAR and Universities and industry is welcome as it demonstrates, at the outset, the additional value of the data being collected beyond its intrinsic long-term value as a baseline resource dataset.

Renewable energy developments utilise sources of energy that are continually replaced and are inexhaustible e.g. solar, wind, hydro, wave, tidal, biomass, and geothermal powers. The exploitation of these energy sources leads to little or no emissions of carbon dioxide and other greenhouse gases which cause global climate change, regarded as the most critical environmental problem at present.

It is recognised that Ireland has some of the best offshore wind energy resources in Europe at its disposal to tackle the growing need for renewable energy. ISMA will assess the feasibility of a number of sites in the Irish Sea for wind energy generation. This project is thus directly applicable to Ireland's national strategic interest in this area. ISMA will assess locations in the Irish Sea where the (sub-) seabed favours the economic construction, operation, and maintenance of wind farms without causing severe environmental damage or impacting on the sustainable development of the marine environment.

References

Van Landeghem, K.J.J., Uehara, K., Wheeler, A.J., Scourse, J. D. and Mitchell, N. (2009) Post-glacial sediment dynamics in the Irish Sea and the formation of giant (up to 38 m high), near-symmetrical trichoidal bedforms. *Continental Shelf Research,* 29 , 1723-1736.

Van Landeghem, K.J.J., Wheeler, A.J., Sutton, G. and Mitchell, N.C. (2009). Variations in sediment wave dimensions across the tidally dominated Irish Sea, NW Europe. *Marine Geology,* 263, 108-119.

Van Landeghem, K.J.J., Wheeler, A.J. and Mitchell, N.C. (2009). Detailed seafloor evidence of palaeo-ice streaming offshore Anglesey, UK: Implications for decline of the Irish Sea Glacier. *Boreas*, 38. 119-131.

SURVEY OBJECTIVES AND RATIONALE

ISMA objectives are:

- To collect high resolution (preferably 120% coverage) bathymetric maps from target areas (Figure B-1.1).

- To collect information on the sub-surface in the target areas using sparker seismics to aid regional stratigraphic correlation and palaeoenvironmental development studies as well as assisting in foundation design for offshore wind turbines.

- To core shallow 3 m sequences using a vibrocore to obtain geotechnical samples from sub-cropping seismic reflectors and samples high sedimentation rate depositional sequences for palaeoenvironmental studies.

- To groundtruth acoustic backscatter maps of the target areas using sediment samplers in order to produce sediment type charts and to assist in hydrodynamic/benthic dynamic interpretations.

- To assess biological taxa presence and distribution in the target areas for the purpose of habitat mapping and potential environmental impact assessments.

- To study the hydrodynamics in the areas through an evaluation of mapped sedbed bedforms, sediment samples, a deployed current meter and water column profile(s).

The target areas reflect areas of potential interest for offshore wind farm develop and sediment transport studies whilst offering extension to the planned INFOMAR coverage.

To fulfil the objectives the following rational was proposed:

- Map areas using the EM3002D multibeam echosounder to provide 100% complete coverage with overlaps. In the north-west of the survey, existing INFOMAR coverage exists although there are some problems with the vertical datum. A repeat grid over this area will allow the INFORMAR data to be incorporated with ISMA data and vice versa. Extensions to the survey out to 80 m are to be attempted either will full seabed coverage or via a survey grid. To calibrate the bathymetric data, 2 tide gauges are to be deployed on the seabed in the area and regular sound velocity profiles taken through the water column.

- A regular grid of seismic lines will be run with approximate 200 m spacing.

- Sediment and biological samples will be taken to provide a spatially distributed coverage of the target areas whilst sampling all backscatter facies (where practical).

- To undertake digital stills camera transects across the area to visually groundtruth the backscatter facies, study smaller scale bedforms and identify megafaunal presence.

- To collect vibro-cores, gravity cores and Reineck box-cores (as appropriate) on targets identified by the seismics and acoustic backscatter.

- To do a limited study of the water masses properties using an acoustic Doppler current profiler (ADCP) and conductivity-temperature-depth (CTD) profiler

- The survey is to be broken up into 2 legs: Leg 1 will collect geophysical data and deploy the ADCP, Leg 2 will groundtruth the geophysical coverage using sediment samples, cores and a benthic camera.

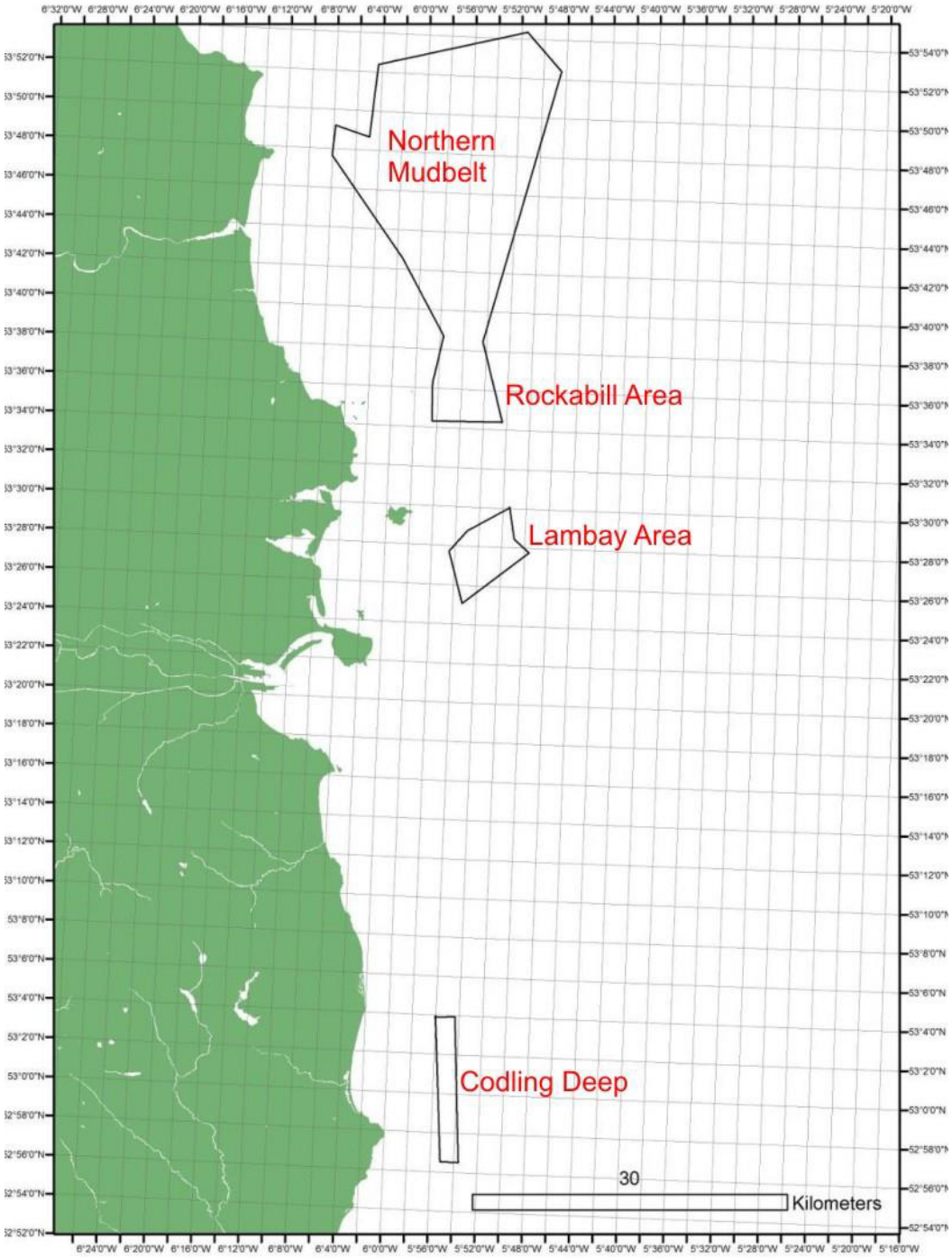

Figure B-1. The proposed survey areas

EQUIPMENT

The following equipment was used during the survey:

Research Vessel – RV Celtic Voyager

The Celtic Voyager is a 31.4 m multi-purpose research vessel. The vessel has wet, dry and chemical laboratories, which are permanently fitted with standard scientific equipment and can accommodate 6 - 8 scientists with a maximum endurance of 14 days. The vessel is manned by an experienced crew who are highly skilled with the handling and deployment of scientific equipment. She is equipped with a Trimble NT Differential GPS and Kongsberg Simrad Seapath 200 motion reference unit. A 10,000 kg general purpose winch hooked through the aft, 4 m high A-frame as well as a 500 kg starboard CTD winch and 1000 kg starboard oceanographic winch used for the sampling and camera operations on this survey.

Figure B-2. The RV Celtic Voyager.

Simrad EM3002D multibeam echosounder

The EM 3002 is a high resolution shallow water multibeam echosounder with dynamically focused beams suitable for 0.5 to 150 m water depth acquiring bathymetry and backscatter data. The transducers are hull mounted and, depending on the accuracy of positioning, the horizontal accuracy (x, y) is usually less than 50 cm and the vertical accuracy (z) less than 15 cm for the processed bathymetry data. Data processing was performed on board with the CARIS HIPS and SIPS software package.

Figure B-3. Hull mounted multibeam transducer on the RV Celtic Voyager (photo of the Marine Institute).

AML Smart SVPlus

The AML Smart SVPlus is a shallow water sound velocity profiler recording sound velocities and pressure through the water column.

Geo-Source 400 Sparker Seismic system

The Geo-Source 400 sparker seismic system consists of the Geo- Spark 6 kJ pulsed power supply which emits a pulse to the sparker source which is towed behind the vessel. The source comprises four electrode modules that are evenly spaced in a planar array. The return signal is picked up in Geo-Sense single channel hydrophone array.

Figure B-4. Geo-Spark 6 kJ pulsed power supply and towed Geo-Source 400 Sparker source.

Sea-Bird SBE 9plus conductivity-temperature-depth (CTD) profiler

The Sea-Bird SBE 9plus CTD profiler was used to determine water mass properties. She was lowered into the water and held at the surface until the sensors equilibrated and then lowered steady to 5 m off the bottom logging in real-time. The capacity to take water samples was not used on this survey. The CTD was deployed on the starboard winch mid-ship.

Figure B-5. Sea-Bird SBE 9plus CTD profiler being deployed

Acoustic Doppler Current Profiler (ADCP)

A TRDI 600 kHz Workhorse Sentinel ADCP (depth rated to 200 m) was deployed on the seabed to profile changes in current speed throughout the water column. The ADCP is housed within TRDI Workhorse Sentinel ADCP Seabed Gimballed Frame with a Sonardyne LRT, pop-up buoy and rope canister that can be acoustically released for recovery. Communication with the ADCP is with a Sonardyne LRT Command Unit with Dunking Transducer. The ADCP was deployed through the A-frame. Near the ADCP, a weight was deployed and attached by chain to the ADCP. Attached to the weight was Dan buoy with a winky light and radar reflector. In addition, a navigation warning was issued.

Figure B-6. The TRDI 600 kHz Workhorse Sentinel ADCP

Shipek sediment sampler

A Duncan & Associates Shipek sampler was used to take the majority of sediment and biological samples in both muddy and gravelly substrates. The sampler scoops a sediment sample from the top 10 cm of the seabed. The Shipek was deployed on the starboard winch mid-ship.

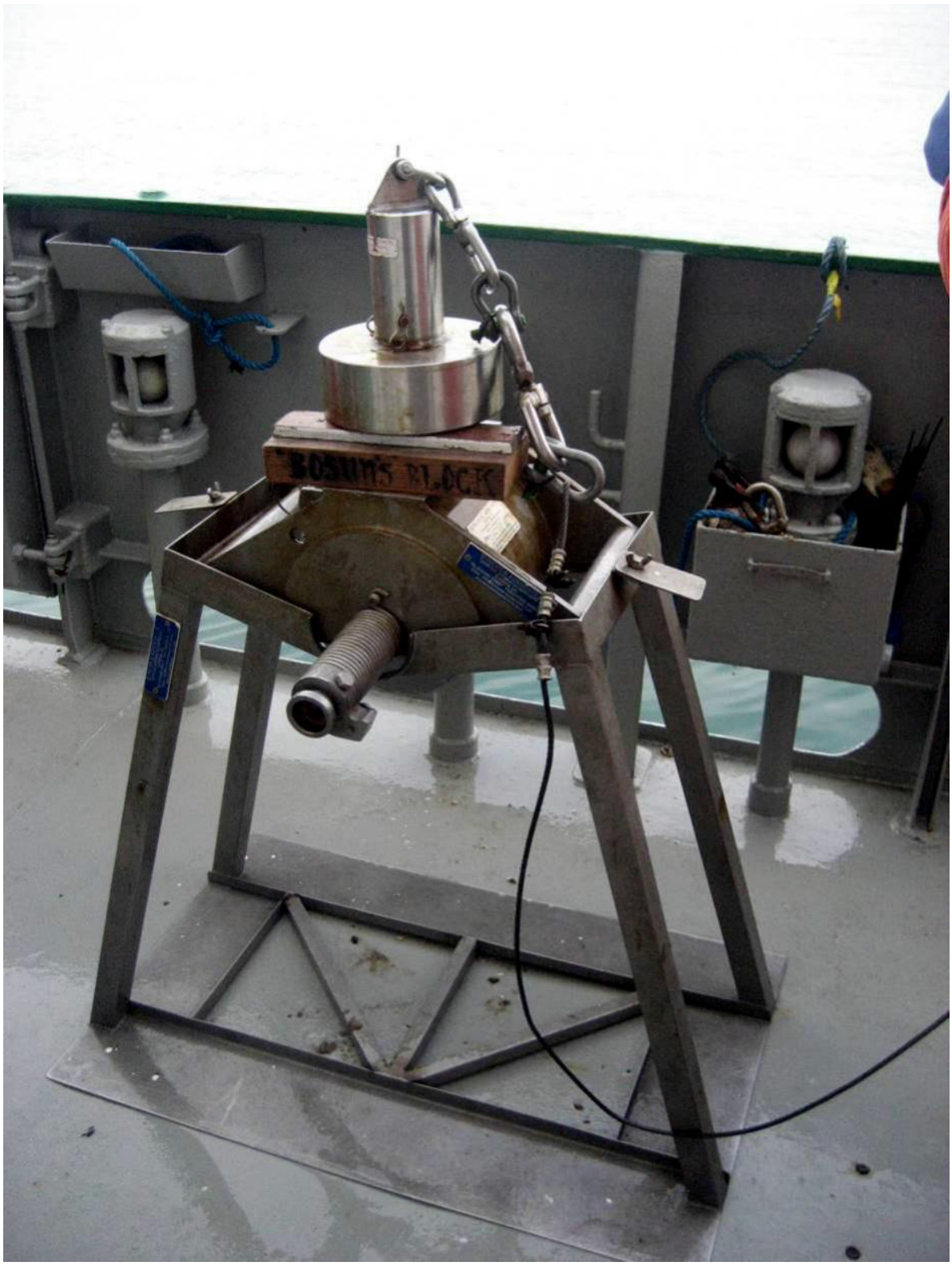

Figure B-7. Shipek sampler on stand

Reineck box core

A Reineck box-corer was used to take undisturbed sediment samples from the upper 30 cm of the seabed. These were then sub-sampled using a push core.

Figure B-8. The Reineck box-corer and retrieved sample showing the push-core inserted.

Gravity Corer

A 1 m Marine Institute gravity corer was used as an alternative coring device to the vibrocore. Although shorter, it has the advantage that it can be deployed at any state of the tide although penetration is limited in sands and gravels but excellent in mud. The gravity corer was deployed through the A-frame. Note that it was used only once but did not produce a sample due to the nature of the seabed. It is therefore not included in the station list.

Figure B-9. Gravity corer with 1 m core barrel.

Geo-Resources 6000 vibrocorer

A 3 m vibrocore was used and deployed via the A-Frame. As the vessel does not have dynamic positioning, the vibrocore could only be deployed at slack water when there was limited windage. The vibrocore was lowered to the bottom, activated for a maximum of 1.5 minutes and recovered. Cores contained in the core-liners were cut into 1 m lengths, labelled, sealed with end caps, taped and wax sealed. They were stored at 2^{o}C.

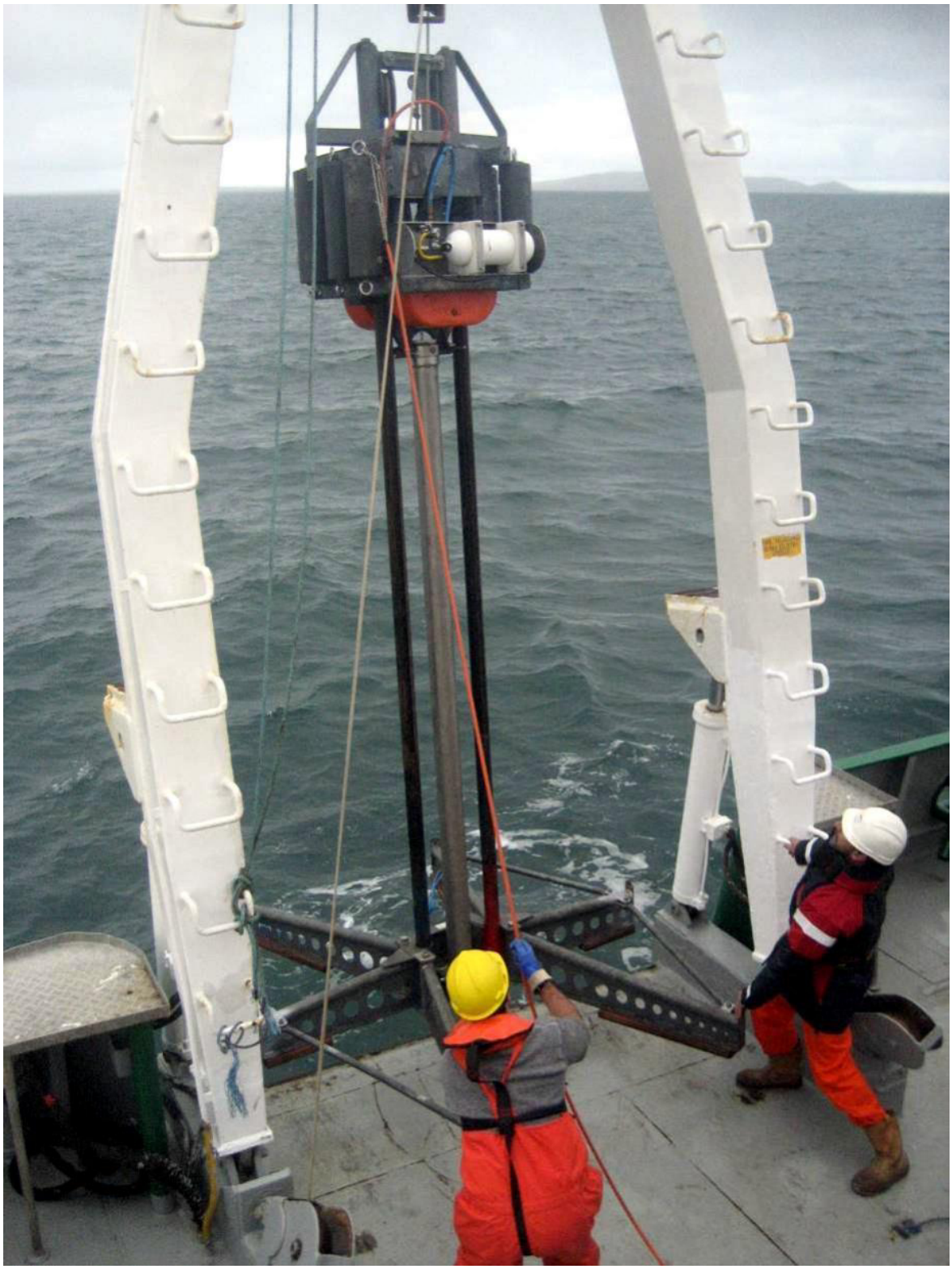

Figure B-10. The Geo-resources 6000 vibrocore being deployed.

Digital stills camera

Imagery of the seabed was collected by a Konsberg Simrad OE14-208 Digital Stills Camera System with a flash unit housed within a Seatronics stainless steel seabed camera frame. The camera was winched to the seabed, a photo was taken, then lifted up, moved a few metres and set back on the bottom again for the next photo to be taken. In this way, transects of high resolution digital still images were generated. A live video feed was also relayed to the ship and viewed on a 14" Sony/JVC Colour Video Monitor for the selection of sites to be photographed. In the video mode, the seabed was illuminated by four 24 V dc Seatronics SeaLed MKII Subsea LED lamps. Photography and illumination was controlled from the surface in real-time. Video data was logged in real-time to a Datavideo DN-300 Hard Disk Video Recorder. Digital stills imagery was stored in the camera and downloaded after recovery. The camera system was deployed on the starboard winch mid-ship. The position of the camera at the seabed was generated from the vessel dGPS.

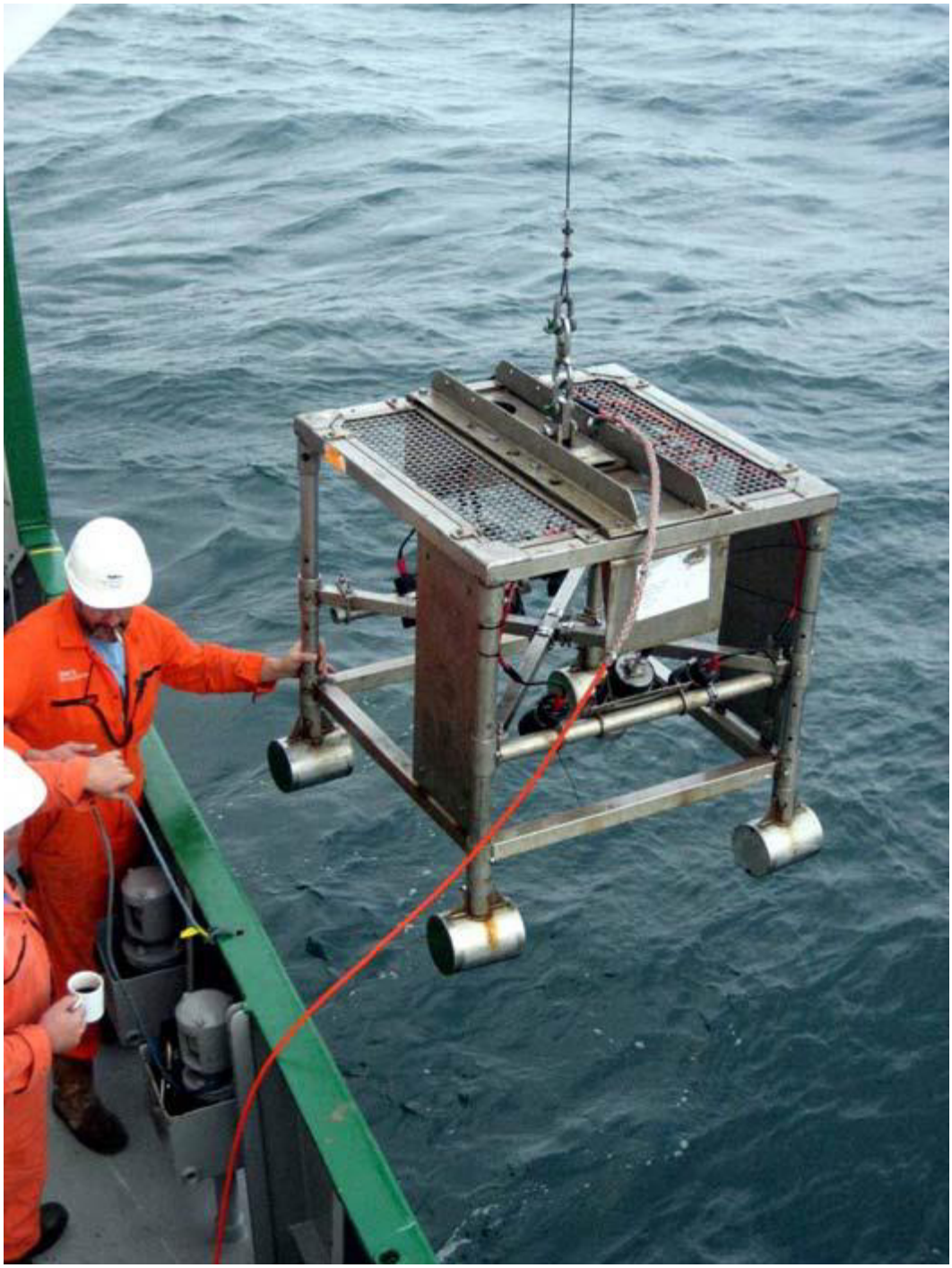

Figure B-11. The digital stills camera, flash and LED lamps housed in the camera frame being deployed off the starboard winch during the survey.

SUMMARY OF AREAS

Northern Mudbelt

The Northern Mudbelt is a very large area about 26 by 20 km and is very uniform. The area is covered by about 10 m of silty mud which is heavily bioturbated by shrimp including the commercial *Nephrop* sp. or Dublin Bay prawn. We saw little change in burrow density although trawl marks on the seabed were clearly visible especially on the backscatter data and increase in density to the north-east. Some live *Nephrops* were observed by the camera. In some areas the vibrocores were able to sample into the underlying glacial tills and below these at about 20 m is bedrock. There are numerous evidences of accumulations of biogenic gas including pockmarks and reduced and partially concreted sediments. At the southern limit of the area, a band of dark backscatter may also be related to gas. Data highlights are presented below:

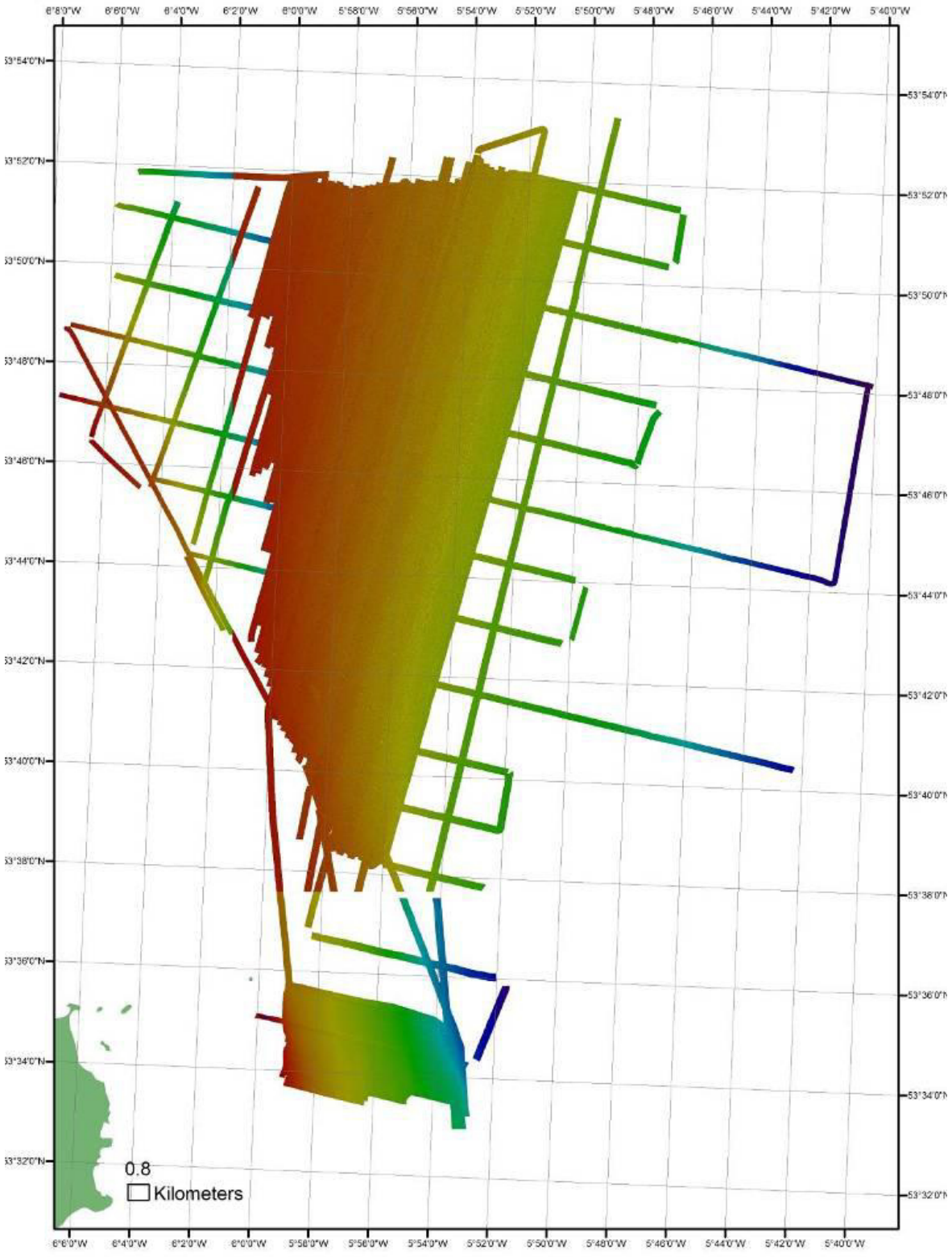

Figure B-12. Multibeam bathymetric coverage in the Northern Mudbelt (northern and central coverage) and the Rockabill area (southern coverage). The image shows a smooth seabed, gentle sloping to the east.

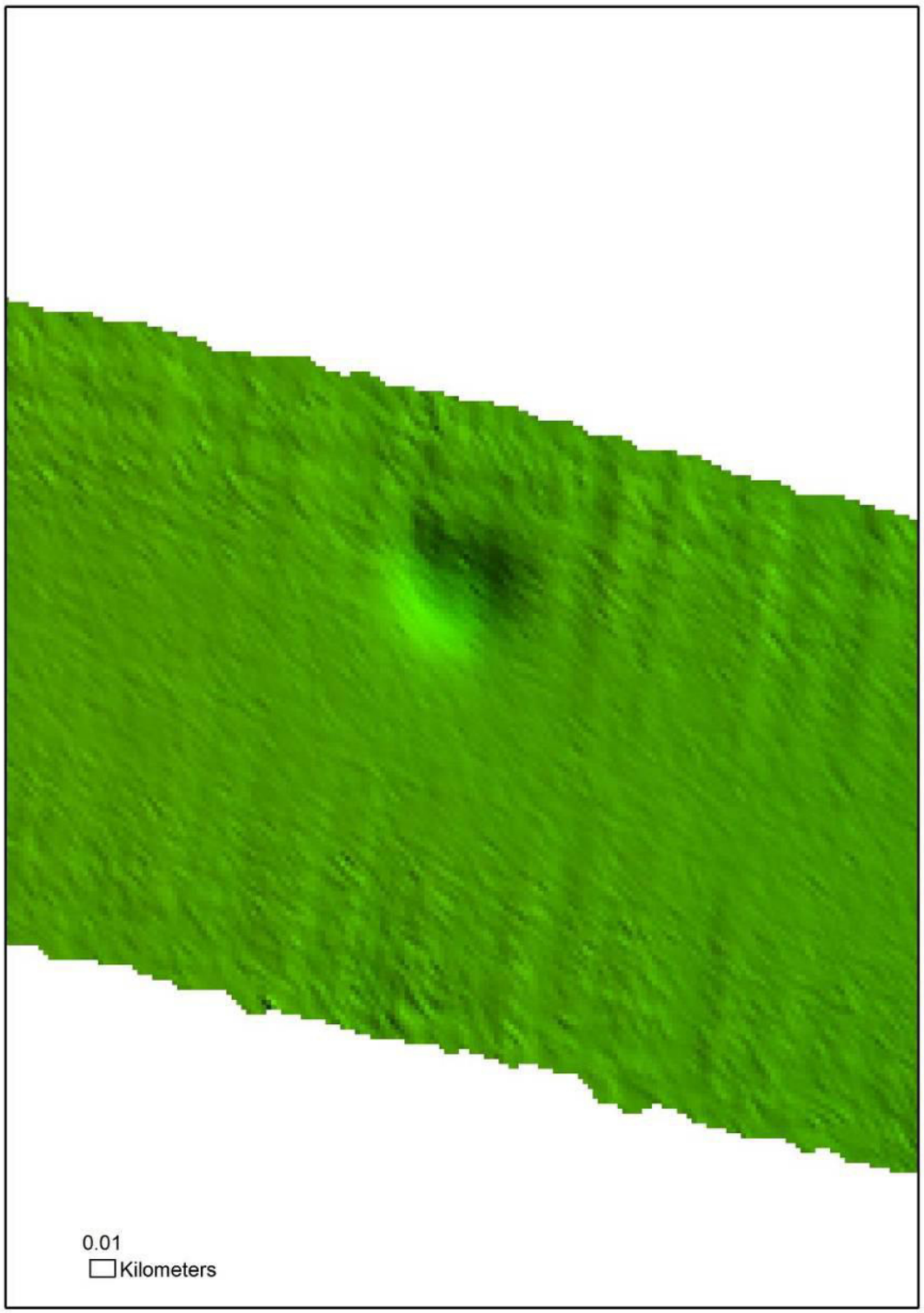

Figure B-13. Multibeam bathymetry showing a pockmark formed by shallow gas escape of which there were several in the area.

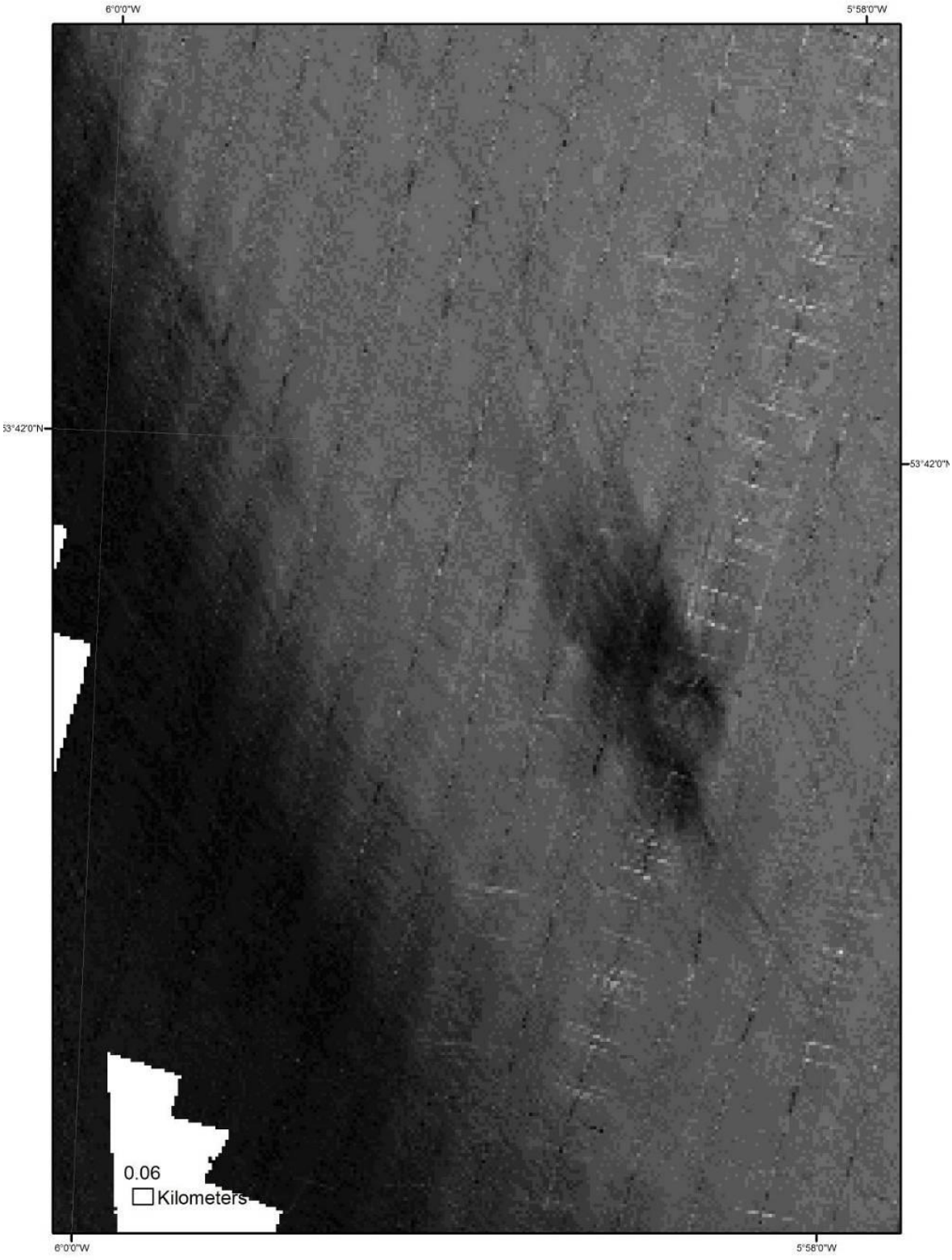

Figure B-14. Multibeam backscatter image showing another pockmark (dark irregular backscatter in the central image) and a zone of high backscatter in the south of the area. The reason for the change in backscatter may be due to an increase in silt content in the pockmark or cementation. The zone of dark backscatter to the southwest may also be due to gas although this is unclear at present.

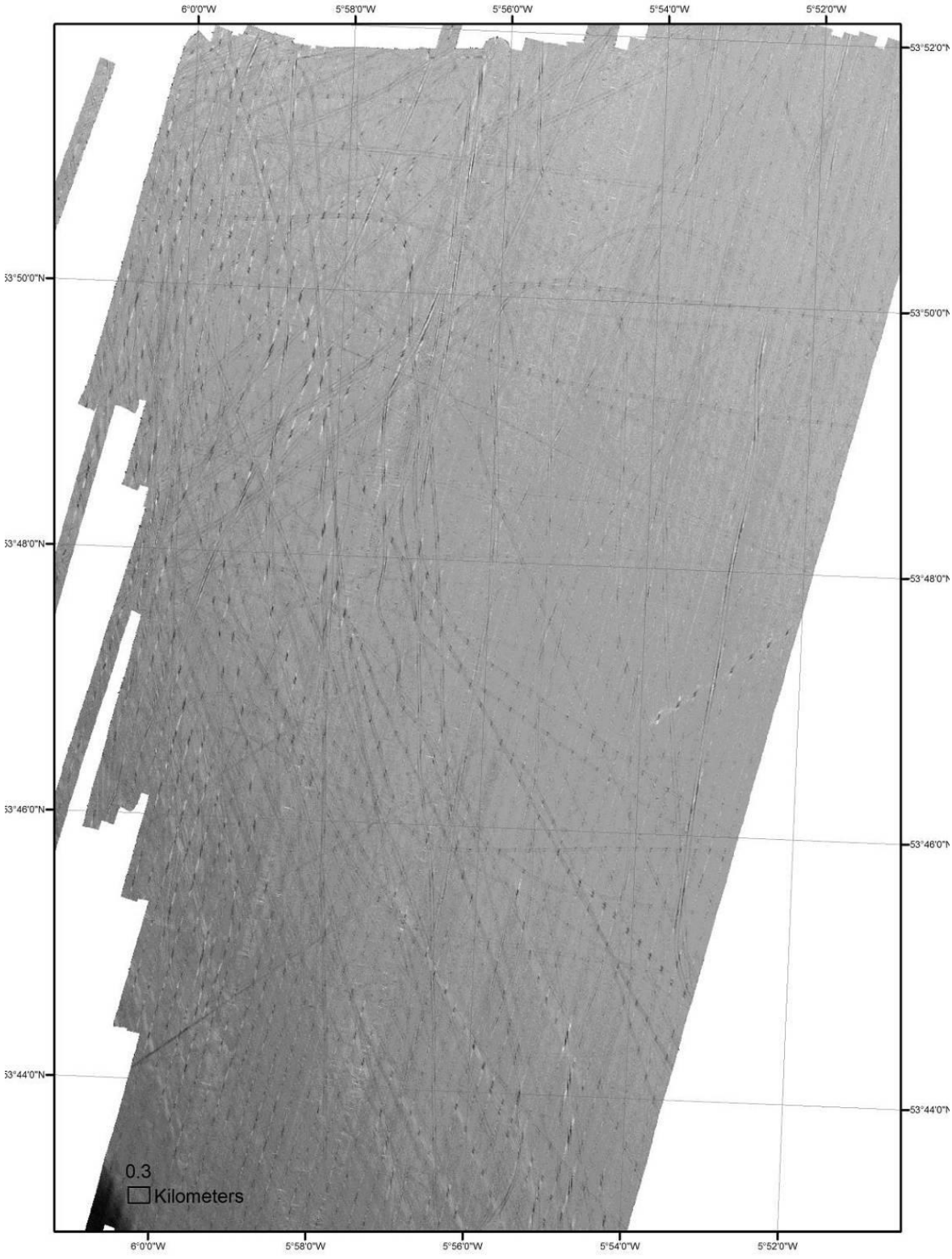

Figure B-15. Multibeam backscatter in most of the Northern Mudbelt showing trawl-marks caused by prawn fishing. Areas of more intense trawling are apparent. It is not known how long a trawl marks remains visible on the seabed in this area.

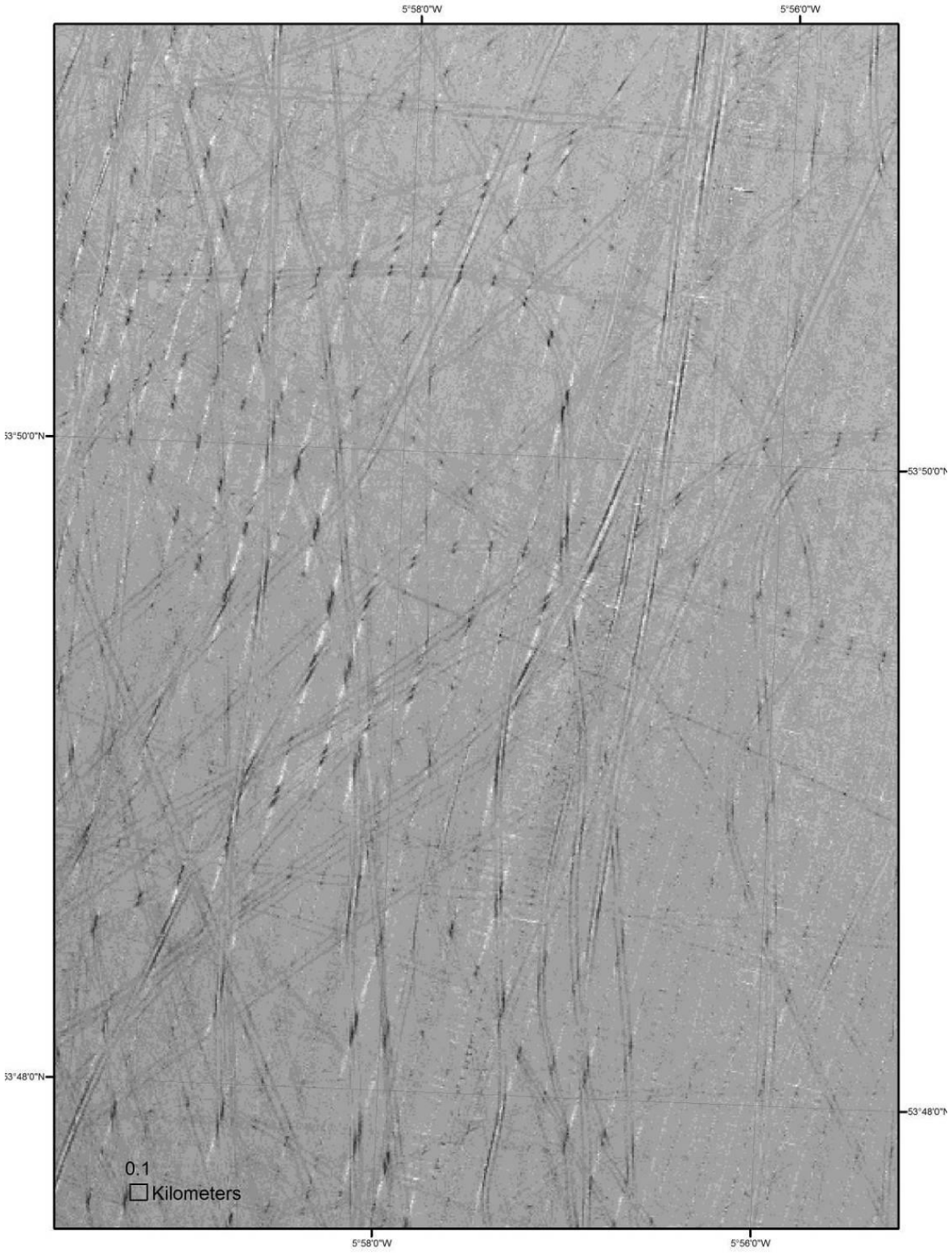

Figure B-16. A close-up of a heavily trawled area.

Figure B-17. A typical sediment sample from the Northern Mudbelt showing soft gloopy mud. Significant silt contents are common.

Figure B-18. A typical shot of the seabed in the Northern Mudbelt showing the irregular microtopography and active bioturbation by worms and larger prawn burrows. Scale of view approximately 50 cm across.

Figure B-19. Another typical shot of the seabed in the Northern Mudbelt showing a Nephrop prawn burrow. Nephrop prawns are the focus of the commercial fishery. Scale of view approximately 50 cm across.

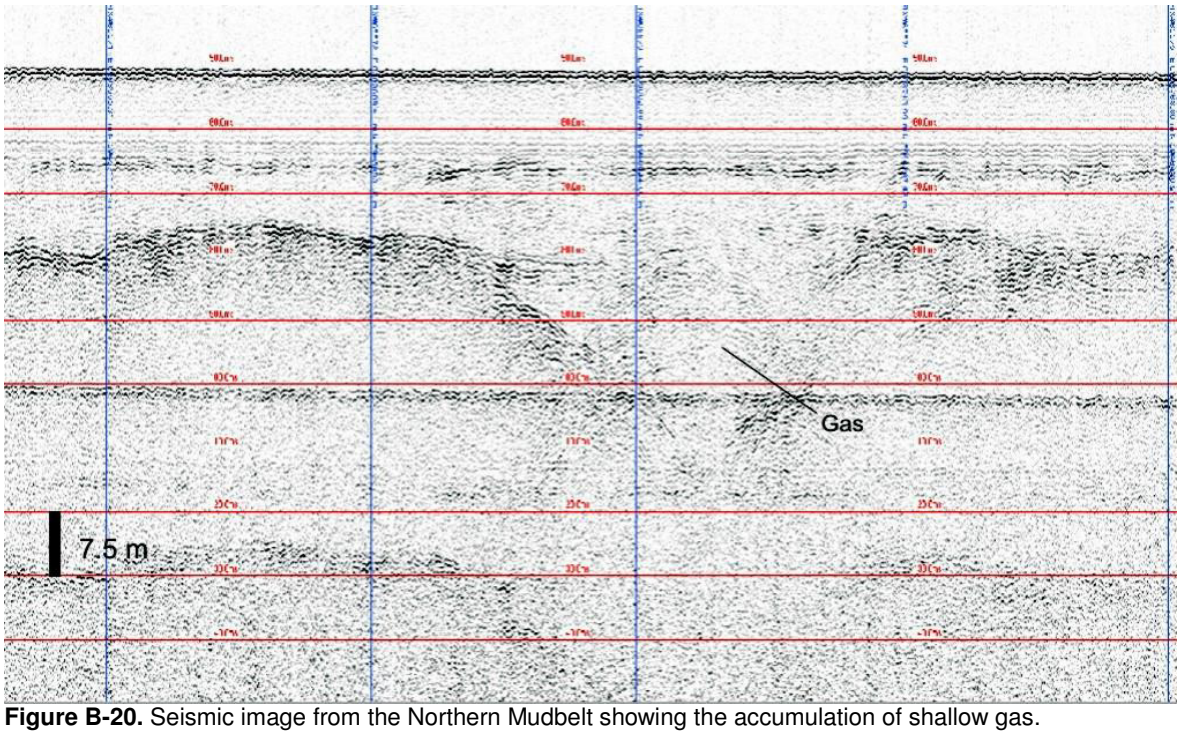

Figure B-20. Seismic image from the Northern Mudbelt showing the accumulation of shallow gas.

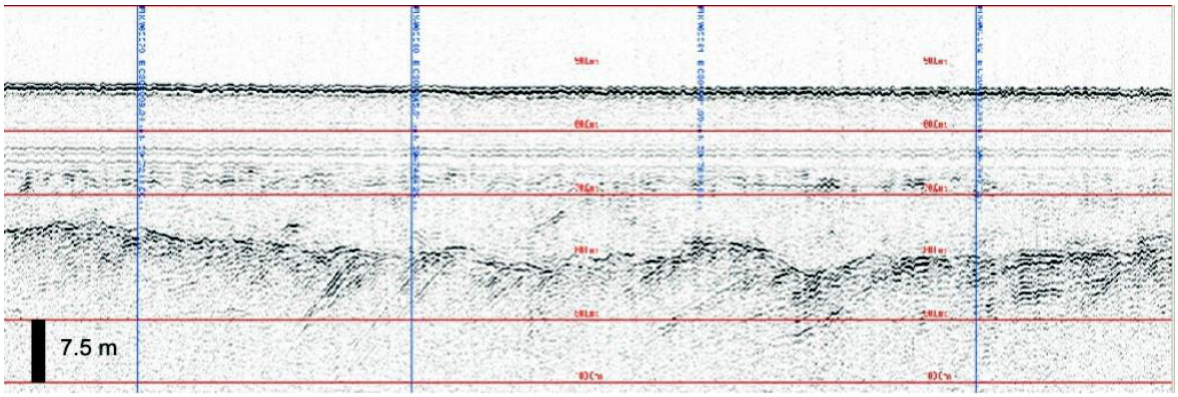

Figure B-21. Seismic image showing bedrock 20 m below the surface. Dipping bedding is clearly discernable.

ROCKABILL

The Rockabill area is a relatively smooth area of seabed gently sloping to the east. Fine grained rippled sand cover the seabed with some seaweed but limited megafauna. Subtle differences in acoustic backscatter probably represent grain-size changes but these were hard to determine by eye from samples or camera imagery. Vibrocores showed the upper few metres consisted of compacted sands overlying till. The till is imaged on the sparker seismics running underlying the area at about 4 m. Data highlights are presented below:

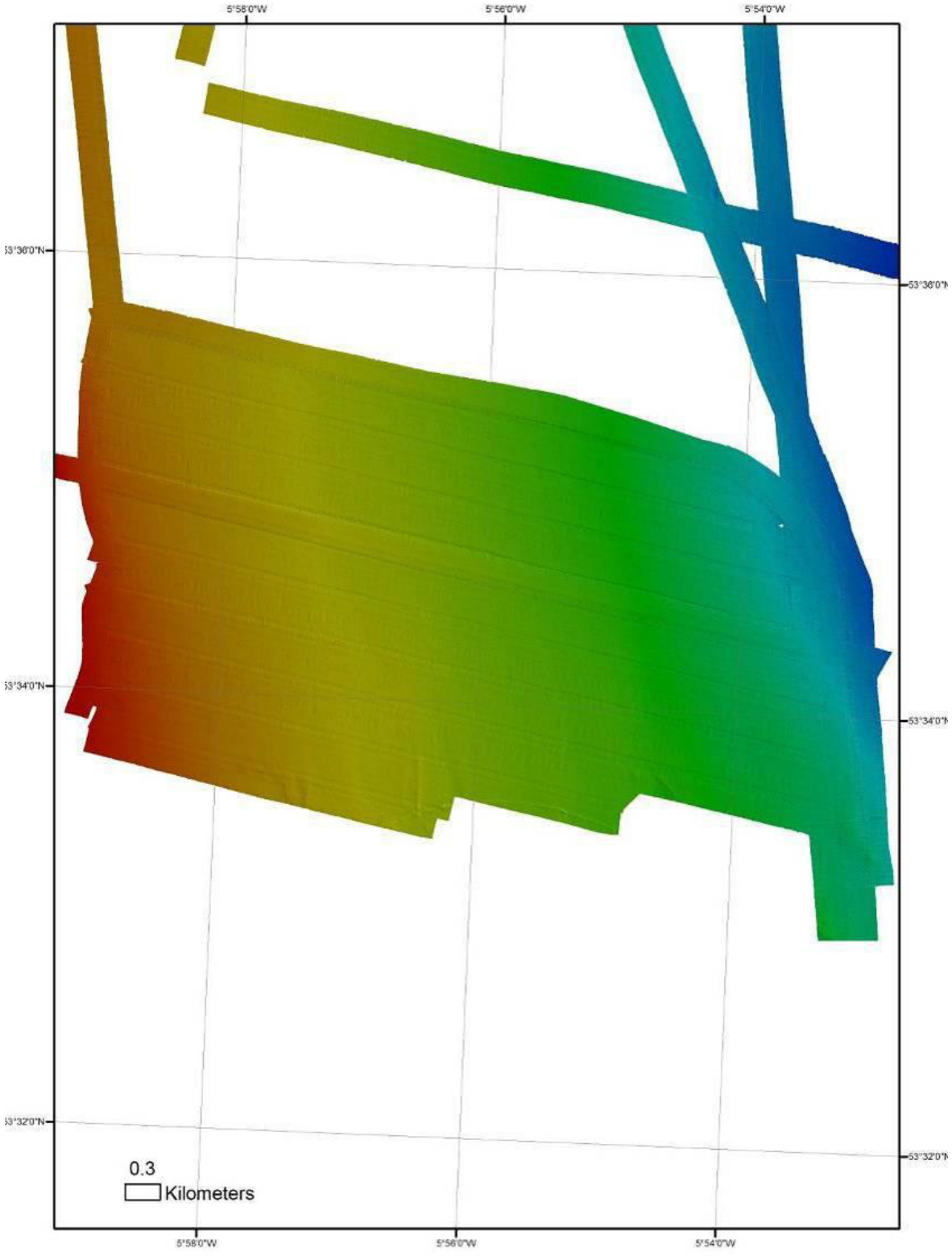

Figure B-22. Multibeam bathymetry image showing the seabed sloping from west to east.

Figure B-23. Typical muddy sand sediment sample from the Rockabill area.

Figure B-24. Typical seabed image showing rippled muddy sands. Scale of view approximately 50 cm across.

Figure B-25. Typical seabed image showing bioturbated muddy sands. Scale of view approximately 50 cm across.

Figure B-26. Red fish and seaweed are the most common biota in the area. Scale of view approximately 50 cm across.

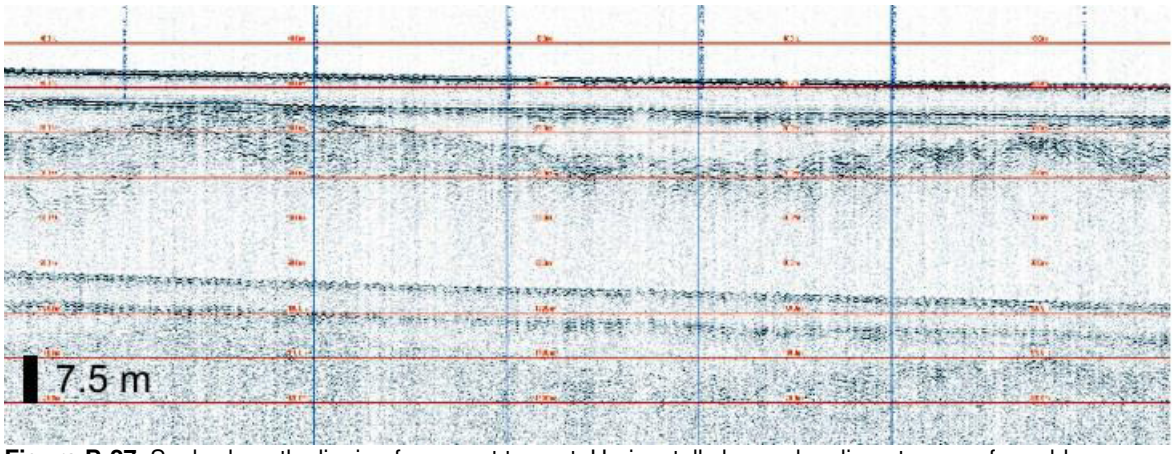

Figure B-27. Seabed gently dipping from west to east. Horizontally layered sediments unconformably overlying deeper successions.

LAMBAY AREA

This is a relatively smooth area of seabed sloping gently to the east with a deep (the Lambay Deep) bordering the eastern margin of the area. The seabed is smooth except for some small bedforms in the south indicating a north-south orientated tidal current flow, and an area of irregular raised topography in the middle. Camera stills from the seabed show that the area is covered by small sand ripples with shell fragments in the troughs. These sediments were sampled by the Shipek although we had difficulties penetrating the sediment to depth. Coring revealed that the upper sequence was composed of compacted sand and in one area this was lithified (explaining our sampling problems). Shear strength in the underlying sediments was expected to be exceptionally high. The lithified sequences were exposed at the surface in the central area and overlain by an onlapping sandy draft. Camera stills showed some megafauna including red fish and sponges.

Data highlights are presented below:

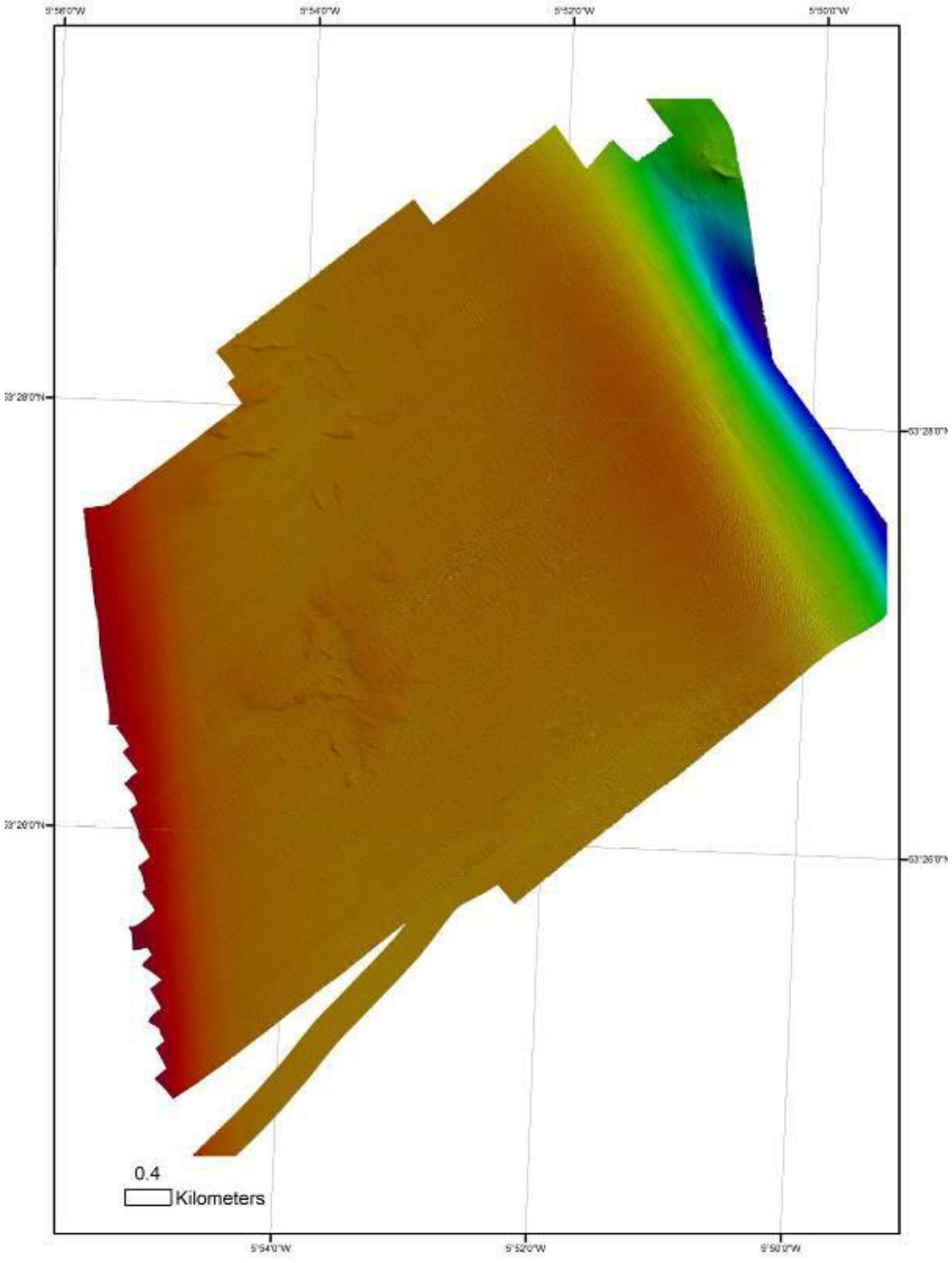

Figure B-28. Bathymetry showing gently sloping seabed and the Lambay deep to the east.

Figure B-29. Bathymetric close-up showing small scale sand waves on the seabed.

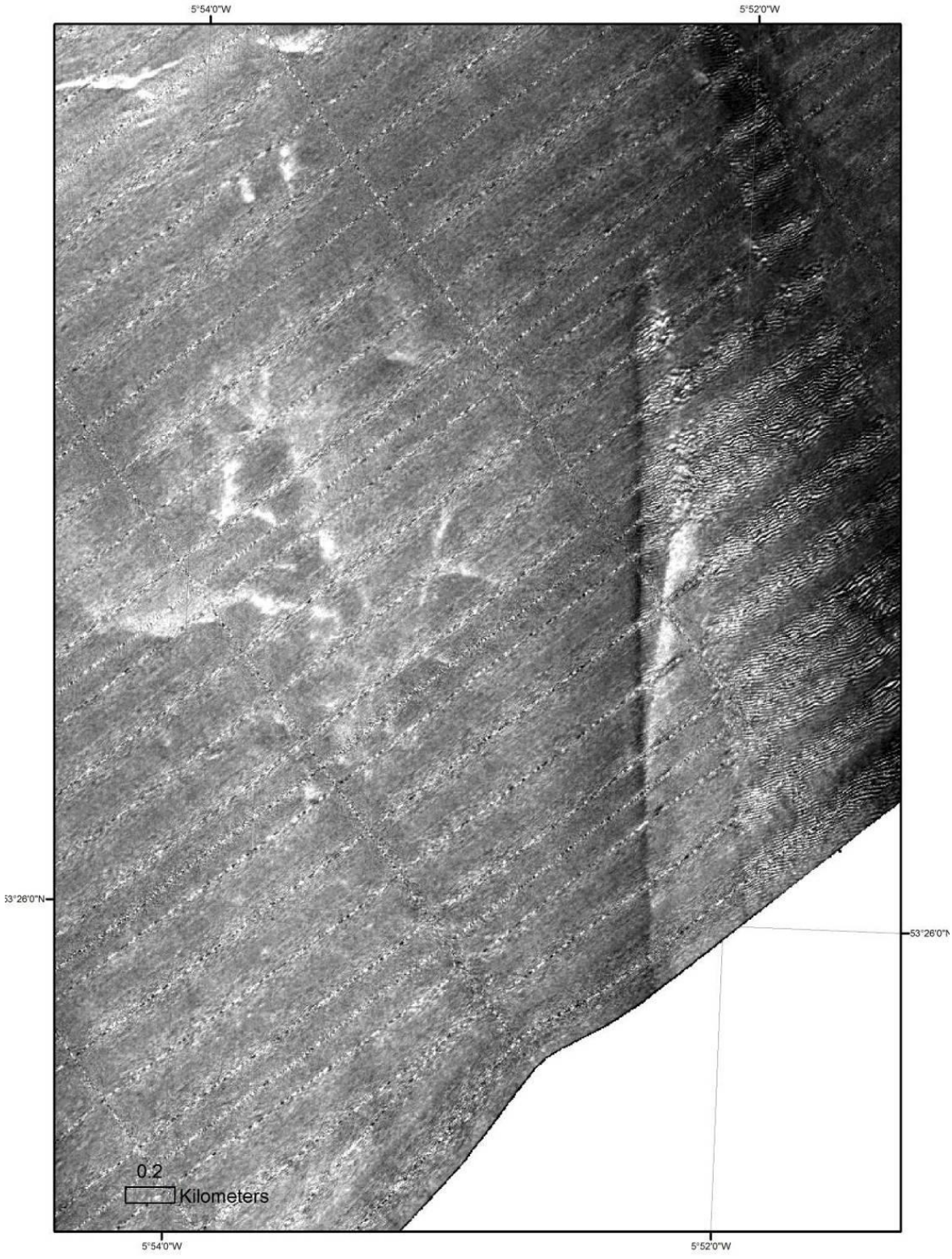

Figure B-30. Multibeam backscatter detail showing strong return (white) indicating lithified sediment outcropping and a linear north-south feature possibly a fault.

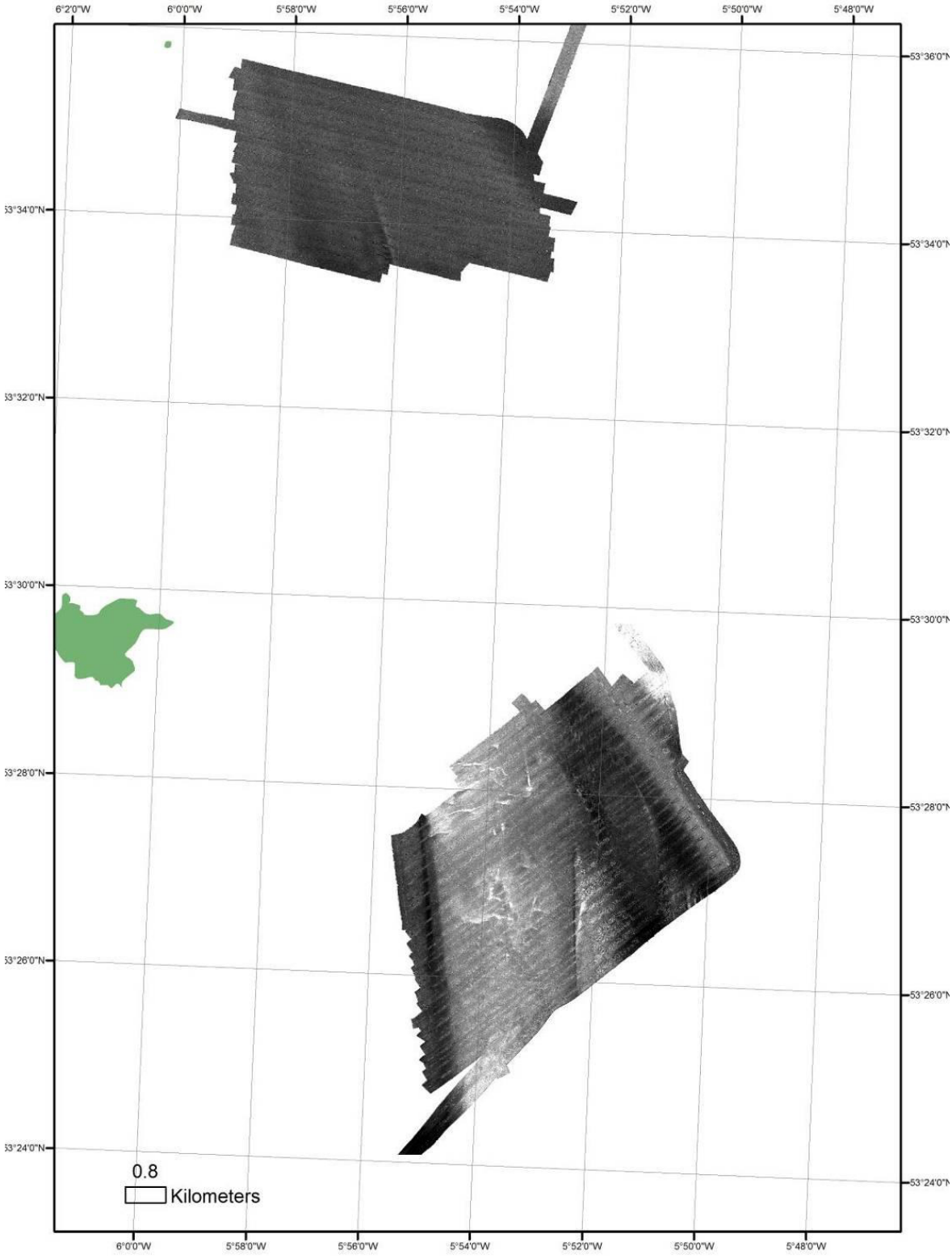

Figure B-31. Contrasting backscatter from the Rockabill (north) and Lambay (south) areas due to difference in grain-size (sandier in Lambay) and exposure of lithified sediments in Lambay.

Figure B-32. Typical sandy sediment sample with shells.

Figure B-33. Typical seabed image showing rippled sands and red fish. Scale of view approximately 50 cm across.

Figure B-34. Seabed showing well developed sand ripples. Scale of view approximately 50 cm across.

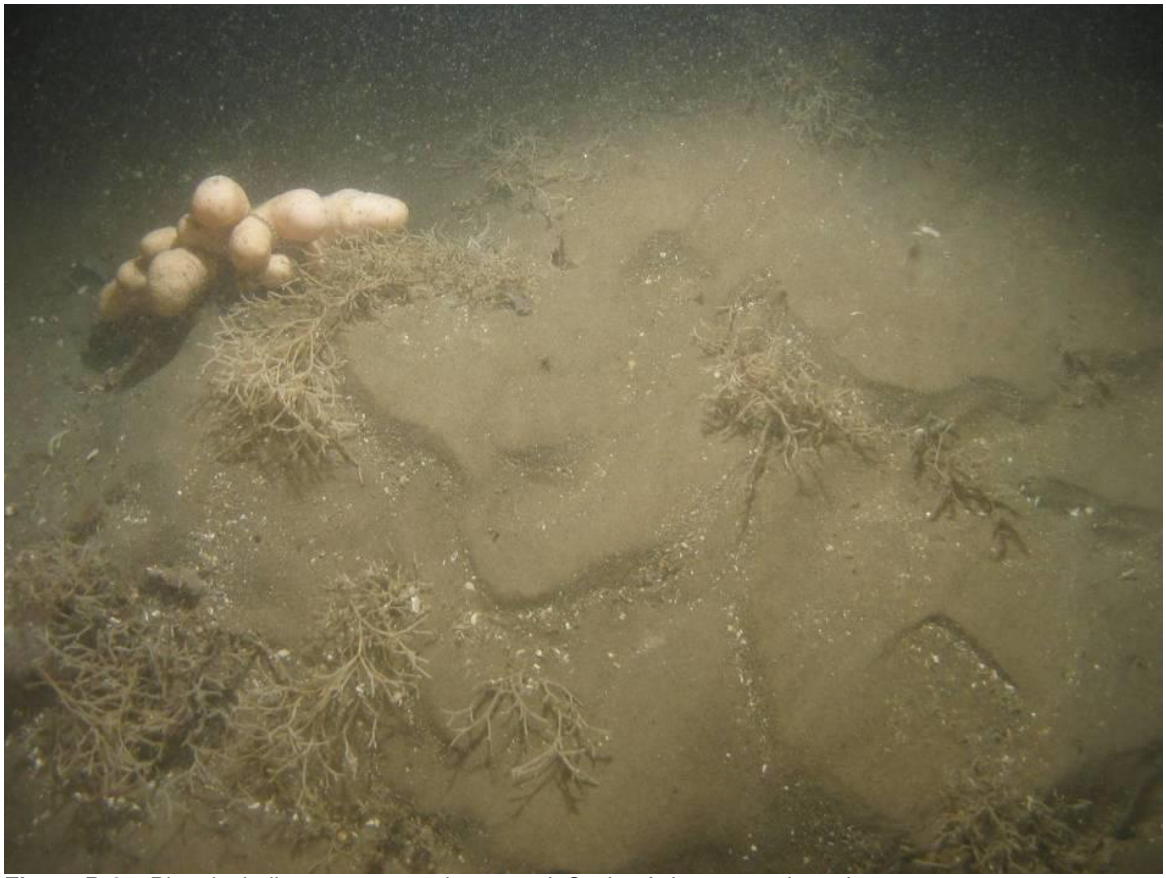

Figure B-35. Biota including sponges and seaweed. Scale of view approximately 50 cm across.

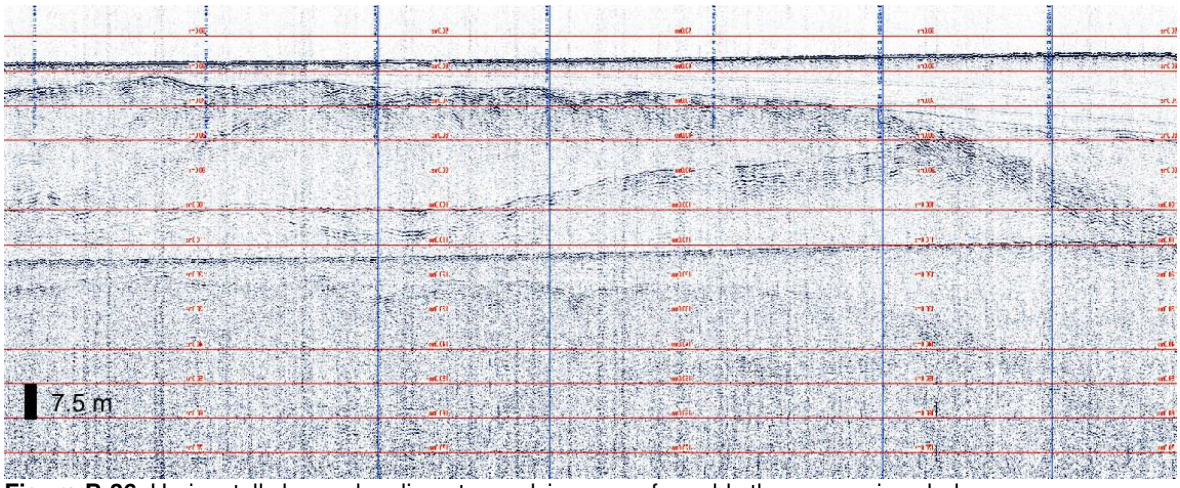

Figure B-36. Horizontally layered sediments overlying unconformably the successions below.

CODLING DEEP

The Codling Deep was the most varied of the areas surveyed in terms of sediment types, topography and biology. It experiences strong current that affects not just the nature of the seabed but also vessel operations. It comprises a long linear irregular depression up to 82 m deep with mobile sand and gravel waves as well as mobile shell hash. These areas have a limited fauna. In contrast, deeper areas are characterised by cobblely ground that was difficult to sample and was covered in a rich diverse fauna. The sub-seabed has complex stratigraphy with numerous erosional surfaces.

Data highlights are presented below:

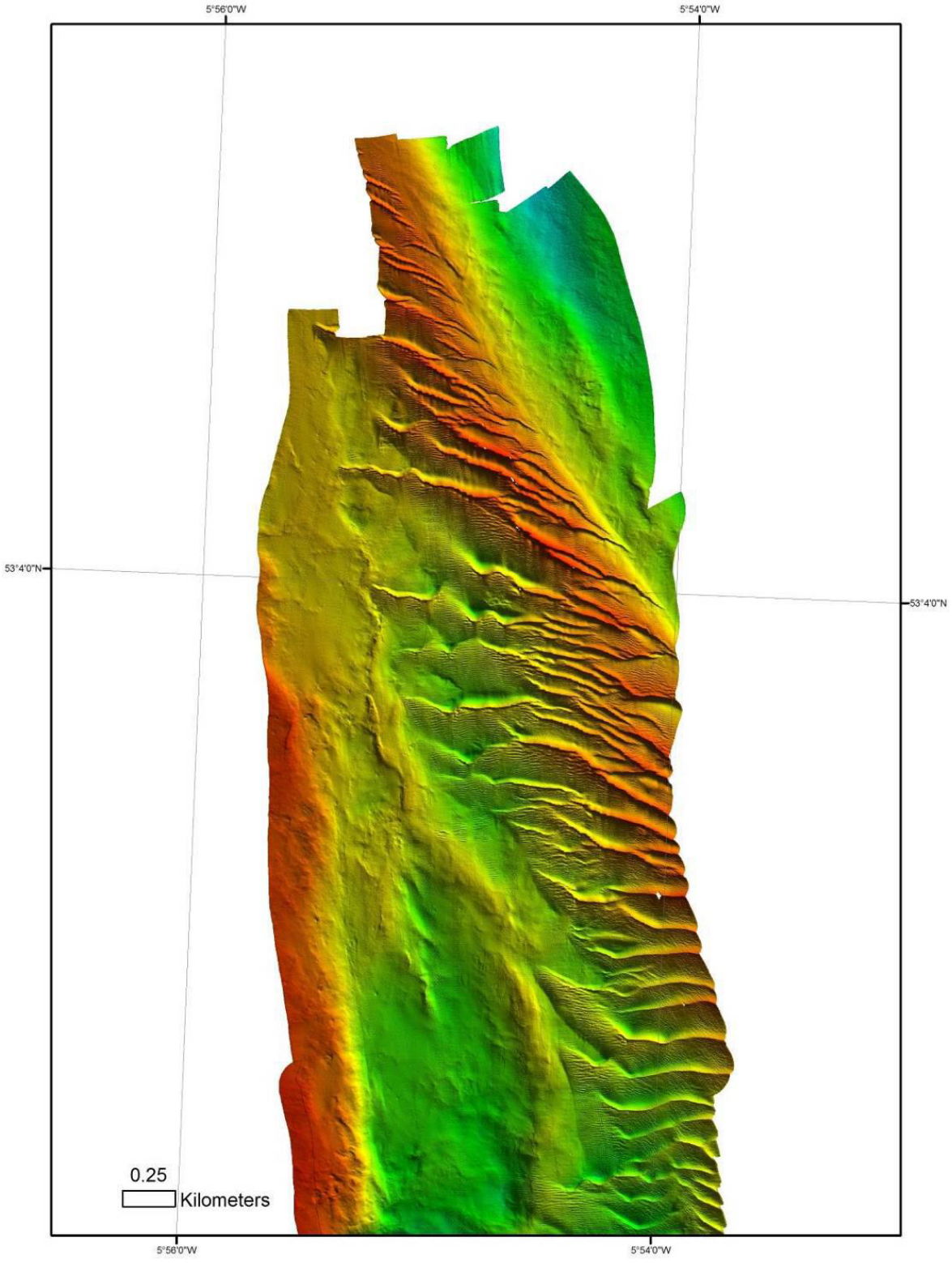

Figure B-37. Bathymetry map showing sediment waves on the edge of the India Bank.

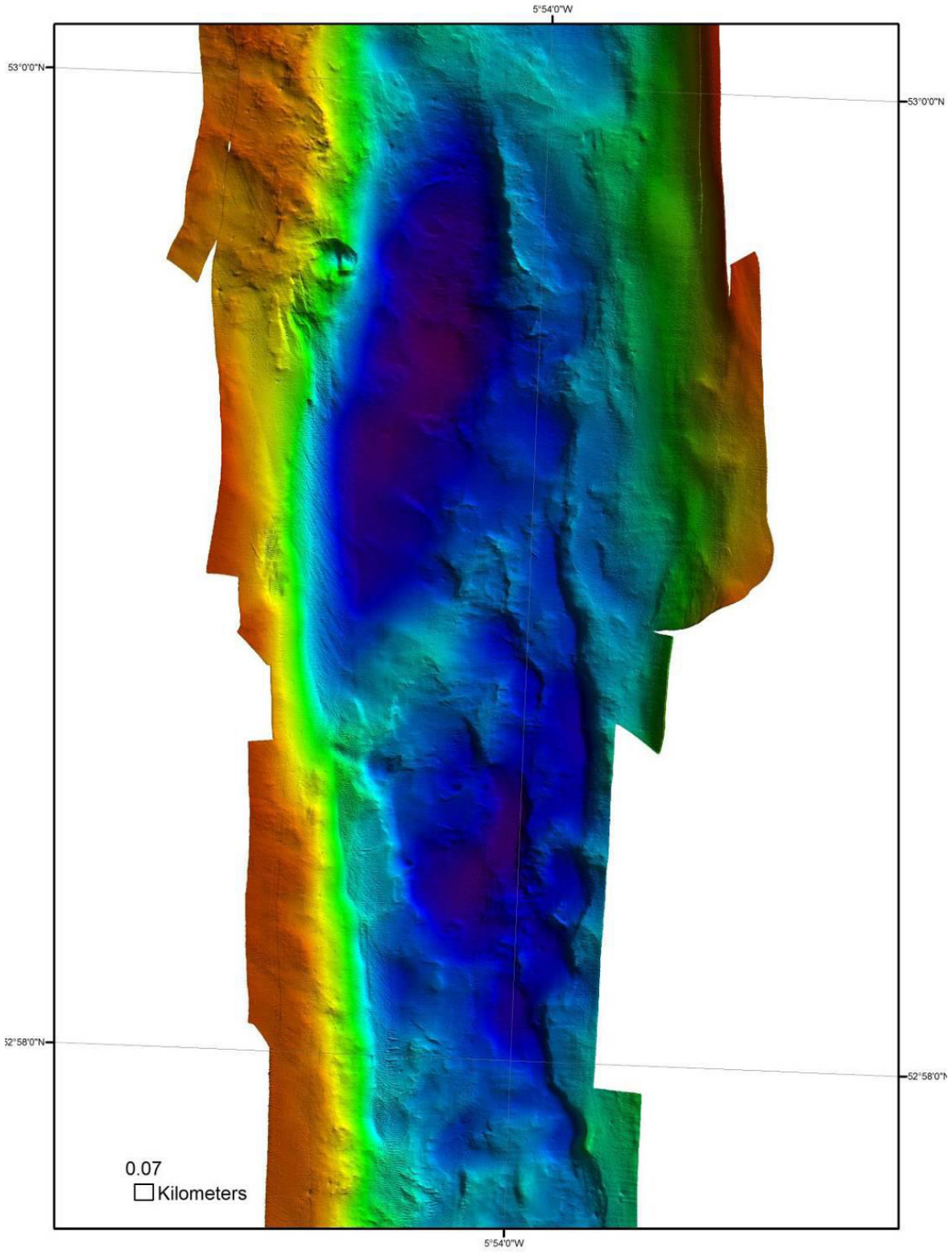

Figure B-38. Bathymetry map showing erosional surfaces in the deep.

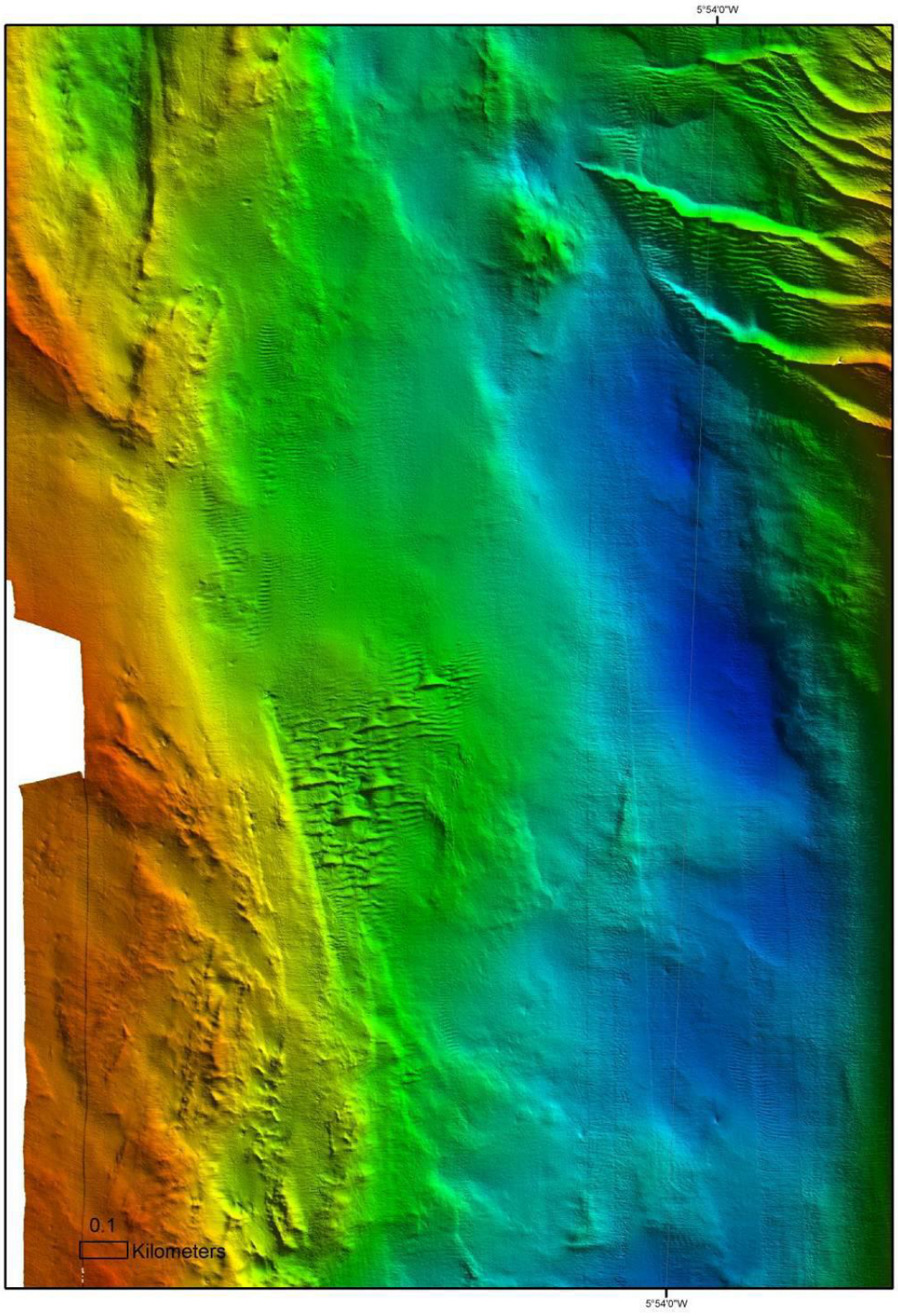

Figure B-39. Bathymetry map showing sediment waves of various sizes.

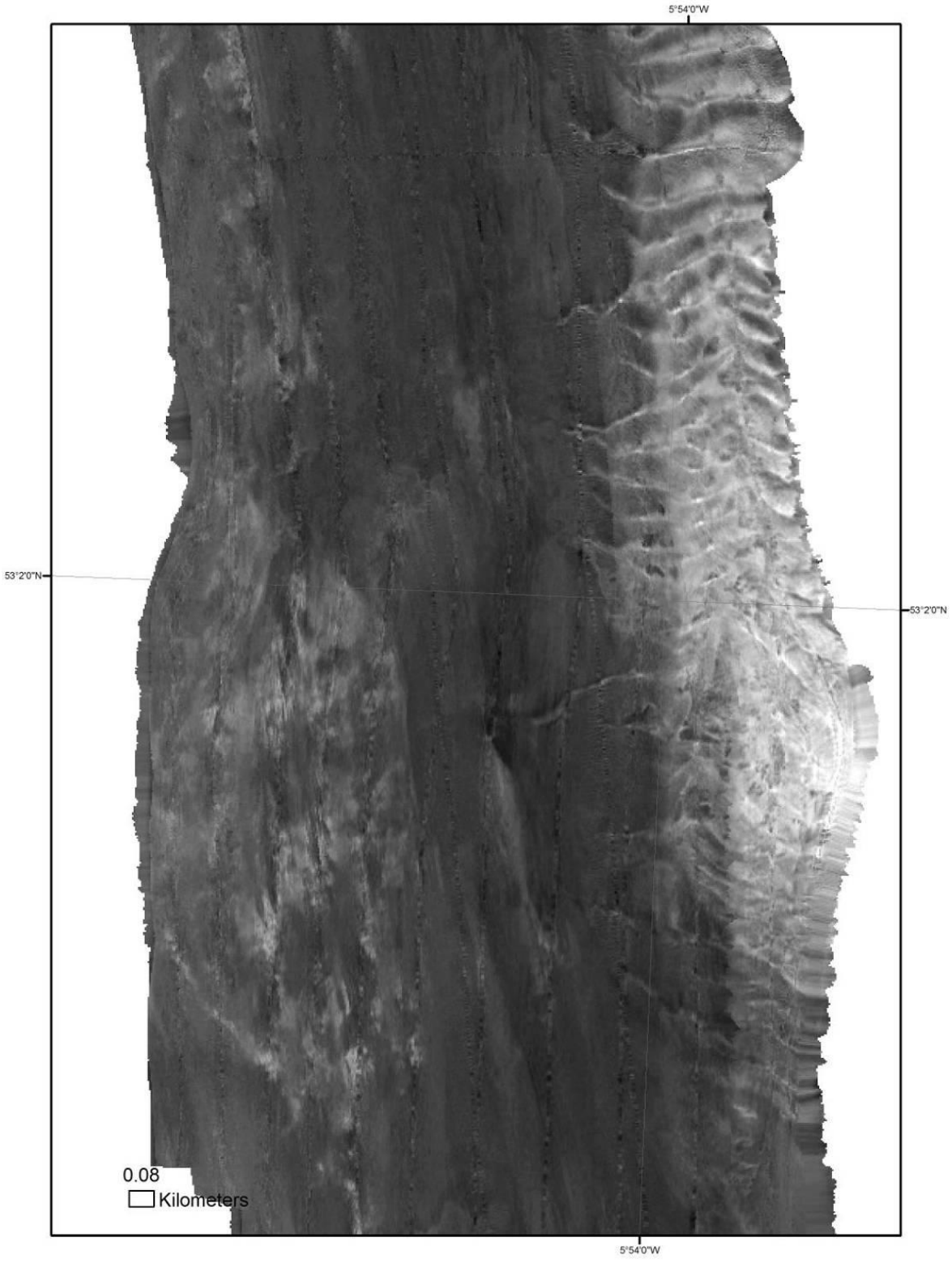

Figure B-40. Backscatter map showing sediment waves (right hand side) and mottled seabed covered with cobbles (left hand side).

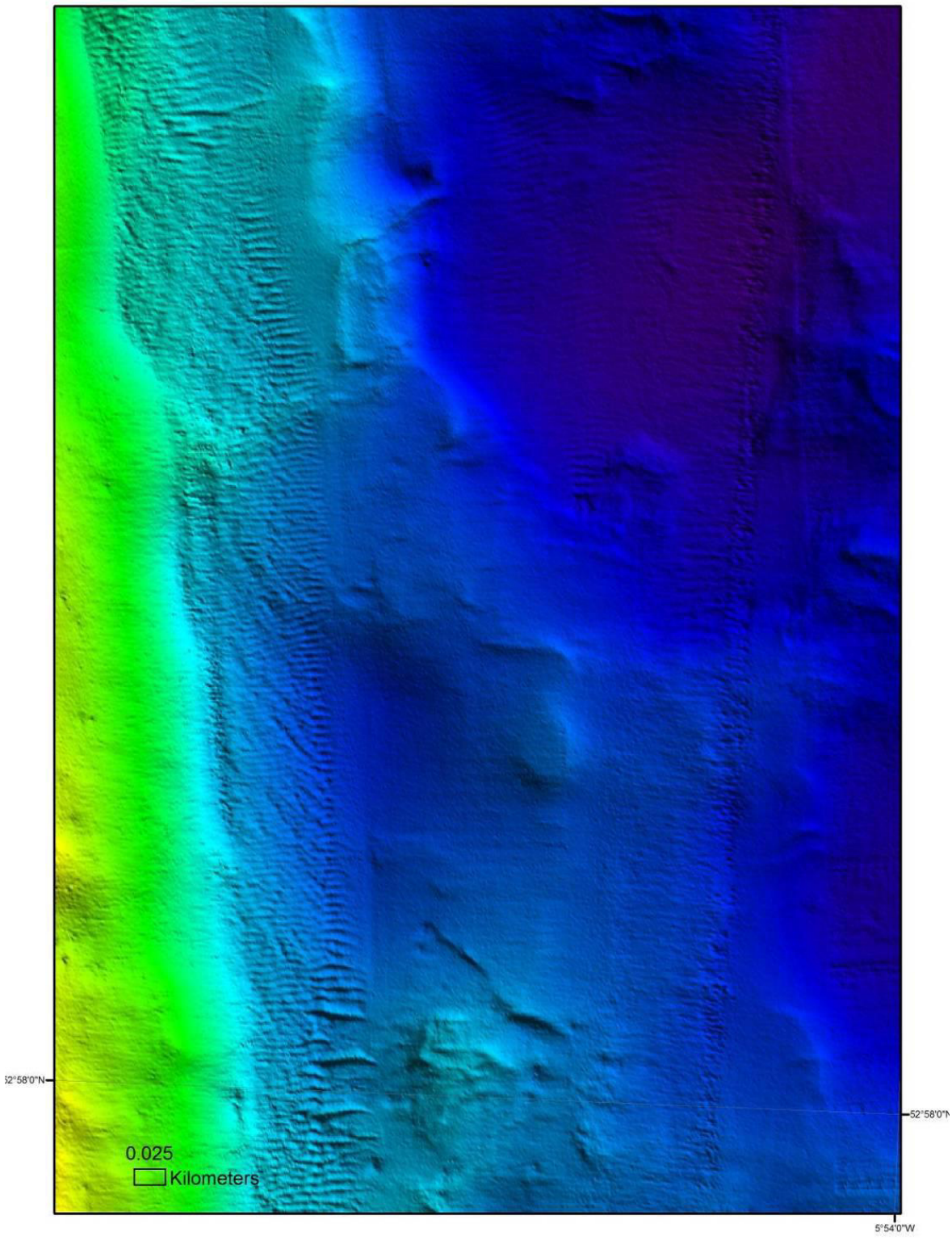

Figure B-41. Bathymetry map showing small scale sediment waves on the edge of the Codling Deep.

Figure B-42. A typical sediment sample of cobbles and shell.

Figure B-43. A typical sediment sample of well sorted coarse sands and shell hash.

Figure B-44. Typical seabed image showing sorted course sands and shell hash from the sediment wave area. Scale of view approximately 50 cm across.

Figure B-45. Typical seabed image showing coarse sands, pebbles, shell and an anemone. Scale of view approximately 50 cm across.

Figure B-46. Typical seabed image showing cobbles covered in barnacles and starfish. Scale of view approximately 50 cm across.

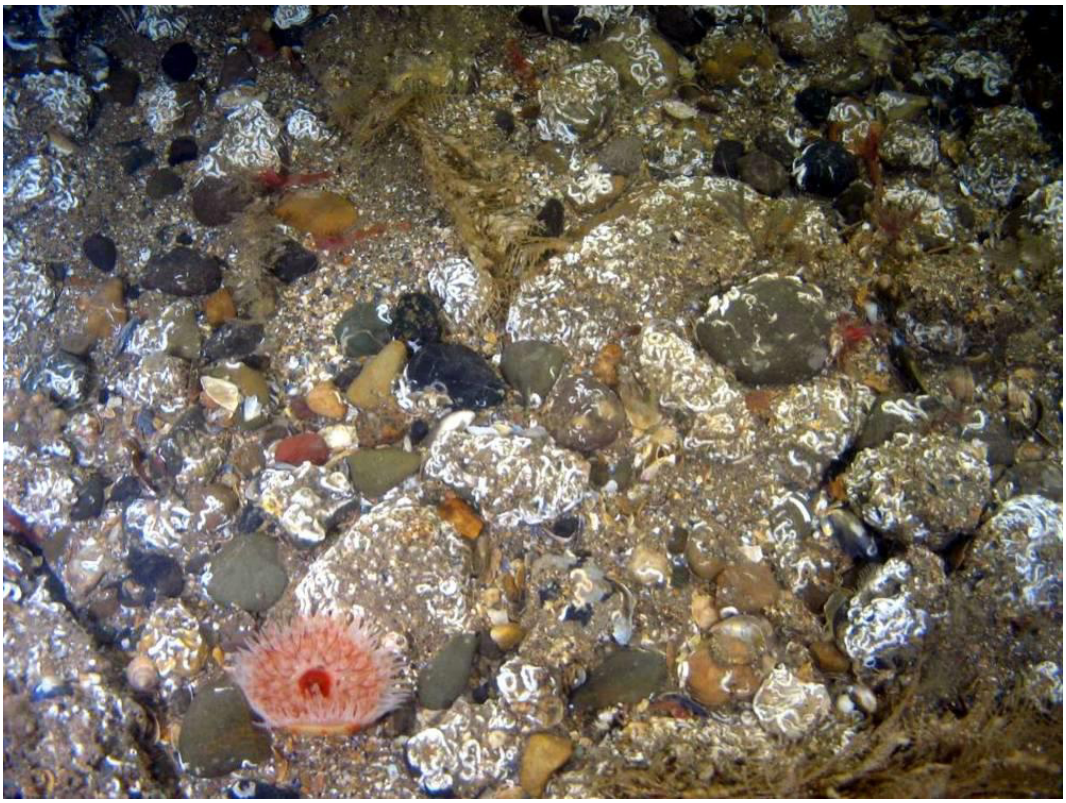

Figure B-47. Typical seabed image showing cobbles covered in serpulid worm tubes and an anemone. Scale of view approximately 50 cm across.

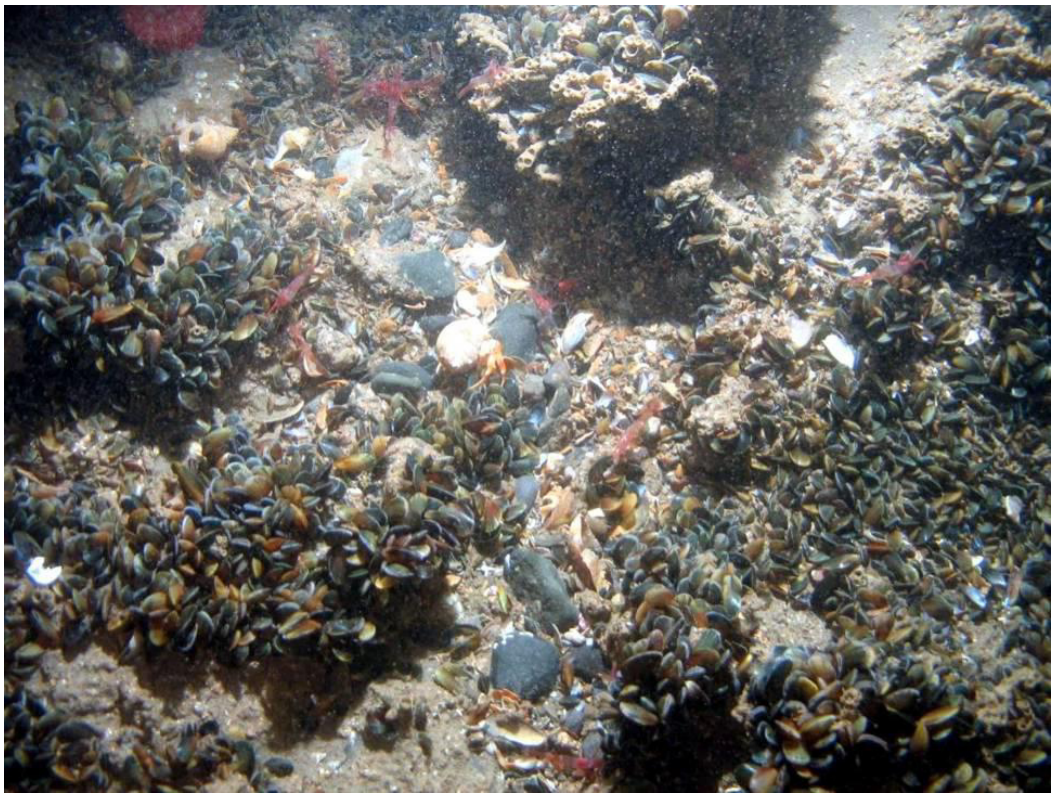

Figure B-48. Typical seabed image showing mussel beds with shrimp, a hermit crab and an anemone. Scale of view approximately 50 cm across.

Figure B-49. Typical seabed image showing seaweed, feather stars, a sponge, shrimp, anemones and agglutinated worm tubes. Scale of view approximately 50 cm across.

Figure B-50. Typical seabed image showing agglutinated worm tubes and seaweed on a sandy seabed. Scale of view approximately 50 cm across.

Figure B-51. Typical seabed image showing rippled sands. Scale of view approximately 50 cm across.

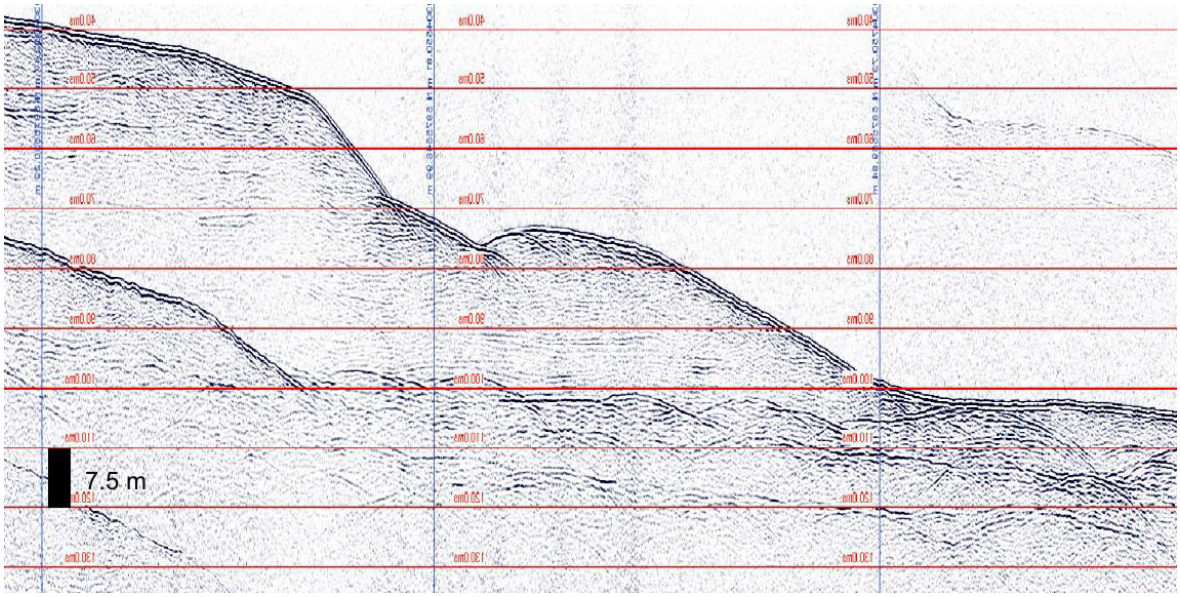

Figure B-52. Seismic profile across the western slope of the Codling Deep.

COVERAGE AND SAMPLE LOCATIONS

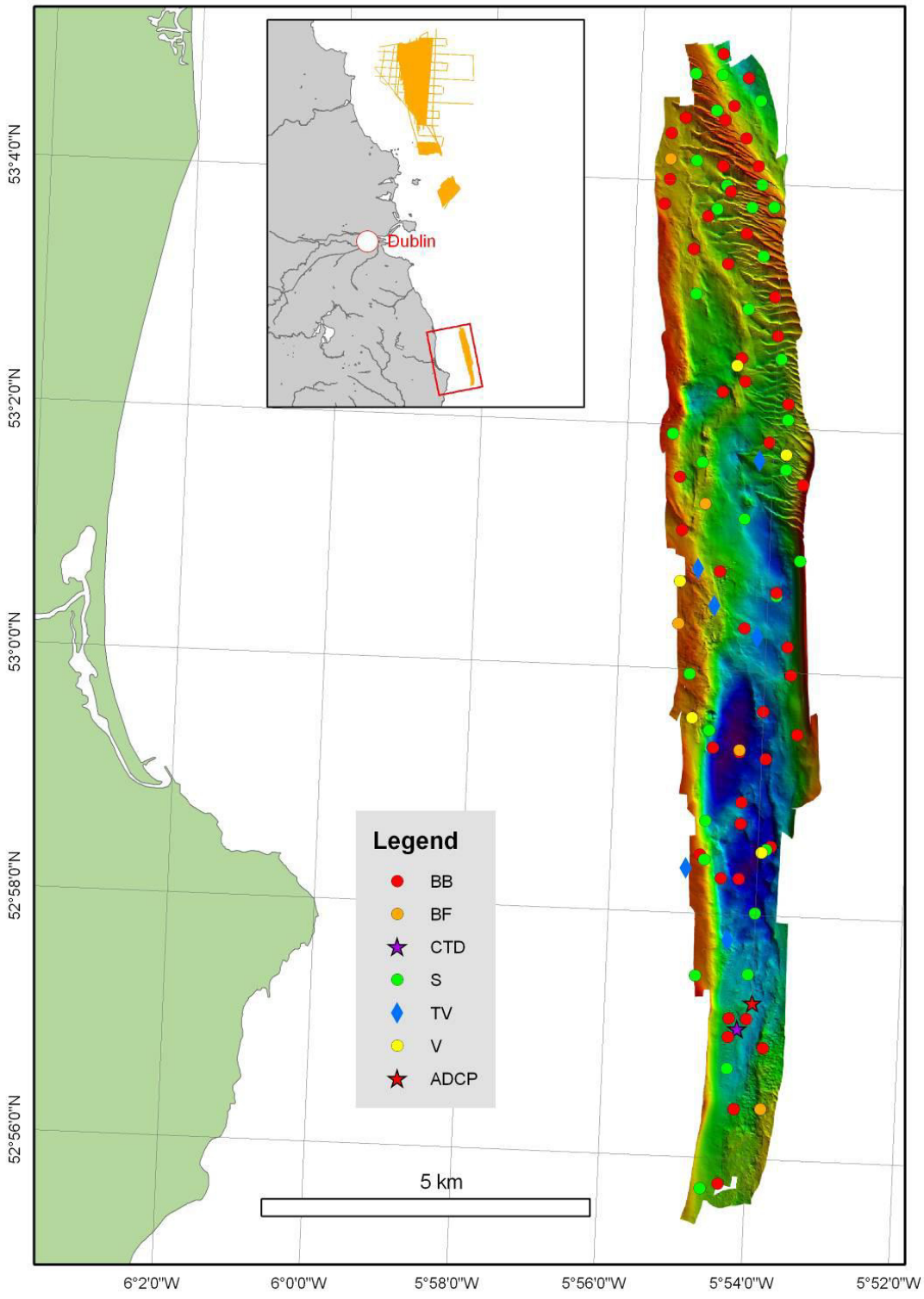

Figure B-53. Codling Deep stations

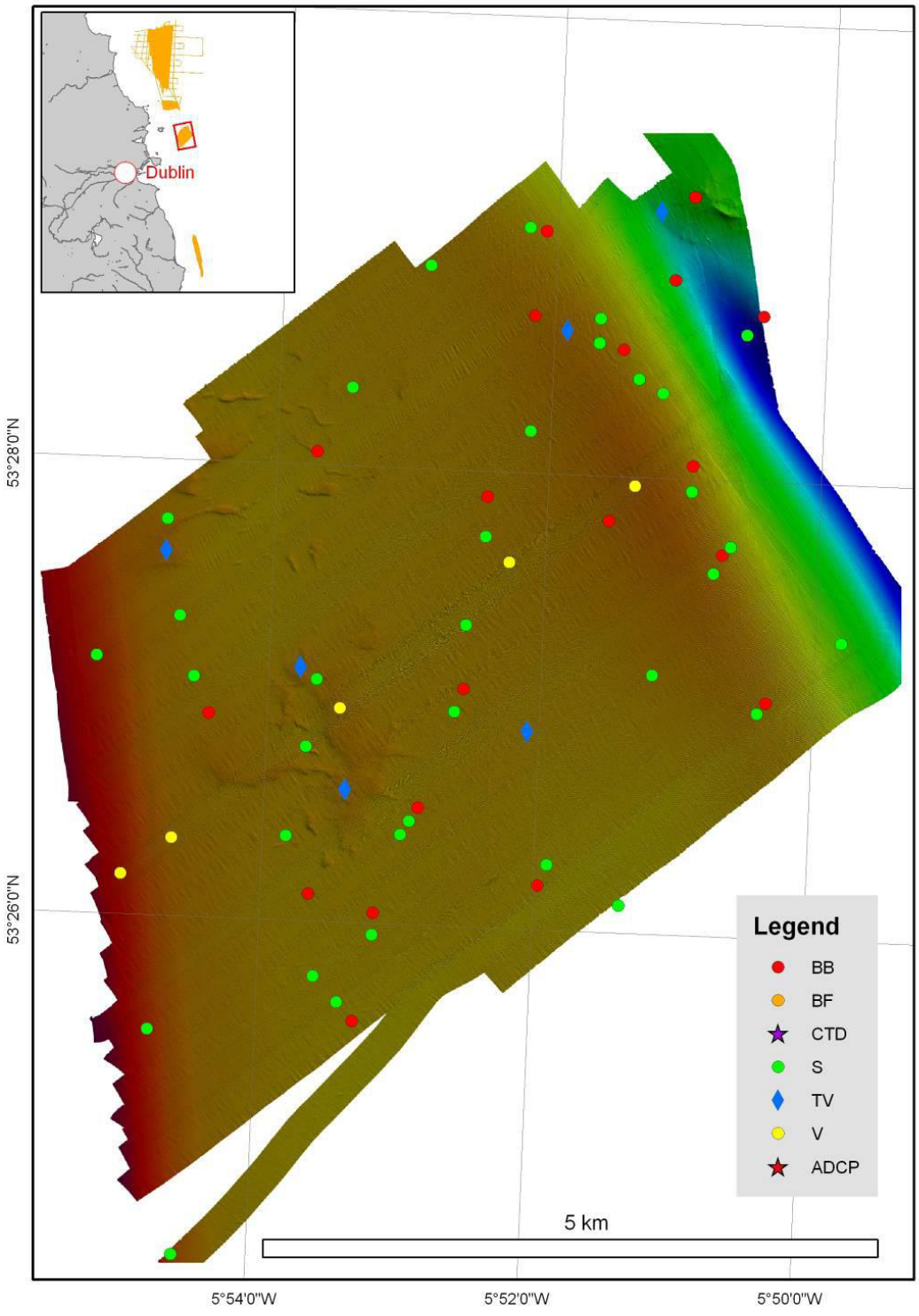

Figure B-54. Lambay area stations

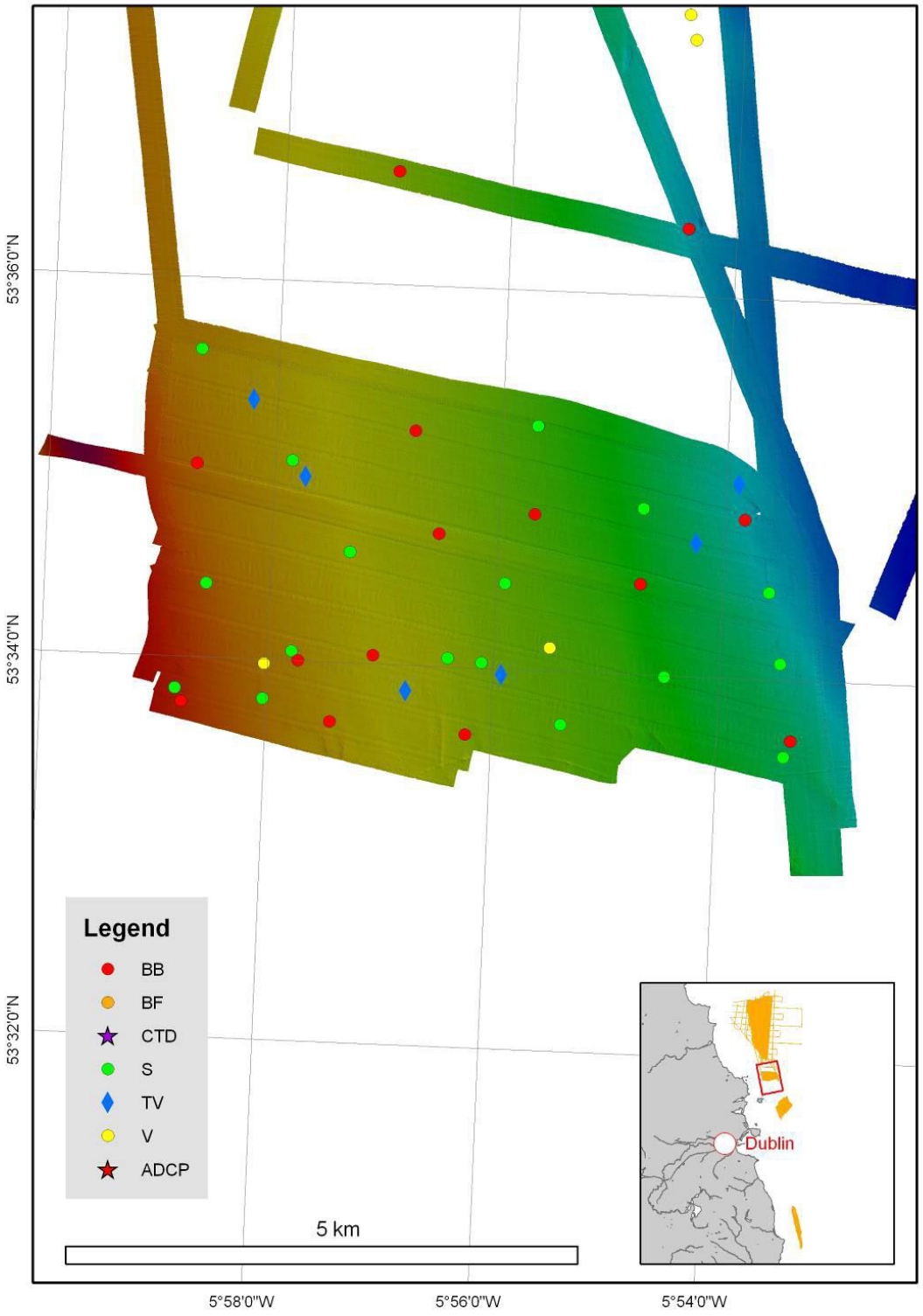

Figure B-55. Rockabill area stations

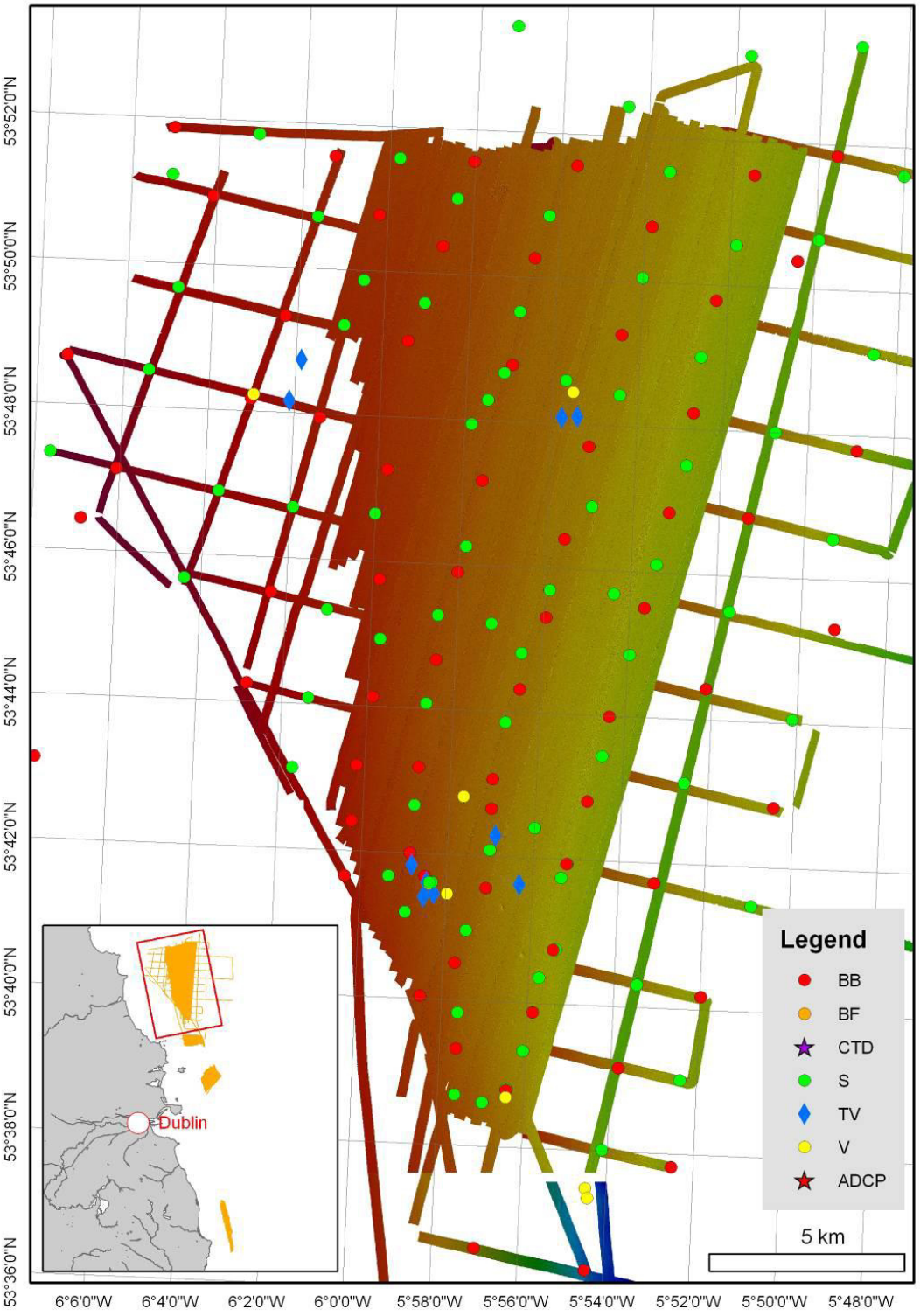

Figure B-56. Northern Mudbelt stations

tation_No	Type	Lat	Long	Date	Time	Depth	Comments
ISMA001	S	53.46231	-5.913	10.10.09	18.25		Fine sand - small sample
ISMA002	S	53.4553	-5.911	10.10.09	18.35		Fine sand - small sample
ISMA003	S	53.45091667	-5.909	10.10.09	1.46		Fine sand - small sample
ISMA004	BB	53.44825	-5.907	10.10.09	18.53		Fine sand - small sample
ISMA005	S	53.43951667	-5.897	10.10.09	19.17		Fine sand - small sample
ISMA006	BB	53.43535	-5.894	10.10.09	19.31		Fine sand - small sample
ISMA007	S	53.42933333	-5.893	10.10.09	19.48		Fine sand - small sample
ISMA008	S	53.42751667	-5.89	10.10.09	19.57		Fine sand - small sample
ISMA009	BB	53.42618333	-5.888	10.10.09	20.03		Fine sand - small sample
ISMA010	S	53.48461667	-5.87	10.10.09	20.38		Fine sand - small sample
ISMA011	BB	53.48438333	-5.868	10.10.09	20.44		Fine sand - small sample
ISMA012	S	53.47816667	-5.861	10.10.09	21.03		Fine sand - small sample
ISMA013	S	53.47638333	-5.861	10.10.09	21.11		Fine sand - small sample
ISMA014	BB	53.47595	-5.858	10.10.09	21.16		Fine sand - small sample
ISMA015	S	53.47383333	-5.856	10.10.09	21.25		Fine sand - small sample
ISMA016	S	53.47286667	-5.853	10.10.09	21.33		Fine sand - small sample
ISMA017	BB	53.46763333	-5.849	10.10.09	21.49		Fine sand - small sample
ISMA018	S	53.46576667	-5.849	10.10.09	21.59		Medium fine sand
ISMA019	S	53.47735	-5.843	10.10.09	22.21		In deep muddy sand
ISMA020	BB	53.47876667	-5.841	10.10.09	22.29		In deep muddy sand
ISMA021	S	53.45983333	-5.846	10.10.09	22.52		Sandy
ISMA022	BB	53.46121667	-5.845	10.10.09	23		Nematode
ISMA023	S	53.46183333	-5.844	10.10.09	23.03		
ISMA024	S	53.4551	-5.83	10.10.09	23.18		
ISMA025	S	53.44973333	-5.84	10.10.09	23.32		Fine Sand

ISMA026	BB	53.45053333	-5.839	10.10.09	23.37		Fine Sand 1 shell
ISMA027	S	53.43536667	-5.856	10.10.09	23.58		Fine sand
ISMA028	BB	53.43661667	-5.866	11.10.09	0.02		Fine sand with shells and biofragments
ISMA029	S	53.43815	-5.865	11.10.09	0.06		Fine Sand
ISMA030	S	53.43253333	-5.886	11.10.09	0.22		Fine Sand
ISMA31	BB	53.43413333	-5.886	11.10.09	0.27		Fine Sand
ISMA032	S	53.43993	-5.883	11.10.09	0.46		Fine Sand
ISMA033	S	53.44093333	-5.882	11.10.09	0.49		Fine Sand Fine Biofragments
ISMA034	BB	53.44193333	-5.881	11.10.09	0.53		Fine Sand Fine Biofragments
ISMA035	S	53.44903333	-5.877	11.10.09	1.18		Fine Sand Fine Biofragments
ISMA036	BB	53.450745	-5.876	11.10.09	1.25		Fine Sand Fine Biofragments
ISMA037	S	53.45541667	-5.876	11.10.09	1.38		Fine Sand Fine Biofragments
ISMA038	S	53.46191667	-5.874	11.10.09	1.56		Fine Sand Fine Biofragments
ISMA039	BB	53.46483333	-5.874	11.10.09	2.04		Fine Sand Fine Biofragments
ISMA040	S	53.46975	-5.869	11.10.09	2.16		Fine Sand
ISMA041	BB	53.47818333	-5.869	11.10.09	2.39		Fine Sand
ISMA042	S	53.48156667	-5.882	11.10.09	2.52		Fine Sand
ISMA043	S	53.55994667	-5.89	11.10.09	3.33		Clayey and Fine Sand
ISMA044	BB	53.56138333	-5.889	11.10.09	3.41		
ISMA045	S	53.56809167	-5.891	11.10.09	3.57		
ISMA046	S	53.57432833	-5.893	11.10.09	4.1		Fine Sand
ISMA047	BB	53.58064833	-5.897	11.10.09	4.21		Fine Sand
ISMA048	BB	53.56085	-5.937	11.10.09	4.44		Fine Sand
ISMA049	S	53.56717	-5.935	11.10.09	4.52		Fine Sand
ISMA050	S	53.57421667	-5.932	11.10.09	5.02		Fine Sand
ISMA051	BB	53.5804	-5.928	11.10.09	5.27		Fine Sand
ISMA052	S	53.58813667	-5.928	11.10.09	5.4		Fine Sand

ISMA053	BB	53.587285	-5.946	11.10.09	5.57		Fine Sand
ISMA054	S	53.57643333	-5.955	11.10.09	6.1		Fine Sand
ISMA055	BB	53.56746667	-5.951	11.10.09	6.23		Fine sand, bio fragents, seastar and sea urchin
ISMA056	S	53.56328333	-5.967	11.10.09	6.41		
ISMA057	S	53.57319	-5.976	11.10.09	7.23		Coarse silt - fine sand and fines in the surface layer
ISMA058	BB	53.58366667	-5.978	11.10.09	7.38		Fine silty sand
ISMA059	S	53.59371333	-5.978	11.10.09	7.52		Fine silty sand
ISMA060	S	53.472425	-5.891	11.10.09	9		Fine sand
ISMA061	BB	53.46764333	-5.895	11.10.09	9.11		Fine sand
ISMA062	S	53.451039	-5.894	11.10.09	9.28		Fine sand
ISMA063	V	53.43905333	-5.911	11.10.09	9.54		Muddy with gravel mainly glacial
ISMA064	V	53.4363	-5.917	11.10.09	10.25		Sand
ISMA065	S	53.64683333	-5.94	11.10.09	12.04		Mud, fine silt and sand
ISMA066	BB	53.646585	-5.94	11.10.09	12.08		Mud- filled bucket
ISMA067	S	53.655765	-5.934	11.10.09	12.21		Silty Clay
ISMA068	S	53.655765	-5.934	11.10.09	12.24		
ISMA069	S	53.6648	-5.931	11.10.09	12.35		Silty Clay - Soft to stiff
ISMA070	BB	53.66463833	-5.931	11.10.09	12.38		Silty Clay - Soft to stiff
ISMA071	S	53.672645	-5.929	11.10.09	12.49		Muddy
ISMA072	S	53.6793	-5.923	11.10.09	13.01		Clayey Mud
ISMA073	BB	53.67920667	-5.924	11.10.09	13.04		Mud
ISMA074	S	53.69587333	-5.922	11.10.09	13.18		Mud
ISMA075	S	53.69912667	-5.92	11.10.09	13.31		Mud
ISMA076	BB	53.699075	-5.92	11.10.09	13.34		Mud
ISMA077	S	53.70704833	-5.933	11.10.09	13.47		Silt and Mud
ISMA078	BB	53.71366	-5.913	11.10.09	13.59		
ISMA079	S	53.71785667	-5.95	11.10.09	14.26		Silt and Clay

ISMA080	BB	53.71785667	-5.95	11.10.09	14.26		Sample taken from same grab as ISMA079
ISMA081	S	53.56753167	-5.963	11.10.09	15.44		
ISMA082	BB	53.56672333	-5.962	11.10.09	15.48		
ISMA083	S	53.56390167	-5.98	11.10.09	16.03		
ISMA084	BB	53.56275667	-5.979	11.10.09	16.07		
ISMA085	S	53.60998333	-5.95	11.10.09	17.15		Mainly silts
ISMA086	BB	53.60998333	-5.95	11.10.09	17.15		Mainly silts
ISMA087	S	53.65568333	-5.96	11.10.09	17.52		
ISMA088	BB	53.65568333	-5.96	11.10.09	17.52		
ISMA089	S	53.66393333	-5.96	11.10.09	18.17		
ISMA090	S	53.67533333	-5.962	11.10.09	18.35		
ISMA091	BB	53.67533333	-5.962	11.10.09	18.35		
ISMA092	S	53.68293333	-5.958	11.10.09	18.48		
ISMA093	S	53.69279333	-5.951	11.10.09	19.04		
ISMA094	BB	53.69279333	-5.951	11.10.09	19.04		
ISMA095	S	53.70156667	-5.95	11.10.09	19.23		
ISMA096	S	53.71107167	-5.95	11.10.09	19.38		
ISMA097	BB	53.71107167	-5.95	11.10.09	19.38		
ISMA098	S	53.73104833	-5.946	11.10.09	19.58		
ISMA099	S	53.73878333	-5.941	11.10.09	20.13		
ISMA100	BB	53.73878333	-5.941	11.10.09	20.13		
ISMA101	S	53.74713333	-5.941	11.10.09	20.35		Mud
ISMA102	S	53.75548333	-5.932	11.10.09	20.42		
ISMA103	BB	53.75548333	-5.932	11.10.09	20.42		
ISMA104	S	53.76185167	-5.931	11.10.09	21.02		
ISMA105	S	53.77365	-5.926	11.10.09	21.21		
ISMA106	BB	53.77365	-5.926	11.10.09	21.21		

ISMA107	S	53.78141667	-5.916	11.10.09	21.37		
ISMA108	S	53.79518333	-5.918	11.10.09	21.57		
ISMA109	BB	53.79518333	-5.918	11.10.09	21.57		
ISMA110	S	53.80726667	-5.907	11.10.09	22.39		
ISMA111	S	53.82110167	-5.907	11.10.09	22.39		
ISMA112	BB	53.82110167	-5.907	11.10.09	22.39		
ISMA113	S	53.83443333	-5.9	11.10.09	22.59		
ISMA114	S	53.84622667	-5.897	11.10.09	23.18		
ISMA115	BB	53.84622667	-5.897	11.10.09	23.18		
ISMA116	S	53.85898	-5.891	11.10.09	23.38		Mud
ISMA117	S	53.85953333	-5.927	12.10.09	0.04		
ISMA118	BB	53.85953333	-5.927	12.10.09	0.04		
ISMA119	S	53.84781667	-5.937	12.10.09	0.22		
ISMA120	S	53.83794333	-5.942	12.10.09	0.39		
ISMA121	BB	53.83794333	-5.942	12.10.09	0.39		
ISMA122	S	53.82553167	-5.947	12.10.09	0.56		
ISMA123	S	53.81325	-5.949	12.10.09	1.13		
ISMA124	BB	53.81325	-5.949	12.10.09	1.13		
ISMA125	S	53.81132833	-5.952	12.10.09	1.31		
ISMA126	S	53.78641667	-5.959	12.10.09	1.52		
ISMA127	BB	53.78641667	-5.959	12.10.09	1.52		
ISMA128	S	53.77108333	-5.964	12.10.09	2.08		
ISMA129	S	53.765145	-5.967	12.10.09	2.26		
ISMA130	BB	53.765145	-5.967	12.10.09	2.26		
ISMA131	S	53.75503667	-5.974	12.10.09	2.42		
ISMA132	S	53.74475	-5.974	12.10.09	2.58		
ISMA133	BB	53.74475	-5.974	12.10.09	2.58		

ISMA134	S	53.73464	-5.977	12.10.09	3.14		
ISMA135	S	53.71999833	-5.979	12.10.09	3.36		
ISMA136	BB	53.71999833	-5.979	12.10.09	3.36		
ISMA137	S	53.711205	-5.98	12.10.09	3.51		
ISMA138	S	53.7002	-5.981	12.10.09	4.08		
ISMA139	BB	53.7002	-5.981	12.10.09	4.08		
ISMA140	S	53.68660667	-5.982	12.10.09	4.27		
ISMA141	S	53.72417	-5.908	12.10.09	5.12		
ISMA142	S	53.733325	-5.906	12.10.09	5.26		
ISMA143	BB	53.733325	-5.906	12.10.09	5.26		
ISMA144	S	53.74763333	-5.899	12.10.09	5.45		
ISMA145	S	53.75853333	-5.894	12.10.09	5.57		
ISMA146	BB	53.75853333	-5.894	12.10.09	5.57		
ISMA147	S	53.76869333	-5.89	12.10.09	6.1		
ISMA148	S	53.78071667	-5.886	12.10.09	6.25		
ISMA149	BB	53.78071667	-5.886	12.10.09	6.25		
ISMA150	S	53.79167667	-5.88	12.10.09	6.36		
ISMA151	S	53.80378333	-5.878	12.10.09	7.1		
ISMA152	BB	53.80378333	-5.878	12.10.09	7.1		
ISMA153	S	53.81672167	-5.876	12.10.09	7.2		
ISMA154	S	53.82988333	-5.871	12.10.09	7.3		
ISMA155	BB	53.82988333	-5.871	12.10.09	7.3		
ISMA156	S	53.8428	-5.864	12.10.09	7.41		
ISMA157	S	53.85905667	-5.858	12.10.09	7.53		
ISMA158	BB	53.85905667	-5.858	12.10.09	7.53		
ISMA159	V	53.56634833	-5.967	12.10.09	10.18		2.83m of good core
ISMA160	V	53.56871333	-5.925	12.10.09	10.43		Only top and bottom of core, rest of core lost

ISMA161	BB	53.08150167	-5.921	12.10.09	21.2		Gravel
ISMA162	S	53.08150167	-5.921	12.10.09	21.2		Gravel
ISMA163	S	53.08431667	-5.915	12.10.09	21.29		
ISMA164	BB	53.08431667	-5.915	12.10.09	21.29		
ISMA165	S	53.08143333	-5.915	12.10.09	21.35		
ISMA166	S	53.07725	-5.912	12.10.09	21.43		
ISMA167	BB	53.07725	-5.912	12.10.09	21.43		
ISMA168	S	53.08113833	-5.909	12.10.09	21.59		
ISMA169	BB	53.08113833	-5.909	12.10.09	21.59		
ISMA170	S	53.07806667	-5.906	12.10.09	22.08		
ISMA171	S	53.06916	-5.906	12.10.09	23.18		Sand Gravel Bioclasts
ISMA172	BB	53.06916	-5.906	12.10.09	23.18		Sand Gravel Bioclasts
ISMA173	S	53.072895	-5.909	12.10.09	23.31		Sandy
ISMA174	BB	53.072895	-5.909	12.10.09	23.31		Sandy
ISMA175	S	53.07525167	-5.914	12.10.09	23.43		Sand , Pebbles and Bioclasts
ISMA176	BB	53.07525167	-5.914	12.10.09	23.43		Sand , Pebbles and Bioclasts
ISMA177	S	53.07654167	-5.916	12.10.09	23.51		Sand, Pebbles, Bioclasts and Gastropods
ISMA178	S	53.07537833	-5.923	13.10.09	0.03		Sand, Pebbles, Bioclasts and Gastropods
ISMA179	BB	53.07537833	-5.923	13.10.09	0.03		Sand, Pebbles, Bioclasts and Gastropods
ISMA180	S	53.073235	-5.926	13.10.09	0.18		Sand, Gravel. Bio-encrustation on gravel clasts
ISMA181	BB	53.073235	-5.926	13.10.09	0.18		Sand, Gravel. Bio-encrustation on gravel clasts
ISMA182	S	53.06968167	-5.926	13.10.09	0.3		Sand, Gravel. Bio-encrustation on gravel clasts
ISMA183	BF	53.06968167	-5.926	13.10.09	0.3		Sand, Gravel. Bio-encrustation on gravel clasts
ISMA184	S	53.069615	-5.92	13.10.09	0.41		Sand, Gravel. Bio-encrustation on gravel clasts
ISMA185	S	53.06893167	-5.914	13.10.09	0.54		Sand, Gravel. Bio-encrustation on gravel clasts
ISMA186	BB	53.06893167	-5.914	13.10.09	0.54		Sand, Gravel. Bio-encrustation on gravel clasts
ISMA187	S	53.06635	-5.913	13.10.09	1.52		Sand, Pebbles and Gravel

ISMA188	S	53.06551667	-5.912	13.10.09	2		Sand and Large Gravel
ISMA189	BB	53.06551667	-5.912	13.10.09	2		Sand and Large Gravel
ISMA190	S	53.06663	-5.905	13.10.09	2.13		Sand and Gravel
ISMA191	S	53.06359667	-5.902	13.10.09	2.26		Sand, Pebbles and Bioclasts
ISMA192	S	53.06359667	-5.902	13.10.09	2.26		Sand, Pebbles and Bioclasts
ISMA193	S	53.063495	-5.907	13.10.09	2.38		Sand, Gravel, Gastropods and Bioclasts
ISMA194	S	53.063095	-5.915	13.10.09	2.52		Sand, Gravel, Gastropods and Bioclasts
ISMA195	S	53.06207167	-5.917	13.10.09	2.57		Sand, Gravel, Gastropods and Bioclasts
ISMA196	BB	53.06207167	-5.917	13.10.09	2.57		Sand, Gravel, Gastropods and Bioclasts
ISMA197	S	53.06687833	-5.926	13.10.09	3.24		Gravel (+ Sand) Starfish,Barnacles on Large Clasts
ISMA198	BB	53.06687833	-5.926	13.10.09	3.24		Gravel (+ Sand) Starfish,Barnacles on Large Clasts
ISMA199	S	53.06352667	-5.927	13.10.09	3.43		
ISMA200	BB	53.06352667	-5.927	13.10.09	3.43		Gravel, Pebbles and Cobbles barnacles on larger clasts
ISMA201	BB	53.06352667	-5.927	13.10.09	3.55		Gravel, Pebbles and Cobbles barnacles on larger clasts
ISMA202	S	53.057465	-5.92	13.10.09	4.54		Gravel, Pebbles and Cobbles barnacles on larger clasts
ISMA203	BB	53.057465	-5.92	13.10.09	4.54		Gravel, Pebbles and Cobbles barnacles on larger clasts
ISMA204	S	53.051345	-5.919	13.10.09	5.45		Sand, gravel, bio fragments; correct lat coordinate??
ISMA205	S	53.04282	-5.908	13.10.09	6.03		Coarse sandy gravel
ISMA206	BB	53.04282	-5.908	13.10.09	6.03		Coarse sandy gravel
ISMA207	V	53.04175833	-5.909	13.10.09	6.23		3 sections (2.7m)
ISMA208	S	53.03967333	-5.907	13.10.09	7.5		Sandy, lots of bioclasts
ISMA209	BB	53.03967333	-5.907	13.10.09	7.5		Sandy, lots of bioclasts
ISMA210	S	53.02085333	-5.906	13.10.09	8.15		Sandy gravel
ISMA211	BF	52.99454833	-5.9	13.10.09	8.54		Gravel with abundant biomatter
ISMA212	BB	52.99454833	-5.9	13.10.09	8.54		Gravel with abundant biomatter
ISMA213	S	52.98814	-5.899	13.10.09	9.2		Sandy gravel
ISMA214	BB	52.98814	-5.899	13.10.09	9.2		Sandy gravel

ISMA215	S	52.97937333	-5.912	13.10.09	9.56		Well sorted fine to medium sand
ISMA216	BB	52.97471833	-5.913	13.10.09	10.2		Sandy gravel + abundant worm tubes
ISMA217	TV	52.97286167	-5.916	13.10.09	11.51		SOL
ISMA218	TV	52.96317333	-5.906	13.10.09	13.28		EOL
ISMA219	BB	52.92984	-5.906	13.10.09	14.28		
ISMA220	S	52.92908833	-5.91	13.10.09	14.44		
ISMA221	S	52.94006833	-5.903	13.10.09	14.59		Cobbles
ISMA222	BB	52.94006833	-5.903	13.10.09	14.59		
ISMA223	S	52.91800333	-5.901	13.10.09	15.13		Cobbles, gravel, crabs, worms and barnacles
ISMA224	BB	52.91800333	-5.901	13.10.09	15.13		
ISMA225	BF	52.94023333	-5.897	13.10.09	15.26		
ISMA226	S	52.95818833	-5.913	13.10.09	15.52		
ISMA227	S	52.95860167	-5.901	13.10.09	16.13		
ISMA228	S	52.966955	-5.9	13.10.09	16.28		Pebbles, gravels and shells
ISMA229	S	52.966955	-5.9	13.10.09	16.28		
ISMA230	S	52.97161667	-5.908	13.10.09	17.23		
ISMA231	BB	52.97161667	-5.908	13.10.09	17.23		
ISMA232	BB	52.97158333	-5.904	13.10.09	17.31		
ISMA233	BF	52.99341	-5.916	13.10.09	18.01		
ISMA234	V	52.993385	-5.916	13.10.09	18.11		
ISMA235	V	53.029825	-5.897	13.10.09	18.38		
ISMA236	S	53.05561667	-5.912	13.10.09	20.08		Shelly gravel
ISMA237	BB	53.05561667	-5.912	13.10.09	20.08		Shelly gravel
ISMA238	S	53.059865	-5.908	13.10.09	20.2		
ISMA239	BB	53.059865	-5.908	13.10.09	20.2		
ISMA240	S	53.05682667	-5.904	13.10.09	20.3		
ISMA241	S	53.05133833	-5.901	13.10.09	20.38		

ISMA242	BB	53.05133833	-5.901	13.10.09	20.38		
ISMA243	S	53.04957833	-5.907	13.10.09	20.46		
ISMA244	S	53.04603667	-5.9	13.10.09	20.58		
ISMA245	BB	53.04603667	-5.9	13.10.09	20.58		
ISMA246	S	53.042845	-5.899	13.10.09	21.04		
ISMA247	S	53.03677333	-5.897	13.10.09	21.14		
ISMA248	BB	53.03677333	-5.897	13.10.09	21.14		
ISMA249	S	53.03457833	-5.897	13.10.09	21.18		
ISMA250	S	53.03145167	-5.901	13.10.09	21.51		
ISMA251	BB	53.03145167	-5.901	13.10.09	21.51		
ISMA252	S	53.02777667	-5.897	13.10.09	22.09		
ISMA253	S	53.02575	-5.893	13.10.09	22.22		
ISMA254	BB	53.02575	-5.893	13.10.09	22.22		
ISMA255	S	53.01536	-5.893	13.10.09	22.32		
ISMA256	S	53.01042833	-5.898	13.10.09	22.53		
ISMA257	BB	53.01087833	-5.898	13.10.09	22.53		
ISMA258	S	53.00349667	-5.895	13.10.09	23.11		
ISMA259	BB	53.00349667	-5.895	13.10.09	23.11		
ISMA260	S	52.99968667	-5.894	13.10.09	23.22		
ISMA261	BB	52.99968667	-5.894	13.10.09	23.22		
ISMA262	S	52.99161167	-5.892	13.10.09	23.41		
ISMA263	BB	52.99161167	-5.892	13.10.09	23.41		
ISMA264	TV	53.02889667	-5.903	14.10.09	0.12		SOL
ISMA265	TV	53.01384167	-5.916	14.10.09	1.44		EOL
ISMA266	BB	53.00591833	-5.905	14.10.09	3.03		Too coarse for sediment sample, Mussels!!!
ISMA267	BF	53.00618667	-5.92	14.10.09	3.29		Shrimp, crabs and wormtubes and no sediment
ISMA268	S	52.98894833	-5.905	14.10.09	4		Gravel, Sand, Wormtubes and Shells

ISMA269	BB	52.98895	-5.905	14.10.09	4		Gravel, Sand, Wormtubes and Shells
ISMA270	S	52.99179167	-5.912	14.10.09	4.3		Sand and Mud. Organic matter concretions?
ISMA271	S	52.989425	-5.911	14.10.09	4.38		Sand , gravel clasts and shells
ISMA272	BB	52.989425	-5.911	14.10.09	4.38		Sand , gravel clasts and shells
ISMA273	BB	52.98206833	-5.904	14.10.09	4.57		Wormtubes, shells, small amount of sand
ISMA274	S	52.97614667	-5.897	14.10.09	5.2		Large pebble+ sand-gravel, lots of shells
ISMA275	BB	52.97614667	-5.897	14.10.09	5.2		Large pebble+ sand-gravel, lots of shells
ISMA276	BB	53.01902333	-5.92	14.10.09	5.43		Shell, gastropods, pebbles with sand-gravel (small amount of sediment)
ISMA277	S	53.02273	-5.915	14.10.09	5.52		Cobbles+encrusted bio, shells, gravel - sand
ISMA278	BB	53.02273	-5.915	14.10.09	5.52		Cobbles+encrusted bio, shells, gravel - sand
ISMA279	BF	53.02273	-5.915	14.10.09	5.52		Cobbles+encrusted bio, shells, gravel - sand
ISMA280	BB	53.02626667	-5.921	14.10.09	6.01		Wormtubes
ISMA281	TV	53.00883667	-5.912	14.10.09	6.22		SOL camera line 3
ISMA282	TV	53.00478667	-5.902	14.10.09	7.42		EOL camera line 3
ISMA283	CTD	52.95109983	-5.903	14.10.09	8.3		Uniform profile (at ADCP site)
ISMA284	BB	52.952505	-5.901	14.10.09	9.14		Fine sand and bivalves
ISMA285	S	52.945625	-5.905	14.10.09	9.26		Fine sand and bivalves
ISMA286	BB	52.9486	-5.897	14.10.09	9.39		Mussels, worms
ISMA287	S	52.94994833	-5.905	14.10.09	9.52		Sand, gastropods, shells
ISMA288	BB	52.94994833	-5.905	14.10.09	9.52		Sand, gastropods, shells
ISMA289	S	52.95249167	-5.905	14.10.09	10.08		Coarse sand, gravel, bivalve shells
ISMA290	BB	52.95249167	-5.905	14.10.09	10.08		Coarse sand, gravel, bivalve shells
ISMA291	S	52.97410167	-5.912	14.10.09	11.1		Wormtubes, crabs and asnd
ISMA292	S	52.97566667	-5.898	14.10.09	11.2		Shells, gravel ,pebbles
ISMA293	S	52.97573	-5.898	14.10.09	11.29		Shells, gravel ,pebbles
ISMA294	BB	52.979195	-5.904	14.10.09	11.56		
ISMA295	BF	52.98922167	-5.905	14.10.09	12.11		Mussels, Shells and Gravel

ISMA296	V	52.975285	-5.899	14.10.09	12.52	71.72	1 section (sand)
ISMA297	V	53.01202833	-5.92	14.10.09	13.24	22.9	3 sections (2.9m); sand
ISMA298	S	52.99938667	-5.917	14.10.09	14.12		Worm Tubes. Sand taken for sampling
ISMA299	S	53.01351667	-5.911	14.10.09	14.4		Shells and Gravel
ISMA300	BB	53.01351667	-5.911	14.10.09	14.4		
ISMA301	S	53.02836167	-5.916	14.10.09	14.55		
ISMA302	S	53.032145	-5.923	14.10.09	15.05		Gravel and Shells
ISMA303	S	53.03812833	-5.912	14.10.09	15.17		Pebbles Gravel and Shells
ISMA304	BB	53.03812833	-5.912	14.10.09	15.17		Pebbles Gravel and Shells
ISMA305	S	53.40863	-5.909	14.10.09	18.02		
ISMA306	V	53.44898333	-5.891	14.10.09	19.32	43.3	1 x 40cm section + core catcher lithified
ISMA307	V	53.46604167	-5.856	14.10.09	19.59	42.05	3 sections sandy
ISMA308	V	53.46009667	-5.871	14.10.09	20.15	44.1	3 sections silty mud
ISMA309	S	53.45225167	-5.853	14.10.09	21.13		
ISMA310	BB	53.46341	-5.859	14.10.09	21.26		
ISMA311	S	53.48118	-5.852	14.10.09	21.43		Silty mud
ISMA312	BB	53.48118	-5.852	14.10.09	21.43		
ISMA313	S	53.48725833	-5.85	14.10.09	21.53		Silty mud with large worm
ISMA314	BB	53.48725833	-5.85	14.10.09	21.53		
ISMA315	S	53.45215	-5.921	14.10.09	22.22		
ISMA316	S	53.42500167	-5.913	14.10.09	22.39		
ISMA317	S	53.446085	-5.895	14.10.09	23.41		Fine Sand and 1 Crab
ISMA318	S	53.56148333	-5.957	15.10.09	0.24		Fine Sand
ISMA319	BB	53.56148333	-5.957	15.10.09	0.24		Fine Sand
ISMA320	S	53.56748	-5.94	15.10.09	0.37		Fine Sand
ISMA321	S	53.56201333	-5.923	15.10.09	0.5		Fine Sand
ISMA322	S	53.566585	-5.908	15.10.09	1.02		Fine Sand

ISMA323	S	53.57465167	-5.912	15.10.09	1.16		Fine Sand
ISMA324	BB	53.57465167	-5.912	15.10.09	1.16		Fine Sand
ISMA325	S	53.58127667	-5.912	15.10.09	1.27		Fine Sand
ISMA326	S	53.57835333	-5.942	15.10.09	1.55		Fine Sand
ISMA327	BB	53.57835333	-5.942	15.10.09	1.55		Fine Sand
ISMA328	S	53.58423333	-5.964	15.10.09	2.02		Fine Sand
ISMA329	S	53.69436333	-6.006	15.10.09	3.07		Clayey, Very Fine Sand
ISMA330	BB	53.69436333	-6.006	15.10.09	3.07		Clayey, Very Fine Sand
ISMA331	S	53.70705333	-6.004	15.10.09	3.19		Clayey. Silt
ISMA332	BB	53.70705333	-6.004	15.10.09	3.19		Clayey. Silt
ISMA333	S	53.71989	-6.003	15.10.09	3.36		Clayey Silt Below Sandy Surface
ISMA334	BB	53.71989	-6.003	15.10.09	3.36		Clayey Silt Below Sandy Surface
ISMA335	S	53.73573333	-5.998	15.10.09	3.5		Clayey Silt Below Sandy Surface
ISMA335	BB	53.73573333	-5.998	15.10.09	3.5		Clayey Silt Below Sandy Surface
ISMA337	S	53.74905333	-5.996	15.10.09	4.03		Clayey Silt Below Sandy Surface
ISMA338	S	53.76276167	-5.997	15.10.09	4.15		Clayey Silt Below Sandy Surface
ISMA339	BB	53.76276167	-5.997	15.10.09	4.15		Clayey Silt Below Sandy Surface
ISMA340	S	53.77777167	-6	15.10.09	4.29		Clayey Silt Below Sandy Surface
ISMA341	S	53.78795833	-5.996	15.10.09	4.4		Clayey Silt Below Sandy Surface
ISMA342	BB	53.78795833	-5.996	15.10.09	4.4		Clayey Silt Below Sandy Surface
ISMA343	S	53.80493333	-5.958	15.10.09	4.53		Clayey Silt Below Sandy Surface
ISMA344	S	53.81771833	-5.99	15.10.09	5.17		Clayey Silt Below Sandy Surface
ISMA345	BB	53.81771833	-5.99	15.10.09	5.17		Clayey Silt Below Sandy Surface
ISMA346	S	53.82658167	-5.984	15.10.09	5.31		Clayey Silt Below Sandy Surface
ISMA347	S	53.83979333	-5.978	15.10.09	5.45		Clayey Silt Below Sandy Surface
ISMA348	BB	53.83979333	-5.978	15.10.09	5.45		Clayey Silt Below Sandy Surface
ISMA349	S	53.85084833	-5.973	15.10.09	5.57		Clayey Silt Below Sandy Surface

ISMA350	S	53.859565	-5.967	15.10.09	6.08		Clayey Silt Below Sandy Surface
ISMA351	BB	53.859565	-5.967	15.10.09	6.08		Clayey Silt Below Sandy Surface
ISMA352	S	53.859585	-5.996	15.10.09	6.23		Clayey Silt Below Sandy Surface
ISMA353	S	53.84635333	-6.003	15.10.09	6.38		Clayey Silt Below Sandy Surface
ISMA354	BB	53.84635333	-6.003	15.10.09	6.38		Clayey Silt Below Sandy Surface
ISMA355	S	53.831305	-6.008	15.10.09	6.52		Clayey Silt Below Sandy Surface
ISMA356	V	53.62475167	-5.908	15.10.09	8.35	50.5	3 sections (2.95m) mud to sand
ISMA357	V	53.62255167	-5.907	15.10.09	8.56	50.5	2 sections (1.9m) + cc
ISMA358	V	53.64495667	-5.94	15.10.09	9.25	44.8	3 sections (2.85m)+cc
ISMA359	V	53.71362167	-5.961	15.10.09	10.12	42	3 sections (2.6m) +cc
ISMA360	TV	53.70488	-5.948	15.10.09	11.3		SOL camera line 4
ISMA361	TV	53.69390833	-5.938	15.10.09	12.52		EOL camera line 4
ISMA362	TV	53.56447333	-5.946	15.10.09	14.25		
ISMA363	TV	53.56623333	-5.932	15.10.09	15.22		
ISMA364	TV	53.578435	-5.904	15.10.09	15.57		
ISMA365	TV	53.58371167	-5.898	15.10.09	16.44		
ISMA366	TV	53.58290333	-5.962	15.10.09	18.02		
ISMA367	TV	53.589485	-5.97	15.10.09	18.45		
ISMA368	S	53.71875833	-6.028	15.10.09	19.59		
ISMA369	BB	53.71875833	-6.128	15.10.09	19.59		
ISMA370	S	53.73492	-6.023	15.10.09	20.13		
ISMA371	S	53.73776833	-6.047	15.10.09	20.32		
ISMA372	BB	53.73776833	-6.047	15.10.09	20.32		
ISMA373	S	53.75533167	-6.017	15.10.09	20.55		
ISMA374	S	53.75883167	-6.039	15.10.09	21.11		
ISMA375	BB	53.75883167	-6.039	15.10.09	21.11		
ISMA376	S	53.77852167	-6.032	15.10.09	21.29		

ISMA377	S	53.79931833	-6.023	15.10.09	21.51		
ISMA378	BB	53.79931833	-6.023	15.10.09	21.51		
ISMA379	S	53.82080167	-6.015	15.10.09	22.13		
ISMA380	S	53.82237167	-6.038	15.10.09	22.3		
ISMA381	BB	53.82237167	-6.038	15.10.09	22.3		
ISMA382	S	53.845445	-6.027	15.10.09	22.59		
ISMA383	S	53.85950833	-6.021	15.10.09	23.18		
ISMA384	BB	53.85950833	-6.021	15.10.09	23.18		
ISMA385	S	53.86388833	-6.051	15.10.09	23.36		Silt Mud
ISMA386	S	53.864575	-6.084	15.10.09	23.54		Silt Mud
ISMA387	BB	53.864575	-6.084	15.10.09	23.54		Silt Mud
ISMA388	S	53.853755	-6.084	16.10.09	0.13		Silt Mud
ISMA389	S	53.84912	-6.068	16.10.09	0.27		Silt Mud
ISMA390	BB	53.84912	-6.068	16.10.09	0.27		Silt Mud
ISMA391	S	53.82790333	-6.08	16.10.09	0.45		Silt Mud
ISMA392	S	53.81136667	-6.122	16.10.09	1.11		Silt Mud
ISMA393	BB	53.81136667	-6.122	16.10.09	1.11		Silt Mud
ISMA394	S	53.80872833	-6.09	16.10.09	1.28		Silt Mud
ISMA395	S	53.803	-6.05	16.10.09	1.49		Silt Mud
ISMA396	BB	53.803	-6.05	16.10.10	2.49		Silt Mud
ISMA397	S	53.78154833	-6.061	16.10.09	2.1		Silt Mud
ISMA398	S	53.78565667	-6.101	16.10.09	2.33		Silt Mud
ISMA399	BB	53.78565667	-6.101	16.10.09	2.33		Silt Mud
ISMA400	S	53.78896833	-6.127	16.10.09	2.52		Silt Mud
ISMA401	S	53.77397667	-6.114	16.10.09	3.13		Silt Mud
ISMA402	BB	53.77397667	-6.114	16.10.09	3.13		Silt Mud
ISMA403	S	53.76124667	-6.073	16.10.09	3.4		Silt Mud

ISMA404	S	53.694815	-5.989	16.10.09	4.34		Silt Mud
ISMA405	S	53.66745833	-5.975	16.10.09	5.07		Silt Mud
ISMA406	BB	53.66745833	-5.975	16.10.09	5.07		Silt Mud
ISMA407	S	53.645135	-5.96	16.10.09	5.27		Silt Mud
ISMA408	S	53.63372333	-5.902	16.10.09	5.54		Silt Mud
ISMA409	S	53.65267	-5.897	16.10.09	6.1		Silt Mud
ISMA410	BB	53.65267	-5.897	16.10.09	6.1		Silt Mud
ISMA411	S	53.67190167	-5.891	16.10.09	6.23		Silt Mud
ISMA412	S	53.69542	-5.886	16.10.09	7.04		Silt Mud
ISMA413	BB	53.69542	-5.886	16.10.09	7.04		Silt Mud
ISMA414	S	53.71875333	-5.876	16.10.09	7.3		Silt Mud
ISMA415	S	53.74047167	-5.869	16.10.09	7.51		Silt Mud
ISMA416	BB	53.74047167	-5.869	16.10.09	7.51		Silt Mud
ISMA417	V	53.80754667	-5.925	16.10.09	8.38		3 sections (2.72m) + cc
ISMA418	V	53.80399833	-6.049	16.10.09	9.19		3 sections (2.49 m) + cc
ISMA419	TV	53.81239667	-6.031	16.10.09	10.1		SOL Mudbelt N
ISMA420	TV	53.80296667	-6.035	16.10.09	10.54		EOL Mudbelt N
ISMA421	TV	53.80189667	-5.923	16.10.09	11.47		SOL Mudbelt N
ISMA422	TV	53.80156333	-5.929	16.10.09	12.27		EOL Mudbelt N
ISMA423	TV	53.48821667	-5.921	16.10.09	15.03		SOL Lambay NW
ISMA424	TV	53.460015	-5.913	16.10.09	15.55		EOL Lambay NW
ISMA425	TV	53.4772	-5.865	16.10.09	16.04		SOL Lambay NE
ISMA426	TV	53.48613833	-5.854	16.10.09	17.4		EOL Lambay NE
ISMA427	TV	53.443065	-5.89	16.10.09	18.43		SOL Lambay Central
ISMA428	TV	53.45188833	-5.896	16.10.09	19.09		EOL Lambay Central
ISMA429	S	53.605945	-5.907	16.10.09	20.27		
ISMA430	BB	53.605945	-5.907	16.10.09	20.27		

ISMA431	S	53.695	-5.975	16.10.09	21.21		
ISMA432	BB	53.695	-5.975	16.10.09	21.21		
ISMA433	S	53.76159167	-5.906	16.10.09	21.59		
ISMA434	S	53.79921667	-5.964	16.10.09	22.4		
ISMA435	S	53.89113333	-5.952	16.10.09	23.23		Silt and Mud
ISMA436	S	53.87362333	-5.908	16.10.09	23.48		Silt and Mud
ISMA437	S	53.88638333	-5.861	17.10.09	0.13		Silt and Mud
ISMA438	S	53.88945333	-5.818	17.10.09	0.34		Silt and Mud
ISMA439	S	53.86411833	-5.826	17.10.09	0.56		Silt and Mud
ISMA440	BB	53.86411833	-5.826	17.10.09	0.56		Silt and Mud
ISMA441	S	53.86008	-5.8	17.10.09	1.13		Silt and Mud
ISMA442	S	53.97610167	-5.804	17.10.09	1.32		Silt and Mud
ISMA443	BB	53.97610167	-5.804	17.10.09	1.32		Silt and Mud
ISMA444	S	53.84463833	-5.832	17.10.09	1.52		Silt and Mud
ISMA445	S	53.83962333	-5.84	17.10.09	2.13		Silt and Mud
ISMA446	BB	53.83962333	-5.84	17.10.09	2.13		Silt and Mud
ISMA447	S	53.81895167	-5.809	17.10.09	2.52		Silt and Mud
ISMA448	S	53.796545	-5.814	17.10.09	3.22		Silt and Mud
ISMA449	BB	53.796545	-5.814	17.10.09	3.22		Silt and Mud
ISMA450	S	53.80010667	-5.846	17.10.09	3.41		Silt and Mud
ISMA451	S	53.780145	-5.855	17.10.09	4.02		Silt and Mud
ISMA452	BB	53.780145	-5.855	17.10.09	4.02		Silt and Mud
ISMA453	S	53.77599833	-5.822	17.10.09	4.2		Silt and Mud
ISMA454	S	53.755405	-5.82	17.10.09	4.42		Silt and Mud
ISMA455	BB	53.755405	-5.82	17.10.09	4.42		Silt and Mud
ISMA456	S	53.758515	-5.861	17.10.09	5.2		Silt and Mud
ISMA457	S	53.73423333	-5.835	17.10.09	5.44		Silt and Mud

ISMA458	S	53.71381833	-5.841	17.10.09	6.03		Silt and Mud
ISMA459	BB	53.71381833	-5.841	17.10.09	6.03		Silt and Mud
ISMA460	S	53.69103167	-5.848	17.10.09	6.23		Silt and Mud
ISMA461	S	53.669715	-5.866	17.10.09	7.04		Silt and Mud
ISMA462	BB	53.669715	-5.866	17.10.09	7.04		Silt and Mud
ISMA463	S	53.65039333	-5.873	17.10.09	7.23		Silt and Mud
ISMA464	S	53.63042333	-5.875	17.10.09	7.38		Silt and Mud
ISMA465	BB	53.63042333	-5.875	17.10.09	7.38		Silt and Mud
ISMA466	TV	53.69030167	-5.975	17.10.09	8.22		SOL run 13 (pockmark feature)
ISMA467	TV	53.69737833	-5.98	17.10.09	8.49		EOL run 13
ISMA468	TV	53.69101333	-5.971	17.10.09	9.1		SOL run 14 (pockmark feature)
ISMA469	TV	53.69355667	-5.974	17.10.09	9.39		EOL run 14
ISMA470	V	53.69328333	-5.973	17.10.09	9.54	41m	3 sections (3m) + cc (in 2 bags)
ISMA471	V	53.69115333	-5.966	17.10.09	10.17	41.7m	3 sections (2.3m) + cc (in 2 bags)
ISMA472	BX	53.81013333	-5.928	17.10.09	12.3		22cm core
ISMA473	S	53.81013333	-5.928	17.10.09	12.3		Intact Burrow
ISMA474	BX	53.75360667	-5.953	17.10.09	13.04		26cm Mud Core
ISMA475	S	53.75360667	-5.953	17.10.09	13.04		
ISMA476	BX	53.69238667	-5.972	17.10.09	13.36		
ISMA477	S	53.69361333	-5.972	17.10.09	13.36		
ISMA478	BX	53.69361333	-5.973	17.10.09	13.51		
ISMA479	S	53.69361333	-5.973	17.10.09	13.51		
ISMA480	BX	53.64351333	-5.949	17.10.09	14.23		
ISMA481	S	53.64351333	-5.949	17.10.09	14.23		
ISMA482	TV	53.39457667	-5.876	17.10.09	16.04		SOL
ISMA483	TV	53.44780667	-5.868	17.10.09	16.04		EOL

SPARKER SEISMIC LINES

Survey	LineID	Line_Type	Date-Time SOL	Long_SOL (dd)	Lat_SOL (dd)	Fix_No_SOL	Date-Time EOL	Long_EOL (dd)	Lat_EOL (dd)	Fix_No_EOL
CV09_UCC_ISMA	15	Sparker	29/09/2009 07:52	-5.899819097	52.99907163	61620	29/09/2009 12:07	-5.910779778	53.08233167	61705
CV09_UCC_ISMA	16	Sparker	29/09/2009 12:20	-5.917102039	53.07347386	61706	29/09/2009 14:37	-5.907185869	52.930468	61786
CV09_UCC_ISMA	17	Sparker	29/09/2009 14:41	-5.90418821	52.92780199	61787	29/09/2009 15:15	-5.894708857	52.96489487	61809
CV09_UCC_ISMA	18	Sparker	29/09/2009 15:23	-5.897161532	52.96574076	61810	29/09/2009 15:36	-5.912026193	52.965474	61815
CV09_UCC_ISMA	19	Sparker	29/09/2009 15:42	-5.913969331	52.96810014	61816	29/09/2009 15:49	-5.914626686	52.97706387	61821
CV09_UCC_ISMA	20	Sparker	29/09/2009 15:56	-5.914340858	52.97712359	61822	29/09/2009 16:09	-5.896513869	52.97756642	61828
CV09_UCC_ISMA	21	Sparker	29/09/2009 16:12	-5.893874812	52.9791635	61829	29/09/2009 16:26	-5.888349207	52.99291528	61838
CV09_UCC_ISMA	22	Sparker	29/09/2009 16:31	-5.891415042	52.99430842	61839	29/09/2009 16:50	-5.918129157	52.99332366	61848
CV09_UCC_ISMA	23	Sparker	29/09/2009 16:55	-5.919708661	52.99438806	61849	29/09/2009 17:11	-5.919807888	53.01229272	61859
CV09_UCC_ISMA	24	Sparker	29/09/2009 17:15	-5.919493781	53.01165449	61860	29/09/2009 17:31	-5.899578609	53.01366308	61867
CV09_UCC_ISMA	25	Sparker	29/09/2009 17:37	-5.894333871	53.01754667	61868	29/09/2009 17:45	-5.891184987	53.02815457	61874
CV09_UCC_ISMA	26	Sparker	29/09/2009 17:48	-5.894055695	53.02962527	61875	29/09/2009 18:09	-5.923783705	53.02950415	61885
CV09_UCC_ISMA	27	Sparker	29/09/2009 18:11	-5.925112336	53.03132091	61886	29/09/2009 18:22	-5.925081017	53.04367849	61893
CV09_UCC_ISMA	28	Sparker	29/09/2009 18:27	-5.922825243	53.04551668	61894	29/09/2009 18:43	-5.899020176	53.04635088	61902
CV09_UCC_ISMA	31	Sparker	29/09/2009 19:40	-5.937246135	53.07587331	61925	29/09/2009 22:29	-5.880481136	53.43113427	62139
CV09_UCC_ISMA	32	Sparker	29/09/2009 23:00	-5.912906888	53.41402093	62140	29/09/2009 23:30	-5.829609352	53.45540642	62176
CV09_UCC_ISMA	33	Sparker	29/09/2009 23:32	-5.830811398	53.45703216	62177	29/09/2009 23:59	-5.911810044	53.41688808	62212
CV09_UCC_ISMA	34	Sparker	30/09/2009 00:03	-5.915309675	53.41779415	62213	30/09/2009 00:33	-5.834377305	53.45801575	62248
CV09_UCC_ISMA	35	Sparker	30/09/2009 00:37	-5.836778092	53.45928786	62249	30/09/2009 01:04	-5.915275778	53.42012826	62283
CV09_UCC_ISMA	36	Sparker	30/09/2009 01:07	-5.916402335	53.42214063	62284	30/09/2009 01:36	-5.838005997	53.46136583	62318
CV09_UCC_ISMA	37	Sparker	30/09/2009 01:39	-5.840535209	53.46263606	62319	30/09/2009 02:05	-5.916746845	53.42466458	62352
CV09_UCC_ISMA	38	Sparker	30/09/2009 02:09	-5.916267149	53.42793946	62353	30/09/2009 02:35	-5.84202925	53.46446534	62385
CV09_UCC_ISMA	39	Sparker	30/09/2009 02:37	-5.842717079	53.46660653	62386	30/09/2009 03:04	-5.916863872	53.4299156	62418
CV09_UCC_ISMA	40	Sparker	30/09/2009 03:07	-5.916320567	53.4326569	62419	30/09/2009 03:31	-5.844603194	53.46829734	62450
CV09_UCC_ISMA	41	Sparker	30/09/2009 03:34	-5.844840266	53.47037215	62451	30/09/2009 04:01	-5.916859139	53.43501509	62482

Survey	LineID	Line_Type	Date-Time SOL	Long_SOL (dd)	Lat_SOL (dd)	Fix_No_SOL	Date-Time EOL	Long_EOL (dd)	Lat_EOL (dd)	Fix_No_EOL
CV09_UCC_ISMA	42	Sparker	30/09/2009 04:04	-5.918199912	53.43690885	62483	30/09/2009 04:28	-5.84648631	53.47258402	62514
CV09_UCC_ISMA	43	Sparker	30/09/2009 04:30	-5.845998273	53.47524588	62515	30/09/2009 04:56	-5.917846834	53.43969202	62546
CV09_UCC_ISMA	44	Sparker	30/09/2009 04:59	-5.92053505	53.44085981	62547	30/09/2009 05:24	-5.846525964	53.47769533	62579
CV09_UCC_ISMA	45	Sparker	30/09/2009 05:26	-5.847780503	53.47957879	62580	30/09/2009 05:52	-5.919549468	53.44398225	62611
CV09_UCC_ISMA	46	Sparker	30/09/2009 05:56	-5.920325911	53.44618	62612	30/09/2009 06:21	-5.848579369	53.48185126	62643
CV09_UCC_ISMA	47	Sparker	30/09/2009 06:23	-5.84833164	53.4844834	62644	30/09/2009 06:50	-5.922386261	53.44771746	62676
CV09_UCC_ISMA	48	Sparker	30/09/2009 06:52	-5.922976591	53.44984735	62677	30/09/2009 07:18	-5.849192732	53.48680092	62709
CV09_UCC_ISMA	49	Sparker	30/09/2009 07:24	-5.859722731	53.48733855	62710	30/09/2009 07:48	-5.923735655	53.45464114	62738
CV09_UCC_ISMA	50	Sparker	30/09/2009 07:52	-5.924641335	53.45703417	62739	30/09/2009 08:11	-5.869059169	53.4845619	62763
CV09_UCC_ISMA	51	Sparker	30/09/2009 08:15	-5.871581243	53.48615292	62764	30/09/2009 08:28	-5.90597455	53.46869716	62779
CV09_UCC_ISMA	52	Sparker	30/09/2009 08:32	-5.909945058	53.46981171	62780	30/09/2009 08:40	-5.886831213	53.48130742	62790
CV09_UCC_ISMA	53	Sparker	30/09/2009 09:25	-5.852276565	53.48752393	62791	30/09/2009 10:16	-5.921707099	53.45301958	62821
CV09_UCC_ISMA	54	Sparker	30/09/2009 10:31	-5.919502492	53.44368261	62822	30/09/2009 11:23	-5.848051104	53.47950163	62853
CV09_UCC_ISMA	55	Sparker	30/09/2009 11:33	-5.842996	53.47299748	62854	30/09/2009 12:25	-5.919132468	53.43496868	62887
CV09_UCC_ISMA	56	Sparker	30/09/2009 12:37	-5.917037579	53.4254406	62888	30/09/2009 13:31	-5.841077359	53.46359978	62921
CV09_UCC_ISMA	57	Sparker	30/09/2009 13:42	-5.832099367	53.45761688	62922	30/09/2009 14:39	-5.913108302	53.41748	62957
CV09_UCC_ISMA	58	Sparker	30/09/2009 14:57	-5.891712664	53.41602313	62958	30/09/2009 15:22	-5.920375689	53.43906854	62974
CV09_UCC_ISMA	59	Sparker	30/09/2009 15:25	-5.922238338	53.44288572	62975	30/09/2009 15:39	-5.926244833	53.45705261	62983
CV09_UCC_ISMA	60	Sparker	30/09/2009 15:46	-5.919014306	53.4602752	62984	30/09/2009 16:22	-5.878868583	53.42884506	63006
CV09_UCC_ISMA	61	Sparker	30/09/2009 16:34	-5.861504003	53.4375366	63007	30/09/2009 17:09	-5.90357856	53.47035183	63030
CV09_UCC_ISMA	62	Sparker	30/09/2009 17:27	-5.890359162	53.48225979	63031	30/09/2009 18:07	-5.844705832	53.44654009	63056
CV09_UCC_ISMA	63	Sparker	30/09/2009 18:20	-5.827414529	53.45538997	63057	30/09/2009 18:53	-5.865879569	53.4853481	63078
CV09_UCC_ISMA	74	Sparker	01/10/2009 07:56	-5.943830848	53.8728157	63877	01/10/2009 10:18	-6.007594702	53.71558517	63967
CV09_UCC_ISMA	75	Sparker	01/10/2009 10:53	-6.04001072	53.72714532	63968	01/10/2009 12:56	-5.978416382	53.86235389	64046
CV09_UCC_ISMA	76	Sparker	01/10/2009 13:01	-5.980201527	53.86608912	64047	01/10/2009 13:51	-6.086396196	53.86436684	64082
CV09_UCC_ISMA	77	Sparker	01/10/2009 14:02	-6.095924704	53.85264771	64083	01/10/2009 17:55	-5.669954259	53.80264167	64226
CV09_UCC_ISMA	78	Sparker	01/10/2009 18:09	-5.671066136	53.80206136	64227	01/10/2009 19:07	-5.685498572	53.73794445	64263
CV09_UCC_ISMA	79	Sparker	01/10/2009 19:13	-5.694608321	53.73779722	64264	01/10/2009 23:13	-6.125708597	53.78881019	64409
CV09_UCC_ISMA	80	Sparker	01/10/2009 23:56	-6.073683458	53.76239517	64410	01/10/2009 02:07	-5.832795875	53.73427383	64491

Survey	LineID	Line_Type	Date-Time SOL	Long_SOL (dd)	Lat_SOL (dd)	Fix_No_SOL	Date-Time EOL	Long_EOL (dd)	Lat_EOL (dd)	Fix_No_EOL
CV09_UCC_ISMA	81	Sparker	02/10/2009 02:13	-5.826107172	53.73102871	64492	02/10/2009 02:28	-5.832227837	53.71527452	64501
CV09_UCC_ISMA	82	Sparker	02/10/2009 02:33	-5.837458069	53.71277922	64502	02/10/2009 04:27	-6.048408329	53.73771625	64573
CV09_UCC_ISMA	83	Sparker	02/10/2009 04:30	-6.050140494	53.73614759	64574	02/10/2009 04:51	-6.029606645	53.71414339	64588
CV09_UCC_ISMA	84	Sparker	02/10/2009 04:55	-6.025759234	53.71145733	64589	02/10/2009 07:47	-5.705061067	53.67372118	64697
CV09_UCC_ISMA	104	Sparker	04/10/2009 08:08	-5.999305335	53.58465035	65476	04/10/2009 09:10	-5.883792363	53.57108939	65515
CV09_UCC_ISMA	105	Sparker	04/10/2009 09:15	-5.876069054	53.57318355	65516	04/10/2009 09:34	-5.861533756	53.59681683	65530
CV09_UCC_ISMA	106	Sparker	04/10/2009 09:39	-5.868257598	53.60071488	65531	04/10/2009 10:34	-5.969257427	53.61190863	65565
CV09_UCC_ISMA	107	Sparker	04/10/2009 10:39	-5.973638372	53.61477047	65566	04/10/2009 11:31	-5.9783768	53.66844283	65597
CV09_UCC_ISMA	108	Sparker	04/10/2009 11:35	-5.978095643	53.67251703	65598	04/10/2009 11:52	-5.971178765	53.69000218	65608
CV09_UCC_ISMA	109	Sparker	04/10/2009 12:29	-5.973743368	53.68463926	65609	04/10/2009 15:20	-5.896679249	53.87317816	65717
CV09_UCC_ISMA	110	Sparker	04/10/2009 15:23	-5.894809451	53.87661505	65718	04/10/2009 15:40	-5.860554744	53.88404005	65730
CV09_UCC_ISMA	111	Sparker	04/10/2009 15:43	-5.859262343	53.88174403	65731	04/10/2009 20:26	-5.968823706	53.56125601	65913
CV09_UCC_ISMA	112	Sparker	04/10/2009 20:32	-5.966033598	53.55740901	65914	04/10/2009 20:49	-5.928656835	53.56443216	65927
CV09_UCC_ISMA	113	Sparker	04/10/2009 20:52	-5.925654137	53.56731417	65928	05/10/2009 01:49	-5.817873189	53.88797292	66110
CV09_UCC_ISMA	114	Sparker	05/10/2009 02:45	-5.907936252	53.87302053	66111	05/10/2009 03:50	-5.782463893	53.85906787	66153
CV09_UCC_ISMA	115	Sparker	05/10/2009 03:53	-5.778816798	53.85666155	66154	05/10/2009 04:05	-5.781836895	53.84240802	66162
CV09_UCC_ISMA	116	Sparker	05/10/2009 04:08	-5.785560221	53.83979503	66163	05/10/2009 05:59	-5.994386198	53.86374209	66233
CV09_UCC_ISMA	117	Sparker	05/10/2009 06:14	-6.01952752	53.85982511	66234	05/10/2009 07:47	-6.072138988	53.76038868	66292
CV09_UCC_ISMA	118	Sparker	05/10/2009 07:51	-6.078773053	53.75934827	66293	05/10/2009 08:10	-6.106231853	53.7735006	66305
CV09_UCC_ISMA	119	Sparker	05/10/2009 08:12	-6.106723085	53.77585699	66306	05/10/2009 09:25	-6.064238119	53.85456776	66352
CV09_UCC_ISMA	120	Sparker	05/10/2009 10:00	-6.09612228	53.8292827	66353	05/10/2009 12:40	-5.792347608	53.7938467	66455
CV09_UCC_ISMA	121	Sparker	05/10/2009 12:45	-5.788611978	53.79086729	66456	05/10/2009 13:01	-5.799047128	53.77413318	66466
CV09_UCC_ISMA	122	Sparker	05/10/2009 13:04	-5.802321207	53.77381119	66467	05/10/2009 16:09	-6.120416255	53.81228238	66574
CV09_UCC_ISMA	123	Sparker	05/10/2009 16:17	-6.122079546	53.81051703	66575	05/10/2009 17:15	-5.997016974	53.68532533	66656
CV09_UCC_ISMA	124	Sparker	05/10/2009 17:32	-5.997942859	53.68448384	66657	05/10/2009 18:42	-5.867238088	53.66947227	66701
CV09_UCC_ISMA	125	Sparker	05/10/2009 18:46	-5.864471854	53.66747287	66702	05/10/2009 19:00	-5.867338227	53.65321365	66710
CV09_UCC_ISMA	126	Sparker	05/10/2009 19:04	-5.871133856	53.65005115	66711	05/10/2009 19:58	-5.972066575	53.66170089	66745
CV09_UCC_ISMA	127	Sparker	05/10/2009 20:01	-5.975822505	53.66097797	66746	05/10/2009 20:17	-5.980217754	53.64504697	66755
CV09_UCC_ISMA	128	Sparker	05/10/2009 20:21	-5.978039578	53.64249501	66756	05/10/2009 21:15	-5.877277452	53.63057509	66790

Appendix C

SURVEY CV12006 CRUISE REPORT

Appendix C

Research Cruise: RV Celtic Voyager – Survey CV12006; NSGeo.
25th March – 7th April 2012

Ship's Crew	Scientific Party (Leg 1)
Philip Baugh - Master	Dr. Boris Dorschel - Chief Scientist (UCC)
Brendan Barry - Chief engineer	James Burns- Student (UU)
Brandon McGovern - Mate	Mark Coughlan - PhD student (UCC)/Night Watch Leader
Lorin McFadden - 00W	Niall Finn – Multibeam Operator Geological Survey of Ireland (GSI)
Tommy Byrne - Motorman	Marian McGrath – Marine Mammal Observer, PhD student (UCC)
Tom Gilmartin - AB	Sarah Kate McHugh - INFF
James Burke - AB	Jhonny Miranda – Sparker Operator Geomarine Survey Systems/Geosurveys
Kevin O'Leary - Cook	Jordan Nixon - Student (UU)

EXECUTIVE SUMMARY

The NSGeo survey is a collaborative research survey undertaken by University College Cork and the INFORMAR programme (Geological Survey of Ireland & Marine Institute). Its purpose is to collect baseline information from areas of potential interest for future offshore wind farm developments. In addition, valuable data and samples are collected for geo-engineering appraisals of the investigated areas towards a comprehensive understanding of geological sub-bottom architecture and contemporary sedimentary processes. The survey targeted three areas in Irish and Northern Irish waters:

Dungarvan area

Saltee Island area

Killkeel and Dundrum Bay area

Due to exceptional weather conditions, **49.7 m of vibro cores** were recovered during 33 successful vibro corer deployments. All vibrocores were opened and described on board and the recovered sediments contain over consolidated tills, sands and muds. In addition, **31 shipek grab samples** were collected. **476 nautical miles (882 km) of sparker seismic lines** were recorded. Due to extremely flat seas, the sparker data sets are of excellent quality. Parallel to the sparker seismic data also multibeam echosounder data were recorded.

BACKGROUND

Ireland has excellent offshore renewable energy resources. Experience with offshore wind farm development (e.g. the Arklow Bank; Scroby Sands) have in the past highlighted the potential for cost inefficiency during offshore development due to e.g. scour, as seabed and sub-seabed properties and dynamics had not been considered appropriately. Maintenance costs incurred through unpredicted seabed scour resulted in extensive additional rock armour of turbine bases at considerable expense, while scour around the rock armour is often even greater than around the original base. This is a cost avoidable with adequate foundation design based on sound geotechnical appraisals of the seabed. The costs of foundation maintenance are therefore of central importance for the economic viability of an offshore installation.

The siting of wind farms requires consideration of foundation design with foundations easily taking up one third of overall investment. Although it is theoretically possible to site wind turbines anywhere offshore, different substrates (and sub-substrates) require different foundation designs (e.g. monopile, tripod, gravity base, steel jacket) and installation approaches (e.g. driving and/or drilling, or suction caissons). Major worries around the Irish coast are for instance large boulders and stiff clays from Pleistocene glacier deposits. An early-development foundation design allows for a tailor-made installation strategy, and thus reduces the costs of transportation, associated crane capacity and the very substantial equipment on the Jack-Up vessels usually required to put these foundations in place. The conditions of the seabed also define where Jack Up vessels best rise on their jack-up legs. Last but not least, seabed mobility will define the strategy of cable emplacement, often the Achilles‘ heel of a wind farm.

The cost of installing wind turbines in inappropriate substrates can prohibitively affect the viability of the development of a wind farm, leading to the concept of cost recoverable foundation solutions and grid emplacement. Because of the nature of the seabed, some marine areas will simply never allow profitable wind farms to be developed there. Knowing what areas of the seabed possess appropriate sedimentary sequences allowing profitable wind farm development is thus a first order need and first step assessment towards a national windfarm development strategy.

During this cruise 3D seabed topographic, hydrodynamic, sedimentological and sub-seabed seismic data was collected from offshore of the south coast of Ireland and from the northern Irish Sea. This was to analyse the marine environmental conditions and thus to optimise the foundation design for offshore renewable energy infrastructure. By recording, mapping and analysing fundamental information on seabed and sub-seabed geotechnical properties, significant knowledge gaps with potentially major bearings on the practicality and costs for both installation and maintenance of offshore renewable energy infrastructure through tailor made designs for foundation and cable emplacement can be addessed. Data collected during this survey will also feed into academic research attempting to understand the development of offshore sedimentary sequences around Ireland. Such sequences provide a palaeo-environmental and potential palaeo-climatic record. Understanding the geological history of glacial low-lying coastal areas (now submerged due to sea-level rise) is of fundamental importance in understanding ice sheet dynamics. The Irish shelf areas have likely been completely covered with glaciers once, but the limits of the British and Irish Ice Sheet (BIIS) during the Last Glacial Maximum, and in particular the marginal setting to the Irish Sea Ice Stream, have been much debated. Both sites on the south coast and in the northern Irish Sea have a key role to play to reconstruct the dynamics of the BIIS. Mapping the sequences using sparker seismics and obtaining vibrocores through these sequences gives us the real possibility of advancing not only our understanding of the Quaternary and archaeological history of offshore Ireland, but to provide general insight into rapidly collapsing ice sheets. Furthermore, data collected during this survey can be used to gain a better understanding of contemporary sediment dynamics in these areas. This data will enable us to look at bedform migration rates and thus general seabed mobility. We will assess bedform morphology and we will compare bedform development with quantified peak + average current intensities and spatial variation in current intensity + orientation. Particle size analysis of collected sediments will allow a

validation of results. An understanding of sediment transport dynamics and bedform migration rates is of importance to all offshore engineering exercises, coastal sediment budgets and management, and generates a fundamental understanding of how the seabed changes over short time scales (not just as a snapshot).

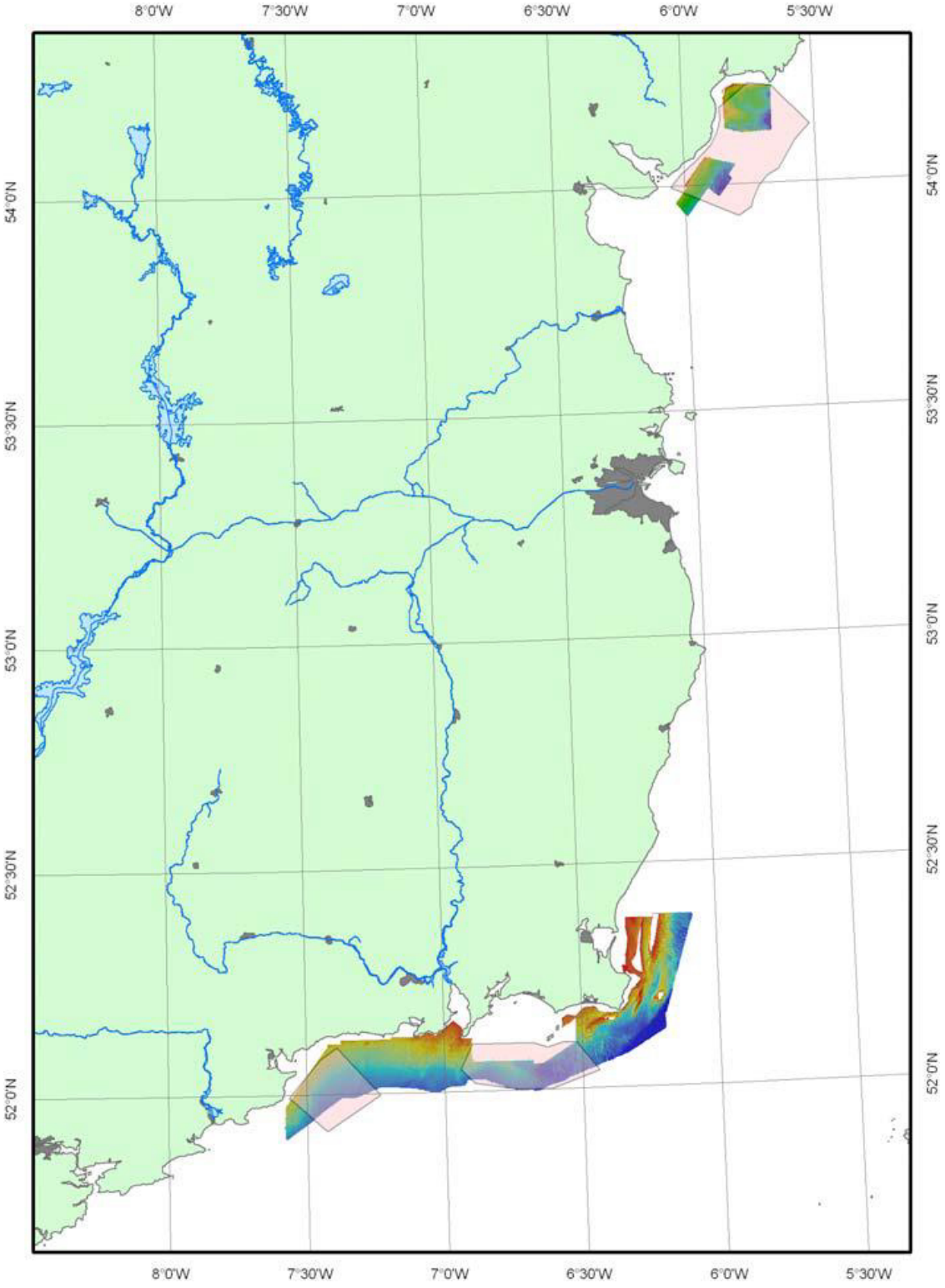

Figure C-1. Overview of the survey areas (shaded in red).

SURVEY RATIONALE AND OBJECTIVES

The key objectives of this cruise are:

- to determine the sub-seabed stratigraphy (the succession of sedimentary layers below the seabed) in high probability areas for renewable energy farm development with particular relevance to the industry's requirements: the lateral extent and variability in e.g. variation in strata thickness, depth, internal sedimentary unit properties and acoustic reflectivity; thus to advise the industry on optimised foundation designs in target areas

- to obtain physical samples from the sub-seabed for geotechnical analysis e.g. shear strength, load capacity, internal friction, density, cohesion etc

- to obtain and analyse physical samples from the sub-seabed to determine the palaeo environmental development of the seabed and submerged coastline and low lying terrestrial areas through time

- to map the spatial distribution and morphological characteristics of sedimentary bedforms and collect physical samples to advance our understanding of seabed mobility in key areas and to advise the industry on optimised cable emplacement strategy in target areas

- to provide this data as (1) base-line data to both government bodies and industry for both site selection and future environmental assessment, and (2) key data to allow for realistic financial modelling for cost-effective installations and maintenance of offshore renewable energy farms.

Data was collected at two sites, north and south of the border, in areas of identified windfarm development potential. The data from this project feeds into a PhD programme (for Marian

McGrath) funded by the Universities of Ireland North-South Postgraduate Research Programme and INFOMAR Programme.

EQUIPMENT

The following equipment was used during the survey:

Research Vessel – RV Celtic Voyager

The Celtic Voyager is a 31.4 m multi-purpose research vessel. The vessel has wet, dry and chemical laboratories, which are permanently fitted with standard scientific equipment and can accommodate 6-8 scientists with a maximum endurance of 14 days. The vessel is manned by an experienced crew who are highly skilled with the handling and deployment of scientific equipment. The Celtic Voyager is equipped with a Trimble NT Differential GPS and Kongsberg Simrad Seapath 200 motion reference unit. A 10,000kg general purpose winch hooked through the aft, 4 m high A-frame as well as a 500 kg starboard CTD winch and 1000kg starboard oceanographic winch.

Figure C-2 The RV Celtic Voyager.

Simrad EM3002D multibeam echosounder

The EM 3002 is a high resolution shallow water multibeam echosounder with dynamically focused beams suitable for 0.5 to 150 m water depth acquiring bathymetry and backscatter data. The transducers are hull mounted and, depending on the accuracy of positioning, the horizontal accuracy (x,y) is usually less than 50 cm and the vertical accuracy (z) less than 15 cm for the processed bathymetry data.

Figure C-3 Hull mounted multibeam transducer on the RVCeltic Voyager (photo of the Marine Institute).

EM1002

The EM1002 is the older version of the multibeam echosounder with a slightly lower resolution than the EM3001.

Geo-Source 400 Sparker Seismic system

The Geo-Source 400 sparker seismic system of the Marine Institute was used during the survey. This sparker seismic system consists of the Geo-Spark 6 kJ pulsed power supply which emits a pulse to the sparker source which is towed behind the vessel. The source comprises four electrode modules that are evenly spaced in a planar array. The return signal is picked up in Geo-Sense single channel hydrophone array.

Figure C-4 Geo-Spark 1500 power supply and towed Geo-Source 400 Sparker source.

Geo-Resources 6000 vibrocorer

A 3 m vibrocore was used and deployed via the A-Frame. As the vessel does not have dynamic positioning, the vibrocore was only deployed at slack water when there was limited windage. The vibrocore was lowered to the bottom, activated for a maximum of 1.5 minutes and recovered. Cores contained in the core-liners were cut into 1 m lengths, caped, sealed with electro tape and labelled.

Immediately after recovery, the vibro cores were labelled, cut and split. The archive halves were cleaned, described and cone penetrometer tested (cpt) with a handheld freefall cone penetrometer. Cpt was performed at 5cm intervals. The work halves where only cleaned for later on-shore sampling. All core halves were wrapped with cling-film and stored at ambient temperature in the wet lab.

Figure C-5. The Geo-resources 6000 vibrocore being deployed.

Shipek sediment sampler

A Duncan & Associates Shipek sampler was used to sediment samples in both muddy, sandy and gravelly substrates. The sampler scoops a sediment sample from the top 10 cm of the seabed. The Shipek grab was deployed on the starboard winch mid-ship. All Shipek grab samples were described, photographed and sub-sampled for later on-shore analyses. All grab samples were stored in the wet lab at ambient temperature.

Figure C-6. Shipek sampler recovered after a successful deployment.

AML Smart SVPlus

The AML SV Plus is a shallow water sound velocity profiler recording sound velocities and pressure through the water column.

Figure C-7. AML Smart SV Plus.

SUMMARY OF AREAS

Dungarvan Area

The Dungarvan Area measured roughly 18 x 18 km encompassing 336 km² of varying degrees of silt, sand and gravel as seen from 3m vibrocores taken within the area. Water depths varied from 20 to 55m. Multibeam data revealed what appeared to be bedrock outcropping at the surface at the western and eastern ends of the area. From initial seismic data it was possible to infer channelling which had been subsequently infilled.

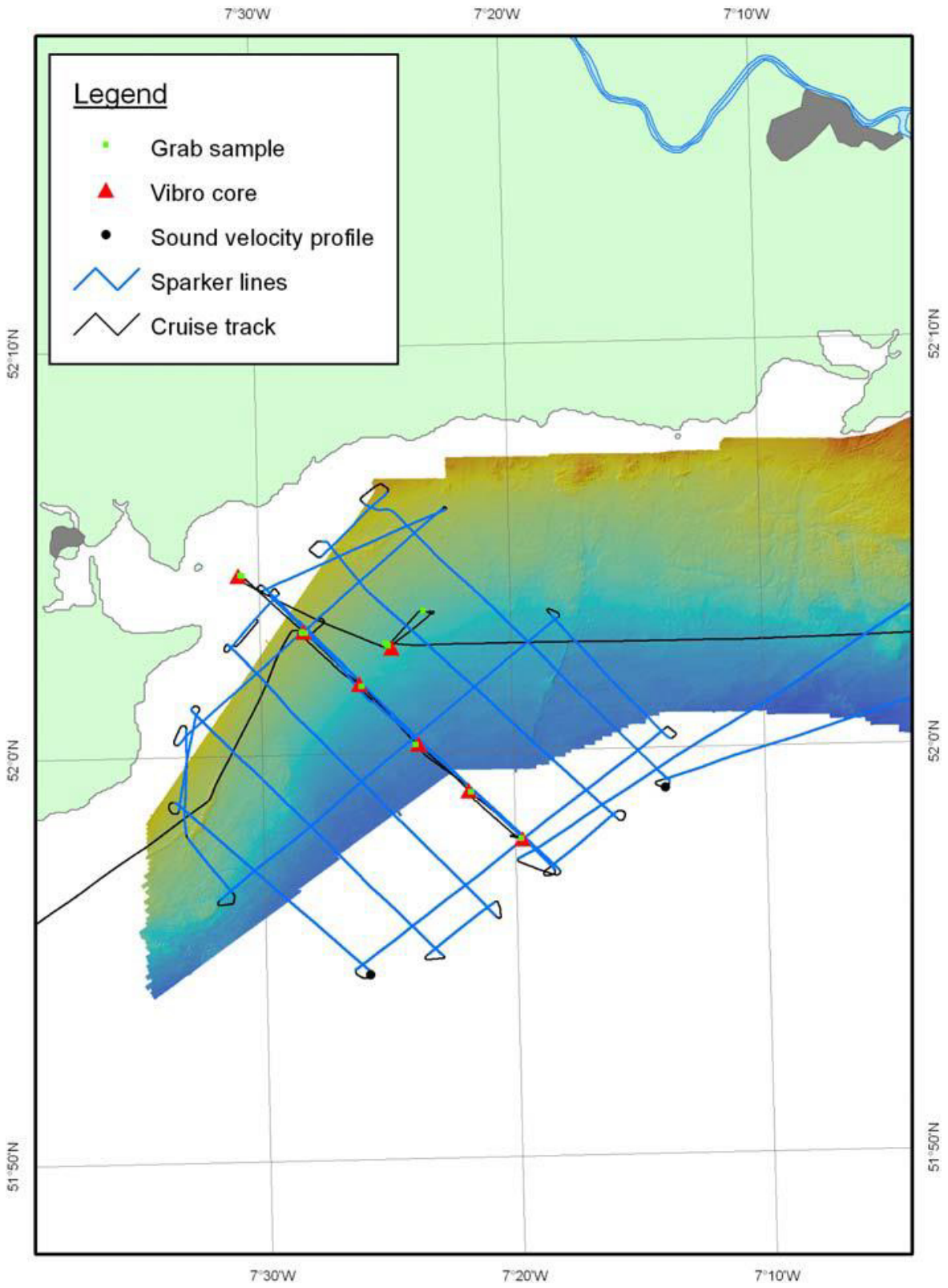

Figure C-8. Dungarvan survey area.

Saltee Island Area

This is a relatively dynamic area with large sand waves noted in the eastern half. The area covered 515km² of the seafloor consisting largely of mobile sands overlying a strong initial reflector interpreted as glacial till. Bedrock was marked by a second strong reflector exhibiting distinct anti and syncline features similar to onshore exposures. Infilled channelling was again prevalent in the area, most likely an extension of the River Barrow. Vibrocores with a maximum depth of 3 m revealed surface sediments to be composed largely of silts and sands with a minor gravel component in certain areas.

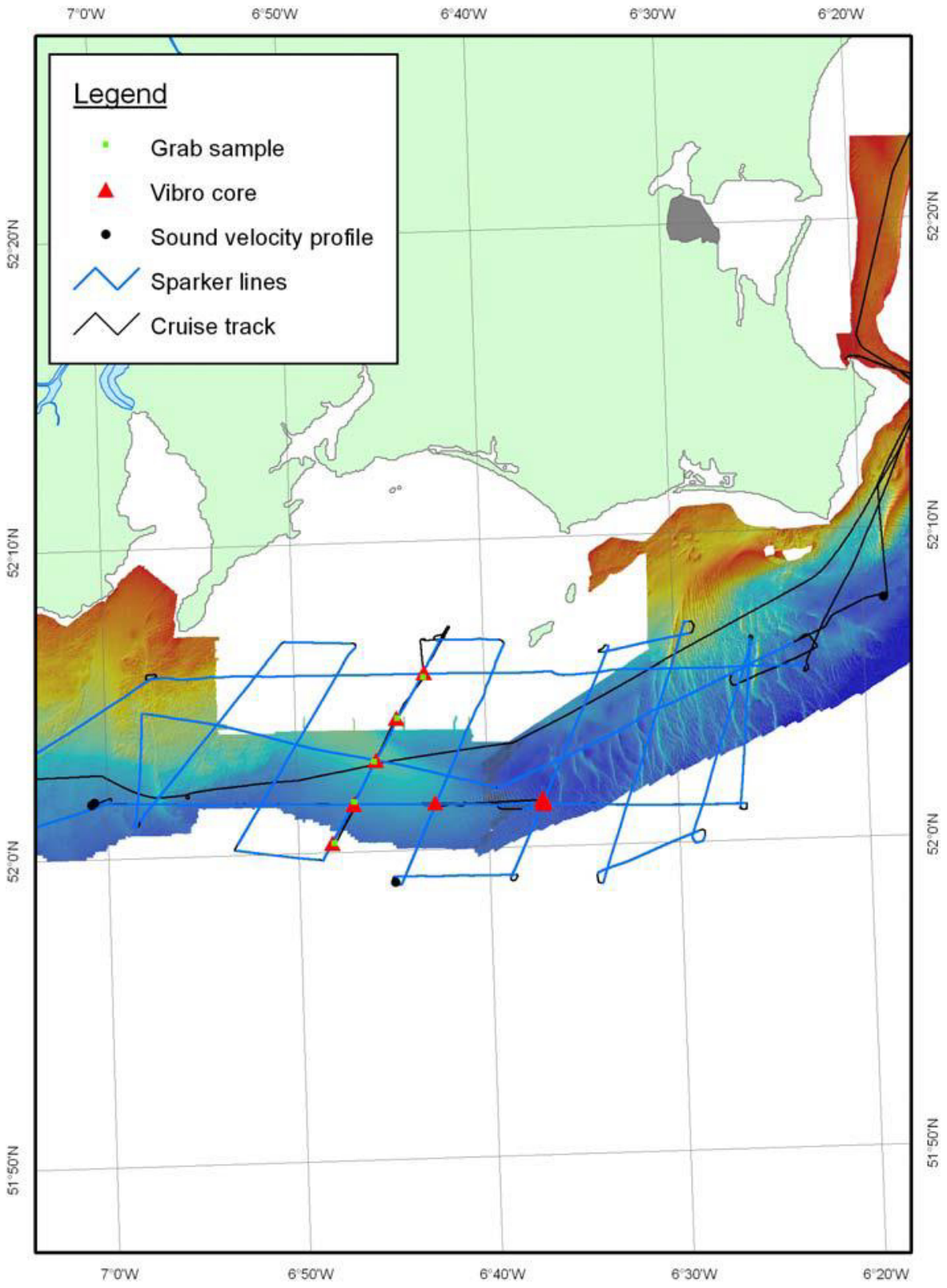

Figure C-9. Saltee Islands survey area.

Killkeel & Dundrum Bay Area

The Killkeel Area located north of Carlingford Lough is 122 km² in size and is distinguished by sand and silt overlying consolidated clay infilling a series of channels which run between outcropping lithified till that contains boulders up to 30 cm in diameter. Attempts to core and grab sample this outcropping till proved unsuccessful. Away from shore in the deeper section of the area surface sediments were mainly sands and silts often with a clay component. Coring attempts in this section were often unsuccessful, possibly due to the uneven topography.

The Dundrum Bay area just north of Killkeel was similarly composed of seemingly outcropping lithified till which led to difficulties coring and sample grabbing close to the shore in the 247 km² area. In the deeper section mainly silts and sands with some gravels were found, often overlying consolidated clays. Channeling was observed on preliminary seismic profiles.

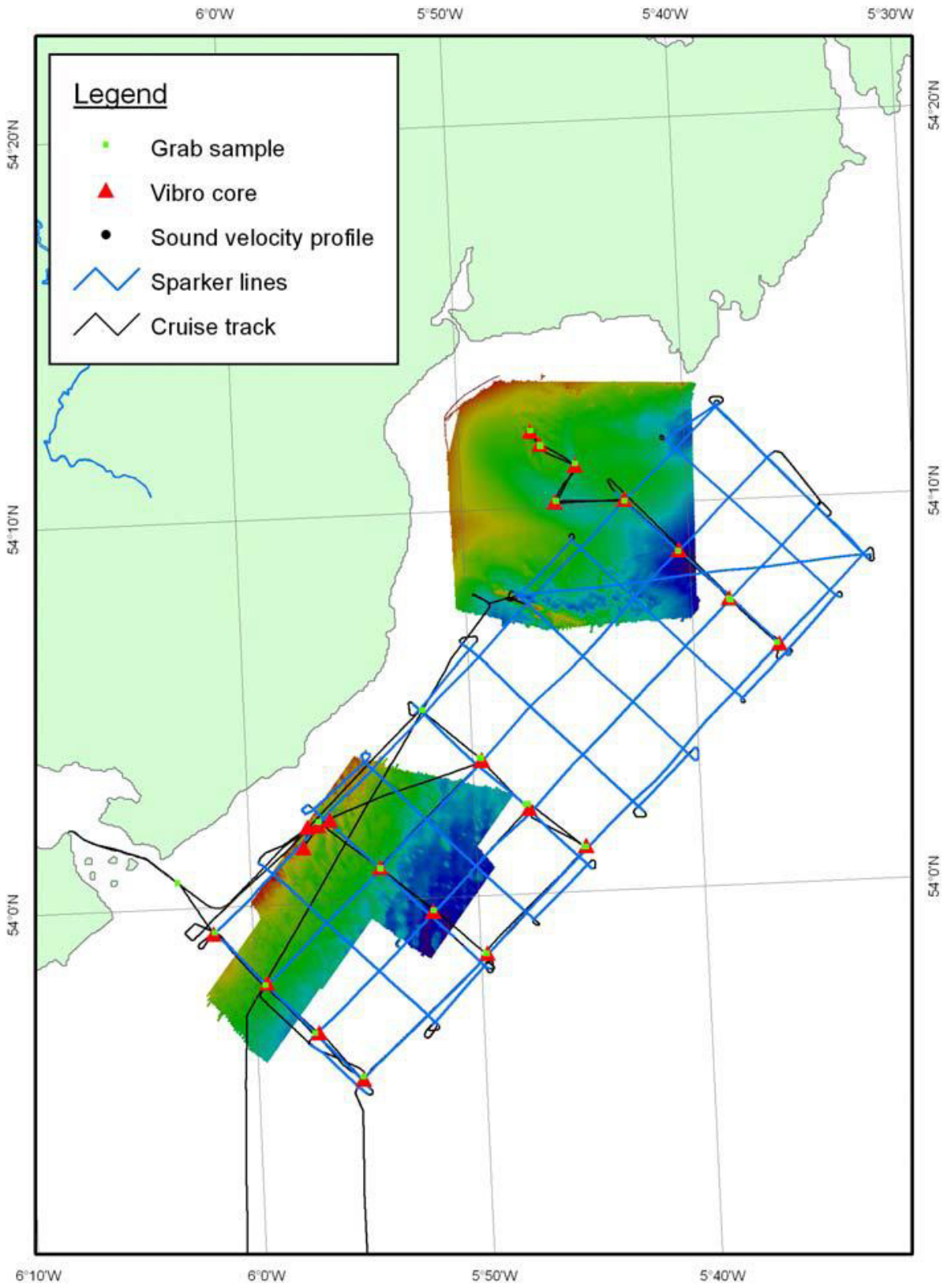

Figure C-10. Killkeel and Dundrum Bay survey area.

Vibro core section list

Cruise	Core	No. of section	Total length	Section	Section	Section
			cm	cm	cm	cm
CV12_UCC	001	2	165	0-65	65-165	
CV12_UCC	002	2	171	0-71	71-171	
CV12_UCC	003	2	135	0-35	65-135	
CV12_UCC	004	1	39	0-39		
CV12_UCC	005	1	31	0-31		
CV12_UCC	016	1	54	0-54		
CV12_UCC	017	2	137	0-37	37-137	
CV12_UCC	022	3	247	0-47	47-147	147-247
CV12_UCC	023	1	56	0-56		
CV12_UCC	024	3	211	0-11	11-111	111-211
CV12_UCC	025	3	272	0-72	72-172	172-272
CV12_UCC	026	3	292	0-92	92-192	
CV12_UCC	036	3	286	0-86	86-186	186-286
CV12_UCC	037	3	257	0-57	57-157	157-257
CV12_UCC	038	3	258	0-58	58-158	158-258
CV12_UCC	039	3	292	0-92	92-192	192-292
CV12_UCC	040	3	285	0-85	85-185	185-285
CV12_UCC	041	3	302	0-102	102-202	202-302
CV12_UCC	043	2	139	0-39	39-139	
CV12_UCC	044	1	35.5	0.35.5		
CV12_UCC	045	3	208	0-11	11-108	108-208
CV12_UCC	046	2	172	0-72	72-172	172-272
CV12_UCC	047	2	128	0-28	28-128	
CV12_UCC	048	1	62	0-62		
CV12_UCC	049	1	39	0-39		
CV12_UCC	053	1	93	0-93		
CV12_UCC	054	2	105	0-13	13-108	

Figure C-11. Cores gathered during this survey. Cores used in this thesis are highlighted in yellow and presented below.

CV12_UCC_038 Date: 01.04.12 Pos: 52°38.6993'N 05°56.4873'W
Water Depth: 42 m Core Length: 258 cm

Lithology

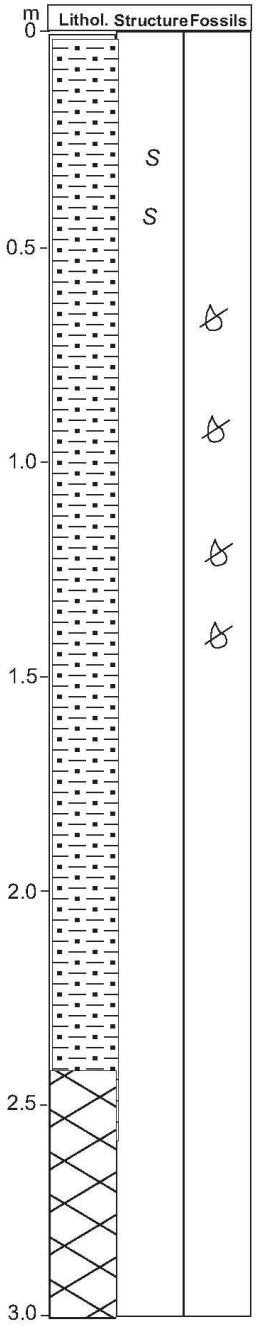

Medium brown muddy silts throughout

Bioturbation represented by dark, organic layers

CV12_UCC_039 Date: 01.04.12 Pos: 53°42.7616'N 05°57.5076'W
Water Depth: 41 m Core Length: 292 cm

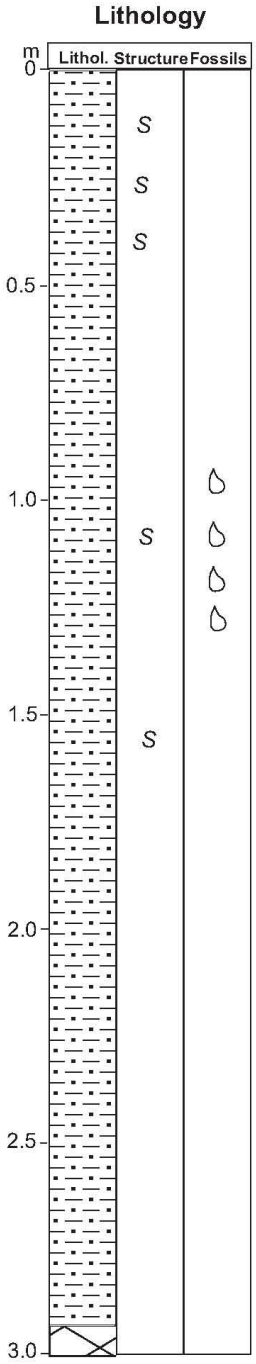

Clayey silt throughout

Bioturbation

Gastropods

Increase in clay component

CV12_UCC_040 Date: 01.04.12 Pos: 53°48.1247'N 06°02.7625'W
Water Depth: ??? m Core Length: 285 cm

Lithology

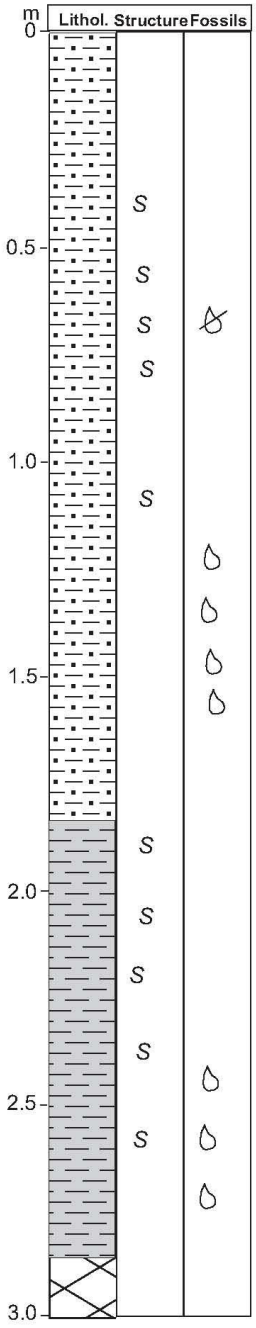

Clayey silt throughout

Bioturbation

Gastropod layer

Increase in clay component

Gastropod layer

CV12_UCC_041 Date: 01.04.12 Pos: 53°48.3841'N 05°55.49212'W
Water Depth: 44 m Core Length: 302 cm

Lithology

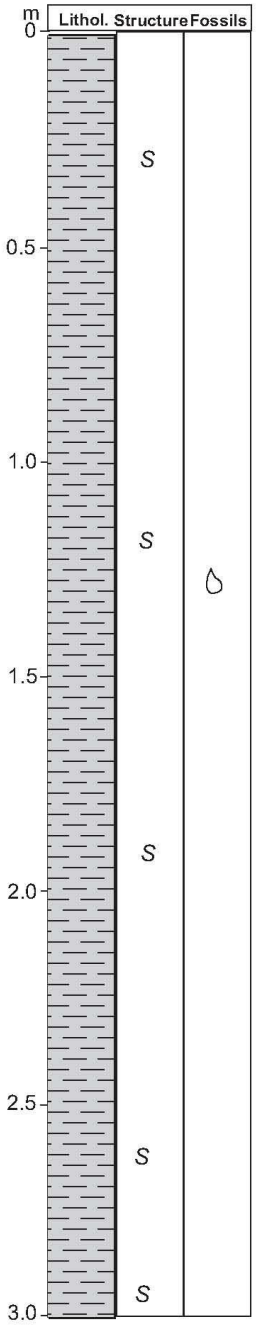

Dark grey/ brown silty clay with subtle bioturbation throughout

Burrow with silty infill

Infilled burrow

Appendix D

SURVEY CE14001 CRUISE REPORT

Appendix D

Research Cruise: RV Celtic Explorer – Survey CE14001; Developing Geotechno-stratigraphies (Leg 2)
10th – 17th January 2014

Ship's crew	Scientific Party
Denis Rowen *Master*	Prof. Andy Wheeler *Chief Scientist (UCC)*
Mark Ivory *Chief Engineer*	Prof. Dr. Tobias Mörz *Scientist/GOST team leader (MARUM)*
Basil Murphy *1st Mate*	Mark Coughlan *Geologist – Night watch leader (UCC)*
John O'Regan *2nd Mate*	Marian McGrath *Geologist - Day watch leader (UCC)*
Ted Sweeney *2nd Engineer*	Aaron Lim *Geologist (UCC)*
Paul Wray (10th -15th Jan) Dave Stuart (15th – 17th Jan) *ETO*	Wolfgang Schunn *Technician/GOST operator (MARUM)*
Frank Kenny *Bosun*	Christian Bathmann *Scientist/GOST operator (MARUM)*
Shane Horan *Bosun's Mate*	Johannes Brock *Scientist/GOST operator (MARUM)*
Michelin Faherty *AB Deckhand*	André Kahl *Scientist/GOST operator (MARUM)*
Martin Goggin *AB Deckhand*	Daniel Otto *Scientist/GOST operator (MARUM)*
Tom Gilmartin *AB Deckhand*	Antoinette McCarthy (10th -15th Jan) *Student (UCC)*
Jimmy Burke *AB Deckhand*	Brennus Voarino (10th -15th Jan) *Student (UCC)*
Philip Gordon *Technician*	
Jimmy Moran *Cook*	
Mark Masson *Assistant Cook*	
Daniel Rose *Engineer Cadet*	

Compiled by
Prof. Andy Wheeler (Chief Scientist)
Mark Coughlan (Night watch leader)
Scientific Party (data input, corrections to drafts and minor text)

EXECUTIVE SUMMARY

This is the second part of a two part survey to define offshore stratigraphies. The initial survey (CE13003) concentrated on NW Celtic Sea and offshore Dungarvan- the Saltees, collecting cores and seismic data for palaeoenvironmental and geotechnical studies. The overall objective to understand the control of palaeoenvironments on sedimentary sequence development and how, in turn, this controls geotechnical sub-seabed properties.

The purpose of this survey was to perform in situ Cone Penetration Testing (CPTu) in order to ground truth previously collected seismic data and obtain geotechnical data regarding the nature of sediment at depth. This involved a collaborative effort undertaken by University College Cork, MARUM (University of Bremen), the Marine Institute and Gaelectric Developments Ltd. The main area of focus was the North-western Mudbelt area of the Irish Sea; a large area earmarked for offshore renewable energy development. The Lambay Deep area was also the subject of a seismic survey to identify buried tunnel valleys and one site for CPT deployment.

Under a 24 hour work routine, **17 sites** were surveyed using the MARUM designed and built Geotechnical Offshore Survey Tool (GOST). In total some **306.17 m** of good, in situ sub-seabed geotechnical data was collected identifying a succession of inferred glacial layer overlaying bedrock, in turn overlain by an unconsolidated marine mud layer. Thickest accumulations of sediment were found towards the centre of the area with bedrock and glacial sediments occurring close to the surface in the west and south.

In the Lambay Deep area, **66.3 km** of sparker lines were shot imagining three valley structures. Two of these valleys were infilled and showed a complex fill history. The third was open and part of the Lambay Deep system.

BACKGROUND

The development of the Pleistocene sedimentary sequences in the Irish Sea is complex and records episodes of glacial and glaciomarine deposition, fluvioglacial erosion and deposition,

marine transgressive surfaces and sea level high stand marine sedimentation. Understanding the history of Irish Sea Pleistocene deposition provides us with a fuller understanding of British-Irish Ice Sheet dynamics and palaeoenvironmental responses to Pleistocene climate and sea level change. By understanding the dynamics of Irish Sea environments in the past, we can appreciate the dynamics of future climate and sea level responses in the Irish Sea.

Although numerous studies on coastal exposures have revealed valuable information, these settings are peripheral to the Irish Sea proper which house, at least in the last glacial, a significant surging Ice Stream and has repeatedly cut major meltwater channels.

Accessing these sequences, which are often buried 10's of metres, is costly. Building on previous studies, both by UCC over the last 10 years and the BGS in the 1970s and 80s, this survey focussed on the seismic investigation of deeps marking former meltwater channels and the groundtruthing of previous seismic studies using an in-situ cone penetrometer (GOST-CPT) that provides geotechnical and inferred sediment composition data has cm resolution down to 40 m.

In addition, the GOST-CPT data is of interests to offshore renewable energy developers who can use this data to assess potential foundation device solution for offshore energy devices. Ireland has one of the best offshore renewable energy resources in the world. The development of this sector has the potential to yield thousands of new jobs as well as providing Ireland with future energy security.

The siting of wind farms, tidal turbines and near-shore wave energy converters requires significant consideration of foundation design with foundations easily taking up one third of overall investment. Although it is theoretically possible to these technologies anywhere offshore with sufficient resource, different substrates (and sub-substrates) require different foundation designs (e.g. monopile, tripod, gravity base, steel jacket) and installation approaches (e.g. driving and/or drilling, or suction caissons). An early-development foundation design allows for a tailor-made installation strategy, and thus reduces the costs of transportation, associated crane capacity and the very

substantial equipment on the Jack-Up vessels usually required to put these foundations in place. The conditions of the seabed also define where Jack Up vessels best rise on their jack-up legs.

SURVEY RATIONALE AND OBJECTIVES

The key objectives of the proposal are:

- to determine the sub-seabed stratigraphy (the succession of sedimentary layers below the seabed) in high probability areas for renewable energy farm development with particular relevance to the industry's requirements: the lateral extent and variability in e.g. variation in strata thickness, depth, internal sedimentary unit properties (boulders!) and acoustic reflectivity; thus to advise the industry on optimised foundation designs in target areas

- to obtain physical samples from the sub-seabed for geotechnical analysis e.g. shear strength, load capacity, internal friction, density, cohesion

- to obtain and analyse physical samples from the sub-seabed to determine the palaeo-environmental development of the seabed and submerged coastline and low-lying terrestrial areas through time

- to map the spatial distribution and morphological characteristics of sedimentary bedforms and collect physical samples to advance our understanding of seabed mobility in key areas and to advise the industry on optimised cable emplacement strategy in target areas

- to provide this data as (a) base-line data to both government bodies and industry for both site selection and future environmental assessment, and (b) key data to allow for realistic financial modelling for cost-effective installations and maintenance of offshore renewable energy farms.

These objectives will be achieved at several sites off the south coast that are potential areas of identified windfarm development.

The data from this project feeds into the existing PhD programmes of Marian McGrath and Mark Coughlan as well as proposed PhD and post-doctoral researcher through the SFI Research Areas call (pending).

EQUIPMENT

Research Vessel - RV Celtic Explorer

The Celtic Explorer is a 65.5 m multi-purpose research vessel. The vessel has wet, dry and chemical laboratories, which are permanently fitted with standard scientific equipment and can accommodate 20-22 scientists along with 13-15 crew who are highly skilled with the handling and deployment of scientific equipment. It has a maximum endurance of 35 days. The Celtic Explorer is equipped with two Trimble 300-D GPS and has Dynamic Positioning (DP).

On the aft deck is a 25 tonne A-frame with 4m outward and inward reach in addition to a 3m, 10 tonne starboard T-frame. The ship also comprises of a midship, forward and aft crane as well as a 6 tonne CTD winch.

Figure D-1. RV Celtic Explorer.

GOST Cone Penetration Test System

Figure D-1 GOST system on deck

The Geotechnical Offshore Seabed Tool (GOST), designed and developed at the MARUM Institute, University of Bremen in Germany, is an innovative geotechnical tool used to characterise the subsoil by means of "push-in tools" such as cone penetration testing or CPT. It is designed to operate from the seafloor in water depths of up to 4,000m with a penetration depth of 6-40 m. Its primary focus is as an offshore site investigation tool in aid in foundation design, cable/pipeline route surveys and environmental mapping.

During continuous operations, GOST can be slightly lifted from the seafloor during transit times and so allow for maximum use of valuable shiptime as there is no need for full recovery and subsequent redeployment at new sites.

The GOST itself weighs between 2 and 8 tonnes depending on the addition of weighted plates for extra stability. It has its own mobile winch with a mobile hydraulic power unit allowing for easy and quick deployment using a three point suspension. It has 8,000kg of hydraulic push power with infinitely variable hydraulic pressure of 0-200bar. The cone tip has a cross section of $5cm^2$ and is composed of hardened stainless steel. Recording measurements such as tip resistance, sleeve friction, differential pore pressure, inclination and acceleration, it has a resolution of 0.06 MPa

allowing for a range up to 120MPa. Additionally, it CAN be fitted with sensors for heat conductivity. Exact control on push velocity during penetration allows for data to comply to the highest international including DIN 4904 requirements. The interface is a digital one of industrial RS485 BUS using direct A/D converting of a measured variable with overvoltage and reverse protection.

Geo-Source 400 Sparker Seismic system

The Geo-Source 400 sparker seismic system of the Marine Institute was used during the survey. This sparker seismic system consists of the Geo-Spark 6 kJ pulsed power supply which emits a pulse to the sparker source which is towed behind the vessel. The source comprises four electrode modules that are evenly spaced in a planar array. The return signal is picked up in Geo-Sense single channel hydrophone array. The system provides high resolution (<30cm) seismic profiles of the Shallow subbottom strata. The device achieves this level of accuracy due to its multi-tip array of sparker nodes, which are evenly spaced and set in-phase producing a very strong downward projection of acoustic energy. The system which is designed to be towed on or just below the water-surface. High resolution seismic profiles of up to 300m depth can be imaged using the Geo-Spark 200 depending on the composition of the water column, sea conditions and the nature of the underlying geology.

Figure D-2 Sparker system.

Sound Velocity probe

The AML SV Plus is a shallow water sound velocity profiler recording sound velocities and pressure through the water column.

Figure D-3 Sound Velocity probe.

SURVEY NARRATIVE

Friday 10th January 2014

Calm, cloudy and occasional drizzle.

Wind speed 7 m s-1. Wind direction 270^{o}. Swell 0.5m

08.00 - Start mobilisation of GOST system to modified deck and modified A-frame. Progress good with a few setbacks overcome.

20.00 - Depart Dublin Port for the Northern Irish Sea Mudbelt. All heavy lifting complete, final checks to GOST system and construction of GOST personnel gantry completed on route.

Saturday 11th January 2014

Calm, Wind speed 10 m s-1 .Direction 230^{o}. Swell 0.5m.

00.03 - Arrive on station for first CPT deployment (**CV14001_001**) in the middle of the mudbelt. Dynamic positioning took 15 minutes to fine tune and stabilise ships position.

02.32 – 30 m of rod constructed on GOST and starting to push into seabed

03.35 – 30 m penetration achieved (**CV14001_001**).

03.45 – On recovery it was discovered that the rod broke, only 3m of rod recovered.

04.05 – GOST system recovered on deck. Transit to most NWerly CPT site.

05:30 - Arrive on station (Station 2, originally Station 6). Maintenance of GOST continues.

09:00 - Deployment of the GOST began in earnest. 10 rods used.

10:00 - GOST began collecting data at Station 2 (**CV14001_002A**).

10:09 - the push was halted due to the probable presence of a stone or cobble. It was decided to retrieve the rod to the seabed, move the GOST a few metres to the side and begin again in hopes of going deeper without causing possible damage to the probe. Hence Station 2 is divided into Station 2a and 2b.

10.23 - GOST began collecting data at Station 2 again (**CV14001_002B**).

10:37 – GOST aborted as hit a stone at 75cm at Station 2B

10:47 – Cone damaged so GOST returned to surface to replace the cone. Cone was tested in the water column which confirmed damage.

11.35 – GOST on deck and damaged cone inspected and replaced with a more robust cone but with decreased data quality.

15.40 – GOST began collecting data at Station 2 again (**CV14001_002C**).

15.45 – Started to push **CV14001_002C** into seabed at 15MPa per second

15.54 – Aborted **CV14001_002C** at 3.3m (Unit E) due to high resistance as in **CV14001_002B**.

16.15 - Transit 1.5 nm to Station 3 at 1.9 kts

17:14 – GOST on the bottom of Station 3 (**CV14001_003**). Started to push cone into seabed. Limit was set at 20mPa and exceeded this limit at 3.75m so the limit was increased to 30mPa. There is a break in the data where the limit was reset so will show as files 3_1 and 3_2. When the 30mPa limit was applied and penetration started it peaked again at 3.75m.

17.45 – GOST aborted at 3.75m at 30 MPa due to concern on the GOST system's limit. GOST was then taken up and with the top few metres of rod decoupled and the system held just in the water tight to the stern. This arrangement enabled us to transit at 3 kts in the dark in an area of potential crab pots.

18.00 – Transit to station 4 at 3 kts commenced.

20.55 - Arrive at Station 4 and start lower GOST to seabed.

21:22 – GOST on the bottom of Station 4 (**CV14001_004**). Started to push cone into seabed. A depth of 3.38 m was reached before the push was aborted when 30 mPa was reached and the GOST recovered and secured to the back of the ship for transit.

22.16 – Began transit to next station (Station 5) at 3 kts.

23.12 - Arrive at Station 5 and start lower GOST to seabed.

23:38 – GOST on the bottom of Station 5 (**CV14001_005a**). Started to push cone into seabed. During recording data was split into 2 files. A stone was encountered at 10 m reaching a peak of 10

mPa. The push was discontinued at 00:12 (Sunday 14th); the GOST raised from the seabed and moved 2/3 m (station 5b) in order to try again.

Sunday 12th January 2014

Calm, Wind speed 19 m s-1, wind direction 141°. Swell 1.0m deteriorating to Wind Speed = 28.0 m s-1 but gusting 38 m s-1, wind direction = 160°, swell height 2.7m. Gale force 8.

00:45 – Second push started at Station 5 (**CV14001_005B**). A peak of 30mPa in the data was encountered at 2.6 m, subsequently the data was divided into 2 parts (A and B). 8 m saw an increase of up to 2 mPa which gradually increased further. At 01:08 the limiter peak of 30 mPa was encountered and so the push stopped. The GOST was recovered. As it was discerned that trawling had recently taken place in the area and hence there was little likelihood of encountering static gear, the GOST held 6 m above the seafloor and moved to the next station (Station 6) at a speed of 1 knot initially. At this stage the sea-state began to noticeably pick up.

01:39 - Began transit to next station (Station 6_aborted).

02:38 - DP bow thruster tripped. RV Celtic Explorer deviates slightly from course on transit.

03:06- On site at Station 6_aborted.

03:09- Just prior to redeployment of GOST. Technical issues arise. Rods have become parted during transit. A cone and some rods are lost. The GOST is recovered for maintenance. Poor and deteriorating weather inhibits redeployment: bow thrusters would not be able to hold position, excessive pitch on the aft deck makes deployment and recovery dangerous, GOST heave compensator would be under severe strain.

11.00 - Weather update:

Bad weather throughout Sunday morning so can not deploy CPT. Wind Speed = 28.0 m s-1 but gusting 38 m s-1, wind direction = 160°, swell height 2.7m. Gale force 8. Weather should improve after 20.00.

18.00 – Weather update:

20:00- After consultation with the bridge and Bosun it was decided to wait until 21:00 to try and deploy the GOST.

21:00- Sea state greatly improved. Decision was taken to deploy GOST

21:02 - On station (new Station 6)

21:18- GOST deployed off the stern. Some initial issues with the gangway were solved by some gentle persuasion from Jimmy and his hammer. Rod string being constructed.

21.30 - Weather update:
Wind Speed = 11.0 m s-1, wind direction = 231°, swell height 1.5m.

22.32 - GOST on the bottom of Station 6 (**CV14001_006**). Started to push cone into seabed. Penetration down to 23.5m into till eventually.

Monday 13th January 2014

Sea progressively calming in the early morning. Wind speed 13 m s-1. Wind direction 209. Swell 1.5 m.

00.44 - Began transit to next station (Station 7) at 1kt initially to see how the GOST system performs in the water. Speed increased to 1.2 kts.

02.01 - On station (new Station 7)

02.06 - GOST on the bottom of Station 7 (**CV14001_007**).

03.30 – Left station 7 (**CV14001_007**). Now on route to next station (**CV14001_008**).

04:17- On station (Station 8)

04:24- GOST on Seabed (**CV14001_0078**)

04:36- Started pushing (**CV14001_008**)

05:18- Stopped pushing at a depth of 19 m. No till was encountered with cone resistance values staying relatively low (<2 mPa). Recovery of the GOST began.

06:06- GOST lifted off the seabed and transit to next station began (Station 9)

06:58- Arrived at Station 9 and GOST was deployed.

07:07- GOST on the seabed at Station 9 (**CV14001_009**)

07:15- Push started

07:57- Pushed stopped having reached a depth of 19 m (**CV14001_009**)

08:04 - GOST lifted off the seabed and move to Station 10 started.

10.17 – GOST deployed at station 10 (**CV14001_0010**). Penetrated to 20m and hit bedrock.

2121.07 – GOST lifted off the seabed and move to Station 11 started on DP at 1.5-2 kts.

12.27 – Vibration on the GOST was too high even at 1.5 kts and unsustainable. GOST recovered on deck.

15.00 - Left station 11 on route to next station 12 at 7 knots.

15.50 - Arrived at Station 11. GOST rods to be built to 30m.

17.01 - GOST deployed at station 11 (**CV001_0011)**.Penetrated to 26.5m and hit probable bedrock.

17.10 – GOST lifted off the seabed and move to Station 12 started on DP at 1.4 kts.

20.09 - GOST deployed at station 12 (**CV001_0012)**.

21.14 – Push stopped. Penetration to 26m.

22:13-GOST lifted off the seabed and move to Station 13 started on DP at 1.5-2 kts.

Tuesday 14th January 2014

Calm. Wind speed 17 m s-1 peaking at 30 m s-1 by afternoon. Wind direction 283. Swell 1- 1.5 m rising to 2m by afternoon

00:20- Arrived on site (Station 13)

00:32- GOST on seabed and pushing begins (**CV001_0013).**

01:43- Pushing stopped having reached a depth of approximately 30 m (**CV001_0013)** (this is the world record for the GOST system). Retrieval of the GOST begins.

02:23- As the GOST is retrieves it is discovered that the cone tip has been lost electronically. Therefore, the GOST must return to deck to have a new cone fitted.

04:25- GOST back on deck to have cone replaced and electronics tested. Some water is believed to have gotten into the data cable so will be cleaned. No big deal. Transit to next site (Station 14) begins.

04:55- On site at Station 14. GOST continues to be serviced on the deck.

05:25- Some bended rods. Data cable was replaced on deck.

08:15- GOST redeployed at Station 14 having been mended.

09:27- GOST on sea bed and started pushing with a limit of 15mPa (**CV001_0014).** At 26m there is more sand so the CPT was increased to 20mPa.

10:34 – GOST stopped at 26.7m as passed the 20mPa limit. GOST recovered from seabed, rods dismantled on way up.

13.51 – GOST on deck and sensor changed. Transit to Station 15 at 7 kts.

15.00 – On station 15 (**CV001_0015)**

15.51 – GOST deployed over the stern, rods being built up to 20 m.

16.59 – GOST is on the seabed (**CV001_0015)** and started pushing. Penetration to 18.32m where we hit a stone or bedrock.

17.58 – GOST system retrieved from seabed and brought up above the water line aft of the vessel to allow transit Station 16 which is a second attempt at Station 3.

19.41 – Start transit to Station 16 (**CV001_0016)** with the GOST tight against the stern of the vessel at 9.2 kts.

21.20 – GOST lowered to the seabed to start (**CV001_0016).**

21.43 – Due to an unfortunate wave we hit the seabed with some force and damaged the cone. CV001_0016 aborted.

21:57- During hauling the cable hopped out of GOST sleeve. Therefore, GOST is returned to the seabed to rectify.

22.15 – Sieve fixed and GOST recovery continued.

23:14 – GOST recovered on deck and fixed. Transit to Station 17 (Lambay) 30 nm away at 9 kts.

Wednesday 15th January 2014

Calm. Wind speed 13 m s-1. Wind direction 207. Swell 1- 1.5 m

02:12- On site (Station 17).

02:22- GOST deployed.

03.31 – GOST on the seabed and started pushing (**CV001_0017).** Penetrated to 20m.

04.22 – GOST system recovery started.

06:26- GOST back on deck and transit back to Dublin begins at 5 kts.

09.30 – tie up in Dublin Port and commence demobilisation of the GOST system.

Thursday 16th January 2014

Moderate. Wind speed 21 m s^{-1}. Wind direction 177. Swell 1.5 – 2.0 m. Dropping during the day

07:58 – Leave Dublin Port and transit to Station 18 at 9 kts.

07.15 – Marine Mammal Observations commences prior to soft-start of the sparker seismic system.

08:27- SVP was deployed in the water but not fully due to strong tides. As a result, it was retrieved, the ship went off DP and allowed to drift to find an easier position.

08:34- SVP was redeployed, this time with an added weight on the line. Currents at 3 kts so vessel but on drift with DP hold drift back to allow SVP to go down as vertical as possible.

08:44- SVP taken (**CE001_0018**) and back on board. Ship moved 2 miles to allow for configuration of Sparker system prior to starting first line.

09.50. - Marine Mammal Observations cease and sparker soft start commences.

09.50-13.30 – Sparker data very poor due to weather hampering configuration. Eventually decent data quality achieved on falling sea, after several configurations of sparker and streamer and different setting reasonable geology is seen. Weather conditions still marginal. Head for SOL.

Weather update: *Wind speed 14 m s^{-1}. Direction 198. Swell 2.5m.*

13.59 – SOL **CE001_0019** at 2kts.

15:20- EOL **CE001_0019**

15:31 – Sparker equipment retrieved onboard. Started steaming for next line (Station 19) at 7 knts.

16.15 – Marine Mammal Observations commences prior to soft-start of the sparker seismic system.

17.00 – Sparker deployed and soft start protocol commenced. Continue transit at 6 kts.

17.30 – Soft start complete. Marine Mammal Observations complete.

19.47 – SOL **CE001_0020** at 4 kts.

20.16 - EOL **CE001_0020.** Transit to next line at 6 kts.

20.36 - SOL **CE001_0021** at 4 kts.

21.14 - EOL **CE001_0021.** Transit to next line at 6 kts

21.27 - SOL **CE001_0022** at 4 kts.

21.14 - EOL **CE001_0022.** Transit to next line at 6 kts.

22.44 - SOL **CE001_0023** at 4 kts.

23.15 - EOL **CE001_0023.** Transit to next line at 6 kts.

22.44 - SOL **CE001_0024** at 4 kts.

Friday 17th January 2014

Weather Update (00.30): Moderate. Wind speed F2. Wind direction NNW. Swell ~1m; Slight sea.

00:54- SOL **CE001_0025** at 5.2 kts

01:30- EOL **CE001_0025**. Transit to next line at 5 kts.

02:04- SOL **CE001_0026** at 5.6 kts.

03:37- EOL **CE001_0026**. Transit to next line was slowed by a ferry crossing nearby.

04:12- SOL **CE001_0027**.

05:09- EOL **CE001_0027**. Transit to next line at 4.8 kts.

05:36- SOL **CE001_0028** at 4.9 kts.

06:18- EOL **CE001_0028.** Transit to next line at 4.3 kts.

06.31- SOL **CE001_0029** at 4.9 kts.

06:57- EOL **CE001_0029.**

07.04 – Sparker system recovered. Transit to Howth.

09.00 – Scientific party disembark at Howth via tender Tom Creen.

AREA MAPS: COVERAGES AND SAMPLE LOCATIONS

NW Irish Sea station map

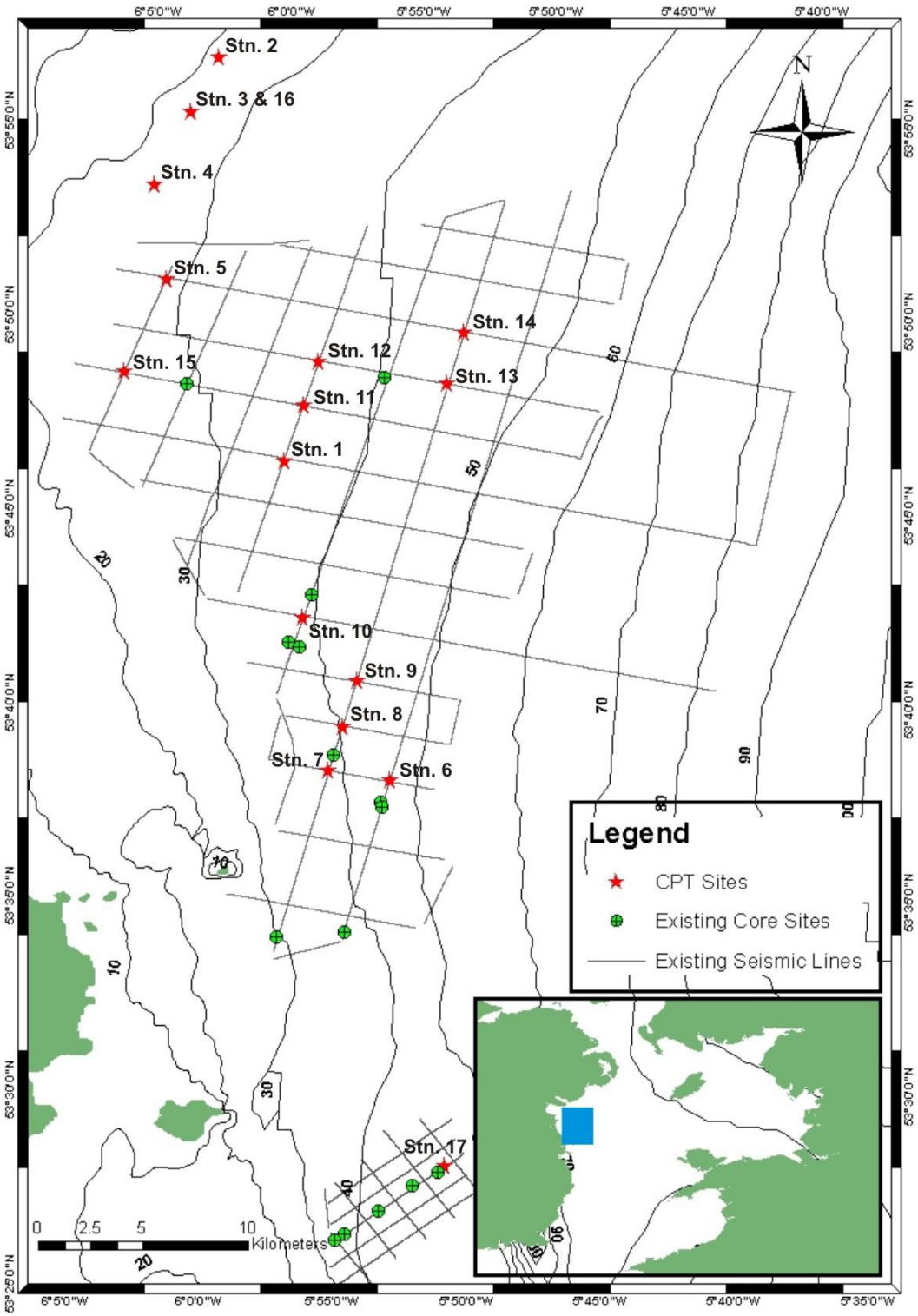

Figure D-5. CPT location map.

Central Sea station map

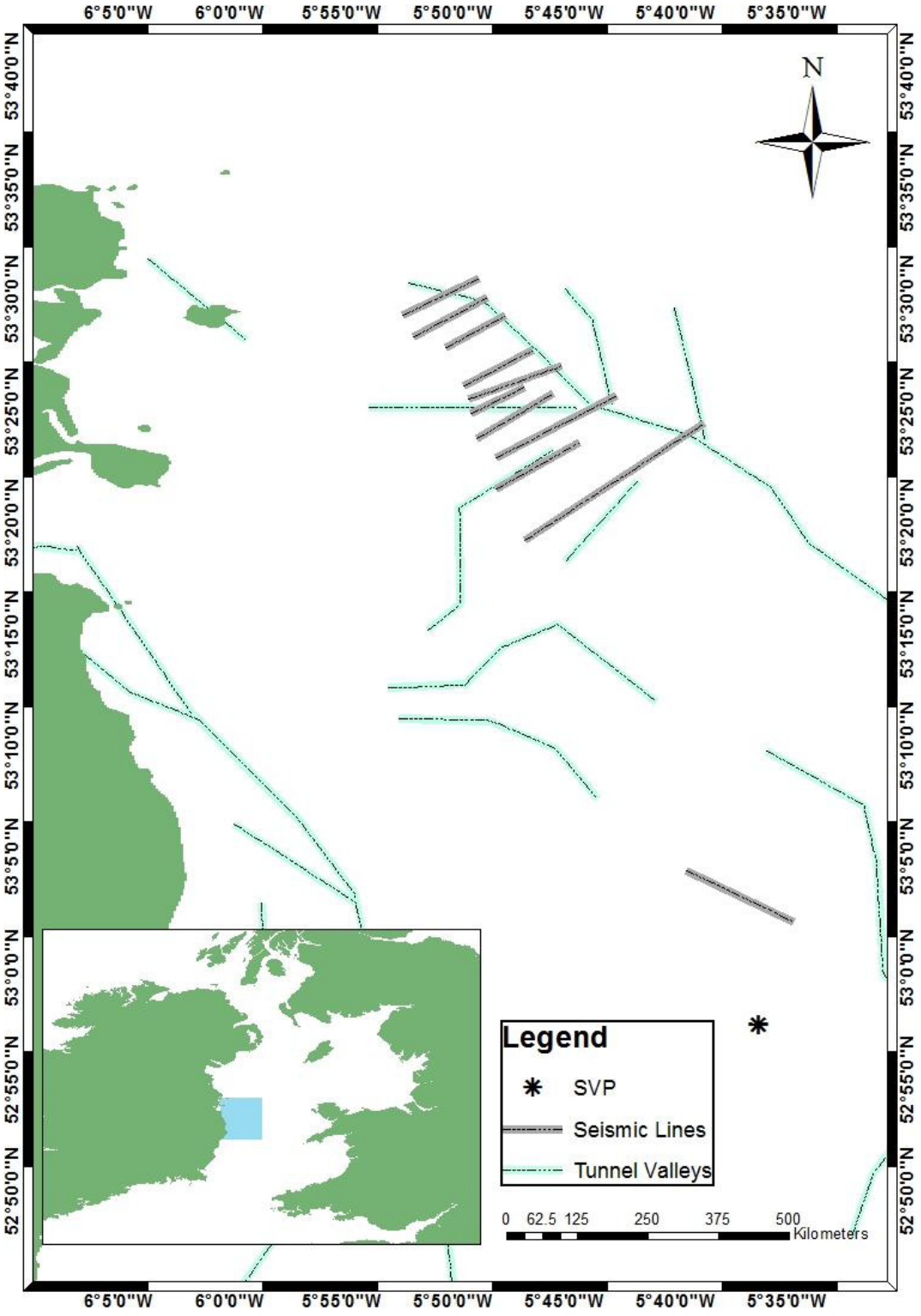

Figure D-6. Seismic line location map.

CPT STATIONS

Survey	Station No.	Area	Date	Time UTC	Latitude (Deg)	Latitude (Dec Min)	Longitude (Deg)	Longitude (Dec Min)	Water Depth (m)	Depth of GOST penetration (m)
CE14_001	1	Mudbelt			53	46.2545	5	59.0872	31.6	30
CE14_001	2a	Mudbelt			53	56.6689	6	2.658	22.1	3.3
CE14_001	2b	Mudbelt			53	56.669	6	2.659	21.3	0.75
CE14_001	2c	Mudbelt			53	56.682	6	2.652	20	3.3
CE14_001	3	Mudbelt			53	55.261	6	3.551	21.4	3.75
CE14_001	4	Mudbelt			53	53.375	6	47.091	29.1	3.65
CE14_001	5a	Mudbelt			53	50.937	6	4.015	28.6	10
CE14_001	5b	Mudbelt			53	50.9346	6	4.01	27.1	8.7
CE14_001	6	Mudbelt			53	37.994	5	54.266	48.8	21.2
CE14_001	7	Mudbelt			53	38.284	5	56.577	36.8	16
CE14_001	8	Mudbelt			53	39.418	5	56.158	37.7	19
CE14_001	9	Mudbelt			53	40.573	5	55.768	43.4	19
CE14_001	10	Mudbelt			53	42.248	5	57.914	37.5	20
CE14_001	11	Mudbelt			53	47.706	5	58.502	32.7	26.5
CE14_001	12	Mudbelt			53	48.819	5	58.045	35.3	26
CE14_001	13	Mudbelt			53	48.309	5	58.231	43.9	30
CE14_001	14	Mudbelt			53	49.58	5	52.701	44.1	26.7
CE14_001	15	Mudbelt			53	48.491	6	5.373	24.3	18.32
CE14_001	16	Mudbelt			53	55.25	6	3.54	23.1	0 (Aborted)
CE14_001	17	Lambay			53	28.0659	5	51.115	37.9	20

SPARKER SEISMIC LINES & SVP

Survey	Station No.	Line No.	Area	Date	Time UTC	Latitude (Deg)	Latitude (Dec Min)	Longitude (Deg)	Longitude (Dec Min)	Water Depth (m)	Comment
CE14_001	18		W. St. George's Channel	16.1.14	08.34	52	57.396	5	36.271	72	SVP
CE14_001	19	1	W. St. George's Channel	16.1.14	13.59	53	2.048	5	34.726	95.5	SOL
CE14_001	19	1	W. St. George's Channel	16.1.14	15.20	53	4.330	5	39.551	-	EOL. Two files
CE14_001	20	2	Lambay	16.1.14	19.47	53	27.844	5	50.353	49.2	SOL
CE14_001	20	2	Lambay	16.1.14	20.16	53	29.256	5	47.650	75.7	EOL
CE14_001	21	3	Lambay	16.1.14	20.36	53	30.070	5	48.486	73.1	SOL
CE14_001	21	3	Lambay	16.1.14	21.14	53	28.303	5	51.808	37.4	EOL
CE14_001	22	4	Lambay	16.1.14	21.27	53	29.259	5	52.290	42.6	SOL
CE14_001	22	4	Lambay	16.1.14	22.01	53	30.956	5	48.847	64.6	EOL
CE14_001	23	5	Lambay	16.1.14	22.44	53	27.719	5	46.438	71.0	SOL
CE14_001	23	5	Lambay	16.1.14	23.15	53	26.087	5	49.520	42.9	EOL
CE14_001	24	6	Lambay	16.1.14	23.46	53	23.721	5	48.967	44.8	SOL
CE14_001	24	6	Lambay	16.1.14	00:26	53	25.7957	5	45.5019	66.2	EOL
CE14_001	25	7	Lambay	17.1.14	00:54	53	23.588	5	44.3280	62.4	SOL
CE14_001	25	7	Lambay	17.1.14	01:30	53	21.4918	5	48.086	43.6	EOL
CE14_001	26	8	Lambay	17.1.14	02:04	53	19.1780	5	46.8267	30.9	SOL
CE14_001	26	8	Lambay	17.1.14	03:37	53	24.4436	5	38.7441	53.4	EOL

Survey	Station No.	Line No.	Area	Date	Time UTC	Latitude (Deg)	Latitude (Dec Min)	Longitude (Deg)	Longitude (Dec Min)	Water Depth (m)	Comment
CE14_001	27	9	Lambay	17.1.14	04.12	53	25.6940	5	42.6492	57.3	SOL
CE14_001	27	9	Lambay	17.1.14	05.09	53	22.8755	5	48.0861	44.7	EOL
CE14_001	28	10	Lambay	17.1.14	05.36	53	24.851	5	49.2460	41.6	EOL
CE14_001	28	10	Lambay	17.1.14	06:18	53	27.045	5	45.1628	65.2	EOL
CE14_001	29	11	Lambay	17.1.14	06.31	53	26.0443	5	46.7910	67.8	EOL
CE14_001	29	11	Lambay	17.1.14	06.57	53	25.5464	5	49.3307	41.3	EOL

Appendix E

RESEARCH EXPERIENCE

PEER REVIEWED PUBLICATIONS (as of September 2014)

- **Coughlan, M**., Wheeler, A.J., Dorschel, B., McCarron, S., Boer, W., van Gaever, P., de Haas, H. and Mörz, T. (Submitted). Mid to Late Holocene Depositional History of the Western Irish Sea Mud Belt. *Marine Geology.*
- **Coughlan, M**., Wheeler, A.J., Hepp, D.A., Hebbeln, D., and Mörz, T. (Submitted). A Revised Stratigraphic Framework for the Quaternary Deposits of the German North Sea Sector: a Geological - Geotechnical Approach. *Quaternary Science Reviews.*
- Wheeler, A. J., Murton, B., Copley, J., Lim, A., Carlsson, J., Collins, P., Dorschel, B., Green, D., Judge, M., Nye, V., Benzie J, Antoniacomi, A., **Coughlan, M.**, Morris, K., 2013. Moytirra: Discovery of the first known deep-sea hydrothermal vent field on the slow-spreading Mid-Atlantic Ridge north of the Azores. *Geochemistry, Geophysics, Geosystems* Volume 14, Issue 10, pages 4170–4184, October 2013.

CONFERENCE PROCEEDINGS

Irish Geological Research Meeting, Galway, February 2011

Renewable Energy Potential of Shallow European Continental Shelves: A Geological Appraisal.

M. Coughlan[1], A.Wheeler[1], B. Dorschel[1] and T.Mörz[2]

[1]*Geology, School of Biological, Earth and Environmental Sciences, University College Cork.*

[2]*Department of Marine Engineering Geology, MARUM, University of Bremen.*

Ireland has some of the best renewable energy sources in Europe, particularly in the offshore sector including wind, wave and tidal energy. These resources are essential in reaching EU targets for greenhouse gas emission as outlined in the Kyoto Protocol.

Within the context of offshore site suitability for renewable energy generation, we aim to carry out a modern geotechnical, stratigraphic and geophysical investigation into the comparable evolution of the Quaternary stratigraphy, palaeoenvironments and ice processes of shallow sea continental shelf strata, namely the north Irish Sea and southern North Sea.

In particular, the Codling Deep has been identified as an area of interest for studies in relation to developing tidal energy potential. The Codling Deep is one of a number of former subglacial tunnel valleys associated with glaciostatic downwarping in the Irish Sea Basin that experiences contemporary high energy hydrodynamic regimes. This project will develop a tidal model for the Codling Deep to establish the hydrodynamic regime and its relationship to bedform development. This study is crucial for energy potential evaluation as well as to further understand and explain

. . . . . .

GEOHAB, Helsinki, May 2011.

Quantifying Seabed Processes with Direct Relevance to Siting Offshore Renewable Energy Installation Foundations.

M. Coughlan[1], A.Wheeler[1], B. Dorschel[1] and T.Mörz[2]

[1]*Geology, School of Biological, Earth and Environmental Sciences, University College Cork.*

[2]*Department of Marine Engineering Geology, MARUM, University of Bremen*

The Irish Sea is a shallow, formerly glaciated, continental shelf consisting of a series of deeps in the south which presently experience high energy regimes to relatively benign mudbelts in the north. As such, the area has been recognized as having the potential to develop a number of sites for offshore renewable energy installations in both the wind and tidal sector.

Therefore, in September 2009 the Irish Sea Marine Assessment (ISMA) was undertaken by University College Cork (UCC), the Geological Survey of Ireland (GSI) and an industrial to target specific areas within the Irish Sea for developing offshore sites. During the course of the assessment a number of surveys were carried out with the intention of building a reliable geological model for the area including seismic, bathymetry, acoustic backscatter, sampling (both sedimentary and biological) and seabed current velocities. Initial analysis of the area noted a marked decrease in current velocities from the southern end to the northern end of the study section, this is represented by a change in seabed sediment particle size and seabed features. Acoustic backscatter is groundtruthed by sediment samples and underwater video camera transects. Additionally, grain size analyses is used in creating sediment facies distribution maps as well as determining seabed processes and velocities which are also mapped. Acoustic doppler current profiler (ADCP) data also aided in establishing the seabed hydrodynamic regime.

Constraining a good geological model of an area is essential in both siting offshore installations as well as assessing the potential impact of these installations on the local environment. The ISMA dataset provides a broad baseline map covering parameters of relevance to siting offshore renewable energy devices and their environmental impacts. The dataset also facilitates further studies focused on more site specific factors and modelling of impacts such as scour, hydrodynamic and sediment transport interactions and ecosystem response. In this way, through a carefully designed seabed mapping exercise, we hope to develop adequate data collection protocols for sustainable offshore renewable energy development.

. . . . . .

Irish Geological Research Meeting, Cork, February 2012.

Impact of Sediment Disturbance on the Western Mud Belt of the Irish Sea as a Paleo-archive and its Engineering Significance

M. Coughlan[1], A.Wheeler[1], B. Dorschel[1] and T.Mörz[2]

[1]*Geology, School of Biological, Earth and Environmental Sciences, University College Cork.*

[2]*Department of Marine Engineering Geology, MARUM, University of Bremen*

The Mud Belt in the Western Half of the Irish Sea is located at the northern termination of a transport path which has its origins further south in St. Georges Channel (Belderson, 1964). As such the area is largely regarded as a depocentre consisting of predominately Holocene muds and silts overlying glacial tills in places which hold a high resolution record allowing for a detailed paleoenvironmental reconstruction of the area.

The area is extensively trawled for the commercial Dublin Bay prawn and is also earmarked for potential offshore windfarm development. However, anthropogenic activities such as trawling as well as bioturbation from various benthic fauna may affect the geotechnical parameters of the sediment in the area, lowering the shear strength and hence making it more prone to scour which is a serious engineering consideration for such offshore installations. Therefore, the purpose of this study is to address the issues outlined above utilizing data acquired in order to characterise the geology of the Mud Belt. In doing so it is envisioned that it will provide a baseline study which will aid in any further management strategy of the area.

. . . . . .

GV and SEDIMENT, Hamburg, September 2012.

Re-evaluating Southern North Sea Stratigraphy from an Engineering Perspective

M.Coughlan[1], A.J. Wheeler,[1] S.Kreiter[2], D.Hepp[2] and T.Moerz[2]

[1] *School of Biological, Earth & Environmental Sciences, University College Cork*

[2]*Department of Marine Engineering Geology, MARUM, University of Bremen*

Due to investigations into oil and gas reserves, many areas of the North Sea have been comprehensively mapped. Such investigations do not take into account engineering considerations pertaining to sediment geotechnical parameters which are the primary concern in developing offshore renewable energy installations. Furthermore, petroleum exploration focuses on deeper layers as the primary target, below the immediate subsurface layers of significance to the construction of turbine foundations.

In this respect, the structure and stratigraphy of the uppermost 100 m or so of the German sector within the North Sea remains relatively under-investigated with existing models based on information from the late 1960's (e.g. Sindowski, 1970). Hitherto, the stratigraphy of the area has often been based on seismic interpretation of data limited by its shallow depth penetration and sedimentological interpretation of mostly short cores that were poorly recovered and constrained in their location. Often the distinction lithologically between various units from differing glacial episodes proved difficult, hence the need for clear seismic indicators.

The general evolution of the North Sea during the Pleistocene to the present can be summarised by marine to fluviodeltaic sedimentation in the Early Pleistocene, followed by at least three stages of glaciation in the Elsterian, Saalian and Weichselian with final stages of ice melting and present day sedimentary environments in the Latest Pleistocene and Holocene. The traditional three stage model of glaciation under scrutiny with evidence for more glacial episodes preserved in North Sea sequence with at least two stages of ice advance during the Saalian. This has resulted in a variety of ground conditions and environmental settings depositing a range of sediment with earlier, pre-glacial sediment, consequently been affected by subsequent ice overburden. Noticeable features in the area include glacier meltwater cut valley systems, successively infilled with sediment. In these valleys notable infills are primarily preserved including thick Lauenburg clay, an important stratigraphic marker. Similarly, basal peats are found at the base of the Holocene sequences and help to determine the boundary between Holocene and Pleistocene sediments, an important feature when it is considered Holocene sediments generally have unsuitable loading capacities compared to underlying deposits. As a result, individual site conditions can differ greatly depending on the presence of these valleys, as well as local salt structures, with varying lithological thicknesses and successions.

With this geological information in mind, the object of this project is to re-evaluate the stratigraphy of specific sites of interest within the German sector of the North Sea from an engineering perspective utilising an extensive seismic, core and geotechnical dataset to identify specific facies, describe their relations and give an overview of their typical soil mechanical properties and hence

develop a more robust geological model these specific sites which will hopefully correlate across the area.

. . . . . .

Irish Geological Research Meeting, Derry, March 2013.

Depositional History of the Western Irish Sea Mud Belt

M.Coughlan[1], A. Wheeler[1], B. Dorschel[2] and T. Moerz[3]

[1] *School of Biological, Earth & Environmental Sciences, University College Cork*

[2] *Alfred Wegner Institute for Polar Research, Bremerhaven*

[3]*Department of Marine Engineering Geology, MARUM, University of Bremen*

The Mud Belt in the western half of the Irish Sea is located at the northern termination of a transport path ,largely marked by sand-wave migration, which has its origins further south. Here, deposition is the dominant process under a low energy regime and, as such, it is a depocentre consisting of predominately Holocene muds and silts overlying glacial tills deposited during the melting of the Devensian ice-sheet extending over an extensive area with water depths ranging up to 100 m.

Until now the potential of the Mud Belt as a high resolution archive of paleoenvironmental and climatic change in the Irish Sea remains relatively unexplored. With climate change a major global issue today, the need for coherent and detailed records establishing past environmental conditions are all the more important. Hence, we aim to investigate whether the sediment record holds a high-resolution paleoarchive of environmental change during the Holocene or has been disturbed by biological (e.g. bioturbation), physical (e.g. wave and tidal) or anthropogenic (e.g. trawling) factors.

In order to do so three vibrocores were recovered from various parts of the Mud Belt. Correlation between the cores was made possible by multi-sensor core logger data with subsequently two cores subjected to detailed stratigraphic analysis by way of gamma spectrometry and accelerator

mass spectrometry (AMS) 14C dating. Furthermore, the cores were subject to particle-size analyses (PSA) and X-ray fluorescence (XRF) analyses to aid in paleoenvironmental reconstruction.

The study hopes to address the issues outlined above utilizing data acquired in order to characterise the geology of the Mud Belt as part of an extensive survey. In doing so it is envisioned that it will also provide a baseline study which will aid in any further management strategy of the area seeing as it is commercially active as a prominent fisheries ground as well as being earmarked for offshore renewable energy development.

. . . . . .

International Association of Sedimentologists, Manchester, September 2013.

Depositional History of the Western Irish Sea Mud Belt and Anthropogenic Impacts

Coughlan, M.[1], Wheeler, A. [1], Dorschel, B. [2], McCarron, S. [3], de Stigter, H. [4], Boer, W. [4], van Gaever, P. [4], de Haas, H. [4] and Mörz, T. [5]

1 School of Biological, Earth & Environmental Sciences, University College Cork, Ireland.
2 Alfred Wegner Institute, Bremerhaven, Germany.
3 Department of Geography, National University of Ireland, Maynooth.
4 Royal Netherlands Institute for Sea Research, The Netherlands.
5 Department of Marine Engineering Geology, MARUM, University of Bremen, Germany.

The Mud Belt in the western half of the Irish Sea is located at the northern termination of a transport path, largely marked by sand-wave migration, which has its origins further south. Here, deposition is the dominant process under a low energy regime and, as such, it is a depocentre consisting of predominately Holocene muds and silts overlying glacial tills deposited during the melting of the Devensian ice-sheet extending over an extensive area with water depths ranging up to 100 m. Furthermore, the area is economically important being extensively trawled for the commercial Dublin Bay prawn and is also earmarked for potential offshore windfarm development.

Until now the potential of the Mud Belt as a high resolution archive of paleoenvironmental and climatic change in the Irish Sea remains relatively unexplored. With climate change and anthropogenic effects on environments a major global issue today, the need for coherent and detailed records establishing past environmental conditions are all the more important. Hence, we aim to investigate whether the sediment record here holds a high-resolution palaeoarchive of environmental change during the Holocene or has been disturbed by biological (e.g. bioturbation), physical (e.g. wave and tidal) or anthropogenic (e.g. trawling) factors.

In order to do so four vibrocores of roughly 3 metre length were recovered from various parts of the Mud Belt in 2009 as part of the Irish Sea Marine Assessment (ISMA) onboard the Irish R.V. Celtic Voyager. Correlation between the cores was made possible by multi-sensor core logger data including gamma ray attenuation, P-wave velocity, magnetic susceptibility and colour spectrometry. Subsequently, two cores were subjected to detailed stratigraphic analysis by way of gamma spectrometry focusing on ^{210}Pb, ^{137}Cs and ^{241}Am levels in the upper 2 metres with accelerator mass spectrometry (AMS) 14C dating carried out on ten samples of the gastropod *Turritella communis*. In addition, the cores were subject to microfossil, particle-size (PSA) and X-ray fluorescence (XRF) analyses to aid in palaeoenvironmental reconstruction with CT X-ray scans used to identify sedimentary structures as well as assess sediment disturbance through bioturbation.

As a result, based on particle size distribution, geochemical and physical properties, we were able to identify 5 lithostratigraphic units across all cores spanning some 7,000 years of depositional history. These units represent broad environmental changes that can be linked to recorded climatic fluctuations during the late Holocene. Definite changes in sedimentation and hydrographical conditions are seen throughout this timeframe and right up to the present day. However, in the more recent past, we see an increased anthropogenic influence on the stratigraphic record through the effects of trawling and input of radionuclides derived from Sellafield discharge.

Therefore, whilst the Mud Belt offers a unique area to study the link between past climate forcing and oceanic circulations in addition to terrestrial changes, human influence is strongly felt, which has implications for future environmental management and evolution of the area.

. . . . . .

Irish Geological Research Meeting, Dublin, March 2014.

A Revised Stratigraphic Framework for the Quaternary Deposits of the German North Sea sector: A Geological-Geotechnical Approach.

M. Coughlan[1,2], A.J. Wheeler[1], D.A. Hepp[2] , D. Hebbeln[2] and T. Mörz[2,3].

[1]*School of Biological, Earth & Environmental Sciences, University College Cork, North Mall, Cork, Ireland.*

[2]*MARUM- Center for Marine Environmental Sciences and Faculty of Geosciences, of Bremen, Leobener Str, 28359 Bremen, Germany.*

[3]*Geo-Engineering.org GmbH, Bremen, Germany.*

With an increasing focus on the study of anthropogenic driven climate change, the need to investigate and understand natural climatic and environmental fluctuations is even greater. The mid- to late-Quaternary has seen changing conditions between glacial and inter-glacial times. Onshore exposure of these transitions is limited; however, offshore marine sediments can offer a record of such changes.

In comparison to neighbouring countries the offshore Quaternary stratigraphy of the German North Sea remains largely under-investigated (Cameron *et al.,* 1987). This can be attributed to the paucity of scientifically published information and data relating to the upper 100m or so of the German North Sea sub-surface as early surveys experienced poor recovery from sedimentary sequences, limited seismic depth penetration and resolution and the geomorphological context for features was not easily identifiable (Graham *et al.,* 2011). As a result, generally oversimplified lithostratigraphies were presented (e.g. Sindowski, 1970).

The advent of increased interest in renewable energy in the offshore sector has brought new advances in offshore site investigation and yielded a new suite of data focusing on the geological and mechanical properties of the upper sedimentary layers in addition to extensive geophysical surveys. As a result, the study of offshore stratigraphy has benefitted from increased groundtruthing by sediment cores with in-situ measurements (such as Cone Penetration Tests or CPT) along with an increased density and much improved resolution of seismic imaging allowing for a dependable interpretation of sedimentary processes and models.

Across four study areas within the German North Sea sector, nine buried valleys and two shallow troughs were mapped. This study aims to reappraise the stratigraphy and geometry of the Quaternary deposits of the German North Sea sector by linking new seismic data with recovered core lithostratigraphies and geotechnical properties. Furthermore, these analyses will garner new insights into depositional history and palaeoenvironments.

. . . . . .

Irish Quaternary Association Annual Spring Meeting, Cork, March 2014.

Palaeo-archive Settings in Shallow Shelf Seas of North-West Europe

M.Coughlan[1], A. Wheeler [1], B. Dorschel [2], S. McCarron[3], H. de Stigter [4], W. Boer[4], P. van Gaever[4], H. de Haas [4], C. Lordan[5] and Mörz, T[6].

[1] *School of Biological, Earth & Environmental Sciences, University College Cork, Ireland.*

[2] *Alfred Wegner Institute, Bremerhaven, Germany.*

[3]*Department of Geography, National University of Ireland, Maynooth.*

[4] *Royal Netherlands Institute for Sea Research, The Netherlands.*

[5]*Marine Institute, Rinville, Oranmore, Co. Galway, Ireland.*

[6]*Department of Marine Engineering Geology, MARUM, University of Bremen, Germany.*

The climatic development of the Mid to Late Quaternary (last 400,000 years) is characterised by fluctuation between glacial and interglacial periods leading to the present interglacial, the

Holocene. In comparison to preceding periods it was believed the Holocene represented a time of relative climatic stability. However, recent work has shown that the Holocene can be divided into cooler periods such as the Little Ice Age alternating with time intervals where climatic conditions ameliorated i.e. Medieval Warm Period, Holocene Thermal Optimum and the present Modern Optimum. In addition, the Holocene is recognised as a period with increasing anthropogenic influence on the environment.

Onshore records recording glacial/interglacial cycles as well as anthropogenic effects are limited. However, sites of sediment accumulation on the shallow continental shelf offer the potential to reconstruct these events. Such sites include tunnel valleys and low energy, depositional settings. In this study we interrogated the sediment stratigraphy at such sites in the North Sea and Irish Sea using traditional techniques, as well as novel applications of geotechnical data, to reconstruct the palaeoenvironmental record.

Within the German North Sea sector a combination of core, seismic and in-situ Cone Penetration Testing (CPT) data was used to identify sedimentary units, place them within a morphological context, relate them to glacial or interglacial periods stratigraphically, and correlate them across the German North Sea. Subsequently, we were able to revise the Mid to Late Quaternary stratigraphy for the North Sea using this new and novel data.

Similarly, Holocene environmental changes were investigated within the Irish Sea at a depositional site with active anthropogenic influence. The methods used included analyses on grain-size distribution, foraminifera, gamma spectrometry, AMS 14C and physical core logging. The investigation revealed a strong fluctuating climatic signal early in the areas history before anthropogenic influence affects the record through trawling.

RESEARCH CRUISES

January 2014 **Research Scientist/Night Shift Leader, Celtic Explorer, CE14001.**

February 2013 **Research Scientist/Night Shift Leader, Celtic Explorer, CE13003.**

March 2012 **Research Scientist, Celtic Voyager CV12006, (NSGeo).**

August 2011 **Research Scientist, Celtic Explorer CE11009, (VENTuRE).**

July 2010 **Research Scientist, R.V POSEIDON POS400, (CORICON).**

September 2009 **Research Scientist, Celtic Voyager CV0926, (ISMA).**

April 2009 **Research Scientist, Celtic Explorer CE0907.**